

Genome-wide identification of Hand2 target regions in mouse embryos using dRMCE, a new genetic tool

Inauguraldissertation

zur Erlangung der Würde eines Doktors der Philosophie
vorgelegt der
Philosophisch-Naturwissenschaftlichen Fakultät
der Universität Basel

von

Marco Osterwalder

aus Gaiserwald, SG

Basel, 2012

Original document stored on the publication server of the University of Basel
edoc.unibas.ch



This work is licenced under the agreement „Attribution Non-Commercial No Derivatives – 2.5 Switzerland“. The complete text may be viewed here:

creativecommons.org/licenses/by-nc-nd/2.5/ch/deed.en



Attribution-Noncommercial-No Derivative Works 2.5 Switzerland

You are free:



to Share — to copy, distribute and transmit the work

Under the following conditions:



Attribution. You must attribute the work in the manner specified by the author or licensor (but not in any way that suggests that they endorse you or your use of the work).



Noncommercial. You may not use this work for commercial purposes.



No Derivative Works. You may not alter, transform, or build upon this work.

- For any reuse or distribution, you must make clear to others the license terms of this work. The best way to do this is with a link to this web page.
- Any of the above conditions can be waived if you get permission from the copyright holder.
- Nothing in this license impairs or restricts the author's moral rights.

Your fair dealing and other rights are in no way affected by the above.

This is a human-readable summary of the Legal Code (the full license) available in German:
<http://creativecommons.org/licenses/by-nc-nd/2.5/ch/legalcode.de>

Disclaimer:

The Commons Deed is not a license. It is simply a handy reference for understanding the Legal Code (the full license) — it is a human-readable expression of some of its key terms. Think of it as the user-friendly interface to the Legal Code beneath. This Deed itself has no legal value, and its contents do not appear in the actual license. Creative Commons is not a law firm and does not provide legal services. Distributing of, displaying of, or linking to this Commons Deed does not create an attorney-client relationship.

Genehmigt von der Philosophisch-Naturwissenschaftlichen Fakultät

auf Antrag von

Prof. Dr. Rolf Zeller (Dissertationsleiter), Prof. Dr. Markus Affolter (Korreferent) und

Dr. Antoine H. F. M. Peters

Basel, den 21. Februar 2012

Prof. Dr. Martin Spiess

Dekan

1. Table of contents

1. Table of contents	5
2. Summary	9
3. Introduction	11
3.1 Limb bud development.....	11
3.1.1 The basics.....	11
3.1.2 AER-Fgfs control proximodistal limb bud outgrowth in an instructive manner	13
3.1.3 The zone of polarizing activity (ZPA) is the source of Shh signalling.....	14
3.1.4 The spatio-temporal control of the anteroposterior limb bud axis by Shh signalling.....	16
3.1.5 Interlinked signalling feedback loops integrate AP and PD limb development	17
3.1.6 Control of the zone of polarizing activity (ZPA) and the pre-patterning mechanism	19
3.1.7 Functions of Hand2 prior to and independent of <i>Shh</i> activation.....	22
3.1.8 <i>Hox</i> genes during limb development	23
3.2 Hand2 as a critical regulator of embryonic development.....	26
3.3 Technology: The identification of bona fide transcriptional targets requires genomic engineering of the endogenous locus.....	28
4. Aim of the Thesis	31
5. Results	33
5.1 Development of dRMCE for high-throughput engineering of conditional alleles	33
5.1.1 Challenges in targeting the <i>Hand2</i> locus.....	33
5.1.2 dRMCE to custom-modify conditional alleles: the proof of principle	34
5.1.3 dRMCE allows efficient re-engineering of thousands of IKMC conditional alleles	41
5.1.4 Defining high-sensitivity epitopes for tagging endogenous Hand2.....	49
5.1.5 Generation of various <i>Hand2</i> knock-in alleles using dRMCE.....	54
5.2 A sensitive tool for detection of the endogenous Hand2 protein	58
5.2.1 Embryoid bodies to validate the <i>Hand2</i> ^{3xFLAG} endogenously tagged protein	58
5.2.2 Tracking the expression dynamics of Hand2 tagged proteins in the mouse limb bud	65
5.2.3 A tool to monitor Hand2 expression in the embryonic heart.....	73
5.2.4 Hand2 and Sox9 proteins are expressed in a largely complementary manner.....	75
5.3 Identification of genome-wide target regions bound by Hand2	78
5.3.1 Refined mapping of Hand2 interaction with the ZRS by ChIP-qPCR.....	78
5.3.2 Genome-scale identification of Hand2 target regions in the mouse embryo using a ChIP-seq approach	84

5.3.3 Hand2 regulates femur development and interacts with a <i>Tbx4</i> hindlimb enhancer.....	92
---	----

6. Discussion..... 97

6.1 dRMCE and next-generation engineering of the mouse genome	98
---	----

6.2 Epitope tagging of endogenous proteins to assess <i>in vivo</i> function.....	99
---	----

6.3 Genome-wide identification of the genomic regions bound to Hand2-containing transcriptional complexes during limb bud development.	100
---	-----

6.4 Candidate target genes of Hand2 in the embryonic heart and branchial arches	104
---	-----

6.5 Conclusions & Outlook.....	107
--------------------------------	-----

7. Materials and Methods..... 109

7.1 Genetic engineering of plasmids	109
---	-----

7.1.1 Cloning procedure	109
-------------------------------	-----

7.1.2 Generation of the <i>Hand2</i> , <i>Hand2</i> ^{1xFLAG} , <i>Hand2</i> ^{NBio} and <i>Hand2</i> ^{CBio} expression vectors.....	109
---	-----

7.1.3 Construction of the pDIRE expression vector.....	110
--	-----

7.1.4 Construction of the <i>Hand2</i> ^{1xFLAG} replacement vector.....	110
--	-----

7.1.5 Construction of the pDRAV replacement backbone vectors	111
--	-----

7.1.6 Generation of the pGT-VP replacement vector series	111
--	-----

7.1.7 Construction of the <i>Hand2</i> ^{3xFLAG} expression and replacement vectors	111
---	-----

7.1.8 Construction of the <i>Hand2</i> ^{LAP} expression and replacement vectors	112
--	-----

7.1.9 Construction of the <i>Hand2</i> ^{Bio-BirA} expression and replacement vectors	112
---	-----

7.2 dRMCE related technical approaches.....	113
---	-----

7.2.1 dRMCE procedure including ES cell culture.....	113
--	-----

7.2.2 ES cell transfection and selection.....	113
---	-----

7.2.3 Detection of dRMCE replacement events by PCR	114
--	-----

7.2.4 <i>In silico</i> data mining to identify conditional alleles compatible with dRMCE	114
--	-----

7.2.5 Screening of PCR selected ES clones by Southern Blot analysis	114
---	-----

7.2.6 Immunodetection of YFP and β -galactosidase in ES cells.....	116
--	-----

7.3 Mice & Molecular Biology	116
------------------------------------	-----

7.3.1 Generation of Hand2-FLAG lines and mouse colony management.....	116
---	-----

7.3.2 Skeletal preparations	117
-----------------------------------	-----

7.3.3 Whole mount <i>in situ</i> hybridisation	117
--	-----

7.3.4 Protein overexpression in HEK293T cells	118
---	-----

7.3.5 Luciferase assay	119
------------------------------	-----

7.3.6 ES cell differentiation	119
-------------------------------------	-----

7.3.7 RNA extraction and cDNA synthesis	120
---	-----

7.3.8 Quantitative real-time PCR analysis (qPCR).....	121
---	-----

7.3.9 Western Blot analysis	122
-----------------------------------	-----

7.3.10 Silver stain	123
---------------------------	-----

7.3.11 Limb bud cell culture	123
------------------------------------	-----

7.3.12 Immunocytochemistry.....	124
---------------------------------	-----

7.3.13 Histology	124
------------------------	-----

7.3.14 Immunohistochemistry.....	125
7.4 Towards a ChIP-seq approach.....	125
7.4.1 Sonication tests	125
7.4.2 Immunoprecipitation (IP).....	126
7.4.3 Chromatin immunoprecipitation (ChIP) using E11.75 limb buds.....	126
7.4.4 ChIP with subsequent next-generation sequencing (ChIP-seq).....	129
7.5 Tables of reagents, frequencies & materials	133
8. Acknowledgements	145
9. References.....	147
10. Appendix.....	163
10.1 Appendix Introduction	163
10.1.1 Morphogenesis of the heart: The basics	163
10.2 Appendix Results	166
10.2.1 Detection of Hand2 protein isoforms in <i>Hand2</i> ^{3xFLAG} expressing tissues	166
10.2.2 ChIP-seq reveals Hand2 candidate target regions in the branchial arches and the developing heart.	166
10.3 Appendix Panels & Tables	170
Appendix Table 1. List of the highest enriched Hand2 ChIP-seq peaks.....	176
Appendix Table 2. GO Biological Processes associated with the top 795 ChIP-seq dataset....	191
Appendix Table 3. GREAT gene association tables of the top 795 peak regions.....	192
Appendix Table 4. List of dRMCE compatible conditional alleles described in the literature.....	195
10.4 Appendix References.....	201
11. Publications.....	203
11.1 Dual RMCE for efficient re-engineering of mouse mutant alleles – Nature Methods, 2010 (First Author)	205
The author file – Nature Methods	217
Next generation engineering of conditional mouse alleles with loxP and FRT sites by dual RMCE – Nature Protocol Exchange.....	219
11.2 Distinct Roles of Hand2 in Initiating Polarity and Posterior Shh Expression during the Onset of Mouse Limb Bud Development – Plos Genetics (Co-Author)	221
11.3 GLI3 Constrains Digit Number by Controlling Both Progenitor Proliferation and BMP-Dependent Exit to Chondrogenesis – Developmental Cell (Co-Author).....	235

2. Summary

Limb bud development is a paradigmatic model to study the molecular signals that orchestrate cell growth and behaviour. Anterior-posterior patterning of the limb bud mesenchyme is dependent on the secreted ligand Sonic hedgehog (Shh). *Shh* expression in the posterior limb bud mesenchyme defines the zone of polarizing activity (ZPA) and controls cell survival and proliferative expansion during limb bud outgrowth. The bHLH transcription factor Hand2 binds to the limb-specific far-upstream *Shh* enhancer termed ZPA regulatory sequence (ZRS) and is essential for *Shh* activation. With the exception of the ZRS, no other direct Hand2 target regulatory regions and genes have been identified. Given that Hand2 is also required for development of the heart and neural crest derivatives, determining the genome-wide range of Hand2 target regions in mouse embryos will contribute to the understanding of underlying gene-regulatory networks. We decided to insert an epitope tag into the endogenous Hand2 protein to be able to precisely determine the range of Hand2 target sequences by ChIP-seq analysis. However, as genetic engineering of the *Hand2* locus by homologous recombination is very inefficient, we developed dRMCE to re-engineer the *Hand2* conditional allele. In doing so, we realized that dRMCE is compatible with thousands of conditional alleles and allows highly efficient custom-modification of the endogenous locus. dRMCE allowed me to rapidly generate a mouse model encoding an epitope tag within the endogenous Hand2 protein, which permits highly sensitive detection and localization of endogenous Hand2 in differentiated ES cells and embryonic tissues. We successfully used this fully functional epitope-tagged Hand2 protein to identify the large range of Hand2 target sequences in mouse embryonic tissues using a ChIP-seq approach. Our results indicate that Hand2 interacts with *Gli3* and *Tbx* regulatory sites in limb buds and binds to a minimal ZRS element associated with human point mutations that cause polydactyly. I show that Hand2 is required for the development of the proximal skeleton of the hindlimb, likely by interacting directly with a *Tbx4* enhancer. Furthermore, I describe the Hand2 target range associated with essential regulators of cardiac or craniofacial development. Thus, my approach begins

to provide insight into the regulatory gene networks regulated by Hand2 during embryogenesis.

3. Introduction

“What can be more curious than that the hand of a man, formed for grasping, that of a mole for digging, the leg of the horse, the paddle of the porpoise, and the wing of the bat, should all be constructed on the same pattern, and should include the same bones, in the same relative positions?”

- Charles Darwin, The Origin of Species, Chapter 13

3.1 Limb bud development

3.1.1 The basics

Tetrapod fore- and hindlimbs originate from lateral plate mesoderm at defined positions and grow out perpendicular to the primary body axis (Zeller et al., 2009). Developing limbs emerge as a bulge of mesenchyme enveloped in an ectodermal pocket and are patterned along the proximodistal (PD), anteroposterior (AP) and dorsoventral (DV) axes (Figure 1A). Along the PD axis, limb buds are divided into three segments giving rise to the skeletal elements, defined as stylopod (humerus/femur), zeugopod (ulna/radius and tibia/fibula) and autopod (carpals/tarsals, metacarpals/metatarsals, phalanges) (Figure 1B). AP axis patterning defines the number and identity of autopodal (digits 1 to 5) and zeugopodal (radius/ulna) skeletal elements (Figure 1B). The most anterior digit is defined as digit 1 (thumb), whereas the most posterior digit is digit 5 (pinky). The limb skeleton provides an excellent anatomical read-out of the molecular alterations underlying genetically altered limb development. The analysis of the molecular mechanisms that control vertebrate limb development have made major contributions to our current understanding of vertebrate organogenesis. The developing limb bud is amenable to experimental manipulation and non-essential for the survival of embryos. Therefore, limb development provides an excellent system to study the molecular mechanisms that coordinate growth with patterning during

embryogenesis (Zeller et al., 2009). Two main signalling centers coordinate limb bud development. The apical ectodermal ridge (AER) is a source of fibroblast growth factors (Fgf) and critical for proximo-distal (PD) limb axis outgrowth and patterning (Figure 1C). The zone of polarizing activity (ZPA) is located in the posterior mesenchyme and produces Sonic Hedgehog (Shh), which is essential to pattern the antero-posterior (AP) axis (Figure 1C). These two organizers are interlinked by feedback signalling interactions and coordinate limb bud outgrowth and patterning.

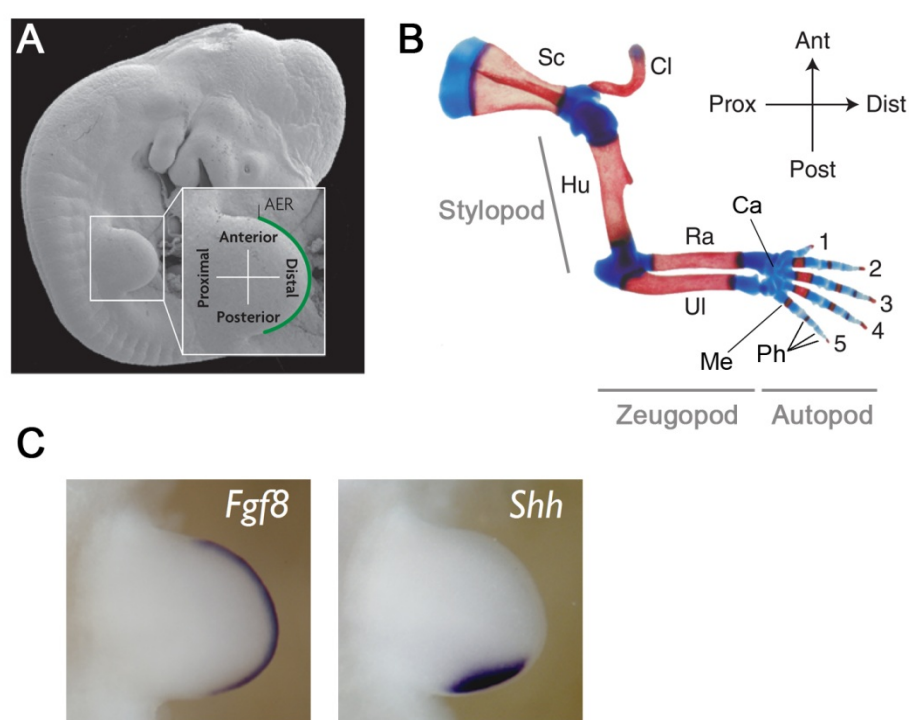


Figure 1. Proximodistal (PD) development defines the sequence of skeletal elements of the limb. **(A)** Scanning electron micrograph of a mouse embryo at embryonic day 10.5 (E10.5). The forelimb bud is enlarged and shows proximodistal (PD) and anteroposterior (AP) axes. The apical ectodermal ridge (AER) appears in green. Adapted from Zeller et al., 2009. **(B)** Skeletal preparation of a newborn mouse forelimb. Cartilage is stained in blue, whereas ossified elements are coloured red. Skeletal elements are indicated. Numbers denote the sequence from the anterior-most (1) to the most posterior (5) digit. Sc, Scapula. Cl, clavicle. Hu, humerus. Ra, radius. UI, ulna. Ca, carpals. Me, metacarpals. Ph, phalanges. Adapted from Benazet & Zeller, 2009. **(C)** Two signalling centers control limb bud outgrowth and patterning. The apical ectodermal ridge (AER) is defined by the *Fgf8* expression domain running along the distal dorsoventral interface. The zone of polarizing activity (ZPA) corresponds to the domain of *Shh* expression. Images displaying *in situ* transcript detection were contributed by Javier Lopez-Rios.

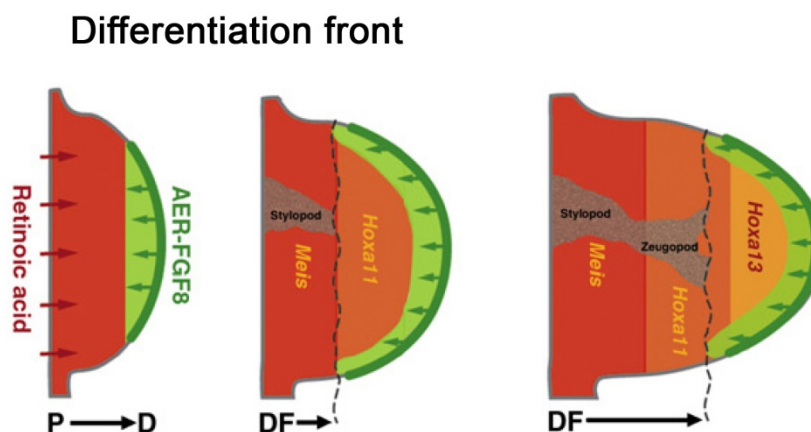
3.1.2 AER-Fgfs control proximodistal limb bud outgrowth in an instructive manner

Proximodistal outgrowth is controlled by the AER, which runs along the distal tip of the limb bud at the dorsoventral interface of the ectoderm. The critical signals produced by the AER are ligands of the Fgf family, which include Fgf4, Fgf8, Fgf9 and Fgf17 (Niswander et al., 1993; Mariani et al., 2008). During the onset of forelimb budding, the T-box transcription factor Tbx5 (Tbx4/Pitx1 in the hindlimb (Duboc & Logan, 2011)) initiates *Fgf10* expression in the forelimb bud mesenchyme (Agarwal et al., 2003). Fgf10 in turn activates *Fgf8* in the AER, which establishes a positive feedback loop between these two Fgf ligands that is essential for PD outgrowth (Ohuchi et al., 1997; Min et al., 1998). Inactivation of *Fgf8* results in smaller limb buds and delays *Shh* activation, which causes skeletal abnormalities (Lewandowski et al., 2000). *Fgf4*, *Fgf9* and *Fgf17* are activated after AER formation and they are individually dispensable for limb development, but required in combination with *Fgf8* to control the PD sequence of skeletal elements in a dose-dependent manner (Mariani et al., 2008). The most severe phenotype is observed in *Fgf4*, *Fgf8* compound mutants, as limb bud outgrowth is disrupted (Sun et al., 2002). In addition, AER-Fgf signalling represses the expression of *Meis* genes, which regulate proximal cell fate (Mariani et al., 2008, Mercader et al., 2000). One current model for control of PD limb bud development is the differentiation-front model (Figure 2; Tabin & Wolpert 2007; Zeller et al., 2009). This model suggests that the naïve limb field is in a “default” state in which cells are fated to contribute to the proximal stylopod as a consequence of RA-mediated expression of the homeobox transcription factors *Meis1/2* (Mariani et al., 2008; Mercader et al., 2000). Mesenchymal cells in the range of AER-Fgf and ectodermal Wnt signals acquire distal fates and retain an undifferentiated, proliferative state (Ten Berge et al., 2008). Polarized cell division and movement of mesenchymal cells promote PD outgrowth by pushing the AER and its mesenchymal target domain progressively more distal (Boehm et al., 2010). Cells exiting the undifferentiated zone are determined by “fixing” their PD fates. The border at which cells leave and become determined is called differentiation front (Figure 2). Cells under the influence of only Wnt

signals proliferate slower and are re-specified to acquire soft connective tissue fates (Ten Berge et al., 2008). In contrast, cells within the core mesenchyme are out of range of Wnt and Fgf signals and are specified towards pre-chondrogenic mesenchyme.¹

Figure 2.

The differentiation front model. Left panel: Retinoic acid (RA) signalling from the flank (red) specifies the proximal chondrogenic part of the early limb bud. The distal part is subjected to Fgf8 signalling from the AER



(green) and thus in an undifferentiated state. Middle panel: In the course of limb bud outgrowth, RA-mediated *Meis1/2* activation in the proximal part leads to pre-chondrogenic condensations of stylopod (humerus) skeletal elements. More distal cells which received Fgf signalling are specified towards zeugopod (ulna, radius) character (marked by *Hoxa11*). The differentiation front (DF, broken line) is established at the interface of proximal chondrogenic and distal undifferentiated cells. Right panel: With progressive limb bud outgrowth, the differentiation front moves distally. Cells leaving the differentiation front undergo differentiation whereas a subpopulation acquires chondrogenic fate. Distal cells under the influence of AER-Fgfs are specified to populate the presumptive autopod, as marked by expression of *Hoxa13*. P, proximal. D, distal. Adapted from Zeller, 2010.

3.1.3 The zone of polarizing activity (ZPA) is the source of Shh signalling

More than 40 years ago, J.W. Saunders showed that transplantation of chicken posterior limb bud tissue into the anterior mesenchyme of a donor limb bud caused mirror image digit duplications (Saunders & Gasseling 1968). This “polarizing organizer” located at the posterior mesenchymal limb bud margin was later termed zone of polarizing activity (ZPA). Finally, the long-range diffusible morphogen produced in the ZPA and polarizing the AP limb

¹ DV patterning is out of scope of this study and therefore not discussed here (see Zeller & Duboule 1997)

bud axis was identified as Sonic hedgehog (Shh), which is a homologue of the *Drosophila* segment polarity gene *hedgehog* (Riddle et al., 1993; Riddle et al., 1995). Hedgehog signalling is a major morphogenetic pathway during vertebrate development and its deregulation causes different types of tumours (reviewed in Varjosalo & Taipale 2008).

Hedgehog (HH) proteins encode a small N-terminal signal sequence, a signalling domain and a large C-terminal autoprocessing. Cleavage of the signal sequence and the C-terminal domain is required for covalent palmitoyl (N-terminally) and cholesterol (C-terminally) modifications, which control diffusion of the HH ligand (Chen et al., 2004; Li et al., 2006). The mature Shh polypeptide forms a posterior to anterior gradient across the limb bud mesenchyme at long distances up to 300µm (Zeng et al., 2001; Zhu and Scott 2004; Li et al., 2006). The 12-span transmembrane protein Ptch1 restricts the spreading of the Shh signal and promotes its internalization and lysosome-mediated degradation (Varjosalo & Taipale 2008). Binding of Shh to Ptch1 leads to accumulation of Smoothed (Smo) at the primary cilia and intracellular signal transduction via activation of Gli transcription factors (Goetz & Anderson 2010). The Gli zinc finger proteins (Gli1, Gli2, Gli3) are the direct downstream effectors of Shh signalling in vertebrates and orthologues of *Cubitus interruptus* (Ci), the effector of Hedgehog signal transduction in *Drosophila* (Matise & Joyner 1999). *Gli1* encodes a transcriptional activator, whereas the full-length Gli2 and Gli3 can be either activator or processed into repressor forms, similar to Ci. In the absence of Shh, the default proteolytic processing of the Gli2/3 full-length isoforms results in the production of the Gli2/3R transcriptional repressors (Wang et al., 2000). Whereas Gli1 and Gli2 are dispensable for limb bud development, Gli3R represents the major Gli repressor form in the limb bud (Wang et al., 2000; Ahn & Joyner et al., 2004). *Gli3* is required to restrict Shh pathway activation to the posterior mesenchyme, whereas its absence triggers ectopic Shh signalling, which causes preaxial (anterior) and central polydactylies (Büscher et al., 1997; Hui & Joyner 1993, Figure 5C).

3.1.4 The spatio-temporal control of the anteroposterior limb bud axis by Shh signalling

In the forelimb bud *Shh* is expressed from about embryonic day 9.5 (E9.5) to E12. The “French Flag model” put forward by Lewis Wolpert proposed that the posterior mesenchyme secretes a morphogen, a molecule that would diffuse in a gradient manner from its source. Threshold levels of the morphogen (illustrated by the three colours of the French flag) would then specify the different digit identities in chicken wing buds and the ZPA itself would not contribute to the digits (Figure 3A). More recently, genetic fate mapping of the ZPA-descendant population (*Shh* descendants) and of *Shh*-responding cells in mouse limb buds (Harfe et al., 2004; Ahn & Joyner 2004) revealed that AP axis patterning is a more dynamic and complex process in which mesenchymal cells acquire a kinetic memory of the time and dose of exposure to SHH, which ultimately is interpreted to establish their AP identities in the limb bud (Figure 3B).

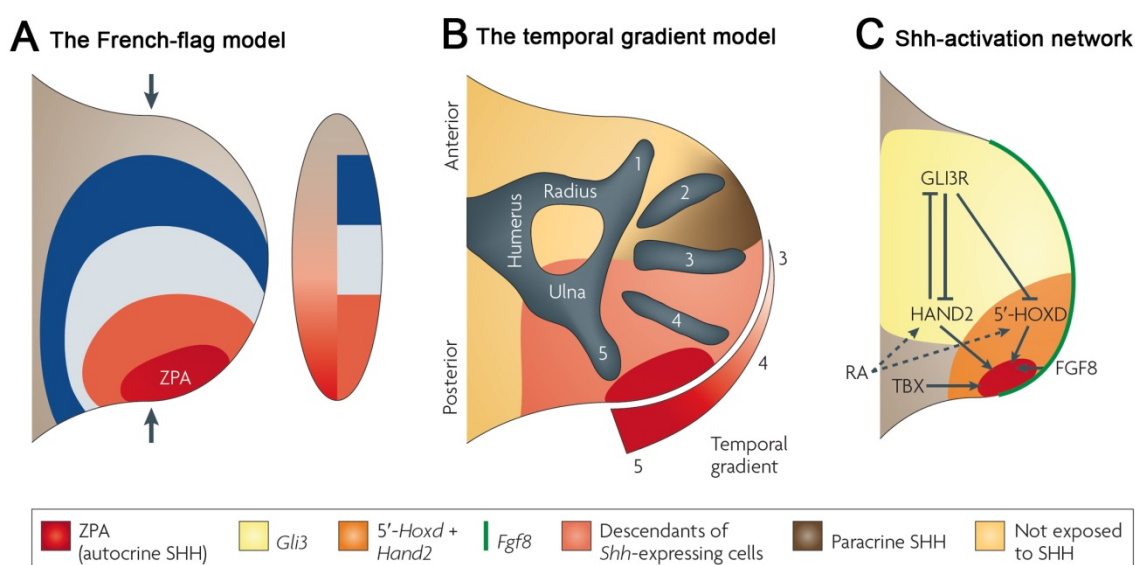


Figure 3. The polarizing zone of activity (ZPA) instructs the anteroposterior (AP) limb bud axis. **(A)** The French-flag model postulates the specification of digit identities through threshold concentrations of the ZPA-secreted morphogen (red gradient). The colours of the French flag correspond to distinct identities of the three chicken digits. **(B)** In mouse limb buds, AP identities are specified by two distinct gradients of *Shh* signalling. A spatial gradient of long-range, morphogenic *Shh* signalling (paracrine) specifies identity of digit 2 (and parts of digit 3). Cells leaving the ZPA (*Shh* descendants) abrogate *Shh* expression and progressively displace non-ZPA cells (receiving morphogenic *Shh* signalling). A temporal gradient is established by *Shh* descendant cells contributing to the more posterior structures,

the later they leave the ZPA. *Shh* descendants contribute to the ulna, digits 5, 4 and parts of digit 3. Specification of the prospective humerus, radius and digit 1 occurs independently of *Shh*. (C) *Shh* expression is activated, maintained and restricted to the ZPA (red) through a specific gene regulatory network. *Hand2* and *5'Hoxd* (overlapping domains in orange), *Tbx2/3* and *Fgf8* are essential for *Shh* activation or maintenance. Gli3R (yellow) restricts *Shh* to the posterior mesenchyme. Retinoic acid (RA) signalling might cooperate with *Hand2* or *Hoxd* genes in ZPA regulation (Niedereither et al., 2002). Modified figure adapted from Zeller et al., 2009.

Constitutive inactivation of *Shh* leads to a truncated limb with just one zeugopodal element and a single digit rudiment (Chiang et al., 1996; Chiang et al., 2001). The proximal-most skeletal structures are not affected and the femur displays normal morphology (Chiang et al., 2001), indicating that the stylopod does not depend on *Shh* activity. The loss of skeletal elements observed in *Shh* deficient limb buds is mainly a result of massive cell death of pre-chondrogenic precursors (Sanz-Esquerro, 2000; Zhu et al., 2008). Interestingly, *Shh* inactivation in the context of *Gli3* deficiency rescues this cell death and results in the polydactylous *Gli3* mutant phenotype with associated loss of digit identities (Hui & Joyner 1993). This demonstrates that *Shh* and *Gli3* are required to establish digit identities and that a major molecular function of Shh signalling is to counteract processing of Gli3 into Gli3R in the posterior mesenchyme (Wang et al., 2000; Te Welscher et al., 2002b; Litingtung et al., 2002). Finally, temporally controlled inactivation of *Shh* using a conditional *Shh* allele has revealed two different essential functions during limb bud outgrowth (Zhu et al., 2008). In a first phase, Shh is required for specification of AP identities in the mesenchyme. In a second phase, Shh promotes survival and proliferative expansion of the mesenchymal progenitors of the autopod primordia (Zhu et al., 2008; Towers et al., 2008).

3.1.5 Interlinked signalling feedback loops integrate AP and PD limb development

Three decades ago, it was already known that the specification of chicken wing digits relies on the cooperative interaction of the ZPA with the AER (Tickle, 1981). It turned out that *Shh* indeed is required to maintain the AER as part of a feedback loop involving Fgfs (Laufer et

al., 1994; Niswander et al., 1994), i.e. both organizers maintain each other's activity as part of an epithelial-mesenchymal feedback loop. The functionality of this Shh-Fgf feedback loop was subsequently shown to depend on *Grem1*, a BMP antagonist positively regulated by the Shh signal (Zuniga et al., 1999; Khokha et al., 2003; Michos et al., 2004; Zuniga et al., 2004). *Grem1* is initially expressed in the posterior-most limb bud mesenchyme and its expression expands anteriorly during limb bud outgrowth. During limb bud initiation (Figure 4A) high levels of Bmp signalling are required to establish a functional AER and to rapidly upregulate *Grem1* expression (Benazet et al., 2009; Ahn et al., 2001; Nissim et al., 2006; Zeller et al., 2009). This fast Bmp-*Grem1* feedback reduces Bmp activity, which is essential for the establishment of the Shh/*Grem1*/Fgf feedback loop during the subsequent propagation phase (Figure 4B). During this proliferative expansion, low Bmp4 activity regulates the length of the AER (Benazet et al., 2009).

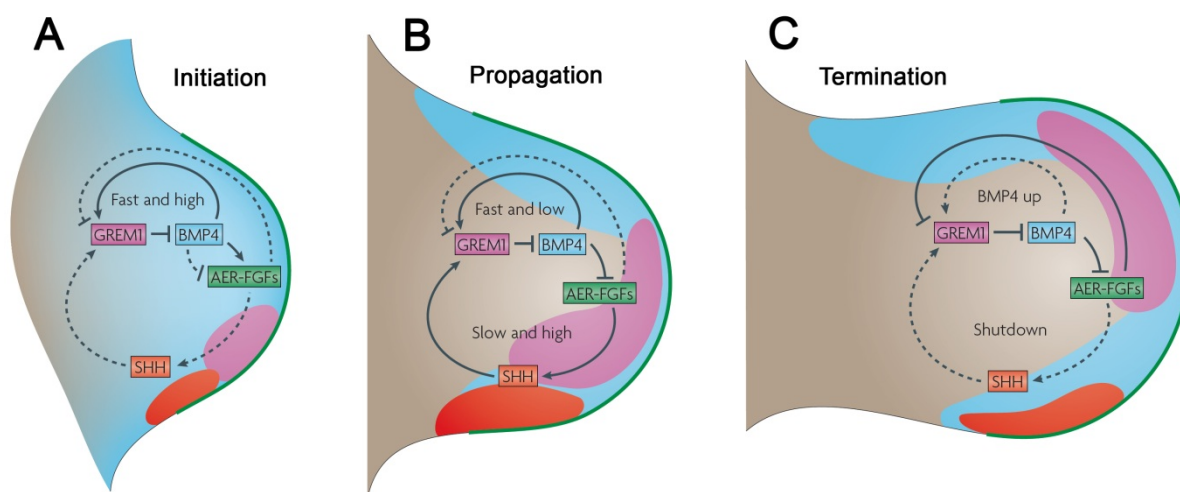


Figure 4. Interlinked signalling feedback loops display self regulatory properties in governing limb bud outgrowth. (A) During the initiation phase, high mesenchymal Bmp4 (blue) levels are required for AER-Fgf (green) maintenance and activation of its own antagonist, *Grem1* (purple). (B) In the propagation phase Bmp4 displays an adverse effect on the AER. High levels of *Grem1* antagonize Bmp4 and allow Fgf signalling from the AER to the underlying mesenchyme (for PD outgrowth) and the activated ZPA. Shh signalling from the ZPA promotes cell survival, proliferative expansion and maintenance of *Grem1* expression. (C) Termination of the feedback loops is dependent on two acts. Firstly, *Shh* descendants (see previous figure) emanating from the ZPA are refractory to *Grem1* expression and displace the *Grem1* domain to the distal-anterior. The increasing distance to the ZPA starts downregulation of *Grem1*. Second, raising AER-Fgf levels show a repressive effect on *Grem1*

and increase the gap between the AER and the *Grem1* domain. This terminates the feedback loop and leads to upregulation of Bmp signalling which plays a role in digit specification. Operating feedback loops are indicated as solid lines, whereas inactive loops are shown as broken lines. Bmp4, bone morphogenetic protein 4. *Grem1*, Gremlin 1. Fgf, fibroblast growth factor. Shh, Sonic hedgehog. Figure adapted from Zeller et al., 2009.

The Shh/*Grem1*/Fgf epithelial-mesenchymal module is required for distal progression of limb bud outgrowth and specification of posterior digits. During this phase, Shh-mediated maintenance of the AER ensures clearance of retinoic acid (RA) from the distal mesenchyme. Expression of the RA-degrading enzyme *Cyp26b1* in the zeugopod and autopod progenitors prevents cells from acquiring proximal character (Probst et al, 2010). The Shh/*Grem1*/Fgf feedback system exhibits self-terminating features as the expanding population of *Shh* descendants becomes refractory to *Grem1* expression (Figure 4C, Benazet et al., 2009; Scherz et al., 2004; Nissim et al., 2006). Thereby, *Grem1* expressing cells are progressively displaced towards the anterior and eventually reside outside of the domain of long-range Shh signalling. In addition, increasing AER-Fgf levels begin to repress *Grem1* in the underlying mesenchyme, which increases the distance of the AER to the *Grem1* domain (Verheyden & Sun, 2008). These combined molecular alterations result in the shut down of *Grem1* expression, which terminates the feedback loop and epithelial-mesenchymal signalling. During termination, Bmp activity rises again and induces chondrogenesis (Bandyopadhyay et al., 2006; Lopez-Rios et al., 2012), possibly in the late determination of digit identities (Benazet et al., 2009; Suzuki et al., 2008; Witte et al., 2010).

3.1.6 Control of the zone of polarizing activity (ZPA) and the prepatterning mechanism

Shh expression is localized to the ZPA by a long-range enhancer termed ZRS (for ZPA regulatory sequence; Lettice et al., 2003), which is located around 800kb upstream of the *Shh* locus in intron 5 of the *Lmbr1* locus (Figure 5A; Zeller & Zuniga, 2007). The ZRS contains a highly conserved 1.1kb core element named mammals-fishes-conserved-sequence 1 (MFCS1; Figure 5A). Genetic deletion of the MFCS1 element leads to a loss of

limb-specific *Shh* expression and reproduces the *Shh* limb phenotype (Figure 5B; Sagai et al., 2005). Remarkably, in species which have lost their limbs during evolution, such as pythons and limbless newts, the ZRS sequence is disrupted (Sagai et al., 2004; Cohn & Tickle, 1999). The ZRS was originally identified as an evolutionary conserved region to which several point mutations / transgene insertions causing congenital polydactylies in humans, cats and mice were mapped (Figure 5A, 5B; Lettice et al., 2003; Lettice et al., 2007; Sagai et al., 2004; Lettice et al., 2002) Point mutations in the ZRS likely perturb the binding affinities for transcription factors which causes ectopic *Shh* expression and results in polydactyly. Acheiropodia (Toledo & Saldanha, 1969) is a rare human autosomal recessive malformation, which causes limb truncations similar to the *Shh* limb skeletal phenotypes observed in mice. Notably, the deletion causing acheiropodia maps to a region containing *Lmbr1* exon 4 adjacent to the ZRS (Figure 5B; Ianakiew et al., 2001). This suggests that regions outside the ZRS may also be involved in the control of *Shh* expression (Zeller & Zuniga, 2007). The ZRS physically interacts with the *Shh* promoter in the posterior and anterior limb bud mesenchyme but the *Shh* locus loops out of its chromosome territory only in ZPA cells, where the mRNA production at a particular time point seems to be restricted to a low number of cells. This indicates that *Shh* transcription occurs in pulses (Amano et al., 2009).

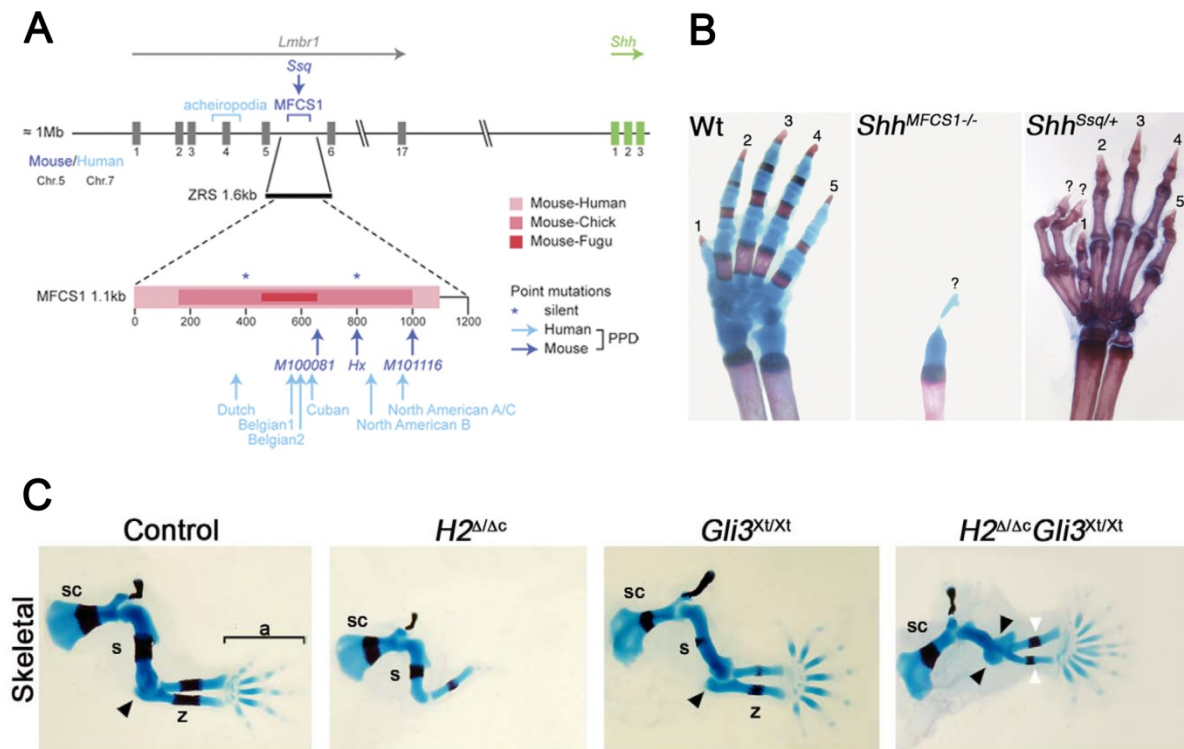


Figure 5. The mouse ZPA regulatory sequence (ZRS) defines a distant cis-regulatory element essential for limb-specific expression of *Shh*. **(A)** Scheme depicting the ZRS encoded in intron 5 of the *Lmbr1* gene, approximately 800kb upstream of the *Shh* locus. The core ZRS region termed mammals-fishes-conserved-sequence 1 (MFCS1) is enlarged. The MFCS1 core sequence (dark pink) displays highest sequence conservation ($\geq 50\%$ between mouse and Fugu). Medium pink marks $\geq 75\%$ conservation between mouse and chick, whereas pale pink denotes $\geq 75\%$ conservation between mouse and human. Identified preaxial polydactyly (PPD) causing point mutations in humans (bright blue) and mice (dark blue) are shown. The position of the Sasquatch (Ssq) transgene insertion is indicated. The region corresponding to the human acheiropodia mutation is delineated. Chr, chromosome. Adapted from Zeller & Zuniga, 2007. **(B)** Distal forelimb phenotypes carrying loss-of-function and gain-of-function ZRS/MFCS1 mutations. Left/mid panels: Wild-type (Wt) and MFCS1 deficient ($Shh^{MFCS1-/-}$) forelimb skeletal phenotypes of mouse embryos shortly before birth. Deletion of the MFCS1 sequence results in a severe distal truncation with only a remaining digital rudiment, a phenocopy of the *Shh* phenotype. Likewise, the ulna and the radius are fused. “?” indicates uncertain identity. Right panel: Anterior PPD of mice carrying one copy of the Ssq allele carrying a transgene insertion in *Lmbr1* intron 5. Digit identities are numbered from 1 (most anterior) to 5 (most posterior). Adapted from Zeller & Zuniga 2007. **(C)** E14.5 skeletal preparations of wild-type (control), $Hand2^{\Delta/\Delta c}$ (Prx1-Cre), $Gli3^{Xt/Xt}$ (*Gli3* Null) and $Hand2^{\Delta/\Delta c}; Gli3^{Xt/Xt}$ mutant limb buds. Inactivation of *Hand2* in the limb bud ($Hand2^{\Delta/\Delta c}$) results in a phenocopy of the *Shh* phenotype. Polydactyly and stylopod defects are more severe in the $Hand2; Gli3$ double mutant than in *Gli3* deficient limb buds. Black arrowheads indicate elbows in wild-type and $Gli3^{Xt/Xt}$ limbs and the symmetrical elbow-like structure in mutants $Hand2^{\Delta/\Delta c}; Gli3^{Xt/Xt}$. White arrowheads mark the symmetrical zeugopod elements. Sc, scapula. S, stylopod. Z, zeugopod. Adapted from Galli et al., 2010.

Which are the transacting factors that activate *Shh* expression and confine it to the ZPA? Appropriate ZPA positioning and *Shh* maintenance were shown to be dependent on retinoic acid (RA) and Fgf8 signalling, respectively (Figure 3C, Niederreither et al., 2002; Lewandoski et al., 2000). A number of transcriptional regulators have been implicated in *Shh* activation in the posterior limb bud mesenchyme (Figure 3C). For instance, members of the 5' *Hoxa* and *Hoxd* gene clusters are required (Kmita et al., 2005; Tarchini et al., 2006), and in particular the Hoxd10 and Hoxd13 proteins interact directly with the ZRS (Capellini et al., 2006). The bHLH transcription factor Hand2 is also essential for *Shh* activation in the posterior mesenchyme (Charité et al., 2000; Yelon et al., 2000; Galli et al., 2010), and ectopic *Hand2* expression in the anterior mesenchyme induces ectopic *Shh*, preaxial polydactyly and/or mirror image digit duplications (Fernandez-Teran et al., 2000; McFadden et al., 2002). Indeed, Hand2 is part of transcriptional complexes that bind to the ZRS in mouse embryonic limb buds and control *Shh* activation (Galli et al., 2010). Interestingly, the ZRS encodes Hand2-specific *Ebox* consensus elements (Galli et al., 2010; Dai & Cserjesi, 2002), but the minimal Hand2 binding sites in the ZRS are not known. Finally, Tbx2 and Tbx3 also contribute to maintenance of the ZPA (Nissim et al., 2007; Davenport et al., 2003) and posterior restriction of *Shh* expression is also dependent on the *Etv4* and *Etv5* transcription factors (Mao et al., 2009; Zhang et al., 2009; Zhang et al., 2010).

3.1.7 Functions of Hand2 prior to and independent of *Shh* activation

Recently, it has been shown that the activity of all four *Hox9* paralogs is required to activate *Hand2* expression in the posterior mesenchyme in forelimb buds (Xu & Wellik, 2011). Prior to the onset of *Shh* expression, *Hand2* interacts in a genetically mutual antagonistic manner with *Gli3*, which polarizes the nascent limb bud mesenchyme along its AP axis and is known as the pre-patterning mechanism (Te Welscher et al., 2002a).

Although *Hand2*-specific functions (i.e *Shh*-independent) in setting up AP polarity are difficult to dissect genetically, we have recently shown that the posterior expression of *Tbx2* and

Tbx3 depends on *Hand2* (Galli et al., 2010). Furthermore, ablation of the pre-patterning mechanism in limb buds lacking both *Hand2* and *Gli3* leads to a complete loss of AP asymmetry (Figure 5C; Galli et al., 2010). This contrasts with the phenotype of either *Gli3* single or *Gli3;Shh* double mutant limb buds, where posterior identity is still largely maintained (Te Welscher et al., 2002b; Lopez-Rios et al., 2012). These studies indicate that in addition to *Shh* expression, *Hand2* controls other early genes in the posterior limb bud. However, the identity of most of these genes and whether their regulation depends on this early pre-patterning still remains to be determined.

3.1.8 *Hox* genes during limb development

Hox genes initiate polarization of the limb bud and are important regulators of patterning and growth in limb development and required to pattern the skeletal elements (Zakany & Duboule 2007; Xu & Wellik 2011). Members of the four mammalian *Hox* clusters, *Hoxa* to *Hoxd*, are located on different chromosomes, encoded in a sequential manner with typically short intergenic regions and comprise a total of 39 genes. The *Drosophila* Abdominal-B (*abdB*) paralogs at the 5' end of the *Hoxa* and *Hoxd* clusters are essential for limb development and are expressed in a collinear fashion (Dollé et al., 1989). Spatial and temporal collinearity describes the correlation between the relative *Hox* gene positions within the gene cluster and the onset and extent of their expression domain in the limb bud mesenchyme. The more 5' a *Hox* gene is located, the more distal and later it is expressed during limb bud development (Dollé et al., 1989). There are two phases of *Hox* expression during limb development. The first wave of *Hoxd* expression is restricted to the posterior by *Gli3* and required for initiation of *Shh* (Zuniga & Zeller 1999; Deschamps, 2004). This early phase of 5' *Hoxd* expression is controlled by the early limb control region (ELCR), located telomeric to *Hoxd1* (Zakany et al., 2004). The second phase of *Hoxd* expression occurs in the distal part of the limb and is required for the formation of the autopod (Zakany & Duboule, 2007) and important for the evolutionary diversity of paired appendages (Sordino et al., 1995; Shubin et al., 2009). In mice, the *Hoxd13* to *Hoxd10* transcripts show “reverse collinearity”, such that *Hoxd13* is

expressed at highest levels whereas *Hoxd12*, *Hoxd11* and *Hoxd10* are expressed at progressively lower levels and more posteriorly restricted. Interestingly, *Hoxd13* represents the only 5'*Hoxd* gene expressed in the prospective thumb territory (Montavon et al., 2008). The second phase of 5'*Hoxa/d* transcription is regulated by the 40kb global control region (GCR), located around 180kb upstream of *Hoxd13* (Spitz et al., 2003). The GCR regulatory landscape falls into the 600kb *Atp5g3/Lnp* gene desert and controls gene expression in limb buds, the dorsal neural tube, midbrain and forebrain (Spitz et al., 2003). The GCR harbours two blocks of highly conserved sequences termed CsA (telomeric) and CsB (centromeric) (Spitz et al., 2003; Gonzalez et al., 2007). CsB controls expression in the distal autopod and posterior zeugopod territories (Gonzalez et al., 2007). A recent study shows that the GCR is only one of many distal enhancer elements scattered throughout the *Atp5g3-Lnp* gene desert (Figure 6A). Supposedly, context-dependent chromatin remodelling allows transcription factor complexes to bind to these cis-regulatory elements and to loop over to control the basic transcriptional machinery at the 5' *Hoxd* promoters (Figure 6B-D; Montavon et al., 2011). The GCR interacts also with 5' *Hoxd* genes in the progenitors of the presumptive digit domains. However, the GCR is only required for *Hoxd13* expression in the posterior handplate. Taken together, transcriptional regulation of the *Hoxd* cluster appears more complex than previously anticipated, whereas establishment of reverse-collinear *Hoxd* expression in the digit domain is controlled by a large "regulatory archipelago" (Montavon et al., 2011). However, the trans-acting factors binding to these different elements have not been identified.

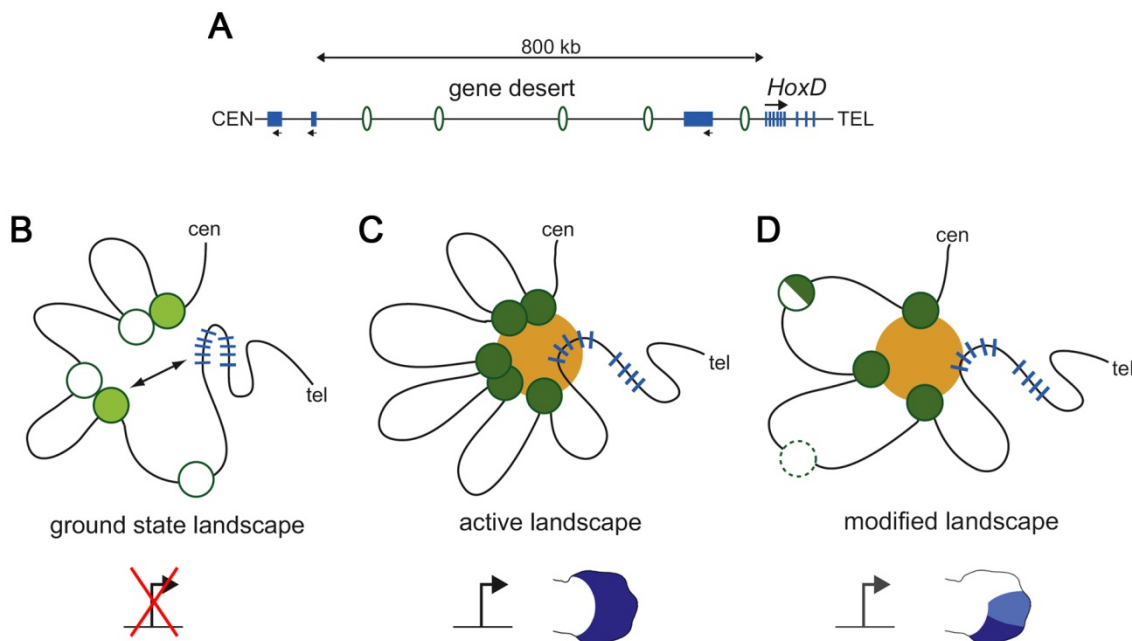


Figure 6. The “regulatory archipelago” controlling second phase *5'Hoxd* expression in the autopod as an example of a large complex regulatory region. **(A)** Map depicting the *Atp5g3/Lnp* “regulatory archipelago” extending over 800 kb upstream of the *Hoxd* cluster. Green ovals indicate regulatory islands. **(B)** In a ground state landscape only some regulatory elements interact with partial enhancer chromatin signatures (light green) which may contact the *Hoxd13* locus. However, these contacts are too weak to recruit the transcriptional activation complex and *Hoxd13* expression remains absent. **(C)** In the presumptive digit territories additional contacts are mediated to establish a fully active conformation, likely through interaction with specific transcription factors. Activating histone marks (dark green) in regulatory islands contribute to the recruitment of the RNA polymerase II (RNAPII) complex (yellow) which efficiently transcribes *Hoxd13* in the autopod domain. **(D)** If the distance changes, or in presence of sequence alterations, the regulatory interactions might decrease and fail to provide the full spectrum of spatiotemporal expression. This would for example explain “incomplete” patterns as expected for *Hoxd12*, *Hoxd11*, etc. Cen, centromeric. Tel, telomeric. Centromeric blue bars: *5'Hoxd* gene cluster. Telomeric blue bars: *3'Hoxd* gene cluster. Modified figure adapted from Montavon et al. 2011.

3.2 Hand2 as a critical regulator of embryonic development

Hand2 (heart, autonomic nervous system and neural crest derivatives expressed transcript 2) belongs to the Twist family of basic helix-loop-helix (bHLH) transcription factors and is a major regulator of organ morphogenesis (Firulli, 2003). bHLH factors contain a basic DNA-binding domain followed by two amphiphatic α -helices which are separated by a loop structure (helix-loop-helix -HLH- motif). The HLH motif is involved in protein interactions (Massari & Murre, 2000). The basic domain shows high affinity to hexameric canonical *Ebox* (CANNTG) sequences. In general, bHLH proteins are grouped in two classes. Class A proteins are ubiquitously expressed (E-proteins) and dimerize with tissue specific class B factors (e.g. Hand2) to form transcriptional regulatory complexes (Massari & Murre 2000). *Hand2* orthologues show a high degree of sequence conservation among vertebrates. Mouse Hand2 consists of 217 amino acids and is expressed in a variety of compartments during embryogenesis. Its biochemical features include a transcriptional activation domain (aa41-85) towards the N-terminus (Dai & Cserjesi, 2002), followed by a highly conserved bHLH domain (aa101-152). *In vitro*, the biochemical DNA binding specificity of Hand2 is directed against the CATCTG *Ebox* with highest affinity, and less against the CATGTG, CACCTG and CACGTG motifs (Dai & Cserjesi, 2002). Hand2 is regulated by phosphorylation at the conserved Thr₁₁₂ and Ser₁₁₄ residues by Protein kinase A (PKA) and protein phosphatase 2A (PP2A) (Firulli et al., 2003), which likely modulates dimerization with other bHLH factors (Firulli et al., 2005, Firulli et al., 2007, Barnes & Firulli 2009).

In addition to its roles during limb development, Hand2 is critical for heart formation in different cardiac lineages (see Appendix for heart morphogenesis). *Hand2* transcripts are detected in myocardial and endocardial cells (Biben et al., 1997) derived from the secondary heart field (SHF; Buckingham et al., 2005; Martin-Puig et al., 2008). *Hand2* expression in the SHF is controlled by the chromatin remodelling protein Smyd1 (Bop) and regulated by Gata factors that interact with an upstream heart enhancer (Gottlieb et al., 2002; McFadden et al.,

2000). *Hand2* deficient embryos display severe heart defects (Srivastava et al., 1997), which cause growth retardation and embryonic lethality by around E10.5. Inactivation of *Hand2* in different subsets of cardiac cells has revealed defined functions (Morikawa & Cserjesi, 2008; Tsuchihashi et al., 2010). However, in cardiac lineages *in vivo* direct *Hand2* target genes remain largely unknown (Laugwitz et al., 2008).

Hand2 is also expressed in neural crest derived cells, contributing to craniofacial structures and the cardiac arterial pole (Firulli & Conway 2004; Morikawa & Cserjesi, 2008). The pharyngeal (branchial) arches represent transient structures populated by neural crest derived cells that contribute to the craniofacial skeleton. *Hand2* is expressed by the distal branchial arch mesenchyme and is essential for cell survival (Srivastava et al., 1995; Thomas et al., 1998; Ayier et al., 2005; Barron et al., 2011). Around E9.5, the *Dlx5/6* homeobox transcription factors induce *Hand2* expression via a branchial arch enhancer in progenitors of the lower jaw skeleton (Thomas et al., 1998; Charité et al., 2001; Yanagisawa et al., 2003; Ruest et al., 2003). In the mandibular arch (first branchial arch) *Hand2* is required for activation and/or maintenance of *Hand1* and *Gooseoid (Gsc)* and promotes repression of *Dlx5/Dlx6* which is essential for development of the tongue (Barron et al., 2011). In addition, *Hand2* seems to inhibit premature osteoblast differentiation in the mandibular primordia by disrupting the interaction of *Runx2* with DNA (Funato et al., 2009).

Hand2 is also expressed in neural crest derived cells contributing to the autonomic nervous system (ANS), including the lineages of sympathetic (SNS), parasympathetic (PSNS) and enteric nervous (EN) systems (Howard et al., 2000; Wu & Howard 2002; Dai et al., 2004; Morikawa et al., 2005). For instance, *Hand2* promotes the noradrenergic fate of sympathetic nervous system (SNS) neurons by regulating *tyrosin hydroxylase (Th)* and *dopamine β -hydroxylase (Dbh)* expression (Howard et al., 2000; Morikawa et al., 2007).

Recently it has been shown that *Hand2* functions in the adult uterine stroma as a progesterone-dependent factor. In particular, *Hand2* expression enables blastocyst

implantation by suppressing Fgf-mediated proliferation of the uterine epithelium (Li et al., 2011).

3.3 Technology: The identification of *bona fide* transcriptional targets requires genomic engineering of the endogenous locus

With the advent of ChIP-seq (Chromatin immunoprecipitation coupled to next-generation sequencing) the identification of genome-wide transcription factor target sites or chromatin remodelling marks has become possible with a resolution of less than 100bp (Park, 2009; Metzker, 2010). For instance, recent pioneering ChIP-seq studies identified enhancers with p300 transcriptional complexes in E11.5 limb buds, forebrain, midbrain and heart (Visel et al., 2009; Blow et al., 2009). ChIP-seq is dependent on high quality antibodies, which represent the major limiting factor in all these approaches. In particular, commercial antibodies often cannot be utilized as they lack specificity. Generation of ChIP-grade quality antibodies to detect the transcription factor of choice is often time consuming or even impossible (Massie & Mills, 2008). Thus, tagging proteins with specific epitopes is a promising alternative that allows the genome-wide study of protein functions in ES cells and mouse embryos (Zhang et al., 2008a; Vokes et al., 2008). Furthermore, to avoid off-target effects due to over-expression, the epitope-tagged protein is best expressed from the endogenous locus to prevent any transgene-associated perturbations (Melton, 1994; Conway et al., 2010).

In the mouse, gene targeting by homologous recombination (HR) in embryonic stem (ES) cells represents the most powerful tool for tailored manipulation of the genome. However, the efficiency of this technology is limited by great variation in targeting frequencies among different loci (Capecchi, 1989). In many cases, targeting frequencies by HR are rather low (e.g. less than 1%), which renders genetic manipulations tedious and labour intensive. In addition, there is an increasing need to re-engineer the same locus by e.g. introducing

epitope tags or specific point mutations to study gene functions at high resolution and in genome-wide context (Zeller et al., 2009).

Site-specific recombinases (SSRs) have revolutionized the field of genetic engineering and have become indispensable for analysis of gene functions and their roles in development and diseases (Barna & Dymecki, 2004). SSRs catalyze the recombination of short, specific target sequences in an efficient manner. Frequently used SSR/target site combinations are the *Cre/loxP* and *Flp/FRT* systems. The most common application using SSRs is the generation of mouse conditional (“floxed”) alleles. Conditional alleles are generated by HR and are defined by *loxP* sites flanking one or several critical exons to allow temporal or tissue-specific ablation of gene functions by Cre recombinase (Gu et al., 1994). Another common feature of this type of alleles is the use of *FRT* sites that flank the resistance cassette to select recombined ES cell colonies. Flp-mediated recombination of *FRT* sites allows removal of the selection cassette in correctly targeted ES cell clones. This removal is important as the selection cassette may interfere with the transcriptional regulation of the targeted and/or neighbouring locus, resulting in hypomorphic conditional alleles (Meyers et al., 1998).

Furthermore, pairs of heterotypic, non-interacting recombinase target sites (RTs) can be inserted by HR to flank a genomic sequence of interest. These sites are targets for efficient re-engineering of the flanked sequence by a technique called RMCE (Recombinase-Mediated Cassette Exchange; Figure 7; Feng et al., 1999; Barna & Dymecki 2004; Wirth et al., 2007). RMCE relies on initial intermolecular recombination of heterotypic RTs followed by intramolecular excision which frequently results in the exchange of the region between RTs (Figure 7). Cre and Flp site-specific recombinases and the Φ C31 integrase have been utilized for RMCE in combination with appropriate heterotypic RTs (Bethke & Sauer; Soukharev et al.; 1999, Seibler et al.; 1998, Lauth et al., 2002; Belteki et al., 2003). RMCE targeting frequencies are in general significantly higher than those of HR at the same locus (Feng et al., 1999). However, as RMCE is a rather recent technology that relies on insertion

of heterotypic RTs, the vast majority of currently available conditional alleles in the mouse are not compatible with RMCE. In particular, the International Knockout Mouse Consortium (IKMC; <http://www.knockoutmouse.org>) aims to target all protein-coding genes in the mouse genome (around 20,000) such that “knockout-first” alleles can be converted into conditional alleles (Collins et al., 2004; Skarnes et al., 2011). To date, more than 10,000 of these alleles have been generated, but they cannot be used for conventional RMCE as they lack heterotypic SSR target sites. Therefore, for an *in depth* analysis of gene functions and interactions, all these *loci* need to be re-engineered by HR, which is laborious, time consuming and expensive. This is in particular true for loci with very low HR targeting frequencies, such as the *Hand2* locus (around 0.2%; Srivastava et al., 1997; Galli et al., 2010).

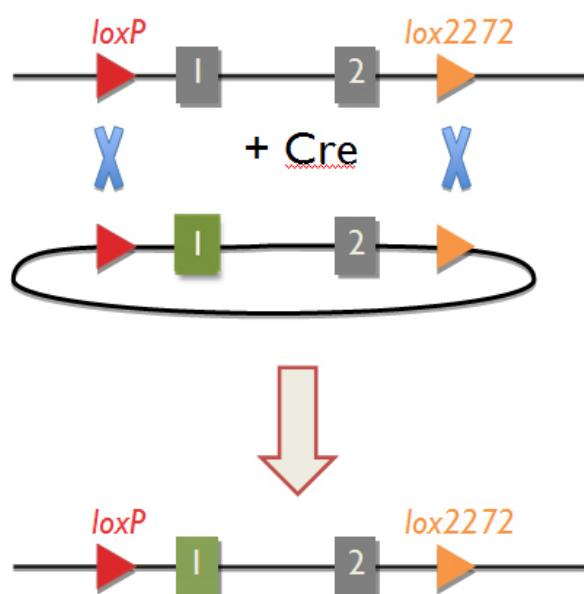


Figure 7 Scheme illustrating the basic principle of recombinase-mediated cassette exchange (RMCE). Top panel: Genomic element of interest flanked by heterotypic Cre recombinase target sites (RTs) *loxP* (standard) and *lox2272* (mutant). Cre-mediated recombination is only catalyzed between homotypic RTs. Upon transfection of a targeting vector which encodes the same heterotypic pair flanking the modified (green) sequence of interest, Cre-mediated intermolecular recombination between one of the homotypic pairs is catalyzed. This leads

to the integration of the targeting vector as an unstable intermediate structure which is then resolved into the final exchanged cassette by intramolecular recombination (lower panel).

4. Aim of the Thesis

Transcription factors are part of complex gene regulatory networks and are key links between extracellular signals and cellular programs. During embryonic development, the morphogenetic signals that coordinate growth with patterning regulate the activity of these transcriptional modulators to balance cell specification, determination and differentiation. The study of limb development has been of paradigmatic value for our molecular understanding of how coordinated cell behaviour orchestrates organ formation. Determining the precise mechanisms of such processes provides not only new developmental and evolutionary insights, but is also of importance for understanding human congenital defects and disease.

Hand2 is an essential transcriptional regulator during embryogenesis, as it is critical for heart development and neural crest-derived tissues (see before). Most importantly, *Hand2* is required to activate *Shh* expression in the limb bud mesenchyme, which in turn participates in orchestrating limb outgrowth and specification of digit identities. In the laboratory of Prof. Rolf Zeller we study mouse limb development with the aim to understand how morphogenetic networks interact during organogenesis. In the context of my PhD project and in light of the new technologies arising, the aim of this study was to identify the range of target genes of the *Hand2* transcription factor during limb bud development. This level of detail is needed to be able to build and understand the gene regulatory networks that operate during organogenesis. As no high-quality antibodies against *Hand2* were available, we planned to generate a mouse model encoding an epitope tag inserted into the endogenous *Hand2* protein. However, technical limitations in the manipulation of the *Hand2* locus in mouse ES cells led us to define another major aim of my studies: to render the existing *Hand2* conditional allele compatible with RMCE. This might raise *Hand2* targeting frequencies tremendously and simplify site-specific genetic modifications. Moreover, if generally applicable, such a technique would allow highly efficient re-engineering of the available

thousands of conditional alleles. I performed proof-of-principle experiments in mouse ES cells using a novel approach, which we termed dRMCE. Subsequently, I generated various ES cell lines expressing different types of epitope-tagged Hand2 proteins. I used ES cell differentiation assays to identify the optimal tagged Hand2 version, which was then processed to generate the final mouse model. In the second part of my PhD studies, I established the necessary procedures to demonstrate that epitope tags provide sensitive tools which allow straightforward, spatiotemporal localization and quantitation of the endogenous Hand2 protein in mouse embryonic tissues. Finally, I established a ChIP protocol for deep sequencing (ChIP-seq), utilizing embryonic tissues from the mouse strain carrying an epitope tagged Hand2 protein. This allowed me to identify the target sequences interacting with Hand2 in a genome-wide manner.

5. Results

5.1 Development of dRMCE for high-throughput engineering of conditional alleles

5.1.1 Challenges in targeting the *Hand2* locus

Due to the lack of available high quality and ChIP-grade antibodies against the mouse Hand2 protein, we decided to target the endogenous *Hand2* locus to generate epitope-tagged Hand2 as a valuable tool for ChIP/IP-based techniques. Selection of an epitope-tag without interference with *in vivo* protein function can be a rather difficult task and requires knowledge about the structure of the encoded protein (see introduction). Tightly balanced Hand2 activities are indispensable for the correct morphogenesis and function of critical organs including the heart (Conway et al., 2010; Olson, 2006). We selected the 1xFLAG immunoreactive peptide (DYKDDDDK, Hopp et al., 1988; Einhauer & Jungbauer, 2001) due to its short extension (8aa) and in order to minimize the risk of interfering with protein functions. In addition, the functionality of an N-terminally 1xFLAG-tagged Hand2 protein (FLAG peptide insertion at amino acid position 12) was validated extensively in tissue culture assays by co-immunoprecipitation and luciferase assays (Galli et al., 2010 and data not shown). Taken together, we considered these properties sufficient to undertake a site-specific *Hand2*^{1xFLAG} knock-in into the *Hand2* locus in mouse embryonic stem cells (ES), which would allow analysis of Hand2 protein functions in mouse models. Prospectively, our approach should establish endogenous epitope-tagged Hand2 as a tool to enable *in-vivo* localization studies and genome-wide characterisation of target sequences. This approach should overcome problems encountered by *in vitro* studies or transgenic approaches based on protein overexpression (Massie & Mills, 2008). However, targeting of the *Hand2* locus by homologous recombination (HR) is inefficient and time consuming and results in only 0.17%

of positive clones (1 in 576, Galli et al., 2010). Similarly low frequencies were obtained by others (Srivastava et al., 1997). In light of this disadvantage, we sought to develop a more directed, non-HR based approach, which would allow efficient insertion of epitope tags into the endogenous *Hand2* coding sequence (CDS).

5.1.2 dRMCE to custom-modify conditional alleles: the proof of principle

Most of the conditional alleles generated up to date are not compatible with conventional recombinase-mediated cassette exchange (RMCE) that usually relies on replacement mediated by heterotypic pairs of *loxP* or *FRT* recombinase target sites (Branda et al., 2004; Wirth et al., 2007). Remarkably, the vast collection of conditional alleles generated by the international knockout mouse consortium (IKMC) is based on a “knockout-first” design (Testa et al., 2004) that implies the use of homotypic pairs of wild-type *loxP* and *FRT* sites. Thus, none of these thousands of engineered alleles are compatible with RMCE approaches.

The IKMC makes use of targeting vectors that encode either promoterless (for genes expressed in ES cells) or promoter-driven selection cassettes (Skarnes et al., 2011). In the case of promoterless alleles the *FRT* flanked selection cassette is placed on the outside of a *loxP* flanked region containing the critical exon(s). Most notably, the *Hand2* conditional allele (Galli et al., 2010) and many other conditional alleles encode the same configuration. Thus, an approach allowing site-specific targeting of conditional alleles with targeting frequencies similar to the ones obtained by RMCE would greatly simplify re-engineering of thousands of available conditional alleles. In particular, this technology would be extremely valuable in the context of loci displaying very low targeting frequencies, such as *Hand2*.

Around 10 years ago, it was reported that combined expression of Cre and Flp recombinases promoted exchange of sequences flanked by single *loxP* and *FRT* sites at random genomic locations (Lauth et al., 2002). However, this approach did not explore whether the dual recombinase system could be utilized to target *loxP* or *FRT* sites present in conditional alleles. Thus, we reasoned that the region of a conditional allele, which is flanked by *loxP* and *FRT* sites, could be replaced efficiently with a sequence of choice using an appropriately

designed replacement vector in combination with optimized iCre and Flpo recombinases (Shimshek et al., 2002; Raymond & Soriano 2007). As two different recombinase systems were involved, we termed this process dual RMCE (dRMCE). The basic dRMCE principle is illustrated schematically in Figure 1A. In theory, the archetype structure of a dRMCE compatible conditional allele (target locus) must encompass *loxP*- and *FRT*-flanked genomic regions and can even have more than two sites of each (see below). However, it is essential that the *FRT*-flanked genomic region is not located within the *loxP* flanked genomic region or *vice versa*. Mouse ES cells are transfected with a plasmid expressing iCre and Flpo recombinases, which will provide a balanced maximal degree of recombination efficiency to prevent second-step Cre mediated excision of the sequence of choice (Lauth et al., 2002). To provide a pulse of simultaneous and optimized Cre and Flp activities in mouse ES cells, we developed the pDIRE expression plasmid (Figure 1B). The pDIRE vector was engineered to provide efficient but transient co-expression of iCre and Flpo recombinases (Shimshek et al., 2002; Raymond et al., 2007). We utilized heterologous promoters for driving recombinase expression (PGK-*FLPo*; EF1 α -*iCre*) to avoid transcriptional quenching by depleting transacting factors. Co-transfection of a replacement vector encoding also an appropriate selection cassette will provide the *loxP*-*FRT*-flanked custom modification of the target sequence. Simultaneous dual recombinase activity will likely induce rapid *cis*-recombination within the genomic target sequence resulting in the deleted locus (Figure 1A). The remaining single *loxP* and *FRT* sites would then serve as docking elements for *trans*-recombination mediated insertion of the *loxP*-*FRT*-flanked region in the replacement vector (Figure 1A). The minimal distance between the *loxP* and *FRT* sites in the deleted allele is of minor importance as dRMCE based replacement is likely achieved in a two-step process (Lauth et al., 2002). As 34bp *FRT* sites are refractory to integration (Jayaram, 1985), Cre likely integrates the replacement vector at the *loxP* site in a first step. This supposedly results in the formation of an intermediate co-integrate structure (Lauth et al., 2002). Given that both recombinases display similar efficiencies, two possible options exist for the second step. Cre-mediated *cis*-recombination of *loxP* sites may revert the co-integrate to the original deleted allele. On the

other hand, Flp-mediated *FRT* recombination in the co-integrate structure would induce the desired substitution of the targeted region by the replacement cassette.

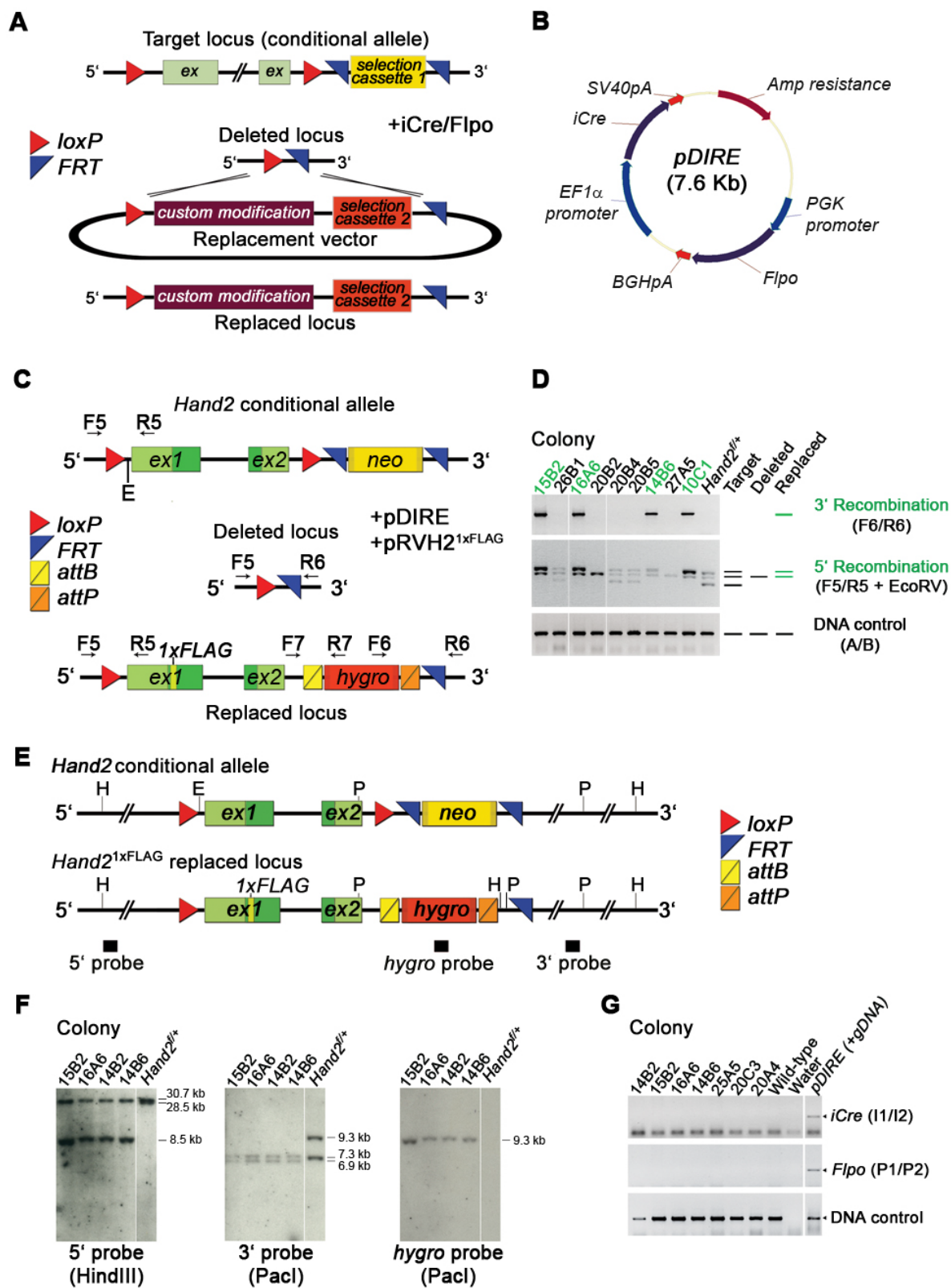


Figure 1. The theoretical concept of dRMCE and the proof-of-principle experiment. **(A)** The principle of dRMCE for re-engineering mouse conditional alleles. The scheme of the target locus shows the best-suited configuration of a conditional mouse allele with the critical exon(s) flanked by two *loxP* sites (red) and an outside selection cassette flanked by two *FRT* sites (blue). Upon transfection, iCre/Flpo-mediated recombination in *cis* ideally results in the deleted allele flanked by one *loxP* and *FRT* site. Single *loxP* and *FRT* sites of the deleted allele represent “docking sites” for iCre/Flpo mediated insertion of the replacement cassette. **(B)** Map of the pDIRE (Dual Improved Recombinase Expression) expression vector. Simultaneous expression of both iCRE and FLPo recombinases in mouse ES cells is provided by the use of heterologous promoters (PGK-*FLPo*; EF1 α -iCre). **(C)** Scheme depicting the targeting of the *Hand2* locus by dRMCE. The available conditional *Hand2* allele (Galli et al., 2010) was used to insert a FLAG epitope tag into the *Hand2* coding region. The replacement vector was co-transfected into heterozygous *Hand2*^{f-neo/+} recipient mouse ES cells with the pDIRE plasmid. dRMCE-mediated correct replacement results in the *Hand2*^{1xFLAG} allele. The *PGK-hygromycin* selection cassette is flanked by the Φ C31 integrase target sites *attB* (yellow) and *attP* (orange) to enable its subsequent removal. Relevant PCR primers for colony screening are indicated (F5-F7, see Material and Methods Table 3 and Table 4). **(D)** PCR screening identified ES clones with correct replacement at both the 3' and 5' ends of the *Hand2* ORF (12.5%; indicated in green, see Material and Methods Table 5A). The scheme at right shows PCR fragment patterns indicative of the different alleles. **(E)** Schematic view of the *Hand2*^{f-neo} and *Hand2*^{1xFLAG} alleles. The positions of restriction sites and the probes used for Southern blot analysis are indicated. H: HindIII, E EcoRV, P: PacI. **(F)** Southern blot analysis confirms that replacement occurred correctly at both the 5' (6.9 kb) and 3' (8.5 kb) ends and reveals the integrity of the *Hand2*^{1xFLAG} locus (Material and Methods Table 7). Random integration of the replacement vector was excluded as only a single copy of the hygromycin-resistance cassette is present in all *Hand2*^{1xFLAG} clones (primers used to generate DIG-labelled probes are shown in Material and Methods Table 7). **(G)** No random integration of the pDIRE vector occurred, as PCR primers that specifically amplify iCre and Flpo sequences fail to detect pDIRE sequences in *Hand2*^{FLAG} clones (primers listed in Material and Methods Table 3). E: *EcoRV* site required to detect correct 5' replacement by PCR screening in combination with *EcoRV* restriction digestion. *Ex*, exon; *neo*, neomycin resistance cassette; *hygro*, hygromycin resistance cassette.

We used the mouse *Hand2* locus to test the feasibility of dRMCE with the aim to insert a peptide epitope into the *Hand2* CDS, (Figure 1C). The *Hand2* locus has previously been targeted by homologous recombination (HR) in mouse ES cells to generate a conditional loss-of-function allele, which is compatible with the dRMCE principle (Figure 1C; *Hand2*^{f-neo}, Galli et al., 2010). The replacement vector design implied insertion of the 1xFLAG epitope into the N-terminal portion of the *Hand2* CDS (see above and Figure 1C). Thereby, the modified *Hand2* CDS is flanked by single *loxP* and *FRT* sites in the same orientation as in the conditional *Hand2*^{f-neo} locus (Figure 1C). A *PGK-hygromycin* selection cassette is inserted downstream of the second *Hand2* coding exon to allow selection of mouse ES cell clones. This selection cassette is flanked by *attB* and *attP* sites (Figure 1C) which enables its removal by the Φ C31 integrase in correctly targeted mouse ES cell clones (Belteki et al., 2003).

The *Hand2*^{1xFLAG} dRMCE replacement vector was co-transfected with the pDIRE expression plasmid into R1 mouse ES cells carrying the conditional *Hand2*^{f-neo} allele (Figure 1C). A major advantage of the dRMCE technology is the rapid screening of clones by conventional PCR. In contrast, HR is dependent on the use of large homology arms, which requires time-consuming screening by Southern blot analysis. Thus, Hygromycin-resistant ES cell colonies were selected and screened by conventional PCR to detect correct replacement events. Of the selected ES cell colonies analysed, 54 of 343 displayed PCR patterns indicative of correct replacement (15.7%). Extended analysis by PCR revealed that 11 of these colonies were mixed, as both the correctly replaced (*Hand2*^{1xFLAG}) and the deleted (*Hand2*^Δ) alleles were present (Figure 1D; Material and Methods Table 5A). The rather high proportion of such mixed ES colonies (20% of the 54 PCR positive colonies) is unlikely to arise by cross-contamination during picking, but rather indicates that *cis*-recombination (resulting in the *Hand2*^Δ allele) occurs prior to *trans*-recombination that gives rise to the *Hand2*^{1xFLAG} allele (Figure 1A; Zheng et al., 2000). Thus, mixed colonies likely emerge if *cis*-recombination (deletion) in the genomic region occurs immediately before cell division and is followed by unequal plasmid segregation or delayed incorporation of the replacement vector.

Subsequently, site-specific integration of the replacement cassette will occur in only one of the daughter cells. Consistent with this interpretation, events involving only *cis*-recombination and resulting in the *Hand2*^Δ allele are accompanied by random integration of the replacement vector in a very large fraction of all hygromycin resistant colonies (131/343; Material and Methods Table 5A). Despite these partial or *cis*-restricted recombination events, 12.5% (43/343) of all mouse ES cell colonies analysed have undergone complete and correct replacement of the *Hand2*^{f-neo} with the *Hand2*^{1xFLAG} allele (Material and Methods Table 5A). This indicates that dRMCE is about 70-fold more efficient than conventional HR at the *Hand2* locus (Galli et al., 2010; Srivastava et al., 1997). Thus, the novel dRMCE approach allows highly efficient further engineering of the difficult-to-target *Hand2* locus.

Four ES cell clones with correct replacement as judged by conventional PCR screening (Figure 1D) were expanded and tested for genomic integrity. As the modified *Hand2* sequence contained specific restriction enzyme (RE) consensus sites to generate diagnostic fragments (Figure 1E), integrity of the *Hand2*^{1xFLAG} locus was assessed by Southern blot analysis (Figure 1F). This confirmed that dRMCE results in correct 5' and 3' replacement of the *Hand2*^{f-neo} by the *Hand2*^{1xFLAG} allele. Importantly, no additional random integration of the replacement vector (Figure 1G) and the pDIRE plasmid (Figure 1H) were detected in these ES cell clones.

In a next step, we confirmed the functionality of the mechanism that allows removal of the selection cassette. As the *hygromycin* resistance cassette is flanked by *attB* and *attP* sites, it can be deleted upon intramolecular recombination using the ΦC31 integrase (Fig 2A; Belteki et al., 2003). This issue might be of relevance, as the *PGK* promoter controlling *hygromycin* expression might perturb endogenous gene expression resulting in undesired hypomorphic phenotypes. Such interference has been observed with e.g. conditional alleles (Meyers et al., 1998). Transient transfection of a vector expressing the codon-optimised version of the ΦC31 integrase (ΦC31o, Raymond & Soriano, 2007) catalysed the deletion of the selection cassette (Figure 2B). This indicates that the selection cassette can be removed in mice by inter-crossing them with ΦC31 “deleter” mice (Raymond & Soriano, 2007).

To assess the germline potential of mouse ES cells engineered by dRMCE, two *Hand2*^{1xFLAG} ES cell clones (clone 14B2 and clone 14B6) were injected into mouse blastocysts, which yielded several highly chimeric mice. Chimeric males from both clones transmitted the *Hand2*^{1xFLAG} allele to their F1 progeny (Figure 2C) with frequencies of 38.7% (12/31; 14B6), 17.4% (4/23; 14B6) and 3.7% (1/27; 14B2). Most importantly, mice homozygous for the *Hand2*^{1xFLAG} allele displayed no phenotypical defects, in contrast to the early lethality of *Hand2*-deficient mouse embryos (Srivastava et al., 1997). Taken together, these results establish that dRMCE does neither affect the germline transmission potential nor cause chromosomal abnormalities (as shown by karyotyping of injected ES clones, data not shown).

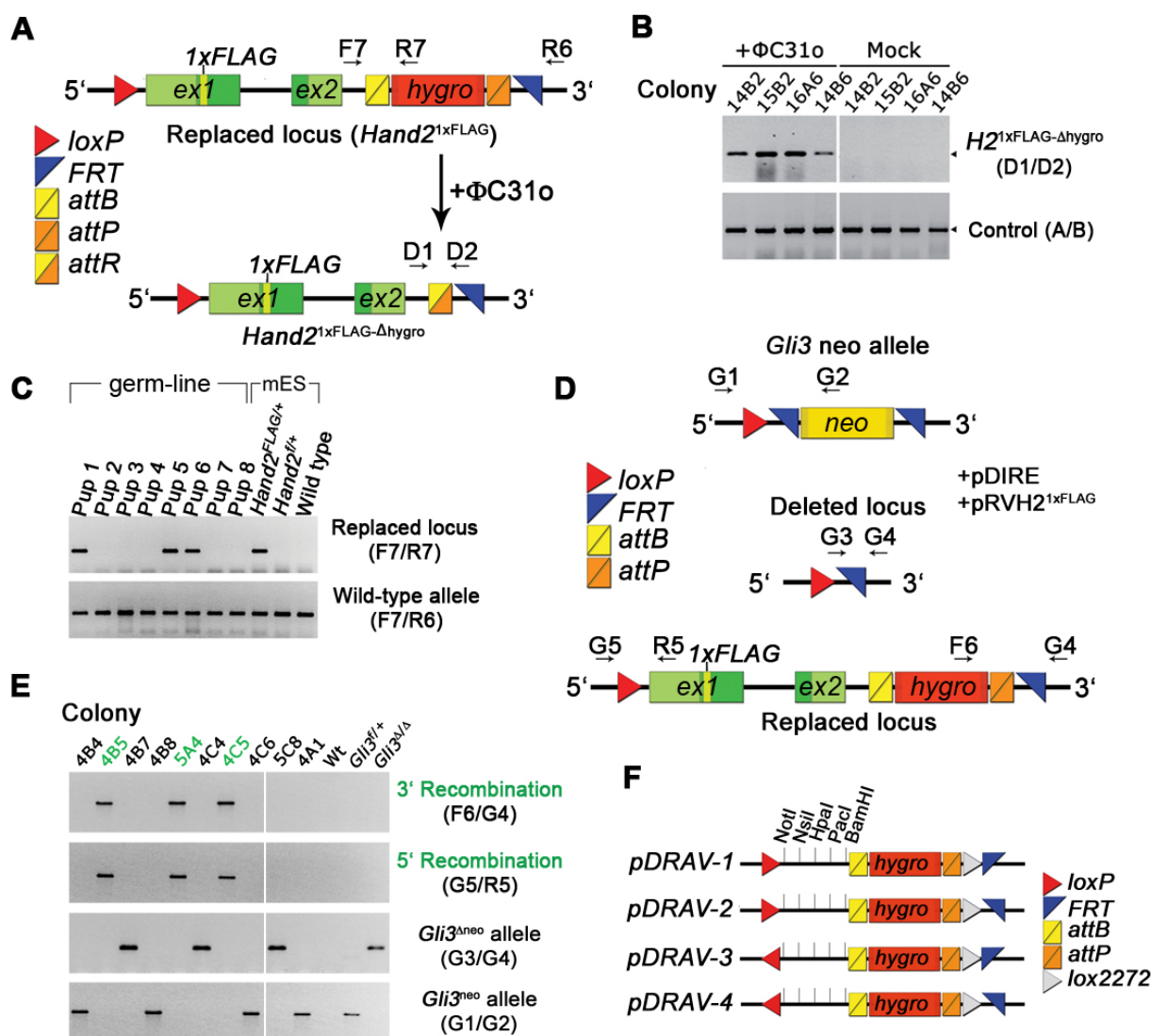


Figure 2. dRMCE does not alter the potential of germline transmission of mouse ES cells and demonstrates high efficiency at the heterologous *Gli3* locus. **(A)** Scheme depicting the correctly replaced *Hand2*^{1xFLAG} locus and the conversion to the *Hand2*^{1xFLAG-Δhygro} allele upon exposure to ΦC31o activity. Recombination between *attB* and *attP* sites produces the non-functional *attR* site. PCR primers used for the detection of ΦC31o-mediated excision of the selection cassette (D1, D2) and genotyping of the offspring of a *Hand2*^{1xFLAG} chimera (F7, R7) are indicated. **(B)** PCR analysis reveals excision of the *PGK-hygromycin* cassette after transfection of a ΦC31o expression vector (Addgene plasmid 13795). **(C)** Agarose gel showing frequent germline transmission (Pups 1, 5 and 6) of the dRMCE-modified *Hand2*^{1xFLAG} allele. **(D)** Heterozygous mouse ES cells carrying the *Gli3*^{neo} allele were used to insert the *Hand2*^{1xFLAG} replacement vector by dRMCE. The primers for PCR screening are indicated (Material and Methods Table 3 and Table 4). **(E)** PCR screening of hygromycin-resistant colonies revealed efficient recombination (33%) between the *Gli3*^{neo} locus and the *Hand2*^{FLAG} cassette resulting in the replaced *Gli3*^{H2} locus (clones with correct replacements are indicated in green; see Material and Methods Table 5B). **(F)** The pDRAV (Dual Recombinase Aceptor Vector) plasmid series encodes single *loxP* and *FRT* sites in all possible orientations. A *lox2272* site (light grey) renders these replacement vectors compatible for conventional RMCE manipulation following dRMCE-mediated replacement of the conditional allele of interest. The polylinker of the pDRAV vectors provides the necessary versatility for the rapid generation of custom-designed dRMCE replacement vectors. The PGK-hygromycin selection cassette is flanked by ΦC31 integrase target sites (*attB*, *attP*). *Ex*, exon; *neo*, neomycin resistance cassette; *hygro*, hygromycin resistance cassette.

5.1.3 dRMCE allows efficient re-engineering of thousands of IKMC conditional alleles

To establish the general potential of the dRMCE technology, we decided to target an unrelated heterologous locus. To this purpose we selected the *Gli3*^{neo} allele (an intermediate product in the generation of the *Gli3* conditional allele; Lopez-Rios et al., 2012) as a target locus. The *Gli3*^{neo} allele encodes a dRMCE compatible configuration as it harbours a single *loxP* site adjacent to the *FRT*-flanked *neomycin* selection cassette (Figure 2D). Heterozygous *Gli3*^{neo} ES cells were transfected with the *Hand2*^{1xFLAG} replacement vector as well as the pDIRE plasmid. Subsequent PCR screening of selected hygromycin resistant ES colonies revealed high targeting efficiency as the *Hand2*^{1xFLAG} replacement cassette was correctly inserted into the *Gli3* locus in 32.7% of all ES colonies analyzed (37/113; Figure 2E; Material and Methods Table 5B, 12). In contrast, HR mediated engineering of the *Gli3* locus resulted in only 3% of correctly targeted ES clones (Lopez-Rios et al., 2012; Table 1).

Targeting the *Gli3* locus with dRMCE also yielded 25% of colonies in which *FRT*-dependent recombination in *cis* was detected together with random integration of the replacement vector (*Gli3*^{Δneo} clones; Figure 2E; Material and Methods Table 5B). In contrast to *Hand2* replacement (Figure 1D; Material and Methods Table 5A), no mixed colonies were identified. Nevertheless, the significant number of *Gli3*^{Δneo} clones detected corroborates the proposal that *cis*- precedes *trans*-recombination (Figure 2D). Taken together, these results show that dRMCE mediated site-specific genomic engineering is about 10 (*Gli3*) to 70-fold (*Hand2*) more efficient than HR and equally efficient as conventional RMCE (data not shown), despite the fact that it depends on the activity of two different recombinases (Table 1).

In order to provide the research community with rapid access to the dRMCE technology, we have constructed four pDRAV (plasmid Dual Recombinase Aceptor Vector) targeting plasmids in which *loxP* and *FRT* sites are encoded in all possible orientations (Figure 2F). In combination with pDIRE (Figure 1B) these vectors allow easy and efficient site-specific insertion of any desired replacement cassette into any compatible conditional allele, even in the presence of multiple recombinase sites (see below).

We have performed *in silico* data mining using the Jackson Mouse Genome Informatics database to define a large collection of over 200 dRMCE compatible conditional alleles that have been generated by the research community and can be directly used for dRMCE approaches (see Appendix Table 4).

Bearing major advantages over HR such as the yield of higher efficiencies and a more rapid vector preparation and screening procedure, dRMCE could serve as an attractive tool for re-engineering the mouse genome to e.g. generate numerous reporter and Cre-lines. The IKMC programs EUCOMM (European Conditional Mouse Mutagenesis Program) and KOMP-CSD (Knockout Mouse Program) aim to conditionally engineer all protein coding genes in C57BL/6 mouse ES cells using “knockout-first” targeting vectors (Collins et al., 2007; Pettit et al., 2009; Skarnes et al., 2011). Currently, more than 10'000 IKMC conditional alleles of individual genes are already available in ES cells (<http://www.knockoutmouse.org>). As these

alleles are in principle compatible with dRMCE, we tested the feasibility of applying dRMCE to the two types of IKMC conditional alleles, which differ mainly by containing either a *promoterless* (Figure 3A) or a *promoter-driven* (Figure 4A) selection cassette (Testa et al., 2004; Skarnes et al., 2011).

Promoterless conditional alleles encode a splice acceptor (SA) in the 5' part of the selection cassette (*SA-T2A-lacZ-T2A-neo*). Interspersed T2A peptide sequences promote equimolar multicistronic expression of consecutive coding sequences by inducing peptide bond inhibition ("ribosomal skip mechanism") (Donnelly et al., 2001; Szymczak et al., 2004). The architecture of the IKMC selection cassette enables expression of the *lacZ* reporter and the *neomycin* selection marker under control of the endogenous locus, which must be transcriptionally active in mouse ES cells (Mountford et al., 1994). As *Smad4* encodes an integrator of Bmp signalling and is expressed in mouse ES cells (Mishra et al., 2005; Fei et al., 2010), we used the IKMC-conditional *Smad4^f* allele to test the feasibility of dRMCE to target the *promoterless* type of IKMC "knockout-first" alleles (Figure 3A). We designed the replacement vector in a way that correct replacement by dRMCE induces a switch from β -galactosidase to Histone 2B-Venus-YFP (H2B-YFP) activity under control of the endogenous *Smad4* locus (Figure 3A). This arrangement enables visual detection of correct dRMCE-mediated replacement in ES cells (see below). Heterozygous C57BL/6 *Smad4^f* ES cells were co-transfected with the pDIRE and pDREV-1 plasmids and 48 randomly selected puromycin resistant colonies were screened by PCR to detect correct replacement and generation of the *Smad4^{YFP}* allele (Figure 3A and 3B). Correct replacement was detected in the majority of all clones (33/48; 68.8%), whereas a small fraction of the colonies appeared mixed (10.4%; for details see Figure 3B and Material and Methods Table 5C). The *Smad4^A* allele was also detected in a subset of the colonies analysed.

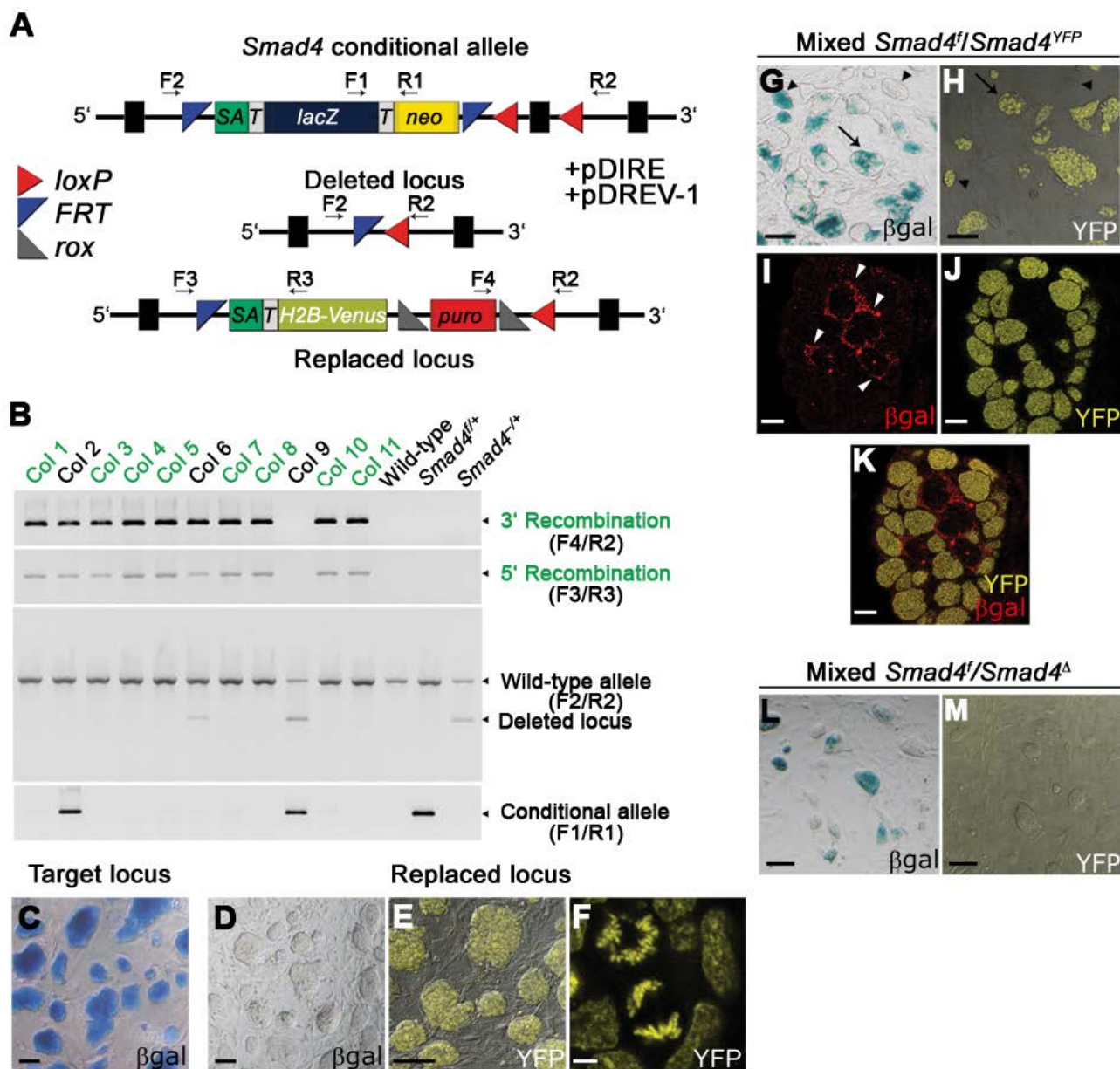


Figure 3. Highly efficient replacement at *Smad4* locus reveals that the vast IKMC collection of conditional alleles is compatible with dRMCE. **(A)** Schematic representation of the replacement in the *Smad4* locus mediated by dRMCE. The target locus is a *Smad4* conditional allele (*Smad4*^f) with a promoterless selection cassette such that the *lacZ* reporter and the neomycin resistance genes are expressed under control of the endogenous *Smad4* promoter. Co-transfection of pDIRE and pDREV-1 vectors mediates replacement likely via an intermediate product, the deleted allele (*Smad4*^A). Correct replacement *in trans* results in the *Smad4*^{YFP} allele (replaced locus). F1-F4 and R1-R3 primers for PCR screening are indicated (Material and Methods Table 3 and Table 4). **(B)** PCR screening reveals a large number of clones (69%) with correct 3' and 5' replacement (indicated in green, see Material and Methods Table 5C). Col, colony; 3' recombination, 5' recombination, correct replacement at the 3' and 5' ends, respectively. **(C)** The parental *Smad4*^{f/+} ES line is β -galactosidase positive and all clones are stained blue. **(D, E)** Clones with correct replacement (*Smad4*^{YFP}) are completely β -galactosidase

negative, but display YFP fluorescence. **(F)** Single dRMCE engineered cells show nuclear localisation (interphase) and association with condensed chromosomes (mitosis) of the fluorescent H2B-Venus protein in *Smad4*^{YFP} cells. **(G, H)** Mixed colonies identified by PCR (e.g. colony 2 in **B**: *Smad4*^f/*Smad4*^{YFP}) are composed of both β -galactosidase and YFP positive cells. While some colonies are mixed (arrows), others are completely β -galactosidase or YFP positive (arrowheads). **(I, J, K)** Co-immunolocalization of β -galactosidase (red, localization to the cytoplasm) and YFP (yellow, nuclear localization) reveals that individual cells exclusively express one reporter. White arrowheads point to cells expressing β -galactosidase in the cytoplasm. **(L, M)** In agreement with screening by PCR, another type of mixed colonies (colony 9 in **B**: *Smad4*^f/*Smad4*^A) contains some β -galactosidase-positive cells, but no YFP-expressing cells. H2B-Venus, YFP fusion protein with histone 2B; *lacZ*, β -galactosidase coding region; *neo*, neomycin resistance cassette; *puro*, puromycin resistance cassette; *rox*, Dre recombinase target sites (Anastassiadis et al., 2009); *SA*, *En2* splice acceptor; *T*, “auto-cleaving” T2A peptide coding region from *Thosea asigna* virus (TaV). Scale bars: 100 μ m (**C-E, G, H, L, M**), 10 μ m (**I-K**), 5 μ m (**F**).

As predicted, dRMCE resulted in a switch from β -galactosidase activity in parental *Smad4* ES cells (Figure 3C) to H2B-YFP fluorescence in *Smad4*^{YFP} clones (Figure 3D-3F). In particular, the H2B-YFP fusion protein displayed nuclear localization (Figure 3E) and was restricted to chromosomes in mitotic *Smad4*^{YFP} ES cells (Figure 3F). This observation verified the functionality of the fusion protein, as reported for the original H2B-GFP construct (Kanda et al., 1998). In addition, the composition of mixed colonies was now assessed at cellular resolution by comparing β -galactosidase activity with H2B-YFP fluorescence (Figure 3G-3M). Colonies positive for both *Smad4*^f and *Smad4*^{YFP} (e.g. colony no. 2, see Figure 3B) displayed β -galactosidase activity (Figure 3G) and H2B-YFP fluorescence (Figure 3H). Co-immunolocalization using antibodies against β -galactosidase and GFP revealed that reporter activity was mutually exclusive (Figure 3I-K). As determined by PCR, a different type of “mixed colonies” (e.g. colony no. 9 in Figure 3B) showed the presence of both the conditional and the deleted alleles (*Smad4*^f and *Smad4*^A). Consistently, β -galactosidase reporter activity was detected in a variable fraction of the total number of cells (Figure 3L), whereas YFP fluorescence remained absent (Figure 3M).

In summary, dRMCE-mediated targeting of the *Smad4* locus demonstrates the potential of dRMCE in highly efficient re-engineering of IKMC conditional alleles encoding a *promoterless*

selection cassette. In particular, the frequency of correct replacement at the *Smad4* locus is about 10-fold higher than in HR-mediated targeting (Chu et al., 2004). A similar frequency of correct recombination can be achieved by HR using a *promoterless* targeting vector in combination with diphtheria-toxin (DTA) negative selection to minimize random integration (IKMC).

To assess dRMCE on loci encoding a *promoter-driven* selection cassette, the conditional *Zfp503* allele was used (Figure 4A). This alternative type of IKMC conditional “knockout-first” allele encodes three *loxP* and two *FRT* sites and is utilized to target genes not expressed in ES cells. However, upon pDIRE-induced transient iCre and Flpo activity, *cis*-recombination may result in two distinct delta allele configurations (Figure 4A). Recipient *Zfp503*^{fl+} ES cells were co-transfected with the pDIRE and pDREV-0 vectors and selected with puromycin (Figure 4A). Again, dRMCE-mediated correct replacement was highly efficient, as the *Zfp503*^{YFP} allele was detected in 52.1% (25/48) of all colonies analyzed (for details see Figure 4B; Material and Methods Table 5D). Even though two allelic variants could be expected due to different sequences of *cis*-recombination, only the type of delta allele (*Zfp503*^A) encoding the *loxP-FRT*-flanked *lacZ* cassette was detected by PCR analysis (Figure 4A, B). This indicates that iCre-mediated *cis*-recombination among the three *loxP* sites precedes Flpo catalyzed *FRT* recombination *in-cis* and likely occurs due to slightly higher iCre efficiency. Indeed, this observation is in agreement with the finding that iCre remains more efficient than Flpo (Anastassiadis et al., 2009).

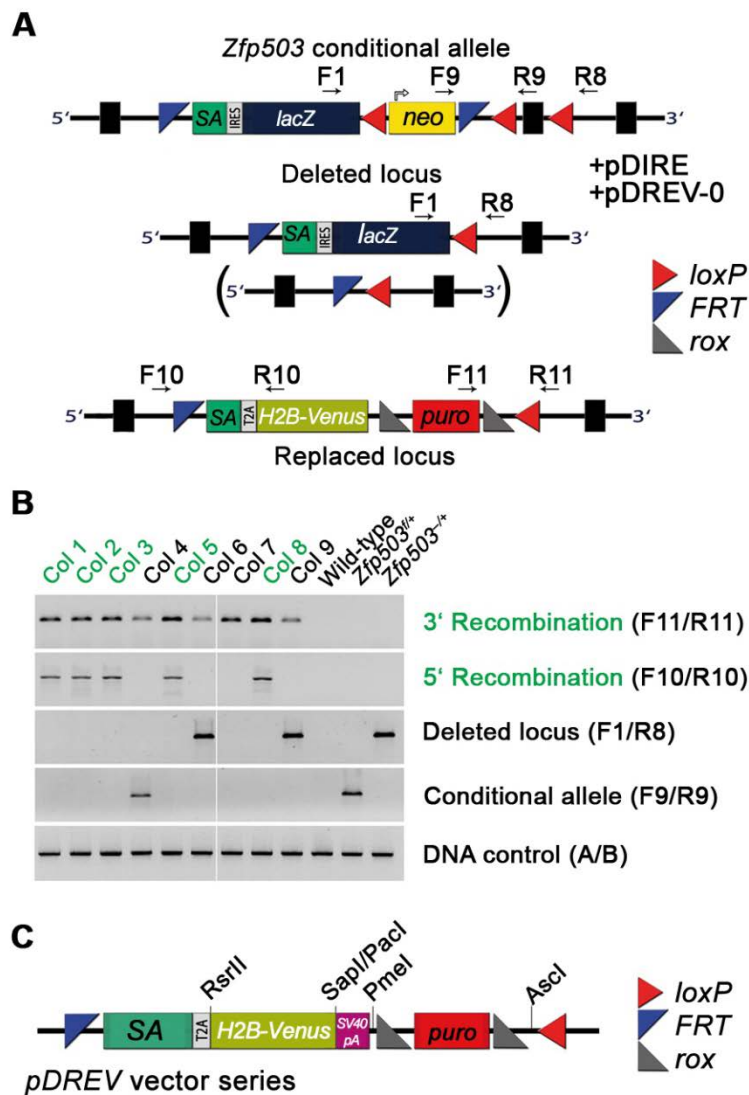


Figure 4. dRMCE is also very efficient for the replacement of IKMC alleles encoding a promoter-driven selection cassette. **(A)** Scheme of the dRMCE strategy for the *Zfp503* conditional allele (*Zfp503^f*), which encodes three *loxP* sites. The scheme illustrates pDIRE mediated *cis*-deletion and subsequent *trans*-insertion, which generates the *Zfp503^{YFP}* allele. Two types of deleted alleles are theoretically possible (the one in brackets was never detected). **(B)** PCR screening reveals the high frequency of clones with

correct replacement (52%, indicated in green, see Material and methods Table 5D for details) and some clones with only partial or no replacement. As *Zfp503* is not expressed in mouse ES cells, β -galactosidase or YFP reporter activity could not be assessed. Col, colony; 3' recombination, 5' recombination, correct replacement at the 3' and 5' ends, respectively. **(C)** The pDREV plasmid series consists of vectors compatible with all three reading frames that allow the quick generation of dRMCE exchange vectors to target IKMC alleles. Cassettes are flanked by a 5' *FRT* site and a 3' *loxP* site for dRMCE mediated re-engineering of IKMC knockout first alleles. pDREV plasmids encode the *En2* splice acceptor (SA) fused *in frame* to the T2A peptide (T) followed by the H2B-Venus fluorescent reporter. Transcription of the reporter is terminated by a *SV40* polyadenylation site, after which a *rox* site flanked *PGK-puromycin* selection cassette is located. The H2B-Venus coding sequence can be substituted in a single cloning step by coding sequences of 3 choice, as it is flanked by rarely occurring

RE sites (RsrII, SapI/PacI). *SA*, *En2* splice acceptor; *IRES*, internal ribosomal entry site, *lacZ*, β -galactosidase coding region; H2B-Venus, YFP fusion protein with histone 2B; *puro*, puromycin resistance cassette; *rox*, Dre recombinase target sites (Anastassiadis et al., 2009).

Taken together, dRMCE represents a highly efficient re-engineering tool for conditional alleles containing multiple recombinase target sites, as represented by the ever increasing number of promoter-driven IKMC “knockout-first” alleles (Skarnes et al., 2011). In particular, dRMCE-mediated targeting of the *Zfp503* locus resulted in correct replacement within half of all the clones analyzed. Therefore, dRMCE was about 5-fold more efficient in targeting of the *Zfp503* locus than conventional HR including positive and negative selection (IKMC).

Table 1 | dRMCE enables re-engineering of different loci at frequencies significantly higher than homologous recombination

Gene locus	dRMCE	Homologous recombination	Fold increase
<i>Hand2</i>	13%	0.2% ^{Galli et al., 2010}	65x
<i>Gli3</i>	33%	3% ^{Lopez-Rios et al., 2012}	11x
<i>Smad4</i>	69%	6% ^{Chu et al., 2004}	12x
<i>Zfp503</i>	52%	11% ^a	5x

^aIKMC.

In summary, dRMCE is a universal and flexible tool that enables custom-modified re-engineering of a vast number of compatible conditional alleles. Notably, locus specific dRMCE targeting frequencies are 5 to 65 times higher than the ones obtained by HR (Table 1). Most importantly, dRMCE is compatible with both types of the ever-growing collection of IKMC “knockout-first” conditional alleles. Thus, dRMCE will allow custom-defined modification of most of the protein-coding genes in the mouse genome in a highly efficient manner. As such tools can be of high value for the research community, we have simplified access to the dRMCE technology by providing a dRMCE toolkit. The pDREV (plasmid Dual Recombinase EuComm Vector) series (Figure 4C) complements the pDIRE (Figure 1A) and pDRAV (Figure 2F) plasmids and represents a highly versatile replacement vector for dRMCE-mediated modification of IKMC conditional alleles. pDREV vectors encode a

cassette (Figure 4C) that promotes localized and thus very sensitive reporter expression (H2B-Venus, see Figure 3). For versatile use, the *H2B-Venus* CDS is flanked by specific RE sites that allow easy insertion of any sequence of interest (Figure 4C). All dRMCE toolkit vectors are available from Addgene (www.addgene.org).

5.1.4 Defining high-sensitivity epitopes for tagging endogenous Hand2

Mouse embryos with inactivated *Hand2* display severe cardiac defects that cause embryonic lethality at E9.5 (Srivastava et al., 1997). On the other hand, a single copy of the *Hand2* allele is sufficient to maintain the wild-type phenotype in *Hand2*^{Δ/+} embryos and mice (Srivastava et al., 1997). Importantly, mice homozygous for the *Hand2*^{1xFLAG} allele were viable, reproduced and revealed no obvious phenotypical defects (data not shown). This demonstrates that endogenous *Hand2*^{1xFLAG} retains wild-type *Hand2* functions during embryogenesis and in adult mice. In a next step, we assessed the regulation of *Hand2*^{1xFLAG} transcripts in mouse embryos by mRNA *in situ* hybridisation (ISH). Embryos homozygous for the *Hand2*^{1xFLAG} allele maintained the wild-type *Hand2* transcript domains in E10.5 limb buds, branchial arches and the heart (Figure 5A). The spatial extension of the *Hand2* expression domains was also not altered at E11.5, as shown for the forelimb buds (Figure 5B). In addition, no phenotypes were detected in *Hand2*^{1xFLAG/Δ} embryos and mice (data not shown). Taken together, these results indicate that transcriptional regulation of the *Hand2*^{1xFLAG} allele was not impaired by the presence of the *hygromycin* selection cassette located 3' to the *Hand2* transcription unit. Notably, reduction of *Hand2* transcripts by around 70% induces formation of a cleft palate (Xiong et al., 2009) and pups with such defects are unable to feed and die one day after birth (Morikawa et al., 2007). Therefore, the endogenous *Hand2* locus retained its temporal and spatial regulation and the epitope-tagged *Hand2*^{1xFLAG} protein appeared fully functional *in vivo*.

In a previous study, we used a commercial polyclonal anti-Hand2 antibody (M-19, Santa Cruz) to detect endogenous Hand2 proteins in Western blots (Galli et al., 2010). The

observed triplet of Hand2 proteins (around 27kD) may represent isoforms with different post-translational modifications, such as phosphorylation (Barnes & Firulli 2009). The epitopes interacting with this M-19 anti-Hand2 antibody are located in the N-terminal domain of the Hand2 protein (Santa Cruz). Notably, the anti-Hand2 antibody recognized Hand2^{1xFLAG} in extracts of transfected HEK cells (data not shown), despite the presence of the 1xFLAG peptide inserted at amino acid position 12.

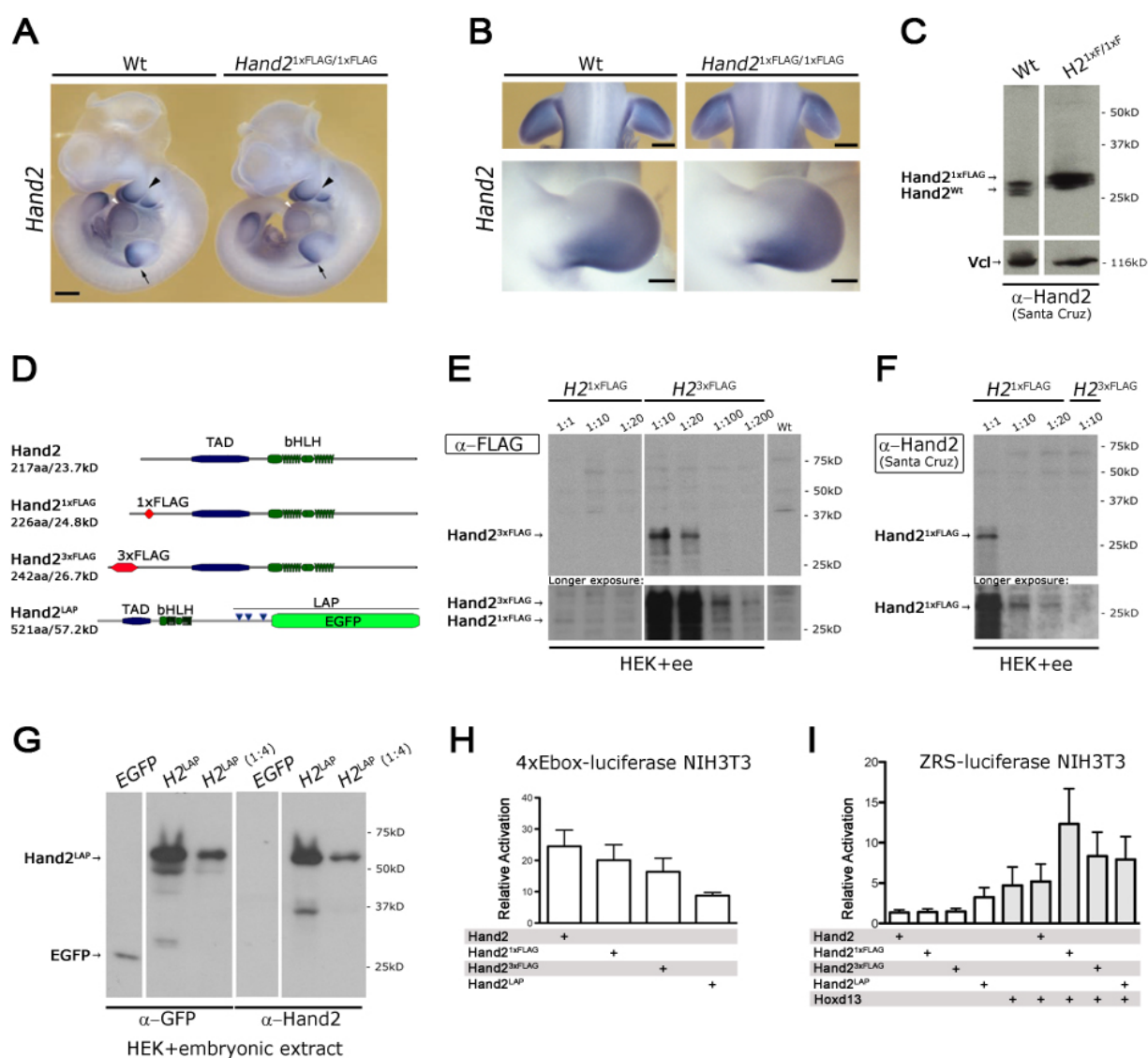


Figure 5. Detection of *Hand2*^{1xFLAG} mRNA and protein: low sensitivity of the 1xFLAG system requires the characterisation of better epitope-tagged Hand2 variants. **(A)** *In situ* detection of *Hand2* transcripts in wild-type (wt) and *Hand2*^{1xFLAG/1xFLAG} mouse embryos at embryonic day 10.5 (E10.5). The *Hand2*^{1xFLAG} allele reproduces wt *Hand2* expression, as marked in the posterior limb bud mesenchyme (arrow), branchial arches (black arrowhead) and heart (white arrowhead). Scale bar, 500µm. **(B)**:

Hand2 expression in forelimb buds in wt and *Hand2*^{1xFLAG/1xFLAG} at E10.5 (upper panel; posterior view) and E11.5 (lower panel; dorsal view) is similar. Scale bar upper panel, 200µm, lower panel 100µm. (C) Western blot using extracts (60µg) from E12.5 limb buds. M-19 anti-Hand2 antibody (Santa Cruz) detected the presence of the endogenous *Hand2*^{1xFLAG} protein based on a 1.1kD shift compared to wt *Hand2*. (D) Schematic figure showing wt and tagged *Hand2* protein versions. The localization of the *Hand2* transcriptional activation domain (TAD), the basic helix-loop-helix domain (bHLH) and the distinct epitope tags is indicated. Blue triangles mark the protease cleave site and S-peptide localizations in the LAP linker region. LAP, localization and affinity purification cassette (Cheeseman et al., 2005). (E) Western blot experiment including dilution series of transfected HEK293T cell extracts in the presence of whole embryo lysates (40µg) to simulate endogenous background. The 3xFLAG tag is 200x more sensitive than the 1xFLAG tag (compare similar band intensities in the blot exposed for longer in 1:1 (*Hand2*^{1xFLAG}) and 1:200 (*Hand2*^{3xFLAG}) dilutions). (F) Western blot with diluted samples of transfected HEK293T cells detects the *Hand2*^{1xFLAG} proteins with the M-19 anti-Hand2 antibody. Each sample contained whole embryonic lysate (40µg) to reproduce endogenous background. Film exposures are identical to the ones shown in E. Longer exposed film reveals around 20 times higher sensitivity in detection of *Hand2*^{1xFLAG} proteins with the M-19 anti-Hand2 antibody compared to detection with the M2 anti-FLAG antibody (in E). In addition, M-19 anti-Hand2 antibodies cannot bind the *Hand2*^{3xFLAG} proteins. (G) Detection of the *Hand2*^{LAP} fusion protein at 57kD in Western blots with anti-GFP (Roche) and M-19 anti-Hand2 antibodies. In anti-GFP probed blots the sensitivity was slightly more increased. The presence of weak, but specific bands reveals potential cleavage products. All samples were derived from transfected HEK293T cells. Lysates from cells transfected with EGFP expression vector were loaded as control. To simulate endogenous background, embryonic extract (40µg) was added to each sample. (H) Relative luciferase activity from an artificial 4xEbox-luciferase reporter plasmid transiently co-transfected with *Hand2*, *Hand2*^{1xFLAG}, *Hand2*^{3xFLAG}, or *Hand2*^{LAP} expression vectors in NIH3T3 cells. (I) Transactivation activity of the ZRS-reporter in NIH3T3 cells reveals a comparable activity between wt and *Hand2*-tagged versions (*Hand2*^{3xFLAG} and *Hand2*^{LAP}), either alone or in combination with *Hoxd13* (Galli et al., 2010) and *Hoxd13* expression vector in NIH3T3 cells. Standard deviations are indicated as error bars.

We performed immunoblotting using mouse embryonic limb buds to validate the sensitivity of the 1xFLAG-system. Thereby we utilized the established M2 anti-FLAG antibody to detect endogenous *Hand2*^{1xFLAG} proteins (Sigma; Einhauer & Jungbauer, 2001; Zhang et al., 2008a). In contrast to *in vitro* overexpressed *Hand2*^{1xFLAG}, endogenous *Hand2*^{1xFLAG} proteins from limb buds homozygous for the *Hand2*^{1xFLAG} allele could not be detected in Western blots or immunocytochemistry (data not shown). However, endogenous *Hand2*^{1xFLAG} proteins were detectable on immunoblots probed with the M-19 anti-Hand2 antibody (Santa Cruz; Figure 5C). The shift in molecular weight due to the inserted FLAG tag (1.1kD) ensured that the

endogenous Hand2^{1xFLAG} was produced at normal levels (Figure 5C). This is in accordance with the unaltered expression pattern in embryos and the lack of phenotypes in mice homozygous for the Hand2^{1xFLAG} allele (Figure 5A and 5B, data not shown). However, these results indicated that the generation of a sensitive tool to study endogenous Hand2 protein had failed using a 1xFLAG epitope tag. Therefore, the choice of epitopes for tagging the endogenous protein should not be based on overexpression in tissue culture systems alone.

As dRMCE allowed straightforward generation of different knock-in alleles, we decided to utilize alternative epitope tags for tagging the endogenous Hand2 protein. We selected the 3xFLAG peptide (Sigma) and the “localization and affinity purification” (LAP) cassette (Cheeseman et al., 2005) due to successful use of these tags for genome-wide studies in mouse ES cells or embryos (Zhang et al., 2008a; Nishiyama et al., 2009; Vokes et al., 2008; Poser et al., 2008). Most notably, the 3xFLAG epitope is of acceptable size (22aa, around 1/10 of the entire Hand2 protein) and should be at least 10 times more sensitive than the 1xFLAG tag (Sigma). Therefore, we constructed a Hand2^{3xFLAG} expression vector encoding a N-terminal fusion of Hand2 to the 3xFLAG peptide (Figure 5D). We performed Western blotting to demonstrate the enhanced sensitivity of Hand2^{3xFLAG} over Hand2^{1xFLAG} proteins (Figure 5E). Dilution series of protein lysates from transfected HEK293T cells mixed with embryonic extracts were used to mimic endogenous conditions. The Hand2^{3xFLAG} protein occupies a calculated molecular weight of 26.7kD and was detected with high sensitivity running around 32kD. In agreement, wild-type Hand2 proteins are also running 3 to 4kD higher in Western blots (around 27kD) than the calculated molecular weight (23.7 kD) (Figure 5D). Most notably, Hand2^{3xFLAG} was detected with about 200 times greater sensitivity than Hand2^{1xFLAG} by Western blotting with M2 anti-FLAG antibodies (Figure 5E). However, in contrast to Hand2^{1xFLAG}, the Hand2^{3xFLAG} protein could no longer be detected by anti-Hand2 antibodies (Figure 5F). This indicates that the 3xFLAG peptide attached to the N-terminus of the Hand2 protein disrupts the epitope structures, which interact with the polyclonal anti-Hand2 antibodies. In addition, we found that detection of the Hand2^{1xFLAG} proteins by the

anti-Hand2 antibody was about 20 times more sensitive than using the M2 anti-FLAG antibody (compare longer exposures of Figure 5E (1:1) to 5F (1:20)). This finding provided the explanation for the failure to detect the endogenous Hand2^{1xFLAG} proteins in samples from limb buds using the M2 anti-FLAG antibody.

The LAP tag was recently used for a high-throughput bacterial artificial chromosome (BAC) transgene approach to study protein-protein and protein-DNA interactions in mouse ES or human tissue culture cells (Poser et al., 2008). The LAP cassette consists of 304 amino acids that encode the extended green fluorescent protein (EGFP) coupled to a linker region with protease cleavage sites for native elution and an S-peptide for affinity purification. To generate such a multifunctional Hand2 chimeric protein, we fused the LAP cassette to the C-terminus of the *Hand2* coding region (Figure 5D), last but not least to prevent disruption of the inherent N-terminal transcriptional activation domain (Dai & Cserjesi, 2002). However, the size of the LAP tag is a major disadvantage, which exceeds the size of Hand2 by almost 1.5 times and may thus impair its function. Western blot analysis using anti-GFP antibody readily detected Hand2^{LAP} proteins in transfected HEK293T cells with sensitivities similar to anti-Hand2 antibodies (Figure 5G). However, the direct comparison to the 3xFLAG-system revealed around 10-20 times lower sensitivity in detecting the Hand2^{LAP} protein (data not shown). Remarkably, higher amounts of Hand2^{LAP} revealed the presence of potential degradation products (Figure 5G).

In a next step, we performed luciferase assays to further evaluate protein activity. In transfected NIH3T3 cells, both Hand2^{3xFLAG} and Hand2^{LAP} proteins were able to transactivate an artificial 4xEbox-Luciferase reporter (Figure 5H). However, the values appeared reduced to two thirds for Hand2^{3xFLAG} and to about one third for Hand2^{LAP} proteins in comparison to the presence of wild-type Hand2. To assess the transactivation potential in a less artificial approach, we used the ZRS luciferase reporter which was transactivated about 10-fold in the presence of Hand2 and Hoxd13 transcription factors (Galli et al., 2010). Upon co-transfection with Hoxd13, the transactivation potential of Hand2^{3xFLAG} and Hand2^{LAP} was enhanced around 8 fold, similar to the published values (Figure 5I). This indicates that the two novel

epitope-tagged Hand2 variants transactivate the ZRS enhancer element and thus retain wild-type Hand2 function. However, a comparatively low ZRS transactivation value was obtained when co-transfecting wild-type Hand2 with Hoxd13. Furthermore, both Hand2^{3xFLAG} and Hand2^{LAP} chimeric proteins could be readily immunoprecipitated from transfected HEK293T cells (data not shown). Moreover, HEK cells transfected with the *Hand2*^{LAP} expression vector displayed nuclear GFP fluorescence, demonstrating correct sub-cellular localization of the fusion protein (data not shown). Taken together, the Hand2^{3xFLAG} and Hand2^{LAP} proteins displayed significantly enhanced sensitivity relative to Hand2^{1xFLAG} in Western blots involving diluted cell extracts to simulate endogenous levels. Moreover, both variants retained the biological function upon assessment of the interaction with Hoxd13 and the ZRS enhancer element in luciferase assays.

5.1.5 Generation of various *Hand2* knock-in alleles using dRMCE

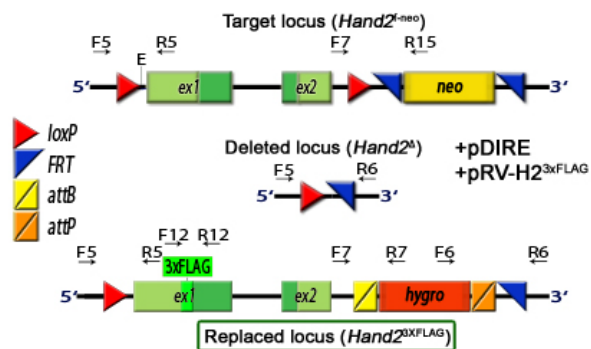
Next, based on the *in vitro* characterisation, we decided to introduce the *Hand2*^{3xFLAG} and *Hand2*^{LAP} versions into the endogenous *Hand2* locus. However, as such *in vitro* tests are rather artificial, the performance of the epitope-tagged protein is best assessed directly at endogenous levels.

First, the necessary dRMCE targeting vectors were generated (pRVH2^{3xFLAG} and pRV-H2^{LAP}, Figure 6A and 6B, see Material and Methods). In addition to the *in vitro* validated Hand2^{3xFLAG} and Hand2^{LAP} versions, a largely untested yet promising epitope-tagging strategy based on a biotinylation approach was included (Figure 6C; De Boer et al., 2003; Kolodziej et al., 2009). Thereby, the biotin acceptor peptide (Bio-tag; Kulman et al., 2006) was fused N-terminally to the *Hand2* CDS. In a catalytic reaction the *E.coli* Biotin ligase (BirA) covalently links a biotin moiety to the Bio-tag acceptor peptide. Biotin displays high affinity for avidin (or streptavidin), which is the strongest non-covalent interaction identified in nature and several magnitudes stronger than antibody-epitope interactions (De Boer et al., 2003). Tagging by biotinylation has been used for the identification of protein interaction networks and ChIP assays in ES cells and cell lines (Wang et al., 2006; Kim et al., 2008; Kolodziej et al., 2009). To provide

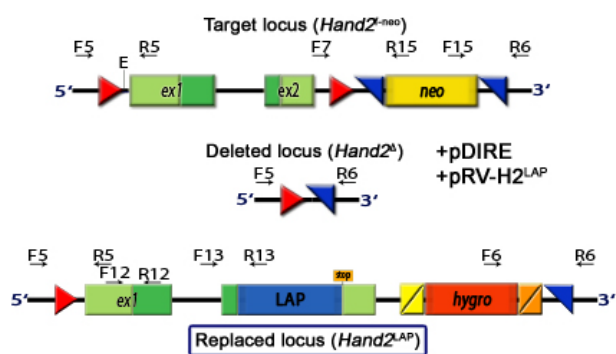
simultaneous stoichiometric quantities of BirA expression in cells with active *Hand2* transcription, a cassette promoting T2A-mediated BirA release was fused C-terminally to the *Hand2* CDS in the dRMCE targeting vector (pRV-H2^{NBio-BirA}; Figure 6C).

Taken together, the multiple *Hand2* targeting approach should demonstrate the high-throughput applicability of dRMCE for a locus displaying very low HR targeting frequencies. For dRMCE R1 ES cells heterozygous for the conditional *Hand2*^{f-neo} allele (Galli et al., 2010) were co-transfected with the pDIRE plasmid (Figure 1B) and pRV-H2^{3xFLAG} (Figure 6A), pRV-H2^{LAP} (Figure 6B) or pRV-H2^{NBio-BirA} (Figure 6C) replacement vectors. Following hygromycin selection 347 ES colonies were isolated in total and screened by conventional PCR for correct 3' and 5' recombination events using appropriate primer pairs (Figure 6D; Material and Methods Tables 3 and 4). 43 of total 347 ES colonies analysed showed correct replacement. Further characterisation of these 43 colonies with primers specific for the conditional (f-neo) and the delta (Δ) allele uncovered merely five mixed ES cell colonies (four with the *Hand2* ^{Δ} allele and one with the *Hand2*^{f-neo} allele). In summary, the highest targeting efficiency was obtained for the generation of the *Hand2*^{3xFLAG} allele (16%, 20/125), whereas the frequencies for the *Hand2*^{LAP} (8.9%, 10/113) and *Hand2*^{NBio-BirA} (7.5%, 8/109) alleles were decreased to about half (Figure 6E, Material and Methods Table 6). Notably, 14 ES colonies with correctly recombined 3' and 5' junctions were expanded and subjected to *in-depth* characterisation by PCR. Importantly, this examination ensured the presence of the introduced modifications and confirmed the clonal nature of most ES colonies (Figure 6D). All such validated and expanded ES clones were aliquotted and frozen in sufficient quantities to allow both ES cell differentiation assays and injection into mouse blastocysts to generate chimeric mice. All *Hand2* knock-in alleles generated were designed to reveal a specific banding pattern by Southern blot analysis (Figure 6F; Material and Methods Table 7).

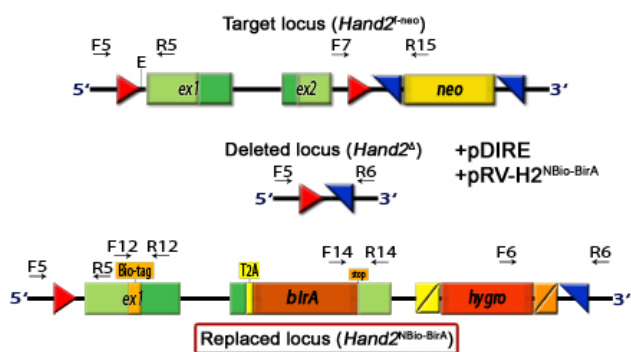
A



B



C

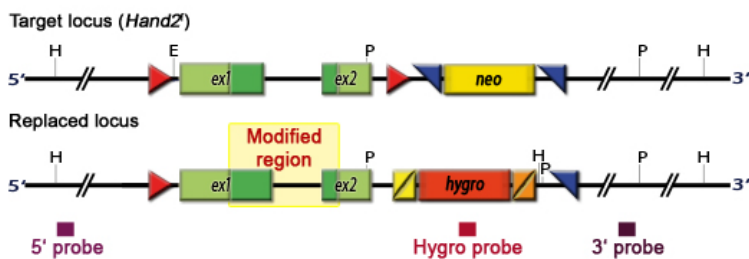


E

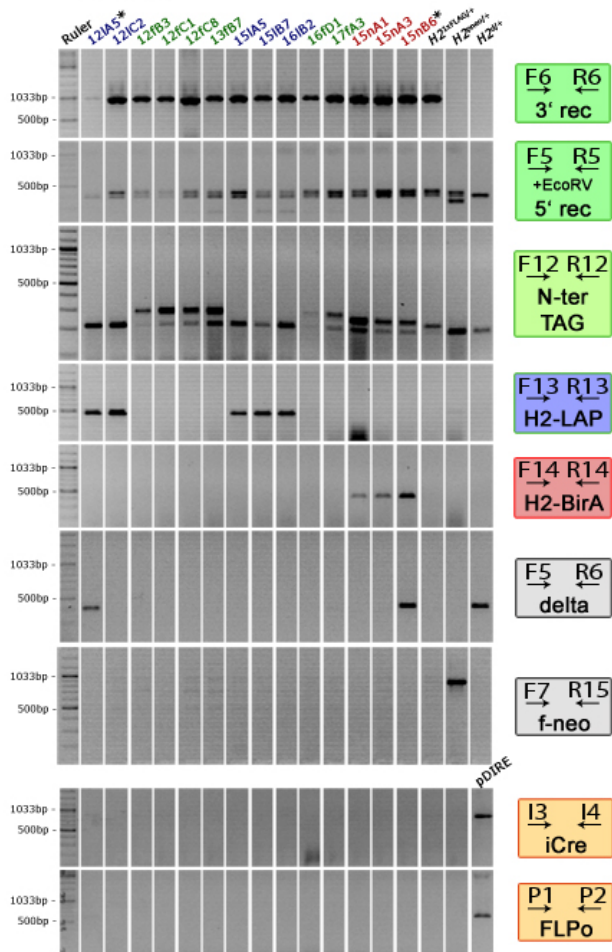
<i>Hand2^{3xFLAG}</i>	n	f	<i>Hand2^{LAP}</i>	n	f
dRMCE (5' and 3')	20	16%	dRMCE (5' and 3')	10	8.9%
Total clones picked	125		Total clones picked	113	

<i>Hand2^{NBio-BirA}</i>	n	f
dRMCE (5' and 3')	8	7.5%
Total clones picked	109	

F



D Colony



G

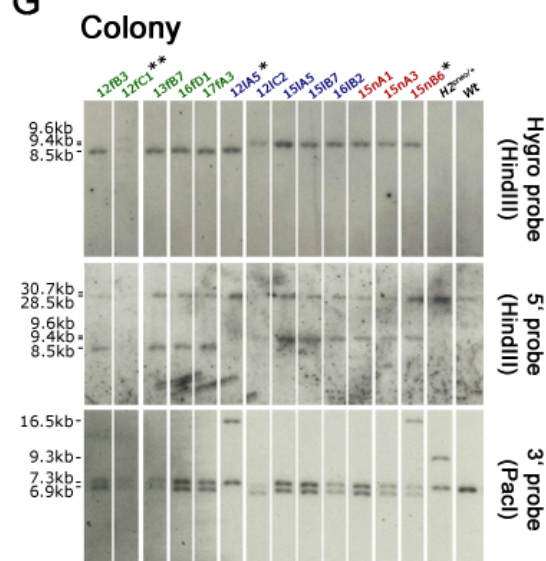


Figure 6. The dRMCE technology allows simultaneous and rapid generation of multiple *Hand2* knock-in alleles. **(A-C)** Schemes illustrating insertion by dRMCE of different epitope-tagged *Hand2* versions. Recipient *Hand2*^{f-neo/+} R1 mouse ES cells heterozygous for the *Hand2* conditional allele (Galli et al., 2010) were co-transfected with pDIRE and the according replacement vector (pRV-H2^{3xFLAG}, pRV-H2^{LAP} or pRV-H2^{NBio-BirA}). Following formation of the deleted allele upon cis-recombination, dRMCE-mediated correct replacement *in trans* results in the *Hand2*^{3xFLAG}, *Hand2*^{LAP} and *Hand2*^{NBio-BirA} alleles. Relevant PCR primers for screening of selected colonies are indicated (see Material and Methods Table 3 and Table 4). **(D)** PCR screening of hygromycin selected ES colonies. Expanded colonies of ES cells transfected with pRV-H2^{3xFLAG} (green), pRV-H2^{LAP} (blue) or pRV-H2^{NBio-BirA} (red) are shown. Identification of PCR screened ES clones with correct replacement at 3' and 5' ends (primer pairs F6/R6 and F5/R5, respectively). PCR with the F12/R12 primer pair flanking the N-terminus allows specific distinction of *Hand2* alleles. Further PCR screening of expanded clones leads to the exclusive detection of *Hand2*^{LAP} and *Hand2*^{NBio-BirA} alleles (F13/R13, F14/R14). Mixed colonies (such as 12IA5 and 15nB6, marked by single asterisks) are excluded using PCR primer pairs F5/R6 and F7/R15 specific for *Hand2*^Δ and *Hand2*^{f-neo} alleles, respectively. Random integration of the pDIRE plasmid is excluded by the use of primers specific for *iCre* (I3/I4) and *Flpo* (P1/P2). 0.1pg of pDIRE plasmid was loaded for PCR control. **(E)** Allele specific frequency of correct dRMCE replacement as determined by PCR screening. Mixed clones are excluded. n, number of ES colonies; f, frequency. **(F)** Scheme depicting the conditional *Hand2*^{f-neo} and dRMCE modified *Hand2* knock-in alleles. RE sites for digestion of diagnostic fragments and probes utilized for Southern blot analysis are indicated. H: HindIII, E: EcoRV, P: PacI. **(G)** Southern blotting confirms locus integrity and correct replacement at both 5' and 3' ends in PCR screened and expanded ES colonies (shown in **D**). Allele specific fragment sizes obtained by RE digest are listed in Material and Methods Table 7. The *Hand2* delta allele (16.5kb, 3' screening) was detected in mixed colonies (12IA5 and 15nB6, marked with single asterisks). Except in clone 12fC1 (two asterisks, duplet band detected) only single copies of the hygromycin-resistance cassette were detected. Primer sequences for generation of DIG-labelled Southern blot probes are depicted in Material and Methods Table 7. E: *EcoRV* site to detect correct 5' replacement by PCR amplification and following digestion of the product with *EcoRV*. *attB* (yellow) and *attP* (orange): Φ C31 integrase target sites allow subsequent removal of the selection cassette. LAP, localization and affinity purification cassette (Cheeseman et al., 2005); *birA*, *Escherichia coli* Biotin Ligase; Ex, exon; *neo*, neomycin resistance cassette; *hygro*, hygromycin resistance cassette; H, *HindIII* site; P, *PacI* site.

Validation of positive ES cell clones by Southern blot analysis is essential to identify unwanted random integration of the replacement vector. With one exception, no random integration events were detected in expanded ES cell colonies using a *hygromycin*-specific probe (Figure 6G). Furthermore, Southern blotting verified the integrity of the *Hand2* locus as only the correct 3' and 5' recombination events were detected. In addition, colonies identified

as mixed by PCR were confirmed using the 3' probe (Figure 6G). In summary, dRMCE permitted the simultaneous generation and subsequent validation of three different *Hand2* knock-in alleles in a time and cost efficient manner. Given the availability of ready-to-use targeting vectors and target ES cells, dRMCE allowed me to perform three successful targetings of the *Hand2* locus within two months, including the validation (PCR and Southern blot) of several positive clones for each construct.

5.2 A sensitive tool for detection of the endogenous Hand2 protein

5.2.1 Embryoid bodies to validate the *Hand2*^{3xFLAG} endogenously tagged protein

Direct validation of genetically modified *Hand2* products is challenging, as *Hand2* is not expressed in ES cells. Hence, we implied the sensitive detection and localization of endogenously tagged Hand2 in differentiated ES cells as a mandatory criterion for generating the mouse model. However, knowledge about the function and regulatory capacity of the Hand2 transcription factor in differentiated pluripotent ES cells is still very limited. As Hand2 displays spatio-temporally distinct functions in cardiac cells derived from the secondary heart field and the neural crest, differentiation assays of ES cells towards the cardiac lineage might serve as a tool to assess the sensitivity and localization of epitope-tagged Hand2 proteins. Indeed, detection of *Hand2* transcripts is reported in ES cells differentiating towards the cardiac lineage (Kouskof et al., 2004).

Dissecting the cellular and molecular mechanisms operating during cardiac lineage commitment and subsequent differentiation into the major functional heart cell types is pivotal to understanding cardiac development, function and disease (Wu et al., 2008; Martin-Puig et al., 2008). ES cell differentiation has already contributed significantly to our molecular understanding of cardiac progenitor specification and helped the characterisation of signalling pathways operating in cardiac precursors (Martin-Puig et al., 2008; Evans, 2008). In general, the availability of an epitope-tagged *Hand2* allele in an ES differentiation system would be a valuable tool to study the role of Hand2 in cardiac progenitor commitment. ES

differentiation assays are usually dependent on the formation of three-dimensional cellular aggregates, so-called embryoid bodies (EBs). EBs are formed spontaneously in ES suspension cultures. The cellular characteristics, such as size and morphology, depend on culture conditions and impact on the differentiation status and capacity of precursor cells (Kurosawa et al., 2007).

To establish an ES cell differentiation system that allows rapid assessment of epitope-tagged endogenous Hand2 proteins, we established a method that allows generation of EBs in liquid suspension culture using bacterial-grade dishes (Kurosawa et al., 2007; Bibel et al., 2007). For further differentiation towards a cardiogenic fate, we transferred the EBs to gelatinized dishes at day 4 of differentiation (d4) to induce attachment and cellular outgrowth (Boheler et al., 2002). Floating embryoid bodies (fEBs) were formed by 4d in suspension culture and were characterized by the appearance of morula-like, spherical aggregates of differing sizes and shapes (Figure 7A). These morphological variations are explained by spontaneous aggregation of floating ES cells and depend on the stochastic probability of cell-cell encounters (Kurosawa et al., 2007). However, using fEBs, the number of contracting foci indicative of the presence of cardiomyocytes in subsequent adherent cultures was sparse. This might be explained by the rather heterogenous nature of fEBs as the variable EB morphology likely induces loss of synchronized differentiation (Kurosawa et al., 2007).

To improve cardiogenic induction, we tested an alternative method relying on low-adherence tubes in order to provide a higher degree of homogeneity in EB morphology and differentiation. Indeed, a simple protocol using five days of cultivation of 2×10^4 ES cells in a 1.5ml conical screw cap tube (Kurosawa et al., 2003) resulted in most cases in a single, large EB (conical tube EB, ctEB; Figure 7B). Ultimately, adherent culture of ctEBs resulted in a far higher number of contracting foci (indicative of cardiomyocytes) than other protocols we tested and that include treatment with Dorsomorphin (Hao et al., 2008) or retinoic acid (Wobus et al., 1997). However, to first assess the temporal kinetics of *Hand2* expression, we established a fEB based ES cell differentiation assay (see Material and Methods) that included collection of samples at different time points (d0: ES cells, d4: EBs, d8, d12, d16:

adherence culture, outgrowth). For this purpose, MEF depleted ES cells were cultured in suspension for 4 days in bacterial-grade dishes. Subsequently, EBs were plated on gelatin-covered surfaces for adherence and massive cell growth. As expected, transcript analysis by quantitative real-time PCR (qPCR) revealed step-wise reduction of the pluripotency markers *Nanog* and *Sox2* (Figure 7C). This pointed to the expected loss of ES cell character due to ongoing differentiation. The quantitative differences in *Nanog* and *Sox2* transcripts in ES cells appeared in accordance with published data (Stadtfield et al., 2008). As *Sox2* contributes to embryonic stemness as well as neural identity (Gubbay et al., 1990; Graham et al., 2003), maintained *Sox2* levels detected at stages with advanced differentiation likely accounted for neural progenitors. Quantification of *Hand2* mRNA in fEB derived differentiating cells revealed a gradual increase in transcription from d8 to d16. (Figure 7D). In comparison to pluripotency markers, this tendency supported the role of *Hand2* as a transcriptional regulator of lineage commitment towards specific cell types. Furthermore, the temporal changes in *Hand2* transcript levels were very similar in wild-type and *Hand2*^{3xFLAG/+} differentiated ES cells, which pointed to normal regulation of the modified *Hand2* locus (Figure 7D). Whereas *Hand2* transcripts were absent in ES cells, levels at d16 were similar to those in embryonic hearts at E10.5. Next, Western blot analysis was performed to assess the expression and sensitivity of the epitope-tagged proteins. Strikingly, using the M2 anti-FLAG antibody, endogenous *Hand2*^{3xFLAG} proteins were readily detectable in differentiated *Hand2*^{3xFLAG/+} cells, but never in wt cells at d12 and d16 (Figure 7E). Only low *Hand2*^{3xFLAG} protein levels were present at d8, which was in agreement with the transcript levels (Figure 7D). Importantly, the three *Hand2* protein isoforms were detected as it is observed for the endogenous *Hand2* protein in mouse embryos (Galli et al., 2010). Moreover, we identified an additional *Hand2* specific protein isoform around 40kD, which is slightly smaller than the background band (Figure 7E). In general, the levels of *Hand2*^{3xFLAG} proteins correlated well with the transcript levels at the corresponding stages.

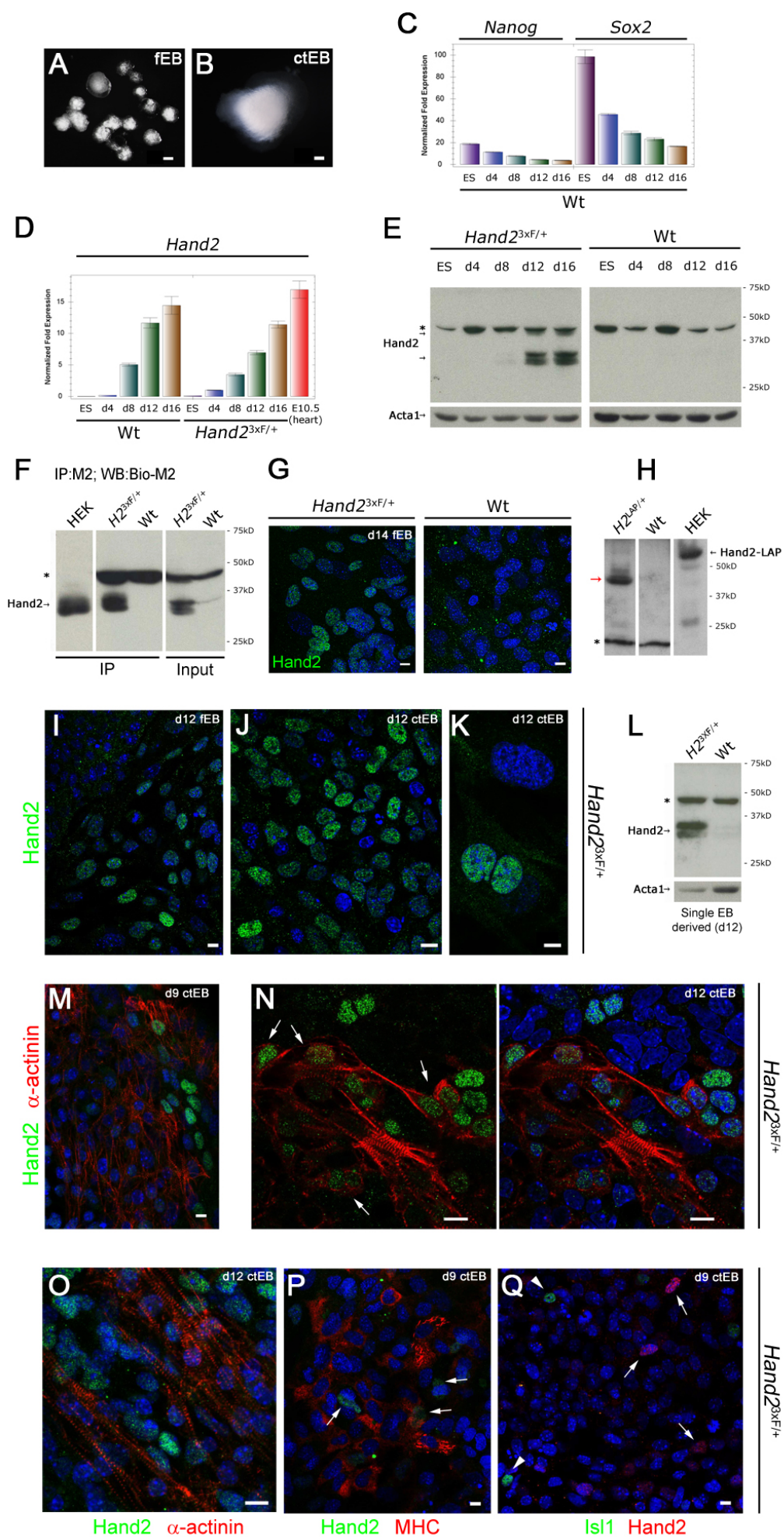


Figure 7. The novel *Hand2*^{3xFLAG} allele produces endogenous levels of tagged Hand2 that is detectable with high sensitivity and allows investigation of Hand2 localization and functions in differentiated ES cells. Asterisk indicates antibody-specific background band detected with M2 anti-FLAG antibodies in Western blots. **(A, B)** Floating embryoid bodies (A, fEBs) are morphologically more heterogeneous and smaller than those produced in conical tubes (B, ctEBs). Scale bars, 100 μ m. **(C)** Real-time quantitative PCR (qPCR) analysis of samples harvested at day of differentiation 0 (d0; ES cells), at d4 (EBs) and d8, d12 and d16 (attached to dish). Representative *Nanog* and *Sox2* transcript levels obtained at specific time points are shown. **(D)** qPCR analysis reveals *Hand2* upregulation in fEB differentiation assays. Error bars represent the mean of qPCR triplicates (C, D). **(E)** Immunoblot using M2 anti-FLAG antibody shows the induction of endogenous *Hand2*^{3xFLAG} expression during ES differentiation. 60 μ g of total protein extracts were loaded. **(F)** *Hand2*^{3xFLAG} can be efficiently immunoprecipitated from total protein extracts obtained from d12 EB cultures. Lysates of control HEK cells transfected with *Hand2*^{3xFLAG} expression vector were diluted 1:20. Input control contained 3.5x less extract than used for IP. **(G)** Immunofluorescence staining of fEBs at d14 performed with M2 anti-FLAG primary antibody. Endogenous *Hand2*^{3xFLAG} proteins (green) co-localize with Hoechst stained nuclei (blue) in *Hand2*^{3xFLAG/+} cells. In wild-type control cells treated identically, nuclear staining remains absent in all cells. Scale bar, 10 μ m. **(H)** Western blot using anti-GFP antibody reveals not only sensitive detection of the C-terminally LAP-tagged endogenous Hand2 protein but also a decreased molecular weight (red arrow) in comparison to correctly sized control *Hand2*^{LAP} protein from transfected HEK cells (black arrow). 60 μ g of total protein extracts were loaded. **(I-K)** Immunolocalization of *Hand2*^{3xFLAG} proteins (green) with the M2 anti-FLAG antibody using *Hand2*^{3xFLAG/+} cells at d12. Different fields of cells show heterogeneous expression of the tagged Hand2 protein, probably correlating with the generation of multiple uncharacterized cell types. Scale bars, 10 μ m. **(L)** Western blotting demonstrates the high sensitivity of the 3xFLAG-system by the detection of endogenous *Hand2*^{3xFLAG} proteins in extracts from d12 cultures originating from only a single embryoid body (ctEB). 20 μ g of total protein extracts were loaded. **(M-O)** Co-immunolocalization of ctEB-derived cardiomyocytes and Hand2 positive cells using antibodies against sarcomeric α -actinin (red) and the 3xFLAG epitope (green). Scale bars, 10 μ m. At d9 of differentiation large clusters of cardiac myocytes were localized, sometimes with interstitial groups of Hand2 positive cells **(M)**. At d12, Hand2 positive nuclei were identified in a fraction of cardiomyocytes (arrows) **(N)**, closely associated with them **(O)** or even absent from clusters of cardiac muscle (data not shown). **(P)** CtEB-derived cardiomyocytes marked by immunofluorescence (red) with the anti-MHC (sarcomeric) antibody revealed nuclei with absent Hand2 proteins. In a sub-fraction, single cells with Hand2 expressing nuclei (green) were detected in close proximity (arrows) by co-staining with the M2 anti-FLAG antibody. Scale bar, 10 μ m. **(Q)** Immunofluorescence using anti-Isl1 antibody revealed single cells containing high levels of nuclear Isl1 protein (green, arrowheads). In these cells Hand2 proteins (red, arrows) were absent. Scale bar, 10 μ m. Secondary antibodies were either labelled with 488-Alexa (green) or 594-Alexa (red). Nuclei were counterstained with Hoechst.

Next, endogenous $Hand2^{3xFLAG}$ proteins were immunoprecipitated from lysates of d12 differentiated $Hand2^{3xFLAG/+}$ ES cells, but not from equivalent wild-type control samples (Figure 7F). The specificity of detecting the endogenous $Hand2^{3xFLAG}$ protein was further demonstrated by immunofluorescence analysis, which revealed the nuclear localization of the $Hand2^{3xFLAG/+}$ proteins in differentiated $Hand2^{3xFLAG/+}$ ES cells at d14 (Figure 7G). In contrast, nuclear staining was not observed in d14 wild-type control cells and only faint non-nuclear background was detected. Taken together, the ES cell differentiation approach allowed rapid examination of sensitivity and localization of the epitope-tagged endogenous Hand2 protein. In particular, validation of endogenous $Hand2^{3xFLAG}$ by Western blot, immunoprecipitation and immunofluorescence revealed the high specificity and sensitivity of the 3xFLAG epitope-tag based approach, which appeared well suited to generate the $Hand2^{3xFLAG}$ mouse model.

Using this ES cell differentiation system, we next validated the other epitope-tagged $Hand2$ alleles generated by dRMCE. In a first step, we assessed C-terminally LAP-tagged endogenous Hand2 proteins in d12 $Hand2^{LAP/+}$ differentiated ES cells using an anti-GFP antibody (Poser et al., 2008). However, immunoblotting revealed an aberrantly sized protein running at around 45kD instead of 57kD (calculated molecular weight) detected in HEK cells transfected with the $Hand2^{LAP}$ expression vector (Figure 7H). This decrease in molecular weight indicated that either the Hand2 protein (23.7kD) or the LAP cassette (33.5kD) was truncated or degraded. Furthermore, $Hand2^{NBio-BirA/+}$ differentiated ES cells were cultured in biotin enriched medium and collected at d12. However, due to unknown reasons, we were never able to detect Bio-tagged endogenous Hand2 by Western blot analysis (data not shown).

In light of these findings our observations illustrate that heterogeneous ES differentiation culture assays may allow easy validation of epitope-tagged factors not expressed in ES cells. In particular, our approach also identified the basic problems in detecting endogenous Hand2 proteins using the $Hand2^{LAP}$ and $Hand2^{NBio-BirA}$ alleles. This avoids the costly and time

consuming generation of mouse models encoding epitope-tagged factors with insufficient sensitivity or decreased protein stability.

Comparison of fEB and ctEB differentiating ES cells at d12 revealed subpopulations of cells with differential levels of nuclear Hand2^{3xFLAG} proteins localized predominantly in proximity to the outgrowing EB (Figure 7I, J). In contrast, most other regions and the remnant EB itself were usually not expressing Hand2 proteins. Hand2 positive cells appeared overall extended and covered larger areas in ES cell cultures differentiated from ctEBs (Figure 7J). Rapid differentiation and proliferation of these heterogeneous populations resulted in a variety of differential cell morphologies. Interestingly, Hand2 protein was also detected in comparatively large nuclei of cells localized at the distant border of the area covered by the outgrowing cells (Figure 7K). Underscoring the impressive sensitivity of the 3xFLAG system, endogenous Hand2^{3xFLAG} proteins were readily detected by Western blot analysis of differentiating cells from one single ctEB (Figure 7L).

We next used the ctEB differentiation method to investigate the characteristics of cells differentiating towards the cardiac lineage. Hand2 positive cells and cardiomyocytes were localized using M2 anti-FLAG and anti-sarcomeric α -actinin antibodies, respectively (Domian et al., 2009). α -Actinin (Actn2) is a component of the sarcomeric Z-disc in cardiomyocytes and skeletal muscle which crosslinks myosin and actin filaments and is required for transmission of contractile force. As little paraxial mesoderm is formed in embryoid bodies, the appearance of clusters of skeletal muscle is rather unlikely in EB derived cell cultures (Darabi et al., 2008). The highest frequency of rhythmically contracting cellular foci, which points to the presence of functional cardiomyocytes (Boheler et al., 2002), was detected at d9 of ctEB differentiation (≤ 5 foci per well). However, the sizes of beating foci varied significantly, likely representing the degree of heterogeneity in the stochastic lineage commitment (Kurosawa et al., 2007). Interestingly, at d9, immunolocalization revealed that Hand2 was only rarely expressed directly by cardiomyocytes. In fact, Hand2 positive cells were detected in a rather complementary pattern in comparison to the still mono-nucleated

cardiomyocytes (Figure 7M). Moreover, some large areas of cardiomyocytes were not associated at all with Hand2 expressing cells (data not shown).

In general, more than 50% of all wells contained contracting foci at d12. Cardiomyocytes appeared larger and at least partially multinucleated with intense striated sarcomeric Z-discs (Figure 7N, O). However, these cardiomyocytes rarely co-expressed Hand2 (Figure 7N). More frequently, cells with nuclear Hand2 proteins were localized in close proximity to cardiomyocytes (Figure 7O). This complementary expression could be related to Hand2 functions in multipotent cardiovascular progenitors (Bhattacharya et al., 2006; Laugwitz et al., 2008) or provide an environment for induction or fusion of cardiomyocytes as during zebrafish heart development (Garavito-Aguilar et al., 2010). Similarly, co-localization of Hand2 with another cardiomyocyte marker, sarcomeric myosin heavy chain (sMHC; Takahashi et al., 2006) at d9 revealed few intercalated Hand2 positive cells between clusters of sMHC expressing cardiomyocytes (Figure 7P). We further examined the localization of cardiovascular Islet1 (Isl1) positive precursors (Moretti et al., 2007; Laugwitz et al., 2008). Isl1 was nuclear in single, isolated cells located close to the outer border of the remnant EB (Figure 7Q). In addition, Isl1 was also detected at lower levels in nuclei of small groups of cells close to the outer border (data not shown). However, Hand2 never co-localized with Isl1 in cell nuclei. Notably, Hand2 is described as an indirect target of Isl1 during secondary heart field development (Laugwitz et al., 2008). Taken together, *Hand2*^{3xFLAG/+} ES cells represent a versatile tool for differentiation assays to elucidate the molecular functions of Hand2 in specification, maturation and differentiation of various cell types, such as cardiac progenitors.

5.2.2 Tracking the expression dynamics of Hand2 tagged proteins in the mouse limb bud

ES cell differentiation assays show that the endogenous *Hand2*^{3xFLAG} protein is produced from the *Hand2* locus and detected by the M2 anti-FLAG antibody with high sensitivity and specificity. Based on this promising validation, we decided to generate *Hand2*^{3xFLAG} mice as a tool to study Hand2 functions during embryonic development. Two karyotyped ES clones

(12φB3, 17φA3) encoding the dRMCE-engineered *Hand2*^{3xFLAG} allele were used for blastocyst injection. Two male chimeras generated by injection of 12φB3 ES cells were highly chimeric and efficiently transmitted the *Hand2*^{3xFLAG} allele to the F1 offspring (Figure 8A). Importantly, mice homozygous and hemizygous for the *Hand2*^{3xFLAG} allele were viable and fertile and did not display any defects throughout postnatal and adult life. Moreover, offspring carrying the *Hand2*^{3xFLAG} allele were obtained in Mendelian ratios. As *Hand2* deficient embryos display various defects and die after E9.5 (Srivastava et al., 1997), our findings indicate that the N-terminally located 3xFLAG epitope does not significantly alter *Hand2* protein function. Diagnostic F12/R12 PCR primers, which flank the 3xFLAG peptide-coding region at the *Hand2* N-terminus, were used for routine genotyping (Material and Methods Table 8). This primer pair allowed simultaneous amplification of DNA fragments indicative of *Hand2*^{3xFLAG} and wild-type *Hand2* alleles (Figure 8B). DNA sequencing of the gel-extracted and purified PCR fragment encoding the 3xFLAG peptide fused to the *Hand2* N-terminus (284bp) revealed the correct nucleotide sequence (Figure 8C). For immediate examination of epitope-tag functionality, we performed Western blot experiments. For this purpose, lysates of limb buds of *Hand2*^{3xFLAG/+} and wild-type embryos at E11.5 and E12.5 were used, as *Hand2* is known to be expressed at high levels in the limb bud mesenchyme. Indeed, *Hand2* isoforms were readily detected (Figure 8D), including again a fourth isoform (at around 40kD), which was already observed in differentiated ES cells (Figure 7E). Furthermore, this analysis illustrated the sensitivity of the 3xFLAG-based system, as the additional band was not detected using anti-*Hand2* antibodies (Figure 8D). Moreover, the *in vivo* *Hand2*^{3xFLAG} protein could not be detected by anti-*Hand2* antibodies, as the N-terminal 3xFLAG peptide likely disrupts the required epitope structure. To rapidly validate the use of the *Hand2*^{3xFLAG} allele for immunolocalization in the mouse embryo, we cultured limb bud cells. This approach was previously used to localize endogenous wild-type *Hand2* proteins in the nucleus of a subset of limb bud cells using the anti-*Hand2* antibody (Galli et al., 2010). Indeed, cells with nuclear *Hand2*^{3xFLAG} proteins were readily observed in cultures from E11.5 and E12.5 *Hand2*^{3xFLAG/+} limb buds (Figure 8F-J). In contrast, no specific signals were

detected in wild-type control limb bud cells (Figure 8E, data not shown). Different levels of Hand2^{3xFLAG} proteins were observed in specific cells of E11.5 Hand2^{3xFLAG/+} limb buds cultured for 3.5h (Figure 8F, 8G). Furthermore, primary limb bud cells from E12.5 embryos revealed the presence of nuclear Hand2^{3xFLAG} after 5 hours (Figure 8H) and even after 20 hours (Figure 8I) of culture. The exact subcellular localization of Hand2^{3xFLAG} proteins could be determined at high resolution (Figure 8J). Taken together, the Hand2^{3xFLAG} allele allows detection and localization of Hand2 proteins in primary limb bud cells with higher sensitivity and reproducibility than commercial anti-Hand2 antibodies.

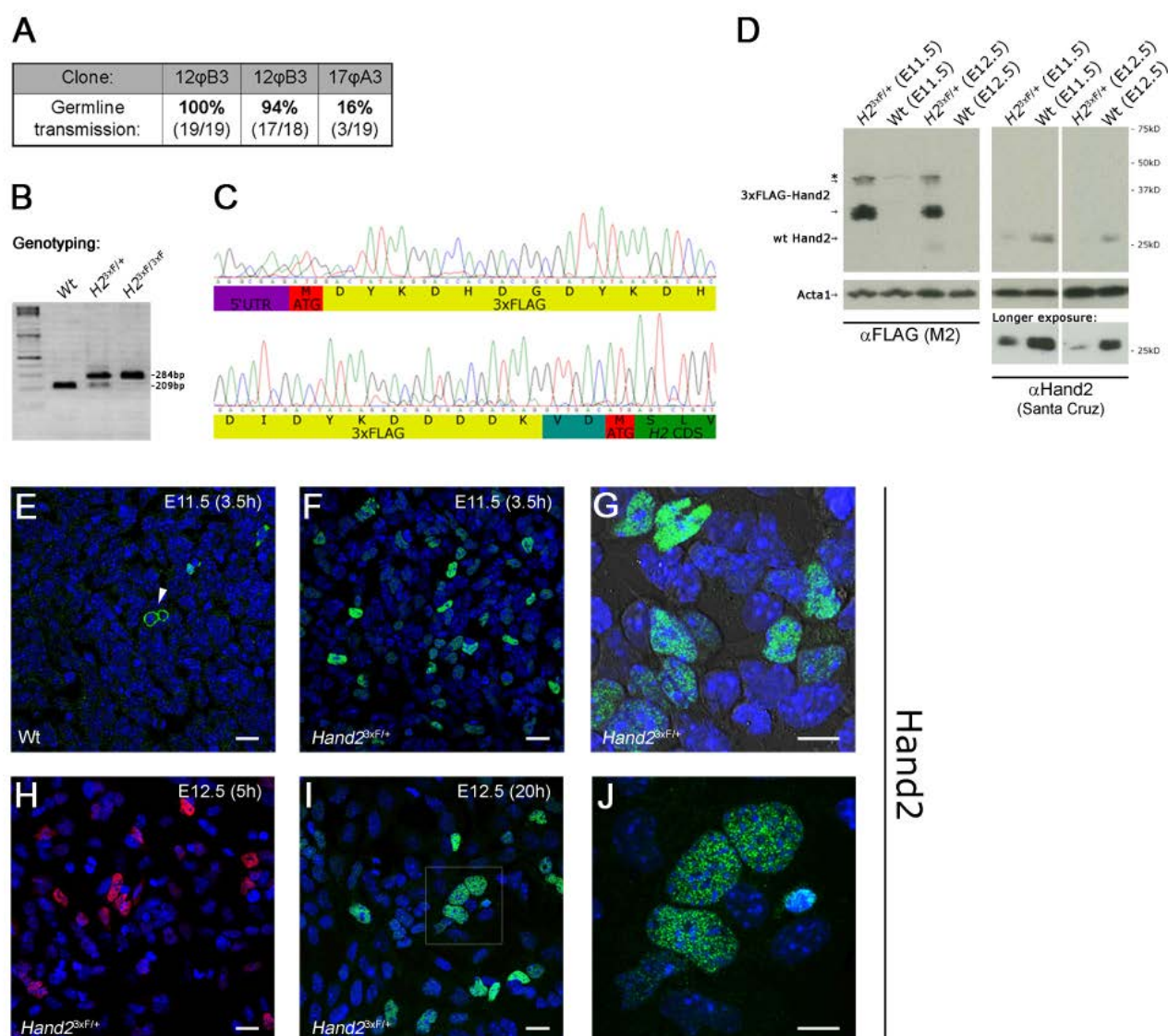


Figure 8. The endogenous Hand2^{3xFLAG} allele enables sensitive detection and sub-cellular localization of Hand2 proteins in embryonic limb bud cells. **(A)** Germline transmission frequencies obtained by

three different *Hand2*^{3xFLAG} male mouse chimeras derived from dRMCE engineered ES clones. The number of agouti pups (indicative of germline transmission) and the total number of offspring is indicated in brackets. **(B)** Agarose gel illustrating the genotyping strategy using the PCR primer pair F12/R12 (Material and Methods Table 8) which allows simultaneous detection and discrimination of wild-type *Hand2* and *Hand2*^{3xFLAG} alleles. **(C)** Correct in-frame fusion was confirmed by sequencing of a PCR fragment (shown in B) amplified from the *Hand2*^{3xFLAG} allele and covering the region encoding the 3xFLAG tag. The nucleotide sequence appears in a colour code (A: green, T: red, G: grey, C: blue) and translated amino acid sequences are indicated. Valin (V) and aspartic acid (D) residues located 5' to the original *Hand2* start codon represent a linker region that served as RE consensus site for cloning. **(D)** Western blot analysis of E11.5 and E12.5 embryonic limb buds heterozygous for the *Hand2*^{3xFLAG} allele compared to wild-type controls, reveals sensitive and specific detection of the *Hand2*^{3xFLAG} protein using M2 anti-FLAG antibody (blot on the left). Arrows indicate the *Hand2* characteristic triplet (Galli et al., 2010) and a fourth *Hand2* isoform at around 40kD. Detection of endogenous *Hand2* proteins by anti-*Hand2* antibodies (Santa Cruz) revealed significantly decreased sensitivity (blot on the right). 60µg of total protein extracts were loaded. **(E-G)** Immunofluorescence using the M2 anti-FLAG antibody in dissociated limb bud cells (at E11.5) cultured for 3.5 hours enables specific detection of *Hand2*^{3xFLAG} proteins with high resolution. **(E)** Primary cell cultures from wild-type limb buds never display any nuclear signal, but only occasional non-nuclear background (arrowhead). Scale bar, 20µm. **(F)** *Hand2* specific nuclear signal is detected in a subset of *Hand2*^{3xFLAG} limb bud cells. Scale bar, 20µm. **(G)** Higher magnification reveals variable levels of *Hand2* protein. Differential interference contrast (DIC) allows visualization of cellular structures. Scale bar, 10µm. **(H-J)** immunofluorescence of limb bud cell cultures of E12.5 *Hand2*^{3xFLAG/+} embryos using M2 anti-FLAG antibodies. **(H)** After 5 hours of culture, *Hand2*^{3xFLAG} proteins were readily detectable in some nuclei. Scale bar, 20µm. **(I)** Primary cells maintained production of the *Hand2* protein after 20h of culture. Scale bar, 20µm. **(J)** Increased magnification shows at high resolution the sub-cellular localization of *Hand2*^{3xFLAG} proteins. Scale bar, 10µm. Cells used for immunofluorescence microscopy were treated with 488-Alexa (green) or 594-Alexa (red) secondary antibodies and nuclei were counterstained with Hoechst.

Transcriptional control requires binding of transcription factors to specific cis-regulatory elements to regulate spatio-temporal gene expression. Thus, introduction of additional sites or the presence of a selection marker in an endogenous locus potentially interferes with cis-regulatory elements located up- or downstream of the transcriptional start site including intronic regions (Carroll, 2008; Splinter & de Laat 2011; Tschopp et al., 2011). Thus, whole mount *in-situ* hybridisation was used to assess the transcriptional integrity of the *Hand2* locus in mouse embryonic limb buds (Figure 9A). We observed no significant alterations of the spatio-temporal *Hand2* transcript distribution in fore- and hindlimb buds of embryos

homozygous or hemizygous for the *Hand2*^{3xFLAG} allele (at E11.75). In all cases the posterior, apical and proximal-anterior *Hand2* expression domains (Charité et al., 2000) were identical to those in age-matched wild-type limb buds (Figure 9A). Next, we investigated the *Shh* transcript distribution in fore- and hindlimb buds at E11.0 to establish the integrity of the zone of polarizing activity (ZPA). As expected, the posterior *Shh* domain was normal, even in the presence of only one tagged *Hand2* allele (Figure 9A). This further illustrates the functionality of endogenous *Hand2*^{3xFLAG} proteins in a complex *in-vivo* system, such as the developing limb bud.

In a next step, we quantified the endogenous *Hand2*^{3xFLAG} proteins in defined embryonic tissues at different stages. *Hand2*^{3xFLAG} proteins were readily detected in a dose-dependent manner in extracts of whole embryos at E9.5 (Figure 9B). From about E9.5 to E11.5, characteristic *Hand2* expression is observed in the limb buds, the heart and the branchial arches. Indeed, the tissue-specific and dose-dependent expression of *Hand2*^{3xFLAG} proteins was verified by Western blots from embryonic tissues at E10.5 and E11.5 (Figure 9C, 9D). As expected, *Hand2* proteins are absent in a negative control tissue such as the midbrain. Highest levels of *Hand2* proteins were detected in branchial arches and limb buds, whereas cardiac tissues revealed lower quantities (Figure 9C, Appendix Figure 2). Interestingly, the top band of the *Hand2* triplet represented the most abundant protein isoform in all samples at E10.75 (Appendix Figure 2), as also observed by Western blotting using the anti-*Hand2* antibody on limb buds (Galli et al., 2010). Impressively, *Hand2*^{3xFLAG} proteins were detected in the heart of a single embryo heterozygous for the *Hand2*^{3xFLAG} allele at E10.5 (Figure 9C). Taken together, this Western blot analysis shows that the endogenous *Hand2*^{3xFLAG} proteins are produced by both alleles in specific mouse embryonic tissues and can be detected in a highly sensitive manner in a single organ.

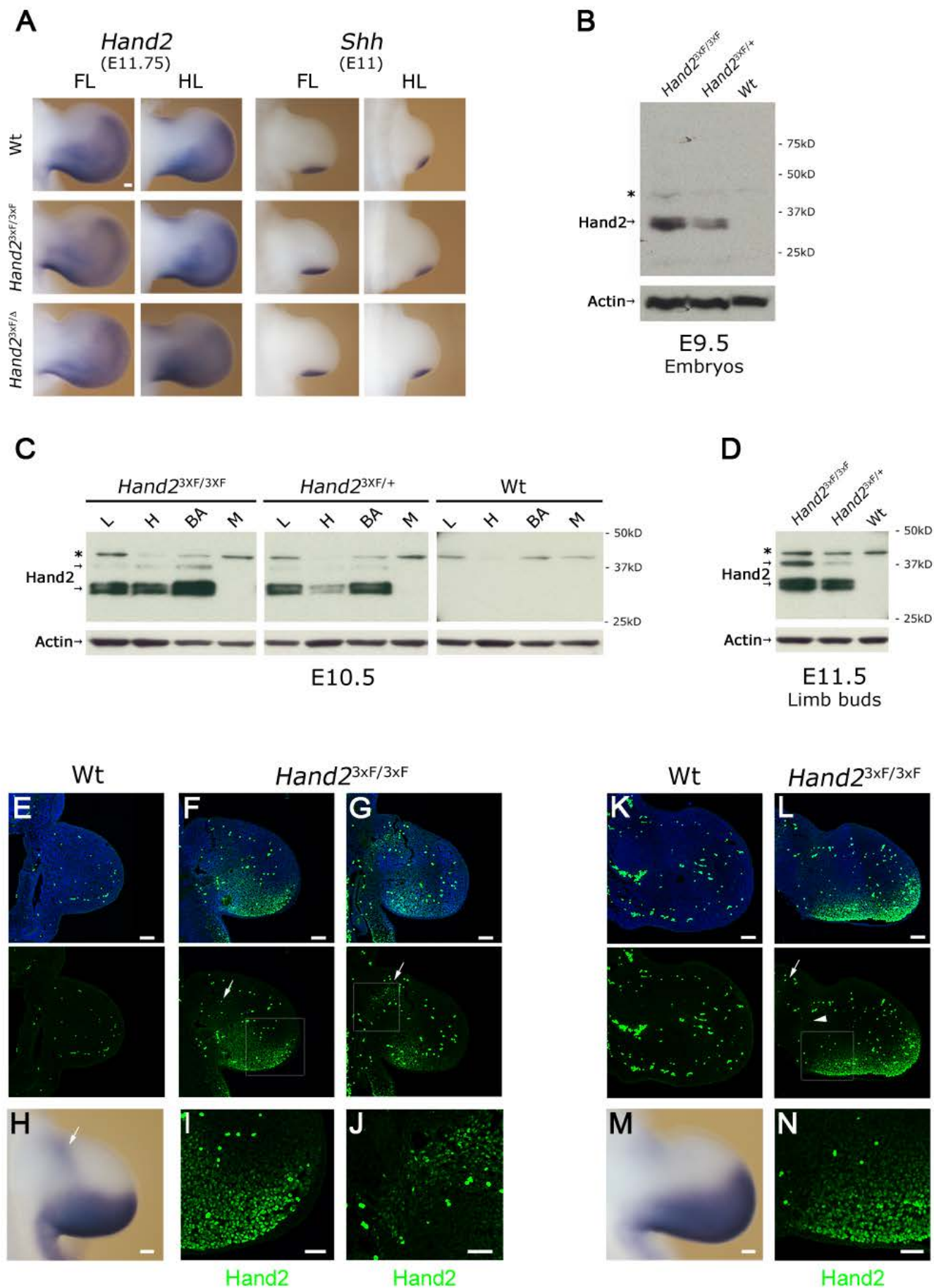


Figure 9. Both transcripts and proteins produced by the *Hand2*^{3xFLAG} allele display normal expression domains and levels in limb buds. **(A)** Left panels: *in situ* mRNA detection reveals unaltered *Hand2* expression in limb buds of embryos homozygous or hemizygous for the *Hand2*^{3xFLAG} allele at E11.75 (54 somites). Right panels: *in situ* hybridization reveals normal *Shh* expression in *Hand2*^{3xFLAG/3xFLAG} and *Hand2*^{3xFLAG/Δ} limb buds at E11 (40 somites). FL, forelimb bud. HL, hindlimb bud. Scale bar, 100μm. **(B)** Western blotting detects endogenous levels of *Hand2*^{3xFLAG} proteins in single embryos homozygous or heterozygous for the *Hand2*^{3xFLAG} allele at E9.5. 60μg of total proteins were loaded. Asterisk indicates an antibody-related background band. **(C)** Immunoblotting using lysates (15μg) from limb buds (L), heart (H), branchial arches (BA) and midbrain (M, negative control) of single embryos homozygous/heterozygous for the *Hand2*^{3xFLAG} allele or wild-type (at E10.5; 36 somites). **(D)** Western blotting detects *Hand2*^{3xFLAG} proteins in lysates (15μg) of limb buds from *Hand2*^{3xFLAG/3xFLAG} and *Hand2*^{3xFLAG/+} embryos at E11.5 (50 somites). **(E-G, I-L, N)** Immunofluorescence detects endogenous *Hand2*^{3xFLAG} proteins (green) in limb buds. Strong cytoplasmic signals in single cells scattered across the whole limb bud represent autofluorescent blood cells. Scale bar, 100μm. **(E)** No specific signal was obtained by immunofluorescence in control forelimb buds at E10.5 (except autofluorescent erythrocytes). **(F, G)** *Hand2* immunolocalization in serial sections of *Hand2*^{3xFLAG/3xFLAG} forelimb buds at E10.5 (36S). Arrows indicate domains of *Hand2* protein expressing cells in the proximal-anterior limb bud. Scale bar, 100μm. **(H)** *Hand2* transcript distribution shown by *in situ* hybridization in wild-type E10.5 limb buds. The proximal-anterior expression domain is indicated (arrow). Scale bar, 100μm. **(I, J)** Enlargement of framed areas in F and G, respectively. Distal-posterior **(I)** and proximal-anterior **(J)** parts of the forelimb bud are shown. Scale bars, 50μm. **(K)** No specific signals were detected in E11.0 wild-type control limb buds. Scale bar, 100μm. **(L)** Localization of *Hand2* positive cells predominantly in the posterior forelimb bud at E11.0. Other groups of cells containing lower levels of *Hand2*^{3xFLAG} proteins are indicated in the proximal-anterior (arrow) and in the core of the limb bud (arrowhead). Scale bar, 100μm. **(M)** *Hand2* transcript distribution in wild-type forelimb buds at E11.0 as revealed by *in situ* hybridisation. Scale bar, 100μm. **(N)** Enlargement of the region framed in L illustrates a graded distribution of *Hand2*^{3xFLAG} protein. Scale bar, 50μm. The M2 anti-FLAG antibody was used in all applications to detect endogenous *Hand2*^{3xFLAG} proteins. In Western blots, anti-actin antibody was used as loading control. In all panels limb buds are oriented with the anterior to the top. A 488-Alexa secondary antibody was used and nuclei were counterstained with Hoechst.

So far, immunolocalization of the endogenous *Hand2* proteins in embryonic tissues (Xiong et al., 2009; Li et al., 2011) has been rather difficult, likely due to the lack of sensitivity and poor performance of the available *Hand2* antibodies. Thus, we performed immunohistochemistry using sections of mouse embryonic forelimb buds to determine the *Hand2* protein distribution. Indeed, specific immunofluorescence was observed in nuclei of cells located mainly in the posterior mesenchyme of forelimb buds homozygous for the *Hand2*^{3xFLAG} allele

at E10.5 (Figure 9F, G). In contrast, specific nuclear staining was not detected in age-matched wild-type controls (Figure 9E). At E10.5, *Hand2* transcripts are predominantly expressed in the posterior mesenchyme with a weaker proximal-anterior domain (Figure 9H; Charité et al., 2000). The distribution of Hand2 positive cells largely matched the characteristic *Hand2* transcript distribution during limb bud development. In contrast to RNA *in situ* hybridisation, analysis of the Hand2 protein distribution provides single cell resolution and allows quantitative analysis of Hand2 transcription factor levels. This is particularly important as Hand2 levels are regulated post-transcriptionally as shown in the developing heart (Zhao et al., 2005). Immunolocalization using the *Hand2*^{3xFLAG} allele revealed a gradient-like distribution of Hand2 proteins in cells within the posterior limb bud mesenchyme with higher levels in close proximity to the epithelium including the AER (Figure 9I). Moreover, we detected Hand2 positive cells in a proximal-anterior area of the limb bud, which co-localized with the proximal-anterior transcript domain detected by RNA *in situ* hybridisation (Figure 9G, H, J; Charité et al., 2000). In addition, transverse sections showed that the *Hand2*^{3xFLAG} proteins are localized in limb bud mesenchymal cells adjacent to epithelial cells in both the dorsal and ventral ectoderm (data not shown). Furthermore, immunolocalization revealed the Hand2 protein distribution in the posterior forelimb bud mesenchyme at E11.5 (Figure 9L), while no positive cells were detected in controls (Figure 9K). Interestingly, the *Hand2* transcript distribution (Figure 9M) extends more anteriorly than the domain of cells positive for Hand2 protein expression. Again, the Hand2 protein levels were highest in close proximity to the posterior epithelium, resulting in a graded decrease of the Hand2 protein distribution towards the anterior (Figure 9N). This gradient extended about 200-250µm into the central mesenchyme, which is within the range of secreted signals and antagonists that regulate limb development, such as Wnts or Fgfs (Ten Berge et al., 2008; Zeller et al., 2009). Thus, our observations suggest that Hand2 could be regulated by signals secreted from the posterior epithelium and AER. However, also the graded distribution of a *Hand2* repressor (such as Gli3R) could explain the differential levels of Hand2 proteins.

5.2.3 A tool to monitor Hand2 expression in the embryonic heart

Localization of endogenous Hand2 proteins at a single cell resolution is of particular interest for understanding the molecular processes involved in cardiac development (Srivastava, 2006; Olson, 2006). The *Hand2*^{3xFLAG} allele in combination with the M2 anti-FLAG antibody allowed identification of single Hand2 positive cells in specific embryonic tissues (Figure 10A, D, G, J). In the developing heart, at E10.0, most cells of the right atrium were positive for the nuclear Hand2 protein, whereas in the transition between the outflow tract (OFT) and the right ventricle (RV) around half of the myocardial cells expressed the Hand2 protein (Figure 10B). Endocardial cells often expressed high levels of Hand2 proteins. We further localized Hand2 positive cells in pericardial and endocardial, but not myocardial cells in the developing left ventricle at E10.0 (Figure 10E). Interestingly, cells expressing high levels of Hand2 are contributing also to the forming endocardial cushion in the atrioventricular canal (Figure 10E, F). Interestingly, in the left atrium we discovered only few Hand2 positive cells likely representing invading cells from the overlying pharyngeal mesoderm (Figure 10D). Furthermore, we observed nuclear Hand2 proteins in the ventrolateral portions of the branchial arches at E10.0 (Figure 10C), overlapping the *Hand2* expression domain (Thomas et al., 1998).

With progressing cardiac development, the ventricular compact and trabecular zones expand between E10.0 and E10.5, due to enhanced proliferation of myocardial cells (Martin-Puig, 2008; Figure 10H, K). At E10.5, a majority of the cells were positive for Hand2 within the compact zone and the trabecular zone of the right ventricle and within the atrial myocardium (Figure 10H, I). As observed at E10.0, endocardial cells frequently expressed high levels of Hand2 protein. Hand2 was further localized in a subset of cells populating the OFT (data not shown) and in nuclei of pericardial cells enveloping the developing heart (Figure 10H, K). In the left ventricle Hand2 proteins were detected in endocardial, but not in myocardial cells, whereas the left atrial chamber revealed a subset of Hand2 positive cells (Figure 10K, L, data not shown). In general, the compartment-specific distribution of Hand2 in distinct

cardiac cell-types was in agreement with the previously described cardiac phenotypes and mRNA expression patterns.

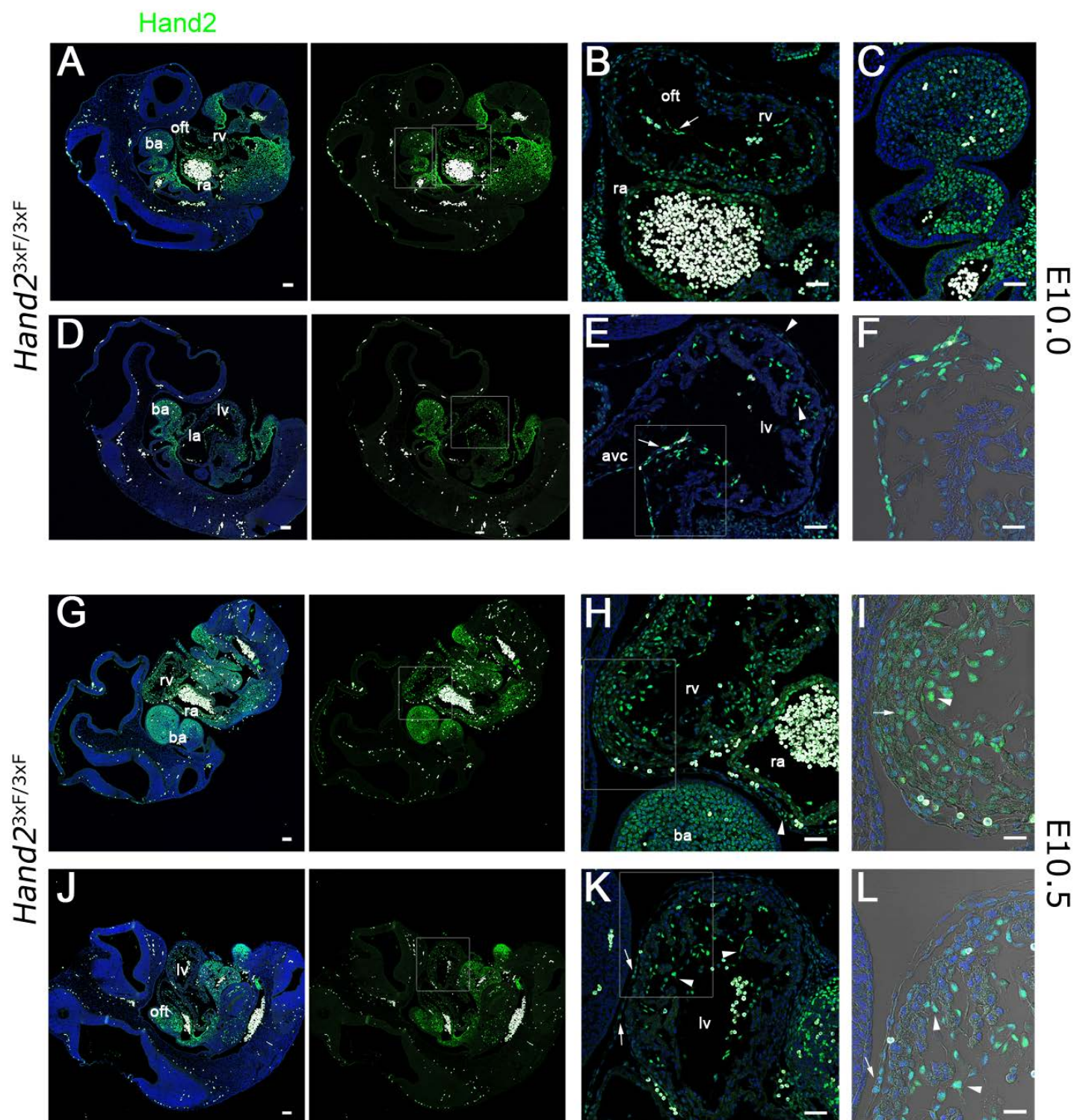


Figure 10. Immunolocalization of Hand2^{3xFLAG} proteins in cardiac tissues. (A, D) Serial sagittal sections show endogenous Hand2^{3xFLAG} proteins in an embryo homozygous for the Hand2^{3xFLAG} allele at E10.0 (29 somites). Scale bar, 100 μ m. (B) Enlargement of the cardiac region framed in A. Nuclear Hand2^{3xFLAG} proteins are localized in the majority of cardiac cells in the developing right atrium (ra).

Nuclei containing Hand2 protein are also observed in around half of the cells populating the right ventricle - outflow tract (OFT) transition. Cells contributing to the endocardial cushion in the OFT are also positive (arrow). Scale bar, 50 μ m. **(C)** Enlargement of the left frame in A illustrates the presence of Hand2 in the ventrolateral mesenchyme of the branchial arches. Scale bar, 50 μ m. **(E)** Enlargement of the area framed in D. Hand2^{3xFLAG} proteins are absent from the left ventricular myocardium, but detected in pericardial and endocardial regions (arrowheads) and in cells demarcating the endocardial cushion anlage in the atrioventricular canal (arrow). Scale bar, 50 μ m. **(F)** Enlargement of the region framed in E. High resolution shows strongly Hand2 positive cells contributing to the endocardial cushion in the atrioventricular canal. Scale bar, 25 μ m. **(G, J)** Immunolocalization of Hand2^{3xFLAG} proteins (green) in a *Hand2*^{3xFLAG} homozygous embryo at E10.5 (34 somites). Scale bar, 100 μ m. **(H)** Hand2 positive cells populate a large fraction of the developing right ventricle and atrium at E10.5. Also cells in the surrounding pericardial layer appear Hand2 positive (arrowhead). **(I)** Zoom of a part of the right ventricle framed in H. Hand2 positive myocardial cells of the compact zone (arrow) and pericardial cells (arrowhead) are shown. **(K)** Pericardial (arrows) and endocardial (arrowheads) cells are often Hand2 positive, whereas ventricular myocytes in the compact zone and trabeculae are negative for Hand2 at E10.5. **(L)** Enlarged area framed in K. Hand2 positive pericardial (arrow) and endocardial (arrowhead) cells are indicated. Ba, branchial arches. Oft, outflow tract. Rv, right ventricle. Ra, right atrium. Lv, left ventricle. La, left atrium. Avc, atrio-ventricular canal. Enlargements of Figures **A, B, D, E, G, H, J, K** are found in the Appendix. Autofluorescent blood cells are shown in white. Sections were treated with 488-Alexa secondary antibody and nuclei were counterstained with Hoechst.

5.2.4 Hand2 and Sox9 proteins are expressed in a largely complementary manner

During limb bud development Sox9 marks pre-chondrogenic cells and is required for chondrocyte differentiation within the mesenchymal condensations that give rise to the primordia of the limb skeleton (Akiyama et al., 2002). In order to obtain a comprehensive view of the distribution of Hand2 positive cells in relation to the pre-chondrogenic mesenchymal cells, we performed an immunofluorescence analysis of E10 to E12.5 forelimb buds homozygous for the *Hand2*^{3xFLAG} allele. Interestingly, at E10, the forelimb bud appeared to be sub-divided into three similar-sized mesenchymal regions (Figure 11A). Whereas cells positive for nuclear Hand2 proteins populated the posterior mesenchyme, Sox9 positive cells were found to be restricted to a proximal anterior part. In addition, a third distal anterior domain was neither positive for Hand2 nor Sox9. However, only few cells co-expressed both Hand2 and Sox9 proteins. These cells were located at the border of the respective

expression domains. At E10.5, Sox9 positive cells were also detected within the central mesenchyme and a small population of cells with low levels of both Hand2 and Sox9 proteins was localized in the proximal-anterior mesenchyme (Figure 11B). At E11, the proximal area of condensing Sox9 positive cells was separated from a broader, more distally located domain of Sox9 expressing cells (Figure 11C). Interestingly, we detected low levels of Hand2 in a fraction of cells located in between these two domains. Furthermore, Hand2 positive cells were located in a proximal-anterior area abutting the proximal domain of Sox9 positive cells (Figure 11C). As already described (Figure 9L), Hand2 proteins were detected at high levels in a broad, elongated posterior domain along which the Hand2 and Sox9 proteins displayed inverse graded distribution. Taken together, cells positive for Hand2 and/or Sox9 formed largely complementary domains at these earlier stages.

At E11.5, the Hand2 and Sox9 protein expression domains displayed still largely complementary patterns (Figure 11D). However, cells co-expressing Hand2 and Sox9 proteins in the proximal-posterior autopod and posterior zeugopod were also apparent (Figure 11D). These regions of co-expression likely harbour the progenitors of the ulna, the carpals and the metacarpals (Zeller et al., 2009). Interestingly, Hand2 proteins were co-expressed in a fraction of Sox9 positive cells located within the forming condensations of the posterior autopod. In agreement with the *Hand2* transcript distribution (Charité et al., 2000), the distribution of Hand2 positive cells extended anteriorly within the distal autopod. Moreover, the proximal-anterior domain of Hand2 positive cells was enlarged and located adjacent to the Sox9 positive condensation of the prospective humerus. Last but not least, the highest levels of Hand2 proteins were detected in cells located in the proximal-posterior part of the outgrowing limb bud (Figure 11D).

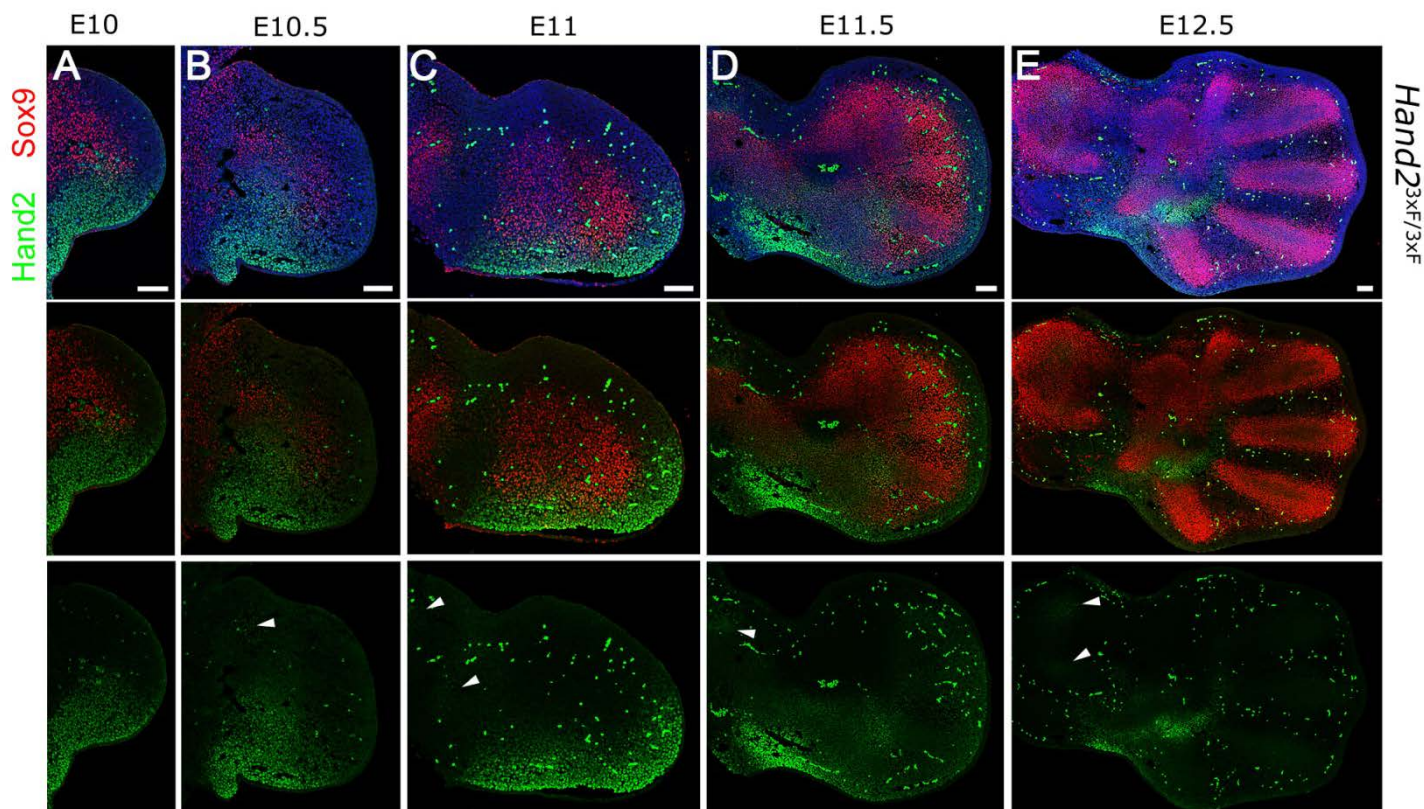


Figure 11. Co-localization of Hand2 and Sox9 proteins during limb bud development. (A-E) Immunolocalization using M2 anti-FLAG and anti-Sox9 antibodies uncovers the spatiotemporal distribution of endogenous Hand2^{3xFLAG} (green) and Sox9 (red) proteins in Hand2^{3xFLAG/3xFLAG} limb buds at E10 (A, 32 somites), E10.5 (B, 36 somites), E11 (C, 43 somites, same limb bud as shown in Figure 9L), E11.5 (D, 52 somites) and E12.5 (E). Arrowheads mark proximal-anterior Hand2 positive cell populations exhibiting lower Hand2 levels than the domain in the posterior. Nuclei (blue) were counterstained with Hoechst. Strong, green cytoplasmic signals in cells scattered across the whole limb bud represent autofluorescent blood cells. Limb buds are oriented with the anterior to the top. Scale bars, 100 μ m.

At E12.5, cells in the core of the mesenchymal condensations differentiate into prehypertrophic chondrocytes and Sox9 levels begin to decrease (Ng et al., 1997; Zhao et al., 1997). At this stage, cells expressing low levels of Hand2 were detected in the mesenchyme surrounding the condensations of the digit primordia and in the interdigital mesenchyme (Figure 11E). Regions with Hand2 positive nuclei were also detected in the proximal-posterior autopod, whereas the cells with highest levels of Hand2 were in general not expressing Sox9 (Figure 11E). Furthermore, a group of Hand2 positive cells was located along the anterior border of the epithelium within the proximal limb bud mesenchyme. Finally,

two domains of Hand2 positive cells were localized within the Sox9 positive humerus primorida (Figure 10E). In summary, this analysis reveals the predominantly complementary nature of the Hand2 and Sox9 protein distributions in the outgrowing limb bud. In addition, Hand2 appears to co-localize with Sox9 within a fraction of cells forming the stylopod condensations, which could reflect its role in chondrocyte maturation (Abe et al., 2009). In summary, we establish that the *Hand2*^{3xFLAG} allele provides novel molecular insights in limb development, by revealing context-dependent distribution of the endogenous Hand2 proteins at single cell resolution.

5.3 Identification of genome-wide target regions bound by Hand2

5.3.1 Refined mapping of Hand2 interaction with the ZRS by ChIP-qPCR

Immunoprecipitation (IP) represents an important prerequisite in light of further genome-wide applications such as ChIP-seq to identify Hand2 interacting sequences or mass spectrometry to analyze protein complexes. In order to establish the usefulness of endogenous Hand2^{3xFLAG} for such approaches, we performed IPs from lysates of embryonic tissues heterozygous for the *Hand2*^{3xFLAG} allele (Figure 12A). The M2 anti-FLAG antibody efficiently immunoprecipitated epitope-tagged Hand2 proteins from limb buds, hearts and branchial arches, but not from midbrain controls (Figure 12A). IP specifically enriched the Hand2 proteins without significant background. Therefore, the *Hand2*^{3xFLAG} allele represents a useful reagent for genome-wide applications to study the role of Hand2 in transcriptional regulation during embryogenesis.

As the *Hand2*^{3xFLAG} allele allowed specific recognition and IP of the endogenous epitope-tagged Hand2 protein, we performed chromatin immunoprecipitation (ChIP) analysis for identification of target sequences bound by Hand2 containing protein complexes. To date, the ZPA regulatory sequence (ZRS) is the only established cis-regulatory region interacting

with Hand2 transcriptional complexes in developing limb buds (Galli et al., 2010). However, specific Hand2 target sequences within the ZRS could not be identified in this previous analysis due to the insufficient specificity of the antibodies used. Interestingly, six Hand2 interacting *Ebox* hexanucleotides were found to reside within the ZRS (Galli et al., 2010; Figure 12B).

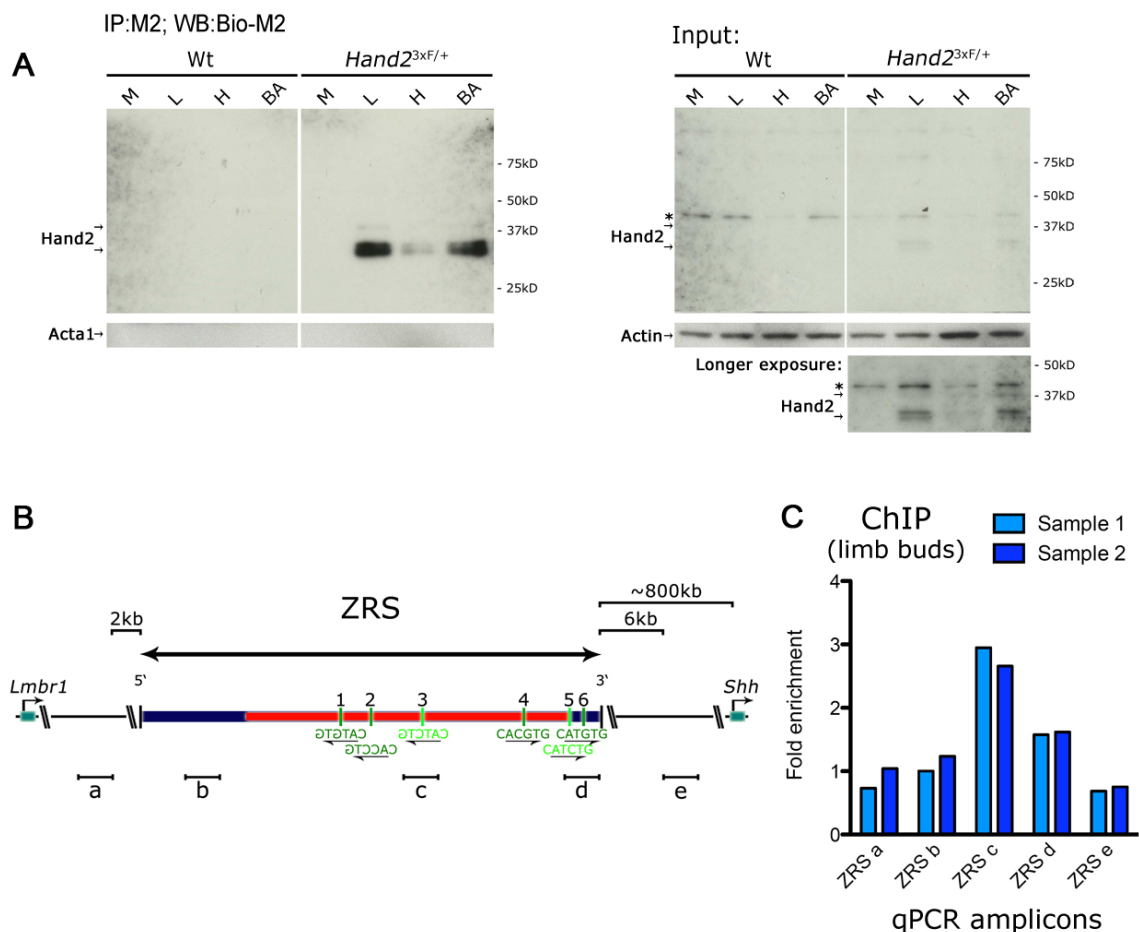


Figure 12. Chromatin immunoprecipitation (ChIP) using limb buds heterozygous for the *Hand2*^{3xFLAG} allele. **(A)** Immunoprecipitation (IP) of Hand2^{3xFLAG} proteins from lysates of midbrains (M, negative control), limb buds (L), hearts (H) or branchial arches (BA) isolated from *Hand2*^{3xFLAG/+} embryos at E10.5. 100µg of protein extracts were used for IP, 10µg were loaded as input control. The M2 anti-FLAG antibody was used for IP, whereas the biotinylated M2 anti-FLAG antibody (Bio-M2) was used for immunoblotting. Asterisk denotes M2 antibody-related background band. Anti-actin antibody was used for loading control. **(B)** Schematic illustration of the location of the mouse ZRS cis-regulatory element which regulates *Shh* expression in the limb bud (scheme adapted from Galli et al., 2010). The ZRS sequence (blue) is encoded within an intron of mouse *Lmbr1* and located ~800kb upstream of the *Shh* locus. The ZRS core element, termed MFCS1, is indicated in red. Potential Hand2 interacting *Ebox* consensus sequences (in green) are numbered "1" to "6". Amplicons (a-e) used for ChIP-qPCR are shown. Negative control amplicons "a" and "e" are located 2kb and 6kb away from the ZRS,

respectively. Amplicons “b”, “c” and “d” are located within the ZRS and used to examine its interaction with Hand2 (Galli et al., 2010). (C) ChIP-qPCR analysis shows specific enrichment of Hand2 proteins around amplicon “c” (two independent ChIP assays). Per sample, fresh (non-frozen) cross-linked chromatin was obtained from pooled limb buds of nine *Hand2*^{3xFLAG/+} or wild-type embryos at E11.75 (~54 somites). The M2 anti-FLAG antibody was used for ChIP. Columns represent fold enrichment compared to a wild-type control. ChIP values are normalized to input and a β -actin negative control region (see Material and Methods).

Therefore, we initially aimed to reproduce the interaction of endogenous Hand2^{3xFLAG} with the ZRS in limb buds. Limb buds of *Hand2*^{3xFLAG/+} and wild-type embryos at E11.75 were used for ChIP analysis. The use of wild-type limb bud tissues as negative control provides an excellent setup to exclude FLAG antibody-related background from ChIP analysis. qPCR analysis of these ChIP samples revealed the about 3 fold enrichment of amplicon “c” over wild-type controls in samples normalized for input and a negative control region (Figure 12C). Negative control amplicons “a” and “e” are located more distant from the ZRS and reflect the background, which might potentially be influenced by e.g. suboptimal sonication conditions (see Material and Methods). In summary, these results indicated that the Hand2 transcription factor interacts with sequences within or close to amplicon “c”, which encodes a high affinity Ebox motif within a region highly conserved in tetrapods.

Next-generation sequencing of ChIP-enriched DNA fragments (ChIP-seq) represents the state-of-the-art technology to assess the range of genome-wide DNA sequences bound by specific transcription factor complexes (Massie & Mills, 2008; Metzker et al., 2010). In addition to the need of excellent and highly specific antibodies, one particular obstacle for ChIP-seq of embryonic tissues is the requirement of large tissue amounts, typically around 1×10^7 cells (Massie & Mills, 2008). Therefore, only few reports describing ChIP-seq applications on embryonic tissues have been published. For example, ChIP-seq analysis of genome-wide targets of the p300 transcriptional co-activator in limb buds, midbrains and forebrains at E11.5 involved tissues collected from around 150 embryos (Visel et al., 2009).

As Hand2 proteins are expressed at high levels by E10.5 (Figure 10G, J), we decided to use forelimb buds, hearts and branchial arches of such embryos for ChIP-seq analysis. To have sufficient quantities for analysis, we pooled these collected tissues from both *Hand2*^{3xFLAG/+} and *Hand2*^{3xFLAG/3xFLAG} embryos (denoted as *Hand2*^{3xF}). As the selected tissues from one embryo at E10.5 yielded similar amounts of total protein as four limb buds at E11.5 (Figure 13C), we reasoned that collection of around 150 embryos should yield sufficient tissue quantities for *Hand2*^{3xF} ChIP-seq analysis. Albeit the fact that Hand2 is a tissue-specific transcription factor, which is likely expressed at overall lower levels than a global transcriptional co-regulator such as p300, we decided to adapt the ChIP-seq approach used by Visel and colleagues for our purposes (see Material and Methods). In particular, we modified the method to efficiently disaggregate cells from embryonic tissues expressing *Hand2*^{3xF} before formaldehyde crosslinking of protein-DNA complexes (Orlando et al., 1997). Temporally controlled formaldehyde crosslinking is important, as prolonged duration can lead to crosslinking of non-related DNA elements and proteins (Massie & Mills, 2008). A tissue grinder was used to disaggregate cells from collected tissues and to prepare nuclei, which largely maintained the morphological integrity (Figure 13A). Concentrated nuclei were used for immunoprecipitation which revealed that the endogenous *Hand2*^{3xFLAG} proteins were detected on Western blots at higher concentrations than without disaggregation (Figure 13B). Importantly, silver staining of all proteins revealed the absence of major non-specific proteins in the IP sample in comparison to the input. However, the immunoprecipitated *Hand2*^{3xFLAG} proteins were not concentrated enough to be detected by silver stain (Figure 13C). In a next step, we performed ChIP-qPCR to validate the feasibility of detecting the interaction of Hand2 with the ZRS in the extracts defined for ChIP-seq. It is important to note that the limb bud mesenchymal cells in which Hand2 interacts with the ZRS are diluted in the extracts prepared from pooled tissues. For ChIP we processed cross-linked chromatin from 100 embryos of wild-type (wt) and *H2*^{3xF} collections each. Indeed, the test qPCR analysis revealed the Hand2-ZRS interaction, represented by a more than five fold enrichment of

amplicon “c” which contains a *bona fide* Hand2 *Ebox* (Figure 13D; compare to Figure 12B and 12C; Galli et al., 2010).

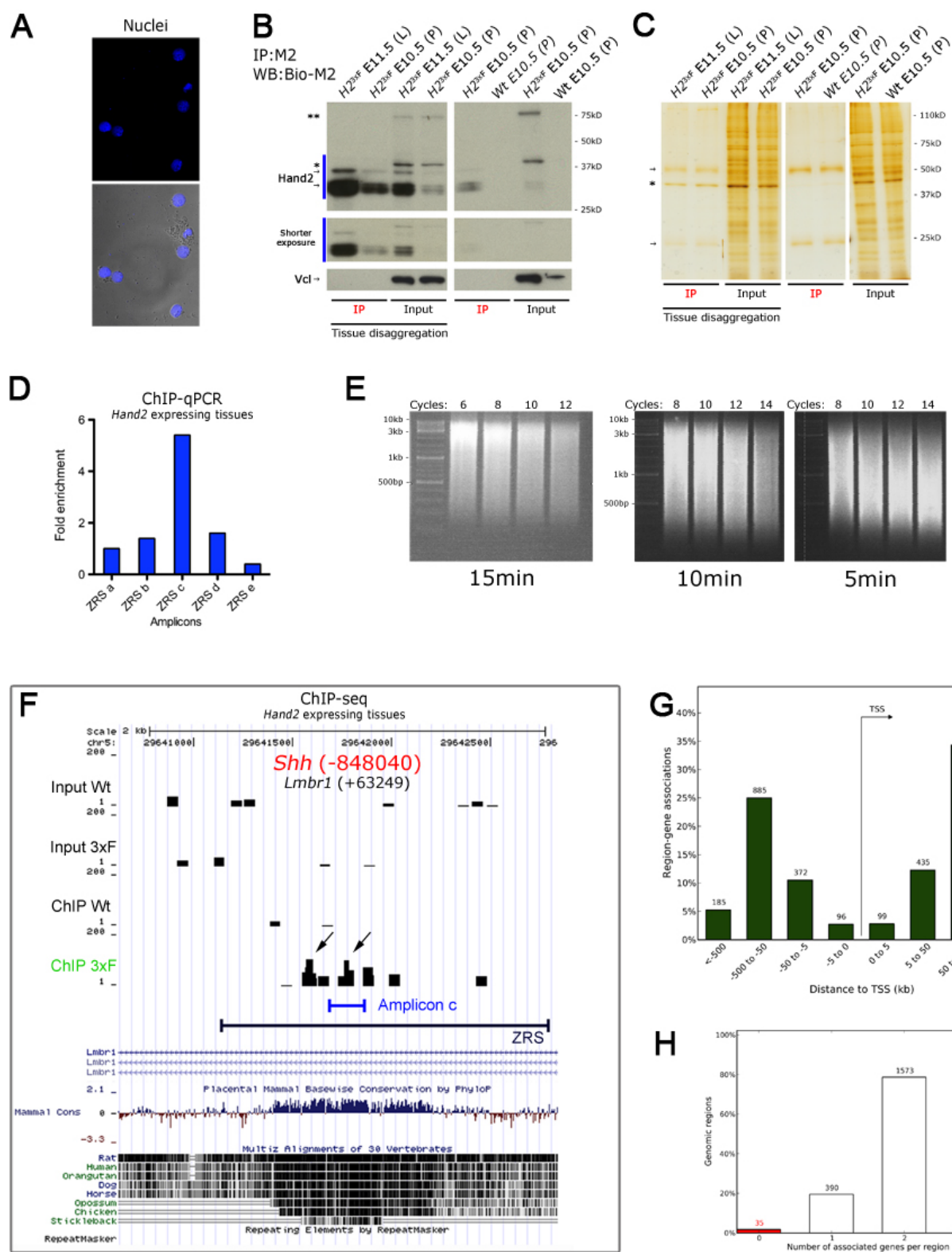


Figure 13. ChIP-seq set-up using the *Hand2*^{3xFLAG} allele to identify genome-wide DNA target sequences interacting with endogenous Hand2 proteins in limb buds, hearts and branchial arches at E10.5. **(A)** Confocal microscopy reveals the morphological integrity of nuclei extracts prepared by tissue homogenization. **(B)** Immunoprecipitation (IP, using M2 anti-FLAG antibody) of Hand2^{3xFLAG} proteins from isolated nuclei or total tissue extracts reveals that the nuclei preparation allows a very efficient concentration of the protein of interest. 200 μ g of total proteins were used for IP and 90% were loaded on the poly-acrylamide gel. 10 times less of sample was used for input lanes. Vinculin (Vcl) was detected as loading control. L, pooled limb buds. P, pools including limb buds, hearts and branchial arches. Asterisks indicate occasional background bands. **(C)** A silver-stained gel illustrates the specificity of the IP as largely no background proteins are pulled down. Amounts loaded corresponded to 10% of IP and input samples used for Western blot (shown in B). Arrows denote IgG heavy chain (50kD) and light chain (25kD) of the monoclonal M2 anti-FLAG antibody used for IP. Asterisk indicates the background band also observed in the immunoblot. **(D)** ChIP-qPCR using large amounts of tissue confirms the feasibility of the planned ChIP-seq approach. Pools of limb buds, hearts and branchial arches from around 100 embryos were processed for ChIP. qPCR reveals more than 5 fold enrichment of the ZRS amplicon “c” in the *Hand2*^{3xF} sample (compare to Figure 12B, C). ChIP was performed using the M2 anti-FLAG antibody. Columns display fold enrichment compared to wild-type control values. The values are normalized to input and a β -actin negative control region (see Material and Methods). **(E)** Test to define optimal sonication and cross-linking conditions for ChIP-seq. Large embryonic tissue quantities were cross-linked for 5, 10 or 15 minutes and used for ChIP-based preparation of chromatin samples (see Material and Methods). Shearing of DNA was performed using a Branson sonicator. **(F)** UCSC browser window depicting the ZRS region in ChIP-seq datasets. Enrichment (in wiggle track format) is observed in the ChIP sample of *Hand2*^{3xF} (3xF) embryos. Wild-type ChIP and input samples are shown as controls. Note that in this particular case the saturation is very low and thus the enrichments were not recognized to be significant. This is due to the low amount of ZPA cells in the total preparation of pooled tissues. The distance of peaks in regulatory domains of nearest genes is shown relative to the transcriptional start site. According information about the ChIP-seq and graphic representations shown can be obtained in the legend to Figure 14. **(G, H)** Region/gene association graphs of the top 2000 regions identified by ChIP-seq analysis (as determined by the GREAT algorithm). The distance of peaks in regulatory domains of nearest genes is shown relative to the transcriptional start site **(G)**; the number of genes associated with a given peak is also shown **(H)**.

Taken together, ChIP-qPCR indicated that our ChIP-seq approach was feasible and showed that endogenous Hand2^{3xFLAG} proteins in a diluted subset of cells display sufficient specificity and sensitivity for the detection of interactions with genomic DNA fragments. To be able to process a ChIP sample for next-generation sequencing, the DNA concentration must be at

least between 2 and 10ng. Indeed, determination of the DNA concentration revealed that about 7ng (in the *H2*^{3xF} sample) of DNA were recovered, which is sufficient for ChIP-seq. Furthermore, the library preparation for Illumina deep sequencing includes size selection of DNA fragments in a range of 200-250bp. Thus, we performed sonication tests including large amounts of chromatin from embryonic tissues to define the optimal crosslinking period of extracted nuclei (Figure 13E). We found that chromatin crosslinked for 5 minutes and sonicated applying 14 cycles (Branson) resulted in sufficient genomic DNA fragmentation as the peak of sheared DNA fragments ranged from 200bp to 1kb (Figure 13E). In contrast, chromatin crosslinked for 10 or 15 minutes could not be sufficiently sheared using equal sonication conditions (Figure 13E).

5.3.2 Genome-scale identification of Hand2 target regions in the mouse embryo using a ChIP-seq approach

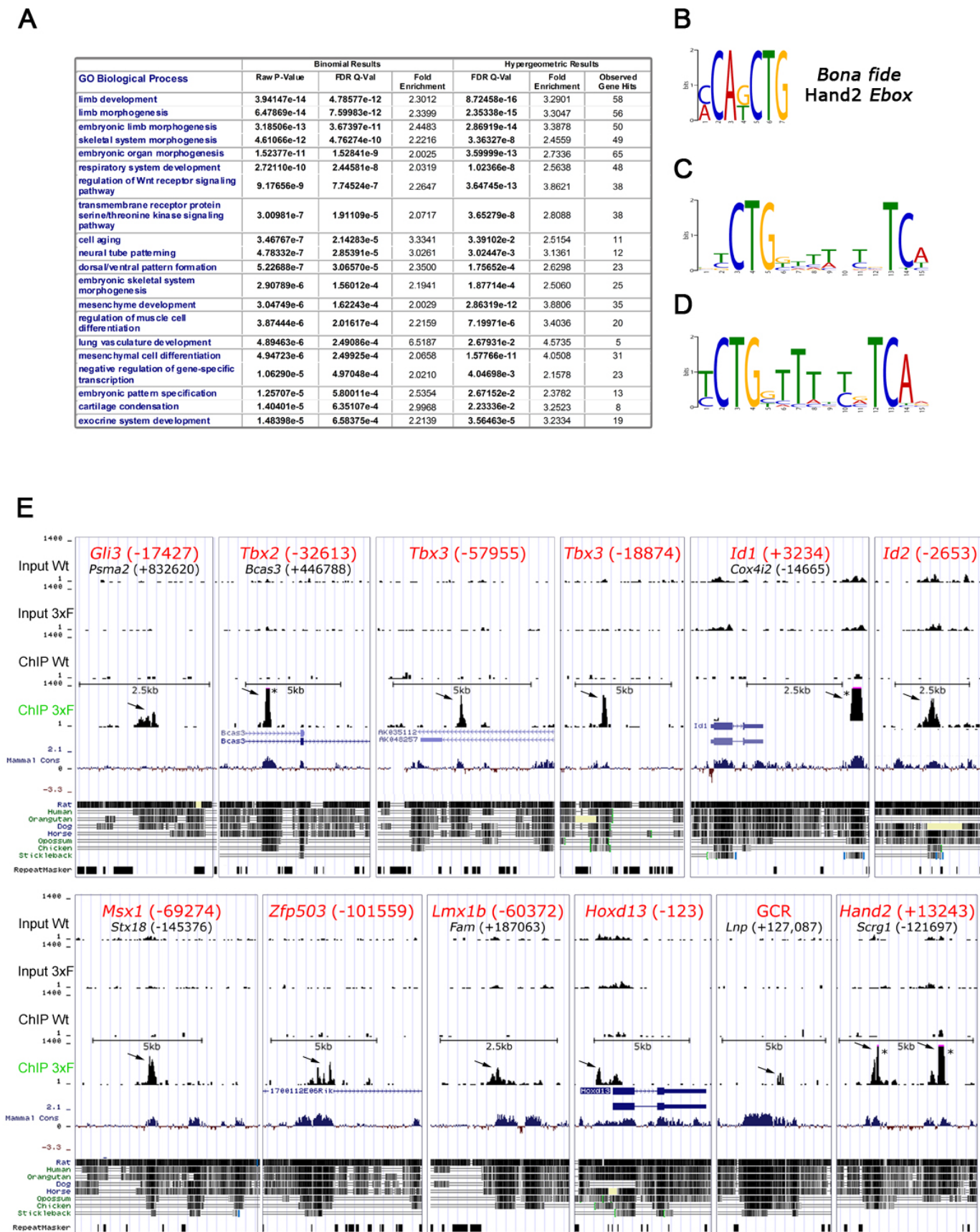
Given that all the necessary conditions were met, we performed ChIP followed by next-generation sequencing (ChIP-seq) using tissues (limb buds, heart, branchial arches) from approximately 150 embryos to compare *Hand2*^{3xF} with wild-type controls at E10.5. ChIP yielded around 20ng of DNA in the *Hand2*^{3xF} (3xF) sample and 6ng of DNA in the wild-type (wt) control sample. As these quantities surpassed the minimal criteria, DNA fragments could be processed for library generation and were sequenced using an Illumina Genome Analyzer. The resulting sequence tags were mapped to the reference mouse genome (UCSC mm9, Jul/2007) and read alignments (tag-to-position information) were transformed into genomic density maps (count-per-position information) by the generation of WIG files (Rhead et al., 2010; Leleu et al., 2010). After the verification of potential enrichment visualized in the UCSC browser, input samples of both conditions were also sequenced. Sequencing of the input controls is essential to confirm that the observed signal enrichment represents transcription factor binding and is not due to biases in the experimental and computational procedures (Rozowsky et al., 2009). We used MACS (Model-based Analysis of ChIP-seq data) for robust peak prediction in sequenced samples to achieve a high spatial

resolution (Zhang et al., 2008b). Furthermore, MACS removes noise in the resulting peaks as it captures local biases due to amplification of ChIP-DNA or library preparation. MACS computes a robust false discovery rate (FDR) in relation to the numbers of peaks from control over ChIP data, which were identified at identical p -value cut-offs (Zhang et al., 2008b). MACS recognized around 56'700 regions in *Hand2*^{3xFLAG} and 65'000 regions in wild-type control ChIP samples with enriched tags in comparison to input values. However, the vast majority of these peaks exhibited low numbers of tag counts which often arise due to regional noise. Such noise occurs due to sequencing and mapping biases or variations in chromatin structure (Redon et al., 2006; Zhang et al., 2008b). Another issue is the extent of saturation. If the overall saturation is high and all peaks are assessed, also peaks with minimal enrichment may reach significance (Park 2009). Indeed, a multitude of minimally enriched peaks are shared between control and ChIP sample and thus overall peak counts are known to be similar between control and ChIP datasets (Leleu et al., 2010). However, a major additional advantage of utilizing epitope-tagged proteins for ChIP-seq is the inclusion of a wild-type control sample, which was treated in an identical manner to allow the identification of antibody-related false hits. By filtering regions significantly enriched in *Hand2*^{3xFLAG} over wild-type control ChIP and input samples, we were able to define a set of around 24'000 candidate Hand2 DNA binding regions. However, a certain number of these sequences are likely false positives, as repetitive or low-complexity regions may generate peaks with no shift in between strands (Leleu et al., 2010). To obtain a more significant dataset, we limited the analysis to the 2000 MACS validated regions with highest enrichment over wild-type controls (top 2000). We used the USCS browser to view the enriched regions in their genomic context (Rhead et al., 2010). Initially, we analyzed the ZRS for Hand2 interactions as this had served as a positive control in setting up ChIP-seq. The conserved ZRS region contained no elements with sufficient enrichment, as determined by MACS. However, two adjacent small peaks were apparent in the ZRS, in particular one mapping to amplicon "c" (Figure 13F). In support of our previous analysis by ChIP-qPCR (Figure 13D), this reveals that an element within amplicon "c" is bound by endogenous Hand2

transcriptional complexes. The low saturation of these peaks might be related to the small number of cells in which Hand2 binds to the ZRS, in comparison to the significantly larger populations analyzed. In a next step, we used GREAT (Genomic Regions Enrichment of Annotations Tool, McLean et al., 2010) to validate the functional significance of the top 2000 enriched regions based on the distribution and proximity to loci annotated to different functional classes defined in gene ontology (GO) terms (Ashburner et al., 2000). GREAT specifies a “regulatory domain” consisting of a “basal” and an “extension” domain (up to 1Mb) for each gene (McLean et al., 2010). Thereby, a given genomic region is associated with genes in whose “regulatory domains” it is located. To eliminate biases due to variable sizes of the gene regulatory domains and association of a large set of genomic regions with a restricted number of genes, GREAT combines a binomial test of the genomic regions with a hypergeometric test of the genes (McLean et al., 2010). GREAT analysis showed that the top 2000 enriched sites mapped most frequently between 50kb and 500kb upstream or downstream of transcriptional start sites (Figure 13G) and most regions were associated with two genes (Figure 13H). Furthermore, GREAT associated the coordinates of putative Hand2 target elements with significantly enriched GO terms “limb development” and “organ morphogenesis” (Figure 14A). In contrast, feeding GREAT with the top 2000 assumed hits in the wild-type control dataset failed to reveal any significant enrichment. This analysis showed that the set of potential Hand2 target regions identified by ChIP-seq was functionally significant and mostly consisted of cis-regulatory elements.

Discovery of the enriched DNA motifs bound specifically by the transcription factor of interest may verify the functional significance of the ChIP-seq approach. Thus, we further processed putative peak regions for motif discovery with MEME-ChIP (Machanick & Bailey, 2011). MEME-ChIP is based on the MEME algorithm (Bailey et al., 2006) and allows processing of large datasets in contrast to other web-based tools. Furthermore, MEME-ChIP is complemented by the DREME algorithm (Bailey et al., 2011) which defines short binding motifs often not identified by using only MEME algorithm. MEME or DREME identified enriched motifs can then be interrogated further for similarity with known motifs in databases

using the TOMTOM algorithm (Gupta et al., 2007). Remarkably, processing the top 2000 Hand2^{3xF} enriched regions, the *bona fide Ebox* previously defined *in vitro* (Dai & Cserjesi, 2002) was identified by DREME as one of the most significant motifs (7th position; Figure 14B). However, use of the MEME-ChIP web-interface for analysis was limited as the peak sequences were centered and trimmed to 100bp prior to motif analysis (Machanick & Bailey, 2011). As some of the identified cis-regulatory elements encoded more than 100bp or displayed a double peak, important additional Hand2 binding motifs might be missed. The most significant motif found by analysis of the same set using the MEME algorithm is shown in Figure 14C. However, the TOMTOM algorithm failed to identify significant similarities of this novel putative Hand2 binding motif to motifs in transcription factor databases. Subsequent manual screening of the top 1000 peak sequences excluded all peaks containing a significant number of repeated elements and low complexity sequences as identified by the RepeatMasker in the UCSC browser. This resulted in a reliable set of 795 putative Hand2 target regions ordered according to enrichment scores (see Appendix Table 1). Analyzing this collection of peaks with MEME yielded a putative Hand2 binding motif very similar to the one obtained by analyzing the top 2000 peaks (Figure 14D). On the other hand, DREME failed to discover the *bona fide Ebox* consensus in this smaller curated dataset. In a next step, GREAT associated this curated dataset with GO terms such as negative regulation (including members of the *Tbx*, *Id* and *Gli* gene families), embryonic morphogenesis and limb development (Appendix Table 2 and Table 3).



identifies primarily genes associated with limb development or embryonic morphogenesis. Top 20 gene ontology (GO) terms at a false discovery rate of 0.05 are shown (with ≥ 2 fold-enrichment and significant according the hypergeometric test, McLean et al., 2010). **(B)** Motif analysis using the DREME algorithm identifies enrichment of the *bona fide* Hand2 Ebox consensus (7th rank) in the dataset including the top 2000 peaks. **(C, D)** Analysis of the top 2000 regions by MEME (C) reveals a novel putative Hand2 binding motif that was also confirmed using the curated dataset (top 795 regions; D). **(E)** Selected candidate Hand2 target regions associated with genes with known functions in limb development. ChIP-seq results are presented in the UCSC browser (www.genome.ucsc.edu) in WIG format. Significant (MACS validated) enrichments appear as peaks (arrows). Asterisks mark truncated peaks (higher than the scale used). Datasets including ChIP and input samples from *Hand2*^{3xFLAG} (3xF) and wild-type (wt) control tissues are also shown. Genes with closest association to the peak are indicated and the distance to the transcriptional start site (in base pairs) is displayed in brackets. The gene with closest association to the target region is marked red. Evolutionary conservation score displaying the placental mammal basewise identity is presented as a conservation histogram (wiggle format). Pairwise alignments of selected species are shown as a grayscale density plot (darker values indicate higher levels of sequence conservation). The UCSC browser utilizes RepeatMasker to indicate interspersed repeats and DNA elements of low complexity (black bars).

We used the USCS genome browser to visualize maps of selected peaks (with specific enrichment) that indicate binding of the Hand2^{3xFLAG} protein to cis-regulatory elements of genes expressed in the developing limb buds (Figure 14E). Notably, a fraction of the most prominent peaks shows also slight enrichment in the input controls. This phenomenon has been observed previously and likely reflects the heterogeneous nature of chromatin (Rozowsky et al., 2009). Differences in chromatin structure can inflict a bias on experimental accessibility. Our analysis revealed non-specific low level enrichment often associated with gene promoters or coding regions. Indeed, such signals seem to be related to open chromatin which is a hallmark of transcriptionally active loci (Rozowsky et al., 2009). Therefore, it is important to note that the final distribution of aligned fragments in the signal maps represents not only specific Hand2 interactions but also bystander effects such as heterogeneous chromatin structure and the density of bases in a defined region (Rozowsky et al., 2009). However, the majority of all top 2000 putative Hand2 target peaks were significantly higher than any of the signals observed in the input and wild-type control samples.

Interestingly, genome-wide identification of candidate *Hand2* target regions in E10.5 embryonic tissues including the limb buds, the heart and the branchial arches identified a significant number of peaks associated with genes required for limb bud development. Often these peaks mapped to conserved non-coding regions (Figure 14E) which indicates high probability of encoding functionally relevant cis-regulatory regions (Wittkopp & Kalay, 2012). Most interestingly, we identified a single peak upstream of the *Gli3* coding region (Figure 14E) which encodes a key mediator of Shh signalling. During early limb bud development, *Hand2* and *Gli3* have been shown to interact in a mutual antagonistic manner (Te Welscher et al., 2002a). The corresponding genomic element is conserved to some extent in euarchontoglires and contains two *Ebox* sequences matching *Hand2* specific motifs defined by *in vitro* studies (CATGTG, CACCTG; Dai & Cserjesi 2002). However, this was the only peak (among the top 2000 regions) significantly enriched within the *Gli3* genomic landscape. Other interesting hits were associated specifically with genes of the *Tbx2* subfamily (*Tbx2-Tbx5*) which are all expressed from early stages onward during limb bud development (Figure 14E). Members of the *Tbx2* subfamily arose by duplication generating the *Tbx2/Tbx4* and *Tbx3/Tbx5* gene clusters (Agulnik et al., 1996). Therefore, similarities in cis-regulatory elements that control the expression of the *Tbx2/Tbx3* or *Tbx4/Tbx5* genes might have been retained. Indeed, *Tbx2* and *Tbx3* display similar spatiotemporal expression patterns with predominant posterior and anterior domains in both fore- and hindlimb buds at E10.5 and E11.5 (Gibson-Brown et al., 1996). Furthermore, we showed that early posterior *Tbx2* and *Tbx3* expression is disrupted in forelimb buds lacking *Hand2* which suggested that their expression could be directly regulated by *Hand2* in a *Shh*-independent manner (Galli et al., 2010). Strikingly, among the top 795 candidate regions obtained by ChIP-seq (see Appendix Table 1) we identified four conserved peaks directly associated with *Tbx2* (-32'613bp, -95085bp, -111969bp, -203850bp). The peak closest to the *Tbx2* transcriptional start site (TSS) is shown in Figure 14E and maps to a highly conserved region in the *Bcas3* intronic region. Moreover, analysis of the top 795 regions revealed two conserved putative cis-regulatory elements upstream of the *Tbx3* TSS (-18874bp, -57955bp) which are shown in

Figure 14E. Interestingly we also observed robust and conserved peaks in proximity to *Tbx4* (-13770bp (see Figure 15), +20326bp) and *Tbx5* (-37965bp) transcriptional start sites. Taken together, our ChIP-seq results suggest that *Hand2* might directly regulate aspects of the tissue-specific expression of *Tbx2* subfamily members.

We further identified highly enriched conserved elements in regions close to the transcriptional start sites of *Id1* (-6634bp, -1065bp, +3253bp) and *Id2* (-2653bp) (Figure 14E). Inhibitor of differentiation (*Id*) genes are targets of Bmp signalling and encode helix-loop-helix proteins which lack a DNA binding domain and negatively regulate bHLH factors (Miyazono & Miyazawa, 2002). *Id1* and *Id2* transcripts are likely co-expressed with *Hand2* in the posterior limb bud mesenchyme (Gray et al., Science 2004). Interestingly, we further discovered a prominent peak in an element located 69kb upstream of the Bmp target *Msx1* (Figure 13E). The core region of this element is highly conserved among tetrapods. *Msx1* is expressed by neural crest derived cells in the mandibular arch and in the limb bud mesenchyme. In the limb buds *Msx1* transcripts seem to overlap significantly with cells positive for *Hand2* proteins (Davidson et al., 1991). However, *Msx1* expression is maintained in *Hand2* deficient mandibular arch mesenchyme (Barron et al., 2011). We also identified peaks associated with other genes related to the Bmp signalling pathway (see Appendix), but these were quite distant from the transcriptional start sites.

Among the top 795 peaks we identified an uncommonly large number of enrichments associated with the *Zfp503* locus (-58598bp, -59366bp, -79769bp, +85683bp, -101559bp, 178740bp), whereas only the peak with highest enrichment is shown in Figure 14E. *Zfp503* is expressed by a broad variety of embryonic tissues including limb bud and distal branchial arch mesenchyme (McGlinn et al., 2008). Indeed, the *Hand2* protein domain (Figure 11C, D) likely overlaps with *Zfp503* expression in the posterior limb bud mesenchyme (McGlinn et al., 2008), which would agree with the potential direct regulation of *Zfp503* expression by *Hand2*. Significant enrichments at conserved elements located up- (-60372bp) and downstream (+96173bp) of the *Lmx1b* TSS were also detected. This is interesting as the LIM homeodomain transcription factor *Lmx1b* is a central player in dorso-ventral limb bud

patterning by integrating Wnt7a signalling from the dorsal ectoderm (Riddle et al., 1995). *Lmx1b* is expressed in the dorsal half of the limb bud mesenchyme and determines dorsal cell fates (Chen et al., 1998, Dreyer et al., 1998). In particular, *Lmx1b* expression might overlap with the Hand2 protein distribution in the dorsal-posterior limb bud mesenchyme.

Interestingly, we also observed enrichment at the proximal promoter of *Hoxd13* (Figure 14E) which participates in the initial polarization of the early limb bud and interacts together with Hand2 and with the ZRS during activation of *Shh* expression (Tarchini et al., 2006; Capellini et al., 2006; Galli et al., 2010). In any case, this peak represented the only significant enrichment observed in proximal association with the 5'*Hoxa* and 5'*Hoxd* clusters, which are required for limb bud development. In addition, a significantly enriched genomic element within the CsB enhancer in the 5'*Hoxd* global control region (GCR) was also identified (Figure 13E; Gonzalez et al., 2007). Therefore, Hand2 proteins might be involved in the regulation of 5'*Hoxd* genes during limb bud development.

Last but not least, we observed major enrichment of two characteristic peaks downstream of the Hand2 locus which mapped to sites of high conservation (+10990bp, +13243bp; Figure 14E). Strikingly, the higher peak mapped precisely to a region identified as a limb specific *Hand2* silencer element which is directly regulated by Gli3R repressor (Vokes et al., 2008). This indicates that Hand2 might directly regulate its own expression as part of a positive auto-regulatory loop.

Taken together, ChIP-seq analysis using *Hand2*^{3xFLAG} expressing embryonic tissues yielded an impressive collection of putative Hand2 binding sequences at high resolution. The identified potential cis-regulatory elements are often highly conserved and associated with genes required for limb bud development or embryonic development in general.

5.3.3 Hand2 regulates femur development and interacts with a *Tbx4* hindlimb enhancer

Hand2 ChIP-seq further revealed two significant peaks associated with the *Tbx4* locus (13kb upstream / 20kb downstream) and mapping to conserved elements. The T-box transcription

factor *Tbx4* is required for hindlimb bud development and expressed in a limb-type specific manner (Chapman et al., 1996; Gibson-Brown et al., 1996; Naiche et al., 2005). Recently, a large scale enhancer analysis of the *Tbx4* locus uncovered two cis-regulatory elements which control reporter gene expression in the hindlimb bud mesenchyme in an area similar to the *Tbx4* domain (Menke et al., 2008). In particular, the upstream *Tbx4* peak we discovered by ChIP-seq (Figure 15A) co-localizes with one of these two enhancers termed hindlimb enhancer A (HLEA). HLEA encodes five Hand2 consensus *Ebox* elements as defined *in vitro* (Dai & Cserjesi 2002). Therefore, we investigated the impact of reducing *Hand2* expression in the proximal part of the hindlimb mesenchyme. To this aim, we used the novel *Hoxa13^{Cre}* knock-in allele (Lopez-Rios et al., 2012), which drives Cre-mediated recombination in the distal part of the forelimb bud starting at around E10.75 and within the entire hindlimb mesenchyme from around E10.0 onwards. Using the *Hoxa13^{Cre}* allele, we generated *Hand2^{p/Δ}*, *Hoxa13^{Cre/+}* (*Hand2^{Δ/ΔA13}*) conditional mutant embryos. RNA *in situ* hybridisation was used to reveal the clearing of *Hand2* transcripts in *Hand2^{Δ/ΔA13}* mutant limb buds from E10.75 onwards (Figure 15B, C). In order to exclude molecular variations due to heterozygosity for *Hoxa13* we used *Hand2^{p/+}*, *Hoxa13^{Cre/+}* (*Hand2^{ΔA13/+}*) limb buds as controls which showed no differences in *Hand2* expression in comparison to wild-type (*Hand2^{p/+}*) limb buds. *Hand2* transcripts had cleared from a small distal-posterior domain following the activation of the *Hoxa13* locus in forelimb buds at E10.75 (Figure 15B). By E11.0 *Hand2* transcripts progressively cleared from the distal mesenchyme, whereas expression remained in the central mesenchyme (Figure 15B) By E11.5 *Hand2* expression was lost from the distal prospective autopod territory, while proximal and central expression remained (Figure 15B). Therefore, *Hand2* transcripts were not cleared in the most prominent Hand2 protein domains observed in corresponding forelimb buds (Figure 11D). In contrast, we detected drastic reduction of *Hand2* transcripts from E10.75 onwards in *Hand2^{Δ/ΔA13}* hindlimb buds. *Hand2* transcript persisted only in the posterior margin of the limb bud (Figure 15C). By E11.5 weak *Hand2* expression persisted in the anterior and posterior proximal mesenchyme (Figure 15C). Taken together, the *Hoxa13^{Cre}* allele allows the analysis of *Hand2* deficient autopod

primordia in forelimb buds in direct comparison to hindlimb buds with drastically reduced *Hand2* expression.

We next analyzed the phenotypical consequences caused by the defined spatio-temporal reduction of *Hand2* transcripts in fore- and hindlimb buds by skeletal staining at E16.5 (Figure 15B, C). *Hand2*^{Δ/ΔA13} mutant forelimbs appeared morphologically normal with the exception of small variations in the carpal bones (Figure 15D). This agrees with earlier conclusions that *Hand2* is essential during initiation of limb bud development (Galli et al., 2010). Interestingly, in *Hand2*^{Δ/ΔA13} mutant hindlimbs the femurs were between 15 and 25% shorter than in control hindlimbs (Figure 15E). Notably, the lower hindlimb elements of E16.5 *Hand2*^{Δ/ΔA13} embryos were abnormally oriented relative to the femur. This was a potential secondary effect caused by the defective morphology or alignment of the developing condyles of the femur (Figure 15E). Similarly, *Tbx4::PrxCre* mutant hindlimbs express low levels of *Tbx4* transcripts and are characterised by hypoplastic femurs and abnormally turned hindlimbs (Naiche & Papaioannou 2007). As *Hand2* expression was almost normal in limb-specific *Tbx4* mutants, this observation is in agreement with the proposal that *Hand2* acts upstream of *Tbx4*. Furthermore, we observed fusion of the proximal tarsal bones, disorganization of distal tarsal elements and variable effects on digit morphology and numbers (4-5 digits) in *Hand2*^{Δ/ΔA13} hindlimbs (Figure 15E), similar to *Hand2::PrxCre* conditional mutant hindlimbs (Galli et al., 2010). These more distal defects are likely a consequence of reduced *Shh* expression, as such phenotypes are also observed in hindlimbs with temporally delayed deletion of *Shh* (Zhu et al., 2008).

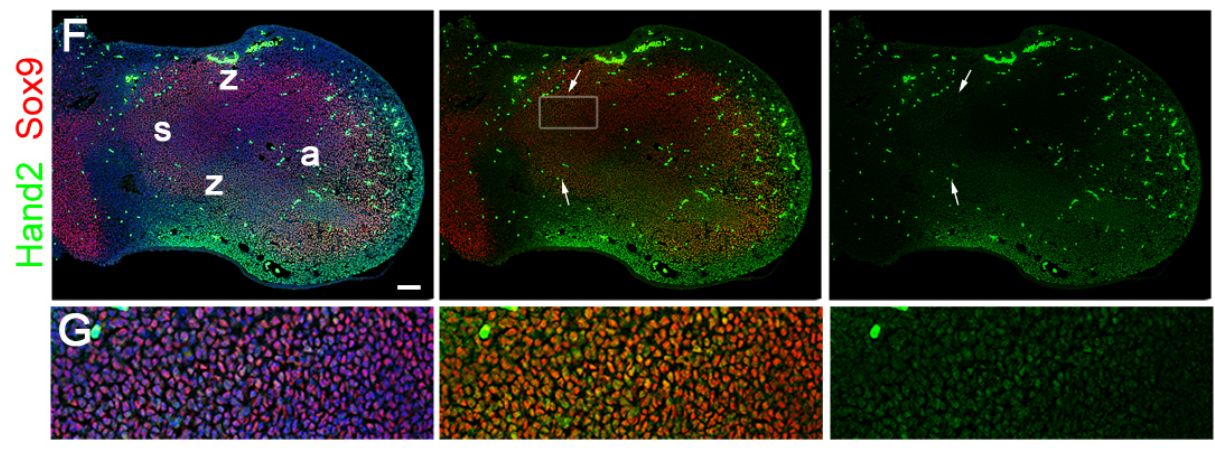
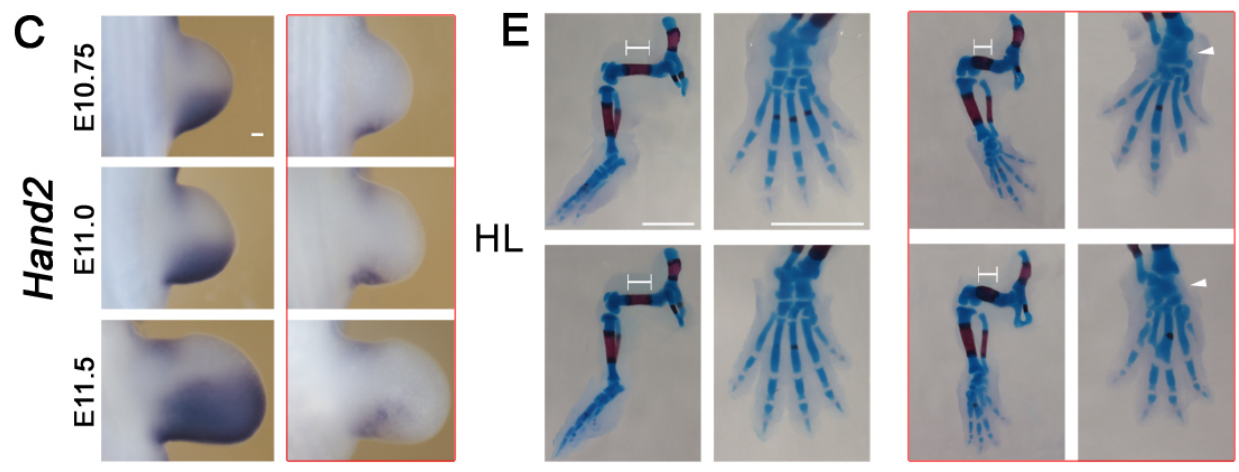
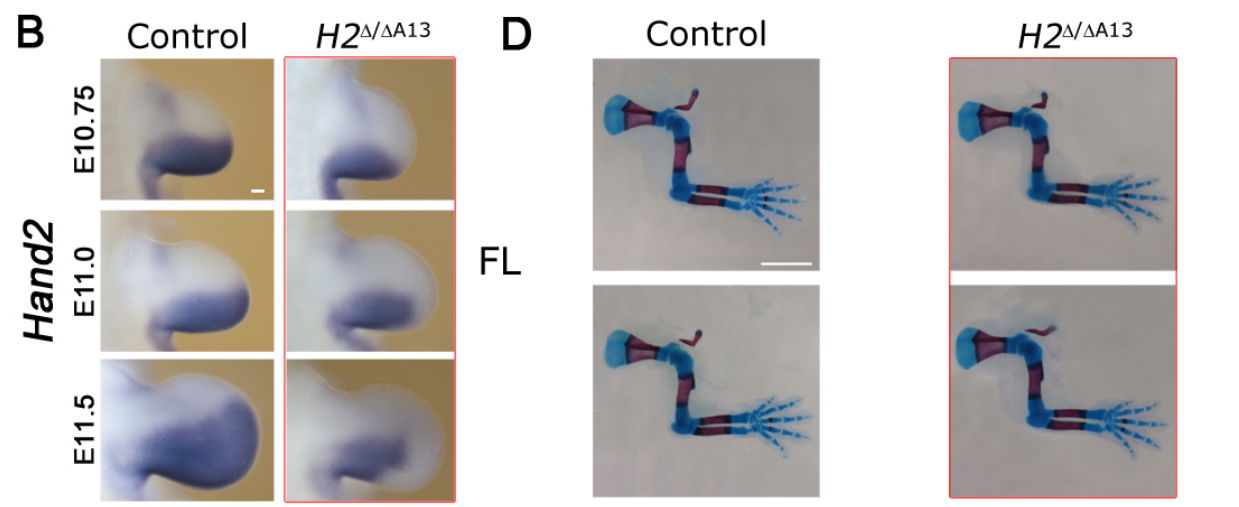
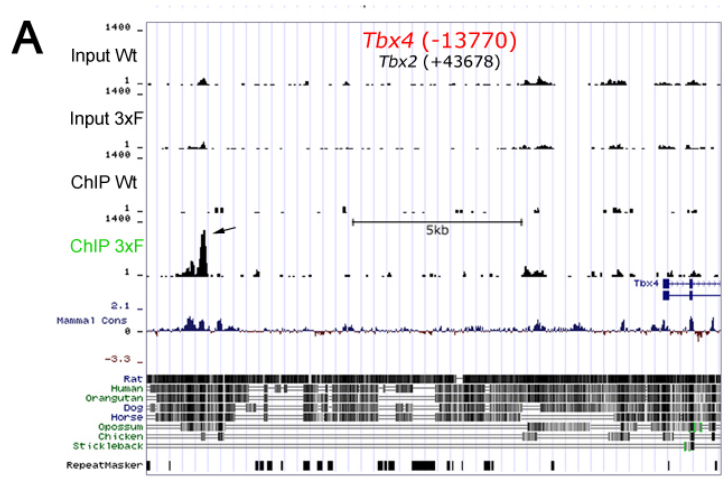


Figure 15. *Hand2* interacts with a previously described *Tbx4* limb-enhancer and contributes to correct morphogenesis of proximal hindlimb structures. **(A)** The ChIP-seq dataset reveals interaction of *Hand2* with the *Tbx4* hindlimb enhancer (HLEA; Menke et al., 2008) around 13.7kb upstream of the *Tbx4* transcriptional start site. Arrow denotes the significantly enriched peak. Information about the ChIP-seq and the graphical features is provided in Figure 14. **(B, C)** Detection of *Hand2* transcripts in *Hand2*^{ΔA13/+} control and conditional *Hand2*^{Δ/ΔA13} (framed in red) limb buds using whole mount *in situ* hybridization. A timecourse at E10.75 (39 somites), E11.0 (42 somites) and E11.5 (50 somites) forelimb **(B)** and hindlimb **(C)** buds reveals efficient clearance of *Hand2* transcripts due to the activity of *Hoxa13*-Cre. Scale bars, 100μm. **(D, E)** Skeletal staining of mouse forelimbs **(D)** and hindlimbs **(E)** at E16.5 using alcian blue (cartilage) and alizarin red (bone). *Hoxa13*^{Cre} mediated inactivation of *Hand2* (*Hand2*^{Δ/ΔA13}) displays no obvious phenotypes in the forelimb bud. In the hindlimb bud various defects are observed. Representative *Hand2*^{p/+} (top) and *Hand2*^{ΔA13/+} (bottom) control fore- and hindlimbs are shown. Mutant *Hand2*^{Δ/ΔA13} fore- and hindlimbs from two different embryos are shown (framed in red) to illustrate the hindlimb-specific defects **(E)**. Brackets indicate the mineralized region in the femur, which is shortened in *Hand2*^{Δ/ΔA13} limbs relative to control limbs. Arrowheads indicate fused proximal tarsal bones observed in *Hand2*^{Δ/ΔA13} limbs. Scale bars, 2mm. **(F)** Fluorescent immunolocalization of endogenous *Hand2*^{3xFLAG} (green) and Sox9 (red) proteins in *Hand2*^{3xFLAG/3xFLAG} hindlimb buds at E11.25 (54 somites). Note the large population of cells co-expressing *Hand2* and Sox9 proteins in the presumptive stylopod domain (arrows and enlarged region shown in **G**). s, forming stylopod condensation. z, presumptive zeugopod elements. a, autopod domain. Nuclei were counterstained with Hoechst (blue). Strong and scattered cytoplasmic signals (appear in green) correspond to autofluorescent blood cells. Scale bars, 100μm. In all panels limb buds are located with the anterior to the top.

Finally, the distribution of *Hand2* and Sox9 proteins in E11.5 hindlimb buds was analyzed to understand whether *Hand2* co-localizes with Sox9 in the presumptive proximal skeletal domains. In general, *Hand2* and Sox9 transcription factors were co-expressed in nuclei of a large number of cells located in the posterior half of the hindlimb bud (Figure 15F). In particular, the cells of the presumptive stylopod domain often co-expressed *Hand2* and Sox9 proteins (Figure 15F, G). As *Tbx4* is expressed by mesenchymal cells in the proximal hindlimb bud (Naiche et al., 2011), our findings indicate that *Hand2* interacts with a *Tbx4* enhancer in the precursors of the proximal hindlimb skeletal elements to regulate correct morphogenesis.

6. Discussion

As part of my PhD research we developed dRMCE, a flexible re-engineering tool for efficient custom modification of available conditional alleles. We show that dRMCE works with high efficiency in engineering of the *Hand2* difficult-to-target locus and is compatible to “knockout-first” conditional alleles of the IKMC consortium. This makes dRMCE amenable for straightforward engineering of the more than 10'000 currently available conditional alleles of individual genes. We used dRMCE to introduce epitope tags into the endogenous *Hand2* locus and tested the tagged Hand2 proteins in differentiated mouse embryonic stem (ES) cells. We demonstrate that endogenous 3xFLAG-tagged Hand2 proteins are detected and localized in differentiated ES cultures and within distinct mouse embryonic tissues with high sensitivity and at high resolution. We further show the utility of the modified *Hand2* allele for chromatin immunoprecipitation (ChIP) of tagged Hand2 proteins in mouse embryos. Thereby, we established a ChIP-seq protocol that allowed us to identify candidate genome-wide target regions of endogenous Hand2 proteins in the mouse limb buds, heart, and branchial arches. We provide evidence that Hand2 interacts with a minimal element of the ZRS that is associated to human point mutations giving rise to polydactyly. Furthermore, our results suggest the interaction of Hand2 with a *Gli3* cis-regulatory region and a Gli3 binding element, which indicates implications in the pre-patterning mechanism. We also present evidence for several cis-regulatory Hand2 binding sites associated with *Tbx* or *Hox* genes which might be involved in pre-specification of the posterior limb bud mesenchyme. Furthermore, we show that Hand2 is essential for femur development and interacts with a *Tbx4* hindlimb enhancer. Last but not least, our analysis identifies putative Hand2-interacting cis-regulatory elements associated with genes that have important roles in heart development or craniofacial morphogenesis.

6.1 dRMCE and next-generation engineering of the mouse genome

dRMCE has many advantages over HR-based gene targeting. The generation of replacement plasmids using the dRMCE backbone is simple, as there is no need to clone long homology arms. An additional advantage of dRMCE over HR is that only a small number of colonies need to be picked. These can be screened and characterized during their clonal expansion and injected into blastocysts without any freezing steps. Although targeting frequencies vary between different loci, we show that dRMCE is much more efficient than HR (up to 65-fold) and is as effective as conventional RMCE, which depends on a single SSR and for which only few alleles are available (Seibler et al., 1998; Soukharev et al., 1999). Most importantly, we have shown that dRMCE does not affect the generation of high quality chimeras that efficiently transmit the engineered allele. Finally, dRMCE is more straightforward, specific, and broadly applicable than other RMCE-type approaches recently developed (Schnütgen et al., 2011; Schebelle et al., 2010; Singla et al., 2010).

dRMCE technology allows a “next-generation” engineering of the mouse genome by taking advantage of the vast collection of available IKMC conditional alleles (currently >10'000). In particular, this method enables directed and highly efficient replacement of the target region with orthologous or paralogous genes, epitope or fluorescent tags, and single or multiple mutations into endogenous genes of interest. This is very important for *in vivo* biochemical studies and the generation of ES cell and mouse models with direct relevance to human diseases. As the goal of the IKMC is to provide conditional alleles for all mouse genes (Skarnes et al., 2011), dRMCE represents the most attractive technique to generate genome-wide reporter- or Cre-libraries with the aim to establish a complete “Cre-zoo” (Rajewski 2007). In addition, such libraries could be generated for any type of recombinase using dRMCE. For example, the GUDMAP consortium (<http://www.gudmap.org>) has recently chosen dRMCE to develop novel transgenic mouse strains to genetically analyze the developing urogenital system. dRMCE technology is also well suited for high-throughput mutagenesis of loci of interest in ES cells or mice, and allows rapid functional screening of

several disease-causing mutations in mouse models. The feasibility of dRMCE allows even those with limited experience in mouse genetics and/or funds to rapidly engineer their mouse gene of interest using a dRMCE-compatible conditional allele.

The University of Basel has protected this technology in both the US and Europe through an International Patent Application (Patent Number(s): WO2011001247-A2; WO2011001247-A3). Furthermore, the University is in negotiations to license this technology to a mouse genome engineering company for the commercialization of mouse models generated using dRMCE.

6.2 Epitope tagging of endogenous proteins to assess *in vivo* function

Epitope tagging of endogenous proteins has numerous advantages in comparison to conventional transgenic approaches. Regulatory sequences that control the spatio-temporal patterns of gene expression are often dispersed over large regions forming genomic landscapes and archipelagos (Zeller & Zuniga et al., 2007; Tschopp et al., 2011; Montavon et al., 2011; Horsthuis et al., 2009). In contrast to conventional transgenes that require prior characterization of the *cis*-regulatory elements to be used to drive expression, direct modification of the endogenous coding sequences bypasses this step and avoids ectopic or aberrant expression. Furthermore, transgenic expression can be perturbed by the genomic location and the number of inserted transgenes (Clark et al., 1994; Williams et al., 2008).

Antibody quality and specificity are critical for ChIP studies (Massie & Mills, 2008; Park et al., 2009). The generation of ChIP-grade antibodies against the protein of interest is a time-consuming process that is not feasible for all labs to generate. Commercial antibodies are expensive and often affected by batch-to-batch variations that affect the reproducibility of results. Even worse, these antibodies might cross-react with other proteins, which will result in false positives (Massie & Mills, 2008; Park et al., 2009). In contrast, epitope-tagging allows the use of established, highly specific ChIP-grade antibodies. A rather large collection of different epitope tags has been established over the years, which allow detection of the tagged protein of interest with high sensitivity (Terpe et al., 2003). For instance, epitope

tagging of endogenous factors in yeast allowed the precise characterization of gene regulatory networks that control metabolic processes and display condition-dependent transcription factor occupancies (Lee et al., 2002; Harbison et al., 2004). Recent reports have also demonstrated the potential of mouse strains encoding epitope-tagged endogenous proteins by efficient quantification and immunolocalization of Sox5, Math5 and Pou4f2 (Fu et al., 2009; Lee et al., 2011). Furthermore, ChIP using endogenous FLAG-tagged Math1 identified an interaction with a *Gli2* regulatory element in the postnatal cerebellum (Flora et al., 2009).

The choice of the appropriate epitope tag and its position are major aspects to consider for balancing sensitivity of detection with the potential to interfere with protein functionality. For example, with respect to Hand2, the small 1xFLAG tag performed optimally in *in vitro* over-expression assays (Galli et al., 2010), but it lacked sufficient sensitivity in levels produced under the control of the endogenous *Hand2* locus. Detection of the LAP-tag (Cheeseman et al., 2005; Poser et al., 2008), on the other hand, was sufficiently sensitive *in vivo* but resulted in the truncation/degradation of the Hand2-LAP tag fusion protein. In contrast, the 3xFLAG-tag fused *in frame* to the endogenous Hand2 protein was detected with high sensitivity and specificity in a variety of assays. This allowed me to show that epitope tagging of an endogenous transcription factor is a good strategy for Hand2 protein localization and to identify the genomic regions with which Hand2 interacts in embryonic tissues.

6.3 Genome-wide identification of the genomic regions bound to Hand2-containing transcriptional complexes during limb bud development.

We have previously established that Hand2 is required for *Shh* activation in the posterior limb bud mesenchyme by directly interacting with the distant ZRS cis-regulatory region (Galli et al., 2010; see Introduction). Here, using ChIP-qPCR and ChIP-seq analysis in combination with endogenous 3xFLAG-tagged Hand2 proteins, we have identified amplicon “c” within the ZRS as the element to which Hand2 binds *in vivo*. This sequence “c” is located within the MFCS1, the evolutionarily conserved core of the ZRS, and contains a Hand2 *bona fide* Ebox

("Ebox3"). In support of this interaction, electrophoretic mobility shift assays (EMSA) revealed direct binding of Hand2 to *Ebox3* (Galli A., unpublished data).

Interestingly, point mutations in humans ("Cuban" G to A transition) and mice (M100081 A to G transition) map only a few base pairs from *Ebox3* (Zguricas et al., 1999; Sagai et al., 2004). Both mutations cause preaxial polydactyly (PPD) in humans and mice, respectively, and correlate with ectopic *Shh* expression in the anterior limb bud margin as revealed by transgenic analysis (Masuya et al., 2006; Lettice et al., 2007). Furthermore, *Ebox3* is separated from these mutations by only a putative *Hoxd* consensus site (Berger et al., 2008), and the entire element encoding *Ebox3*, *Hoxd* consensus, and Cuban/M100081 point mutations spans around 20bp. *Hoxd13* also interacts with the ZRS (Capellini et al., 2006) and both factors form a transcriptional complex that transactivates the ZRS in cell-based assays (Galli et al., 2010). Taken together, these data indicate that a transcriptional activation complex containing both Hand2 and *Hoxd13* binds to the 20bp element (see before) to control *Shh* expression in the limb bud mesenchyme. It is tempting to speculate that the PPD-causing mutations alter and/or increase the binding affinity of such transcriptional complexes, leading to ectopic expression of *Shh* in regions of transcriptional competence (i.e. activated chromatin). This agrees with the observation that the MFCS1 enhancer and the *Shh* promoter are in contact by long-range chromatin folding in both the anterior and posterior limb bud mesenchyme (Amano et al., 2009). While *Shh* is only transcribed in the posterior margin, this chromatin conformation may provide enhanced competence for ectopic *Shh* activation in the anterior mesenchyme, as observed with the point mutations in the ZRS.

The early and mutual genetic antagonism between *Hand2* and *Gli3* pre-patterns the nascent limb bud along its AP axis prior to the activation of *Shh* (Te Welscher et al., 2002a; Galli et al., 2010). *Gli3R* binding sites have been recently identified downstream of the *Hand2* locus, which could participate in the early posterior restriction of *Hand2* expression (Vokes et al.,

2008). ChIP-seq analysis revealed that Hand2 also interacts with one of these Gli3R binding sites and to a region located 17kb upstream of the *Gli3* transcriptional start site. This latter element in the *Gli3* locus might be involved in excluding *Gli3* expression from the posterior mesenchyme. It is possible that these reciprocal binding sites are part of the molecular mechanism that underlies the pre-patterning by which *Gli3* and *Hand2* mutually down-regulate the expression of the other. Therefore, it will be particularly interesting to investigate the dynamics of binding at sites downstream of the *Hand2* locus that are potentially occupied by both the Hand2 and Gli3R transcriptional regulators.

My results also indicate that Hand2 directly interacts with cis-regulatory regions controlling the *Hoxd* cluster, such as the GCR and the *Hoxd13* promoter. In particular, I find evidence for an interaction of Hand2 with the conserved CsB cis-regulatory region within the GCR. This cis-regulatory sequence drives reporter expression in the autopod and in the proximal posterior limb bud mesenchyme (Gonzalez et al., 2007). The complex and dynamic regulation of the spatio-temporal expression of 5'*Hoxd* genes during limb development is not well understood, and our study suggests that Hand2 could be one of the transacting factors that regulates its expression. Interestingly, *Gli3* is required to posteriorly restrict 5'*Hoxd* genes, as they are up-regulated in the anterior mesenchyme of *Gli3*-deficient limb buds (Zuniga & Zeller 1999). Furthermore, Gli3R binding sites have also been identified within the *Hoxd* complex (Vokes et al., 2008), and it will be interesting to investigate further if Hand2 and Gli3 interact in the transcriptional regulation of 5'*Hoxd* genes.

Finally, our genome-wide analysis of Hand2 binding sites revealed several hits in conserved elements associated with *Tbx* family genes. *Tbx2* and *Tbx3* are expressed in the anterior and posterior proximal mesenchyme at early limb bud stages and contribute to positioning and maintenance of the ZPA (Nissim et al., 2007; Davenport et al., 2003). In particular, *Hand2* controls the posterior expression of both these genes in early limb buds (Galli et al., 2010). The ChIP-seq analysis performed in this study indicates that Hand2 binds to several

conserved and likely cis-regulatory regions close to *Tbx2* and *Tbx3* coding sequences. This provides evidence that *Hand2* is a direct regulator of these genes in the limb bud mesenchyme and potentially in other embryonic organs where they are co-expressed, such as the developing branchial arches and heart. Furthermore, the ChIP-seq analysis reveals an interaction of *Hand2* with the HLEA region, which encodes a hindlimb enhancer regulating *Tbx4* expression (Menke et al., 2008). Targeted disruption of the HLEA fragment causes down-regulation of *Tbx4* expression in hindlimb buds and results in reduced bone size. Similarly, *Tbx4*-deficient limb buds display hypoplastic femurs and abnormally turned hindlimbs (Naiche & Papaioannou 2007). Strikingly, hindlimb buds with very low *Hand2* expression (*Hand2*^{ΔΔA13}) develop hypoplastic femurs and abnormal turning similar to the *Tbx4* mutants (Figure 14E). These defects cannot result from reduced *Shh* expression, as the femur is normal in *Shh* deficient limb buds (Chiang et al., 2001). Our results suggest that *Hand2* directly interacts with this *Tbx4* cis-regulatory region in the mesenchymal precursors of proximal hindlimb skeletal primordia to regulate femur morphogenesis. In agreement, severe defects in proximal skeletal elements are observed in *Hand2;Gli3* compound mutant limb buds (Galli et al., 2010). If these phenotypes result from patterning defects, abnormal chondrogenesis or osteogenesis still remains to be determined. There is evidence that *Hand2* promotes endochondral ossification, but also represses chondrogenesis (Abe et al., 2009). Indeed, the expression domains of *Hand2* and *Sox9* are rather complementary during the proliferative expansion and distal progression of limb bud development, which would point to an inhibitory effect of *Hand2* on prechondrogenic condensation. In line with a potential inhibitory effect on cartilage formation, *Hand2* interacts with a region located just upstream of the *Col1a1* transcription unit (data not shown; peak with highest enrichment in the curated ChIP-seq dataset; see Appendix). *Col1a1* encodes a main component of type I collagen, which is characteristic of fibrous connective tissues. In this context, it is tempting to speculate that during limb bud development, *Hand2* participates in the determination of chondrogenic and connective tissue cell types in the limb bud mesenchyme (Ten Berge et al., 2008, see Introduction).

Microarray analysis of *Hand2*-deficient limb buds will reveal the genes whose expression is regulated by Hand2. This analysis is ongoing and the resulting dataset will be overlapped with the ChIP-seq results described here. Expression of candidate target genes associated with cis-regulatory regions will be further studied in *Hand2*-deficient limb buds. Potential cis-regulatory regions regulated by Hand2 will then be assayed for their ability to drive lacZ expression in transgenic mouse embryos using tetraploid aggregation chimeras (Tanaka et al., 2009). However, a recent study showed that regulatory elements ultimately have to be genetically inactivated or replaced to gain a complete functional understanding of their relevance (Montavon et al., 2011).

6.4 Candidate target genes of Hand2 in the embryonic heart and branchial arches

Hand2 displays important functions in different cardiac lineages and its constitutive inactivation results in embryonic lethality due to right ventricular hypoplasia and aortic arch artery defects (Morikawa & Cserjesi 2008; Tsuchihashi et al. 2010; Srivastava et al. 1997). In particular, Hand2 is part of a regulatory network operating in SHF (secondary heart field) lineages that include the *Nkx2-5*, *Isl1*, and *Tbx1* transcriptional regulators (Vincent & Buckingham, 2010; see Appendix). *Hand2* is also essential for craniofacial development through the regulation of genes in the branchial arches (Charité et al., 2001; Yanagisawa et al., 2003; Barron et al. 2011). However, direct Hand2 target regions during heart and branchial arch development have not been defined *in vivo* and associated regulatory elements remain largely unknown (Laugwitz et al., 2008).

In addition to Hand2 binding regions in genomic loci functioning during limb bud development, the ChIP-seq analysis performed in this study identified Hand2 binding regions close to genes expressed during heart and branchial arch development. For instance, we identified an interaction between Hand2 and a conserved sequence element located 3kb upstream of the *Nkx2-5* locus (see Appendix). During cardiac looping, *Nkx2-5* marks the

ventricular myocardium and is required for myogenesis (Lyons et al., 1995). Transgenic analysis of a 3.3kb element just upstream of the *Nkx2-5* coding region drives *lacZ* reporter gene expression in myocardial cells of the outflow tract and the basal part of the right ventricle (Tanaka et al., 1999). Both of these tissues also express *Hand2*, but *Nkx2-5* expression appears unaltered in *Hand2*-deficient hearts (Srivastava et al., 1997). However, both *Hand2* and *Nkx2-5* and their genetic interaction, are essential for specification and expansion of the ventricular myocardium (Srivastava et al., 1997; Seidmann et al., 2000; Yamagishi et al., 2001; Tsuchihashi et al., 2010). *Hand2* could also regulate *Nkx2-5* in pro-epicardial cells, as both transcription factors fulfill critical functions in the formation of the epicardium (Zhou et al., 2008b; Barnes et al., 2011). In particular, *Hand2* is required for differentiation and survival of epicardial cells. In agreement, we also identified *Hand2* binding regions in the loci of epicardial markers such as *Wt1* and *Tbx18* (data not shown), which might be essential to regulate the pericardial expression of these genes (Zhou et al., 2008a; Cai et al., 2008).

A conserved *Hand2* interacting element far upstream of the *Tbx20* locus was also identified (see Appendix). *Tbx20* is another key regulator of cardiac development and potentially co-localizes with *Hand2* in right ventricular myocytes, endocardial cells, and the lateral plate mesoderm (Stennard et al., 2005 rev). Inactivation of *Tbx20* in mouse embryos causes defects similar to those observed in *Hand2*-deficient hearts. Therefore this interaction should be explored further, as the *Hand2* binding region may be a functionally relevant *cis*-regulatory module during cardiac development.

Finally, *Connexin40* (*Cx40/Gja5*) encodes a cardiac-specific gap junction protein, the inactivation of which causes dysrhythmias and septational defects (Kirchhoff et al., 2000). *Cx40* has been previously suggested to be a direct target of *Hand2* (Holler et al., 2010), and indeed, I have identified a *Hand2* binding region downstream of the *Cx40* locus that needs to be further investigated (see Appendix).

Interestingly, expression of *Hand1* in the mandibular arch largely depends on *Hand2* (Barron et al., 2011) and therefore might depend on a direct Hand2 interaction. Indeed, our ChIP-seq analysis identified a Hand2 binding region around 100kb upstream of *Hand1* (data not shown), which has to be further characterized.

The ChIP-seq analysis indicates that *Gsc* (*gooseoid*) is another direct Hand2 target, as I have identified several Hand2 binding regions clustered upstream of the *Gsc* locus (see Appendix). *Gsc* is expressed in branchial arches, limb buds and ventrolateral mesoderm, and its inactivation leads to inner ear and craniofacial defects including a hypoplastic mandible (Gaunt et al., 1993, Yamada et al., 1995). Expression of *Gsc* is indeed lost in *Hand2*-deficient first and second pharyngeal arches, which results in severe mandibular hypoplasia similar to that observed in *Gsc*-deficient embryos (Barron et al., 2011; Yamada et al. 1995). Furthermore, *Gsc* inactivation causes stylopod phenotypes represented by proximally malformed humerus and femur (Belo et al., 1998). These limb phenotypes might be related to the proximal defects we have observed in hindlimbs following conditional inactivation of *Hand2* (Figure 15E). This raises the possibility that stylopod morphogenesis depends on the regulation of *Gsc* expression by Hand2, possibly via the putative cis-regulatory regions I have identified. Indeed, this hypothesis is supported by our recent microarray analysis that reveals the significant reduction of *Gsc* expression in *Hand2*-deficient limb buds (data not shown). Together, these results provide evidence that *Gsc* may represent a *bona fide* transcriptional target of Hand2 in mouse embryos, and that this interaction might be required for normal morphogenesis of skeletal elements in different embryonic tissues (branchial arches and limb buds).

6.5 Conclusions & Outlook

This thesis has aimed at identifying candidate Hand2 transcriptional regulatory regions using a genome-wide ChIP-seq approach. I hope this will contribute to the mechanistic understanding of the regulatory networks controlled by Hand2 and operating during limb bud, cardiac, and craniofacial development. In my experiments, the starting material consisted of pools of embryonic tissues expressing a 3xFLAG-tagged Hand2 protein, so the precise spatio-temporal pattern of the Hand2 occupancy of these regions will have to be monitored by ChIP-qPCR. The deep sequencing dataset will be overlapped with the transcriptome analysis of *Hand2*-deficient tissues to identify likely functionally relevant interactions. Candidate cis-regulatory regions will be further studied for the presence of histone modifications such as H3K27ac, which allows predictions with respect to enhancer activity (Creyghton et al., 2010). In the future, chromatin conformation capture techniques will allow me to define the spatio-temporal nature of the physical interactions between distant genomic regions and to study the conformation of active and inactive cis-regulatory regions (Simonis et al., 2007) In particular, this will help me define 3D-interactions of Hand2 binding regions with the proximal promoter of genes of interest. Last but not least, the *Hand2*^{3xFLAG} mouse model and ES cells are valuable tools to identify Hand2-interacting proteins by immunoprecipitation with mass spectrometric analysis. Finally, motif analysis based on ChIP-seq data will help in identifying the cooperative DNA sequences of interacting proteins. This may contribute to determining the composition and genomic location of the transcriptional complexes in active chromatin of the morpho-regulatory targets of Hand2.

We have established a streamlined protocol for epitope-tagging of endogenous proteins and used this for genome-wide analysis of transcription factor binding sites. In our laboratory, we have generated mouse strains that express endogenous 3xFLAG-tagged Hand2, Gli3, and Smad4 transcriptional regulators. The use of such standardized experimental approaches with the appropriate controls produces unbiased and directly comparable datasets. For

example, the use of negative controls, such as ChIP using an unrelated antibody or non-expressing tissue, is not required anymore. Additionally, these controls would not exclude off-target effects. Therefore, the generation of equivalent datasets of targets of the Hedgehog (Gli3) and BMP (Smad4) pathways will be greatly simplified by the technology and approaches I have developed during my PhD research. The overlap of these and available ChIP-seq datasets of transcription factors, components of the basic transcriptional machinery, and/or chromatin modifications will move us toward a mechanistic and systems biology view of gene regulation and interactions. Our 3xFLAG-tagged endogenous proteins can be used for proteomics approaches to define tissue-specific protein interactions. My research provides a systems biology-type approach to study the dynamic properties of protein-DNA interactions and should help us to understand how cellular fates and properties are instructed by the activation of defined sets of transcriptional targets.

7. Materials and Methods

7.1 Genetic engineering of plasmids

7.1.1 Cloning procedure

Restriction enzyme (RE) digested vectors and inserts were agarose gel extracted and purified with the QIAquick Gel Extraction Kit (QIAGEN). De-phosphorylation of vectors was accomplished using the rAPid alkaline phosphatase kit (Roche). Ligation reactions were performed at RT for 10-15min using the T4 Ligase (NEB) system. Dialysis was conducted for 30min utilizing nitrocellulose containing MFTM-Membrane Filters (Millipore). Electroporation of plasmids into electrocompetent bacteria (XL1 blue) was achieved using a MicroPulserTM (BioRad). Plasmid DNA purification of grown bacteria was performed using the QIAGEN Plasmid Midi Kit or the NucleoBond[®] Xtra Midi kit (Macherey Nagel). The Expand High Fidelity^{PLUS} PCR System (Roche) was applied for the generation of PCR fragments for cloning.

To generate linkers, 100 μ M of each oligonucleotide stock were added to 1x annealing buffer (10x stock: 1M NaCl, 100mM Tris pH7.4) in a total volume of 50 μ l. Annealing of oligonucleotides occurred in a 85-95°C waterbath in a glass beaker at RT, gradually cooling down to room temperature (for several hours). 1 μ l of 1:10, 1:100 and 1:1000 dilutions of the annealed template was used in 0.5X annealing buffer for ligation. To prevent formation of concatomers, vectors were not de-phosphorylated, as oligonucleotides did not harbour a 5' phosphate. In general, the appropriate nucleotide composition of the vectors constructed was confirmed by sequencing, using the Big Dye terminator cycle sequencing kit (Applied BioSystems).

7.1.2 Generation of the *Hand2*, *Hand2*^{1xFLAG}, *Hand2*^{NBio} and *Hand2*^{CBio} expression vectors

Plasmids were constructed using *Hand2* and *Hand2*^{1xFLAG} (Galli et al., 2010) expression vector templates for PCR amplification of coding sequences which were flanked by appropriate RE consensus sites. Bio-tagged *Gli3* vectors (provided by Javier Lopez-Rios) were utilized to attach a

Biotin acceptor peptide (Bio-tag: NBio, CBio) (Kulman et al., 2006) either N- or C-terminally of the *Hand2* coding sequence (CDS). In a final step, *Hand2*, *Hand2*^{1xFLAG}, *Hand2*^{NBio} and *Hand2*^{CBio} coding sequences were cloned into pcDNA3 (Invitrogen) to generate the expression vectors. In all cases a Kozak consensus sequence (GCCGCCACC) is preceding the start codon to provide optimal initiation conditions for translation.

7.1.3 Construction of the pDIRE expression vector

The *iCre* coding sequence was amplified by PCR from the pBOB-CAG-iCRE-SD plasmid (Addgene Plasmid 12336) using primers with specific restriction sites (primers A1 and A2, Table 1). Following *Sall*/*NotI* digestion, the *iCre* fragment was cloned into pBluescript II KS (Stratagene, also denoted as pBSIIKS below). Subsequently, the human *EF1 α* promoter (Mizushima & Nagata, 1990) was inserted 5' as a *HindIII*-*BamHI* fragment derived from the pBS513 EF1alpha-Cre plasmid (Addgene Plasmid 11918). The SV40pA was inserted as a *SpeI*-*SpeI* fragment after PCR amplification (using primers A3 and A4, Table 1) from the pEGFP-N1 plasmid (GenBank Accession #U55762). These cloning steps resulted in the *pEF1 α -iCre* cassette, which was completely sequenced. This *iCre* expression unit was isolated as a *EcoRV*-*EcoRV* fragment and inserted into the *PsiI* site of the pPGKFLPobpA plasmid (Addgene Plasmid 13793) to generate the pDIRE expression vector (Figure 1B). To prevent potential promoter competition, the pDIRE vector was designed such that *iCre* is expressed under the control of the *EF1 α* promoter, while FLPo expression is controlled by the PGK promoter (Figure 1B).

7.1.4 Construction of the *Hand2*^{1xFLAG} replacement vector

Linkers were inserted into pBluescript II KS (Stratagene) to produce the following restriction/recombinase site configuration: *SacI-loxP-NarI-NotI-BamHI-Sall-ClaI-FRTinv-HindIII-KpnI*. A *NarI-NotI* fragment of the *Hand2* 5'UTR and a *NotI-BamHI* fragment corresponding to the rest of the *Hand2* transcription unit (with a 1xFLAG-epitope tag inserted into the PflMI site of coding exon 1) were sequentially inserted into the pBluescript backbone. In the final step, a DNA fragment encoding the *attB*-pGK-*Hygro*-*attP* resistance cassette with 3' *HindIII* and *PacI* sites for Southern blot screening was cloned into the *BamHI/Sall* sites of the pBluescript backbone, which resulted in the pRV-H2^{1xFLAG} (pRV-H2) final dRMCE replacement vector (Figure M1, 1C). A detailed scheme of all the cloning steps is illustrated in Figure M1 (pX) and according linkers sequenced are listed in Table 2 (Linkers L1-L7).

7.1.5 Construction of the pDRAV replacement backbone vectors

The four pDRAV vectors are shown in Figure 2F. The pBluescript II KS (Stratagene) plasmid was modified by inserting linkers to produce all possible orientations of the *loxP* and *FRT* sites, and a *lox2272* sequence, which would permit subsequent conventional RMCE (Linkers L5, L6, L8, L9). The *attB*-pGK-*Hygro*-*attP* resistance cassette was cloned into the *BamHI*-*Sall* sites. The multiple cloning sites of all pDRAV plasmids consist of unique *NotI*-*NsiI*-*HpaI*-*PacI*-*BamHI* restriction sites that can be used to insert the sequences of interest. *HpaI*, *PacI* and *BamHI* are well suited for Southern analysis of genomic DNA.

7.1.6 Generation of the pGT-VP replacement vector series

(made by Javier- Lopez-Rios and Barry Rosen)

A 1.75Kb DNA fragment encoding the required elements (T2A/H2B-Venus/SV40 polyadenylation site/*rox*/*XhoI*/*rox*/*loxP*) was synthesized by GeneArt (Regensburg, Germany) and cloned as a *BglIII*/*HindIII* fragment into the vector series L1L2-gt0/gt1/gt2 in all three possible reading frames. The PGK-*puromycin* selection cassette was excised as a *SalI* restriction fragment from the *pPGKpuro* plasmid (Addgene Plasmid 11349) and inserted into the *XhoI* site of the L1L2-gt-H2B-Venus plasmid series. This resulted in the definitive pGTx-VP replacement vector collection, which are compatible with all three open reading frames (Figure 4C).

7.1.7 Construction of the *Hand2*^{3xFLAG} expression and replacement vectors

To generate the *Hand2*^{3xFLAG} expression vector (pcDNA3-Nt3xFLAG-*Hand2*), a *SalI*-*EcoRI* fragment encoding the *Hand2* CDS was cloned into pBluescript II KS (Stratagene) containing a Kozak-3xFLAG cassette inserted into *KpnI*-*Sall*. Subsequently, the *KpnI*-*EcoRI* fragment encoding N-terminal 3xFLAG-tagged *Hand2* was cloned into pcDNA3 (Invitrogen).

In order to construct the *Hand2*^{3xFLAG} targeting vector, a PCR product encoding the following nucleotide sequence was generated using appropriate primers (Table 1: A5, A6): 5'-BssHII-*Hand2* 5'UTR portion-ATG-3xFLAG-ATG-*Hand2* 5' CDS-PfIMI-3'. The *Hand2*^{3xFLAG} expression vector was utilized as template for the PCR reaction. The fragment generated was then cloned into a BssHII/PfIMI digested vector containing the *NotI*-*BamHI* fragment encompassing a large part of the *Hand2*

transcription unit (pBSIIKS-H2-NotI-BamHI, illustrated in Figure M1). To generate the final *Hand2*^{3xFLAG} replacement vector (Figure 6A) for dRMCE (pRV-H2^{3xFLAG}), the *NotI-BamHI* fragment encoding N-terminal 3xFLAG-tagged *Hand2* was inserted into NotI/BamHI digested pRV-H2^{1xFLAG} (see above and Figure M1).

7.1.8 Construction of the *Hand2*^{LAP} expression and replacement vectors

The *Hand2*^{LAP} expression vector was generated by PCR amplification of a *SacI-LAP-SacI* fragment from pR6Kamp-LAP (received from Ina Poser, Poser et al., 2008) using the primer pair A7/A8 (Table 1). This fragment was inserted into the *SacI* site of pBSIIKS-Hand2-CBio (see above), which resulted in a vector encoding the *Hand2* CDS fused C-terminally to the LAP cassette (pBSIIKS-*Hand2*-LAP). A 2918bp *KpnI-EcoRI* fragment of this plasmid (encoding the Hand2-LAP fusion protein) was then inserted into Asp718/*EcoRI* digested pcDNA3 (Invitrogen) to generate the final expression vector (pcDNA3-*Hand2*-LAP). Assembly of the *Hand2*^{LAP} replacement vector for dRMCE was initiated by PCR amplification of a 453bp fragment including the 3' part of the LAP cassette followed by TAATGA stop codons and the 5' part of the *Hand2* 3'UTR (using primers A9 and A10). After digestion with *AflIII/SpeI*, the fragment was cloned into pBSIIKS-*Hand2*-LAP (see above). Digestion with *BglIII/SpeI* allowed the release of the following 1379bp fragment: *BglIII-Hand2* CDS (Exon2)-LAP cassette-TAATGA-*Hand2* 3'UTR portion-*SpeI*. This sequence was cloned into *BglIII-SpeI* of pBSIIKS-H2-NotI-BamHI (Figure M1). NotI/BamHI digestion of the resulting vector released a 4175bp fragment, which was cloned into *NotI-BamHI* of pRV-H2^{1xFLAG} (see above and Figure M1) to obtain the final dRMCE targeting vector encoding the *Hand2*-LAP cassette (pRV-H2^{LAP}, see Figure 6A).

7.1.9 Construction of the *Hand2*^{Bio-BirA} expression and replacement vectors

To fuse the T2A peptide *in frame* to the C-terminus of Hand2, a linker sequence (L10) was inserted into the *SacI* site of the 3' *Hand2* CDS in pBSIIKS-NBio-H2 (see above). This generated the following configuration: NBio-*Hand2* CDS-T2A-*EcoRV-XhoI-SpeI-EcoRI-SacI*. Subsequently, a PCR fragment (using primers A11/A12) encoding the *E.coli* biotin ligase (BirA) was cloned into *EcoRV-XhoI* to construct the NBio-*Hand2* CDS-T2A-BirA unit (pBSIIKS-NBio-Hand2-T2A-BirA). This module was inserted into *KpnI-EcoRI* of pcDNA3 (Invitrogen) to generate the *Hand2*^{Bio-BirA} expression vector (pcDNA3-NBio-*Hand2*-T2A-BirA). Furthermore, a 375bp PCR fragment (amplified with the A13/A10

primer pair) containing the 5' part of the *Hand2* 3' UTR was cloned into *XhoI-SpeI* of pBSIIKS-NBio-Hand2-T2A-BirA. In another reaction, using primers A14/A15, a PCR fragment encoding the NBio-tag flanked by *Hand2* 5' UTR and *Hand2* CDS sequences was inserted into *BssHII-PfIMI* of pBSIIKS-H2-NotI-BamHI (Figure M1) resulting in the generation of pBSIIKS-NBio-H2-NotI-BamHI. A 1496bp fragment of pBSIIKS-NBio-Hand2-T2A-BirA, which encoded the 3' portion of the *Hand2* CDS fused to the T2A-BirA unit, was cloned into *BglII-SpeI* of pBSIIKS-H2-NotI-BamHI. In a final step, the *NotI-BamHI* fragment from the resulting construct was cloned into *NotI-BamHI* digested pRV-H2^{1xFLAG} (see above and Figure M1) which resulted in the final pRV- H2^{Bio-BirA} dRMCE targeting vector (see Figure 6A).

7.2 dRMCE related technical approaches

7.2.1 dRMCE procedure including ES cell culture

A detailed step-by-step protocol describing the dRMCE procedure and informing about required materials and reagents was developed. This protocol is available from the nature protocol exchange web platform (<http://www.nature.com/protocolexchange/protocols/1906>).

7.2.2 ES cell transfection and selection

50µg of the appropriate replacement vector were co-electroporated with 50µg of pDIRE into mouse ES cells (1.5 x10⁷ cells per cuvette; 240kV and 475µF). *Hand2*^{f-neo} or *Gli3*^{f/+} R1 cells were plated in DMEM (4.5g/l glucose) containing 15% FCS (HyClone), 2mM D-Glutamine, 1x non-essential aminoacids, 2mM sodium pyruvate, 1x Penicilin/Streptomycin, 0.1mM β-mercaptoethanol and 10³units/ml LIF/ESGRO (Chemicon; all other reagents from Gibco-Invitrogen). *Smad4*^{f/+} or *Zfp503*^{f/+} JM8 ES cells were grown in Knock-out DMEM (4.5g/l glucose) containing 10% FBS, 2mM D-Glutamine, 1x Penicillin/Streptomycin, 0.1mM β-mercaptoethanol and 10³units/ml LIF/ESGRO (Chemicon; all other reagents from Gibco-Invitrogen). The culture medium was changed daily and from the second day onwards, resistant colonies were selected in the presence of 175µg/ml hygromycin or 0.5µg/ml puromycin (Sigma). After eight days in selection media, drug-resistant colonies were picked and analysed by PCR. A selection of *Hand2*^{1xFLAG}, *Hand2*^{3xFLAG}, *Hand2*^{LAP} and *Hand2*^{Bio-BirA} clones with

correct replacement were expanded and frozen in several aliquots. Correct recombination events and the absence of random integration were verified by Southern Blot analysis.

7.2.3 Detection of dRMCE replacement events by PCR

The primer pairs used for screening of ES clones by conventional PCR are indicated in the respective figures. The sequences of all primers used in the screening process of ES clones are listed in Table 3. Information about the relevant amplicons with according base pair extensions is shown in Table 4. The 5' screening strategy for the *Hand2*^{FLAG}, *Hand2*^{3xFLAG}, *Hand2*^{LAP} and *Hand2*^{Bio-BirA} alleles is based on the loss of a single diagnostic *EcoRV* site in comparison to the *Hand2*^{f-neo} allele due to the identical size of the 5' PCR products. Amplification using the F2/R2 primer pair yielded a doublet at 435bp (*Hand2*^{FLAG}, *Hand2*^{3xFLAG}, *Hand2*^{LAP} and *Hand2*^{Bio-BirA} and *Hand2*^{f-neo} alleles) and at 389bp (wild-type allele). In the *Hand2*^{f-neo} allele, this duplet was converted into a triplet by *EcoRV* digestion. As *EcoRV* digestion was performed partially in PCR buffer a faint upper band remained visible. Exact, locus-specific recombination frequencies obtained upon dRMCE mediated gene targeting were determined by PCR screening and are presented in Table 5.

7.2.4 *In silico* data mining to identify conditional alleles compatible with dRMCE

The Mouse Genome Informatics database (www.informatics.jax.org) was interrogated for *loxP* and *FRT* site-containing conditional alleles, which were then individually analysed for their compatibility with dRMCE. The list of currently available compatible conditional alleles of mouse genes is included in the appendix (Table 1).

7.2.5 Screening of PCR selected ES clones by Southern Blot analysis

DIG-dUTP-labelled probes for Southern Blot were synthesized using the PCR DIG Probe Synthesis Kit (Roche). Sequences of the primers used are listed below (Table 7). ES cell clones were grown to 80-100% confluency in 10cm dishes, rinsed two times with D-PBS and frozen at -20°C. Concentrated DNA was obtained using the DNA extraction method described in the dRMCE protocol (Nature Protocols Exchange). Appropriately scaled volumes (2-3ml) of lysis buffer containing 10% proteinase K were used to lyse the cells in the 10cm dish and 750µl/sample were processed. Finally, the DNA pellet was resuspended in 150-200µl of 10 mM Tris-Cl, 100 µM EDTA (pH 8.0) and stored at 4°C for at

least overnight. 6-10 μ g of extracted DNA were digested in a 1.5ml Eppendorf tube with the appropriate RE for 5 to 6h in a total reaction volume of 45 μ l (1x RE Buffer, 100 μ g/ml RNase A, 30 units of RE, in H₂O). Prior to loading on the agarose gel, 5 μ l of 10x loading buffer were added to the reaction mix and the sample was heated at 55°C for 20min. The entire sample was loaded into a well of a 0.75% agarose gel containing 20 μ l EtBr and the DNA was separated in TBE overnight at 30-40V. The next day, TBE buffer was exchanged and the gel was run for additional 3 to 4h at 50V until the appropriate separation of bands was achieved. Prior to transfer, the gel was depurinated in 0.25M HCl for 10min, washed in denaturation solution (0.5M NaOH, 1.5M NaCl) 2 times for 15min and washed in neutralization solution (0.5M Tris-HCl pH 7.5, 1.5M NaCl) 2 times for 15min. Equilibration was then conducted in 20xSSC (3M NaCl, 150 mM sodium citrate, pH 7.0) for at least 15min. A short rinse in H₂O preceded denaturation, neutralization and equilibration steps. For capillary transfer, a gel-size fitted positively charged nylon membrane (Roche) was pre-soaked in H₂O and equilibrated in 2xSSC. The transfer stack was set accordingly and capillary transfer was conducted overnight in 20%SSC. The next day paper tissues were exchanged and transfer continued for additional 3 to 4h. After disassembly of the transfer stack, the membrane was incubated in 2xSSC for 5min and dried for 1h at RT. Subsequently, the membrane was baked at 80°C for 2h in a sheath of 3MM paper and stored at RT. For prehybridization, the membrane was placed in a rolling bottle with DNA facing site up and incubated in prewarmed hybridization solution ((5xSSC, 50% deionized formamide, 0.1% N-lauroylsarcosine, 0.02% SDS, 2% Blocking Solution, in H₂O) at 42°C for at least 30min. Blocking Solution was prepared by dissolving 10% (w/v) Blocking Reagent (Roche) in 1x maleic acid buffer (0.1 M maleic acid, 0.15 M NaCl, pH 7.5) at 60-65°C. The prehybridization solution was then replaced with prewarmed hybridization solution containing DIG labelled probe. Re-used probe was heated to 68°C for 10min before. Hybridization was done overnight at 42°C in a rolling bottle. The probe solution was recovered the next day and the membrane was washed 2 times for 15min in 2xSSC, 0.1% SDS at RT and two times for 15min in preheated 0.2xSSC, 0.1%SDS at 68°C in the rolling bottle. Subsequently, the membrane was rinsed 1min in maleic acid wash buffer (0.1 M maleic acid, 0.15 M NaCl, 0.3% Tween20, pH 7.5) and blocked with 1% fresh Blocking Solution for 30min to 3h at RT. Still in the rolling bottle, the membrane was then incubated in 1% Blocking Solution containing anti-digoxigenin-AP antibody (1:20'000) for 30min at RT. The membrane was then transferred into a plastic tray and washed in maleic acid wash buffer 3 times for 15min at RT. Incubation in detection buffer (0.1M Tris-

HCl, 0.1M NaCl, pH9.5) followed for 2 min. To develop the signal, the membrane was placed onto an overhead foil and covered with detection buffer containing 6 μ l/ml CDP Star (Roche) for 5min at RT. The signal was visualized by exposure of the membrane (placed in a sealed bag) to Kodak BioMax MR film from 2-3 hours to overnight.

7.2.6 Immunodetection of YFP and β -galactosidase in ES cells

(performed by Javier Lopez-Rios)

ES colonies were grown on ibidi μ -slides (8 well) and fixed in cold acetone for 5min. After 3x5min washes in PBS, cells were blocked in 10% goat serum (in PBS) for 1h and incubated overnight at 4°C with rabbit α GFP-Alexa Fluor-488 (1:1000) and mouse α β -galactosidase (1:50) primary antibodies. After 3x10min washes in PBS, cells were treated with goat α mouse-Alexa Fluor-594 (1:1000) secondary antibody for 1h at RT. After 3x10min washes in PBS, fluorescent images were acquired with a Leica SP5 confocal microscope and software.

7.3 Mice & Molecular Biology

7.3.1 Generation of Hand2-FLAG lines and mouse colony management

Chimeric mice were generated by injection of *Hand2*^{1xFLAG/+} or *Hand2*^{3xFLAG/+} R1 ES cell clones (subjected to dRMCE) into C57BL/6J mouse blastocysts by the Transgenic Mouse Core Facility (Biozentrum, University of Basel). Male chimeras with ~60-100% agouti coat colour were crossed to C57BL/6J females to obtain germline transmission (agouti coat colour). Mice carrying the engineered *Hand2*^{1xFLAG} or *Hand2*^{3xFLAG} allele were obtained with the expected Mendelian ratios. Lines were kept in a mixed 129SvJ/C57BL/6J background. *Hand2*^{1xFLAG/1xFLAG} embryos were obtained by mating homozygous with/or heterozygous parents. For experimental use, *Hand2*^{3xFLAG/+} or *Hand2*^{3xFLAG/3xFLAG} males were crossed to wt NMRI females or C57BL/6J females, *Hand2* ^{Δ /+} females (Galli et al., 2010), *Hand2*^{3xFLAG/+} or *Hand2*^{3xFLAG/3xFLAG} females to obtain *Hand2*^{3xFLAG/+}, *Hand2*^{3xFLAG/3xFLAG} or *Hand2*^{3xFLAG/ Δ} embryos. The *Hand2*^{floxed} allele (Galli et al., 2010) was maintained in a 129SvJ/C57BL/6J mixed background. Homozygous parents were mated to obtain *Hand2*^{floxed/floxed} females that were crossed to *Hand2* ^{Δ /+}; *Hoxa13*^{Cre/+} males in order to generate *Hand2*^{floxed/ Δ} ; *Hoxa13*^{Cre/+} (*Hand2* ^{Δ / Δ A13}) embryos. Genotyping of mice and embryos was based on the extraction of DNA from ear-punch biopsies (mice)

or extra-embryonic membranes and head tissues (embryos). A piece of liver tissue was used for genotyping of E16.5 fetuses. Genotypes were determined by agarose gel electrophoresis following PCR amplification of diagnostic fragments. All primer sequences used for genotyping are listed below (Table 8). 5% of DMSO were used in PCR reactions for genotyping of the *Hand2*^{3xFLAG} allele. All animal experiments were performed in accordance with Swiss law and have been approved by the regional veterinary authorities.

7.3.2 Skeletal preparations

E16.5 fetuses were decapitated and kept in tap water overnight to soften the skin. The next day, specimens were placed into tap water heated to 70°C for 20-30 seconds, de-skinned and eviscerated. Subsequently, specimens were fixed in 95% EtOH for 3 days or more. Cartilage was stained in Alcian Blue staining solution (0.3g/l Alcian Blue 8GX, 20% glacial acetic acid in 95% EtOH) for 16hrs on a horizontal mixer. Specimens were fixed again in 95% EtOH for 24hrs and cleared for 15 to 20 min in 1%KOH. Ossified bone was stained by Alizarin red (50mg/l Alizarin Red, in 1%KOH) for 1.5 (E16.5 embryos) or 2 hours (newborn mice). Subsequently, embryos were rinsed in 1%KOH for 30min and clearing proceeded in 1%KOH/glycerol 80:20 for one (E16.5 embryos) or two (newborn mice) days. Clearing continued for several days (for each step) in a glycerol series including 60:40, 40:60 and 20:80 of 1%KOH/glycerol. Skeletal preparations were dissected and stored in 80% glycerol. Specimens were photographed using a Leica MZ FLIII stereomicroscope.

7.3.3 Whole mount *in situ* hybridisation

Whole mount *in situ* mRNA hybridisation (WISH) was performed using a modified version of the protocol from David Wilkinson (Wilkinson, 1993). All washes were carried out for 5min at RT on a rocking platform, if not otherwise noted.

Embryos were collected in cold PBS and fixed overnight at 4°C in 4%PFA in PBS in glass vials. Dehydration was conducted applying a 25%, 50%, 75%, 2x 100% MeOH/PBT series, after which embryos were stored in 100% MeOH at -20°C. For WISH, embryos were rehydrated in a reversed MeOH/PBT series (100%, 75%, 50%, 25%), transferred to 2ml Eppendorf tubes and washed 2 times in PBT. Embryos were then bleached in 6% hydrogen peroxide (in PBT) for 15min and washed 3 times in PBT. As exclusively mesenchyme specific riboprobes were used, incubation with proteinase K

(10 μ g/ml, in PBT) followed for 15min (E10.5), 20min (E11.5) or 25min (E12.5). Embryos were then treated with freshly prepared 2mg/ml glycine in PBT to inactivate proteinase K and washed with PBT 2 times. Embryos were refixed for 20min using fresh 0.2% glutaraldehyde, 0.1% Tween in fresh 4% PFA (in PBS), washed with PBT 2 times and incubated in 1ml prehybridisation mix (50% deionized, extra pure formamide, 5x SSC pH 4.5, 2% BCl. Blocking Powder, 0.1% Tween20, 0.5% CHAPS, 50 μ g/ml yeast RNA, 5mM EDTA, 50 μ g/ml heparin) for 1h at 70°C. Hybridisation followed by incubating the embryos in 1ml prehybridisation mix containing digoxigenin-labelled RNA riboprobe (10 μ l/ml) overnight at 70°C.

The day after, embryos were treated with a series of 100%, 75%, 50%, 25% prehybridization mix/2x SSC (0.3 M NaCl, 0.03 M Sodium citrate, pH4.5) at 70°C and washed 2 times with 2x SSC, 0.1% CHAPS for 30min at 70°C. After incubation with RNaseA (20 μ g/ml, in 2x SSC, 0.1% CHAPS) for 45min at 37°C to remove unbound riboprobe, embryos were washed with maleic acid buffer pH 7.5 (100mM maleic acid disodium, 150mM NaCl) 2 times for 10min at RT and 2 times for 30min at 70°C. Embryos were then washed 3 times with TBST (140mM NaCl, 2.7mM KCl, 25mM Tris HCl pH7.5, 0.1% Tween) and blocked in 10% sheep serum in TBST for at least 1h. After blocking, embryos were exposed to antibody treatment by incubation in TBST containing 1% sheep serum and 1:5000 anti-digoxigenin-AP antibody overnight at 4°C. The next day, embryos were rinsed with TBST two times and washed 5 times in TBST for 1h to 1.5h at RT on a rocking platform. After, embryos were washed in TBST overnight at 4°C on a rocking platform. On the fourth day, embryos were treated with fresh NTMT (100mM NaCl, 100mM Tris HCl pH9.5, 50mM MgCl₂, 1% Tween-20) 3 times for 10min and colour development was obtained upon incubation with BM purple AP solution (1ml/sample) at RT on a rocking platform. At the time the appropriate, probe-specific signal intensity was reached, embryos were treated with NTMT for 5min and washed at least 5 times with PBT and 2 times in PBS. Pictures were acquired using Leica MZ FLIII or MZ16A stereomicroscopes and the Leica Application Suite V3 software. For storage, embryos were post-fixed in 4% PFA (in PBS) and kept at 4°C.

7.3.4 Protein overexpression in HEK293T cells

In vitro protein overexpression in HEK293T cells was accomplished by transfecting cells with the FuGENE[®] 6 transfection reagent (Roche). Cells were grown to 50-80% confluency in 6-well plates and 2 μ g of *Hand2*, *Hand2*^{FLAG}, *Hand2*^{3xFLAG} expression vectors and empty pcDNA3 (Invitrogen) control

vector were transfected. After overnight incubation (18-24h), cells were rinsed 2 times in ice cold D-PBS, harvested and lysed in RIPA buffer (see below for composition) on ice by gentle pipetting. To remove debris and DNA, samples were centrifuged at 13'000rpm for 10min at 4°C. The supernatant was transferred to a new tube and used for Western Blot (described below).

7.3.5 Luciferase assay

Approximately 4×10^4 mouse NIH3T3 fibroblasts were plated per well of a 24-well plate and transfected using Lipofectamine LTX (Invitrogen) following the manufacturer's protocol. Cells were transfected with a total amount of 500ng of plasmid DNA complemented with pcDNA3 (Invitrogen). pGL4-TATA-4x Ebox and pGL4-TATA-mZRS reporter constructs (Galli et al., 2010) were co-transfected with 100ng of Hand2, Hand2^{FLAG}, Hand2^{3xFLAG} (see above for construction) and/or Hoxd13 (Galli et al., 2010) expression vectors. A Renilla luciferase vector (Promega) was co-transfected for normalization. Luciferase assays were performed using the Dual-Luciferase[®] Reporter Assay System following the manufacturer's protocol. Assays were performed 2 times in duplicates. Endogenous expression of *Hand2* or *Hoxd13* was not detected in NIH3T3 cells (Galli et al., 2010).

7.3.6 ES cell differentiation

After normal culture, R1 ES cells were cultured without feeder cells for two passages (maintaining 1:4 ratios) on 0.2% gelatine-coated 10cm dishes. Subsequently, ES cells were trypsinized and numbers were determined using a Neubauer hemocytometer. Two different techniques were applied to generate embryoid bodies (EBs) which give rise to a great variety of cell lineages including cardiomyocytes (Boheler et al., 2002): Floating embryoid bodies (fEBs, non-adherent cellular aggregates) were formed following the initial instructions of a protocol that involves generation of EBs (Bibel et al., 2007). Induction of EB formation was initiated on time point day zero (d0). Approximately 4×10^6 ES cells were plated onto a 10cm bacteriological Greiner Petri dish in 15ml of differentiation medium (DMEM (high glucose), 15% FBS (Gibco), 1x Penicillin-Streptomycin (100x stock), 2 mM L-Glutamine (100x stock), 0.1 mM β -mercaptoethanol (500x stock), 0.1 mM MEM Non Essential Amino Acids (100x stock), 1 mM MEM Sodium Pyruvate (100x stock)). Cells were incubated for 2 days at 37°C in 7.5% CO₂. To exchange the medium, the newly formed cellular aggregates were transferred to a 50ml Falcon tube by gentle pipetting. After 5min, EBs were located at the bottom of the tube due

to gravitation force. Used medium was aspirated and EBs were resuspended in fresh 15ml of differentiation medium by gently pipetting 2 times and transferred to a new 10cm Petri dish. For pipetting of cellular aggregates 25ml pipettes were used in order to prevent disaggregation of EBs due to narrow openings. After further 2 days (on day 4) medium was exchanged again and EBs were plated onto 6 wells of a 0.2% gelatine coated 6-well-plate in an equal distribution (for qPCR and WB). For immunofluorescence experiments, 10-20 EBs were plated per well of a ibidi μ -slide (8 well). Differentiated ES cells were harvested for qPCR/WB or processed for immunofluorescence at defined time points (d0-d16).

An alternative conical tube (CT) method to generate larger, single EBs was applied to obtain cultures generating higher numbers of contracting foci (Kurosawa et al., 2003). After ES cell culture and removal of MEFs (outlined above), 2×10^4 cells were incubated in a conical polypropylene 1.5ml screw cap micro tube (Sarstedt) in 1ml differentiation media (see above). Cells were incubated for 5 days at 37°C with 5% CO₂ to exert cellular aggregation at the bottom of the tube. Grown, large-diameter EBs were then transferred to 0.2% gelatine-coated 24-well plates (2-3 per well). Attachment culture was performed in differentiation medium at 37°C with 5% CO₂. First contracting of cardiomyocytes was detected on the third day (d8) after initiation of attachment culture (Kurosawa et al., 2003). ES-derived, differentiated cells were harvested or processed for WB/IF experiments at indicated stages of differentiation.

7.3.7 RNA extraction and cDNA synthesis

ES cells were grown and EBs were plated on gelatinised 6-well plates as described above. After the required time span of differentiation, cells were rinsed once with 4ml of D-PBS (prewarmed to 37°C), collected in 1.5ml of D-PBS using a cell scraper (Sarstedt) and transferred to a 1.5ml Eppendorf tube. Cells were then centrifuged at 2000rpm for 3min and pellets were resuspended in 80-200 μ l of the RNA stabilizing solution RNeasy[®] (Ambion) and incubated overnight at 4°C to ensure appropriate penetration. The next day, cold D-PBS was added to a final 1:1 mixture and cells were centrifuged at 5000rpm for 3min at 4°C. Finally, the supernatant was removed and the pellet was frozen at -80°C.

Samples of an entire differentiation series (collected at the different time points) were simultaneously subjected to RNA extraction. RNA extraction was conducted using the RNeasy[®] Micro kit (QIAGEN) and following the manufacturer's "protocol for purification of total RNA from animal and human cells". Samples were treated with DNase on the column.

For cDNA synthesis, 1µg of total RNA was mixed in a nuclease-free 1.5ml Eppendorf tube with 0.5µl Oligo(dT) and 0.5µl of a 10mM dNTP mix in a total volume of 20µl in RNase free H₂O. The sample was then heated to 65°C for 5min using a heating block and placed on ice for at least 1min. After brief centrifugation, the following reagents were added to the reaction tube: 4µl 5x First Strand Buffer (Invitrogen), 1µl 0.1M DTT, 1µl RNaseOUT™ (Invitrogen), 1µl Superscript™ III RT (Invitrogen). Reverse transcription was conducted by incubation on a heating block at 50°C for 1h. Subsequent heating at 70°C for 15min inactivated the reaction. cDNA was stored at -20°C until use for quantitative real-time PCR (see below).

7.3.8 Quantitative real-time PCR analysis (qPCR)

0.07µl of cDNA (1µg/µl) were diluted in 10.5µl H₂O. A mixture containing 12.5µl of iQ™ SYBR® Green Supermix (Bio-Rad) and 2µl of primer mix (3.75µM of each primer in EB buffer (QIAGEN)) were added per well of a 96-well skirted PCR plate (Bio-Rad). The diluted cDNA sample was added and qPCR reaction was performed using the CFX96 Real Time System (Bio-Rad). Normalization of relative mRNA levels was performed using primers hybridizing to cDNA of ribosomal protein L19 (*Rpl19*) transcripts. Normalized fold expression ($2^{-\Delta\Delta C_q}$) is shown and includes subtraction of normalized C_q (quantification cycle) values of sample and calibrator. Chart data are presented as relative to zero. For *Nanog/Sox2* qPCR, a mean C_q of 29.76 was set to 1.00, whereas for qPCR with *Hand2* primers a C_q of 29.84 was set to 1.00. Standard deviations of qPCR triplicates are indicated. Primers used for qPCR reactions are listed below (Table 9).

To compute enrichment of DNA fragments in chromatin immunoprecipitated samples, specific primers amplifying genomic DNA sequences were used. 2µl (ChIP of limb buds) or 1µl (test ChIP including larger amounts of Hand2 expressing tissues) of ChIP or Input sample were added to H₂O in a total volume of 10.5µl. For qPCR, this mixture was added to 12.5µl of iQ™ SYBR® Green Supermix (Bio-Rad) mixed with 2µl of primer solution (3.75µM of each primer). The fold of enrichment was computed as the fold of C_q values obtained for a region of interest (ROI) normalized to Wt and input samples subtracted to the fold of C_q values obtained for a negative control region (NEG) normalized to Wt and input samples:

$$\Delta\Delta C_{qROI} = (C_{qROI} \text{ ChIP FLAG} - C_{qROI} \text{ ChIP Wt}) - (C_{qROI} \text{ Input FLAG} - C_{qROI} \text{ Input Wt})$$

$$\Delta\Delta C_{qNEG} = (C_{qNEG} \text{ ChIP FLAG} - C_{qNEG} \text{ ChIP Wt}) - (C_{qNEG} \text{ Input FLAG} - C_{qNEG} \text{ Input Wt})$$

$$\text{Fold enrichment} = 2^{-(\Delta\Delta Ct_{ROI} - \Delta\Delta Ct_{NEG})}$$

All primers used are listed below (Table 9).

7.3.9 Western Blot analysis

Embryos and tissues were dissected in ice-cold PBS and indicated tissues were collected in PBS in Eppendorf tubes stored on ice. After removal of the PBS, samples were immediately snap-frozen in liquid nitrogen and stored at -80°C . According volumes (depending on tissue size) of fresh RIPA buffer (50mM Tris HCl pH7.5, 150mM NaCl, 1% NP40, 0.25% Sodium Deoxycholate, 1mM EDTA, 1:1000 pefabloc, 1X Complete Mini protease inhibitor cocktail, phosphatase inhibitors: 1mM activated Na_3VO_4 , 1mM NaF) were added to frozen pellets on ice. Samples were then gently pipetted up and down until complete cell lysis was obtained. After resting the tubes 15min on ice, samples were centrifuged for 10min at 13'000rpm at 4°C and the supernatant was transferred to new tubes. Protein concentrations were determined using the microplate BCA (bicinchoninic acid) Protein Assay (Pierce). For SDS-PAGE, protein extracts were added to new tubes and mixed with SDS sample buffer (25% 0.5M Tris pH6.8, 2% SDS, 0.0025% Bromophenol blue, 20% Glycerol, freshly added 5% β -mercaptoethanol; final 20%). Samples were denatured by heating at 98°C for 5min in a heat block and subsequently cooled on ice for 5min. Separation of proteins was conducted on a SDS polyacrylamid gel in running buffer (25mM Tris, 192mM Glycine, 0.1% SDS) and blotted on a hydrophobic PVDF Immobilon-P transfer membrane. For immunoblot detection of Hand2 proteins a final acrylamide concentration of 10% or 12% was used in resolving gels, whereas 6% of acrylamide was used for Gli3 western blots. The membrane was activated in 100% MeOH for 10s and equilibrated in transfer buffer (25mM Tris, 192mM Glycine, 20% MeOH) for 10min. Wet transfer was conducted at 4°C at 100 V for 1.5h (Hand2) or 2h (Gli3). Following transfer, the membrane was rinsed in TBST (10mM Tris-HCl pH8, 150mM NaCl, 0.05% Tween 20), blocked in 5% milk powder in TBST for 1h and incubated with primary antibody in 5% milk powder in TBST overnight at 4°C (mouse M2 anti-FLAG 1:1000, Bio-M2 (FLAG) 1:1000, goat α Hand2 (M-19) 1:500, mouse α GFP 1:1000, mouse α Gli3 (6F5) 1:1000). After four washes with TBST for 15min, the membrane was incubated with secondary antibody (goat α mouse HRP 1:10'000, goat α rabbit HRP 1:10'000, donkey α goat HRP 1:10'000, Streptavidin-HRP) in 5% milk powder in TBST for 1h at RT. The membrane was then washed with TBST 4 times for 15min and bands were detected using the VisualizerTM Western Blot Detection Kit (blots including embryonic

samples) or a 1:1 mixture between Visualizer™ Western Blot Detection Kit and SuperSignal® West Pico Chemiluminescent Substrate (blots including extracts from differentiated ES cells or HEK cells). Membranes were exposed to Kodak BioMax MR films or Amersham Hyperfilm™ ECL. When control antibodies were included, membranes were washed extensively with TBST, blocked 30min to 1h and incubated with primary antibodies (rabbit α Actin 1:4000, mouse α Vinculin 1:4000) for at least 45min at RT or overnight at 4°C. The following steps were performed as described above. Control bands were detected with SuperSignal® West Pico Chemiluminescent Substrate.

7.3.10 Silver stain

After SDS-PAGE (10% of sample used for immunoblot were loaded), the gel was fixed in 50% EtOH, 12% acetic acid for 1h (to denature and precipitate proteins within the gel matrix) and washed in 30% EtOH 3 times for 20min and then overnight. Subsequently, the gel was rehydrated in H₂O and incubated in 8 μ M sodium thiosulfate (fresh 0.8mM stock) for 1min. Following a 20sec rinse in H₂O, the gel was stained in 11.8mM silver nitrate, 0.02% formaldehyde for 20min. After rinsing 2 times in H₂O for 20sec, coloured protein bands were developed to the desired extent in 566mM sodium carbonate, 0.02mM sodium thiosulfate, 0.02% formaldehyde. Thereby, silver ions binding to proteins are reduced to metallic silver.

7.3.11 Limb bud cell culture

All four embryonic limb buds were dissected in cold D-MEM/F12 medium (containing 10% FBS and 0.5% Pen/Strep) and collected in 3ml of cold D-MEM/F12 medium in 15ml falcon tubes on ice. Limb buds were rinsed once with D-PBS (with Mg²⁺/Ca²⁺). After removing PBS by aspiration, limb buds were digested in 750 μ l of prewarmed digestion buffer (1x HBSS, 1mg/ml Collagenase D, 50 μ g/ml DNase) for 10min at 37°C. In order to prevent sticking of cells to the plastic of normal pipette tips, Biosphere tips were used to dissociate digested limb buds by gently pipetting up and down 15-20 times. Then, 750 μ l of digestion buffer were added and samples were incubated for further 10min at 37°C, after which cells were gently pipetted up and down (not more than 20 times) until complete dissociation was achieved. After adding 1.5ml of inactivation buffer (2% FBS, 10mM EDTA in PBS) tubes were transferred onto ice and 3ml DMEM/F12 medium were added. Cell suspensions were then centrifuged at 1650rpm for 5min, whereupon the supernatant was removed. Cell pellets were

resuspended in 260 μ l of prewarmed (at 37°C) DMEM/F12 medium and plated in one well of a ibidi μ -slide (8 well). Cells were cultured at 37°C, 5% CO₂ for 3.5h, 5h or 20h and processed for immunofluorescence (see below).

7.3.12 Immunocytochemistry

R1 ES derived cells or cultured limb bud cells (see above) were treated in a volume of 300 μ l or 200 μ l (for antibody containing solutions) per well of an ibidi μ -slide (8 well). Cells were rinsed with PBS two times and fixed with 4% PFA in PBS for 30min or 1h at RT. Then, the cells were rinsed with PBS and permeabilized in Triton X-100 (0.1%) in PBS for 10min. After rinsing with PBS, cells were blocked in 10% goat serum in PBS for 30min and rinsed with PBS again. Antibodies were diluted in 1% goat serum in PBS (mouse M2 anti-FLAG, 1:1000, mouse anti- α -actinin (sarcomeric), 1:500, mouse anti-MHC (sarcomeric), 1:300, mouse anti-Isl1, 1:200). Cells were then treated with primary antibody containing solution overnight at 4°C, whereas ibidi slides were kept in a moist chamber. The next day, cells were washed with PBT 3 times for 10min and incubated with secondary antibody containing solution (goat α mouse Alexa Fluor-488, goat α mouse Alexa Fluor-594, goat α rabbit Alexa Fluor-594). Following four washes of 5min with PBT, cell nuclei were counter-stained with Hoechst-33258 in PBT for 5min. Finally, cells were washed with PBT 2 times for 5min and kept in PBS at 4°C in a moist chamber. A Leica SP5 confocal microscope and software were used to obtain high resolution images.

7.3.13 Histology

Embryos were dissected in ice cold PBS and fixed overnight at 4°C in 4% PFA in PBS. Whole embryos or dissected embryonic tissues were washed 2 times for 5 minutes in ice cold PBS and dehydrated to 100% EtOH. In this course, samples were treated once with 25% ice cold EtOH/PBS for 10min, 2 times with 50% ice cold EtOH/PBS for 10min and 2 times with 75% ice cold EtOH/H₂O for 10min. Embryonic samples were transferred to room temperature for 45min and were then incubated 2 times with 100% EtOH for 10min. Following dehydration, samples were cleared in Xylene 2 times for 20min at room temperature, treated with 50:50 (v/v) xylene/paraffin for 30min at 60°C and incubated three times for at least 1hr in heated fresh paraffin at 60°C. Samples were embedded in fresh paraffin (heated to 60°C) using a stereo microscope for proper positioning. The resulting paraffin blocks were

stored at 4°C. 7µm paraffin sections were cut, mounted on SuperFrost/Plus slides (Microm) to be processed for immunofluorescence (see below).

7.3.14 Immunohistochemistry

Paraffin sections of embryonic tissues were deparaffinised with two washes in Xylene for 10min each. Sections were then washed 2 times with 100% EtOH for 10min, rehydrated in an EtOH/H₂O series and washed in PBS 2 times for 5min. Subsequently, sections were subjected to antigen retrieval by autoclaving them for 5min in 10mM Sodium Citrate (pH 6.0) with 0.05% Tween-20. After cooling at RT for 30min, sections were washed 2 times with PBS for 5min and 4 times with PBT (PBS with 0.1% Tween) for 5 min. Sections were blocked in 10% goat serum in PBT for 1hr at RT and incubated with the primary antibody overnight at 4°C in a moist chamber. Antibodies were diluted in 1% goat serum in PBT (mouse M2 anti-FLAG1:500, rabbit α Sox9 1:500 or 1:1000, rabbit α Ki67 1:200). After three washes of PBT for 10min, sections were incubated in secondary antibody containing solution (goat α mouse Alexa Fluor-488 1:1000, goat α rabbit Alexa Fluor-594 1:1000) for 1h at RT. Sections were then washed 3 times with PBT for 10min and 2 times with PBS for 5min. Following incubation with Hoechst-33258 in PBS for 5min to stain cell nuclei, sections were washed two times with PBS for 5min and then covered with a drop of the anti-fade agent Mowiol. Subsequently, a coverslip was added and slides were dried overnight in the dark at room temperature. Fluorescent, high resolution images were captured using a Leica SP5 confocal microscope and software.

7.4 Towards a ChIP-seq approach

7.4.1 Sonication tests

To define sonication conditions resulting in ChIP-seq grade chromatin fragmentation, E11.5 limb buds (from ~60 embryos) or E10.5 embryonic tissues (tissues from ~50 embryos, excluding tissues used for FLAG ChIPs) were processed as described in the ChIP-seq section above. The protocol was followed up to the sonication step using the S-250A Branson sonifier. After sonication, samples were frozen, reverse crosslinked, RNase and PK treated and purified (eluted in 32µl EB buffer) as described below (ChIP). To determine the degree of DNA fragmentation, 20µl (E11.5 limb buds) or 10µg (embryonic tissues) of sample were loaded on an agarose gel.

7.4.2 Immunoprecipitation (IP)

Embryonic tissues were collected, snap-frozen and stored at -80°C as described for Western Blots (above). Antibody-coupled magnetic Dynabeads[®] Protein G were prepared by washing total volume of bead suspension ($10\mu\text{l}/\text{sample}$) in 1ml fresh and cold BSA/PBS (250mg Albumin in 50ml D-PBS with $\text{Mg}^{2+}/\text{Ca}^{2+}$). The bead suspension was then centrifuged for 1min at 3000rpm at 4°C , rinsed 3 times with cold BSA/PBS on a magnetic rack and finally resuspended in BSA/PBS ($25\mu\text{l}/\text{sample}$) containing $0.9\mu\text{g}$ M2 anti-FLAG antibody per sample. The suspension was then transferred to a 2ml conical screw cap micro tube and incubated overnight at 4°C on a rotating platform. The next day, antibody-coupled magnetic beads were rinsed with BSA/PBS 3 times on a magnetic rack, resuspended in BSA/PBS ($10\mu\text{l}/\text{sample}$) and kept on ice. Embryonic sample pellets were lysed with according volumes (dependent on tissue amounts) of IP-RIPA buffer (final 3X Complete Mini Protease Inhibitor Cocktail, otherwise identical to RIPA described for WB). The total protein concentration was determined as described above (WB). For IP, sample volumes containing $100\mu\text{g}$ ($200\mu\text{g}$ for IP, Figure 7F) of total protein were transferred to a 2ml conical screw cap micro tube and complemented with IP-RIPA buffer to a final volume of $150\mu\text{l}$. Subsequently, $10\mu\text{l}$ of prepared antibody-coupled bead suspension were added and samples were incubated at 4°C on a rotating platform for 12h. After five washes in 1ml common RIPA buffer, beads were resuspended in $20\mu\text{l}$ of IP-RIPA buffer and $8\mu\text{l}$ of SDS sample buffer (containing 5% β -mercaptoethanol, see above) were added to the sample. Samples were heated at 98°C for 5min and cooled down on ice for 5min, after which the supernatant containing denatured pulled-down proteins was transferred to a new tube. Immunoblotting (complete sample loaded) including SDS-PAGE and Bio-M2 anti-FLAG primary antibody in combination with Streptavidin-HRP was performed as described above (WB).

Initially, the following parameters were used for IP of differentiated ES cell lysates: 0.6-0.8mg of lysate were incubated with $1.5\mu\text{g}$ of M2 anti-FLAG antibody at 4°C on a rotating platform and after 2.5hrs, $15\mu\text{l}$ of Dynabeads[®] were washed and added. Incubation was performed for 5.5hrs at 4°C .

7.4.3 Chromatin immunoprecipitation (ChIP) using E11.75 limb buds

The following protocol represents a modified version of the “ChIP protocol for small embryonic samples” from Steven A. Vokes (2008). The day prior to starting ChIP, M2 anti-FLAG antibody was

coupled to magnetic Dynabeads[®] Protein G was prepared as described above (IP). For ChIP, embryos were isolated in ice cold PBS and limb buds were dissected in ice-cold feeder cell culture medium. Per sample, fore- and hindlimb buds of 9 embryos (in total 36 limb buds) were pooled in a 15ml Falcon tube containing ice-cold EMFI media. Medium was then decanted and limb buds were rinsed in ice cold D-PBS (with Mg^{2+}/Ca^{2+}). All but 1ml of D-PBS was removed using an aspirator and limb buds were transferred to a 2ml conical screw cap microtube (Sarstedt). After removal of the D-PBS with a pipette, 800 μ l of Collagenase D working solution (1x HBSS, 1mg/ml Collagenase D) was added and the sample was incubated for 5min at 37°C. In order to dissociate the cells, the sample was then gently pipetted up and down 20 times using Biosphere tips and incubated another 5min at 37°C. Subsequently, the sample was gently pipetted up and down again until a single cell suspension was obtained (never exceeding 20 times of pipetting). After adding 800 μ l of inactivation buffer (2%FBS, 10mM EDTA, in D-PBS), the sample was transferred onto ice. To induce protein-DNA crosslinks, 160 μ l of crosslinking buffer (1.25ml 4M NaCl, 100 μ l 0.5M EDTA 8.0, 50 μ l 0.5M EGTA 8.0, 2.5ml 1M HEPES NaOH 8.0, 31.25ml H₂O) containing 11% fresh formaldehyde (from a 36.5% stock) were added. The sample was crosslinked for 30min at RT on a rocking platform. The crosslinking reaction was stopped by adding 88 μ l of 2.5M Glycine and the sample was placed on ice for 5min. After centrifuging at 2000rpm for 5min at 4°C, the pellet was resuspended in 1ml cold D-PBS (with Mg^{2+}/Ca^{2+}), mixed by gentle pipetting and centrifuged again at 2000rpm for 5min at 4°C. Subsequently, the pellet was resuspended in 1ml ice-cold lysis buffer (2ml 1M HEPES KOH pH7.5, 1.4ml 4M NaCl, 80 μ l 0.5M EDTA 8.0, 4ml Glycerol, 2ml 10% NP40, 1ml 10% Triton-X 100, 28.72ml H₂O, 1X Complete Mini protease inhibitor cocktail), placed on ice for 10min and centrifuged at 2500rpm for 8min at 4°C. To extract proteins, the pellet was resuspended in 1ml Buffer 2 (1.6ml 4M NaCl, 64 μ l 0.5M EDTA 8.0, 32 μ l 0.5M EGTA 8.0, 160 μ l 2M Tris 8.0, 29.5ml H₂O, 1X Complete Mini protease inhibitor cocktail), incubated for 10min on ice and centrifuged at 2500rpm for 8min at RT. The pellet was then resuspended in 300 μ l Buffer 3 (40 μ l 0.5M EDTA 8.0, 20 μ l 0.5M EGTA 8.0, 100 μ l 2M Tris 8.0, 19.64ml H₂O, 3X Complete Mini protease inhibitor cocktail) and transferred to a 1.5ml Eppendorf tube. A Diagenode's Bioruptor was used for sonication as follows: the sample was sonicated in a bath of ice-cold water at high frequency for 50min in five cycles of 10min (30" on, 30" off). After each cycle, the water was replaced with ice-cold H₂O containing ice cubes. Following sonication, a 16 μ l aliquot was transferred to a new tube and frozen at -20°C to be used to determine

the quality of sonication. The remaining volume was estimated with a pipette and *N*-Lauroylsarcosine (20% stock) was added to 0.5%, incubated on a rocking platform for 10min and centrifuged at 3500rpm for 10min 4°C. In the meantime, the complexes of dynabeads coupled to M2 anti-FLAG antibodies (after overnight incubation) were rinsed and resuspended as described before (IP). After centrifugation, the supernatant of the sample was transferred to a new tube and topped up to 1.02ml with Buffer 3. Importantly, 20µl were then transferred to a separate tube and frozen at -20°C to be used as input sample. For IP, the sample was split in duplicates, whereas 150µl of ChIP Cocktail Mix (16.25µl 4M NaCl, 6.5µl 10% Sodium Deoxycholate, 65µl 10% Triton-X100, 62.5ml H₂O) and 10µl of prepared suspension containing the bead-antibody complexes were added to the 500µl of sample in a 2ml conical screw cap micro tube (Sarstedt). Immunoprecipitation was done using a rotating platform at 4°C for 13.5h. Afterwards, bead containing samples were transferred to 1.5ml Eppendorf tubes and rinsed 5 times with 1ml of ice-cold RIPA buffer (for 200ml: 20ml 10% NP40, 14ml 10% Sodium Deoxycholate (fresh), 400µl 0.5M EDTA 8.0, 10ml 1M Hepes-KOH pH7.5, 4.24g Lithium Chloride, 155.6 ml ddH₂O) on the magnetic rack. Samples were then rinsed once in 1ml of TE-NaCl (100mM Tris pH8, 10mM EDTA, 50mM NaCl) and centrifuged at 3000rpm for 1min at 4°C. On the magnetic rack residual buffer was removed and beads were resuspended in 100µl of fresh Elution Buffer (2.5µl 2M Tris pH8, 2µl 0.5M EDTA pH8, 10µl 10% SDS, 85.5µl H₂O). Elution occurred at 65°C for 15min on a heating block with shaking at 1300rpm. After centrifugation at 13'000 rpm for 1min, the supernatant was collected and transferred to a PCR tube. In the meantime, the frozen input sample and the sonication quality test sample were thawed and transferred to a new PCR tube containing 100µl of fresh Elution Buffer. All samples were then reverse crosslinked overnight at 65°C (on a PCR block). The next day, 100µl of TE (100mM Tris pH8, 10mM EDTA) and final 0.2µg/µl of RNaseA (from Bovine pancreas) were added and samples were incubated at 37°C for 1hr. Proteinase K was then added to a final concentration of 0.2µg/µl and samples were incubated at 55°C for 2hrs. The QIAquick Gel Extraction Kit (cat no. 28704) was utilized for DNA purification, whereas in the final step DNA was eluted 2 times in 30µl of EB buffer (see manufacturer's protocol). Each sample was aliquotted (20µl) and frozen at -20°C. qPCR was used for amplification of ChIP-enriched fragments and the fold enrichment was computed using the usual controls (see qPCR section above).

7.4.4 ChIP with subsequent next-generation sequencing (ChIP-seq)

Elements of different protocols were combined to establish ChIP followed by next-generation sequencing of enriched DNA fragments (ChIP-seq). The protocols for tissue collection and freezing of crosslinked samples were obtained from Axel Visel (Visel et al., 2009) and used in a modified version. In particular, disaggregation was carried out prior to crosslinking in order to minimize the sticking of tissues to the components of the glass douncer. We crosslinked nuclei instead of tissue and therefore the crosslinking time was reduced to 5min to maintain sonication efficiency. A modified version of the ChIP-chip approach (Kim et al., 2007) was used in combination with a scaled variant of the “ChIP protocol for small embryonic samples” from Steven A. Vokes (2008). D-PBS containing $Mg^{2+}Ca^{2+}$ was utilized and Complete Mini protease inhibitor cocktail was added from a 50X stock (one 50x tablet dissolved in 1ml of H_2O).

E10.5 embryos were dissected in ice-cold PBS the parts containing branchial arches, heart and limb buds were transferred in PBS to a single 2ml Eppendorf tube on ice. In case of low number of embryos in a litter, embryonic tissues of the same genotypes (wild-type or *Hand2*^{3xFLAG}) from different litters were pooled during a dissection session (optimal amounts were covered from around 13-18 embryos). Collected tissue pools were rinsed once with 1.5ml cold D-PBS, transferred to another 1.5ml of D-PBS in a 2ml glass douncer and disaggregated with 25 strokes of pestle A, followed by 25 strokes using pestle B. The solution of disaggregated tissue with nuclei was then transferred back to a new 2ml Eppendorf tube. To collect remnant nuclei, the douncer was rinsed with 0.5ml D-PBS which was added to the sample. After centrifugation at 3000rpm for 2min at 4°C, the supernatant was discarded and the pellet consisting of nuclei and debris was resuspended in 1.5ml D-PBS (RT) containing 150µl 11x crosslinking buffer. Crosslinking was carried out on a horizontally shaking platform for 5min (best sonication efficiency) to 15min at RT, after which 75µl of 2.5M Glycin was added to quench the formaldehyde and inactivate crosslinking. The sample was incubated 5min on a horizontal shaker and centrifuged at 3000rpm for 2min at 4°C. The supernatant was discarded and the pellet resuspended in 1.5ml cold D-PBS. Following centrifugation at 3000rpm for 2min at 4°C, the supernatant was discarded, the pellet snap-frozen in liquid N₂ and stored at -80°C in 2ml Eppendorf tubes.

The day before starting ChIP, antibody coupled magnetic beads were prepared as described above (see IP section). The volumes were adapted from Vokes' protocol and scaled: 250µl of bead

suspension were washed, resuspended in 625 μ l of BSA/PBS and incubated overnight with 25 μ g of M2 anti-FLAG antibody. The following day, the bead-antibody complexes were washed and finally resuspended in 250 μ l BSA/PBS. For ChIP, the snap-frozen, crosslinked nuclei of 100 (Test-ChIP) to 150 (ChIP-seq) embryos were processed by thawing them on ice for 3-5min. Pellets were resuspended in ice cold Lysis buffer (50mM Hepes pH7.5, 140mM NaCl, 1mM EDTA pH8, 10% Glycerol, 0.5% NP40, 0.25% Triton X-100, 1X Complete Mini protease inhibitor cocktail) and pooled in a 50ml Falcon tube in a total volume of 30ml. After incubation on a rocking platform at 4°C for 10min, the sample was centrifuged at 2500rpm for 10min at 4°C. The supernatant was then discarded and the pellet resuspended in 24ml of Protein Extraction Buffer (200mM NaCl, 1mM EDTA pH8, 0.5mM EGTA pH8, 10mM Tris-HCl pH8, 1X Complete Mini protease inhibitor cocktail). Subsequently, the sample was incubated on a rocking platform at RT for 10min and centrifuged at 2500rpm for 10min at 4°C. The supernatant was discarded and the pellet was resuspended in 7ml of cold Chromatin Extraction Buffer (1mM EDTA pH8, 0.5mM EGTA pH8, 10mM Tris-HCl pH8, 3X Complete Mini protease inhibitor cocktail). The sample was then transferred to a 15ml polypropylene conical Falcon tube for sonication. Sonication was conducted on ice using a S-250A Branson sonifier with an attached 3.2mm micro tip. Per sample, 10 cycles (1 cycle: sonication for 30s (output 6), followed by resting on ice (at least 90s)) were carried out for the Test-ChIP, whereas 16 cycles were performed for the ChIP-seq experiment. The sample was then distributed to 1.5ml Eppendorf tubes and centrifuged 13'000rpm for 10min at 4°C to pellet the debris. All supernatant was then pooled in a new 15ml Falcon tube on ice. Two 30 μ l aliquots were then frozen at -20°C for input controls and to test the quality of sonication on an agarose gel. As at least a total volume of 5.5ml was recovered from sonication, 1.375ml of sample were then aliquoted into four 2ml conical screw cap microtubes (Sarstedt) for immunoprecipitation. 447 μ l of ChIP Cocktail Mix (179.6 μ l TE, 17.8 μ l 10% Sodium Deoxycholate, 178.3 μ l 10% Triton-X100, 2X Complete Mini protease inhibitor cocktail) and 28 μ l of antibody coupled to magnetic beads were added to each tube. Thereby, ratios were as described by the Vokes protocol. In total, 11.2 μ g of M2 anti-FLAG antibody were used for each sample. IP was performed for 10hrs at 4°C on a rotating platform as this allowed efficient detection of proteins by Western blots following IP. Subsequently, samples were transferred to 1.5ml Eppendorf tubes and rinsed 7 times with 1ml of ice-cold RIPA buffer (50mM Hepes pH8, 1mM EDTA pH8, 1% NP-40, 0.7% Sodium Deoxycholate, 0.5M LiCl, 1X Complete Mini protease inhibitor cocktail) on a magnetic rack. Samples were then rinsed in

1ml of TE-NaCl (100mM Tris pH8, 10mM EDTA, 50mM NaCl) and centrifuged at 1000rpm for 3min at 4°C. After removing any residual liquid on the magnetic rack, beads were resuspended in 100µl of freshly prepared Elution Buffer (10mM Tris-HCl pH8, 1mM EDTA pH8, 1% SDS) to strip the protein:DNA complex from the antibody. Elution was carried out on a heating block at 65°C for 15min at 1300rpm. Samples were then centrifuged at 13'000rpm for 1min. The supernatant was collected on a magnetic rack and transferred to a PCR reaction tube. The 30µl aliquots frozen for input control and test of sonication quality were thawed. After adding 100µl of Elution buffer, all samples were transferred into PCR tubes. Finally, all samples were reverse crosslinked overnight at 65°C in a PCR block. The following day, 100µl TE (100mM Tris pH8, 10mM EDTA) and 0.2µg/µl RNaseA (from Bovine pancreas) final concentration were added and incubated at 37°C for 1h. After that, Proteinase K (final 0.2µg/µl) was added to each tube and proteins were digested at 55°C for 2hrs. For subsequent purification of DNA fragments, the QIAquick Gel Extraction Kit (cat no. 28704) was used (following the supplier's protocol). Elution of DNA fragments was performed in two steps (first in 30µl, then in 12µl EB buffer) to aim at a final elution volume of 30-40µl as required for deep sequencing.

Agarose gel electrophoresis assessed the quality of the control sample (3µg loaded) and revealed the most abundant DNA fragments in a range between 200bp to 1.5kb (data not shown), which was rated as sufficient for deep sequencing by Dr. Christian Beisel (Head of the Laboratory of Quantitative Genomics, D-BSSE, ETH Zurich). The DNA concentration was determined by Ina Nissen using the PicoGreen[®] assay. All the samples fulfilled the criteria to be processed for deep sequencing (at least 2-10ng required):

Sample	Conc.	Total amount (in 33µl)
1) Input Wt	85ng/µl	2.805mg
2) Wt	0.185ng/µl	6.105ng
3) Input 3xF	69ng/µl	2.277mg
4) 3xF	0.615ng/µl	20.295ng

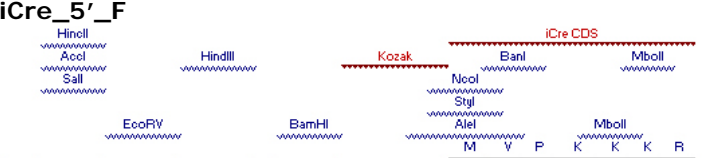
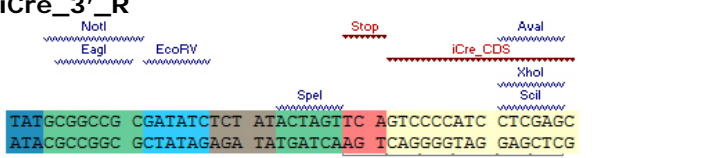
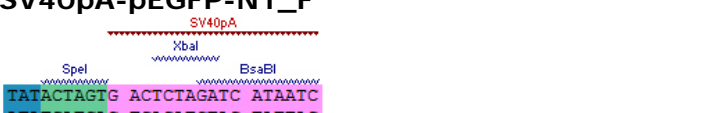
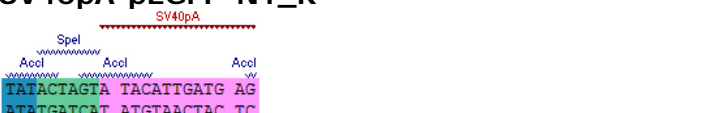
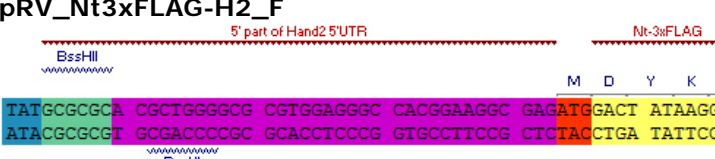
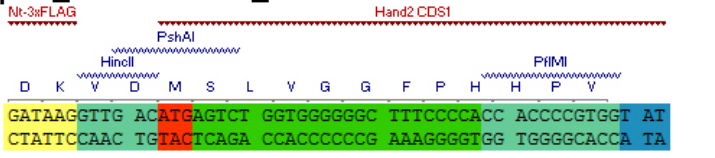
Libraries for deep sequencing were generated by Ina Nissen using the Illumina ChIP-seq DNA Sample Prep kit according to Illumina's instructions. Following end repair and adaptor ligation, library DNA fragments were size selected (~200-250bp) and extracted from an agarose gel. Isolated fragments were then PCR amplified for 18 cycles using Illumina primers. After purification, samples were loaded on an Illumina flow cell for solid-phase amplification (cluster generation). Sequencing of libraries was carried out on the Genome Analyzer II (Illumina) following the manufacturer's instructions. Data processing, alignment of data sets, BigWig generation and data analysis by Model-based analysis of

ChIP-Seq (MACS, Zhang et al., 2008b) were performed by Manuel Kohler and Christian Beisel. MACS was used to define a whole-genome dataset of peaks normalized to enrichment in Wt and Input data to exclude local sequencing biases and detection of false positives (due to e.g. non-specific antibody binding). To determine the significance of the putative *cis*-regulatory regions and to associate peak coordinates with gene loci, we used the Genomic Regions Enrichment of Annotations Tool (GREAT, McLean et al., 2010). For associated genomic regions (regulatory domains) the basal plus extension association rule was used (constitutive 5kb upstream and 1kb downstream with a maximal extension of 1Mb). Mouse NCBI build 37 (UCSC mm9, Jul 2007) was used as genomic background.

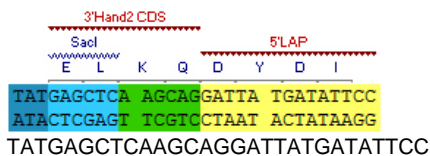
7.5 Tables of reagents, frequencies & materials

Table 1. Primers utilized for the generation of complex PCR fragments for cloning

Colours are used to highlight different modules (Spacers: dark blue, RE sites: turquoise or teal, Kozak: dark yellow, start codon: dark red, *Hand2* CDS: green, tags: yellow, stop codon: red, UTRs: violet).

Primer	Sequence	Length
A1	<p>iCre_5'_F</p>  <p>TATGTCGACG ATATCAAGCT TTAGGATCCG CCGCCACCAT GGTGCCCAAG AAGAAGAGG ATACAGCTGC TATAGTTCGA AATCCTAGGC GCGGTGGTA CCACGGGTTT TCITCTCC</p>	59bp
A2	<p>iCre_3'_R</p>  <p>TATGCGGCCG CGATATCTCT ATAAGTTC AGTCCCCATC CTCGAGC ATACGCGGCG GCTATAGAGA TATGATCAAG TCAGGGTAG GAGCTCG</p> <p>* D G D E L</p> <p>TATGCGGCCGCGATATCTCTATACTAGTTCAGTCCCCATCCTCGAGC ⇒ Template: pBOB-CAG-iCRE-SD (Addgene Plasmid 12336)</p>	47bp
A3	<p>SV40pA-pEGFP-N1_F</p>  <p>TATACTAGTG ACTCTAGATC ATAATC ATATGATCAC TGAGATCTAG TATTAG</p>	26bp
A4	<p>SV40pA-pEGFP-N1_R</p>  <p>TATACTAGTA TACATTGATG AG ATATGATCAT ATGTAAC TAC</p> <p>TATACTAGTATACATTGATGAG ⇒ Template: pEGFP-N1 (GenBank Accession #U55762)</p>	22bp
A5	<p>pRV_Nt3xFLAG-H2_F</p>  <p>TATGCGCGCA CGCTGGGGCG CGTGGAGGGC CACGGAAGGC GAGATG GACT ATAAGGAC ATACGCGCGT GCGACCCCGC GCACCTCCCG GTGCCITCCG CTCTACCTGA TAITCCTG</p> <p>TATGCGCGCACGCTGGGGCGCGTGGAGGGCCACGGAAGGCGAGATGGACTATAAGGAC</p>	58bp
A6	<p>pRV_Nt3xFLAG-H2_R</p>  <p>GATAAAGGTTG ACATGAGTCT GGTGGGGGGC TTTCCCAACC ACCCCGTGGT AT CTATTCCAAC TGTACTCAGA CCACCCCGG AAGGGGTGG TGGGGACCA TA</p> <p>ATACCACGGGGTGGTGGGGAAAGCCCCCACCAGACTCATGTCAACCTTATC ⇒ Template: pcDNA3-Nt3xFLAG-Hand2</p>	52bp
	pEV_H2-CtLAP_F	

A7



TATGAGCTCA AGCAGGATTA TGATATTCC
ATACTCGAGT TCGTCTAAT ACTATAAGG

TATGAGCTCAAGCAGGATTATGATATTCC

29bp

A8

pEV_H2-CtLAP_R



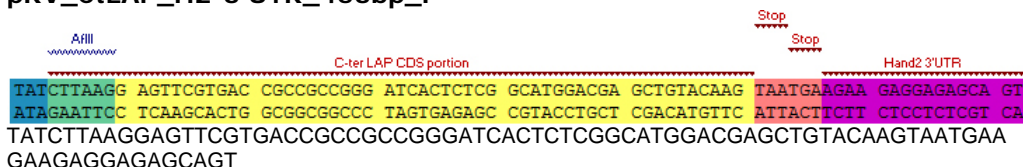
ATAGAGCTCGAATTCAGTTCATTACTTGTACAG

⇒ Template: Cterm_R6K-amp-LAP cassette (from Ina Poser, Buchholz Lab)

36bp

A9

pRV_CtLAP_H2-3'UTR_453bp_F

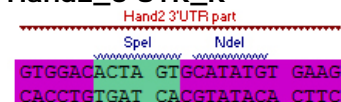


TATCTTAAGGAGTTCTGTGACCGCCCGGGATCACTCTCGGCATGGACGAGCTGTACAAGTAATGAA
GAAGAGGAGAGCAGT

82bp

A10

Hand2_3'UTR_R



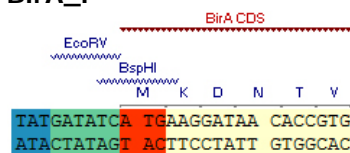
CTTCACATATGCAGTGTCCAC

⇒ Template: pBSIIKS-H2-NotI-BamHI (used in pRV-H2^{FLAG} generation)

24bp

A11

BirA_F

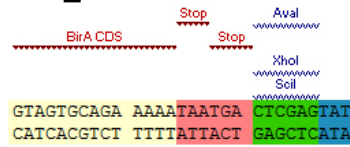


TATGATATCATGAAGGATAACACCGTG

27bp

A12

BirA_R



ATACTCGAGTCATTATTTTTCTGCACTAC

⇒ Template: pcDNA3.1: BirA (BirA-pFLAG-Z1) (Kulman et al., 2006)

28bp

A13

Hand2_3'UTR_375bp_F



TATCTCGAGAGAAGAGGAGAGCAGTG
ATAAGAGCTCTTCTCCTCTCGTCAC

26bp

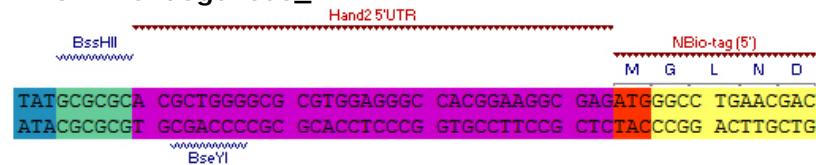
A10

(see above)

⇒ pBSIIKS-H2-NotI-BamHI (used in pRV-H2^{FLAG} generation)

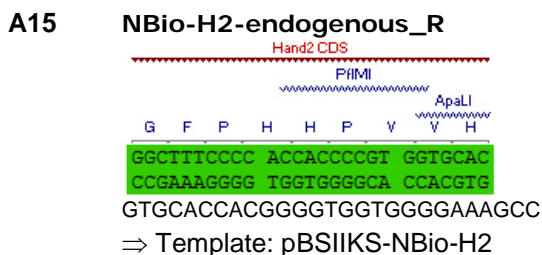
A14

NBio-H2-endogenous_F



TATGCGCGCACGTGGGGCGCGTGGAGGGCCACGGAAGGCGAGATGGGCCTGAACGAC

58bp

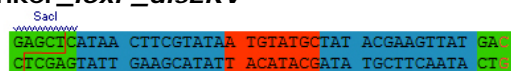


28bp

Table 2. Linkers and the corresponding primer sequences (F: forward primer, R: reverse primer) used for cloning steps in the generation of *Hand2* dRMCE replacement vectors (pRV-H2) or vectors of the pDRAV series (cloning strategy for pRV-H2^{1xFLAG} shown in Figure M1). Linkers were designed to provide RE-compatible 5' and 3' ends (indicated with red lines). RE sites are shown in various green. Recombinase target sites are labelled in different colours, whereas the central core (spacer) is marked. Different modules of the T2A peptide are highlighted (dark yellow: conserved sites, red: 2B proline).

Primer	Sequence	Length
L1	Linker_lox2272-RE	
	<p>1 GAGCTTATA TATGGCCCTC TCAAGGCTTC AGTTCCCA TAACCTCGTA TAAAGTATCC TATACGAAGT TATATCSATA TGAAGCTT CTGAGTATT ATAGCCGCGG AGTGGCCGSC AGTCTCTAGG TCACAGCTCT ATTGARGACT ATTTCATAGG ATATGCTTCA ATATAGCTAT ACTTCGAACC</p> <p>101 TACC ATGS</p>	
F:	CATGATATCGGCGCCTCAGCGGCCGCTCAGGATCCAGTGTGCGACATAAAGTTCGTATAAAGTATCCTA TACGAAGTTATATCGATATGAAGCTTGGTAC	98bp
R:	CAAGCTTCATATCGATATAAAGTTCGTATAGGATACTTTATACGAAGTTATGTCGACACTGGATCCTGAG CGGCCGCTGAGGCCCGGATATCATGAGCT	98bp
L2	Linker_attB-RE	
	<p>1 GATCTGTGCG GGTGCCAGGGCGTGCCTTGGGCTCCCCGGGCGCGTACTCCACCTCACCTCGAGGTGT CCTAGACCGC CCACGGTCCC GCAGGGAC CCGAGGGGCC CGGCGATGAG GTGAGTGA GCTCCACAT GCAGCTACAT CAGCTCTC ATGG</p>	
F:	GATCCTGCGGGTGCAGGGCGTGCCTTGGGCTCCCCGGGCGCGTACTCCACCTCACCTCGAGGTGT AACGCGTATGTAGTCGACGAGGTAC	92bp
R:	CTCGTCTACTACATACGCGTTACACCTCGAGGTGAGGTGAGTACGCGCCCGGGGAGCCCAAGGGCA CGCCCTGGCACCCGAG	84bp
L3	Linker_loxP	
	<p>1 GAGCTCATAA CTTCTATAA TGTATGCTAT ACGAAGTTAT GATATC CTGAGTATT GAAGCATATT ACATACGATA TCTTCAATA CTATAG</p>	
F:	CATAACTTCGTATAATGTATGCTATACGAAGTTATGAT	38bp
R:	ATCATAACTTCGTATAGCATACTTATACGAAGTTATGAGCT	42bp
L4	Linker_attP	
	<p>1 ACGCGTGTGC CCCAACTGGG GTAACCTTIG AGTTCTCTCA GTTGGGGCG TAGGGTCTC GAC TCGCAACAGC GGGTTGACCC CATTGGAAAC TCAAGAGAGT CAACCCCGCG ATCCAGCAG CTG</p>	
F:	CGCGTGTGCCCAACTGGGGTAACCTTTGAGTTCTCTCAGTTGGGGGCGTAGGGTCTG	57bp
R:	TCGACGACCTACGCCCAACTGAGAGAACTCAAAGGTTACCCAGTTGGGGCACA	57bp
L5	Linker_FRT_inv	
	<p>1 ATCGATGAAG TTCTATAGT TTCTAGAGAA TAGGAAGTTC AAGCTT TAGCTACTTC AAGGATATGA AAGATCTT ATCCTTGAAG TTCGAA</p>	
F:	CGATGAAGTTCTATACTTTCTAGAGAATAGGAAGTTC	39bp
R:	AGCTTGAAGTTCTATCTCTAGAAAAGTATAGGAAGTTCAT	41bp

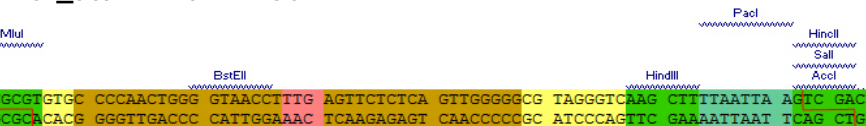
L6 Linker_loxP_disERV

1 

F: CATAACTTCGTATAATGTATGCTATACGAAGTTATGAC 38bp

R: GTCATAACTTCGTATAGCATACATTATACGAAGTTATGAGCT 42bp

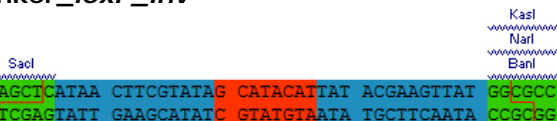
L7 Linker_attP-HindIII-Pacl



F: CGCGTGTCCCCAACTGGGGTAACCTTTGAGTTCTCTCAGTTGGGGCGTAGGGTCAAGCTTTTAA 71bp
TTAAG

R: TCGACTTAATTAAGCTTGACCCTACGCCCAACTGAGAGAACTCAAAGGTTACCCAGTTGGGG 71bp
CACA

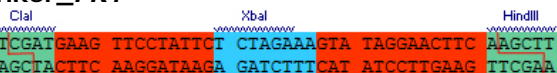
L8 Linker_loxP_inv



F: CATAACTTCGTATAGCATACATTATACGAAGTTATGG 37bp

R: CGCCATAACTTCGTATAATGTATGCTATACGAAGTTATGAGCT 43bp

L9 Linker_FRT



F: CGATGAAGTTCTATTCTCTAGAAAGTATAGGAAGTTCA 39bp

R: AGCTTGAAGTTCTATACTTTCTAGAGAATAGGAAGTTTCA 41bp

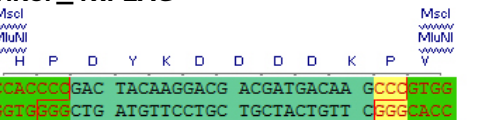
L10 Linker_T2A-RE



F: CAAGCAGGAGGGCAGAGGAAGTCTGCTAACATGCGGTGACGTCGAGGAGAATCCTGGCCAGATATCT 98bp
ACACTCGAGTACAAGTGTGAATTCGAGCT

R: CGAATCACTAGTTGTAAGTGTAGATATCTGGGCCAGGATTCTCCTCGACGTCACCGCATGTTAGC 98bp
AGACTTCTCTGCCCTCCTGCTTGAGCT

L11 Linker_1xFLAG



F: GACTACAAGGACGACGATGACAAGCCC 27bp

R: CTTGTCATCGTCGTCCTTGTAGTCGGG 27bp

(The same sequence was used for the 1xFLAG construct described in Galli et al., 2010)

Table 3. Primer sequences (dRMCE) designed to screen ES clones for correct site-specific recombination events in endogenous *Hand2*, *Gli3*, *Smad4* and *Zfp503* loci.

General primers

IKMC knockout-first alleles

Primer	Sequence
F1	AGCAGAGCGGGTAAACTGGC
R1	GCATCAGAGCAGCCGATTGTC
F9	CCAACCTGCCATCACGAGATT

pDREV

Primer	Sequence
R3	TGGACGAAATGCCGGTGTCA
F4	GCAAAACCAAATTAAGGGCCA
R10	TGGACCTGCTTCAGAACCTTGTA
F11	CTCTTGATTCCCACCTTGTGGTTC

pDRAV

Primer	Sequence
F6	ATGCGACGCAATCGTCCGATC
R7	CATCTGCACGAGACTAGTGAGACG

pDIRE

Primer	Sequence
I1	GACTACCTCCTGTACCTGCAAGCCAG
I2	CTGCCAATGTGGATCAGCATTCTC
I3	CAGAGATACCTGGCCTGGTCTGG
I4	CCTGAACATGTCCATCAGGTTCTT
P1	CAGCCTGAGCTTCGACATCGTGAAC
P2	CTCAGGAACTCGTCCAGGTACACC

Locus specific primers

Primer	Sequence
F2	AACTAACTCTGTGTTTCAGAGCCCCG
R2	GCTGCCCAAATCAATAGCCA
F3	GCAATCCAAACCAAGCATTGTC
F5	CCTCGGCAATTAGCAACGTGAACATC
R5	GTCTCGCTCCTCAGGCTCTCTCG
R6	CCCTCCTCCACCACCACTGCTCAT
F7	CTGTGCCTGGTGCTTCGTTTTGTG
R8	TTGAACTGCGAACAGGGGAA
R9	TTCTGAGGAAGGCGACTTTGG
F10	CTTCCTGTGGGGTTTCTTTC
R11	GCACAAAACGAAACTCAAACGC
F12	TGGAGGGCCACGGAAGGCGAGATG
R12	GACAGGGCCATACTGTAGTCG
F13	GTCTTTCCATTTCTCTCCCTCTCG
R13	CAGGGTCAGCTTGCCGTAGGTGGC
F14	CTCTTCGAACAAGAAGGATTGGCAC
R14	GGAATGCTTTTCTTCAAATATCCACC
R15	CAGGACATAGCGTTGGCTACCCG
A	TCCAAGTCGATGGATATGCAACG (<i>Grem1</i>)
B	ATGAATCGCACCCGCATACACTG (<i>Grem1</i>)
D1	GGAGAAGTGCCTGCGCCTTGTG
D2	AGCTTGACCCTACGCCCCCAACTGA
G1	AGCTGGTAGCCTTAAAATAAGCCAA
G2	TTCTCGTGCTTTACGGTATCG

G3	GCAGCCCAAGCTGATCCTCTA
G4	GCCTGAAAGAGGTCATCATCACC
G5	TTTGGTATTTGAGAAAGGGGCTC

Table 4. Locus specific amplicons (dRMCE)*Hand2* locus

Primer pair	Allele	Amplicon size
F6/R6	<i>Hand2</i> ^{1xFLAG} (3') <i>Hand2</i> ^{3xFLAG} (3') <i>Hand2</i> ^{LAP} (3') <i>Hand2</i> ^{Bio-BirA} (3')	965bp
F5/R5	<i>Hand2</i> ^{1xFLAG} (5') <i>Hand2</i> ^{3xFLAG} (5') <i>Hand2</i> ^{LAP} (5') <i>Hand2</i> ^{Bio-BirA} (5')	435bp
F5/R5	<i>Hand2</i> ^{f-neo} (5')	435bp (EcoRV: 340bp + 95bp)
F5/R6	<i>Hand2</i> ^Δ	411bp
D1/D2	<i>Hand2</i> ^{1xFLAG-Δhygro}	198bp
F12/R12	<i>Hand2</i> ^{1xFLAG}	236bp
F12/R12	<i>Hand2</i> ^{3xFLAG}	284bp
F12/R12	<i>Hand2</i> ^{Bio-BirA}	260bp
F12/R12	<i>Hand2</i> ^{f-neo} <i>Hand2</i> ^{LAP}	209bp
F13/R13	<i>Hand2</i> ^{LAP}	466bp
F14/R14	<i>Hand2</i> ^{Bio-BirA}	448bp
F7/R15	<i>Hand2</i> ^{f-neo}	841bp

Gli3 locus

Primer pair	Allele	Size
F6/G4	<i>Gli3</i> ^{H2} (3')	1055bp
G5/R5	<i>Gli3</i> ^{H2} (5')	613bp
G3/G4	<i>Gli3</i> ^Δ	394bp
G1/G2	<i>Gli3</i> ^{neo}	1065bp

Smad4 locus

Primer pair	Allele	Amplicon size
F4/R2	<i>Smad4</i> ^{YFP} (3')	456bp
F3/R3	<i>Smad4</i> ^{YFP} (5')	1594bp
F2/R2	<i>Smad4</i> ^Δ	565bp
	<i>Smad4</i> ^{wt}	1265bp
F1/R1	<i>Smad4</i> ^f	558bp

Zfp503 locus

Primer pair	Allele	Amplicon size
F11/R11	<i>Zfp503</i> ^{YFP} (3')	396bp
F10/R10	<i>Zfp503</i> ^{YFP} (5')	1449bp
F1/R8	<i>Zfp503</i> ^Δ	987bp
F9/R9	<i>Zfp503</i> ^f	599bp

Table 5. Exact dRMCE recombination frequencies obtained with targeting different loci.

<i>Hand2</i>	n	%
dRMCE (5' and 3')	43	12.54%
Mixed clones (dRMCE + Δ)	11	03.21%
<i>Hand2</i> Δ	131	38.19%
Negative for dRMCE/ Δ	158	46.06%
Total clones picked	343	

<i>Gli3</i>	n	%
dRMCE (5' and 3')	37	32.7%
Mixed clones (dRMCE + Δ /flox)	0	0%
<i>Gli3</i> Δ^{neo}	28	24.78%
<i>Gli3</i> ^{neo}	48	42.48%
Total clones picked	113	

<i>Smad4</i>	n	%
dRMCE (5' and 3')	33	68.8%
Mixed clones (dRMCE + Δ /flox)	5	10.4%
Negative for dRMCE	10	20.8%
Total clones picked	48	

<i>Zfp503</i>	n	%
dRMCE (5' and 3')	25	52.1%
Mixed clones (dRMCE + Δ /flox)	0	0%
Negative for dRMCE	23	47.9%
Total clones picked	48	

Table 6. dRMCE targeting frequencies (2nd *Hand2* targeting)

Overall targeting frequencies obtained with the three different replacement constructs:

<i>Hand2</i> locus	n	%
dRMCE (5' and 3')	38	10.95%
Negative for dRMCE / mixed clones	309	89.05%
Total clones picked	347	

Targeting frequencies for individual alleles:

<i>Hand2</i> ^{3xFLAG}	n	%
dRMCE (5' and 3')	20	16%
Total clones picked	125	
<i>Hand2</i> ^{LAP}	n	%
dRMCE (5' and 3')	10	8.85%
Total clones picked	113	
<i>Hand2</i> ^{NBio}	n	%
dRMCE (5' and 3')	8	7.34%
Total clones picked	109	

Table 7. Primers and fragment sizes for probe synthesis for Southern Blotting

Probe	Forward primer	Reverse primer	Origin
5' <i>Hand2</i> (HindIII)	5'- CTGATAATGGTGCTGTCAGTGAGG-3	5'- GGGAACAGGTAGACTGGGTAAGATG-3'	A.Galli
3' <i>Hand2</i> (PacI)	5'- TGAGCCACCAAACTACTGTCTTATG-3	5'- CAGAGGATAGAAATGAATGGAAATGG-3'	New
<i>Hygro</i> (HindIII)	5'- TTCGACAGCGTCTCCGACCT-3	5'- TTCCTTGCGGTCCGAATGGG-3'	J. Lopez-Rios

Probe	Screening RE	Allele	Fragment size
<i>Hygro</i>	HindIII	<i>Hand2</i> ^{3xFLAG}	8'558bp
<i>Hygro</i>	HindIII	<i>Hand2</i> ^{LAP}	9'398bp
<i>Hygro</i>	HindIII	<i>Hand2</i> ^{NBio}	9'566bp
5' <i>Hand2</i>	HindIII	<i>Hand2</i>	28'541bp
5' <i>Hand2</i>	HindIII	<i>Hand2</i> ^f	30'664bp
5' <i>Hand2</i>	HindIII	<i>Hand2</i> ^Δ	23'264bp
5' <i>Hand2</i>	HindIII	<i>Hand2</i> ^{3xFLAG}	8'558bp
5' <i>Hand2</i>	HindIII	<i>Hand2</i> ^{LAP}	9'398bp
5' <i>Hand2</i>	HindIII	<i>Hand2</i> ^{NBio}	9'566bp
3' <i>Hand2</i>	PacI	<i>Hand2</i>	7'250bp
3' <i>Hand2</i>	PacI	<i>Hand2</i> ^f	9'345bp
3' <i>Hand2</i>	PacI	<i>Hand2</i> ^Δ	16'512bp
3' <i>Hand2</i>	PacI	<i>Hand2</i> ^{3xFLAG}	6'909bp
3' <i>Hand2</i>	PacI	<i>Hand2</i> ^{LAP}	6'909bp

3' <i>Hand2</i>	Pacl	<i>Hand2</i> ^{NBio}	6'909bp
-----------------	------	------------------------------	---------

Table 8. Genotyping primers (mice)

Locus	Forward primer	Reverse primer	Size	Allele
<i>Hand2</i>	5'- CCTCGGCAATTAGCAACGTGAACATC -3' (F5)	5'- GTCCTCGCTCCTCAGGCTCTCTCG -3' (R5)	389bp 435bp	Wt 1xFLAG/ 3xFLAG
<i>Hand2</i>	5'- CTGTGCCTGGTGCTTCGTTTTGTG -3' (F7)	5'- CATCTGCACGAGACTAGTGAGACG -3' (R7)	404bp	1xFLAG/ 3xFLAG
<i>Hand2</i>	5'- TGGAGGGCCACGGAAGGCGAGATG -3' (F12)	5'- GACAGGGCCATACTGTAGTCG -3' (R12)	209bp 236bp 284bp	Wt 1xFLAG 3xFLAG
<i>Hand2</i>	5'- CCTCGGCAATTAGCAACGTGAACATC -3' (F5)	5'- CCCTCCTCCACCACCACTGCTCAT -3' (R6)	411bp	Null
<i>Hand2</i>	5'- CTGTGCCTGGTGCTTCGTTTTGTG -3' (F7)	5'- CCCTCCTCCACCACCACTGCTCAT -3' (R6)	240bp 440bp	Wt floxed
<i>Hoxa13</i>	5'- CACTGGGGTCTTCTCCATGCGGGCTC -3	5'- CAGCATTGCTGTCACTTGGTCGTG -3'	388bp	Cre

Table 9. qPCR primers

cDNA	Forward primer	Reverse primer	Origin
<i>Hand2</i>	5'- AAGAGGAAGAAAGAGCTGAATGAGAT-3	5'- CGTTGCTGCTCACTGTGCTT-3'	Galli et al., 2010
<i>Nanog</i>	5'- TTGCTTACAAGGGTCTGCTACT-3	5'- ACTGGTAGAAGAATCAGGGCT-3'	Stadtfeld et al., 2008
<i>Sox2</i>	5'- AGGGCTGGGAGAAAGAAGAG-3	5'- CCGCGATTGTTGTGATTAGT-3'	Stadtfeld et al., 2008

ChIP amplicon	Forward primer	Reverse primer	Origin
ZRS a	5'- TTCGTTTGATGACTAAATGAGGTAAT -3	5'- TCTCCTTATAAATTGCAGGTCTAAAAA -3'	Galli et al., 2010
ZRS b	5'- TGGCATGAGAGAGTTAGTGGTC -3	5'- TCACAGCACTGTGTTCTCCTC -3'	
ZRS c	5'- GTCACAGTTTGAGATTGTCCTGGT -3'	5'- TGAAAGAATCCAATGAACGCTCATG -3'	
ZRS d	5'- GCACATCTGGAATGCATGCAGG -3'	5'- GCTTAAGTTTGTGTTAAGTCACAATC -3'	
ZRS e	5'- CCAAAGGCTCTAGGTTGCTG -3	5'- GCCCTCCCCTAATCTTCC -3'	
<i>Actb</i>	5'- AACTGTGCCATCTACGAGG -3'	5'- CGCTCGTTGCCAATAGTGATG -3'	

Table 10. List of primary antibodies

Antigen		Host	Distributor/Specification	Use
α -Actinin (sarcomeric)	monoclonal	mouse	Sigma (EA-53) A7811	IF
Actin	polyclonal	rabbit	Sigma, A2066	WB
FLAG (M2)	monoclonal	mouse	Sigma, F1804	WB, IF, IP, ChIP
FLAG BioM2-Biotin	monoclonal	mouse	Sigma, F9291	WB
GFP	monoclonal	mouse	Roche 11814460001	WB
GFP-Alexa Fluor-488	polyclonal	rabbit	Invitrogen, A-21311	IF
Gli3 (N-ter)	monoclonal	mouse	Genentech (6F5)	WB
Hand2 (N-ter)	polyclonal	goat	Santa Cruz (M-19) sc-9409	WB, IF
Isl1	monoclonal	mouse	DSHB (40.2D6, Hybridoma sup.)	IF
Ki67	polyclonal	rabbit	Millipore AB9260	IF
MHC (sarcomeric)	monoclonal	mouse	DSHB (MF20)	IF
Sox9	polyclonal	rabbit	Millipore AB5535	IF
Vinculin	monoclonal	mouse	Sigma V9131	WB
β -Galactosidase	monoclonal	mouse	DSHB (40-1a)	IF

Table 11. List of secondary antibodies

Antigen	Distributor/Specification	Use
donkey α goat IgG-HRP	Santa Cruz, sc-2020	WB
goat α mouse IgG (H+L) Alexa Fluor-488 F(ab') ₂	Invitrogen, A11017	IF
goat α mouse IgG (H+L) Alexa Fluor-594 F(ab') ₂	Invitrogen, A11020	IF
goat α mouse IgG, HRP conjugate	Millipore, 12-349	WB
goat α rabbit IgG (H+L) Alexa Fluor [®] 594	Invitrogen, A11037	IF
goat α rabbit IgG, HRP conjugate	Millipore, 12-348	WB
Streptavidin-HRP	Jackson, 016-030-084	WB
Anti-Digoxigenin-AP, Fab fragments from sheep	Roche, 11 093 274 910	ISH

Table 12. List of additional reagents

Product	Manufacturer/REF.
HBSS	Gibco, 14175-053
Collagenase D	Roche, 11 088 866 001
DNase	Roche
D-MEM/F12	Gibco, 11039
Pen/Strep	Gibco 15140-122
D-PBS (1X), liquid	Gibco, 14190-144
D-PBS with Mg ²⁺ /Ca ²⁺ (1X), liquid	Gibco 14040-117
RNAlater [®]	Ambion, AM7020
Oligo(dT) ₁₂₋₁₈	Invitrogen, 18418-012
RNaseOUT [™] Ribonuclease Inhibitor	Invitrogen, 10777-019
SuperScript [™] III Reverse Transcriptase	Invitrogen, 18080-044
iQ [™] SYBR [®] Green Supermix	Bio-Rad, 170-8882
Complete Mini Protease Inhibitor Cocktail tablets (10x)	Roche, 11 836 153 001
Complete Mini Protease Inhibitor Cocktail tablets (50x)	Roche, 04 693 116 001
Ribonuclease A (from bovine pancreas)	Sigma, R4642
Proteinase K (from Tritirachium album)	Merck, 124568
30% Acrylamide/Bis Solution, 29:1, 500 ml	Bio-Rad, 161-0156
Pefabloc SC (AEBSF)	Roche, 11 585 916 001
BCA Protein Assay Kit	Thermo Scientific Pierce, 23250
Visualizer [™] Western Blot Detection Kit, Rabbit	Millipore (upstate), 64-202
SuperSignal [®] West Pico Chemiluminescent Substrate	Thermo Scientific Pierce, 34087
Kodak BioMax MR films	Sigma, 8070 1302
Amersham Hyperfilm [™] ECL	GE Healthcare, 28-9068-37
Albumin from bovine serum	Sigma, A3059-10G
Dynabeads [®] Protein G	Invitrogen, 100.03D
36.5% formaldehyde	Sigma,
N-Lauroylsarcosine sodium salt	Sigma, L9150
Expand High Fidelity ^{PLUS} PCR System	Roche, 03 300 226 001
T4 DNA Ligase	NEB, M0202
PCR DIG Probe Synthesis Kit	Roche, 11 636 090 910
Blocking Reagent (for Southern Blot)	Roche, 1 096 176
CDP Star	Roche, 12 041 677 001
Alcian Blue 8GX	Sigma, A3157
Alizarin Red	Sigma A5533
BCI. Blocking Powder	Boehringer, 1096176
Yeast RNA	Sigma, R8759
Heparin	Sigma H5515
BM Purple AP Substrate precipitating	Roche, 11 442 074 001

Table 13. List of specific materials

Product	Manufacturer/REF.
Nylon membranes, positively charged	Roche (Boehringer Mannheim), 1 417 240
Immobilon-P transfer membrane	Millipore, IPV00010
ibidi μ -slide 8 well	Ibidi, 80826
1.5ml conical screw cap micro tube	Sarstedt, 72.692.005
2ml conical screw cap micro tube	Sarstedt, 72.694.006
Cell Scraper, 25cm (1.7cm blade)	Sarstedt, 83.1830
Hard-Shell [®] Thin-Wall 96-Well Skirted PCR Plates	Bio-Rad, HSP-9601
BioSphere Tips	Sarstedt, 70.1186.200
Tissue Grind Pestle LC 2ml (douncer pestle A)	Kimble Chase (Gerresheimer), 885301-0002
Tissue Grind Pestle SC 2ml (douncer pestle B)	Kimble Chase (Gerresheimer), 885302-0002
Tissue Grind Tube Size 2ml (douncer glass tube)	Kimble Chase (Gerresheimer), 885303-0002
Micro tip 3,2mm (for 13mm horn)	Branson 101-148-062, VWR 142-3746

8. Acknowledgements

I'm deeply indebted to Rolf Zeller and want to thank him first of all for letting me do a PhD thesis in his lab. Thank you for the great supervision, the teaching and crucial scientific input. I am grateful for the excellent scientific and technical help and all the inspiring suggestions. Thanks for the possibilities and support in using state-of-the-art techniques. And thank you for your great scientific way of thinking and enthusiasm which is a pure source of motivation.

In particular, I want to thank Javier Lopez-Rios for his outstanding supervision and for being a very good friend. Thank you for the excellent training lessons and the patience during all these years. Thanks for your stimulating discussions and great scientific knowledge. I'm very grateful for all the extremely exciting science we have experienced. You were "indispensable" all along my PhD - with the exception of a "timeout" after curling when we planned the first dRMCE.

I'm incredibly grateful to my friend Antonella Galli who provided great support and helpful expert advice, above all in the ES room, in picking and expanding ES clones.

Many thanks to Bill Skarnes and Barry Rosen from "The Wellcome Trust Sanger Institute" in Hinxton for their support in making dRMCE compatible to thousands of alleles.

I am very thankful to Daniela Klewe-Nebenius and Thomas Hennek from the Transgenic Mouse Core Facility of the University of Basel for generating the chimeric mice for us.

Special thanks go to Angelika Offinger and Cornelia Meyer-Sägesser who did an outstanding job in taking care about the mice.

I am indebted to Christian Beisel of the Laboratory of Quantitative Genomics (D-BSSE, ETHZ) for answering crucial questions with regards to ChIP-seq, processing our samples for deep sequencing and providing an initial analysis of datasets.

I want to thank Ina Nissen for the library preparations and Manuel Kohler for the alignment and the basic analysis of the ChIP-seq datasets.

Many thanks to Markus Affolter for the interesting seminars and discussions and for doing the Koreferat and being part of the thesis committee.

I'm indebted to Antoine Peters for taking part in the thesis committee and the exam.

Special thanks to Dimitri Robay for being an excellent neighbour and for great discussions and advice.

Thanks go to Pascal Lorentz for the introduction into confocal microscopy and patience in answering technical questions.

My special thanks go to Dario Speziale who is a great collaborator and friend.

I'm very thankful to Isabelle Ginez for the preparation of nice sections.

I want to thank Simone Probst, Alexandre Gonçalves, Jean-Denis Benazet and Alexandra Schauerte for interesting discussions, technical support and excellent lab outings.

Thanks to Frédéric Laurent for his scientific enthusiasm and for using dRMCE.

I am grateful to Aimée Zuniga, Chris Müller, Gretel Nusspaumer, Ashleigh Nugent, Fabia Imhof, Emanuele Pignatti, Paola Valdivieso, Erkan Ünal, Catherine Vaillant, Sumit Jaiswal, Adrian Hermann, Sandro Nuciforo and Patric Schlenker for interesting discussions, support and a great atmosphere in the lab.

Last but not least, I want to thank Susanne, my family and all my friends who have supported me. I am deeply grateful to my family for the outstanding support and the interest in what I'm doing. And thank you, Susanne, for your enthusiasm, patience, realism, support in assembling this thesis and everything else.

9. References

- Abe, M., Michikami, I., Fukushi, T., Abe, A., Maeda, Y., Ooshima, T., and Wakisaka, S. (2010). Hand2 regulates chondrogenesis in vitro and in vivo. *Bone* 46, 1359-1368.
- Agarwal, P., Wylie, J.N., Galceran, J., Arkhitko, O., Li, C., Deng, C., Grosschedl, R., and Bruneau, B.G. (2003). Tbx5 is essential for forelimb bud initiation following patterning of the limb field in the mouse embryo. *Development (Cambridge, England)* 130, 623-633.
- Agulnik, S.I., Garvey, N., Hancock, S., Ruvinsky, I., Chapman, D.L., Agulnik, I., Bollag, R., Papaioannou, V., and Silver, L.M. (1996). Evolution of mouse T-box genes by tandem duplication and cluster dispersion. *Genetics* 144, 249-254.
- Ahn, K., Mishina, Y., Hanks, M.C., Behringer, R.R., and Crenshaw, E.B., 3rd (2001). BMPR-IA signaling is required for the formation of the apical ectodermal ridge and dorsal-ventral patterning of the limb. *Development (Cambridge, England)* 128, 4449-4461.
- Ahn, S., and Joyner, A.L. (2004). Dynamic changes in the response of cells to positive hedgehog signaling during mouse limb patterning. *Cell* 118, 505-516.
- Aiyer, A.R., Honarpour, N., Herz, J., and Srivastava, D. (2005). Loss of Apaf-1 leads to partial rescue of the HAND2-null phenotype. *Dev Biol* 278, 155-162.
- Akiyama, H., Chaboissier, M.C., Martin, J.F., Schedl, A., and de Crombrughe, B. (2002). The transcription factor Sox9 has essential roles in successive steps of the chondrocyte differentiation pathway and is required for expression of Sox5 and Sox6. *Genes & development* 16, 2813-2828.
- Amano, T., Sagai, T., Tanabe, H., Mizushina, Y., Nakazawa, H., and Shiroishi, T. (2009). Chromosomal dynamics at the Shh locus: limb bud-specific differential regulation of competence and active transcription. *Dev Cell* 16, 47-57.
- Anastassiadis, K., Fu, J., Patsch, C., Hu, S., Weidlich, S., Duerschke, K., Buchholz, F., Edenhofer, F., and Stewart, A.F. (2009). Dre recombinase, like Cre, is a highly efficient site-specific recombinase in *E. coli*, mammalian cells and mice. *Dis Model Mech* 2, 508-515.
- Ashburner, M., Ball, C.A., Blake, J.A., Botstein, D., Butler, H., Cherry, J.M., Davis, A.P., Dolinski, K., Dwight, S.S., Eppig, J.T., *et al.* (2000). Gene ontology: tool for the unification of biology. The Gene Ontology Consortium. *Nature genetics* 25, 25-29.
- Bailey, T.L., Williams, N., Misleh, C., and Li, W.W. (2006). MEME: discovering and analyzing DNA and protein sequence motifs. *Nucleic Acids Res* 34, W369-373.
- Bandyopadhyay, A., Tsuji, K., Cox, K., Harfe, B.D., Rosen, V., and Tabin, C.J. (2006). Genetic Analysis of the Roles of BMP2, BMP4, and BMP7 in Limb Patterning and Skeletogenesis. *PLoS Genet* 2, e216.
- Barnes, R.M., and Firulli, A.B. (2009). A twist of insight - the role of Twist-family bHLH factors in development. *Int J Dev Biol* 53, 909-924.
- Barnes, R.M., Firulli, B.A., VanDusen, N.J., Morikawa, Y., Conway, S.J., Cserjesi, P., Vincentz, J.W., and Firulli, A.B. (2011). Hand2 loss-of-function in Hand1-expressing cells reveals distinct roles in epicardial and coronary vessel development. *Circ Res* 108, 940-949.
- Barron, F., Woods, C., Kuhn, K., Bishop, J., Howard, M.J., and Clouthier, D.E. (2011). Downregulation of Dlx5 and Dlx6 expression by Hand2 is essential for initiation of tongue morphogenesis. *Development (Cambridge, England)* 138, 2249-2259.
- Belo, J.A., Leyns, L., Yamada, G., and De Robertis, E.M. (1998). The prechordal midline of the chondrocranium is defective in Goosecoid-1 mouse mutants. *Mechanisms of development* 72, 15-25.

- Belteki, G., Gertsenstein, M., Ow, D.W., and Nagy, A. (2003). Site-specific cassette exchange and germline transmission with mouse ES cells expressing phiC31 integrase. *Nat Biotechnol* 21, 321-324.
- Benazet, J.D., Bischofberger, M., Tiecke, E., Goncalves, A., Martin, J.F., Zuniga, A., Naef, F., and Zeller, R. (2009). A self-regulatory system of interlinked signaling feedback loops controls mouse limb patterning. *Science* 323, 1050-1053.
- Benazet, J.D., and Zeller, R. (2009). Vertebrate limb development: moving from classical morphogen gradients to an integrated 4-dimensional patterning system. *Cold Spring Harb Perspect Biol* 1, a001339.
- Berger, M.F., Badis, G., Gehrke, A.R., Talukder, S., Philippakis, A.A., Pena-Castillo, L., Alleyne, T.M., Mnaimneh, S., Botvinnik, O.B., Chan, E.T., *et al.* (2008). Variation in homeodomain DNA binding revealed by high-resolution analysis of sequence preferences. *Cell* 133, 1266-1276.
- Bethke, B., and Sauer, B. (1997). Segmental genomic replacement by Cre-mediated recombination: genotoxic stress activation of the p53 promoter in single-copy transformants. *Nucleic Acids Res* 25, 2828-2834.
- Bhattacharya, S., Macdonald, S.T., and Farthing, C.R. (2006). Molecular mechanisms controlling the coupled development of myocardium and coronary vasculature. *Clin Sci (Lond)* 111, 35-46.
- Bibel, M., Richter, J., Lacroix, E., and Barde, Y.A. (2007). Generation of a defined and uniform population of CNS progenitors and neurons from mouse embryonic stem cells. *Nat Protoc* 2, 1034-1043.
- Biben, C., and Harvey, R.P. (1997). Homeodomain factor Nkx2-5 controls left/right asymmetric expression of bHLH gene eHand during murine heart development. *Genes & Development* 11, 1357-1369.
- Blow, M.J., McCulley, D.J., Li, Z., Zhang, T., Akiyama, J.A., Holt, A., Plajzer-Frick, I., Shoukry, M., Wright, C., Chen, F., *et al.* (2010). ChIP-Seq identification of weakly conserved heart enhancers. *Nature genetics* 42, 806-810.
- Boehm, B., Westerberg, H., Lesnicar-Pucko, G., Raja, S., Rautschka, M., Cotterell, J., Swoger, J., and Sharpe, J. (2010). The role of spatially controlled cell proliferation in limb bud morphogenesis. *PLoS Biol* 8, e1000420.
- Boheler, K.R., Czyz, J., Tweedie, D., Yang, H.T., Anisimov, S.V., and Wobus, A.M. (2002). Differentiation of pluripotent embryonic stem cells into cardiomyocytes. *Circ Res* 91, 189-201.
- Branda, C.S., and Dymecki, S.M. (2004). Talking about a revolution: The impact of site-specific recombinases on genetic analyses in mice. *Developmental cell* 6, 7-28.
- Bruneau, B.G., Bao, Z.Z., Tanaka, M., Schott, J.J., Izumo, S., Cepko, C.L., Seidman, J.G., and Seidman, C.E. (2000). Cardiac expression of the ventricle-specific homeobox gene *Irx4* is modulated by Nkx2-5 and dHand. *Dev Biol* 217, 266-277.
- Buckingham, M., Meilhac, S., and Zaffran, S. (2005). Building the mammalian heart from two sources of myocardial cells. *Nature reviews Genetics* 6, 826-835.
- Buscher, D., Bosse, B., Heymer, J., and Ruther, U. (1997). Evidence for genetic control of Sonic hedgehog by Gli3 in mouse limb development. *Mech Dev* 62, 175-182.
- Capecchi, M.R. (1989). Altering the genome by homologous recombination. *Science* 244, 1288-1292.
- Capellini, T.D., Di Giacomo, G., Salsi, V., Brendolan, A., Ferretti, E., Srivastava, D., Zappavigna, V., and Selleri, L. (2006). Pbx1/Pbx2 requirement for distal limb patterning is mediated by the hierarchical control of Hox gene spatial distribution and Shh expression. *Development (Cambridge, England)* 133, 2263-2273.
- Carroll, S.B. (2008). Evo-devo and an expanding evolutionary synthesis: a genetic theory of morphological evolution. *Cell* 134, 25-36.

- Chapman, D.L., Garvey, N., Hancock, S., Alexiou, M., Agulnik, S.I., Gibson-Brown, J.J., Cebra-Thomas, J., Bollag, R.J., Silver, L.M., and Papaioannou, V.E. (1996). Expression of the T-box family genes, Tbx1-Tbx5, during early mouse development. *Dev Dyn* 206, 379-390.
- Charite, J., McFadden, D.G., Merlo, G., Levi, G., Clouthier, D.E., Yanagisawa, M., Richardson, J.A., and Olson, E.N. (2001). Role of Dlx6 in regulation of an endothelin-1-dependent, dHAND branchial arch enhancer. *Genes & development* 15, 3039-3049.
- Charité, J., McFadden, D.G., and Olson, E.N. (2000). The bHLH transcription factor dHAND controls *Sonic hedgehog* expression and establishment of the zone of polarizing activity during limb development. *Development (Cambridge, England)* 127, 2461-2470.
- Cheeseman, I.M., and Desai, A. (2005). A combined approach for the localization and tandem affinity purification of protein complexes from metazoans. *Sci STKE* 2005, pl1.
- Chen, H., Lun, Y., Ovchinnikov, D., Kokubo, H., Oberg, K.C., Pepicelli, C.V., Gan, L., Lee, B., and Johnson, R.L. (1998). Limb and kidney defects in Lmx1b mutant mice suggest an involvement of LMX1B in human nail patella syndrome. *Nature genetics* 19, 51-55.
- Chen, M.H., Li, Y.J., Kawakami, T., Xu, S.M., and Chuang, P.T. (2004). Palmitoylation is required for the production of a soluble multimeric Hedgehog protein complex and long-range signaling in vertebrates. *Genes Dev* 18, 641-659.
- Chiang, C., Litingtung, Y., Harris, M.P., Simandl, B.K., Li, Y., Beachy, P.A., and Fallon, J.F. (2001). Manifestation of the Limb Prepattern: Limb Development in the Absence of Sonic Hedgehog Function. *Dev Biol* 236, 421-435.
- Chiang, C., Litingtung, Y., Lee, E., Young, K.E., Corden, J.L., Westphal, H., and Beachy, P.A. (1996). Cyclopia and defective axial patterning in mice lacking *Sonic hedgehog* gene function. *Nature* 383, 407-413.
- Chu, G.C., Dunn, N.R., Anderson, D.C., Oxburgh, L., and Robertson, E.J. (2004). Differential requirements for Smad4 in TGFbeta-dependent patterning of the early mouse embryo. *Development (Cambridge, England)* 131, 3501-3512.
- Clark, A.J., Bissinger, P., Bullock, D.W., Damak, S., Wallace, R., Whitelaw, C.B., and Yull, F. (1994). Chromosomal position effects and the modulation of transgene expression. *Reprod Fertil Dev* 6, 589-598.
- Cohn, M.J., and Tickle, C. (1999). Developmental basis of limblessness and axial patterning in snakes. *Nature* 399, 474-479.
- Collins, F.S., Rossant, J., and Wurst, W. (2007). A mouse for all reasons. *Cell* 128, 9-13.
- Conway, S.J., Firulli, B., and Firulli, A.B. (2010). A bHLH code for cardiac morphogenesis. *Pediatr Cardiol* 31, 318-324.
- Cranston, A., Dong, C., Howcroft, J., and Clark, A.J. (2001). Chromosomal sequences flanking an efficiently expressed transgene dramatically enhance its expression. *Gene* 269, 217-225.
- Creyghton, M.P., Cheng, A.W., Welstead, G.G., Kooistra, T., Carey, B.W., Steine, E.J., Hanna, J., Lodato, M.A., Frampton, G.M., Sharp, P.A., *et al.* (2010). Histone H3K27ac separates active from poised enhancers and predicts developmental state. *Proc Natl Acad Sci U S A* 107, 21931-21936.
- Dai, Y.S., and Cserjesi, P. (2002). The basic helix-loop-helix factor, HAND2, functions as a transcriptional activator by binding to E-boxes as a heterodimer. *The Journal of biological chemistry* 277, 12604-12612.
- Dai, Y.S., Hao, J., Bonin, C., Morikawa, Y., and Cserjesi, P. (2004). JAB1 enhances HAND2 transcriptional activity by regulating HAND2 DNA binding. *J Neurosci Res* 76, 613-622.
- Darabi, R., Gehlbach, K., Bachoo, R.M., Kamath, S., Osawa, M., Kamm, K.E., Kyba, M., and Perlingeiro, R.C. (2008). Functional skeletal muscle regeneration from differentiating embryonic stem cells. *Nat Med* 14, 134-143.

- Davenport, T.G., Jerome-Majewska, L.A., and Papaioannou, V.E. (2003). Mammary gland, limb and yolk sac defects in mice lacking Tbx3, the gene mutated in human ulnar mammary syndrome. *Development (Cambridge, England)* 130, 2263-2273.
- Davidson, D.R., Crawley, A., Hill, R.E., and Tickle, C. (1991). Position-dependent expression of two related homeobox genes in developing vertebrate limbs. *Nature* 352, 429-431.
- de Boer, E., Rodriguez, P., Bonte, E., Krijgsveld, J., Katsantoni, E., Heck, A., Grosveld, F., and Strouboulis, J. (2003). Efficient biotinylation and single-step purification of tagged transcription factors in mammalian cells and transgenic mice. *Proc Natl Acad Sci U S A* 100, 7480-7485.
- Deschamps, J. (2004). *Developmental Biology*. Hox genes in the limb: a play in two acts. *Science* 304, 1669-1672.
- Dollé, P., Izpisua-Belmonte, J.C., Falkenstein, H., Renucci, A., and Duboule, D. (1989). Coordinate expression of the murine Hox-5 complex homeobox-containing genes during limb pattern formation. *Nature* 342, 767-772.
- Domian, I.J., Chiravuri, M., van der Meer, P., Feinberg, A.W., Shi, X., Shao, Y., Wu, S.M., Parker, K.K., and Chien, K.R. (2009). Generation of functional ventricular heart muscle from mouse ventricular progenitor cells. *Science* 326, 426-429.
- Donnelly, M.L., Luke, G., Mehrotra, A., Li, X., Hughes, L.E., Gani, D., and Ryan, M.D. (2001). Analysis of the aphthovirus 2A/2B polyprotein 'cleavage' mechanism indicates not a proteolytic reaction, but a novel translational effect: a putative ribosomal 'skip'. *J Gen Virol* 82, 1013-1025.
- Dreyer, S.D., Zhou, G., Baldini, A., Winterpacht, A., Zabel, B., Cole, W., Johnson, R.L., and Lee, B. (1998). Mutations in LMX1B cause abnormal skeletal patterning and renal dysplasia in nail patella syndrome. *Nature genetics* 19, 47-50.
- Duboc, V., and Logan, M.P. (2011). Regulation of limb bud initiation and limb-type morphology. *Dev Dyn* 240, 1017-1027.
- Einhauer, A., and Jungbauer, A. (2001). The FLAG peptide, a versatile fusion tag for the purification of recombinant proteins. *J Biochem Biophys Methods* 49, 455-465.
- Evans, T. (2008). Embryonic Stem Cells as a Model for Cardiac Development and Disease. *Drug Discov Today Dis Models* 5, 147-155.
- Fei, T., Xia, K., Li, Z., Zhou, B., Zhu, S., Chen, H., Zhang, J., Chen, Z., Xiao, H., Han, J.D., *et al.* (2010). Genome-wide mapping of SMAD target genes reveals the role of BMP signaling in embryonic stem cell fate determination. *Genome Res* 20, 36-44.
- Feng, Y.Q., Seibler, J., Alami, R., Eisen, A., Westerman, K.A., Leboulch, P., Fiering, S., and Bouhassira, E.E. (1999). Site-specific chromosomal integration in mammalian cells: highly efficient CRE recombinase-mediated cassette exchange. *J Mol Biol* 292, 779-785.
- Fernandez-Teran, M., Piedra, M.E., Kathiriya, I.S., Srivastava, D., Rodriguez-Rey, J.C., and Ros, M.A. (2000a). Role of dHAND in the anterior-posterior polarization of the limb bud: implications for the Sonic hedgehog pathway. *Development (Cambridge, England)* 127, 2133-2142.
- Fernandez-Teran, M., Piedra, M.E., Kathiriya, I.S., Srivastava, D., Rodriguez-Rey, J.C., and Ros, M.A. (2000b). Role of dHAND in the anterior-posterior polarization of the limb bud: implications for the Sonic hedgehog pathway. *Development (Cambridge, England)* 127, 2133-2142.
- Firulli, A.B. (2003). A HANDful of questions: the molecular biology of the heart and neural crest derivatives (HAND)-subclass of basic helix-loop-helix transcription factors. *Gene* 312, 27-40.
- Firulli, B.A., Krawchuk, D., Centonze, V.E., Vargesson, N., Virshup, D.M., Conway, S.J., Cserjesi, P., Laufer, E., and Firulli, A.B. (2005). Altered Twist1 and Hand2 dimerization is associated with Saethre-Chotzen syndrome and limb abnormalities. *Nat Genet* 37, 373-381.

- Firulli, B.A., Redick, B.A., Conway, S.J., and Firulli, A.B. (2007). Mutations within helix I of Twist1 result in distinct limb defects and variation of DNA binding affinities. *The Journal of biological chemistry* 282, 27536-27546.
- Flora, A., Klisch, T.J., Schuster, G., and Zoghbi, H.Y. (2009). Deletion of Atoh1 disrupts Sonic Hedgehog signaling in the developing cerebellum and prevents medulloblastoma. *Science* 326, 1424-1427.
- Fu, X., Kiyama, T., Li, R., Russell, M., Klein, W.H., and Mu, X. (2009). Epitope-tagging Math5 and Pou4f2: new tools to study retinal ganglion cell development in the mouse. *Dev Dyn* 238, 2309-2317.
- Funato, N., Chapman, S.L., McKee, M.D., Funato, H., Morris, J.A., Shelton, J.M., Richardson, J.A., and Yanagisawa, H. (2009). Hand2 controls osteoblast differentiation in the branchial arch by inhibiting DNA binding of Runx2. *Development (Cambridge, England)* 136, 615-625.
- Galli, A., Robay, D., Osterwalder, M., Bao, X., Benazet, J.D., Tariq, M., Paro, R., Mackem, S., and Zeller, R. (2010). Distinct roles of Hand2 in initiating polarity and posterior Shh expression during the onset of mouse limb bud development. *PLoS Genet* 6, e1000901.
- Garavito-Aguilar, Z.V., Riley, H.E., and Yelon, D. (2010). Hand2 ensures an appropriate environment for cardiac fusion by limiting Fibronectin function. *Development (Cambridge, England)* 137, 3215-3220.
- Gaunt, S.J., Blum, M., and De Robertis, E.M. (1993). Expression of the mouse goosecoid gene during mid-embryogenesis may mark mesenchymal cell lineages in the developing head, limbs and body wall. *Development (Cambridge, England)* 117, 769-778.
- Gibson-Brown, J.J., Agulnik, S.I., Chapman, D.L., Alexiou, M., Garvey, N., Silver, L.M., and Papaioannou, V.E. (1996). Evidence of a role for T-box genes in the evolution of limb morphogenesis and the specification of forelimb/hindlimb identity. *Mechanisms of development* 56, 93-101.
- Goetz, S.C., and Anderson, K.V. (2010). The primary cilium: a signalling centre during vertebrate development. *Nature reviews Genetics* 11, 331-344.
- Gonzalez, F., Duboule, D., and Spitz, F. (2007). Transgenic analysis of Hoxd gene regulation during digit development. *Dev Biol* 306, 847-859.
- Gottlieb, P.D., Pierce, S.A., Sims, R.J., Yamagishi, H., Weihe, E.K., Harriss, J.V., Maika, S.D., Kuziel, W.A., King, H.L., Olson, E.N., *et al.* (2002). Bop encodes a muscle-restricted protein containing MYND and SET domains and is essential for cardiac differentiation and morphogenesis. *Nature genetics* 31, 25-32.
- Graham, V., Khudyakov, J., Ellis, P., and Pevny, L. (2003). SOX2 functions to maintain neural progenitor identity. *Neuron* 39, 749-765.
- Gray, P.A., Fu, H., Luo, P., Zhao, Q., Yu, J., Ferrari, A., Tenzen, T., Yuk, D.I., Tsung, E.F., Cai, Z., *et al.* (2004). Mouse brain organization revealed through direct genome-scale TF expression analysis. *Science* 306, 2255-2257.
- Gu, H., Marth, J.D., Orban, P.C., Mossmann, H., and Rajewsky, K. (1994). Deletion of a DNA polymerase beta gene segment in T cells using cell type-specific gene targeting. *Science* 265, 103-106.
- Gubbay, J., Collignon, J., Koopman, P., Capel, B., Economou, A., Munsterberg, A., Vivian, N., Goodfellow, P., and Lovell-Badge, R. (1990). A gene mapping to the sex-determining region of the mouse Y chromosome is a member of a novel family of embryonically expressed genes. *Nature* 346, 245-250.
- Gupta, S., Stamatoyannopoulos, J.A., Bailey, T.L., and Noble, W.S. (2007). Quantifying similarity between motifs. *Genome Biol* 8, R24.
- Hao, J., Daleo, M.A., Murphy, C.K., Yu, P.B., Ho, J.N., Hu, J., Peterson, R.T., Hatzopoulos, A.K., and Hong, C.C. (2008). Dorsomorphin, a selective small molecule inhibitor of BMP signaling, promotes cardiomyogenesis in embryonic stem cells. *PLoS One* 3, e2904.

- Harbison, C.T., Gordon, D.B., Lee, T.I., Rinaldi, N.J., Macisaac, K.D., Danford, T.W., Hannett, N.M., Tagne, J.B., Reynolds, D.B., Yoo, J., *et al.* (2004). Transcriptional regulatory code of a eukaryotic genome. *Nature* **431**, 99-104.
- Harfe, B.D., Scherz, P.J., Nissim, S., Tian, H., McMahon, A.P., and Tabin, C.J. (2004). Evidence for an expansion-based temporal Shh gradient in specifying vertebrate digit identities. *Cell* **118**, 517-528.
- Holler, K.L., Hendershot, T.J., Troy, S.E., Vincentz, J.W., Firulli, A.B., and Howard, M.J. (2010). Targeted deletion of Hand2 in cardiac neural crest-derived cells influences cardiac gene expression and outflow tract development. *Dev Biol* **341**, 291-304.
- Hopp, T.P., Prickett, K.S., Price, V.L., Libby, R.T., March, C.J., Pat Cerretti, D., Urdal, D.L., and Conlon, P.J. (1988). A Short Polypeptide Marker Sequence Useful for Recombinant Protein Identification and Purification. *Nat Biotech* **6**, 1204-1210.
- Horsthuis, T., Buermans, H.P., Brons, J.F., Verkerk, A.O., Bakker, M.L., Wakker, V., Clout, D.E., Moorman, A.F., t Hoen, P.A., and Christoffels, V.M. (2009). Gene expression profiling of the forming atrioventricular node using a novel tbx3-based node-specific transgenic reporter. *Circ Res* **105**, 61-69.
- Howard, M.J., Stanke, M., Schneider, C., Wu, X., and Rohrer, H. (2000). The transcription factor dHAND is a downstream effector of BMPs in sympathetic neuron specification. *Development* (Cambridge, England) **127**, 4073-4081.
- Hui, C., and Joyner, A. (1993). A mouse model of greig cephalopolysyndactyly syndrome: the extra-toesJ mutation contains an intragenic deletion of the Gli3 gene. *Nat-Genet* **3**, 241-246.
- Ianakiev, P., van Baren, M.J., Daly, M.J., Toledo, S.P., Cavalcanti, M.G., Neto, J.C., Silveira, E.L., Freire-Maia, A., Heutink, P., Kilpatrick, M.W., *et al.* (2001). Acheiropodia is caused by a genomic deletion in C7orf2, the human orthologue of the Lmbr1 gene. *Am J Hum Genet* **68**, 38-45.
- Jayaram, M. (1985). Two-micrometer circle site-specific recombination: the minimal substrate and the possible role of flanking sequences. *Proc Natl Acad Sci U S A* **82**, 5875-5879.
- Kanda, T., Sullivan, K.F., and Wahl, G.M. (1998). Histone-GFP fusion protein enables sensitive analysis of chromosome dynamics in living mammalian cells. *Curr Biol* **8**, 377-385.
- Khokha, M.K., Hsu, D., Brunet, L.J., Dionne, M.S., and Harland, R.M. (2003). Gremlin is the BMP antagonist required for maintenance of Shh and Fgf signals during limb patterning. *Nat Genet* **34**, 303-307.
- Kim, J., Chu, J., Shen, X., Wang, J., and Orkin, S.H. (2008). An extended transcriptional network for pluripotency of embryonic stem cells. *Cell* **132**, 1049-1061.
- Kim, T.H., Barrera, L.O., and Ren, B. (2007). ChIP-chip for genome-wide analysis of protein binding in mammalian cells. *Curr Protoc Mol Biol Chapter 21*, Unit 21 13.
- Kirchhoff, S., Kim, J.S., Hagendorff, A., Thonnissen, E., Kruger, O., Lamers, W.H., and Willecke, K. (2000). Abnormal cardiac conduction and morphogenesis in connexin40 and connexin43 double-deficient mice. *Circ Res* **87**, 399-405.
- Kmita, M., Tarchini, B., Zakany, J., Logan, M., Tabin, C.J., and Duboule, D. (2005). Early developmental arrest of mammalian limbs lacking HoxA/HoxD gene function. *Nature* **435**, 1113-1116.
- Kolodziej, K.E., Pourfarzad, F., de Boer, E., Krpic, S., Grosveld, F., and Strouboulis, J. (2009). Optimal use of tandem biotin and V5 tags in ChIP assays. *BMC Mol Biol* **10**, 6.
- Kouskoff, V., Lacaud, G., Schwantz, S., Fehling, H.J., and Keller, G. (2005). Sequential development of hematopoietic and cardiac mesoderm during embryonic stem cell differentiation. *Proc Natl Acad Sci U S A* **102**, 13170-13175.
- Kulman, J.D., Satake, M., and Harris, J.E. (2007). A versatile system for site-specific enzymatic biotinylation and regulated expression of proteins in cultured mammalian cells. *Protein Expr Purif* **52**, 320-328.

- Kurosawa, H. (2007). Methods for inducing embryoid body formation: in vitro differentiation system of embryonic stem cells. *J Biosci Bioeng* 103, 389-398.
- Kurosawa, H., Imamura, T., Koike, M., Sasaki, K., and Amano, Y. (2003). A simple method for forming embryoid body from mouse embryonic stem cells. *J Biosci Bioeng* 96, 409-411.
- Laufer, E., Nelson, C.E., Johnson, R.L., Morgan, B.A., and Tabin, C. (1994). Sonic hedgehog and Fgf-4 act through a signaling cascade and feedback loop to integrate growth and patterning of the developing limb bud. *Cell* 79, 993-1003.
- Laugwitz, K.L., Moretti, A., Caron, L., Nakano, A., and Chien, K.R. (2008). Islet1 cardiovascular progenitors: a single source for heart lineages? *Development (Cambridge, England)* 135, 193-205.
- Lauth, M., Spreafico, F., Dethleffsen, K., and Meyer, M. (2002). Stable and efficient cassette exchange under non-selectable conditions by combined use of two site-specific recombinases. *Nucleic Acids Res* 30, e115.
- Lee, T.I., Rinaldi, N.J., Robert, F., Odom, D.T., Bar-Joseph, Z., Gerber, G.K., Hannett, N.M., Harbison, C.T., Thompson, C.M., Simon, I., *et al.* (2002). Transcriptional regulatory networks in *Saccharomyces cerevisiae*. *Science* 298, 799-804.
- Lee, W.J., Kraus, P., and Lufkin, T. (2011). Endogenous tagging of the murine transcription factor Sox5 with hemagglutinin for functional studies. *Transgenic Res.*
- Leleu, M., Lefebvre, G., and Rougemont, J. (2010). Processing and analyzing ChIP-seq data: from short reads to regulatory interactions. *Brief Funct Genomics* 9, 466-476.
- Lettice, L.A., Heaney, S.J., Purdie, L.A., Li, L., de Beer, P., Oostra, B.A., Goode, D., Elgar, G., Hill, R.E., and de Graaff, E. (2003). A long-range Shh enhancer regulates expression in the developing limb and fin and is associated with preaxial polydactyly. *Human molecular genetics* 12, 1725-1735.
- Lettice, L.A., Hill, A.E., Devenney, P.S., and Hill, R.E. (2008). Point mutations in a distant sonic hedgehog cis-regulator generate a variable regulatory output responsible for preaxial polydactyly. *Human molecular genetics* 17, 978-985.
- Lettice, L.A., Horikoshi, T., Heaney, S.J., Van Baren, M.J., Van Der Linde, H.C., Breedveld, G.J., Joesse, M., Akarsu, N., Oostra, B.A., Endo, N., *et al.* (2002). Disruption of a long-range cis-acting regulator for Shh causes preaxial polydactyly. *Proc Natl Acad Sci U S A* 99, 7548-7553.
- Lewandoski, M., Sun, X., and Martin, G.R. (2000). Fgf8 signalling from the AER is essential for normal limb development. *Nat Genet* 26, 460-463.
- Li, Q., Kannan, A., DeMayo, F.J., Lydon, J.P., Cooke, P.S., Yamagishi, H., Srivastava, D., Bagchi, M.K., and Bagchi, I.C. (2011). The antiproliferative action of progesterone in uterine epithelium is mediated by Hand2. *Science* 331, 912-916.
- Li, Y., Zhang, H., Litingtung, Y., and Chiang, C. (2006). Cholesterol modification restricts the spread of Shh gradient in the limb bud. *Proc Natl Acad Sci U S A* 103, 6548-6553.
- Litingtung, Y., Dahn, R.D., Li, Y., Fallon, J.F., and Chiang, C. (2002). Shh and Gli3 are dispensable for limb skeleton formation but regulate digit number and identity. *Nature* 418, 979-983.
- Lopez-Rios, J., Speziale, D., Robay, D., Scotti, M., Osterwalder, M., Nusspaumer, G., Galli, A., Holländer, G., Kmita, M., and Zeller, R. (2012). GLI3 Constrains Digit Number by Controlling Both Progenitor Proliferation and BMP-dependent Exit to Chondrogenesis. *Dev Cell (in press)*.
- Lyons, I., Parsons, L.M., Hartley, L., Li, R., Andrews, J.E., Robb, L., and Harvey, R.P. (1995). Myogenic and morphogenetic defects in the heart tubes of murine embryos lacking the homeo box gene Nkx2-5. *Genes & development* 9, 1654-1666.
- Machanick, P., and Bailey, T.L. (2011). MEME-ChIP: motif analysis of large DNA datasets. *Bioinformatics* 27, 1696-1697.

- Mao, J., McGlinn, E., Huang, P., Tabin, C.J., and McMahon, A.P. (2009). Fgf-dependent Etv4/5 activity is required for posterior restriction of Sonic Hedgehog and promoting outgrowth of the vertebrate limb. *Dev Cell* 16, 600-606.
- Mariani, F.V., Ahn, C.P., and Martin, G.R. (2008). Genetic evidence that FGFs have an instructive role in limb proximal-distal patterning. *Nature* 453, 401-405.
- Martin-Puig, S., Wang, Z., and Chien, K.R. (2008). Lives of a heart cell: tracing the origins of cardiac progenitors. *Cell Stem Cell* 2, 320-331.
- Massari, M.E., and Murre, C. (2000). Helix-loop-helix proteins: regulators of transcription in eucaryotic organisms. *Mol Cell Biol* 20, 429-440.
- Massie, C.E., and Mills, I.G. (2008). ChIPping away at gene regulation. *EMBO Rep* 9, 337-343.
- Masuya, H., Sezutsu, H., Sakuraba, Y., Sagai, T., Hosoya, M., Kaneda, H., Miura, I., Kobayashi, K., Sumiyama, K., Shimizu, A., *et al.* (2007). A series of ENU-induced single-base substitutions in a long-range cis-element altering Sonic hedgehog expression in the developing mouse limb bud. *Genomics* 89, 207-214.
- Matise, M.P., and Joyner, A.L. (1999). Gli genes in development and cancer. *Oncogene* 18, 7852-7859.
- McFadden, D.G., Charite, J., Richardson, J.A., Srivastava, D., Firulli, A.B., and Olson, E.N. (2000). A GATA-dependent right ventricular enhancer controls dHAND transcription in the developing heart. *Development (Cambridge, England)* 127, 5331-5341.
- McFadden, D.G., McAnally, J., Richardson, J.A., Charite, J., and Olson, E.N. (2002a). Misexpression of dHAND induces ectopic digits in the developing limb bud in the absence of direct DNA binding. *Development (Cambridge, England)* 129, 3077-3088.
- McFadden, D.G., McAnally, J., Richardson, J.A., Charite, J., and Olson, E.N. (2002b). Misexpression of dHAND induces ectopic digits in the developing limb bud in the absence of direct DNA binding. *Development (Cambridge, England)* 129, 3077-3088.
- McGlinn, E., Richman, J.M., Metzis, V., Town, L., Butterfield, N.C., Wainwright, B.J., and Wicking, C. (2008). Expression of the NET family member Zfp503 is regulated by hedgehog and BMP signaling in the limb. *Dev Dyn* 237, 1172-1182.
- McLean, C.Y., Bristor, D., Hiller, M., Clarke, S.L., Schaar, B.T., Lowe, C.B., Wenger, A.M., and Bejerano, G. (2010). GREAT improves functional interpretation of cis-regulatory regions. *Nat Biotechnol* 28, 495-501.
- Melton, D.W. (1994). Gene targeting in the mouse. *Bioessays* 16, 633-638.
- Menke, D.B., Guenther, C., and Kingsley, D.M. (2008). Dual hindlimb control elements in the Tbx4 gene and region-specific control of bone size in vertebrate limbs. *Development (Cambridge, England)* 135, 2543-2553.
- Mercader, N., Leonardo, E., Piedra, M.E., Martinez, A.C., Ros, M.A., and Torres, M. (2000). Opposing RA and FGF signals control proximodistal vertebrate limb development through regulation of Meis genes. *Development (Cambridge, England)* 127, 3961-3970.
- Metzker, M.L. (2010). Sequencing technologies - the next generation. *Nature reviews Genetics* 11, 31-46.
- Meyers, E.N., Lewandoski, M., and Martin, G.R. (1998). An Fgf8 mutant allelic series generated by Cre- and Flp-mediated recombination. *Nature genetics* 18, 136-141.
- Michos, O., Panman, L., Vintersten, K., Beier, K., Zeller, R., and Zuniga, A. (2004). Gremlin-mediated BMP antagonism induces the epithelial-mesenchymal feedback signaling controlling metanephric kidney and limb organogenesis. *Development (Cambridge, England)* 131, 3401-3410.

Min, H., Danilenko, D.M., Scully, S.A., Bonlon, B., Ring, B.D., Tarpley, J.E., DeRose, M., and Simonet, W.S. (1998). Fgf-10 is required for both limb and lung development and exhibits striking functional similarity to *Drosophila* branchless. *Genes & Development* 12, 3156-3161.

Mishra, L., Derynck, R., and Mishra, B. (2005). Transforming growth factor-beta signaling in stem cells and cancer. *Science* 310, 68-71.

Miyazono, K., and Miyazawa, K. (2002). Id: a target of BMP signaling. *Sci STKE* 2002, pe40.

Mizushima, S., and Nagata, S. (1990). pEF-BOS, a powerful mammalian expression vector. *Nucleic Acids Res* 18, 5322.

Montavon, T., Le Garrec, J.F., Kerszberg, M., and Duboule, D. (2008). Modeling Hox gene regulation in digits: reverse collinearity and the molecular origin of thumbness. *Genes Dev* 22, 346-359.

Montavon, T., Soshnikova, N., Mascrez, B., Joye, E., Thevenet, L., Splinter, E., de Laat, W., Spitz, F., and Duboule, D. (2011). A regulatory archipelago controls Hox genes transcription in digits. *Cell* 147, 1132-1145.

Moretti, A., Caron, L., Nakano, A., Lam, J.T., Bernshausen, A., Chen, Y., Qyang, Y., Bu, L., Sasaki, M., Martin-Puig, S., *et al.* (2006). Multipotent embryonic isl1+ progenitor cells lead to cardiac, smooth muscle, and endothelial cell diversification. *Cell* 127, 1151-1165.

Morikawa, Y., and Cserjesi, P. (2008). Cardiac neural crest expression of Hand2 regulates outflow and second heart field development. *Circ Res* 103, 1422-1429.

Morikawa, Y., D'Autreaux, F., Gershon, M.D., and Cserjesi, P. (2007). Hand2 determines the noradrenergic phenotype in the mouse sympathetic nervous system. *Dev Biol* 307, 114-126.

Morikawa, Y., Dai, Y.S., Hao, J., Bonin, C., Hwang, S., and Cserjesi, P. (2005). The basic helix-loop-helix factor Hand 2 regulates autonomic nervous system development. *Dev Dyn* 234, 613-621.

Mountford, P., Zevnik, B., Duwel, A., Nichols, J., Li, M., Dani, C., Robertson, M., Chambers, I., and Smith, A. (1994). Dicistronic targeting constructs: reporters and modifiers of mammalian gene expression. *Proc Natl Acad Sci U S A* 91, 4303-4307.

Naiche, L.A., Arora, R., Kania, A., Lewandoski, M., and Papaioannou, V.E. (2011). Identity and fate of Tbx4-expressing cells reveal developmental cell fate decisions in the allantois, limb, and external genitalia. *Dev Dyn* 240, 2290-2300.

Naiche, L.A., Harrelson, Z., Kelly, R.G., and Papaioannou, V.E. (2005). T-box genes in vertebrate development. *Annu Rev Genet* 39, 219-239.

Naiche, L.A., and Papaioannou, V.E. (2007). Tbx4 is not required for hindlimb identity or post-bud hindlimb outgrowth. *Development (Cambridge, England)* 134, 93-103.

Niederreither, K., Vermot, J., Schuhbauer, B., Chambon, P., and Dolle, P. (2002). Embryonic retinoic acid synthesis is required for forelimb growth and anteroposterior patterning in the mouse. *Development (Cambridge, England)* 129, 3563-3574.

Nishiyama, A., Xin, L., Sharov, A.A., Thomas, M., Mowrer, G., Meyers, E., Piao, Y., Mehta, S., Yee, S., Nakatake, Y., *et al.* (2009). Uncovering early response of gene regulatory networks in ESCs by systematic induction of transcription factors. *Cell Stem Cell* 5, 420-433.

Nissim, S., Allard, P., Bandyopadhyay, A., Harfe, B.D., and Tabin, C.J. (2007). Characterization of a novel ectodermal signaling center regulating Tbx2 and Shh in the vertebrate limb. *Dev Biol* 304, 9-21.

Nissim, S., Hasso, S.M., Fallon, J.F., and Tabin, C.J. (2006). Regulation of Gremlin expression in the posterior limb bud. *Dev Biol* 299, 12-21.

Niswander, L., Tickle, C., Vogel, A., Booth, I., and Martin, G.R. (1993). FGF-4 replaces the apical ectodermal ridge and directs outgrowth and patterning of the limb. *Cell* 75, 579-587.

- Ohuchi, H., Nakagawa, T., Itoh, N., and Noji, S. (1999). FGF10 can induce Fgf8 expression concomitantly with En1 and R-fng expression in chick limb ectoderm, independent of its dorsoventral specification. *Dev Growth Differ* 41, 665-673.
- Olson, E.N. (2006). Gene regulatory networks in the evolution and development of the heart. *Science* 313, 1922-1927.
- Orlando, V., Strutt, H., and Paro, R. (1997). Analysis of chromatin structure by in vivo formaldehyde cross-linking. *Methods* 11, 205-214.
- Park, P.J. (2009). ChIP-seq: advantages and challenges of a maturing technology. *Nature reviews Genetics* 10, 669-680.
- Pettitt, S.J., Liang, Q., Rairdan, X.Y., Moran, J.L., Prosser, H.M., Beier, D.R., Lloyd, K.C., Bradley, A., and Skarnes, W.C. (2009). Agouti C57BL/6N embryonic stem cells for mouse genetic resources. *Nat Methods* 6, 493-495.
- Poser, I., Sarov, M., Hutchins, J.R., Heriche, J.K., Toyoda, Y., Pozniakovsky, A., Weigl, D., Nitzsche, A., Hegemann, B., Bird, A.W., *et al.* (2008). BAC TransgeneOmics: a high-throughput method for exploration of protein function in mammals. *Nat Methods* 5, 409-415.
- Probst, S., Kraemer, C., Demougin, P., Sheth, R., Martin, G.R., Shiratori, H., Hamada, H., Iber, D., Zeller, R., and Zuniga, A. (2011). SHH propagates distal limb bud development by enhancing CYP26B1-mediated retinoic acid clearance via AER-FGF signalling. *Development (Cambridge, England)* 138, 1913-1923.
- Rajewsky, K. (2007). From a dream to reality. *Eur J Immunol* 37 Suppl 1, S134-137.
- Raymond, C.S., and Soriano, P. (2007). High-efficiency FLP and PhiC31 site-specific recombination in mammalian cells. *PLoS One* 2, e162.
- Redon, R., Ishikawa, S., Fitch, K.R., Feuk, L., Perry, G.H., Andrews, T.D., Fiegler, H., Shapero, M.H., Carson, A.R., Chen, W., *et al.* (2006). Global variation in copy number in the human genome. *Nature* 444, 444-454.
- Rhead, B., Karolchik, D., Kuhn, R.M., Hinrichs, A.S., Zweig, A.S., Fujita, P.A., Diekhans, M., Smith, K.E., Rosenbloom, K.R., Raney, B.J., *et al.* (2010). The UCSC Genome Browser database: update 2010. *Nucleic Acids Res* 38, D613-619.
- Riddle, R.D., Ensini, M., Nelson, C., Tsuchida, T., Jessell, T.M., and Tabin, C. (1995). Induction of the LIM homeobox gene *Lmx1* by WNT7a establishes dorsoventral pattern in the vertebrate limb. *Cell* 83, 631-640.
- Riddle, R.D., Johnson, R.L., Laufer, E., and Tabin, C. (1993). *Sonic hedgehog* mediates the polarizing activity of the ZPA. *Cell* 75, 1401-1416.
- Rozowsky, J., Euskirchen, G., Auerbach, R.K., Zhang, Z.D., Gibson, T., Bjornson, R., Carriero, N., Snyder, M., and Gerstein, M.B. (2009). PeakSeq enables systematic scoring of ChIP-seq experiments relative to controls. *Nat Biotechnol* 27, 66-75.
- Ruest, L.B., Dager, M., Yanagisawa, H., Charite, J., Hammer, R.E., Olson, E.N., Yanagisawa, M., and Clouthier, D.E. (2003). dHAND-Cre transgenic mice reveal specific potential functions of dHAND during craniofacial development. *Dev Biol* 257, 263-277.
- Sagai, T., Hosoya, M., Mizushima, Y., Tamura, M., and Shiroishi, T. (2005). Elimination of a long-range cis-regulatory module causes complete loss of limb-specific Shh expression and truncation of the mouse limb. *Development (Cambridge, England)* 132, 797-803.
- Sagai, T., Masuya, H., Tamura, M., Shimizu, K., Yada, Y., Wakana, S., Gondo, Y., Noda, T., and Shiroishi, T. (2004). Phylogenetic conservation of a limb-specific, cis-acting regulator of Sonic hedgehog (Shh). *Mamm Genome* 15, 23-34.

- Sanz-Ezquerro, J.J., and Tickle, C. (2000). Autoregulation of Shh expression and Shh induction of cell death suggest a mechanism for modulating polarising activity during chick limb development. *Development (Cambridge, England)* 127, 4811-4823.
- Saunders, J.W., Jr, and Gasseling, M.T. (1968). Ectodermal-mesenchymal interactions in the origin of limb symmetry. In *Epithelial-Mesenchymal Interactions*, R. Fleischmeyer, and R.E. Billingham, eds. (Baltimore, Williams and Wilkin), pp. 78-97.
- Schebelle, L., Wolf, C., Stribl, C., Javaheri, T., Schnutgen, F., Ettinger, A., Ivics, Z., Hansen, J., Ruiz, P., von Melchner, H., *et al.* (2010). Efficient conditional and promoter-specific in vivo expression of cDNAs of choice by taking advantage of recombinase-mediated cassette exchange using FIEEx gene traps. *Nucleic Acids Res* 38, e106.
- Scherz, P.J., Harfe, B.D., McMahon, A.P., and Tabin, C.J. (2004). The limb bud Shh-Fgf feedback loop is terminated by expansion of former ZPA cells. *Science* 305, 396-399.
- Schnutgen, F., Ehrmann, F., Poser, I., Hubner, N.C., Hansen, J., Floss, T., deVries, I., Wurst, W., Hyman, A., Mann, M., *et al.* (2011). Resources for proteomics in mouse embryonic stem cells. *Nat Methods* 8, 103-104.
- Seibler, J., Schubeler, D., Fiering, S., Groudine, M., and Bode, J. (1998). DNA cassette exchange in ES cells mediated by Flp recombinase: an efficient strategy for repeated modification of tagged loci by marker-free constructs. *Biochemistry* 37, 6229-6234.
- Shimshek, D.R., Kim, J., Hubner, M.R., Spergel, D.J., Buchholz, F., Casanova, E., Stewart, A.F., Seeburg, P.H., and Sprengel, R. (2002). Codon-improved Cre recombinase (iCre) expression in the mouse. *Genesis* 32, 19-26.
- Shubin, N., Tabin, C., and Carroll, S. (2009). Deep homology and the origins of evolutionary novelty. *Nature* 457, 818-823.
- Simonis, M., Kooren, J., and de Laat, W. (2007). An evaluation of 3C-based methods to capture DNA interactions. *Nat Methods* 4, 895-901.
- Singla, V., Hunkapiller, J., Santos, N., Seol, A.D., Norman, A.R., Wakenight, P., Skarnes, W.C., and Reiter, J.F. (2010). Floxin, a resource for genetically engineering mouse ESCs. *Nat Methods* 7, 50-52.
- Skarnes, W.C., Rosen, B., West, A.P., Koutsourakis, M., Bushell, W., Iyer, V., Mujica, A.O., Thomas, M., Harrow, J., Cox, T., *et al.* (2011). A conditional knockout resource for the genome-wide study of mouse gene function. *Nature* 474, 337-342.
- Sordino, P., van der Hoeven, F., and Duboule, D. (1995). Hox gene expression in teleost fins and the origin of vertebrate digits. *Nature* 375, 678-.
- Soukharev, S., Miller, J.L., and Sauer, B. (1999). Segmental genomic replacement in embryonic stem cells by double lox targeting. *Nucleic Acids Res* 27, e21.
- Spitz, F., Gonzalez, F., and Duboule, D. (2003). A global control region defines a chromosomal regulatory landscape containing the HoxD cluster. *Cell* 113, 405-417.
- Splinter, E., and de Laat, W. (2011). The complex transcription regulatory landscape of our genome: control in three dimensions. *Embo J* 30, 4345-4355.
- Srivastava, D. (2006). Making or breaking the heart: from lineage determination to morphogenesis. *Cell* 126, 1037-1048.
- Srivastava, D., Cserjesi, P., and Olson, E.N. (1995). A subclass of bHLH proteins required for cardiac morphogenesis. *Science* 270, 1995-1999.
- Srivastava, D., Thomas, T., Lin, Q., Kirby, M.L., Brown, D., and Olson, E.N. (1997). Regulation of cardiac mesodermal and neural crest development by the bHLH transcription factor, dHAND. *Nature genetics* 16, 154-160.

- Stadtfeld, M., Nagaya, M., Utikal, J., Weir, G., and Hochedlinger, K. (2008). Induced pluripotent stem cells generated without viral integration. *Science* 322, 945-949.
- Stennard, F.A., and Harvey, R.P. (2005). T-box transcription factors and their roles in regulatory hierarchies in the developing heart. *Development (Cambridge, England)* 132, 4897-4910.
- Sun, X., Mariani, F.V., and Martin, G.R. (2002). Functions of FGF signalling from the apical ectodermal ridge in limb development. *Nature* 418, 501-508.
- Suzuki, T., Hasso, S.M., and Fallon, J.F. (2008). Unique SMAD1/5/8 activity at the phalanx-forming region determines digit identity. *Proc Natl Acad Sci U S A* 105, 4185-4190.
- Szymczak, A.L., Workman, C.J., Wang, Y., Vignali, K.M., Dilioglou, S., Vanin, E.F., and Vignali, D.A. (2004). Correction of multi-gene deficiency in vivo using a single 'self-cleaving' 2A peptide-based retroviral vector. *Nat Biotechnol* 22, 589-594.
- Tabin, C., and Wolpert, L. (2007). Rethinking the proximodistal axis of the vertebrate limb in the molecular era. *Genes Dev* 21, 1433-1442.
- Takahashi, T., Kawai, T., Ushikoshi, H., Nagano, S., Oshika, H., Inoue, M., Kunisada, T., Takemura, G., Fujiwara, H., and Kosai, K. (2006). Identification and isolation of embryonic stem cell-derived target cells by adenoviral conditional targeting. *Mol Ther* 14, 673-683.
- Tanaka, M., Hadjantonakis, A.K., Vintersten, K., and Nagy, A. (2009). Aggregation chimeras: combining ES cells, diploid, and tetraploid embryos. *Methods Mol Biol* 530, 287-309.
- Tanaka, M., Wechsler, S.B., Lee, I.W., Yamasaki, N., Lawitts, J.A., and Izumo, S. (1999). Complex modular cis-acting elements regulate expression of the cardiac specifying homeobox gene *Csx/Nkx2.5*. *Development (Cambridge, England)* 126, 1439-1450.
- Tarchini, B., Duboule, D., and Kmita, M. (2006). Regulatory constraints in the evolution of the tetrapod limb anterior-posterior polarity. *Nature* 443, 985-988.
- te Welscher, P., Fernandez-Teran, M., Ros, M.A., and Zeller, R. (2002a). Mutual genetic antagonism involving *GLI3* and *dHAND* prepatterns the vertebrate limb bud mesenchyme prior to *SHH* signaling. *Genes Dev* 16, 421-426.
- te Welscher, P., Zuniga, A., Kuijper, S., Drenth, T., Goedemans, H.J., Meijlink, F., and Zeller, R. (2002b). Progression of Vertebrate Limb Development through *SHH*-Mediated Counteraction of *GLI3*. *Science* 298, 827-830.
- ten Berge, D., Brugmann, S.A., Helms, J.A., and Nusse, R. (2008). Wnt and FGF signals interact to coordinate growth with cell fate specification during limb development. *Development (Cambridge, England)* 135, 3247-3257.
- Terpe, K. (2003). Overview of tag protein fusions: from molecular and biochemical fundamentals to commercial systems. *Appl Microbiol Biotechnol* 60, 523-533.
- Testa, G., Schaft, J., van der Hoeven, F., Glaser, S., Anastassiadis, K., Zhang, Y., Hermann, T., Stremmel, W., and Stewart, A.F. (2004). A reliable lacZ expression reporter cassette for multipurpose, knockout-first alleles. *Genesis* 38, 151-158.
- Thomas, T., Kurihara, H., Yamagishi, H., Kurihara, Y., Yazaki, Y., Olson, E.N., and Srivastava, D. (1998). A signaling cascade involving endothelin-1, *dHAND* and *msx1* regulates development of neural-crest-derived branchial arch mesenchyme. *Development (Cambridge, England)* 125, 3005-3014.
- Tickle, C. (1981). The number of polarizing region cells required to specify additional digits in the developing chick wing. *Nature* 289, 295-298.
- Toledo, S.P., and Saldanha, P.H. (1969). A radiological and genetic investigation of acheiropody in a kindred including six cases. *J Genet Hum* 17, 81-94.

- Towers, M., Mahood, R., Yin, Y., and Tickle, C. (2008). Integration of growth and specification in chick wing digit-patterning. *Nature* **452**, 882-886.
- Tschopp, P., Fraudeau, N., Bena, F., and Duboule, D. (2011). Reshuffling genomic landscapes to study the regulatory evolution of Hox gene clusters. *Proc Natl Acad Sci U S A* **108**, 10632-10637.
- Tsuchihashi, T., Maeda, J., Shin, C.H., Ivey, K.N., Black, B.L., Olson, E.N., Yamagishi, H., and Srivastava, D. (2011). Hand2 function in second heart field progenitors is essential for cardiogenesis. *Dev Biol* **351**, 62-69.
- Varjosalo, M., and Taipale, J. (2008). Hedgehog: functions and mechanisms. *Genes Dev* **22**, 2454-2472.
- Verheyden, J.M., and Sun, X. (2008). An Fgf/Gremlin inhibitory feedback loop triggers termination of limb bud outgrowth. *Nature* **454**, 638-641.
- Vincent, S.D., and Buckingham, M.E. (2010). How to make a heart: the origin and regulation of cardiac progenitor cells. *Curr Top Dev Biol* **90**, 1-41.
- Visel, A., Blow, M.J., Li, Z., Zhang, T., Akiyama, J.A., Holt, A., Plajzer-Frick, I., Shoukry, M., Wright, C., Chen, F., *et al.* (2009). ChIP-seq accurately predicts tissue-specific activity of enhancers. *Nature* **457**, 854-858.
- Vokes, S.A., Ji, H., Wong, W.H., and McMahon, A.P. (2008). A genome-scale analysis of the cis-regulatory circuitry underlying sonic hedgehog-mediated patterning of the mammalian limb. *Genes & development* **22**, 2651-2663.
- Wang, B., Fallon, J.F., and Beachy, P.A. (2000). Hedgehog-Regulated Processing of Gli3 Produces an Anterior/Posterior Repressor gradient in the Developing Vertebrate Limb. *Cell* **100**, 423-434.
- Wang, J., Rao, S., Chu, J., Shen, X., Levasseur, D.N., Theunissen, T.W., and Orkin, S.H. (2006). A protein interaction network for pluripotency of embryonic stem cells. *Nature* **444**, 364-368.
- Wirth, D., Gama-Norton, L., Riemer, P., Sandhu, U., Schucht, R., and Hauser, H. (2007). Road to precision: recombinase-based targeting technologies for genome engineering. *Curr Opin Biotechnol* **18**, 411-419.
- Witte, F., Bernatik, O., Kirchner, K., Masek, J., Mahl, A., Krejci, P., Mundlos, S., Schambony, A., Bryja, V., and Stricker, S. (2010a). Negative regulation of Wnt signaling mediated by CK1-phosphorylated Dishevelled via Ror2. *Faseb J* **24**, 2417-2426.
- Witte, F., Chan, D., Economides, A.N., Mundlos, S., and Stricker, S. (2010b). Receptor tyrosine kinase-like orphan receptor 2 (ROR2) and Indian hedgehog regulate digit outgrowth mediated by the phalanx-forming region. *Proc Natl Acad Sci U S A* **107**, 14211-14216.
- Wittkopp, P.J., and Kalay, G. (2012). Cis-regulatory elements: molecular mechanisms and evolutionary processes underlying divergence. *Nature reviews Genetics* **13**, 59-69.
- Wobus, A.M., Kaomei, G., Shan, J., Wellner, M.C., Rohwedel, J., Ji, G., Fleischmann, B., Katus, H.A., Hescheler, J., and Franz, W.M. (1997). Retinoic acid accelerates embryonic stem cell-derived cardiac differentiation and enhances development of ventricular cardiomyocytes. *J Mol Cell Cardiol* **29**, 1525-1539.
- Wu, S.M., Chien, K.R., and Mummery, C. (2008). Origins and fates of cardiovascular progenitor cells. *Cell* **132**, 537-543.
- Wu, X., and Howard, M.J. (2002). Transcripts encoding HAND genes are differentially expressed and regulated by BMP4 and GDNF in developing avian gut. *Gene Expr* **10**, 279-293.
- Xiong, W., He, F., Morikawa, Y., Yu, X., Zhang, Z., Lan, Y., Jiang, R., Cserjesi, P., and Chen, Y. (2009). Hand2 is required in the epithelium for palatogenesis in mice. *Dev Biol* **330**, 131-141.
- Xu, B., and Wellik, D.M. (2011). Axial Hox9 activity establishes the posterior field in the developing forelimb. *Proc Natl Acad Sci U S A* **108**, 4888-4891.

- Yamada, G., Mansouri, A., Torres, M., Stuart, E.T., Blum, M., Schultz, M., De Robertis, E.M., and Gruss, P. (1995). Targeted mutation of the murine gooseoid gene results in craniofacial defects and neonatal death. *Development (Cambridge, England)* *121*, 2917-2922.
- Yamagishi, H., Yamagishi, C., Nakagawa, O., Harvey, R.P., Olson, E.N., and Srivastava, D. (2001). The combinatorial activities of Nkx2.5 and dHAND are essential for cardiac ventricle formation. *Dev Biol* *239*, 190-203.
- Yanagisawa, H., Clouthier, D.E., Richardson, J.A., Charite, J., and Olson, E.N. (2003). Targeted deletion of a branchial arch-specific enhancer reveals a role of dHAND in craniofacial development. *Development (Cambridge, England)* *130*, 1069-1078.
- Yelon, D., Baruch, T., Halpern, M.E., Ruvinsky, I., Ho, R.K., Silver, L.M., and Stainier, D.Y.R. (2000). The bHLH transcription factor Hand2 plays parallel roles in zebrafish heart and pectoral fin development. *Development (Cambridge, England)* *127*, 2573-2582.
- Zakany, J., and Duboule, D. (2007). The role of Hox genes during vertebrate limb development. *Current opinion in genetics & development* *17*, 359-366.
- Zakany, J., Kmita, M., and Duboule, D. (2004). A dual role for Hox genes in limb anterior-posterior asymmetry. *Science* *304*, 1669-1672.
- Zeller, R. (2010). The temporal dynamics of vertebrate limb development, teratogenesis and evolution. *Curr Opin Genet Dev.* *20(4)*:384-90.
- Zeller, R. and Duboule D. (1997). Dorso-ventral limb polarity and origin of the ridge: on the fringe of independence? *Bioessays* *19(7)*:541-6.
- Zeller, R., Lopez-Rios, J., and Zuniga, A. (2009). Vertebrate limb bud development: moving towards integrative analysis of organogenesis. *Nat Rev Genet* *10*, 845-858.
- Zeller, R. and Zuniga, A. (2007). Shh and Gremlin1 chromosomal landscapes in development and disease. *Current opinion in genetics & development* *17*, 428-434.
- Zeng, X., Goetz, J.A., Suber, L.M., Scott, W.J., Jr., Schreiner, C.M., and Robbins, D.J. (2001). A freely diffusible form of Sonic hedgehog mediates long-range signalling. *Nature* *411*, 716-720.
- Zguricas, J., Heus, H., Morales-Peralta, E., Breedveld, G., Kuyt, B., Mumcu, E.F., Bakker, W., Akarsu, N., Kay, S.P., Hovius, S.E., *et al.* (1999). Clinical and genetic studies on 12 preaxial polydactyly families and refinement of the localisation of the gene responsible to a 1.9 cM region on chromosome 7q36. *J Med Genet* *36*, 32-40.
- Zhang, X., Guo, C., Chen, Y., Shulha, H.P., Schnetz, M.P., LaFramboise, T., Bartels, C.F., Markowitz, S., Weng, Z., Scacheri, P.C., *et al.* (2008a). Epitope tagging of endogenous proteins for genome-wide ChIP-chip studies. *Nat Methods* *5*, 163-165.
- Zhang, Y., Liu, T., Meyer, C.A., Eeckhoutte, J., Johnson, D.S., Bernstein, B.E., Nusbaum, C., Myers, R.M., Brown, M., Li, W., *et al.* (2008b). Model-based analysis of ChIP-Seq (MACS). *Genome Biol* *9*, R137.
- Zhang, Z., Sui, P., Dong, A., Hassell, J., Cserjesi, P., Chen, Y.T., Behringer, R.R., and Sun, X. (2010). Preaxial polydactyly: interactions among ETV, TWIST1 and HAND2 control anterior-posterior patterning of the limb. *Development (Cambridge, England)* *137*, 3417-3426.
- Zhang, Z., Verheyden, J.M., Hassell, J.A., and Sun, X. (2009). FGF-regulated Etv genes are essential for repressing Shh expression in mouse limb buds. *Dev Cell* *16*, 607-613.
- Zhao, Y., Samal, E., and Srivastava, D. (2005). Serum response factor regulates a muscle-specific microRNA that targets Hand2 during cardiogenesis. *Nature* *436*, 214-220.
- Zheng, B., Sage, M., Sheppard, E.A., Jurecic, V., and Bradley, A. (2000). Engineering mouse chromosomes with Cre-loxP: range, efficiency, and somatic applications. *Mol Cell Biol* *20*, 648-655.

Zhou, B., Ma, Q., Rajagopal, S., Wu, S.M., Domian, I., Rivera-Feliciano, J., Jiang, D., von Gise, A., Ikeda, S., Chien, K.R., *et al.* (2008a). Epicardial progenitors contribute to the cardiomyocyte lineage in the developing heart. *Nature* *454*, 109-113.

Zhou, B., von Gise, A., Ma, Q., Rivera-Feliciano, J., and Pu, W.T. (2008b). Nkx2-5- and Isl1-expressing cardiac progenitors contribute to proepicardium. *Biochem Biophys Res Commun* *375*, 450-453.

Zhu, A.J., and Scott, M.P. (2004). Incredible journey: how do developmental signals travel through tissue? *Genes & Development* *18*, 2985-2997.

Zhu, J., Nakamura, E., Nguyen, M.T., Bao, X., Akiyama, H., and Mackem, S. (2008). Uncoupling Sonic hedgehog control of pattern and expansion of the developing limb bud. *Dev Cell* *14*, 624-632.

Zuniga, A., Haramis, A.P., McMahon, A.P., and Zeller, R. (1999). Signal relay by BMP antagonism controls the SHH/FGF4 feedback loop in vertebrate limb buds. *Nature* *401*, 598-602.

Zuniga, A., Michos, O., Spitz, F., Haramis, A.P., Panman, L., Galli, A., Vintersten, K., Klasen, C., Mansfield, W., Kuc, S., *et al.* (2004). Mouse limb deformity mutations disrupt a global control region within the large regulatory landscape required for Gremlin expression. *Genes Dev* *18*, 1553-1564.

Zuniga, A., and Zeller, R. (1999). Gli3 (Xt) and formin (ld) participate in the positioning of the polarising region and control of posterior limb-bud identity. *Development (Cambridge, England)* *126*, 13-21.

10. Appendix

10.1 Appendix Introduction

10.1.1 Morphogenesis of the heart: The basics

Cardiac precursors arise from invaginating mesodermal cells in the anterior primitive streak at the onset of gastrulation (Harris & Black, 2010), and soon segregate into two distinct lineages (Meilhac et al., 2004) that will give rise to the first and second (anterior) heart fields. After E6.5, these expanding cardiac progenitors migrate to anterior-lateral positions located below the head folds (Wu et al., 2008). At around E7.0, these cells are lying at the junction between cranial and lateral mesoderm and establish a curved structure termed the cardiac crescent. These regions represent the two main cardiac precursor populations known as the first heart field, derived from the lateral plate mesoderm, and the secondary (anterior) heart field, derived from the splanchnic mesoderm, which are marked by the expression of *Nkx2-5* and *Islet1*, respectively. Within the cardiac crescent, mesodermal cells are specified into myocardial, endocardial and smooth muscle cell precursors (Harris & Black, 2010). At around E8, cells of the cardiac crescent coalesce at the midline to form the transient primary heart tube. The heart tube is consisting of an inner endothelial lining and an outer layer of myocardial cells which enclose the cardiac jelly, a scaffold composed of extracellular matrix (Martin-Puig et al., 2008). Between E8.5 and E10, the rapidly growing heart tube undergoes rightward looping to adopt a configuration in which the prospective atrial chambers become located cranially to the ventricular compartments. Simultaneously, at around E9.0, cardiac neural crest cells emanating from the pharyngeal mesoderm invade the embryonic heart to contribute to cardiac structures. At around this stage the contiguous heart tube extends from the caudal venous pole to the cranial arterious pole and consists of the future right and left atrial compartments, the atrioventricular canal, the prospective left and right ventricular chambers and the outflow tract (OFT). The OFT constitutes of a tubular transition which couples the heart tube with transient symmetrical aortic arteries located in the pharyngeal

arches (Snider et al., 2007). During development of the heart tube, myocardial cells proliferate in specified atrial and ventricular areas (Aanhaanen et al., 2009). In the expanding ventricular chambers, the so-called compact zone forms, which consists of up to four layers of cardiac myocytes. Simultaneously, cells of the nearby proepicardial organ (PEO) start to envelop the looping heart tube to form the epicardial layer. By around E10.5, the cardiac tube has reached a stage of intense proliferation, differentiation and migration in which the ventricular inner layer will form an expanding trabecular myocardium (Martin-Puig et al., 2008). Trabeculae extending towards the interior of the ventricle are composed of cardiac jelly and mainly trabecular myocytes and represent fingerlike protrusions. These structures enhance the overall myocardial surface to ensure proper oxygenation until a functional coronary circulation is established. Trabecular myocytes display a decreased mitotic index and advanced differentiation with progressed organization of sarcomeres (Wessels & Sedmera, 2003). During the remodelling phase of cardiac development, at around E12.5, the inter-ventricular and the inter-atrial septum formation is completed, generating two separated atrial and ventricular chambers. Concomitant twisting of the heart tube anchors the outflow tract between the atrial chambers on the ventral side, whereas the inflow areas extend dorsally across the ventricles. The division of cardiac chambers is completed by the fusion of the inner-atrial and interventricular septa with the atrioventricular septum (Harvey et al., 2002).

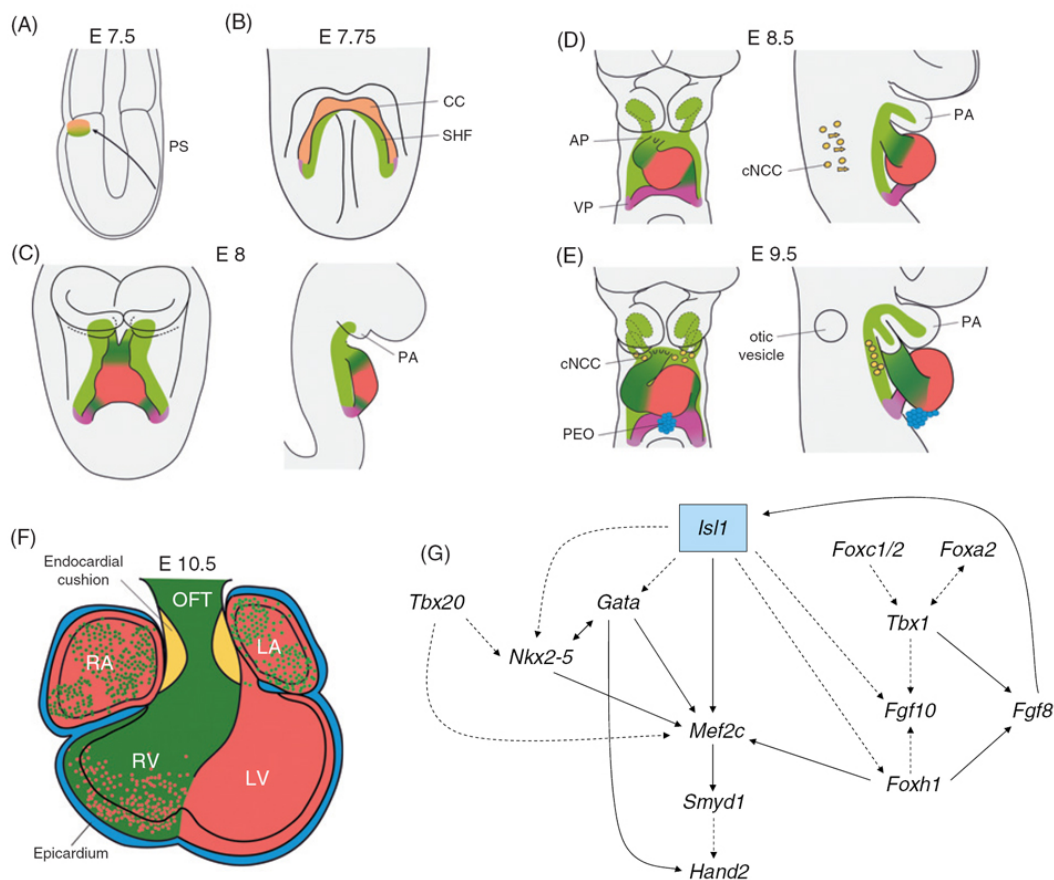
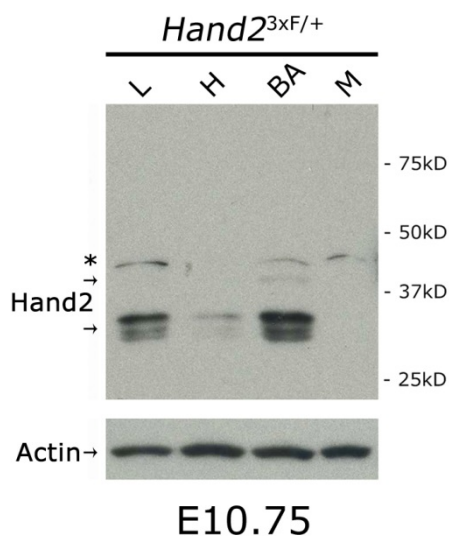


Figure 1. Cardiac progenitors and their contributions to the mouse embryonic heart. **(A)** Cardiac precursors migrate anteriorly from the primitive streak (PS). **(B)** The first heart field (FHF, red) is defined by the cardiac crescent (CC) whereas the secondary heart field (SHF, green) is located medial to it. **(C)** The primary heart tube forms by fusion of cardiac precursors at the midline. PA, pharyngeal arches. **(D-E)** Stages of rightward heart looping and expansion of the ventricular chambers. AP, arterial pole. VP, venous pole. cNCC, cardiac neural crest cells (yellow). PEO, proepicardial organ (blue). **(F)** Compartments and heart field contributions of the looped heart tube at E10.5. OFT, outflow tract. RA, right atrium. LA, left atrium. RV, right ventricle. LV, left ventricle. **(G)** Core gene regulatory network regulating SHF development. Note that no direct *Hand2* targets have been characterized *in vivo* in cardiac development so far. Panels A-F adapted from Vincent & Buckingham, 2010. Panel G adapted from Laugwitz et al. 2008.

10.2 Appendix Results

10.2.1 Detection of Hand2 protein isoforms in *Hand2*^{3xFLAG} expressing tissues

Figure 2. Western blotting using M2 anti-FLAG antibody and extracts (30µg) of pooled limb buds (L), hearts (H), branchial arches (BA) or midbrains (M, negative control) from embryos heterozygous for the *Hand2*^{3xFLAG} allele at E10.75 (38S). Three isoforms of similar sizes are detected as published for the limb bud (Galli et al., 2010). Arrows indicate bands specific for Hand2. Asterisk denotes an antibody-related background band. Actin was detected as loading control.



10.2.2 ChIP-seq reveals Hand2 candidate target regions in the branchial arches and the developing heart.

Hand2 is broadly expressed within the distal mesodermal compartments of the branchial arches and partially overlaps with *Hand1*, which is expressed in the distal mesenchyme of the first pharyngeal arch (Cserjesi et al., 1995; Thomas et al., 1998). Consistent with this, we localized Hand2 protein in the nuclei of cells populating the distal mesenchyme of the branchial arches (Figure 3A). Similar to the outgrowing limb bud (Figure 10A-C), Hand2 proteins in the distal mesenchyme appeared complementary to the proximal Sox9 domain and cells at the border expressed both transcription factors (Figure 3A and data not shown). These patterns raised the possibility that *Sox9* might be a direct transcriptional target of Hand2. Our Hand2 ChIP-seq analysis did not reveal any enrichment within the *Sox9* locus. However, a peak located ~232 kb downstream of the *Sox9* locus was detected in a highly conserved region (data not shown). In contrast, the ChIP-seq analysis revealed an unusual number of robust peaks in the intergenic region between the *Gsc* (*Goosecoid*) and *Dicer1*

genes (Figure 3B). Most interestingly, the expression of *Gsc* in the distal-posterior mesenchyme of the first and second branchial arches is downregulated in *Hand2* deficient branchial arches (Barron et al., 2011). Thus, *Hand2* might directly regulate *Gsc* expression in the branchial arches via these upstream regions (Figure 3B).

Hand2 regulates survival, proliferation and differentiation of cardiac progenitors (Srivastava et al., 2006; Morikawa & Cserjesi, 2008; Tsuchihashi et al., 2010; Barnes et al., 2011). Therefore, the *Hand2* and *Sox9* distributions were analysed in the developing heart (Figure 3C). *Sox9* is expressed by epicardial cells (Smith et al., 2011) and endocardial cushion cells (Akiyama et al., 2004). In contrast, *Hand2* is expressed by pericardial cells (Figure 3C) and no cells co-expressing *Hand2* and *Sox9* were detected in this population. However, the *Sox9* positive cells in endocardial cushions also express the *Hand2* (Figure 3C). This observation is in agreement with the requirement for *Hand2* for endocardial cushion organization and interventricular septum formation (Liu et al., 2009; Togi et al., 2006).

Nkx2-5 is one of the earliest regulators involved in inducing myocardial differentiation in the cardiac crescent and a marker of the first heart field (Buckingham et al., 2005). At a later stage, *Nkx2-5* is homogenously expressed by the outflow tract, atrial and ventricular lineages (Tanaka et al., 1999). Our *Hand2* ChIP-seq analysis revealed a significant enrichment 3.1kb upstream of the *Nkx2-5* transcriptional start site (TSS; Figure 3D). Strikingly, this peak encompasses a highly conserved element and is located within the 3.3kb proximal promoter region which drives strong *lacZ* reporter expression in myocardial cells of the outflow tract and the right ventricle (Tanaka et al., 1999), compartments in which *Hand2* is also localized (this study).

An additional prominent peak was associated to *Tbx20*, encoding another important cardiac transcriptional regulator (Figure 3D). This peak also overlaps with an evolutionary highly conserved element. *Tbx20* may co-localize with *Hand2* in right ventricular myocytes and endocardial cells and its inactivation causes defects that are similar to those observed in

Hand2 constitutive mutants (Stennard & Harvey, 2005). ChIP-seq analysis also revealed significant enrichment close to the *Connexin 40* (*Cx40/Gja5*) locus, localizing to an element showing high degree of evolutionary conservation located 31kb downstream of the *Cx40* TSS (Figure 3D).

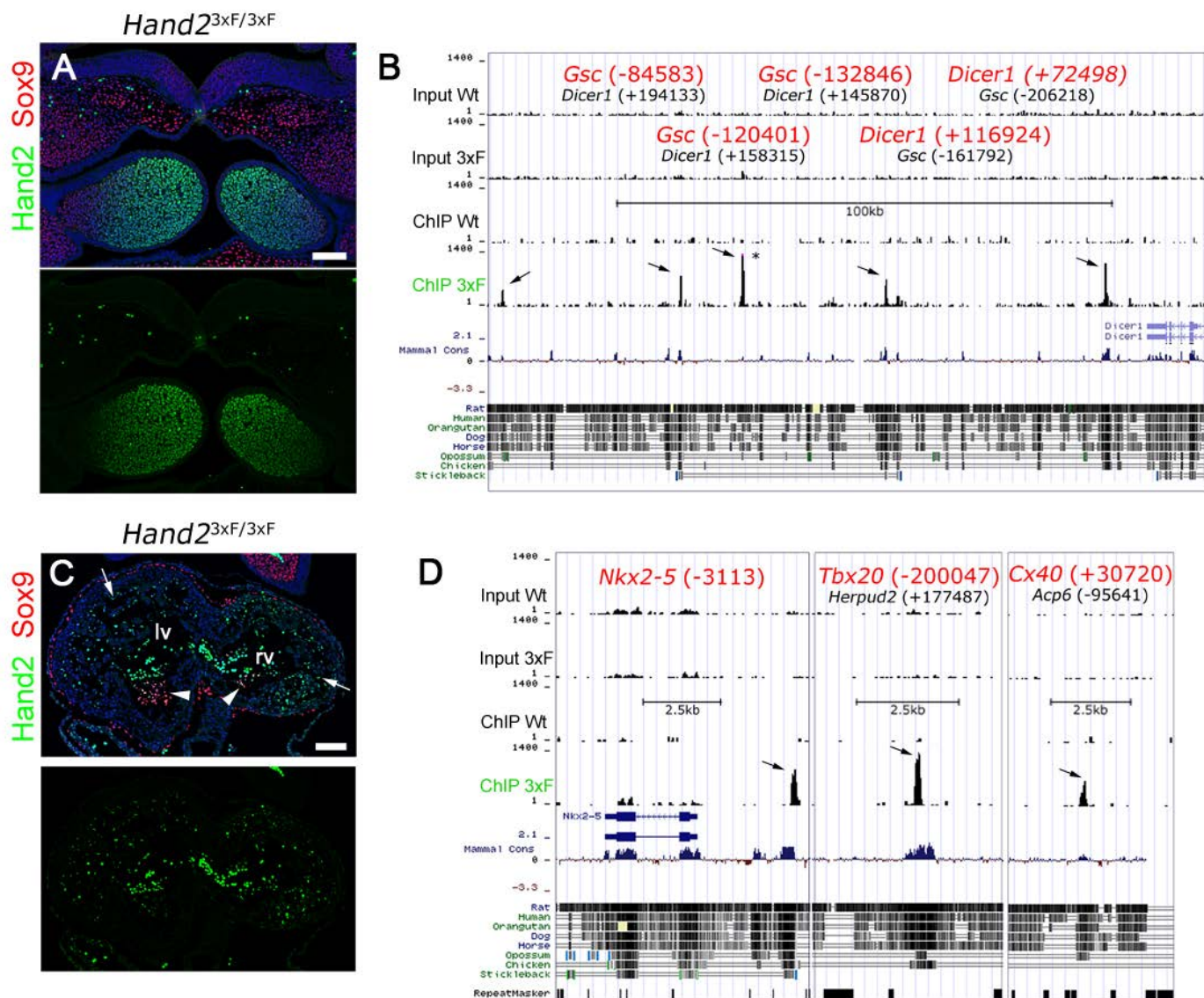
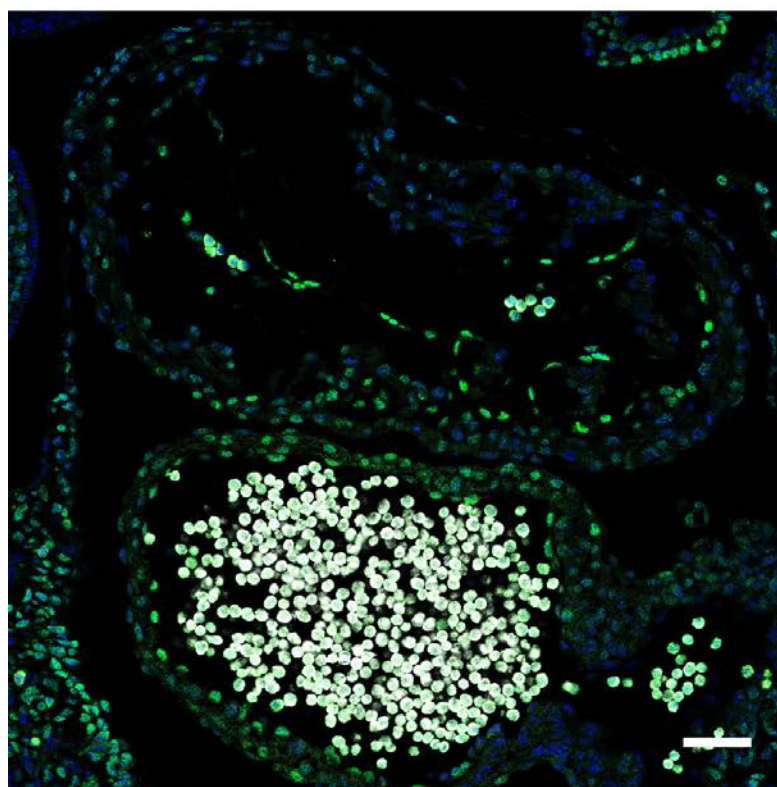


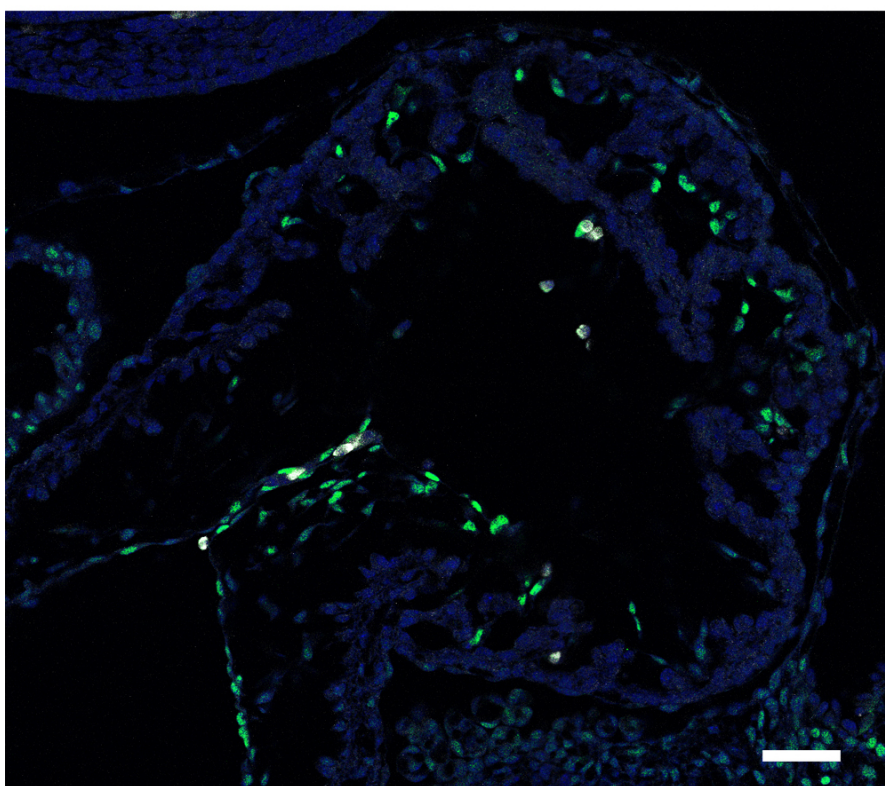
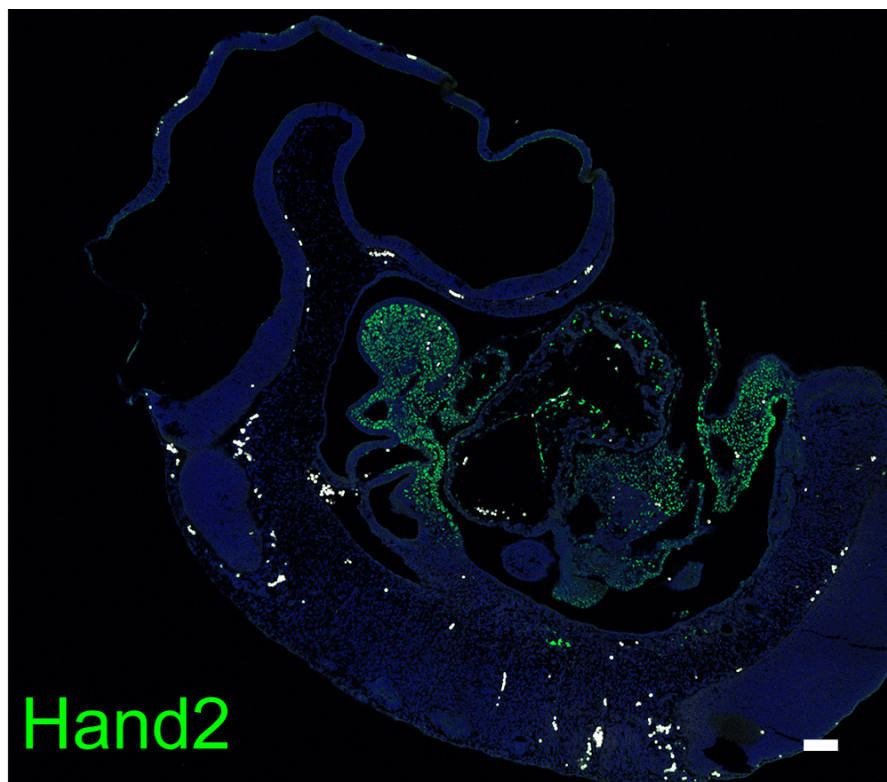
Figure 3. ChIP-seq reveals putative *Hand2* target regions associated to genes expressed in branchial arches and the developing heart. **(A)** Immunolocalization of endogenous *Hand2*^{3xFLAG} (green fluorescence) and Sox9 (red fluorescence) proteins. The first mandibular pharyngeal arch (1st brachial arch) of a *Hand2*^{3xFLAG/3xFLAG} embryo at E10.5 (36 somites) reveals progressively higher *Hand2* levels towards the distal mesenchyme. Scattered, strong cytoplasmic signals (in green) represent autofluorescent blood cells. Nuclei were stained with Hoechst (blue). Scale bar, 100 μ m. **(B)** ChIP-seq analysis identifies potential *Hand2* interacting elements in the *Gsc/Dicer1* intergenic region. Distance to the transcriptional start site is displayed in brackets (in base pairs). Information about additional graphic features can be obtained in the legend of Figure 14. **(C)** Coronal section showing nuclear

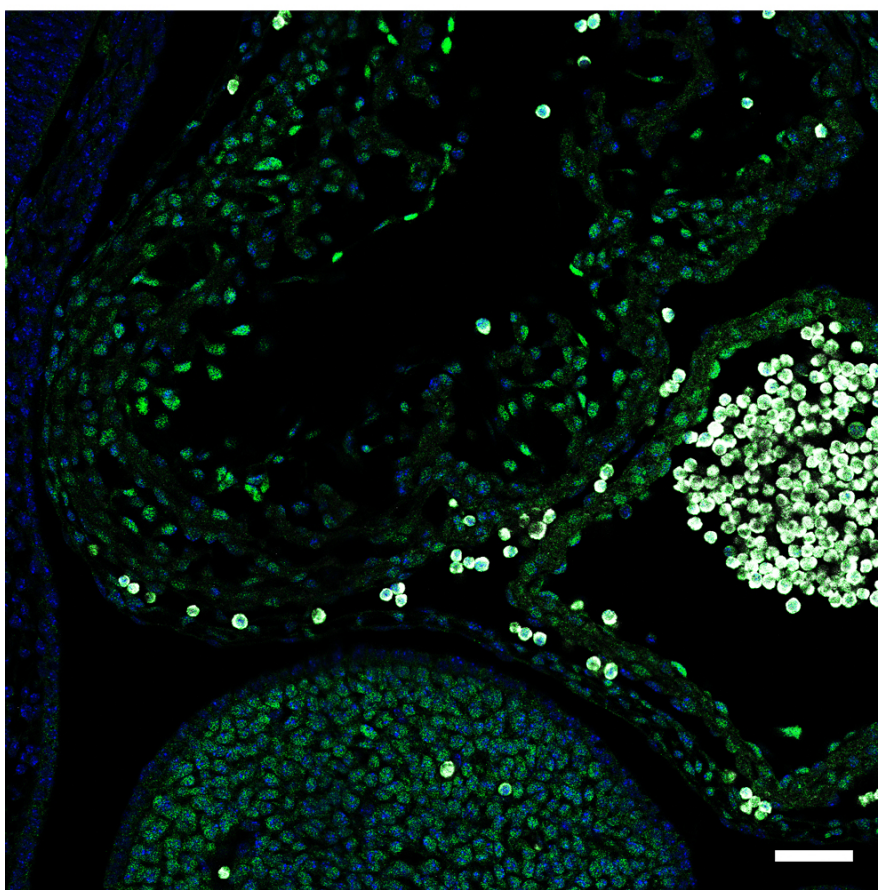
immunolocalization of endogenous Hand2^{3xFLAG} and Sox9 proteins in the embryonic heart at E10.5 (36 somites). Arrowheads indicate endocardial cushion cells co-expressing Hand2 and Sox9 proteins. Note the detection of Sox9 protein in epicardial cells surrounding the ventricular chambers. Arrows mark endocardial cells lining ventricular chambers. Hand2 is also detected in right ventricular myocytes. Lv, left ventricle. Rv, right ventricle. Hoechst stained nuclei appear blue. Strong and scattered cytoplasmic signals represent autofluorescent blood cells (appear as well in green). Scale bar, 100 μ m. **(D)** The Hand2 ChIP-seq dataset reveals enrichments associated with *Nkx2-5*, *Tbx20* and *Cx40*. Distance to the transcriptional start site is enclosed in brackets. The nomenclature used in the UCSC browser is described in Figure 14. Arrows denote significantly enriched peaks. Enlargements of panels **A** and **C** are found below (in the Appendix).

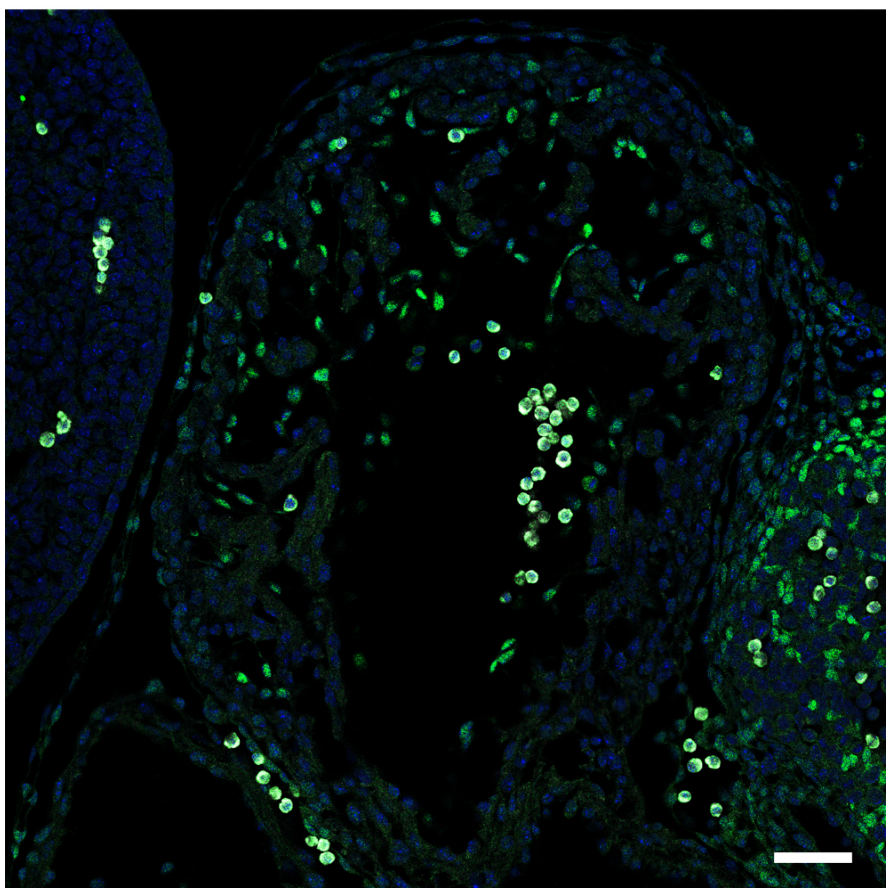
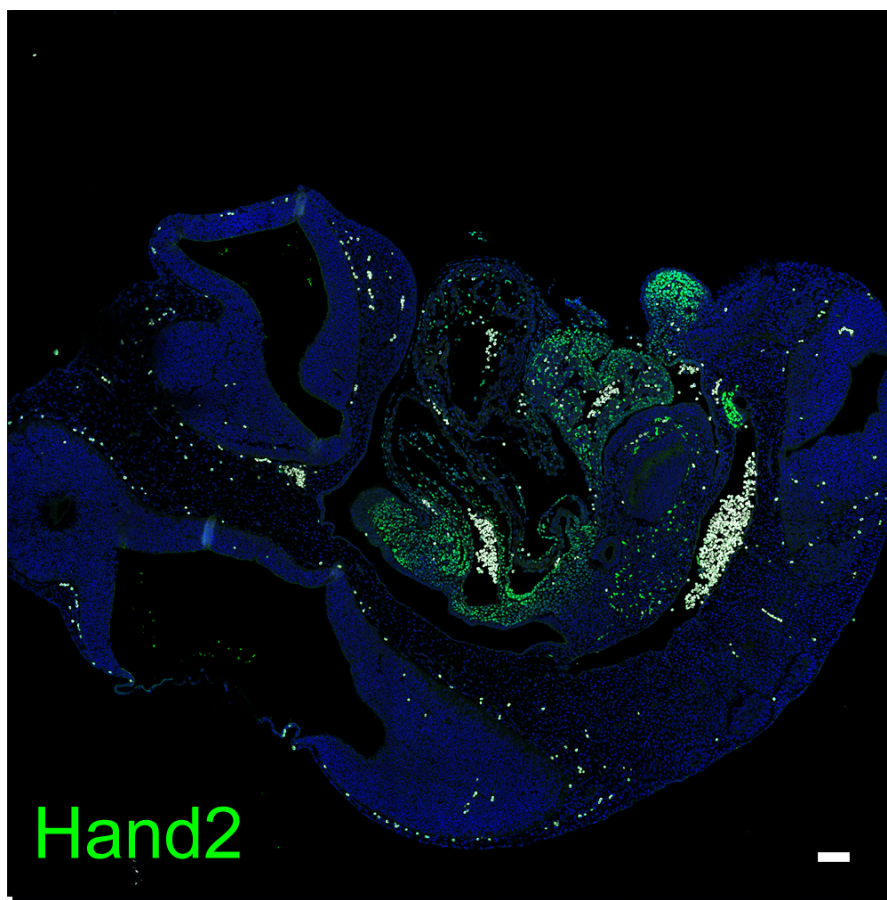
10.3 Appendix Panels & Tables

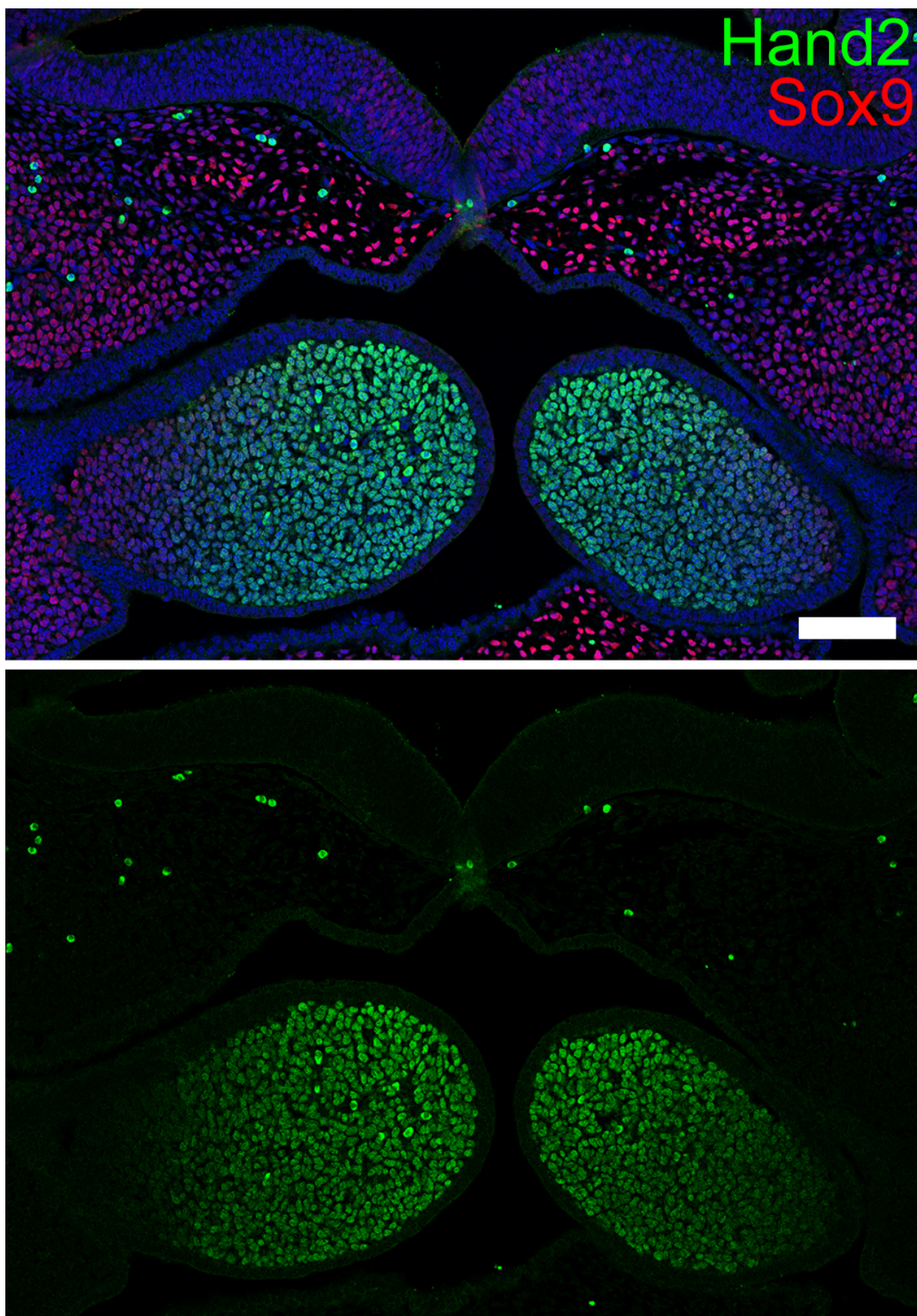
Enlargement of **Figures 10A and 10B** (Results).

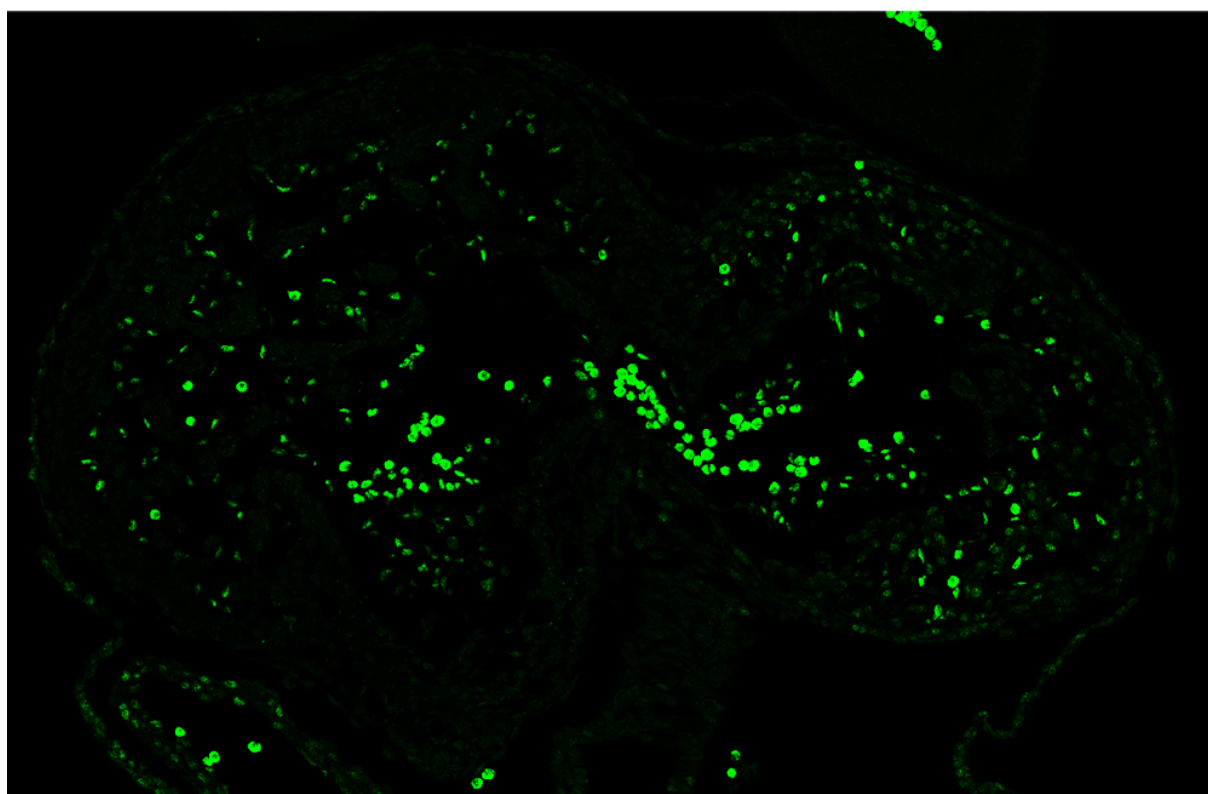
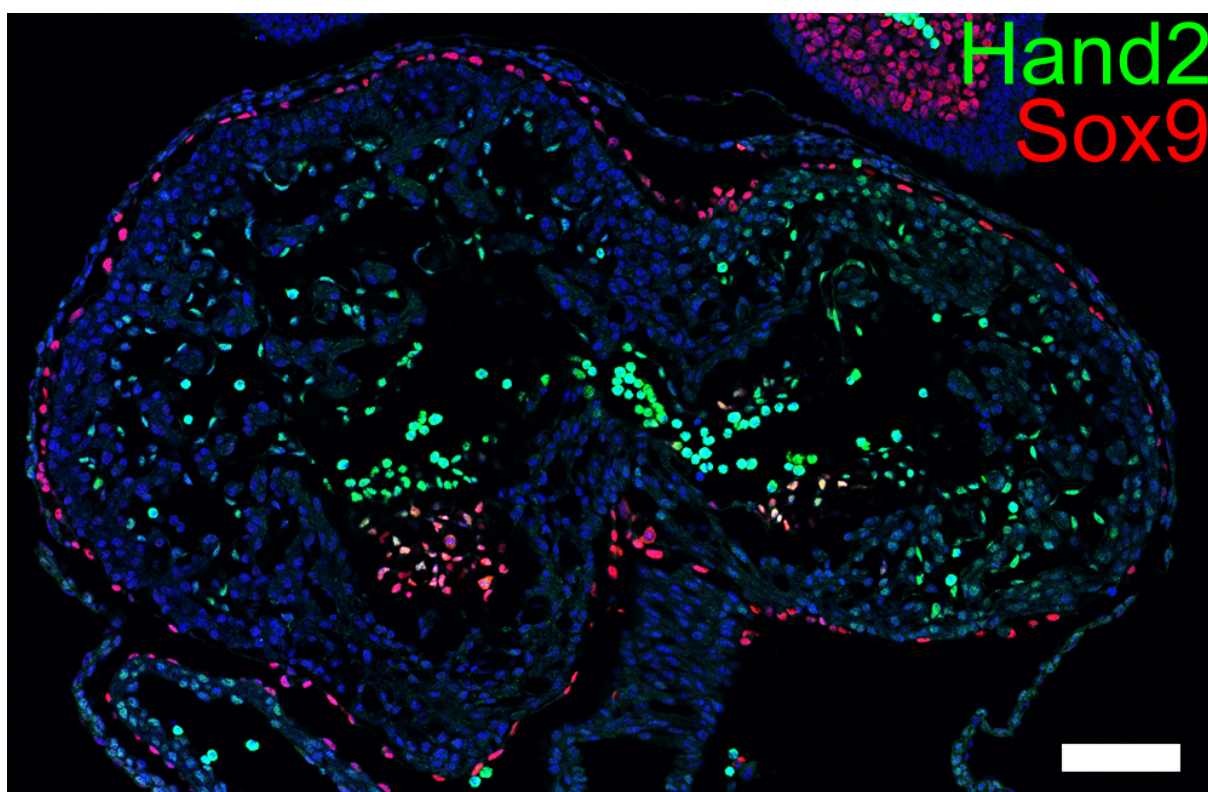


Enlargement of **Figures 10D and 10E** (Results).

Enlargement of **Figures 10G and 10H (Results)**.

Enlargement of **Figures 10J and 10K (Results)**.

Enlargement of **Figure 3A** (Appendix).

Enlargement of **Figure 3C** (Appendix).

Appendix Table 1. List of the highest enriched Hand2 ChIP-seq peaks

in limb buds, hearts and branchial arches at E10.5. The curated dataset containing the top 795 peaks is shown (excluding enrichments mapping to repeat masked elements or low complexity regions). These peaks represent *bona fide* enrichments of regions bound to the Hand2^{3xFLAG} protein and are sorted according to enrichment by MACS (Zhang et al., 2008b).

Chromosome	Start	End	Original Peak No.	Enrichment (MACS)	Closest genes (distance in bp)
chr11	94790090	94790771	uc.3	3053.15	Xylt2 (-251624), Col1a1 (-7153)
chr4	41606336	41607214	uc.4	2916.11	Enho (-19440), Cntfr (+35702)
chr7	17475989	17476786	uc.5	2882.34	Gng8 (-747)
chr5	144125381	144126453	uc.6	2609.95	Kdelr2 (-39582), Grid2ip (+6900)
chr8	28217081	28218061	uc.7	2446.34	Gpr124 (+21258), Brf2 (+21533)
chr6	72166533	72167397	uc.8	2081.42	Atoh8 (+18606), St3gal5 (+119358)
chr11	117824524	117825069	uc.9	2068.34	Tha1 (-89957), Socs3 (+5679)
chr8	122799735	122800977	uc.10	2057.42	Gse1 (-212410), 6430548M08Rik (+162304)
chr7	149518446	149519321	uc.11	2012.27	Krtap5-4 (+29477), 6330512M04Rik (+39280)
chr7	149507249	149508298	uc.12	1999.9	Krtap5-4 (+18367), 6330512M04Rik (+50390)
chr12	105843930	105844653	uc.13	1977.79	Gsc (-132846), Dicer1 (+145870)
chr2	167422727	167423406	uc.14	1710.88	Ube2v1 (+34438), Snai1 (+59340)
chr11	4472635	4474387	uc.15	1642.76	Hormad2 (-132426), Mtmr3 (+21307)
chr8	59812649	59813397	uc.17	1548.89	Scrg1 (-121697), Hand2 (+13243)
chr2	33399437	33400278	uc.18	1514.2	Zbtb43 (-75806), Lmx1b (+96173)
chr6	36846471	36847222	uc.19	1494.99	Ptn (-85486), Dgki (+403129)
chr1	196436708	196437126	uc.20	1487.8	Plxna2 (-9106)
chr11	85613263	85613744	uc.21	1418.2	Tbx2 (-32613), Bcas3 (+446788)
chr6	51118584	51119139	uc.24	1199.22	Npvf (-514470), Nfe2l3 (-263807)
chr15	83469536	83470351	uc.25	1179.27	Ttll12 (-44404), Scube1 (+85507)
chr15	9015708	9016193	uc.26	1176.07	1110020G09Rik (+14942), Skp2 (+54256)
chr7	149668933	149669570	uc.27	1161.4	Mrpl23 (-49770), Lsp1 (+11504)
chr10	43298171	43299291	uc.28	1159.47	Cd24a (-244)
chr12	105917122	105918205	uc.29	1141.34	Gsc (-206218), Dicer1 (+72498)
chr7	149757309	149757930	uc.30	1083.5	H19 (+6431), Mrpl23 (+38598)
chr2	166285259	166286096	uc.33	1009.76	Sulf2 (-304522), Prex1 (+253654)
chr16	15052942	15053500	uc.34	999.89	Efcab1 (+146482), Ube2v2 (+541390)
chr2	152564914	152565574	uc.35	996.56	Cox4i2 (-14665), Id1 (+3234)
chr14	22909705	22911058	uc.36	987.74	Zfp503 (-101559)
chr5	111964812	111965427	uc.37	986.33	Mn1 (+117934), Cryba4 (+716402)
chr15	102201229	102201579	uc.39	967.91	Sp7 (-4702)
chr17	45643665	45644122	uc.40	964.65	Aars2 (+104)
chr11	120025538	120026256	uc.41	947.43	Bahcc1 (-68364), Slc38a10 (-13232)
chr1	137696957	137697553	uc.42	945.52	Lad1 (-17920), Tnni1 (+1257)
chr8	123612724	123613148	uc.44	893.65	Foxf1a (+4562), Mthfsd (+19282)
chr9	40538499	40539178	uc.45	890.72	Hspa8 (-70517), 9030425E11Rik (+44792)
chr5	140012066	140012594	uc.46	890.36	Zfand2a (-51885), Uncx (-7522)
chr13	78923491	78924011	uc.47	885.72	Nr2f1 (-585508)
chr8	33403630	33403914	uc.49	879.58	Nrg1 (-375097)
chr18	55138092	55138594	uc.50	863.31	Zfp608 (+11224)
chr2	59460514	59461193	uc.51	857.74	Tanc1 (+10753), Wdsub1 (+259809)
chr9	30784203	30784774	uc.53	842.87	Zbtb44 (-53740), Adamts8 (+34341)
chr14	121533524	121534073	uc.54	837.4	Farp1 (+99003), Stk24 (+244653)
chr5	38284683	38285513	uc.55	836.33	Stx18 (-145376), Msx1 (-69274)
chr13	51354222	51355034	uc.56	832.65	S1pr3 (-149505), Spin1 (+158361)

chr11	64485126	64485891	uc.57	831.93	Elac2 (-307028), Hs3st3a1 (+236675)
chr6	61166510	61166902	uc.58	829.52	Mmrrn1 (+272395)
chr5	150122904	150123722	uc.59	814.85	Alox5ap (+46679), Hsph1 (+315577)
chr8	127766142	127766892	uc.60	811.41	Disc1 (+188422), Sipa1l2 (+250216)
chr1	57153009	57153583	uc.62	799	1700066M21Rik (-281168), Satb2 (-125118)
chr7	89157010	89157882	uc.63	792.4	Sh3gl3 (-162282), Bnc1 (-20261)
chr13	25703729	25704404	uc.64	790.39	Nrsn1 (-342202)
chr5	122068592	122069221	uc.65	787.49	9330129D05Rik (+40)
chr16	14992428	14992872	uc.66	786.32	Efcab1 (+85911), Ube2v2 (+601961)
chr13	113590715	113591732	uc.67	783.88	Ppap2a (+224)
chr3	94276483	94277120	uc.68	783.02	2310007A19Rik (+711)
chr10	79395323	79396020	uc.69	759.09	Grin3b (-37797), Arid3a (+5855)
chr19	56174171	56174688	uc.70	756.93	Habp2 (-187998), Tcf7l2 (+358130)
chr7	82007395	82008218	uc.71	752.78	Slco3a1 (-308141), Sv2b (+446341)
chr9	25334439	25335059	uc.72	752.7	Eepd1 (+45567)
chr12	13204947	13205414	uc.73	741.27	Mycn (-256539), Ddx1 (+50799)
chr13	3708266	3708956	uc.74	741.26	Asb13 (+75289), Calml3 (+94953)
chr8	122714791	122715418	uc.75	736.71	Gse1 (-297661), 6430548M08Rik (+77053)
chr6	55401680	55402520	uc.76	734.84	Adcyap1r1 (+126)
chr2	35359559	35360188	uc.79	727.59	Dab2ip (-117627), Ggta1 (-42929)
chr9	32350436	32350895	uc.80	723.05	Fli1 (-1713)
chr3	152828689	152829276	uc.81	719.66	St6galnac5 (-183812), St6galnac3 (+559114)
chr8	95484239	95484782	uc.82	716.69	Slc6a2 (-435)
chr6	90994590	90994915	uc.83	713.9	Iqsec1 (-234636), Nup210 (+72067)
chr13	53278543	53279047	uc.84	705.04	Nfil3 (-202387), Ror2 (+102683)
chr2	115686486	115687056	uc.85	695.55	Meis2 (+204023), BC052040 (+279319)
chr1	74321340	74322170	uc.86	693.91	Gpbar1 (-3419)
chr17	43214067	43214312	uc.89	687.29	Gpr110 (-193106), Tnfrsf21 (+60686)
chr10	37117049	37117803	uc.90	682.09	Marcks (-258694)
chr17	80128089	80128701	uc.91	679.33	Cyp1b1 (-14014), At1l2 (+167068)
chr5	43847019	43847759	uc.92	678.89	C1qtnf7 (-145772), Cpeb2 (+222191)
chr6	90413417	90413800	uc.93	669.23	Klf15 (+989)
chr9	32479668	32480629	uc.94	667.66	Fli1 (-131196), Ets1 (-23478)
chr7	143261933	143262512	uc.95	666.71	Mgmt (-824071), Mki67 (-354161)
chr6	36626567	36627375	uc.96	665.77	Ptn (+134390), Chrm2 (+153761)
chr4	131474581	131475346	uc.97	656.85	Sfrs4 (+45410), Epb4.1 (+130029)
chr11	98784028	98784528	uc.98	654.72	Rara (-14732), Cdc6 (+15075)
chr13	103315687	103316419	uc.99	648.47	Pik3r1 (-777881), Cd180 (-167585)
chr8	87179697	87180499	uc.101	646.45	Ier2 (+6653), Cacna1a (+240835)
chr5	120062520	120062926	uc.102	642.09	Tbx3 (-57955)
chr4	108105906	108106534	uc.103	630.63	Gpx7 (-26902), Zcchc11 (-25811)
chr4	123811484	123812040	uc.104	621.26	Pou3f1 (-523127), Rragc (+217086)
chr2	172750341	172750965	uc.106	620.35	Bmp7 (+15141), Tcfap2c (+374162)
chr8	48146489	48147143	uc.107	619.67	Enpp6 (+74537), Ing2 (+613696)
chr4	13169038	13169693	uc.108	619.26	Runx1t1 (-501083)
chr7	149739649	149740543	uc.109	616.78	Mrpl23 (+21074), H19 (+23955)
chr8	122701090	122701970	uc.110	615.47	Gse1 (-311236), 6430548M08Rik (+63478)
chr4	13406972	13407547	uc.112	612.58	Runx1t1 (-263189)
chr11	118331433	118331796	uc.114	610.18	Engase (-6659), C1qtnf1 (+36448)
chr19	59341916	59342305	uc.115	607.03	Slc18a2 (+6694), Pdzd8 (+78159)
chr1	78308187	78308640	uc.116	605.97	Sgpp2 (+1493), Farsb (+177007)
chr16	4658654	4659292	uc.117	603.55	Vasn (+19028), Coro7 (+20747)
chr19	56160883	56161549	uc.118	601.36	Habp2 (-201212), Tcf7l2 (+344916)
chr1	24012264	24012834	uc.119	599.3	1110058L19Rik (-70)
chr10	66384205	66384645	uc.120	596.23	Reep3 (+175180)
chr2	167421260	167421936	uc.121	596.21	Ube2v1 (+35907), Snai1 (+57871)

chr11	85689403	85690186	uc.122	594.55	Tbx4 (-13770), Tbx2 (+43678)
chr17	29553092	29553722	uc.123	593.93	Pim1 (-74583), Fgd2 (+55548)
chr4	141777259	141777886	uc.124	590.25	9030409G11Rik (-11452)
chr11	117280304	117280791	uc.125	585.88	Tnrc6c (-235055), Sept9 (+219573)
chr17	29144308	29145182	uc.126	585.72	Stk38 (+137)
chr2	154285624	154286381	uc.127	584.96	Cbfa2t2 (+23783), Necab3 (+98586)
chr5	120101469	120102138	uc.128	580.61	Tbx3 (-18874)
chr4	29407884	29408657	uc.129	574.75	Epha7 (+667976)
chr8	59810372	59811168	uc.131	572.83	Scrg1 (-123950), Hand2 (+10990)
chr11	105154396	105154705	uc.132	571.26	Mrc2 (+591)
chr1	194622447	194623035	uc.133	570.26	Hhat (-25328), Syt14 (+239151)
chr5	122398645	122399084	uc.134	570.05	Sh2b3 (-112055), Cux2 (+98969)
chr1	170340084	170340782	uc.135	562.72	Pbx1 (+21956), Lmx1a (+720744)
chr16	30068240	30069077	uc.136	560.25	Hes1 (+3216), Cpn2 (+198959)
chr8	27462799	27463559	uc.137	559.86	Erlin2 (-671152), Thap1 (+194538)
chrX	49980125	49980935	uc.138	559.86	Phf6 (-284913), Gpc3 (-13432)
chr14	27964448	27965123	uc.139	558.16	Arhgef3 (-86439), Il17rd (+112599)
chr12	112127373	112127998	uc.140	557.96	Cinp (-362)
chr7	139640126	139640673	uc.141	555.92	Chst15 (-131562), Oat (+127681)
chr9	32637572	32638339	uc.142	551.31	Ets1 (+134329)
chr4	150183406	150183828	uc.143	547.61	Slc45a1 (-157334), Errfi1 (-45583)
chr2	32173313	32174268	uc.145	545.43	Golga2 (+30018), Dnm1 (+35033)
chr4	109792129	109792586	uc.146	541.28	Dmrt2 (+141728), Elavl4 (+167758)
chr4	41610440	41611008	uc.147	539.52	Enho (-23389), Cntfr (+31753)
chr17	84481087	84481699	uc.148	539.33	Hao (-235263), Zfp36l2 (+105894)
chr13	119271903	119272528	uc.149	537.59	Fgf10 (-231290), Mrps30 (-96157)
chr2	51263771	51264297	uc.150	537.56	Rnd3 (-259403), Tas2r134 (-218997)
chr18	83071455	83071851	uc.151	536.41	Zfp236 (-209527), Zfp516 (-53358)
chr4	47657925	47658423	uc.152	536.15	Nr4a3 (-405944), Sec61b (+170641)
chr10	44949635	44950309	uc.153	533.06	Popdc3 (-59139), Prep (+162952)
chr12	72746689	72747362	uc.154	532.8	Daam1 (-185039), Dact1 (+336055)
chr4	13759981	13760477	uc.155	531.08	Runx1t1 (+89780), Slc26a7 (+788696)
chr12	105678232	105679009	uc.156	528.24	Gsc (+32825), Serpina3n (+33703)
chr18	55111545	55112380	uc.157	525.63	Zfp608 (+37604)
chr4	154083612	154084407	uc.158	525.43	Ttc34 (-146299), Actrt2 (-42034)
chr6	99051348	99052010	uc.159	524.97	Foxp1 (+61344)
chr14	26537884	26538509	uc.160	524.4	Ppif (+24541), Zcchc24 (+50145)
chr5	65806792	65807364	uc.161	524.05	Ugdh (+20003), Lias (+24342)
chr11	113902024	113902358	uc.163	522.59	Cdc42ep4 (-289717), Sdk2 (+25074)
chr11	26389852	26390365	uc.164	521.44	Fancl (+103025), Vrk2 (+103811)
chr6	127097815	127098235	uc.167	519.14	9630033F20Rik (-38471), Ccnd2 (+3041)
chr6	29463209	29463808	uc.168	518.39	Irf5 (-13224), Kcp (-5575)
chr8	11585389	11586522	uc.169	517.34	Arhgef7 (-142149), Ing1 (+29890)
chr11	85723635	85724147	uc.170	516.17	Tbx4 (+20326), Brip1 (+290804)
chr10	12810291	12810935	uc.171	515.73	Plagl1 (+19)
chr12	98441957	98442773	uc.172	511.43	NONE
chr14	22867868	22868509	uc.173	505.44	Zfp503 (-59366)
chr1	87803398	87803814	uc.174	504.38	Itm2c (+12521), Gpr55 (+54024)
chr18	61122833	61123373	uc.175	503.3	Camk2a (+37817), Slc6a7 (+50750)
chr14	106294128	106294481	uc.176	502.13	Spry2 (+1731), Ndfip2 (+636284)
chr6	6339504	6340309	uc.177	501.66	Slc25a13 (-172789), Shfm1 (+188751)
chr12	91882371	91882824	uc.178	500.89	Dio2 (+94280)
chr7	138913913	138914256	uc.179	500.8	Gpr26 (-244058), Bub3 (+210180)
chr9	43801275	43801792	uc.181	500.4	Thy1 (-49933), Pvr11 (+248875)
chr18	54501847	54502493	uc.182	498.74	Csnk1g3 (+480403), Zfp608 (+647397)
chr9	97601396	97601814	uc.183	498.56	Trim42 (-331228), Cistn2 (+331981)

chr17	28297152	28297676	uc.184	496.22	Zfp523 (-16949), Scube3 (+17943)
chr4	9752639	9753386	uc.185	494.99	Asph (-156740), Gdf6 (-18506)
chr1	59538184	59538638	uc.186	493.92	Fzd7 (-580)
chr16	90706518	90706900	uc.187	492.78	2610039C10Rik (+20907), Hunk (+320067)
chr18	11510629	11511279	uc.188	491.36	Rbbp8 (-305397), Gata6 (+458446)
chr3	121291688	121292503	uc.189	488.83	F3 (-134359), Slc44a3 (-56834)
chr19	10295937	10296402	uc.190	487.28	1810006K21Rik (+17478), Gm98 (+19068)
chr4	62416410	62417011	uc.191	486.69	Zfp618 (-209897), Rgs3 (+136005)
chr16	96069770	96070586	uc.192	486.16	Psmg1 (+142332), Ets2 (+146164)
chr3	103541711	103542329	uc.193	484.89	Olfml3 (-96)
chr7	150491715	150492138	uc.194	483.32	Cdkn1c (+155028), Kcnq1 (+198768)
chr8	48448559	48449059	uc.196	480.35	Ing2 (+311703), Enpp6 (+376530)
chr18	61812750	61813702	uc.197	480.05	Il17b (-34363), Csnk1a1 (+97990)
chr17	48110953	48111504	uc.198	479.42	Foxp4 (-49648), 9830107B12Rik (+171989)
chr11	89159599	89160111	uc.199	478.2	Nog (+4018), Gm525 (+224700)
chr7	26496697	26497167	uc.201	475.68	Tgfb1 (+24911), Hnrmpul1 (+42807)
chr8	123362711	123363298	uc.202	474.41	Foxf1a (-245369), Irf8 (+102729)
chr9	118771988	118772460	uc.203	471.35	Ctdspl (-63430), Itga9 (+256397)
chr6	100171163	100171728	uc.205	468.11	Prok2 (-495060), Rybp (+65906)
chr6	30571725	30572264	uc.206	464.78	Cpa1 (-17226), Cpa5 (+10985)
chr9	32631346	32631863	uc.207	464.37	Ets1 (+127978)
chr9	24778576	24779010	uc.209	462.07	Tbx20 (-200047), Herpud2 (+177487)
chr13	56213739	56214309	uc.210	461.09	Pitx1 (-281238), H2afy (+22887)
chr14	9237658	9238395	uc.211	461	Oit1 (-26750)
chr5	74557511	74558070	uc.213	458.93	Usp46 (-93355), Rasl11b (-33560)
chr5	5342660	5343291	uc.214	457.57	Fzd1 (-584760), Pftk1 (+37275)
chr2	169525235	169525665	uc.215	455.63	Tshz2 (+66304), Zfp217 (+431270)
chr14	118050375	118050947	uc.216	452.5	Dct (+400807), Gpc6 (+726124)
chr12	113571548	113572168	uc.217	451.48	A530016L24Rik (-155820), Kif26a (+187439)
chr5	147731318	147732110	uc.218	450.37	Gtf3a (-28519), Rasl11a (+75067)
chr4	108556549	108556872	uc.219	448.67	Nrd1 (-116699), Rab3b (+5036)
chr3	104621255	104621832	uc.220	447.35	Mov10 (-63)
chr15	43376722	43377217	uc.221	442.02	Ttc35 (+68195), Tmem74 (+324605)
chr6	148416134	148416849	uc.222	439.24	Tmtc1 (-23618), Ipo8 (+363497)
chr6	18386247	18386822	uc.223	438.51	Cttnbp2 (+78290), Cfr (+265848)
chr11	35248520	35249060	uc.224	438.12	Pank3 (-334207), Slit3 (+313832)
chr2	104804425	104805107	uc.225	437.62	Prrg4 (-114759), Eif3m (+52418)
chr15	84996755	84997386	uc.226	437.19	Fbln1 (-39367), Smc1b (-34684)
chr5	151945563	151946108	uc.228	436.29	Stard13 (+46932), Kl (+190654)
chr11	98993503	98994187	uc.229	435.59	Tns4 (-43225), Ccr7 (+22546)
chr11	85533816	85534479	uc.230	431.51	Tbx2 (-111969), Bcas3 (+367432)
chr9	52045081	52045681	uc.231	429.93	Zc3h12c (-69165), Al593442 (+442153)
chr11	85441985	85442549	uc.232	429.51	Tbx2 (-203850), Bcas3 (+275551)
chr1	165804043	165804678	uc.233	428.8	Scyl3 (-55834), Kifap3 (+94551)
chr17	26981434	26981812	uc.234	428.35	Nkx2-5 (-3113)
chr4	13669741	13670974	uc.235	427.44	Runx1t1 (-91)
chr7	56705551	56706427	uc.236	426.96	Dbx1 (+186216), Nav2 (+204430)
chr4	154563733	154564302	uc.237	425.51	Rer1 (-103612), Ski (+32626)
chrX	6657033	6657686	uc.238	425.28	Akap4 (+12715), Clcn5 (+108452)
chr9	18525378	18525785	uc.239	424.33	Olf24 (+34495), Mbd3l1 (+242743)
chr1	176965586	176966133	uc.240	422.62	Grem2 (-113910), Rgs7 (+456816)
chr7	106105596	106106651	uc.241	422.05	Wnt11 (+118769), Uvrag (+183530)
chr14	10282463	10282978	uc.242	421.2	NONE
chr11	34717799	34718215	uc.243	420.41	Slit3 (-216951), Ccdc99 (-70864)
chr16	30190916	30191543	uc.244	419.42	Cpn2 (+76388), Hes1 (+125787)
chr11	31900204	31900555	uc.245	417.14	Nsg2 (-79)

chr11	11778546	11779109	uc.246	417.04	Figl1 (-69863), Ddc (+11576)
chr2	31195191	31195807	uc.247	416.12	BC040753 (-98083), Freq (+94056)
chr17	25220212	25220855	uc.248	416.01	Tmem204 (-2475)
chr14	25871653	25871925	uc.249	415.97	Zmiz1 (-406989), Rps24 (+561886)
chr4	117938136	117938600	uc.250	415.77	Kdm4a (-85720), Ptpfr (+25634)
chr16	8671575	8672460	uc.251	415.57	Carhsp1 (+228)
chr12	105873007	105873469	uc.252	415	Gsc (-161792), Dicer1 (+116924)
chr1	165783026	165783673	uc.253	414.77	Scyl3 (-76845), Kifap3 (+73540)
chr10	120085048	120085585	uc.254	413.26	Hmga2 (-171326), Msrb3 (+250710)
chr7	137970831	137971247	uc.257	406.75	Plekha1 (-38385), Tacc2 (+250041)
chr12	29682684	29683168	uc.258	406.52	Myt1l (-530323), Ttc15 (-247608)
chr1	93310500	93311118	uc.259	406.36	Hes6 (-1010)
chr8	26653656	26654515	uc.260	406.36	Fgfr1 (+24842), Letm2 (+53873)
chr4	32262759	32263394	uc.262	406.14	Bach2 (-62848), Map3k7 (+211995)
chr8	48202384	48203145	uc.263	405.86	Enpp6 (+130486), Ing2 (+557747)
chr11	24108639	24109163	uc.264	404.96	Bcl11a (+130845)
chr3	81025348	81025948	uc.265	404.75	Ctso (-710890), Pdgfc (+185310)
chr5	114250253	114250667	uc.267	403.2	Tmem119 (-99)
chr15	11998235	11998766	uc.268	402.5	Sub1 (-72739), Zfr (-49105)
chr1	13761050	13761548	uc.269	402.03	Xkr9 (+102447), Eya1 (+538981)
chr13	110783184	110783838	uc.270	400.35	Rab3c (+286903)
chr4	126754423	126754899	uc.271	400.18	Zmym6 (+34)
chr1	92640166	92640975	uc.273	398.45	Col6a3 (+67837), Cops8 (+140571)
chr17	29600437	29600809	uc.274	397.99	Pim1 (-27367), Fgd2 (+102764)
chr2	154280279	154280955	uc.276	395.06	Cbfa2t2 (+18397), Necab3 (+103972)
chr14	69552812	69553578	uc.277	392.76	Adam28 (-279296), Stc1 (-94151)
chr8	117688629	117689582	uc.278	392.58	Maf (+541688), Wwox (+725554)
chr10	28031045	28031497	uc.279	392.29	Themis (-356930), Ptpkr (+236645)
chr4	114494101	114494801	uc.280	391.83	Foxd2 (+87052), Gm12824 (+415122)
chr1	74945077	74945598	uc.281	391.63	Cryba2 (-5629), Ccdc108 (+36835)
chr14	55496299	55496628	uc.282	390.12	Homez (-17137), Bcl2l2 (-5798)
chr1	37181415	37182379	uc.283	390.09	Tmem131 (-185525), Cnga3 (-94209)
chr15	81846233	81847069	uc.284	390.06	Xrcc6 (-148)
chr10	68715896	68716496	uc.285	389.7	Rhobtb1 (+40791), Cdc2a (+99464)
chr2	101843214	101843710	uc.288	389.08	Prr5l (-205598), Ldlrad3 (+183072)
chr13	55855804	55856375	uc.289	389.06	Catsper3 (-29850), Pcbd2 (+27361)
chr1	195376806	195377398	uc.290	388.51	Camk1g (-180626)
chr3	96500627	96501435	uc.291	387.18	Pias3 (+639)
chr5	152453278	152454132	uc.292	386.82	Rfc3 (+78)
chr7	6866246	6866897	uc.293	385.3	Aurkc (-81524), Usp29 (+183120)
chr5	31210717	31211267	uc.294	385	2310016E02Rik (-897)
chr5	115823891	115824414	uc.296	383.46	Msi1 (-55541), Cox6a1 (-25189)
chr2	167408764	167409217	uc.297	382.86	Snai1 (+45264), Ube2v1 (+48514)
chr19	43097301	43097677	uc.298	382.77	Hps1 (-243023), Hpse2 (+365312)
chr9	36837758	36838621	uc.299	382.76	Pknox2 (+116709), Fez1 (+186943)
chr3	141901212	141902017	uc.300	382.71	Bmpr1b (-256400), Pdlim5 (+157015)
chr3	94279965	94280538	uc.301	381.94	2310007A19Rik (-2739), Tnrc4 (-2501)
chr19	45765385	45765905	uc.303	380.29	Fbxw4 (-30962), Fgf8 (+51718)
chr11	99712184	99712809	uc.304	380.16	Krtap4-16 (+422)
chr7	143989479	143990038	uc.305	377.94	Mgmt (-96535)
chr5	58581524	58582258	uc.306	377.81	Pcdh7 (+472631)
chrX	50021339	50021913	uc.307	375.64	Phf6 (-243817), Gpc3 (-54528)
chr18	69953921	69954668	uc.308	374.39	Rab27b (+258728), Tcf4 (+448920)
chr17	17575399	17576364	uc.309	374.27	Riok2 (+64342), Lnpep (+185571)
chr1	163950282	163951034	uc.310	373.1	Pigc (+51339), Dnm3 (+457507)
chr10	13096031	13096657	uc.311	372.13	Fuca2 (-124490), Plagl1 (+285750)

chr7	6697052	6697641	uc.312	370.99	Aurkc (-250749), Usp29 (+13895)
chr19	10088246	10088760	uc.313	370.4	Rab3il1 (-4215)
chr5	135264000	135264586	uc.314	370.4	Eln (-41169), Wbscr28 (+118310)
chr8	59118032	59118637	uc.315	370.4	Hand2 (-681445), Fbxo8 (+88404)
chr2	4203760	4204276	uc.316	369.35	Frmd4a (+130100), Prpf18 (+369114)
chr11	43447448	43447978	uc.318	368.23	Fabp6 (-32700), Ttc1 (+113762)
chr15	61183328	61183676	uc.319	367.44	Myc (-633394), A1bg (-430599)
chr19	43686624	43687181	uc.320	366.72	Nkx2-3 (+88)
chr2	174684159	174685011	uc.321	365.96	Edn3 (+98311), LOC664987 (+208679)
chr10	74142871	74143330	uc.323	363.47	Gnaz (-286875), Pcdh15 (+858486)
chr11	76325054	76325550	uc.324	363.39	Abr (-2381)
chr1	74019120	74019698	uc.325	363.32	Tnp1 (-956936), Tns1 (+151612)
chr15	53130822	53131150	uc.326	362.54	Ext1 (+46752), Med30 (+586986)
chr13	15537840	15538418	uc.327	362.05	Gli3 (-17427), Psma2 (+832620)
chr7	77958098	77958639	uc.329	361.19	Nr2f2 (-452890)
chr4	134308935	134309397	uc.330	360.8	Man1c1 (-48961), Ldlrap1 (+14753)
chr4	122859616	122860072	uc.331	359.22	Hpcal4 (-903)
chr12	105795752	105796305	uc.332	358.99	Gsc (-84583), Dicer1 (+194133)
chr11	63066369	63067179	uc.333	358.71	Pmp22 (+121762), Hs3st3b1 (+669012)
chr15	4594717	4594929	uc.334	358.66	C6 (-82387), Plcx3 (+269332)
chr17	73409903	73410333	uc.336	358.47	Lclat1 (-47216), Lbh (+142473)
chr8	118776487	118777078	uc.337	358.14	Maf (-545989), Dynlrb2 (-252132)
chr2	118860461	118860971	uc.338	358.08	Rpusd2 (+190)
chr18	4137425	4137944	uc.339	357.63	Lyzl1 (-28145), Bambi (+629730)
chr4	150120162	150120597	uc.340	356.57	Errfi1 (-108820), Slc45a1 (-94097)
chr17	48234378	48235218	uc.341	356.06	Foxp4 (-173217), 9830107B12Rik (+48420)
chr12	110675898	110676420	uc.342	354.94	Begain (-369732), Dlk1 (-15274)
chr12	80646357	80646921	uc.343	354.03	Rad51l1 (+248370), Zfp36l1 (+567361)
chr11	117641461	117642104	uc.344	353.7	Tmc8 (-2581), Tmc6 (+152)
chr4	95350940	95351822	uc.345	353.28	Hook1 (-282689), Fgyy (+127183)
chr2	80244838	80245268	uc.346	353.03	Frzb (+42500), Dnajc10 (+89430)
chr13	102571563	102572039	uc.347	352.85	Cd180 (-911837), Pik3r1 (-33629)
chr4	117324659	117325143	uc.348	352.81	Dmap1 (+29929), Eri3 (+101802)
chr1	91948411	91949024	uc.349	351.73	Gbx2 (-120967), Iqca (+101258)
chr3	143237152	143238043	uc.350	351.29	Pkn2 (-692644), Lmo4 (+627698)
chr4	32385969	32386506	uc.351	350.02	Bach2 (+60313), Gja10 (+303119)
chr1	156402861	156403439	uc.352	349.82	Cacna1e (+169900), Glul (+656075)
chr15	101058523	101058831	uc.353	349.67	Nr4a1 (-38600), Grasp (+4039)
chr12	105831608	105832086	uc.354	348.39	Gsc (-120401), Dicer1 (+158315)
chr9	48628747	48629374	uc.355	347.78	Nnmt (-215879), Zbtb16 (+14989)
chr2	63111865	63112452	uc.356	347.17	Kcnh7 (-89815), Fign (+823905)
chr13	21494152	21494727	uc.357	346.46	Zkscan3 (+184)
chr7	6196125	6196776	uc.360	345.19	Zfp667 (-41731), Zscan5b (+22571)
chr13	56780323	56781004	uc.361	344.99	Smad5 (-23707), Tgfb1 (+69700)
chr4	43100403	43100958	uc.362	344.49	4930417M19Rik (-179350), Unc13b (+28825)
chr4	119028924	119029302	uc.363	344.03	Ppih (-35985), Ppcs (+65912)
chr12	109198423	109199039	uc.364	343.19	Bcl11b (+42893)
chr2	167970853	167971303	uc.365	343.19	Adnp (+61484), Pard6b (+64574)
chr14	26241035	26241461	uc.367	340.49	Zmiz1 (-37530), Rps24 (+931345)
chr13	118024306	118024721	uc.368	340.41	Hcn1 (-366773), Emb (+15134)
chr12	80635548	80636117	uc.369	340.32	Rad51l1 (+237564), Zfp36l1 (+578167)
chr9	14488786	14489243	uc.371	338.42	Piwil4 (+56162), Cwc15 (+183952)
chr4	70792031	70792693	uc.372	338.3	Megf9 (-596400)
chr10	45613497	45613927	uc.373	338.2	Hace1 (+316017)
chr3	52848010	52848605	uc.374	338.15	Stoml3 (-444407), Lhfp (+2839)
chr12	72625280	72625541	uc.375	338.1	Daam1 (-306654), Dact1 (+214440)

chr9	61450155	61450613	uc.376	338.08	Tle3 (+230211), Rplp1 (+311933)
chr8	130333556	130334220	uc.377	337.77	Nrp1 (-549085), Pard3 (+745932)
chr2	63921639	63922479	uc.378	337.6	Kcnh7 (-899715), Fign (+14005)
chr8	123824866	123825722	uc.379	336.27	Foxl1 (+173709), Fbxo31 (+277412)
chr16	4552717	4553261	uc.380	335.18	Srl (-29936), Tcfap4 (+6731)
chr5	93315110	93315975	uc.381	335.09	Sept11 (-206940), Shroom3 (+203082)
chr1	180908751	180909181	uc.382	334.98	Kif26b (+449710), Smyd3 (+539168)
chr7	149515950	149516907	uc.383	334.57	Krtap5-4 (+27022), 6330512M04Rik (+41735)
chr11	51282738	51283286	uc.384	334.36	Agxt2l2 (-115247), Col23a1 (+179590)
chr2	152560633	152561256	uc.385	334.25	Id1 (-1065)
chr6	65628170	65628534	uc.386	333.46	Prdm5 (-100604), A930038C07Rik (+6747)
chr4	150674792	150675266	uc.387	333.11	Vamp3 (-242967), Camta1 (+560826)
chr5	136879231	136879894	uc.388	332.77	Sh2b2 (-158790), Cux1 (+162135)
chr3	94743705	94744357	uc.389	332.55	Rfx5 (-14906), Selenbp1 (+7026)
chr10	117342601	117343160	uc.390	331.98	Mdm1 (-235962), Rap1b (-59851)
chr4	81794426	81794995	uc.391	331.79	Mpdz (-706002), Nfib (+356501)
chr14	22888258	22888925	uc.392	331.7	Zfp503 (-79769)
chr8	105932778	105933515	uc.394	330.95	Cdh5 (-692378), Cdh11 (-624136)
chr7	144413244	144413846	uc.395	330.63	Ebf3 (+92583), Mgmt (+327251)
chr7	122297725	122298063	uc.396	330.57	Insc (+408614), Sox6 (+840706)
chr13	53850336	53850856	uc.397	330.56	Msx2 (-282447), Drd1a (+300431)
chr14	105776803	105777453	uc.398	329.77	Ndfip2 (+119107), Spry2 (+518908)
chr15	82768326	82769170	uc.399	329.46	Tcf20 (-26184), Nfam1 (+84820)
chr14	77210764	77211503	uc.400	329.31	Enox1 (-345489), Serp2 (-254640)
chr2	51421026	51421678	uc.401	329.24	Rnd3 (-416721), Tas2r134 (-61679)
chr6	6249102	6249669	uc.402	328.8	Slc25a13 (-82268), Shfm1 (+279272)
chr4	13020118	13021067	uc.404	328.32	Fam92a (-921431), Runx1t1 (-649856)
chr11	102485285	102486025	uc.405	327.66	Adam11 (-137098), Fzd2 (+19910)
chr17	72312154	72312657	uc.406	327.36	BC027072 (-210181), Alk (+641241)
chr13	57933241	57933622	uc.407	326.85	Trpc7 (-936483), Spock1 (+76204)
chr11	57742924	57743528	uc.408	326.45	Cnot8 (-174429), Hand1 (-97577)
chr10	22536083	22536473	uc.410	326.19	Tbpl1 (-85025), Tcf21 (+3656)
chr4	132594320	132595602	uc.411	324.55	Wasf2 (-91587), Ahdc1 (+27540)
chr2	152555122	152555629	uc.412	324.23	Id1 (-6634), Mcts2 (+42492)
chr9	107808926	107809412	uc.413	324.22	Mst1r (-51)
chr2	119130561	119131353	uc.414	322.87	Dll4 (-20563), Vps18 (+16479)
chr1	166976966	166977513	uc.417	322.5	Xcl1 (-111599), Tbx19 (+113664)
chr4	98443481	98443863	uc.418	322.24	Usp1 (-146829), Inadl (+381155)
chr7	137255259	137255729	uc.419	321.44	Fgfr2 (+154828), Brwd2 (+520117)
chrX	104207451	104207963	uc.420	320.7	P2ry10 (-76965), Lpar4 (+91743)
chr10	116402283	116402973	uc.421	319.63	Best3 (-20742), Rab3ip (-15192)
chr4	10075505	10075983	uc.422	318.88	Gdf6 (+304225), Plekhf2 (+859022)
chr1	52289557	52290519	uc.423	317.37	Gls (+38)
chr11	64694066	64694631	uc.424	317.35	Elac2 (-98188), Hs3st3a1 (+445515)
chr1	77334730	77335478	uc.425	317.11	Epha4 (+176559)
chr9	71728367	71728891	uc.426	317.11	Cgnl1 (-109220), Tcf12 (+230997)
chr5	45334387	45334894	uc.427	316.57	Ldb2 (-143695), Qdpr (+506827)
chr2	141056711	141057189	uc.428	315.43	Flrt3 (-559745)
chr4	83302544	83303016	uc.429	315.43	Psip1 (-170486), Bnc2 (+889529)
chr7	26615100	26615510	uc.430	315.21	Cyp2b10 (-67378), Cyp2s1 (-13756)
chr4	106538242	106538739	uc.431	314.88	Acot11 (-66055), Ssbp3 (-45584)
chr16	64145568	64146192	uc.432	313.23	Epha3 (-281897), 4930453N24Rik (+624885)
chr4	134722244	134723017	uc.433	312.59	Runx3 (+46071), Clic4 (+106044)
chr10	120467224	120467469	uc.434	312.52	Wif1 (-3713)
chr8	107688136	107688764	uc.435	312.19	Cbfb (-6124), Ces8 (+32750)
chr7	131479129	131479720	uc.436	312.17	Zkscan2 (-835462)

chr5	135371168	135371547	uc.439	310.71	Eln (-148234), Wbscr28 (+11245)
chr2	128539404	128539951	uc.440	310.45	Tmem87b (-104361), Mertk (+14945)
chr1	180990295	180990724	uc.441	309.71	Smyd3 (+457624), Kif26b (+531254)
chr11	96753464	96753866	uc.442	309.61	Cdk5rap3 (+24130), Copz2 (+42475)
chr17	87913504	87914064	uc.443	309.56	Epcam (-121535), Calm2 (-67509)
chr16	21216013	21216495	uc.444	309.29	Vps8 (-206937), Ephb3 (+11386)
chr16	94060020	94060546	uc.445	309.29	Cldn14 (-51201), Sim2 (-25222)
chr6	148641670	148642315	uc.447	307.87	Tmtc1 (-249119), Ipo8 (+137996)
chr11	96282245	96283307	uc.448	307.01	Skap1 (-43162), Hoxb1 (+55704)
chr2	59363221	59363738	uc.449	307.01	Tanc1 (-86621), Dapl1 (+40766)
chr6	48523425	48523866	uc.451	305.74	Rarres2 (-977)
chr12	37517463	37517928	uc.452	304.9	Meox2 (-317437), 4930579E17Rik (+409590)
chr2	152531760	152532305	uc.453	304.72	Id1 (-29977), Mcts2 (+19149)
chr12	74561345	74562102	uc.454	304.64	Tmem30b (+85658), Slc38a6 (+173882)
chr5	114246725	114247307	uc.455	304.47	Tmem119 (+3345), Iscu (+24195)
chr9	49768089	49768393	uc.456	303.98	1600029D21Rik (-534389), Ncam1 (-161067)
chr4	128318977	128319425	uc.457	303.48	Phc2 (-63041), Tlr12 (-23338)
chr8	49995047	49995458	uc.458	303.07	Odz3 (-235209)
chr1	94668962	94669627	uc.459	302.95	Otos (-123877), Gpc1 (-58968)
chr12	12588041	12588755	uc.460	302.63	Fam49a (+319453), Mycn (+360244)
chr6	30475560	30476427	uc.461	301.78	Tmem209 (-16288), Cpa2 (-15648)
chr17	75473293	75473747	uc.462	301.57	Rasgrp3 (-391433), Ltbp1 (+68651)
chr5	104525016	104525459	uc.463	301.54	Sparcl1 (+17869), Nudt9 (+49208)
chr1	194660697	194661361	uc.464	300.5	Hhat (-63616), Syt14 (+200863)
chr19	45800064	45800484	uc.466	299.89	Fbxw4 (-65591), Fgf8 (+17089)
chr12	43378215	43379045	uc.468	299.24	NONE
chr7	77249631	77250360	uc.469	299.21	Nr2f2 (+255483)
chr6	97831869	97832459	uc.470	298.77	Mitf (+75112)
chr19	36873578	36873981	uc.471	298.72	Ppp1r3c (-62686), Tnks2 (-34942)
chr6	50763146	50763533	uc.472	298.55	Nfe2l3 (-619329), Npvf (-158948)
chr5	120246503	120246910	uc.473	298.36	Tbx5 (-37965), Tbx3 (+126029)
chr11	95437026	95437501	uc.474	297.96	Nxph3 (-61385), Ngfr (+11748)
chr9	58650575	58651041	uc.475	297.83	Hcn4 (-20511), Nptn (+220761)
chrX	48270490	48271041	uc.476	297.42	2610018G03Rik (+76153), Rap2c (+100429)
chr10	98764669	98765178	uc.477	297.24	Dusp6 (+39059), Csl (+457368)
chr8	90355258	90355932	uc.478	297.22	Cbln1 (-359104), Zfp423 (+127899)
chr13	28782573	28783219	uc.479	296.19	Sox4 (+262655), Prl5a1 (+548543)
chr19	9041228	9041779	uc.480	295.94	Eef1g (-27)
chrX	49263817	49264176	uc.482	295.64	Usp26 (-112994), Gpc4 (+254103)
chr19	58194304	58194728	uc.483	294.57	Gfra1 (+334568), Atrnl1 (+508992)
chr17	49721909	49722239	uc.485	293.41	Kif6 (-32423), Daam2 (-18412)
chr1	120801470	120802081	uc.486	293.39	Gli2 (+148420), Tcfcp2l1 (+277254)
chr5	142234838	142235319	uc.487	293.3	Foxk1 (-642372), Sdk1 (+517591)
chr1	16219653	16220178	uc.488	292.7	Rdh10 (+123953), Stau2 (+289467)
chr3	52203114	52203430	uc.489	292.55	Foxo1 (+131013), Cog6 (+617873)
chr1	186068543	186069069	uc.490	292.42	Dusp10 (+210466), Hlx (+487566)
chr13	93363818	93364485	uc.491	291.71	Spz1 (-17965), Serinc5 (-16941)
chr11	64782467	64783041	uc.492	291.28	Elac2 (-9783), Hs3st3a1 (+533920)
chr7	150557160	150557735	uc.493	291.02	Cdkn1c (+89507), Kcnq1 (+264289)
chr2	26977507	26977839	uc.495	290.94	Fam163b (+20321), Adamtsl2 (+42772)
chr1	74226524	74227056	uc.496	290.76	Il8ra (+14415), Il8rb (+26222)
chr2	28808413	28808897	uc.497	290.61	Ttf1 (-107128), Barhl1 (-36714)
chr17	24278221	24278792	uc.498	290.57	Pdpk1 (+54)
chr8	111240674	111241084	uc.499	290.53	Pmfbp1 (-777048), Zfhx3 (+2335)
chr7	103809181	103809783	uc.500	290.44	Nars2 (-290555), Odz4 (+450335)
chr5	21164559	21164950	uc.502	290.35	Armc10 (+12953), Napepld (+42408)

chr1	160393915	160394224	uc.503	289.59	Astn1 (+101599), Pappa2 (+493499)
chr17	62647012	62647389	uc.505	289.17	Efna5 (+583465)
chr14	22722792	22723488	uc.506	289.04	Comtd1 (-55008), Zfp503 (+85683)
chr18	48267950	48268405	uc.507	288.88	Gm5506 (+63189)
chr16	92230755	92231294	uc.508	288.85	Kcne2 (-61609), Mrps6 (+172458)
chr11	24102598	24103213	uc.509	288.56	Bcl11a (+124850)
chr7	141917266	141917542	uc.510	288.56	Nps (-542898), Dock1 (+55034)
chr7	83922008	83922639	uc.511	288.46	Klhl25 (+929100)
chr14	71182992	71183609	uc.512	288.4	Gfra2 (-106636), Dok2 (+9113)
chr4	120489603	120490104	uc.513	287.48	Kcnq4 (-70073), Nfyc (+8466)
chr17	75413227	75413757	uc.514	287.2	Rasgrp3 (-451461), Ltbp1 (+8623)
chr19	8945878	8946561	uc.515	286.32	Ubxn1 (+171)
chr1	167678305	167678729	uc.516	286.16	Mpz1 (-113845), Creg1 (-15394)
chr7	149738510	149738892	uc.517	285.65	Mrpl23 (+19679), H19 (+25350)
chr13	108625438	108625946	uc.518	285.5	Kif2a (-813498), Zswim6 (+54566)
chr4	57859261	57859650	uc.519	285.04	Ptpn3 (-544747), Akap2 (-7576)
chr13	28721693	28722339	uc.520	284.86	Sox4 (+323535), Prl5a1 (+487663)
chr2	169576220	169577127	uc.521	284.12	Tshz2 (+117528), Zfp217 (+380046)
chr1	165107104	165107662	uc.522	283.79	4921528O07Rik (-91582), Prrx1 (+136398)
chr4	135703625	135704640	uc.523	283.73	E2f2 (-24176), Id3 (+4396)
chr6	149083090	149083484	uc.526	283.36	Dennd5b (-33085), 4833442J19Rik (-6832)
chr3	99469807	99470413	uc.529	283.16	Spag17 (-219230), Tbx15 (+412427)
chr17	49115703	49116264	uc.530	283.01	Mocs1 (-451705), Lrln2 (+44077)
chr4	134995104	134995473	uc.531	282.88	Rcan3 (-5569), Nipal3 (+55130)
chr7	127245537	127246141	uc.532	282.83	Tmem159 (-101)
chr4	148314778	148315238	uc.533	282.55	Casz1 (+136507), Pex14 (+158913)
chr3	40886532	40887570	uc.534	282.39	Pgrmc2 (-83)
chr11	98908421	98908858	uc.535	282.07	Igfbp4 (+6066), Tns4 (+41980)
chr1	64925110	64925634	uc.536	281.09	Fzd5 (-141048), Plekhh3 (+78026)
chr11	53880792	53881332	uc.537	280.7	Slc22a4 (-39470), Pdlim4 (+1457)
chr2	173875535	173876051	uc.538	280.7	Stx16 (-26759), Vapb (+312721)
chr4	83671895	83672379	uc.539	280.3	Psip1 (-539843), Bnc2 (+520172)
chr14	22867062	22867780	uc.540	279.65	Zfp503 (-58598)
chr11	94743110	94744277	uc.541	279.53	Xylt2 (-204887), Col1a1 (-53890)
chr18	81727678	81728210	uc.542	278.94	Sall3 (-544627), Galr1 (+848225)
chr12	87533005	87533400	uc.543	278.87	Esrrb (-229391), Tgfb3 (-113212)
chr8	49975650	49976139	uc.544	278.87	Odz3 (-215851)
chr16	30063143	30064678	uc.547	278.29	Hes1 (-1532)
chr4	116393369	116393959	uc.548	277.98	Tesk2 (+104)
chr3	99770001	99770631	uc.549	277.37	Spag17 (+80976), Wdr3 (+196010)
chr12	78698871	78699759	uc.550	277.35	Gphn (-628406), Fut8 (+359307)
chr10	76048844	76049290	uc.551	277.3	Ftcd (+10674), Col6a2 (+37082)
chr9	104648281	104648461	uc.552	276.81	Acpp (-408319), Mrpl3 (-307227)
chr13	47016547	47017049	uc.553	276.8	Nup153 (-193580), Kif13a (+8289)
chr19	20618183	20618639	uc.554	276.33	Anxa1 (-153250), Aldh1a1 (-58061)
chr6	91186341	91186816	uc.555	276.32	Fbln2 (+23821), Wnt7a (+174784)
chr13	36621383	36622022	uc.556	275.26	Nrn1 (+204620), Fars2 (+412423)
chr17	28216480	28217282	uc.558	274.91	Tcp11 (+648)
chr1	93980456	93980916	uc.559	274.11	AK028549 (-281172), Hdac4 (+64385)
chr4	43419101	43419642	uc.560	273.86	Tesk1 (-35777), Rusc2 (+24518)
chr11	63071515	63072113	uc.561	273.72	Pmp22 (+126802), Hs3st3b1 (+663972)
chr4	63071220	63071953	uc.562	273.37	Akna (-7108), Whrn (+85398)
chr15	76292026	76292984	uc.563	273.18	Scx (+4637), Bop1 (+15194)
chr13	51475065	51475611	uc.564	273.05	S1pr3 (-28795), Spin1 (+279071)
chr6	84344441	84344828	uc.565	273.03	Cyp26b1 (+199105), Dysf (+375252)
chr4	85935665	85936221	uc.566	272.68	Rraga (-285634), Adamts1 (+236124)

chr2	141705408	141705921	uc.567	272.25	NONE
chr6	4955501	4956060	uc.569	271.92	Ppp1r9a (+102461), Pon1 (+188043)
chr2	32770342	32770814	uc.570	271.38	Fam129b (+38924), Lrsam1 (+46193)
chrX	98455770	98456336	uc.571	271.21	Gm614 (+3278), Foxo4 (+6186)
chr5	65559891	65560442	uc.572	271.06	Klh5 (+37697), Rfc1 (+166711)
chr7	36910613	36911176	uc.573	270.91	Tshz3 (-572242), Zfp507 (-322887)
chr8	112741507	112742088	uc.575	270.84	Ftsjd1 (-62)
chr3	66874419	66875029	uc.576	270.83	Mlf1 (-303295), Rsrc1 (+85130)
chr7	134856215	134856673	uc.578	270.47	Bcl7c (-4164), Ctf1 (+194)
chr12	28471504	28471861	uc.579	270.43	Sox11 (-444100), Allc (+795665)
chr9	111863488	111863646	uc.581	270.43	Stac (-270847), Arpp21 (+226703)
chr10	20206661	20207184	uc.582	269.59	Bclaf1 (+174648), Pde7b (+237951)
chr17	79083429	79083910	uc.583	269.15	Strn (+52230), Vit (+176190)
chr11	63359099	63359498	uc.584	269.14	Hs3st3b1 (+376487), Pmp22 (+414287)
chr16	7099783	7100500	uc.585	268.99	A2bp1 (+30214)
chr15	66509462	66509825	uc.587	268.37	Tg (+7312), Sla (+134511)
chr4	32390450	32391236	uc.588	268.25	Bach2 (+64918), Gja10 (+298514)
chr6	6416256	6416699	uc.589	267.99	Slc25a13 (-249360), Shfm1 (+112180)
chr6	5031052	5031572	uc.590	267.78	Pon1 (+112512), Ppp1r9a (+177992)
chr12	97961581	97962027	uc.591	267.11	NONE
chr1	167045039	167045477	uc.592	266.93	Xcl1 (-179617), Tbx19 (+45646)
chr19	44982461	44982908	uc.593	266.82	Sema4g (-81149), Pax2 (+150801)
chr18	69681279	69681650	uc.595	265.68	Tcf4 (+176090), Rab27b (+531558)
chr9	36784446	36784985	uc.596	265.44	Fez1 (+133469), Pknox2 (+170183)
chr10	120309497	120309869	uc.597	265.35	Hmga2 (-395692), Msrb3 (+26344)
chr4	32389864	32390422	uc.598	265.34	Bach2 (+64218), Gja10 (+299214)
chr13	114602374	114602871	uc.599	264.76	Arl15 (+17907), Ndufs4 (+575628)
chr14	79641062	79641400	uc.600	264.2	AU017455 (+5872), 1300010F03Rik (+392246)
chr4	108032584	108033183	uc.601	264.07	Fam159a (+23070), 2010305A19Rik (+32127)
chr3	149150922	149151468	uc.602	263.66	Lphn2 (-533496)
chr4	57683596	57684013	uc.603	263.54	Ptpn3 (-369096), Akap2 (-183227)
chr9	41684783	41685201	uc.604	263.24	Ubash3b (-719415), Sorl1 (+247380)
chr13	56105202	56105744	uc.605	263.15	Pitx1 (-172687), H2afy (+131438)
chr1	180730186	180730690	uc.606	262.88	Kif26b (+271182), Smyd3 (+717696)
chr15	38218170	38218767	uc.608	262.64	Klf10 (+11993), Odf1 (+69511)
chr4	114464177	114464743	uc.610	261.43	Foxd2 (+117043), Gm12824 (+385131)
chrX	18019340	18019650	uc.612	261.34	4930578C19Rik (+18905), Kdm6a (+279702)
chr6	35304677	35305432	uc.613	261.18	BC064033 (-28914), Mtpn (+184833)
chr11	74645177	74646022	uc.615	260.54	Mnt (+1174), Sgsm2 (+64982)
chr9	47560310	47560697	uc.616	260.48	Fam55d (-409694), Cadm1 (+222069)
chr14	115835826	115836386	uc.618	260.19	Gpc5 (+344632)
chr16	89992069	89992827	uc.619	259.94	Sod1 (-228539), Tiam1 (-17504)
chr2	91771698	91772867	uc.620	259.68	Mdk (+156)
chr17	30605254	30605707	uc.621	259.31	Btbd9 (+107751), Zfand3 (+463449)
chr12	31195735	31196209	uc.622	259.17	Sntg2 (-137779), Tmem18 (-73336)
chr9	87963586	87964058	uc.623	258.88	Tbx18 (-337727), Nt5e (-258656)
chr6	36827242	36827808	uc.624	258.73	Ptn (-66164), Dgki (+422451)
chr13	116266015	116266369	uc.625	258.67	Itga1 (-374020), Isl1 (+833704)
chr6	52812002	52812356	uc.626	258.67	Tax1bp1 (+148456), Jazf1 (+206410)
chr16	26185880	26186314	uc.627	258.48	Leprel1 (-80227), Cldn1 (+185828)
chr4	132934021	132934398	uc.628	258.45	Slc9a1 (+8523), Trnp1 (+120255)
chr2	144502610	144502928	uc.629	258.39	1700010M22Rik (-146633), Dtd1 (+77080)
chr4	11881881	11882497	uc.630	258.23	Pdp1 (+11408), Cdh17 (+196885)
chr7	103934357	103934973	uc.631	258.23	Nars2 (-165372), Odz4 (+575518)
chr16	34079608	34080043	uc.632	258.19	Umps (-112737), KALRN (+17350)
chr6	32394301	32394657	uc.634	258	Podxl (-880542), Plxna4 (+143713)

chr10	13000644	13001039	uc.635	257.96	Fuca2 (-219992), Plagl1 (+190248)
chr9	41020483	41021055	uc.636	257.28	Ubash3b (-55192), Sorl1 (+911603)
chr1	173420535	173420956	uc.637	256.36	Refbp2 (-12863), F11r (+53054)
chr3	108394122	108394958	uc.646	255.86	Clcc1 (-62625), Taf13 (+19923)
chr17	26813157	26813455	uc.647	255.78	Atp6v0e (-35)
chr6	36840124	36840789	uc.648	255.24	Ptn (-79096), Dgki (+409519)
chr16	93071905	93072486	uc.649	255.15	Cbr1 (-535886), Runx1 (-245885)
chr13	34242074	34242465	uc.650	255.12	Tubb2b (-20047), Slc22a23 (+194781)
chr17	14677041	14677576	uc.651	254.91	Thbs2 (+153960), Smoc2 (+260796)
chr14	33638529	33639020	uc.652	254.88	Fam170b (-8373), Prrx1 (+225662)
chr16	44695675	44696518	uc.653	254.81	Boc (-137114), Gtpbp8 (+50379)
chr2	93378228	93378764	uc.654	254.66	Alx4 (-104095), Cd82 (-75393)
chr2	5037774	5038618	uc.655	254.63	Optn (-53212), Ccdc3 (-20626)
chr2	141883709	141884157	uc.657	254.47	Kif16b (+843267)
chr7	17461828	17462514	uc.659	253.87	Gng8 (-14964), Prkd2 (+33757)
chr15	78662777	78663798	uc.660	253.63	Card10 (-29816), Cdc42ep1 (-9789)
chr14	22987268	22987857	uc.662	253.28	Zfp503 (-178740)
chr13	111502682	111503179	uc.663	253.02	Actbl2 (-542290), Plk2 (+317679)
chr8	97436887	97437814	uc.664	252.83	Dok4 (-37139), Gpr114 (-10243)
chr13	32600633	32601131	uc.665	252.76	Wrnip1 (-293017), Gmds (-170469)
chr8	90806644	90806970	uc.666	252.71	Adcy7 (-84)
chr11	96258326	96258876	uc.668	252.65	Skap1 (-67337), Hoxb1 (+31529)
chr15	102088604	102088854	uc.669	252.51	Rarg (-815)
chr5	143723545	143724104	uc.671	251.99	Fscn1 (+1791), Rnf216 (+150848)
chr2	154873121	154873644	uc.673	251.61	Ahcy (+26779), a (+34077)
chr15	50579647	50579986	uc.674	251	Trps1 (+141770)
chr11	99009078	99009709	uc.675	250.82	Tns4 (-58774), Ccr7 (+6997)
chr2	106301713	106303102	uc.676	250.67	Dnajc24 (-458702), Mpped2 (-231208)
chr10	98761371	98761974	uc.678	250.07	Dusp6 (+35808), Csl (+460619)
chr6	146485639	146486105	uc.680	249.5	Itpr2 (-35438), 4933424B01Rik (+40485)
chr15	5819181	5819739	uc.681	249.31	Ptger4 (-625629), Dab2 (-517288)
chr7	28121491	28122045	uc.682	249	Ltbp4 (+863)
chr10	84604070	84604584	uc.686	248.66	Mterfd3 (-13581), Cry1 (+43472)
chr1	138474252	138475075	uc.687	248.34	Zfp281 (-46814), Kif14 (+110239)
chr11	88341902	88342457	uc.688	248.22	Msi2 (+237363), Mrps23 (+324260)
chr5	99951640	99952111	uc.689	248.16	Rasgef1b (-269930), Hnrnpd (+456081)
chr7	52314644	52315196	uc.690	247.59	Nosip (-2879), Prrg2 (+2101)
chr14	27077507	27078092	uc.691	247.24	Duxbl (-3944)
chrX	11735343	11735809	uc.692	247.24	Atp6ap2 (-429420), Bcor (-78396)
chr2	37636993	37637524	uc.693	247.01	Crb2 (+5490), Dennd1a (+505645)
chr14	23934164	23934832	uc.694	246.89	Kcnma1 (+888929)
chr13	101870438	101870915	uc.695	246.56	Slc30a5 (-267295), Pik3r1 (+667495)
chr14	102802710	102803188	uc.698	246.3	Kctd12 (+578905), Lmo7 (+673804)
chr3	101415520	101416091	uc.699	246.25	Atp1a1 (-7226), Slc22a15 (+312563)
chr4	10129025	10129419	uc.700	245.94	Gdf6 (+357703), Plekhf2 (+805544)
chr13	47013783	47014356	uc.701	245.79	Nup153 (-190852), Kif13a (+11017)
chr14	26798122	26798785	uc.702	245.52	Duxbl (-4037)
chr14	60358241	60358679	uc.703	245.3	Shisa2 (+114342), Atp8a2 (+347211)
chr16	50797033	50797473	uc.704	244.74	Bbx (-364751)
chr10	13425703	13425988	uc.706	244.37	Pex3 (-152898), Aig1 (+162790)
chr7	53040820	53041312	uc.708	244.31	Lmtk3 (+1749), Cyth2 (+28620)
chr12	72328470	72329051	uc.709	243.95	Timm9 (-91099), Dact1 (-82210)
chr19	9127247	9127782	uc.710	243.49	Scgb1a1 (+34931), Ahnak (+63741)
chr11	51346731	51347150	uc.711	243.44	Agxt2l2 (-51318), Col23a1 (+243519)
chr5	118085815	118086141	uc.713	242.66	Nos1 (-230870), Ksr2 (+221969)
chr14	58042600	58043316	uc.714	242.42	Ift88 (+50)

chr9	65460903	65461396	uc.715	242.42	Rbpms2 (-17239), Pif1 (+26138)
chr18	38209534	38210335	uc.717	242.4	Arap3 (-52707), Pcdh1 (+159481)
chr1	173051110	173051308	uc.718	242.27	Fcgr3 (-61675), Sdhc (+29525)
chr11	63300808	63300998	uc.726	242.03	Pmp22 (+355891), Hs3st3b1 (+434883)
chr7	52348203	52348620	uc.727	241.85	Rcn3 (-829)
chr4	108022403	108022886	uc.728	241.52	2010305A19Rik (+21888), Fam159a (+33309)
chr2	32175049	32175712	uc.729	241	Golga2 (+31608), Dnm1 (+33443)
chr13	60327708	60328255	uc.730	240.63	Dapk1 (-375326), Gas1 (-49256)
chr12	35476823	35477419	uc.731	240.58	Hdac9 (-263367), Prps11 (-192312)
chr5	46964603	46964975	uc.732	240.32	Lcorl (-716010)
chr6	122343154	122343393	uc.734	239.58	Phc1 (-56241), Rimklb (+93049)
chr2	118369808	118370498	uc.735	239.31	Srp14 (-64721), Bmf (+5261)
chr11	76313526	76314019	uc.736	239.09	Abr (+9148), Timm22 (+93081)
chr19	42799614	42799893	uc.737	238.75	Loxl4 (-112458), Pyroxd2 (+27511)
chr2	110363565	110364073	uc.738	238.67	Fibin (-160669), Slc5a12 (-73636)
chr11	34725512	34725931	uc.739	238.65	Slit3 (-209236), Ccdc99 (-78579)
chr15	4178048	4178337	uc.741	238.26	Plcx3 (-147298), Oxct1 (+201765)
chr9	87451337	87451667	uc.742	238.12	4922501C03Rik (-301135), Tbx18 (+174593)
chr18	81428560	81429072	uc.743	237.69	Sall3 (-245499)
chr15	97122203	97122716	uc.744	237.44	Amigo2 (-44742), Rpap3 (+413793)
chr12	25783160	25784060	uc.745	237.36	Id2 (-2653)
chr13	56683312	56684064	uc.746	237.36	Lect2 (-33789), Tgfb1 (-27276)
chr9	16792483	16793034	uc.747	237.24	Fat3 (-610084)
chr4	90748462	90749349	uc.749	237.07	Elavl2 (+289840), Zfp352 (+863395)
chr12	96030619	96031045	uc.750	236.7	Flrt2 (-899604)
chr4	58690702	58691221	uc.754	235.99	Lpar1 (-124797), Olfr267 (+107630)
chr6	110086968	110087487	uc.755	235.99	Grm7 (-508364)
chr2	104307268	104307837	uc.756	235.56	Hipk3 (+27093), Cd59a (+371595)
chr7	100943533	100944205	uc.757	235.37	Prcp (+920106)
chr3	130626288	130626500	uc.758	235.25	Rpl34 (-193168), Lef1 (-186995)
chr9	35186597	35186908	uc.760	235	Cdon (-72877), Rpusd4 (+111287)
chr11	52876551	52876984	uc.761	234.78	Hspa4 (+237213), Fstl4 (+298560)
chr8	80208385	80208697	uc.762	234.65	Tmem184c (-74021), Ednra (+39810)
chr2	57549261	57549887	uc.763	234.1	Galt5 (-300992), Gpd2 (+459485)
chr5	127799599	127800254	uc.764	233.9	Tmem132c (+77731), Slc15a4 (+297835)
chr1	37277085	37277363	uc.765	233.82	Inpp4a (-79514), Cnga3 (+1118)
chr11	85550717	85551346	uc.767	233.47	Tbx2 (-95085), Bcas3 (+384316)
chr7	150451039	150451775	uc.768	233.43	Kcnq1 (+158248), Cdkn1c (+195548)
chr14	47281623	47282153	uc.769	233.37	Bmp4 (-271614), Cdkn3 (-98328)
chr3	101199256	101199740	uc.770	233.15	Igsf3 (+18450), Atp1a1 (+209082)
chr16	57366275	57366906	uc.771	233.06	Filip1l (+13201), 2610528E23Rik (+240389)
chr4	106539463	106539965	uc.772	232.94	Acot11 (-67278), Ssbp3 (-44361)
chr5	68032750	68033270	uc.773	232.91	Shisa3 (+33888), Atp8a1 (+205660)
chr4	119095269	119095624	uc.774	232.83	Ppcs (-422), Zmynd12 (+158)
chr13	94159063	94159748	uc.775	232.78	Homer1 (+84956), Jmy (+110238)
chr4	114452646	114453209	uc.776	232.77	Foxd2 (+128575), Gm12824 (+373599)
chr2	161292782	161293180	uc.777	232.59	Chd6 (-358189)
chr15	84049381	84049932	uc.778	232.4	Parvb (-12816), Samm50 (+26994)
chr17	86136493	86137162	uc.779	232.4	Six2 (-49234), Srbd1 (+407687)
chr8	94239618	94240122	uc.780	232.4	Irx3 (+85403), Fto (+402446)
chr16	96046533	96047331	uc.781	232.36	Ets2 (+122918), Psmg1 (+165578)
chr13	52798817	52799259	uc.782	232.35	Syk (+106787), Auh (+226008)
chr1	12796804	12797162	uc.783	232.28	Sulf1 (+88357), Slco5a1 (+184233)
chrX	99042493	99042909	uc.784	232.23	Pin4 (-272103), Cxcr3 (-113215)
chr9	21301036	21301761	uc.785	232.19	Tmed1 (+13231), Dnm2 (+72010)
chr3	116504645	116505004	uc.786	231.97	Slc35a3 (-89627), Agl (+6259)

chr1	20456311	20456897	uc.787	231.79	Pkhd1 (+151534)
chr12	81330813	81331761	uc.788	231.38	Zfp36l1 (-117287), Actn1 (+30071)
chr16	90449852	90450494	uc.790	230.79	Hunk (+63531), 2610039C10Rik (+277443)
chr4	83696002	83696539	uc.791	230.74	Psip1 (-563977), Bnc2 (+496038)
chr15	13125979	13126521	uc.793	230.58	Cdh6 (-22856)
chr6	6736045	6736587	uc.794	230.58	Shfm1 (-207658), Dlx6 (-77018)
chr15	96831279	96831774	uc.795	230.43	Slc38a2 (-301398), Slc38a4 (+54860)
chr6	61090303	61090799	uc.796	230.18	Mmm1 (+196240)
chr11	63814503	63814954	uc.797	230.13	Hs3st3b1 (-78943), Cox10 (+78187)
chr17	4778294	4778534	uc.798	230.06	Ldhal6b (+640353)
chr13	74024999	74025365	uc.799	229.83	Nkd2 (-40103), Trip13 (+50033)
chr18	78464026	78464556	uc.802	229.58	Slc14a1 (-144230), Slc14a2 (+329398)
chr9	47036854	47037307	uc.804	229.46	Cadm1 (-301354), Zfp259 (+955934)
chr17	59111504	59112004	uc.805	229.21	2610034M16Rik (+19044)
chr1	163948007	163948606	uc.806	228.98	Pigc (+48988), Dnm3 (+459858)
chr15	50529961	50530510	uc.807	228.98	Trps1 (+191351)
chr1	187660507	187660962	uc.808	228.95	Lyplal1 (+280454), Slc30a10 (+382008)
chr1	62859854	62860011	uc.810	228.46	Nrp2 (+110042), Ndufs1 (+363463)
chr12	32633887	32635069	uc.831	228.32	Hbp1 (+610)
chr3	96866852	96867266	uc.832	228.1	Acp6 (-95641), Gja5 (+30720)
chr6	4513129	4513962	uc.833	228.08	Casd1 (-37520), Col1a2 (+57849)
chr8	122859833	122860315	uc.834	227.9	Gse1 (-152692), 6430548M08Rik (+222022)
chr12	95910258	95910812	uc.835	227.86	NONE
chr14	77081342	77081769	uc.836	227.82	Enox1 (-475067), Serp2 (-125062)
chr1	138484206	138484811	uc.837	227.71	Zfp281 (-36969), Kif14 (+120084)
chr1	164147399	164147859	uc.838	227.66	Pigc (+248310), Dnm3 (+260536)
chr2	33556081	33556725	uc.839	227.5	Lmx1b (-60372), Fam125b (+187063)
chr10	73291436	73291897	uc.840	227.41	Pcdh15 (+7052)
chr6	50934491	50934999	uc.841	227.29	Nfe2l3 (-447924), Npvf (-330353)
chr5	21048987	21049449	uc.842	227.21	Lrrc17 (-127)
chr11	52905006	52905515	uc.843	227.05	Hspa4 (+208720), Fstl4 (+327053)
chr12	101425628	101426125	uc.844	227.04	BC002230 (-28014), Calm1 (-11874)
chrX	141933323	141933741	uc.845	227	Amot (-11943)
chr11	57530736	57531345	uc.846	226.87	Sap30l (-84098), Galnt10 (+72097)
chr16	87646473	87646850	uc.847	226.57	Bach1 (-52537), ORF63 (+93087)
chr6	65709203	65709866	uc.848	226.57	Prdm5 (-19421), A930038C07Rik (+87930)
chr15	84046601	84047161	uc.849	226.52	Parvb (-15592), Samm50 (+24218)
chr7	36860255	36860815	uc.850	226.52	Tshz3 (-622602), Zfp507 (-272527)
chr5	143026017	143026626	uc.851	226.5	Radil (+709)
chr16	34082221	34082659	uc.852	226.4	Umps (-115351), KALRN (+14736)
chr2	93150088	93150551	uc.853	226.4	Tspan18 (+24324), Trp53i11 (+122579)
chr9	121957137	121957636	uc.854	226.4	Snrk (-68997), C85492 (-52243)
chr12	111079514	111079743	uc.855	226.34	Dio3 (-437811), Rtl1 (-246016)
chr2	141554800	141555178	uc.856	226.27	NONE
chr4	148511192	148511846	uc.857	226.02	Apitd1 (+190)
chr5	32435206	32435942	uc.861	225.06	Fosl2 (-3271)
chr18	60815853	60816450	uc.862	224.62	Synpo (-26413), Ndst1 (+57134)
chr3	30157418	30157765	uc.865	223.3	evi-1 (-260922), Mecom (+250817)
chr11	112875519	112875790	uc.866	223.29	Sox9 (+232131), Slc39a11 (+551420)
chr9	63120114	63120794	uc.867	223.26	Lbxcor1 (-125667), Map2k5 (+105205)
chr12	80129822	80130382	uc.868	222.7	Plekhh1 (-48)
chr13	53300487	53300898	uc.869	222.66	Nfil3 (-224285), Ror2 (+80785)
chr8	35137968	35138499	uc.870	222.66	Rbpms (-97921), Dctn6 (+33331)
chr11	51351840	51352418	uc.871	222.6	Agxt2l2 (-46130), Col23a1 (+248707)
chr13	45179112	45179503	uc.872	222.55	Mylip (-305803), Dtnbp1 (-81843)
chr5	140069721	140070142	uc.873	222.52	Uncx (+50080), Micall2 (+142355)

chr8	93159626	93160055	uc.874	222.52	Tox3 (-287690), Chd9 (-192895)
chr4	82750141	82750576	uc.875	222.47	Snappc3 (-313289), Frem1 (-83353)
chr18	84576711	84577293	uc.877	221.74	Zfp407 (+181894), Zadh2 (+319452)
chr4	58559405	58559937	uc.878	221.73	Lpar1 (+6494), Musk (+260837)
chr1	185596538	185596932	uc.879	221.71	Dusp10 (-261605), Tlr5 (+711816)
chr16	63501338	63501776	uc.880	221.69	Epha3 (+362426), Pros1 (+647397)
chr4	10257325	10257765	uc.883	221.18	Gdf6 (+486026), Plekhf2 (+677221)
chr2	51437872	51438457	uc.884	221.11	Rnd3 (-433534), Tas2r134 (-44866)
chr11	117268851	117269576	uc.887	220.68	Tnrc6c (-246389), Sept9 (+208239)
chr18	81419889	81420331	uc.888	220.66	Sall3 (-236793)
chr15	74157202	74157600	uc.889	220.6	Bai1 (-189225), Ptp4a3 (+578559)
chr18	54981286	54981740	uc.890	220.5	Zfp608 (+168054), Csnk1g3 (+959746)
chr3	83788384	83788783	uc.892	220.32	Tlr2 (-143054), D930015E06Rik (+55499)
chr3	51505143	51506029	uc.893	220.3	Mgst2 (+40471), Maml3 (+403342)
chr2	158865764	158866354	uc.895	220.05	Dhx35 (+245503)
chr8	36636582	36637372	uc.897	219.68	Eri1 (-78390), Mfhas1 (-13875)
chr12	80914787	80915234	uc.899	219.39	Zfp3611 (+298989), Rad5111 (+516742)
chr8	111418349	111418843	uc.901	219.32	Pmfbp1 (-599331), Zfhx3 (+180052)
chr17	44941510	44941913	uc.902	219.23	Runx2 (+10034), Supt3h (+27592)
chr8	105557741	105558237	uc.904	218.84	Cdh11 (-248978)
chr14	26937894	26938468	uc.906	218.61	Duxbl (-4167)
chr5	45077423	45077874	uc.907	218.38	Tapt1 (-459804), Ldb2 (+113297)
chr1	182215886	182216434	uc.908	218.16	Itpkb (-44447), Psen2 (-29729)
chr8	35129266	35129816	uc.909	218.16	Rbpms (-89228), Dctn6 (+42024)
chr6	111833891	111834349	uc.915	216.64	Lmcd1 (-389692)
chr5	133642806	133643219	uc.916	216.54	NONE
chr1	180733336	180733590	uc.917	216.46	Kif26b (+274207), Smyd3 (+714671)
chr16	95612585	95612915	uc.919	216.17	Kcnj15 (+133492), Erg (+139222)
chr7	149702133	149702505	uc.921	215.91	Mrpl23 (-16703), Lsp1 (+44571)
chr19	4897176	4897354	uc.923	215.77	Bbs1 (+9347), Zdhhc24 (+18561)
chr1	135422310	135422739	uc.925	215.69	Sox13 (-101736), Snrpe (+84332)
chr14	26381178	26381724	uc.926	215.69	Ppif (-132205), Zmiz1 (+102673)
chr3	79807214	79807693	uc.927	215.69	1110032E23Rik (+117602), Gria2 (+799259)
chr2	36062515	36063078	uc.930	215.19	Rbm18 (-70573), Ptgs1 (-23149)
chr9	106145438	106145849	uc.931	214.98	Alas1 (+4641), Tlr9 (+20715)
chrX	97155653	97155860	uc.944	214.82	Eda (-15188), Tmem28 (+139349)
chr6	72605244	72605681	uc.946	214.54	Tgoln2 (-38469), Tcf7l1 (+133487)
chr6	94840843	94841426	uc.947	214.54	Kbtbd8 (-226765), Lrig1 (-190996)
chr2	11981822	11982494	uc.948	214.37	Fbxo18 (-283004), Itga8 (+241389)
chr11	119745070	119745587	uc.949	214.01	Chmp6 (-29795), Rptor (+281020)
chr18	57428608	57429177	uc.950	213.66	Prrc1 (-85502), Megf10 (+135764)
chr18	77912467	77912847	uc.951	213.66	Rnf165 (-108782), Haus1 (+93862)
chr8	127600266	127600835	uc.953	213.66	Disc1 (+22456), Sipa1l2 (+416182)
chr2	75214749	75215220	uc.954	213.48	Hnrnpa3 (-282331), Mtx2 (+551116)
chr12	78105878	78106589	uc.955	213.4	Fut8 (-233774), Max (-42999)
chr12	34652446	34652935	uc.956	213.24	Twist1 (+10155), Hdac9 (+561063)
chr2	162927527	162927897	uc.957	213.24	Tox2 (-123478), Gtsf1l (-12375)
chr2	45082587	45083212	uc.958	212.95	Zeb2 (-114101)
chr8	97424830	97425365	uc.960	212.76	Dok4 (-24886), Gpr114 (-22496)
chr9	48483367	48483704	uc.961	212.76	Nnmt (-70354), Zbtb16 (+160514)
chr8	49394319	49394844	uc.962	212.23	Dctd (+210136), Odz3 (+365462)
chr10	3806074	3806417	uc.963	212.22	Rgs17 (-617895), Oprm1 (-248275)
chr18	75261639	75262148	uc.965	212.04	Smad7 (-265125), Dym (+83468)
chr10	94506603	94507081	uc.966	211.81	Plxnc1 (-99630), Cradd (+279889)
chr9	41036923	41037454	uc.967	211.8	Ubash3b (-71612), Sorl1 (+895183)
chr15	51630030	51630661	uc.968	211.78	Trps1 (-908759), Eif3h (+66661)

chr11	86298412	86298800	uc.969	211.71	Rnft1 (+447)
chr7	137938498	137938979	uc.973	211.11	Plekha1 (-70685), Tacc2 (+217741)
chr9	80110196	80110677	uc.974	211.11	Myo6 (+97590), Impg1 (+248608)
chr12	105875367	105875803	uc.975	210.61	Gsc (-164139), Dicer1 (+114577)
chr11	114691450	114691948	uc.977	210.45	Gprc5c (-21155), Gpr142 (+31461)
chr9	32659867	32660505	uc.978	210.42	Ets1 (+156559)
chr10	57845535	57846019	uc.979	210.41	Ranbp2 (-63823), Lims1 (+59482)
chr7	137208000	137208392	uc.980	210.37	Fgfr2 (+202126), Brwd2 (+472819)
chr7	137152154	137152504	uc.982	210.15	Fgfr2 (+257993), Brwd2 (+416952)
chr4	131040461	131041078	uc.984	209.97	Ptpru (+353423), Matn1 (+540470)
chr18	71440768	71441120	uc.986	209.57	Mbd2 (+712998)
chr7	38123025	38123581	uc.989	209.45	Zfp536 (+431468), Tshz3 (+640166)
chr12	111734725	111735135	uc.990	209.25	Dync1h1 (-104675), Ppp2r5c (+10981)
chr2	16407570	16407969	uc.991	209.25	Plxdc2 (+129821)
chr3	141212741	141213193	uc.992	209.25	Unc5c (+84439), Bmpr1b (+432248)
chr15	79780828	79781416	uc.993	209.17	Cbx7 (-18046), Pdgfb (+64116)
chr10	80237243	80237558	uc.994	208.43	Dot1l (+19450), Plekhj1 (+23970)
chr6	15354798	15355291	uc.995	208.33	Mdfic (-315616), Foxp2 (+219539)
chr4	144587359	144587805	uc.996	208.14	Dhrs3 (+104602), Vps13d (+192987)
chr19	28540237	28540638	uc.998	207.97	Rfx3 (-454808), Glis3 (+214129)
chr17	45722061	45722488	uc.999	207.83	Hsp90ab1 (-12065), Slc29a1 (+7067)
chr17	86631309	86631693	uc.1000	207.67	Epas1 (-521703), Prkce (+63752)

Appendix Table 2. GO Biological Processes associated with the top 795 ChIP-seq dataset

Functional classification of the curated top 795 peaks of the ChIP-seq analysis. Terms enriched by GREAT analysis and associated with the gene ontology (GO) “**Biological Process**” are shown (McLean et al. 2010). The *basal plus extension* association rule (5kb upstream, 1kb downstream, 1Mb maximum extension) was used. Top 20 binomial enriched terms are shown. FDR threshold, 0.05. Significant p-values are displayed in bold. Terms appear bold when significant for both the binomial and hypergeometric tests.

GO Biological Process	Binomial Results			Hypergeometric Results		
	Raw P-Value	FDR Q-Val	Fold Enrichment	FDR Q-Val	Fold Enrichment	Observed Gene Hits
negative regulation of metabolic process	6.45495e-18	3.19105e-15	2.1416	3.87500e-13	2.2665	104
negative regulation of gene expression	1.22989e-17	5.67470e-15	2.3069	4.08231e-15	2.6634	88
negative regulation of macromolecule metabolic process	3.40382e-17	1.38576e-14	2.1440	5.32716e-13	2.3098	99
negative regulation of cellular metabolic process	4.28187e-15	1.18539e-12	2.0725	7.89088e-11	2.1992	91
negative regulation of cellular biosynthetic process	5.75502e-15	1.53194e-12	2.1630	5.79209e-12	2.4031	84
negative regulation of transcription, DNA-dependent	7.69401e-15	1.97223e-12	2.3342	1.10349e-12	2.8088	68
negative regulation of RNA metabolic process	8.66558e-15	2.06808e-12	2.3296	1.48338e-12	2.7875	68
negative regulation of biosynthetic process	9.86632e-15	2.27616e-12	2.1459	1.21791e-11	2.3696	84
embryonic morphogenesis	1.04685e-14	2.33717e-12	2.2750	5.90346e-19	3.3215	80
negative regulation of transcription	1.23094e-14	2.66230e-12	2.2152	1.33253e-12	2.5975	77
negative regulation of nucleobase, nucleoside, nucleotide and nucleic acid metabolic process	3.31682e-14	6.95628e-12	2.1524	3.50448e-12	2.4911	80
negative regulation of nitrogen compound metabolic process	3.70032e-14	7.31712e-12	2.1488	5.73925e-12	2.4674	80
negative regulation of macromolecule biosynthetic process	9.03480e-14	1.69000e-11	2.1192	7.38271e-11	2.3467	80
limb development	1.04306e-13	1.89973e-11	3.1784	4.88426e-17	5.2718	42
negative regulation of transcription from RNA polymerase II promoter	1.88423e-13	3.03273e-11	2.4753	9.63013e-11	2.9858	52
limb morphogenesis	3.11913e-13	4.69293e-11	3.2163	3.19889e-16	5.2233	40
skeletal system development	5.45128e-13	7.69966e-11	2.3917	1.02430e-11	2.9126	59
embryonic limb morphogenesis	8.76086e-12	1.01057e-9	3.2996	2.07522e-14	5.2474	35
respiratory system development	1.77241e-11	1.91670e-9	2.8821	8.17558e-10	3.9003	33
lung development	7.44624e-11	7.69185e-9	2.8733	5.57274e-9	3.9174	30

Appendix Table 3. GREAT gene association tables of the top 795 peak regions

associated to the GO Biological Process terms “limb development” and “embryonic morphogenesis”. Genes are sorted alphabetically. The distance to the transcriptional start site is shown in brackets.

GO Biological process: Limb development

Alx4 (-104095)	Lmx1b (+96173)
Asph (-156740)	Lmx1b (-60372)
Bmp4 (-271614)	Meox2 (-317437)
Bmp7 (+15141)	Msx1 (-69274)
Bmpr1b (+432248)	Msx2 (-282447)
Bmpr1b (-256400)	Mycn (+360244)
Cyp26b1 (+199105)	Mycn (-256539)
Dicer1 (+114577)	Nog (+4018)
Dicer1 (+116924)	Nr2f2 (+255483)
Dicer1 (+145870)	Nr2f2 (-452890)
Dicer1 (+158315)	Pbx1 (+21956)
Dicer1 (+194133)	Pitx1 (-172687)
Dicer1 (+72498)	Pitx1 (-281238)
Dlx6 (-77018)	Plxna2 (-9106)
evi-1 (-260922), Mecom (+250817)	Prrx1 (+136398)
Fbxw4 (-30962), Fgf8 (+51718)	Psen2 (-29729)
Fbxw4 (-65591), Fgf8 (+17089)	Rarg (-815)
Fgf10 (-231290)	Rdh10 (+123953)
Fgfr1 (+24842)	Ski (+32626)
Fgfr2 (+154828)	Tbx3 (-18874)
Fgfr2 (+202126)	Tbx3 (-57955)
Fgfr2 (+257993)	Tbx4 (+20326)
Gas1 (-49256)	Tbx4 (-13770)
Gja5 (+30720)	Tbx5 (-37965), Tbx3 (+126029)
Gli2 (+148420)	Twist1 (+10155)
Gli3 (-17427)	Wnt7a (+174784)
Ift88 (+50)	Zbtb16 (+14989)
Lef1 (-186995)	Zbtb16 (+160514)

GO Biological process: Embryonic morphogenesis

Aldh1a1 (-58061)	Lmx1b (-60372)
Alx4 (-104095)	Map3k7 (+211995)
Amot (-11943)	Msx1 (-69274)
Bmp4 (-271614)	Msx2 (-282447)
Bmp7 (+15141)	Myc (-633394)
Cdon (-72877)	Mycn (+360244)
Cyp26b1 (+199105)	Mycn (-256539)
Dlx6 (-77018)	Myo6 (+97590)
Esrrb (-229391), Tgfb3 (-113212)	Ndst1 (+57134)
evi-1 (-260922), Mecom (+250817)	Nkx2-5 (-3113)
Ext1 (+46752)	Nog (+4018)
Eya1 (+538981)	Nr4a3 (-405944)
Fbxw4 (-30962), Fgf8 (+51718)	Odz4 (+450335)
Fbxw4 (-65591), Fgf8 (+17089)	Odz4 (+575518)
Fgf10 (-231290)	Pax2 (+150801)
Fgfr1 (+24842)	Pbx1 (+21956)
Fgfr2 (+154828)	Pcdh15 (+7052)
Fgfr2 (+202126)	Pcdh15 (+858486)
Fgfr2 (+257993)	Pitx1 (-172687)
Foxf1a (+4562)	Pitx1 (-281238)
Foxf1a (-245369)	Prrx1 (+136398)
Foxp4 (-173217)	Psen2 (-29729)

Foxp4 (-49648)
Frzb (+42500)
Gas1 (-49256)
Gbx2 (-120967)
Gja5 (+30720)
Gli2 (+148420)
Gli3 (-17427)
Gsc (+32825)
Gsc (-120401), Dicer1 (+158315)
Gsc (-132846), Dicer1 (+145870)
Gsc (-161792), Dicer1 (+116924)
Gsc (-164139), Dicer1 (+114577)
Gsc (-206218), Dicer1 (+72498)
Gsc (-84583), Dicer1 (+194133)
Hand2 (+10990)
Hand2 (+13243)
Hand2 (-681445)
Hes1 (+125787)
Hes1 (+3216)
Hes1 (-1532)
Hlx (+487566)
Hoxb1 (+31529)
Hoxb1 (+55704)
Id2 (-2653)
Ift88 (+50)
Itga8 (+241389)
Kcnq4 (-70073)
Lef1 (-186995)
Lmo4 (+627698)
Lmx1b (+96173)
Rarg (-815)
Rdh10 (+123953)
Ror2 (+102683)
Ror2 (+80785)
Satb2 (-125118)
Shroom3 (+203082)
Six2 (-49234)
Ski (+32626)
Socs3 (+5679)
Sod1 (-228539)
Spry2 (+1731)
Spry2 (+518908)
Tbx15 (+412427)
Tbx18 (+174593)
Tbx18 (-337727)
Tbx20 (-200047)
Tbx3 (-18874)
Tbx3 (-57955)
Tbx4 (+20326)
Tbx4 (-13770)
Tbx5 (-37965), Tbx3 (+126029)
Tcf21 (+3656)
Tcf7l2 (+344916)
Tcf7l2 (+358130)
Twist1 (+10155)
Ugdh (+20003)
Wnt7a (+174784)
Zbtb16 (+14989)
Zbtb16 (+160514)
Zeb2 (-114101)

Supplementary Table 4

Gene	Allele symbol	MGI number	PMID
Adm	<i>Adm</i> ^{tm1Mtnz}	MGI:3811632	18723674
Aifm1	<i>Aifm1</i> ^{tm2Pngr}	MGI:3686777	16287843
Akap5	<i>Akap5</i> ^{tm1Jscoe}	MGI:3809936	18711127
Akt2	<i>Akt2</i> ^{tm1Mbb}	MGI:2158455	11387480
Apba1	<i>Apba1</i> ^{tm1Sud}	MGI:3697697	12547917
Apba2	<i>Apba2</i> ^{tm1Sud}	MGI:3697709	17167098
Apba3	<i>Apba3</i> ^{tm1Sud}	MGI:3697711	17167098
Apc	<i>Apc</i> ^{tm2Rak}	MGI:3688435	17002498
Bambi	<i>Bambi</i> ^{tm1Jian}	MGI:3758816	17661381
Bdnf	<i>Bdnf</i> ^{tm1Krj}	MGI:3582638	12890780
Bhlhe40	<i>Bhlhe40</i> ^{tm1Rhli}	MGI:3775802	18234890
Birc5	<i>Birc5</i> ^{tm1Mak}	MGI:3046203	14757745
Bmp2	<i>Bmp2</i> ^{tm1Jfm}	MGI:3583785	15986484
Bmp4	<i>Bmp4</i> ^{tm1Jfm}	MGI:3041440	15070745
Bmp4	<i>Bmp4</i> ^{tm3.1Blh}	MGI:2181190	11857779
Bmp4	<i>Bmp4</i> ^{tm4Blh}	MGI:3797048	18404215
Braf	<i>Braf</i> ^{tm1Wds}	MGI:3711006	17396120
Cacna1g	<i>Cacna1g</i> ^{tm1Stl}	MGI:3530499	15677322
Card6	<i>Card6</i> ^{tm1Aldu}	MGI:3776907	18160713
Cdc73	<i>Cdc73</i> ^{tm1Btt}	MGI:3794030	18212049
Cdh2	<i>Cdh2</i> ^{tm1Glr}	MGI:3522469	15662031
Cdh22	<i>Cdh22</i> ^{tm1Hsav}	MGI:3837802	19194496
Chat	<i>Chat</i> ^{tm1Jrs}	MGI:3045899	12441053
Chd4	<i>Chd4</i> ^{tm1.1Kge}	MGI:3641408	15189737
Cnn2	<i>Cnn2</i> ^{tm1.1Jin}	MGI:3820422	18617524
Cnr1	<i>Cnr1</i> ^{tm1Ltz}	MGI:2182922	12152079
Cops5	<i>Cops5</i> ^{tm1Rpar}	MGI:3775801	18268034
Cops8	<i>Cops8</i> ^{tm1Nwe}	MGI:3762119	17906629
Ctnnd1	<i>Ctnnd1</i> ^{tm1Abre}	MGI:3617486	16399075
Ctnnd1	<i>Ctnnd1</i> ^{tm1Lfr}	MGI:3640772	16815331
Cxadr	<i>Cxadr</i> ^{tm1Know}	MGI:3815066	18636119
Cxadr	<i>Cxadr</i> ^{tm1Mds}	MGI:3711225	16543498
Dab1	<i>Dab1</i> ^{tm1Bwh}	MGI:3777252	18029196
Daxx	<i>Daxx</i> ^{tm2Led}	MGI:3840084	N/A (Direct Data Submission)
Dgat1	<i>Dgat1</i> ^{tm2Far}	MGI:3842432	19028692
Dicer1	<i>Dicer1</i> ^{tm1Smr}	MGI:3641051	16099834
Dsc3	<i>Dsc3</i> ^{tm2Pko}	MGI:3812225	18682494
Efnb1	<i>Efnb1</i> ^{tm1Rha}	MGI:3653699	12919674

Efnb1	<i>Efnb1</i> ^{tm1Sor}	MGI:3039289	15037550
Efnb2	<i>Efnb2</i> ^{tm4Kln}	MGI:3026687	14699416
Egln1	<i>Egln1</i> ^{tm2Fong}	MGI:3778917	16966370
Egln2	<i>Egln2</i> ^{tm2Fong}	N/A	16966370
Egln3	<i>Egln3</i> ^{tm2Fong}	N/A	16966370
En1	<i>En1</i> ^{tm8.1Alj}	MGI:3789091	17537797
Epb4.1I1	<i>Epb4.1I1</i> ^{tm1Aliv}	MGI:3838852	19225127
Epb4.1I2	<i>Epb4.1I2</i> ^{tm1Aliv}	MGI:3838851	19225127
Erap1	<i>Erap1</i> ^{tm1Gnie}	MGI:3830213	17277129
Erbp4	<i>Erbp4</i> ^{tm1Fej}	MGI:2680217	12954715
Erbp4	<i>Erbp4</i> ^{tm1Htig}	MGI:3603749	15863464
Esrrb	<i>Esrrb</i> ^{tm1.1Nat}	MGI:3720481	17765677
Ets2	<i>Ets2</i> ^{tm4Rgo}	MGI:3769393	17977525
Etv5	<i>Etv5</i> ^{tm1Sun}	N/A	19386269
Ezr	<i>Ezr</i> ^{tm2Aim}	MGI:3052159	15177033
F3	<i>F3</i> ^{tm1Nmk}	MGI:3803978	17663739
Fgf8	<i>Fgf8</i> ^{tm1.1Mrt}	MGI:1857843	9462741
Fgf9	<i>Fgf9</i> ^{tm1Fwan}	MGI:3621451	16496342
Flcn	<i>Flcn</i> ^{tm1Btt}	MGI:3829641	18974783
Flt4	<i>Flt4</i> ^{tm2Ali}	MGI:3804462	18519586
Foxd3	<i>Foxd3</i> ^{tm3Lby}	MGI:3790794	18367558
Frs2	<i>Frs2</i> ^{tm1Fwan}	MGI:3768912	17868091
Fzd5	<i>Fzd5</i> ^{tm2Nat}	MGI:3796577	18509025
Fzr1	<i>Fzr1</i> ^{tm1Mama}	MGI:3800718	18552834
Gabpa	<i>Gabpa</i> ^{tm1Sjb}	MGI:3665312	17485447
Gabrg2	<i>Gabrg2</i> ^{tm2Lusc}	MGI:2680624	14572465
Gad1	<i>Gad1</i> ^{tm1Rpa}	MGI:3527168	17582330
Gata3	<i>Gata3</i> ^{tm1Bchd}	MGI:3719567	16319112
Gata3	<i>Gata3</i> ^{tm3Gsv}	MGI:3696958	17151017
Gba	<i>Gba</i> ^{tm1Clk}	MGI:3698018	17079175
Gbx2	<i>Gbx2</i> ^{tm1Alj}	MGI:2388609	12367504
Gdf1	<i>Gdf1</i> ^{tm1Dmus}	MGI:3806582	18615710
Gfra1	<i>Gfra1</i> ^{tm2Jmi}	MGI:3715156	17507417
Gjc1	<i>Gjc1</i> ^{tm1Weil}	MGI:3530292	15659592
Gli2	<i>Gli2</i> ^{tm6Alj}	MGI:3664541	16571625
Gli3	<i>Gli3</i> ^{tm1Zlr}	N/A	N/A (this report)
Glud1	<i>Glud1</i> ^{tm1.1Pma}	MGI:3835667	19015267
Gna13	<i>Gna13</i> ^{tm2Cgh}	MGI:3583876	15919816
Gpr22	<i>Gpr22</i> ^{tm1Jwad}	MGI:3805679	18539757
Gpsm1	<i>Gpsm1</i> ^{tm1Lajb}	MGI:3807517	18450958
Gpx4	<i>Gpx4</i> ^{tm2Marc}	MGI:3810783	18762024
Grid2ip	<i>Grid2ip</i> ^{tm1Mmsh}	MGI:3796571	18509461
Hand1	<i>Hand1</i> ^{tm2Eno}	MGI:3514024	15576406

Hand2	<i>Hand2</i> ^{tm1Zlfr}	N/A	N/A (this report)
Hfe	<i>Hfe</i> ^{tm1Wsr}	MGI:3775647	14618243
Hhex	<i>Hhex</i> ^{tm2Cwb}	MGI:3721426	17580084
Hoxb1	<i>Hoxb1</i> ^{tm7Mrc}	MGI:3046794	15198977
Hus1	<i>Hus1</i> ^{tm2Rsw}	MGI:3702082	15919177
Ift20	<i>Ift20</i> ^{tm1Gjp}	MGI:3817416	18981227
Ikbkg	<i>Ikbkg</i> ^{tm1.1Mpa}	MGI:2679024	10911992
Insig1	<i>Insig1</i> ^{tm1Mbjg}	MGI:3603523	16100574
Isl1	<i>Isl1</i> ^{tm2Gan}	MGI:3797783	18434421
Itga3	<i>Itga3</i> ^{tm1Hap}	MGI:3833130	19104148
Itgb1	<i>Itgb1</i> ^{tm3Mlkn}	MGI:3624806	16618804
Itgb4	<i>Itgb4</i> ^{tm1Mfel}	MGI:3803792	18579745
Itgb8	<i>Itgb8</i> ^{tm2Lfr}	MGI:3608910	16251442
Itpr2	<i>Itpr2</i> ^{tm1Chen}	MGI:3640971	15933266
Kcnj10	<i>Kcnj10</i> ^{tm1Kdmc}	MGI:3761690	17942730
Klf2	<i>Klf2</i> ^{tm1Mlkn}	MGI:3765423	17141159
Lama5	<i>Lama5</i> ^{tm2Jhm}	MGI:3612315	15936333
Lamc1	<i>Lamc1</i> ^{tm1Strl}	MGI:2681365	14638863
Ldb3	<i>Ldb3</i> ^{tm4Chen}	MGI:3831620	19028670
Lims1	<i>Lims1</i> ^{tm1.1Chen}	MGI:3575965	15798193
Map3k3	<i>Map3k3</i> ^{tm2Bisu}	MGI:3836798	19265138
Mef2d	<i>Mef2d</i> ^{tm3Eno}	MGI:3772400	18079970
Mfn1	<i>Mfn1</i> ^{tm2Dcc}	MGI:3779080	17693261
Mfn2	<i>Mfn2</i> ^{tm3Dcc}	MGI:3779081	17693261
Mib1	<i>Mib1</i> ^{tm2Kong}	MGI:3804448	18043734
Mir17-92	<i>Mir17-92</i> ^{tm1Tyj}	MGI:3795513	18329372
Mll2	<i>Mll2</i> ^{tm1.1Afst}	MGI:3623310	16540515
Mttr2	<i>Mttr2</i> ^{tm1Abol}	MGI:3513251	15557122
Myb	<i>Myb</i> ^{tm1.1Jof}	MGI:3037362	12941699
Myd88	<i>Myd88</i> ^{tm1Defr}	MGI:3809600	18656388
Myot	<i>Myot</i> ^{tm1Moza}	MGI:3697713	17074808
Nampt	<i>Nampt</i> ^{tm1Oleo}	MGI:3818627	18802071
Ncor1	<i>Ncor1</i> ^{tm1Anh}	MGI:3821874	19052228
Ndufs4	<i>Ndufs4</i> ^{tm1Rpa}	MGI:3527173	18396137
Neurog2	<i>Neurog2</i> ^{tm5(Neurog2)Fgu}	MGI:3664585	N/A (personal communication)
Notch2	<i>Notch2</i> ^{tm3Grid}	MGI:3617328	16397869
Nr5a2	<i>Nr5a2</i> ^{tm1Sakl}	MGI:3795276	18323469
Nr5a2	<i>Nr5a2</i> ^{tm1Sjns}	MGI:3720193	17670946
Nrp2	<i>Nrp2</i> ^{tm1.1Mom}	MGI:3712029	12019322
Ntrk2	<i>Ntrk2</i> ^{tm2Kln}	MGI:1933974	10571233
Numa1	<i>Numa1</i> ^{tm1.1Dwc}	MGI:3838102	19255246
Numb	<i>Numb</i> ^{tm1Ynj}	MGI:1932085	10841580
Olig2	<i>Olig2</i> ^{tm1Qrlu}	MGI:3614399	16436615

Otx2	<i>Otx2</i> ^{tm4.1Sia}	MGI:2178753	11820816
Oxtr	<i>Oxtr</i> ^{tm1.1Wsy}	MGI:3800791	18356275
Pax3	<i>Pax3</i> ^{tm5Buck}	MGI:3687384	16951257
Pax6	<i>Pax6</i> ^{tm2Pgr}	MGI:1934348	11069887
Pax9	<i>Pax9</i> ^{tm1.1Hpt}	MGI:3723638	17610273
Paxip1	<i>Paxip1</i> ^{tm2Gdr}	MGI:3767658	17925232
Pbx3	<i>Pbx3</i> ^{tm1Og}	MGI:3773271	18155191
Pclo	<i>Pclo</i> ^{tm2Sud}	MGI:3785835	N/A (Direct Data Submission)
Pcsk5	<i>Pcsk5</i> ^{tm2Prat}	MGI:3789183	18378898
Pdgfc	<i>Pdgfc</i> ^{tm1Hdin}	MGI:3768436	17941048
Pggt1b	<i>Pggt1b</i> ^{tm1Mbrg}	MGI:3713756	17476360
Pik3cb	<i>Pik3cb</i> ^{tm1Bvan}	MGI:3795849	18544649
Pik3r1	<i>Pik3r1</i> ^{tm1Lca}	MGI:3607981	16227599
Pkd1	<i>Pkd1</i> ^{tm2Ggg}	MGI:3612341	15579506
Pkd1	<i>Pkd1</i> ^{tm2Som}	MGI:3793791	18263604
Pkhd1	<i>Pkhd1</i> ^{tm1Ggg}	MGI:3759214	17575307
Pkp3	<i>Pkp3</i> ^{tm1Fvr}	MGI:3798859	18079750
Pla2g15	<i>Pla2g15</i> ^{tm1Jash}	MGI:3665282	16880524
Plec1	<i>Plec1</i> ^{tm4Gwi}	MGI:3721885	17606998
Plxnb1	<i>Plxnb1</i> ^{tm1Ltam}	MGI:3790772	17519029
Pofut1	<i>Pofut1</i> ^{tm1Ysa}	MGI:3808704	18547789
Prss8	<i>Prss8</i> ^{tm1.2Hum}	MGI:2384523	11857812
Ptch1	<i>Ptch1</i> ^{tm1Hahn}	MGI:3764517	17536012
Ptger3	<i>Ptger3</i> ^{tm1Csml}	MGI:3764893	17676060
Ptk2	<i>Ptk2</i> ^{tm1Lfr}	MGI:2684666	14642275
Ptk2	<i>Ptk2</i> ^{tm1Mmsh}	MGI:3777585	18279360
Pyy	<i>Pyy</i> ^{tm1Batt}	MGI:3771166	16950139
Rasa1	<i>Rasa1</i> ^{tm1Pdk}	MGI:3772459	18064675
Rasgrf1	<i>Rasgrf1</i> ^{tm4.1Pds}	MGI:3611767	17030618
Rela	<i>Rela</i> ^{tm1Asba}	MGI:3775205	18250470
Ret	<i>Ret</i> ^{tm13Jmi}	MGI:3690534	17065462
Ret	<i>Ret</i> ^{tm1Kln}	MGI:3662623	16600854
Rfx3	<i>Rfx3</i> ^{tm1Wrth}	MGI:3045791	15121860
Rictor	<i>Rictor</i> ^{tm1Mgn}	MGI:3526066	16962829
Rims1	<i>Rims1</i> ^{tm3Sud}	MGI:3822548	19074017
Rtel1	<i>Rtel1</i> ^{tm1Hdin}	MGI:3772370	18064678
S100a10	<i>S100a10</i> ^{tm1Jnw}	MGI:3665443	17035534
Sall4	<i>Sall4</i> ^{tm2Tre}	MGI:3692449	17060609
Scn1b	<i>Scn1b</i> ^{tm2Isom}	MGI:3768513	17868089
Scn8a	<i>Scn8a</i> ^{tm1Mm}	MGI:3043395	15286995
Scn9a	<i>Scn9a</i> ^{tm1Jnw}	MGI:3053097	15314237
Scnn1b	<i>Scnn1b</i> ^{tm1.1Hum}	MGI:3832670	19036848
Scnn1g	<i>Scnn1g</i> ^{tm1.1Hum}	MGI:3832674	19036848

Sfpi1	<i>Sfpi1</i> ^{tm1Dgt}	MGI:3045206	15146183
Sfpi1	<i>Sfpi1</i> ^{tm1.2Nutt}	MGI:3578011	15867096
Sh2d4a	<i>Sh2d4a</i> ^{tm1Pdk}	MGI:3809251	18641339
Shh	<i>Shh</i> ^{tm2Chg}	MGI:3628824	16611729
Slc6a9	<i>Slc6a9</i> ^{tm1.1Bois}	MGI:3622080	16554468
Smad3	<i>Smad3</i> ^{tm1Zuk}	MGI:3822465	18809571
Snai1	<i>Snai1</i> ^{tm1.1Stjw}	MGI:3838175	19188491
Socs1	<i>Socs1</i> ^{tm3Wehi}	MGI:2656917	12705851
Sox12	<i>Sox12</i> ^{tm1Weg}	MGI:3804456	18505825
Sox17	<i>Sox17</i> ^{tm2Sjm}	MGI:3717121	17655922
Sp6	<i>Sp6</i> ^{tm1lbmm}	MGI:3778292	18297738
Sp7	<i>Sp7</i> ^{tm2Crm}	MGI:3608932	16203988
Sphk1	<i>Sphk1</i> ^{tm2Cgh}	MGI:3707997	17363629
Sphk2	<i>Sphk2</i> ^{tm1.1Cgh}	MGI:3708000	17363629
Spry1	<i>Spry1</i> ^{tm1Jdli}	MGI:3574403	15691764
Spry2	<i>Spry2</i> ^{tm1Mrt}	MGI:3578632	15809037
Spry4	<i>Spry4</i> ^{tm1.1Mrt}	MGI:3702553	16890158
Supv3l1	<i>Supv3l1</i> ^{tm2Jkl}	MGI:3833740	19145458
Syt9	<i>Syt9</i> ^{tm1Sud}	MGI:3715453	17521570
Tbx1	<i>Tbx1</i> ^{tm1Dsr}	MGI:3510038	15469978
Tcf3	<i>Tcf3</i> ^{tm1Mbu}	MGI:3803637	18538592
Tex11	<i>Tex11</i> ^{tm1Jpt}	MGI:3797589	18369460
Thap11	<i>Thap11</i> ^{tm1Tpz}	MGI:3797582	18585351
Thoc1	<i>Thoc1</i> ^{tm2.1Dwg}	MGI:3698314	17211872
Thrb	<i>Thrb</i> ^{tm1Mkni}	MGI:3836780	19244534
Tor1a	<i>Tor1a</i> ^{tm2Yql}	MGI:3772564	17956903
Tpp2	<i>Tpp2</i> ^{tm1Gnie}	MGI:3783749	18362329
Traf3	<i>Traf3</i> ^{tm1Rbr}	MGI:3777324	18313334
Tslp	<i>Tslp</i> ^{tm1.1Pcn}	MGI:3837749	18650845
Ttn	<i>Ttn</i> ^{tm1Her}	MGI:2651645	12464612
Txnrd1	<i>Txnrd1</i> ^{tm1Marc}	MGI:3574358	15713651
Txnrd2	<i>Txnrd2</i> ^{tm1Marc}	MGI:3512408	15485910
Uba7	<i>Uba7</i> ^{tm1Dzh}	MGI:3521787	16382139
Upf2	<i>Upf2</i> ^{tm1Btp}	MGI:3790198	18483223
Vcl	<i>Vcl</i> ^{tm1Ross}	MGI:3769142	17785437
Vprbp	<i>Vprbp</i> ^{tm1.1Yxi}	MGI:3814062	18606781
Wnt3	<i>Wnt3</i> ^{tm2Amc}	MGI:2450903	12569130
Wnt7b	<i>Wnt7b</i> ^{tm1Amc}	MGI:3526431	16163358
Wnt9a	<i>Wnt9a</i> ^{tm1Chha}	MGI:3701348	16818445
Yy1	<i>Yy1</i> ^{tm2Yshi}	MGI:3625967	16611997

10.4 Appendix References

- Aanhaanen, W.T., Brons, J.F., Dominguez, J.N., Rana, M.S., Norden, J., Airik, R., Wakker, V., de Gier-de Vries, C., Brown, N.A., Kispert, A., *et al.* (2009). The Tbx2+ primary myocardium of the atrioventricular canal forms the atrioventricular node and the base of the left ventricle. *Circ Res* *104*, 1267-1274.
- Akiyama, H., Chaboissier, M.C., Behringer, R.R., Rowitch, D.H., Schedl, A., Epstein, J.A., and de Crombrughe, B. (2004). Essential role of Sox9 in the pathway that controls formation of cardiac valves and septa. *Proc Natl Acad Sci U S A* *101*, 6502-6507.
- Barnes, R.M., Firulli, B.A., VanDusen, N.J., Morikawa, Y., Conway, S.J., Cserjesi, P., Vincentz, J.W., and Firulli, A.B. (2011). Hand2 loss-of-function in Hand1-expressing cells reveals distinct roles in epicardial and coronary vessel development. *Circ Res* *108*, 940-949.
- Barron, F., Woods, C., Kuhn, K., Bishop, J., Howard, M.J., and Clouthier, D.E. (2011). Downregulation of Dlx5 and Dlx6 expression by Hand2 is essential for initiation of tongue morphogenesis. *Development* *138*, 2249-2259.
- Buckingham, M., Meilhac, S., and Zaffran, S. (2005). Building the mammalian heart from two sources of myocardial cells. *Nat Rev Genet* *6*, 826-835.
- Cserjesi, P., Brown, D., Lyons, G.E., and Olson, E.N. (1995). Expression of the novel basic helix-loop-helix gene eHAND in neural crest derivatives and extraembryonic membranes during mouse development. *Dev Biol* *170*, 664-678.
- Harris, I.S., and Black, B.L. (2010). Development of the endocardium. *Pediatr Cardiol* *31*, 391-399.
- Harvey, R.P. (2002). Patterning the vertebrate heart. *Nat Rev Genet* *3*, 544-556.
- Laugwitz, K.L., Moretti, A., Caron, L., Nakano, A., and Chien, K.R. (2008). Islet1 cardiovascular progenitors: a single source for heart lineages? *Development* *135*, 193-205.
- Liu, N., Barbosa, A.C., Chapman, S.L., Bezprozvannaya, S., Qi, X., Richardson, J.A., Yanagisawa, H., and Olson, E.N. (2009). DNA binding-dependent and -independent functions of the Hand2 transcription factor during mouse embryogenesis. *Development* *136*, 933-942.
- Martin-Puig, S., Wang, Z., and Chien, K.R. (2008). Lives of a heart cell: tracing the origins of cardiac progenitors. *Cell Stem Cell* *2*, 320-331.
- McLean, C.Y., Bristor, D., Hiller, M., Clarke, S.L., Schaar, B.T., Lowe, C.B., Wenger, A.M., and Bejerano, G. (2010). GREAT improves functional interpretation of cis-regulatory regions. *Nat Biotechnol* *28*, 495-501.
- Meilhac, S.M., Esner, M., Kelly, R.G., Nicolas, J.F., and Buckingham, M.E. (2004). The clonal origin of myocardial cells in different regions of the embryonic mouse heart. *Dev Cell* *6*, 685-698.
- Morikawa, Y., and Cserjesi, P. (2008). Cardiac neural crest expression of Hand2 regulates outflow and second heart field development. *Circ Res* *103*, 1422-1429.
- Smith, C.L., Baek, S.T., Sung, C.Y., and Tallquist, M.D. (2011). Epicardial-derived cell epithelial-to-mesenchymal transition and fate specification require PDGF receptor signaling. *Circ Res* *108*, e15-26.
- Snider, P., Olaopa, M., Firulli, A.B., and Conway, S.J. (2007). Cardiovascular development and the colonizing cardiac neural crest lineage. *ScientificWorldJournal* *7*, 1090-1113.
- Srivastava, D. (2006). Making or breaking the heart: from lineage determination to morphogenesis. *Cell* *126*, 1037-1048.

- Stennard, F.A., and Harvey, R.P. (2005). T-box transcription factors and their roles in regulatory hierarchies in the developing heart. *Development* 132, 4897-4910.
- Tanaka, M., Wechsler, S.B., Lee, I.W., Yamasaki, N., Lawitts, J.A., and Izumo, S. (1999). Complex modular cis-acting elements regulate expression of the cardiac specifying homeobox gene *Csx/Nkx2.5*. *Development* 126, 1439-1450.
- Thomas, T., Kurihara, H., Yamagishi, H., Kurihara, Y., Yazaki, Y., Olson, E.N., and Srivastava, D. (1998). A signaling cascade involving endothelin-1, dHAND and *msx1* regulates development of neural-crest-derived branchial arch mesenchyme. *Development* 125, 3005-3014.
- Togi, K., Yoshida, Y., Matsumae, H., Nakashima, Y., Kita, T., and Tanaka, M. (2006). Essential role of *Hand2* in interventricular septum formation and trabeculation during cardiac development. *Biochem Biophys Res Commun* 343, 144-151.
- Tsuchihashi, T., Maeda, J., Shin, C.H., Ivey, K.N., Black, B.L., Olson, E.N., Yamagishi, H., and Srivastava, D. (2011). *Hand2* function in second heart field progenitors is essential for cardiogenesis. *Dev Biol* 351, 62-69.
- Vincent, S.D., and Buckingham, M.E. (2010). How to make a heart: the origin and regulation of cardiac progenitor cells. *Curr Top Dev Biol* 90, 1-41.
- Wessels, A., and Sedmera, D. (2003). Developmental anatomy of the heart: a tale of mice and man. *Physiol Genomics* 15, 165-176.
- Wu, S.M., Chien, K.R., and Mummery, C. (2008). Origins and fates of cardiovascular progenitor cells. *Cell* 132, 537-543.
- Zhang, Y., Liu, T., Meyer, C.A., Eeckhoute, J., Johnson, D.S., Bernstein, B.E., Nusbaum, C., Myers, R.M., Brown, M., Li, W., *et al.* (2008b). Model-based analysis of ChIP-Seq (MACS). *Genome Biol* 9, R137.

11. Publications

Dual RMCE for efficient re-engineering of mouse mutant alleles

– Nature Methods, 2010 (First Author)

The author file – Nature Methods

Next generation engineering of conditional mouse alleles with loxP and FRT sites by dual RMCE – Nature Protocol Exchange

Distinct Roles of Hand2 in Initiating Polarity and Posterior *Shh* Expression during the Onset of Mouse Limb Bud Development

– PloS Genetics (Co-Author)

GLI3 Constrains Digit Number by Controlling Both Progenitor Proliferation and BMP-Dependent Exit to Chondrogenesis

– Developmental Cell (Co-Author)

Dual RMCE for efficient re-engineering of mouse mutant alleles

Marco Osterwalder¹, Antonella Galli^{1,3}, Barry Rosen², William C Skarnes², Rolf Zeller¹ & Javier Lopez-Rios¹

We have developed dual recombinase-mediated cassette exchange (dRMCE) to efficiently re-engineer the thousands of available conditional alleles in mouse embryonic stem cells. dRMCE takes advantage of the wild-type *loxP* and *FRT* sites present in these conditional alleles and in many gene-trap lines. dRMCE is a scalable, flexible tool to introduce tags, reporters and mutant coding regions into an endogenous locus of interest in an easy and highly efficient manner.

Gene targeting by homologous recombination in mouse embryonic stem cells is a powerful tool for tailored manipulation of the mouse genome. However, the efficiency of this technology is limited by the great variation in targeting frequencies for different loci¹. In particular, targeting frequencies for a substantial number of loci are very low (<1%), which renders repeated genetic manipulation tedious, especially as the screening strategy usually involves Southern blotting or long-range PCR. In light of the increasing need to re-engineer more subtle mutations at the same locus, recombinase-mediated cassette exchange (RMCE; reviewed in ref. 2) was developed to facilitate this process. RMCE takes advantage of pairs of heterotypic, noninteracting recombination sites for a particular site-specific recombinase, but these sites first need to be introduced into the locus of interest through conventional homologous recombination. Subsequently, co-transfection of such modified mouse embryonic stem cells with the custom-designed RMCE exchange vector and the appropriate recombinase expression plasmid will result in replacement at the endogenous locus².

It was previously established that coexpression of both Cre and Flp recombinases catalyzes the exchange of sequences flanked by single *loxP* and *FRT* sites (their respective standard target sites) integrated into the genome at a random location³. However, this study did not explore whether such an approach could be used to modify conditional mouse alleles carrying single or multiple *loxP* and *FRT* sites. Therefore, we decided to develop dual RMCE (dRMCE) as a re-engineering tool applicable to the vast numbers of mouse conditional alleles that harbor wild-type *loxP* and *FRT* sites and therefore are not compatible with conventional

RMCE. In particular, dRMCE will expand the long-term value of the rapidly increasing collection of targeted alleles produced by the International Knockout Mouse Consortium (IKMC; <http://www.knockoutmouse.org/>). This large-scale program is generating 'knockout-first' conditional alleles for most protein-coding genes in mouse embryonic stem cells, and several thousand alleles are already available⁴.

The general dRMCE strategy takes advantage of the fact that most conditional alleles encode a selection cassette flanked by *FRT* sites, in addition to *loxP* sites that flank functionally relevant exons ('floxed' exons; **Fig. 1a**). The *FRT*-flanked selection cassette is in general placed outside the *loxP*-flanked region, which renders these alleles directly compatible with dRMCE. Simultaneous expression of Cre and Flp recombinases should rapidly induce *cis* recombination and formation of the deleted allele, which would then serve as a 'docking site' at which to insert the replacement vector by *trans* recombination (**Fig. 1a**). The correctly replaced locus would encode the custom modification and a different drug-selection cassette flanked by single *loxP* and *FRT* sites.

In developing dRMCE, we used optimized versions of the Cre (iCre)⁵ and Flp (Flpo)⁶ recombinases to assemble the pDIRE expression vector (see **Supplementary Fig. 1a** and **Supplementary Data** for complete vector sequences). We also developed the pDREV vector series (**Supplementary Fig. 1b** and **Supplementary Data**) that allows insertion and efficient expression of reporters and/or coding regions of choice in any IKMC knockout-first allele. We tested the feasibility of dRMCE-mediated replacement using loci representing these readily available knockout-first alleles as well as standard conditional loss-of-function mutations generated by individual researchers.

The floxed *Smad4* (*Smad4^f*) knockout-first allele generated by the IKMC contains a promoterless gene-trap selection cassette (*lacZ-T2A-neo*) that is flanked by *FRT* sites and followed by *loxP* sites flanking a critical *Smad4* coding exon (**Fig. 1b**). This results in expression of a *lacZ* reporter and the neomycin resistance (*neo*) genes under control of the endogenous *Smad4* promoter, which is active in embryonic stem cells. Heterozygous *Smad4^f* mouse embryonic stem cells were co-transfected with the pDIRE and pDREV-1 vectors, the latter of which encodes an *H2B-Venus YFP* reporter (**Fig. 1b**). Puromycin-resistant colonies were screened by short-range PCR at the 3' (*loxP*) and the 5' (*FRT*) junctions for correct replacement events, which resulted in the *YFP*-tagged *Smad4* allele (*Smad4^{YFP}*; **Fig. 1c**). Most of the colonies were correctly replaced and of clonal origin (69%: 33 out of 48 clones; **Supplementary Table 1**). In contrast to the β -galactosidase-positive *Smad4^f* cells (**Fig. 1d**), *Smad4^{YFP}* colonies have lost the *lacZ* reporter and have become *YFP* positive (**Fig. 1e,f**).

¹Developmental Genetics, Department of Biomedicine, University of Basel, Basel, Switzerland. ²The Wellcome Trust Sanger Institute, Wellcome Trust Genome Campus, Hinxton, Cambridge, UK. ³Present address: Department of Medicine and Genetics & Development, Herbert Irving Comprehensive Cancer Center, Columbia University Medical Center, New York, New York, USA. Correspondence should be addressed to J.L.-R. (javier.lopez-rios@unibas.ch) or R.Z. (rolf.zeller@unibas.ch).

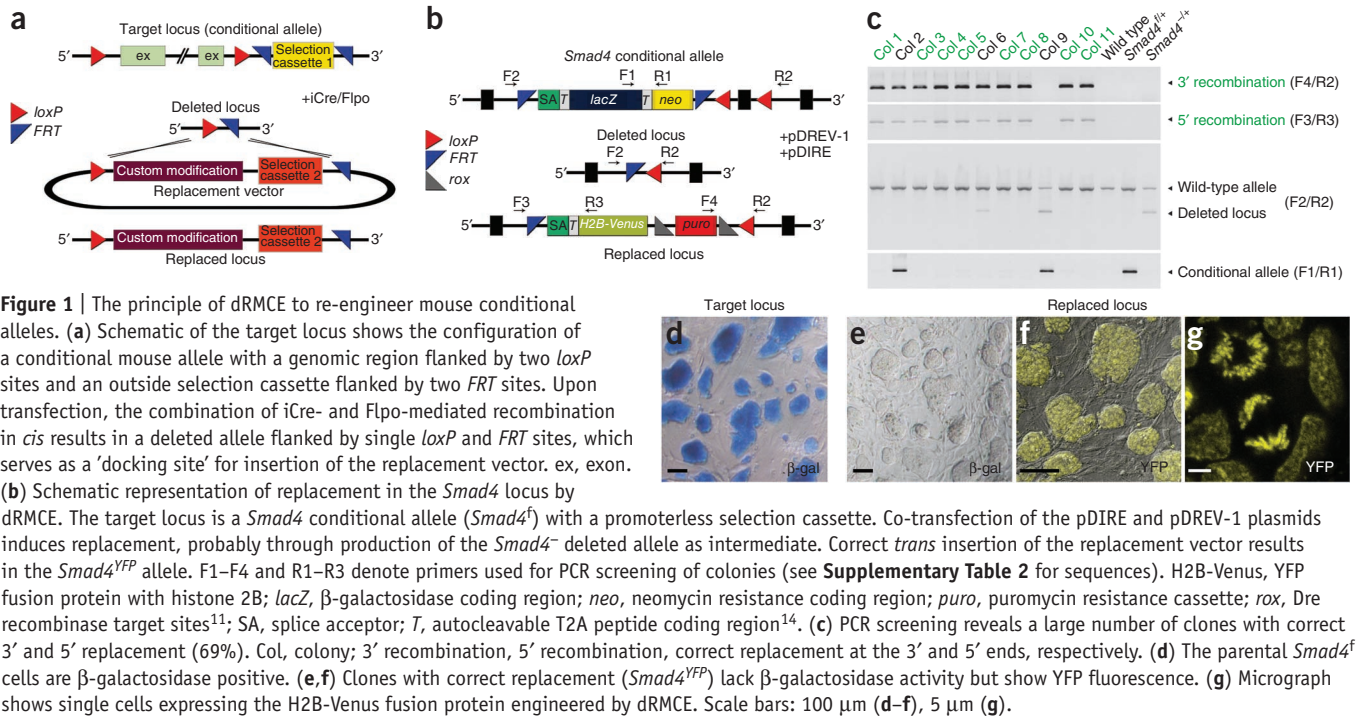


Figure 1 | The principle of dRMCE to re-engineer mouse conditional alleles. **(a)** Schematic of the target locus shows the configuration of a conditional mouse allele with a genomic region flanked by two *loxP* sites and an outside selection cassette flanked by two *FRT* sites. Upon transfection, the combination of iCre- and Flpo-mediated recombination in *cis* results in a deleted allele flanked by single *loxP* and *FRT* sites, which serves as a 'docking site' for insertion of the replacement vector. ex, exon.

(b) Schematic representation of replacement in the *Smad4* locus by dRMCE. The target locus is a *Smad4* conditional allele (*Smad4^f*) with a promoterless selection cassette. Co-transfection of the pDIRE and pDREV-1 plasmids induces replacement, probably through production of the *Smad4⁻* deleted allele as intermediate. Correct *trans* insertion of the replacement vector results in the *Smad4^{YFP}* allele. F1–F4 and R1–R3 denote primers used for PCR screening of colonies (see **Supplementary Table 2** for sequences). H2B-Venus, YFP fusion protein with histone 2B; *lacZ*, β -galactosidase coding region; *neo*, neomycin resistance coding region; *puro*, puromycin resistance cassette; *rox*, Dre recombinase target sites¹¹; SA, splice acceptor; T, autocleavable T2A peptide coding region¹⁴. **(c)** PCR screening reveals a large number of clones with correct 3' and 5' replacement (69%). Col, colony; 3' recombination, 5' recombination, correct replacement at the 3' and 5' ends, respectively. **(d)** The parental *Smad4^f* cells are β -galactosidase positive. **(e, f)** Clones with correct replacement (*Smad4^{YFP}*) lack β -galactosidase activity but show YFP fluorescence. **(g)** Micrograph shows single cells expressing the H2B-Venus fusion protein engineered by dRMCE. Scale bars: 100 μ m (**d–f**), 5 μ m (**g**).

The H2B-Venus fusion protein appeared to be functional, as it was nuclear and bound to chromosomes during mitosis (**Fig. 1g**)⁷.

A small number of colonies were mixed, as judged by PCR analysis (**Fig. 1c** and **Supplementary Table 1**). These mixed colonies were easily recognized because they were composed of cells positive for either β -galactosidase activity (*Smad4^f* allele) or YFP fluorescence (*Smad4^{YFP}* allele) but not both (**Supplementary Fig. 2**). Some other mixed colonies contained cells carrying the *Smad4* loss-of-function allele (*Smad4⁻*; **Fig. 1c** and **Supplementary Fig. 2**). This analysis indicated that mixed colonies originate as a consequence of incomplete recombination. Therefore, dRMCE-mediated replacement must always be validated by confirming the absence of both the floxed and the deleted allele.

The floxed *Zfp503* (*Zfp503^f*) knockout-first allele from the IKMC encodes a promoter-driven selection cassette and three *loxP* and two *FRT* sites (**Supplementary Fig. 3a**). We co-transfected recipient heterozygous *Zfp503^f* mouse embryonic stem cells with the pDIRE and pDREV-0 plasmids and selected colonies on the basis of their resistance to puromycin. Generation of the correctly replaced YFP-tagged *Zfp503* (*Zfp503^{YFP}*) allele was again highly efficient (52%; **Supplementary Fig. 3b** and **Supplementary Table 1**).

To establish dRMCE as a universally applicable method for re-engineering of conditional alleles, we also targeted two other loci. We first selected the *Hand2* locus, as it is very difficult to target by homologous recombination (0.17%)⁸, and chose to use dRMCE to introduce a Flag epitope tag into the endogenous *Hand2* coding region (*Hand2^{Flag}*). To this end, we co-transfected mouse embryonic stem cells heterozygous for the floxed *Hand2* (*Hand2^f*) allele with the pDIRE and a pDRAV-type *Hand2^{Flag}* replacement vectors (**Fig. 2a** and **Supplementary Fig. 1**). Molecular analysis revealed that 13% of all drug-resistant colonies had undergone correct replacement (**Fig. 2b** and **Supplementary Table 1**). Second, we carried out dRMCE-mediated replacement of a *Gli3* conditional allele (J.L.-R. and

R.Z., unpublished data) with the *Hand2^{Flag}* vector, resulting in 33% correct replacement (**Supplementary Table 1** and data not shown). These results indicate that dRMCE permits highly efficient re-engineering of conditional alleles with wild-type *loxP* and *FRT* sites in one step, irrespective of the difficulty of targeting the parental locus by homologous recombination.

To assess the potential effects of dRMCE on germline transmission, we injected two correctly engineered *Hand2^{Flag}* mouse embryonic stem cell clones (**Supplementary Fig. 4**) separately into mouse blastocysts, which resulted in several highly chimeric offspring in each case (80–100% as judged by coat color). These chimeric males transmitted the *Hand2^{Flag}* allele to their F₁ progeny within the first two litters (**Fig. 2c**). These results indicated that dRMCE neither compromises germline transmission potential nor causes frequent chromosomal abnormalities, as judged by karyotyping of all clones⁹ before injection (data not shown). Furthermore, the mouse embryonic stem cells used by the IKMC to generate their conditional alleles have been proven to remain highly germline competent even after multiple rounds of gene targeting and exposure to site-specific recombinases¹⁰.

Most notably, dRMCE-mediated engineering did not alter the temporal and spatial expression of *Hand2* transcripts in mouse embryos homozygous for the *Hand2^{Flag}* allele (**Fig. 2d** and **Supplementary Fig. 5**). The *Hand2^{Flag}* allele was fully functional, as homozygous embryos and mice were phenotypically wild type, which contrasts with the lethality of *Hand2*-deficient mouse embryos⁸. In summary, dRMCE allowed re-engineering of conventional targeted alleles with frequencies of 10–70% correct replacement (**Table 1**). Minimally, this represented a 5- to 65-fold increase in efficiency in comparison to homologous recombination, which is particularly beneficial for difficult to target loci. Even at the lowest efficiency (13% for *Hand2*, **Table 1**), very few colonies needed to be analyzed to identify correctly replaced clones (for example, one 48-well plate of colonies).

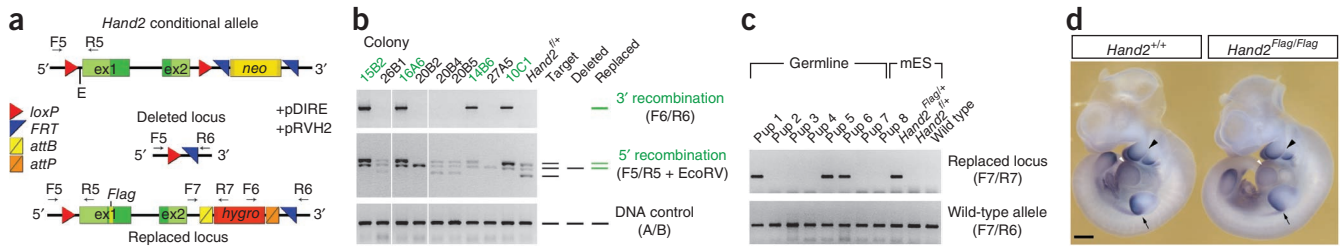


Figure 2 | dRMCE for efficient modification of difficult-to-target loci. **(a)** Schematic shows the conditional *Hand2* allele (*Hand2^f*) used as a target locus for insertion of a Flag epitope tag into the *Hand2* coding region. After co-transfection of the replacement vector (pRVH2) and pDIRE plasmid into heterozygous *Hand2^f* mouse embryonic stem cells, dRMCE-mediated replacement results in the *Hand2^{Flag}* allele. The *PGK-hygro* (hygromycin resistance gene) selection cassette is flanked by the *attB* and *attP* target sites for excision by the ϕ C31 recombinase. F5–F7 and R5–R7 denote primers used for PCR screening and genotyping. E, EcoRV site required to detect correct 5' replacement by combining PCR amplification with an EcoRV restriction digestion. **(b)** PCR screening at both ends of the locus identified *Hand2* colonies with correct replacement (13%). Scheme at right shows PCR fragment patterns indicative of particular genomic configurations. 3' recombination, 5' recombination, correct replacement at the 3' and 5' ends, respectively. A, B, primers to amplify a region serving as positive control (see **Supplementary Table 2** for sequences). **(c)** Gels show germline transmission of the *Hand2^{Flag}* allele (lanes 1, 5, 6). Above, PCR analysis to detect *Hand2^{Flag}* allele. Below, PCR detection of wild-type allele. **(d)** *In situ* detection of *Hand2* transcripts in a wild-type (*Hand2^{+/+}*; left) and *Hand2^{Flag/Flag}* (right) mouse embryo at embryonic day 10.5. Note expression in the posterior limb bud mesenchyme (arrow), branchial arches (black arrowhead) and heart (white arrowhead). Scale bar, 500 μ m.

To facilitate the generation of dRMCE targeting vectors for the large number of alleles containing both *loxP* and *FRT* sites (**Fig. 1a**), we prepared a tool kit consisting of the pDIRE expression vector and various dRMCE vectors (**Supplementary Fig. 1** and **Supplementary Data**). In all cases, the selection cassette can be removed either in cells or directly in mice by breeding them to Dre¹¹ or ϕ C31o⁶ deleter mouse strains. The vector backbones allow the use of validated vector-specific primers for PCR screening in combination with locus-specific primers (**Supplementary Table 2**).

Taken together, our data indicate that dRMCE is a highly efficient and universal tool for re-engineering of conditional mouse alleles. dRMCE also provides a one-step alternative to the Floxin strategy¹² recently developed for gene trap lines available from the International Gene Trap Consortium (IGTC; <http://www.genetrap.org/>)¹³. dRMCE is conceptually straightforward and allows a wide range of precise genomic modifications to be engineered. For example, dRMCE can be used to express mutant gene products and introduce epitope or fluorescent tags or heterologous genes into the endogenous locus of choice. Because of its efficiency, the dRMCE technology is well suited for high-throughput approaches such as functional screening of disease-causing mutations in pathways or genes of interest directly in mouse embryonic stem cells (for example, upon induced differentiation into specific cell types) or in mice generated from engineered clones. Finally, dRMCE technology provides nonspecialists with access to advanced mouse genetic engineering and enhances the long-term value of the existing large collections of genetically altered mouse embryonic stem cell lines.

Table 1 | dRMCE allows re-engineering of different loci at frequencies much higher than homologous recombination

Gene locus	dRMCE	Homologous recombination	Fold increase
<i>Smad4</i>	69%	6% ¹⁵	12 \times
<i>Zfp503</i>	52%	11% ^a	5 \times
<i>Hand2</i>	13%	0.2% ^b	65 \times
<i>Gli3</i>	33%	3% ^b	11 \times

^aIKMC. ^bUnpublished.

METHODS

Methods and any associated references are available in the online version of the paper at <http://www.nature.com/naturemethods/>.

Note: Supplementary information is available on the Nature Methods website.

ACKNOWLEDGMENTS

We are grateful to D. Klewe-Nebenius and T. Hennek (University of Basel) for generating the chimeric mice. We thank I. Verma (Salk Institute, San Diego, California, USA), B. Sauer (Stowers Institute, Kansas City, Missouri, USA), R. Jaenisch (Whitehead Institute, Cambridge, Massachusetts, USA) and P. Soriano (Mount Sinai School of Medicine, New York, New York, USA) for plasmids obtained via Addgene and A.-K. Hadjantonakis (Sloan-Kettering Institute, New York, New York, USA) for suggesting the use of the H2B-Venus fusion protein. We thank A. Schauerte and P. Lorentz for expert technical assistance and are indebted to P. Bovolenta, G. Nusspaumer, A. Zuniga and members of our research groups for helpful input and discussions. Our research is supported by the Swiss National Science Foundation (to R.Z.), by a Marie Curie Intra-European Fellowship and a European Reintegration Grant (to J.L.-R.) and by both cantons of Basel, Switzerland.

AUTHOR CONTRIBUTIONS

M.O., J.L.-R. and R.Z. conceived and designed the experiments. M.O., J.L.-R. and B.R. designed and constructed the dRMCE tool-kit vectors. B.R. and W.C.S. provided the IKMC mouse embryonic stem cell lines. M.O., A.G., J.L.-R. and B.R. performed the experiments. J.L.-R., W.C.S. and R.Z. wrote the paper.

COMPETING FINANCIAL INTERESTS

The authors declare competing financial interests: details accompany the full-text HTML version of the paper at <http://www.nature.com/naturemethods/>.

Published online at <http://www.nature.com/naturemethods/>.

Reprints and permissions information is available online at <http://npg.nature.com/reprintsandpermissions/>.

- Glaser, S., Anastassiadis, K. & Stewart, A.F. *Nat. Genet.* **37**, 1187–1193 (2005).
- Brandt, C.S. & Dymecki, S.M. *Dev. Cell* **6**, 7–28 (2004).
- Lauth, M., Spreafico, F., Dethleffsen, K. & Meyer, M. *Nucleic Acids Res.* **30**, e115 (2002).
- Collins, F.S., Rossant, J. & Wurst, W. *Cell* **128**, 9–13 (2007).
- Shimshak, D.R. *et al. Genesis* **32**, 19–26 (2002).
- Raymond, C.S. & Soriano, P. *PLoS ONE* **2**, e162 (2007).
- Kanda, T., Sullivan, K.F. & Wahl, G.M. *Curr. Biol.* **8**, 377–385 (1998).
- Galli, A. *et al. PLoS Genet.* **6**, e1000901 (2010).
- Nagy, A. *Manipulating the Mouse Embryo: A Laboratory Manual* 3rd edn. (Cold Spring Harbor Laboratory Press, Cold Spring Harbor, New York, USA, 2003).
- Pettitt, S.J. *et al. Nat. Methods* **6**, 493–495 (2009).
- Anastassiadis, K. *et al. Dis. Model. Mech.* **2**, 508–515 (2009).
- Singla, V. *et al. Nat. Methods* **7**, 50–52 (2010).
- Skarnes, W.C. *et al. Nat. Genet.* **36**, 543–544 (2004).
- Szymczak, A.L. *et al. Nat. Biotechnol.* **22**, 589–594 (2004).
- Chu, G.C., Dunn, N.R., Anderson, D.C., Oxburgh, L. & Robertson, E.J. *Development* **131**, 3501–3512 (2004).

ONLINE METHODS

DRMCE protocols and plasmids. The step-by-step protocols used for DRMCE are available online through the Nature Protocols Network (<http://www.natureprotocols.com/>). All DRMCE plasmids are available from the Addgene repository (<http://www.addgene.org/>).

Construction of the pDIRE expression vector. The *iCre* coding sequence was amplified by PCR from the pBOB-CAG-iCre-SD plasmid (Addgene) using primers with specific restriction sites. After digestion with Sall and NotI, the *iCre* fragment was cloned into pBluescript IKS (Stratagene). The human *EF1A* promoter was later inserted 5' as a HindIII-BamHI fragment derived from the pBS513 *EF1alpha-Cre* plasmid (Addgene). The SV40 polyadenylation (SV40 pA) site was inserted as a SpeI-SpeI fragment after PCR amplification from the pEGFP-N1 plasmid. These cloning steps resulted in the p*EF1α-iCre* cassette, which was completely sequenced. This *iCre* expression unit was isolated as an EcoRV-EcoRV fragment and inserted into the PstI site of the pPGK*FlpobpA* plasmid (Addgene) to generate the pDIRE expression vector (**Supplementary Fig. 1a** and **Supplementary Data**). To prevent potential promoter competition, the pDIRE vector was designed such that *iCre* is expressed under the control of the *EF1A* promoter, while the expression of *Flpo* is controlled by the PGK promoter.

Construction of the pDREV replacement vector series. The H2B-Venus fusion protein was selected as a versatile and sensitive reporter because *Venus* is one of the brightest and best validated fluorescent proteins and the fusion of Venus with H2B⁷ allows tracking of individual H2B-expressing cells *in vivo*. A 1.75-kb DNA fragment encoding *H2B-Venus* downstream of the autocleavable T2A peptide¹⁴ and upstream of the SV40 pA site and the *rox*, XhoI, *rox* and *loxP* sites was synthesized by GeneArt and cloned as a BglII-HindIII fragment into the pL1L2_GT vector series (B.R. and W.C.S., unpublished data) engineered in all three reading frames (**Supplementary Fig. 1b**). The *PGK-puro* selection cassette was excised as a Sall restriction fragment from the pPGKpuro plasmid (Addgene) and inserted into the XhoI site of the *L1L2-gt-H2B-Venus* plasmid series. This resulted in the definitive pDREV replacement vector collection (pDREV-0, pDREV-1 and pDREV-2), which is compatible with all three open reading frames (**Supplementary Fig. 1b** and **Supplementary Data**).

Construction of the pDRAV replacement backbone vectors. The pBluescript IKS plasmid was modified by inserting linkers to produce all possible orientations of the *loxP* and *FRT* sites together with a *lox2272* site that permits subsequent use of conventional RMCE. The *attB-pGK-Hygro-attP* resistance cassette was cloned into the BamHI and Sall sites. The multiple cloning sites of all pDRAV plasmids consist of unique NotI-NsiI-HpaI-PacI-BamHI restriction sites that can be used to insert the sequences of interest.

Construction of the *Hand2-Flag* replacement vector (pRVH2). Linkers were inserted into pBluescript IKS plasmid to produce the following restriction/recombinase site configuration: SacI-*loxP*-NarI-NotI-BamHI-Sall-ClaI-*FRT*-HindIII-KpnI.

A NarI-NotI fragment of the *Hand2* 5' untranslated region and a NotI-BamHI fragment corresponding to the remainder of the *Hand2* transcription unit (with a Flag-epitope tag inserted into coding exon 1) were sequentially inserted into the pBluescript IKS backbone. A DNA fragment encoding the *attB-pGK-hygro-attP* resistance cassette with HindIII and PacI sites (to enable Southern blot screening) was cloned into the BamHI and Sall sites of the pBluescript IKS backbone to produce the final replacement vector (**Fig. 2a**).

Mouse embryonic stem cell transfection and selection. 50 μg of the appropriate replacement vector were coelectroporated with 50 μg of pDIRE plasmid into mouse embryonic stem cells (1.5×10^7 cells per cuvette; 240 kV, 475 μF). IKMC mouse embryonic stem cells¹⁰ were grown in Knockout DMEM (4.5 g l⁻¹ glucose) containing 10% FBS, 2 mM D-glutamine, 1× penicillin-streptomycin, 0.1 mM β-mercaptoethanol and 10³ U ml⁻¹ LIF/ESGRO (Chemicon; all other reagents from Gibco-Invitrogen). R1 embryonic stem cells were grown in DMEM (4.5 g l⁻¹ glucose) containing 15% FCS (HyClone), 2 mM D-glutamine, 1× non-essential amino acids, 2 mM sodium pyruvate, 1× penicillin-streptomycin, 0.1 mM β-mercaptoethanol and 10³ U ml⁻¹ LIF/ESGRO. The culture medium was changed daily and from the second day onward; resistant colonies were selected in the presence of 175 μg ml⁻¹ hygromycin or 0.5 μg ml⁻¹ puromycin (Sigma). After 8 d in selection medium, drug-resistant colonies were picked and analyzed by PCR. Clones with correct replacement were expanded, frozen in several aliquots and the correct replacement verified by Southern blot analysis. General protocols for handling, culture and manipulation of mouse embryonic stem cells are available as a standard textbook⁹. Detailed protocols for the culture of IKMC targeted mouse embryonic stem cells can be downloaded from the EUCOMM website (<http://www.eucomm.org/information/protocols/>).

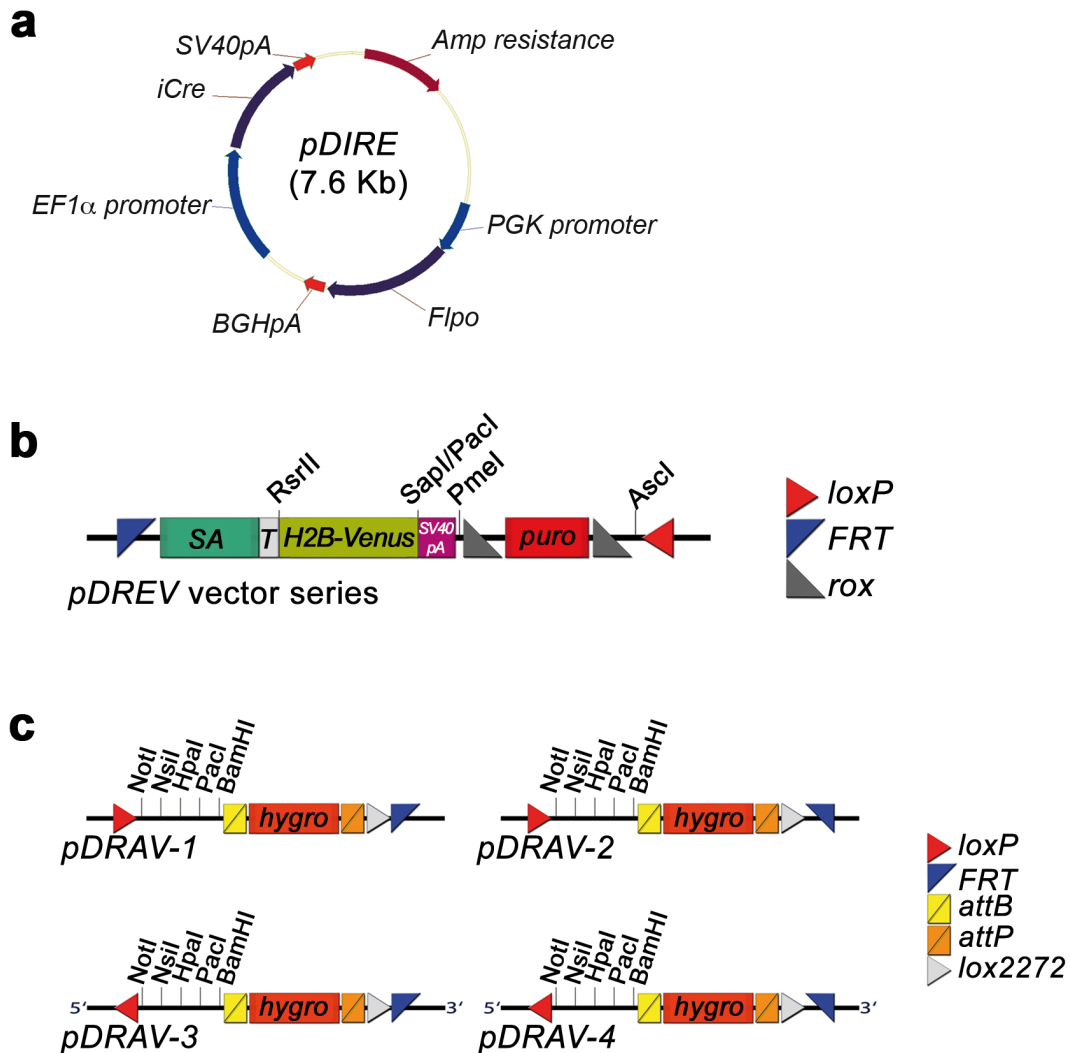
Immunodetection of YFP and β-galactosidase. Embryonic stem cell colonies were grown on eight-well micro-Slides (Ibidi), fixed with cold acetone and incubated with rabbit anti-GFP-Alexa Fluor-488 (1:1,000; Invitrogen) and mouse anti-β-galactosidase (1:50; Developmental Studies Hybridoma Bank, Department of Biology, University of Iowa) primary antibodies, followed by an incubation step with a goat anti-mouse-Alexa Fluor-594 (1:1,000; Invitrogen). Fluorescent images were acquired using a Leica SP5 confocal microscope and software.

Whole-mount *in situ* hybridization. Mouse embryos were processed for whole-mount *in situ* hybridization using digoxigenin-labeled *Hand2* antisense riboprobes⁸. Images were acquired using a Leica MZ16A stereomicroscope and software.

Image processing. All images were processed and composites made using the Adobe Photoshop CS4 software package. Only contrast and brightness of the original images were adjusted minimally and within the linear range when necessary.

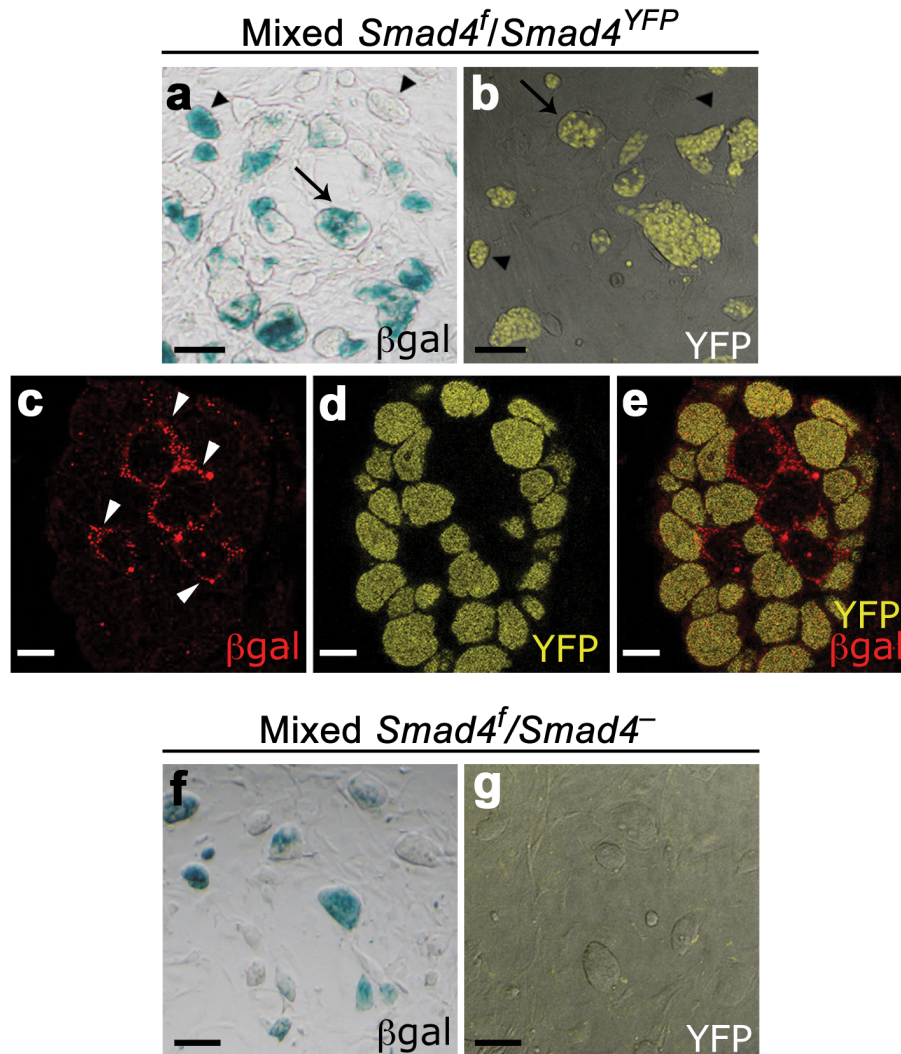
Mice. All animal experiments were performed in accordance with Swiss law and have been approved by the veterinary authorities of Basel.

Supplementary Figure 1. The dRMCE tool-kit.



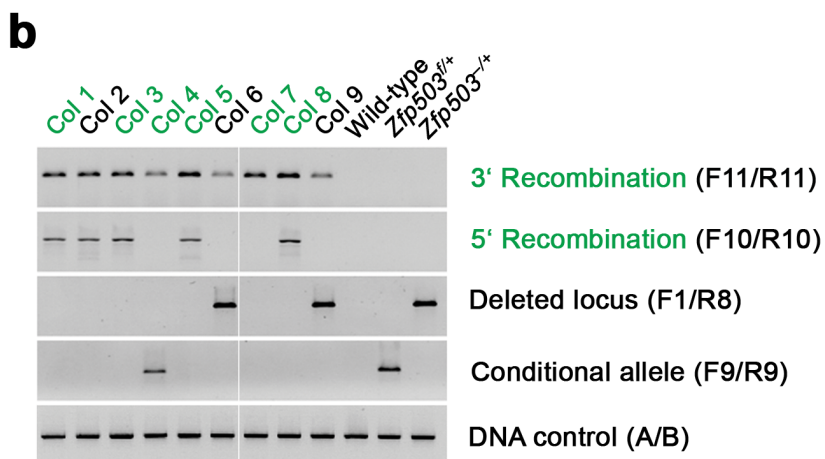
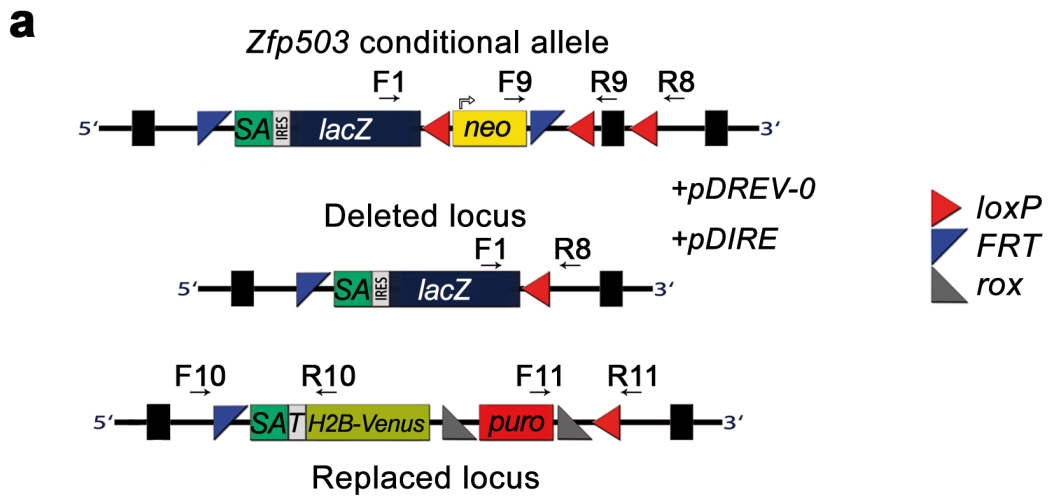
(a) Map of the *pDIRE* (plasmid Dual Improved Recombinase Expression) vector. Simultaneous expression of both iCre and Flpo recombinases in mouse embryonic stem cells is achieved by the use of heterologous promoters (*PGK-Flpo*; *EF1 α -iCre*). (b) The *pDREV* (plasmid Dual Recombinase EuComm Vector) series encode a 5' *FRT* site and 3' *loxP* site for re-engineering of the IKMC knockout first alleles. These plasmids encode the T2A self-cleaving peptide (T) and H2B-Venus fluorescent reporter fused in-frame to the splice acceptor of the mouse *En2* gene followed by the *SV40* polyadenylation site and *PGK-puromycin* selection cassette (flanked by *rox* sites). The *H2B-Venus* coding sequence can be substituted by any coding sequences of choice in a single cloning step. (c) The *pDRAV* (plasmid Dual Recombinase Aceptor Vector) series encodes the *loxP* and *FRT* sites in all possible orientations. The *PGK-hygromycin* selection cassette is flanked by ϕ 31 target sites. A *lox2272* site has also been inserted to enable subsequent engineering. The polylinker in the *pDRAV* series provides the necessary versatility for rapid generation of custom-designed dRMCE replacement vectors. The complete sequences of the *pDIRE*, *pDREV* and *pDRAV* vectors are included as a **Supplementary Data File**.

Supplementary Figure 2. Differential reporter activity distinguishes different types of mixed colonies.



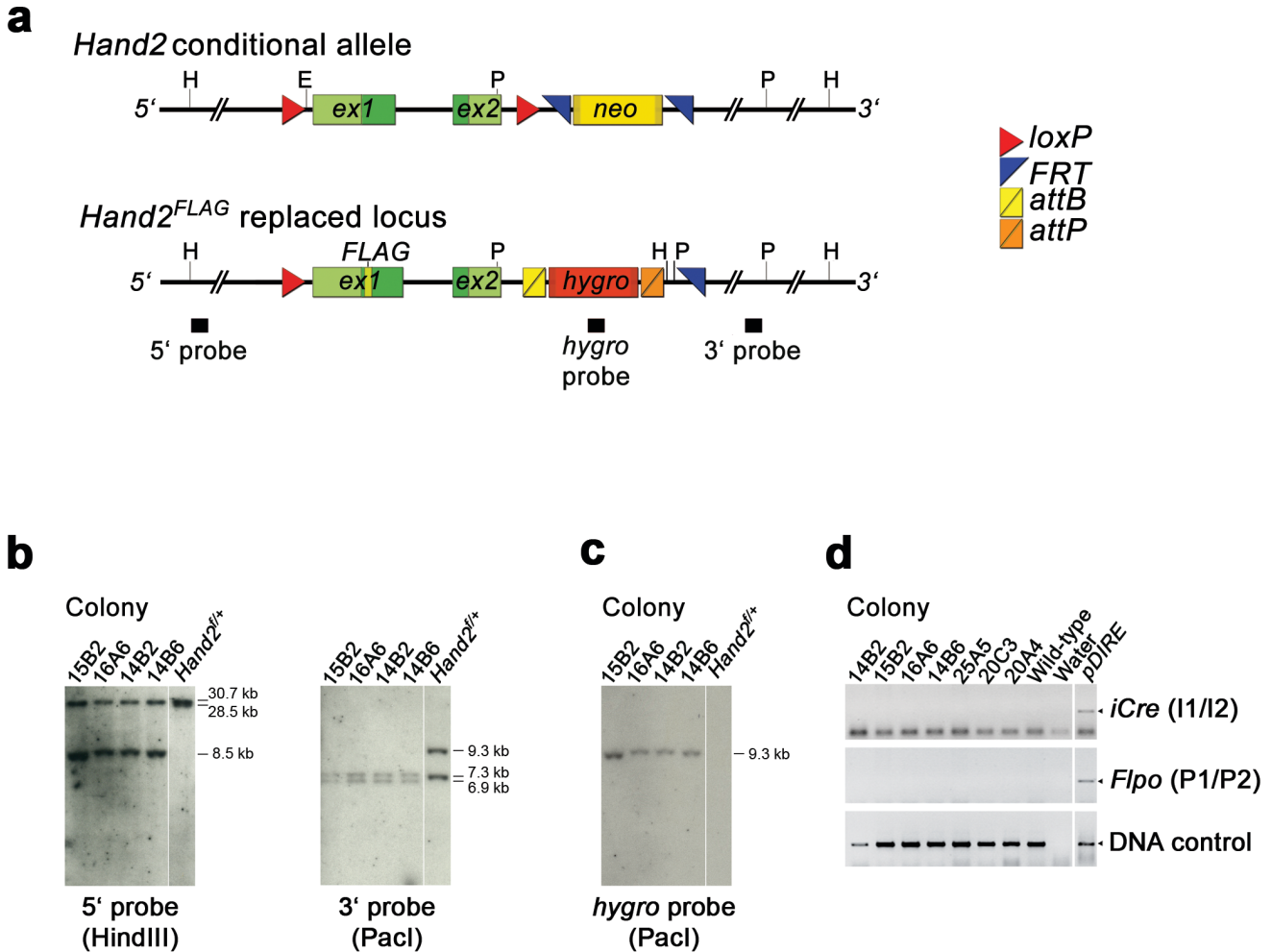
(a, b) Colony 2 is composed of both β -galactosidase (*Smad4^f*) and YFP-positive cells (*Smad4^{YFP}* allele) in agreement with PCR analysis (Fig. 1c). Some colonies are mixed (arrows), while others are either completely β -galactosidase or YFP-positive (arrowheads). (c, d, e) Co-immunolocalization of β -galactosidase (red) and YFP (yellow) in a mixed colony reveals that cells either express one or the other reporter (see panel e). β -galactosidase localizes to the cytoplasm (white arrowheads in panel c), while the YFP protein is nuclear. (f, g) In a mixed colony composed of heterozygous *Smad4^f* and *Smad4⁻* cells, some cells retain β -galactosidase while no YFP fluorescence is detected. Scale bars: 100 μ m (panels a, b, f and g); 10 μ m (panels c-e).

Supplementary Figure 3. dRMCE works efficiently with promoter-driven IKMC knockout-first alleles.



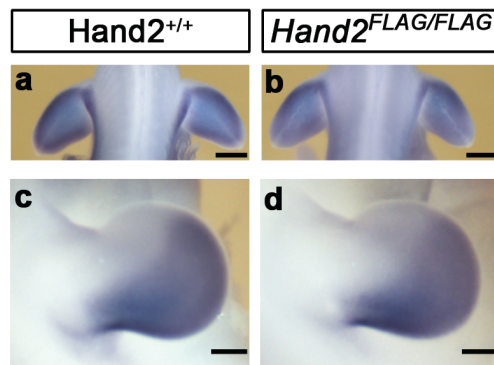
(a) Scheme of the dRMCE strategy for the *Zfp503* conditional allele (*Zfp503*^f), which encodes three *loxP* sites. The scheme illustrates the likely sequence of complete *cis*-deletion and subsequent *trans*-insertion that results in correct replacement and generation of the *Zfp503*^{YFP} allele. (b) PCR screening reveals the high frequency of clones with correct replacement (indicated in green) and some clones with only partial or no replacement. Detection of β -galactosidase activity or YFP fluorescence is not possible as *Zfp503* is not expressed by mouse embryonic stem cells. 3'Recombination, 5'Recombination: correct replacement at the 3' and 5' end, respectively.

Supplementary Figure 4. No random integration of the dRMCE plasmids in *Hand2*^{FLAG/+} mouse embryonic stem cell clones.



(a) Schematic view of the *Hand2*^f and *Hand2*^{FLAG} alleles. The positions of restriction sites and the probes used for Southern blot analysis are indicated. H: HindIII, E: EcoRV, P: PacI. (b) Southern blot analysis confirms that replacement occurred correctly at the 5' (8.5 kb band) and 3' (6.9 kb band) ends and reveals the integrity of the *Hand2*^{FLAG} locus. (c) A single copy of the *hygromycin*-resistance cassette is present in all *Hand2*^{FLAG} clones. (d) PCR primers that amplify *iCre* and *Flpo* sequences fail to detect *pDIRE* sequences in *Hand2*^{FLAG} clones.

Supplementary Figure 5. *Hand2* expression in limb buds of mouse embryos.



(**a, b**) Forelimbs of wild-type (*Hand2*^{+/+}) and *Hand2*^{FLAG/FLAG} mouse embryos at ~E10.5 (posterior view). (**c, d**) Forelimbs of mouse embryos of both genotypes at ~E11.5 (oriented with anterior to the top, posterior to the bottom). Scale bars: 200 μ m (panels **a, b**); 500 μ m (panels **c, d**).

Supplementary Table 1. Frequencies of dRMCE-mediated correct replacement at the *Smad4*, *Zfp503*, *Hand2* and *Gli3* loci in mouse embryonic stem cells.

Gene Locus	Number of Colonies	Correct Replacement	Mixed Colonies	Negative
<i>Smad4</i>	48	33 (69%)	5	10
<i>Zfp503</i>	48	25 (52%)	0	23
<i>Hand2</i>	343	43 (13%)	11	289
<i>Gli3</i>	113	37 (33%)	0	76

Supplementary Table 2. Sequences of the PCR primers used in this study and primer pairs/amplicon sizes that were designed to specifically detect the different alleles of the *Smad4*, *Zfp503* and *Hand2* loci.

Primers of general use

In IKMC knockout-first alleles

Primer	Sequence
F1	AGCAGAGCGGGTAAACTGGC
R1	GCATCAGAGCAGCCGATTGTC
F9	CCAACCTGCCATCACGAGATT

In pDREV

Primer	Sequence
R3	TGGACGAAATGCCGGTGTCA
F4	GCAAAACCAAATTAAGGGCCA
R10	TGGACCTGCTTCAGAACCTTGTA
F11	CTCTTGATTCCCACTTTGTGGTTC

In pDRAV

Primer	Sequence
F6	ATGCGACGCAATCGTCCGATC
R7	CATCTGCACGAGACTAGTGAGACG

In pDIRE

Primer	Sequence
I1	GACTACCTCCTGTACCTGCAAGCCAG
I2	CTGCCAATGTGGATCAGCATTCTC
P1	CAGCCTGAGCTTCGACATCGTGAAC
P2	CTCAGGAACTCGTCCAGGTACACC

Locus specific primers

Primer	Sequence
F2	AACTAACTCTGTGTTTCAGAGCCCCG
R2	GCTGCCCAAATCAATAGCCA
F3	GCAATCCAAACCAAGCATTGTC
F5	CCTCGGCAATTAGCAACGTGAACATC
R5	GTCTCGCTCCTCAGGCTCTCTCG
R6	CCCTCCTCCACCACCACTGCTCAT
F7	CTGTGCCTGGTGCTTCGTTTTGTG
R8	TTGAACTGCGAACAGGGGAA
R9	TTCTGAGGAAGGCGACTTTGG
F10	CTTCCTGTGGGGTTTCTTTC
R11	GCACAAAACGAAACTCAAACGC
A	TCCAAGTCGATGGATATGCAACG (<i>Grem1</i>)
B	ATGAATCGCACCGCATACACTG (<i>Grem1</i>)

Locus specific amplicons

Smad4 locus

Primer pair	Allele	Size
F4/R2	<i>Smad4</i> ^{YFP} (3')	456bp
F3/R3	<i>Smad4</i> ^{YFP} (5')	1594bp
F2/R2	<i>Smad4</i> ⁻	565bp
	<i>Smad4</i> ^{wt}	1265bp
F1/R1	<i>Smad4</i> ^f	558bp

Zfp503 locus

Primer pair	Allele	Size
F11/R11	<i>Zfp503</i> ^{YFP} (3')	396bp
F10/R10	<i>Zfp503</i> ^{YFP} (5')	1449bp
F1/R8	<i>Zfp503</i> ⁻	987bp
F9/R9	<i>Zfp503</i> ^f	599bp

Hand2 locus

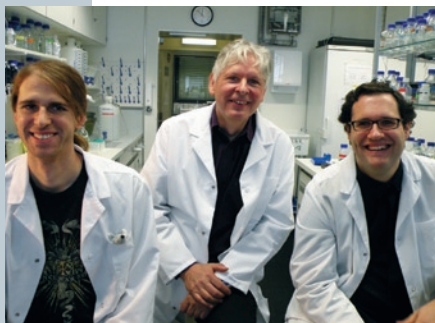
Primer pair	Allele	Size
F6/R6	<i>Hand2</i> ^{FLAG} (3')	965bp
F5/R5	<i>Hand2</i> ^{FLAG} (5')	435bp
F5/R5	<i>Hand2</i> ^f (5')	435bp (EcoRV: 340bp + 95bp)
F5/R6	<i>Hand2</i> ⁻	411bp
F7/R6	<i>Hand2</i> ^{wt}	240bp
F7/R7	<i>Hand2</i> ^{FLAG} (mice)	404bp

THE AUTHOR FILE

Rolf Zeller and Javier Lopez-Rios

Gene cutting and pasting just got a whole lot faster.

It is one of the arbitrary facts of nature that some genes are more amenable to tinkering than others. Unfortunately the gene that Marco Osterwalder, a graduate student at University of Basel Medical



First author Marco Osterwalder (left) is pictured with corresponding authors Rolf Zeller (middle) and Javier Lopez-Rios (right).

Faculty, was most interested in studying was in the latter category. *Hand2* is essential for heart and limb development, and replacing the endogenous mouse gene with an engineered construct, he thought, would help identify a wealth of interaction partners.

But replacing endogenous genes is a tedious, exacting process, explains Javier Lopez-Rios, a postdoc who works with Osterwalder. Constructing a vector containing the replacement construct can take a month or two, and using it to transfect mouse embryonic stem cells takes another couple of weeks. Then screening is necessary to identify the very few cells modified correctly. “You have to pick hundreds of clones,” says Lopez-Rios. Each clone is checked for appropriate modification using PCR or Southern blotting, and if no appropriate clones are found, the process starts over again. Creating a mouse with a new version of the gene by conventional homologous recombination can take up to 18 months.

Generation of the *Hand2* ‘conditional knockout’ by homologous recombination involved screening ~1,500 clones, which took three scientists several months. “It was kind of the story in the lab; this is really the locus from hell,” Lopez-Rios recalls. Therefore, nobody in the group except Osterwalder was keen on modifying this locus any further.

And then Lopez-Rios had an idea. The *Hand2* ‘conditional knockout’ encodes sites that allow two DNA recombinases to excise the protein-coding region on cue, but some sites remain even after the gene is deleted. Maybe, Lopez-Rios thought, these left-over sites could serve as an anchor to pull a new gene construct in. Even better, the International

Knockout Mouse Consortium has engineered ‘conditional knockouts’ for thousands of genes using the same configuration of recombinase sites.

Lopez-Rios and Osterwalder sketched out a possible approach and showed it to Rolf Zeller. “I said it looks like it would work on the drawing board,” Zeller recalls, “but if it would be so easy, why hasn’t anyone done it?” The scientists were not keen to spend another year and a half doing homologous recombination, so they decided to give it a try. “It worked just like we drew it on the blackboard of the seminar room,” Zeller recalls. “Per construct, you pick many fewer colonies. It’s a gain of time, it’s less stress, and you get your result much quicker. It’s one of those cases where laziness makes for good science,” he laughs.

Osterwalder is now back studying limb development and can create more tools than Zeller originally considered possible. The goal of his project is to modify the Hand2 protein with a tag that will capture its interaction partners, and now Osterwalder is screening several tags to find the most effective one. “It’s something we never would have thought of doing if we had to use homologous recombination,” says Zeller. He believes there is even potential for the technique to be used in high-throughput screening to test the effects of various mutations on protein function.

“It’s one of those cases where laziness makes for good science.”
—Rolf Zeller

What’s more, the technique is easy to learn. A graduate student who has never worked with embryonic stem cells is already inserting different tags into an endogenous gene, says Zeller. In contrast, the use of homologous recombination would be tedious and require copious training, he explains. He has previously been reluctant to push such projects for fear that part of a young scientist’s career might be wasted with a long-term project that didn’t work.

Plasmids with the insertion vectors have already been deposited with AddGene for public distribution, says Zeller. And, given that the International Knockout Mouse Consortium has created conditional knockouts for about half of the mouse genome, the technique could be quickly applied to thousands of genes, he says. “What we really hope is that this technology will be useful for a lot of people.”

Monya Baker

Osterwalder, M. *et al.* Dual RMCE for efficient re-engineering of mouse mutant alleles. *Nat. Methods* **7**, 893–895 (2010).

Next generation engineering of conditional mouse alleles with loxP and FRT sites by dual RMCE.

Marco Osterwalder , Javier Lopez-Rios & Rolf Zeller

Developmental Genetics, Department of Biomedicine, University of Basel

Journal name: Protocol Exchange
Year published: (2010)
DOI: doi:10.1038/protex.2010.210
Published online 16 December 2010

Abstract

We have developed dual RMCE (dRMCE) as a rapid, cost-saving and easy to use tool that allows re-engineering the vast majority of existing conditional alleles and generation of mice without the need to resort again to homologous recombination or other more complex or time consuming strategies. dRMCE mobilizes the normal loxP and FRT sites present in most conditional alleles and many gene-trap alleles for site-specific targeting of the endogenous locus with a custom designed replacement cassette. dRMCE is well-suited for the easy and rapid modification of endogenous genes by e.g. inserting molecular tags, introduce disease-causing mutations, swap domains and/or insertion of exogenous genes in mouse ES cell lines. To facilitate access to the technology, we have developed a "dRMCE tool-kit" (available from Addgene) that comprises the dual-recombinase expression vector and several backbone plasmids for easy generation of replacement vectors.

The procedures described here focus mostly on the dRMCE technology. However, we also provide information essential for ES cell culture as far as it is relevant for successful replacement of the locus of interest by dRMCE, generation of highly chimeric mice and germ-line transmission of the modified allele.

This protocol complements the information provided by Osterwalder et al., 2010.

Distinct Roles of Hand2 in Initiating Polarity and Posterior *Shh* Expression during the Onset of Mouse Limb Bud Development

Antonella Galli^{1a*}, Dimitri Robay¹, Marco Osterwalder¹, Xiaozhong Bao², Jean-Denis Bénazet¹, Muhammad Tariq^{3a,b}, Renato Paro^{3,4}, Susan Mackem², Rolf Zeller^{1*}

1 Developmental Genetics, Department of Biomedicine, University of Basel, Basel, Switzerland, **2** Cancer and Developmental Biology Laboratory, National Cancer Institute, Bethesda, Maryland, United States of America, **3** Department of Biosystems Science and Engineering, ETH Zurich, Basel, Switzerland, **4** Faculty of Sciences, University of Basel, Basel, Switzerland

Abstract

The polarization of nascent embryonic fields and the endowment of cells with organizer properties are key to initiation of vertebrate organogenesis. One such event is antero-posterior (AP) polarization of early limb buds and activation of morphogenetic Sonic Hedgehog (SHH) signaling in the posterior mesenchyme, which in turn promotes outgrowth and specifies the pentadactylous autopod. Inactivation of the *Hand2* transcriptional regulator from the onset of mouse forelimb bud development disrupts establishment of posterior identity and *Shh* expression, which results in a skeletal phenotype identical to *Shh* deficient limb buds. In wild-type limb buds, *Hand2* is part of the protein complexes containing *Hoxd13*, another essential regulator of *Shh* activation in limb buds. Chromatin immunoprecipitation shows that *Hand2*-containing chromatin complexes are bound to the far upstream *cis*-regulatory region (ZRS), which is specifically required for *Shh* expression in the limb bud. Cell-biochemical studies indicate that *Hand2* and *Hoxd13* can efficiently transactivate gene expression via the ZRS, while the *Gli3* repressor isoform interferes with this positive transcriptional regulation. Indeed, analysis of mouse forelimb buds lacking both *Hand2* and *Gli3* reveals the complete absence of antero-posterior (AP) polarity along the entire proximo-distal axis and extreme digit polydactyly without AP identities. Our study uncovers essential components of the transcriptional machinery and key interactions that set-up limb bud asymmetry upstream of establishing the SHH signaling limb bud organizer.

Citation: Galli A, Robay D, Osterwalder M, Bao X, Bénazet J-D, et al. (2010) Distinct Roles of Hand2 in Initiating Polarity and Posterior *Shh* Expression during the Onset of Mouse Limb Bud Development. *PLoS Genet* 6(4): e1000901. doi:10.1371/journal.pgen.1000901

Editor: Clifford J. Tabin, Harvard Medical School, United States of America

Received: September 11, 2009; **Accepted:** March 9, 2010; **Published:** April 8, 2010

This is an open-access article distributed under the terms of the Creative Commons Public Domain declaration which stipulates that, once placed in the public domain, this work may be freely reproduced, distributed, transmitted, modified, built upon, or otherwise used by anyone for any lawful purpose.

Funding: This research was supported by the Swiss National Science Foundation (grants 3100A0-100240 and -113866) and the University of Basel (to RZ); the Center for Cancer Research, NCI and NIH (to SM); the EU Epigenome Network of Excellence; and the ETH Zurich (to RP). The funders had no role in study design, data collection and analysis, decision to publish, or preparation of the manuscript.

Competing Interests: The authors have declared that no competing interests exist.

* E-mail: ag2994@columbia.edu (AG); rolf.zeller@unibas.ch (RZ)

^a Current address: Departments of Medicine and Genetics & Development, Columbia University Medical Center, New York, New York, United States of America

^b Current address: Department of Biology, School of Science and Engineering, Lahore University of Management Sciences, Lahore, Pakistan

Introduction

An important step during the initiation of vertebrate organogenesis is the setting-up of morphogenetic signaling centers that coordinately control cell specification and proliferation. One paradigm model to study these processes is the developing limb bud and recent studies have revealed how morphogenetic Sonic hedgehog (SHH) signaling from the zone of polarizing activity (ZPA) and Fibroblast growth factor (FGF) signaling from the apical ectodermal ridge (AER) coordinate cell specification with proliferation along both major limb bud axes [1]. AER-FGF signaling mainly controls the establishment of the proximo-distal (PD) limb bud axis (sequence: stylopod-zeugopod-autopod) [2], while SHH signaling by the polarizing region controls antero-posterior (AP) axis formation (radius and ulna, thumb to little finger) [3,4]. Cells receiving the SHH signal inhibit the constitutive processing of *Gli3* to its repressor form (*Gli3R*) and upregulate the expression of the *Gli1* transcriptional activator, which results in

positive regulation of SHH target genes [5–7]. In limb buds of mouse embryos lacking *Gli3*, the expression of initially posteriorly restricted genes such as *Hand2*, *5'HoxD* genes and the BMP antagonist *Gremlin1* (*Grem1*) expands anteriorly from early stages onwards and an anterior ectopic *Shh* expression domain is established at late stages [8]. However, the resulting digit polydactyly arises in a SHH-independent manner, as limbs of embryos lacking both *Shh* and *Gli3* are morphologically and molecularly identical to *Gli3* deficient mouse embryos [9,10]. These and other studies indicate that *Gli3* acts initially up-stream of SHH signaling to restrict the expression of genes activated prior to *Shh* to the posterior limb bud [11] and that SHH-mediated inhibition of *Gli3R* production is subsequently required to enable distal progression of limb bud development [9].

The molecular interactions that polarize the nascent limb bud along its AP axis and activate SHH signaling in the posterior limb bud mesenchyme have only been partially identified. Previous studies implicated the basic helix-loop-helix (bHLH) transcription

Author Summary

During early limb bud development, posterior mesenchymal cells are selected to express *Sonic Hedgehog* (*Shh*), which controls antero-posterior (AP) limb axis formation (axis from thumb to little finger). We generated a conditional loss-of-function *Hand2* allele to inactivate *Hand2* specifically in mouse limb buds. This genetic analysis reveals the pivotal role of *Hand2* in setting up limb bud asymmetry as initiation of posterior identity and establishment of the *Shh* expression domain are completely disrupted in *Hand2* deficient limb buds. The resulting loss of the ulna and digits mirror the skeletal malformations observed in *Shh*-deficient limbs. We show that *Hand2* is part of the chromatin complexes that are bound to the *cis*-regulatory region that controls *Shh* expression specifically in limb buds. In addition, we show that *Hand2* is part of a protein complex containing *Hoxd13*, which also participates in limb bud mesenchymal activation of *Shh* expression. Indeed, *Hand2* and *Hoxd13* stimulate ZRS-mediated transactivation in cells, while the Gli3 repressor form (Gli3R) interferes with this up-regulation. Interestingly, limb buds lacking both *Hand2* and *Gli3* lack AP asymmetry and are severely polydactylous. Molecular analysis reveals some of the key interactions and hierarchies that govern establishment of AP limb asymmetries upstream of SHH.

factor *Hand2* (*dHand*) in these early determinative processes upstream of SHH signaling [1]. In particular, the development of fin and limb buds of *Hand2* deficient mouse and zebrafish embryos arrests at an early stage and no *Shh* expression is detected [12,13]. This early developmental arrest in conjunction with massive generalized apoptosis of *Hand2* deficient mouse limb buds precluded an *in depth* analysis of the molecular circuits and signaling systems that control initiation and progression of limb bud development. Furthermore, transgene-mediated over-expression of *Hand2* induces digit duplications in mouse limb buds [14]. The functional importance of *Hand2* as a transcriptional regulator in these processes was further corroborated by an engineered mutation that inactivates the *Hand2* DNA binding domain in mouse embryos, which results in limb bud defects resembling the *Hand2* null phenotype [15]. Cell-biochemical analysis showed that *Hand2* interacts with so-called *Ebox* DNA sequence elements most likely as a heterodimer with other bHLH transcription factors such as *E12* [16,17] and *Twist1*, which is also required for early limb bud development [18,19].

Genetic analysis in mouse embryos showed that *Gli3* is required to restrict *Hand2* expression to the posterior limb bud mesenchyme as part of a mutually antagonistic interaction [11]. This interaction was proposed to pre-pattern the limb bud mesenchyme along its AP axis prior to activation of SHH signaling. However, the functional importance of this pre-patterning mechanism for normal progression of limb development remained unknown. Additional pathways are also required for establishment of the *Shh* expression domain in the posterior limb bud mesenchyme such as retinoic acid signaling from the flank and AER-FGF8 signaling [20,21]. During the onset of limb bud development, the expression of the 5' most members of the *HoxD* gene cluster is restricted to the posterior mesenchyme by *Gli3* [22,23]. During these early stages, the 5'*HoxA* and 5'*HoxD* transcriptional regulators are required to activate *Shh* expression in the posterior limb bud mesenchyme [24–26]. Consistent with this genetic analysis, the *Hoxd10* and *Hoxd13* proteins interact directly with the *cis*-regulatory region that controls *Shh* expression in limb buds [27]. This evolutionary

conserved *cis*-regulatory region is called ZPA regulatory sequence (ZRS) and is located about 800 Kb up-stream of the *Shh* gene [28]. Genetic inactivation of the highly conserved core region of the ZRS (termed MFCS1) results in limb bud-specific loss of *Shh* expression and a *Shh* loss-of-function limb skeletal phenotype [29]. Interestingly, this limb bud specific *cis*-regulatory region is absent from vertebrate species that have lost their limbs during evolution [30]. Transgenic analysis in mouse embryos revealed that ZRS-*LacZ* transgenes recapitulate major aspects of *Shh* expression in limb buds [28]. However, this study did not reveal specific *cis*-regulatory elements or sub-regions within the ZRS that regulate transcription, but rather indicated that the entire ZRS is required for correct *Shh* expression. A recent study shows that the ZRS interacts directly with the *Shh* transcription unit in both the anterior and posterior limb bud mesenchyme [31]. However, the *Shh* locus loops out of its chromosomal territory only in the posterior mesenchyme, which results in initiation of transcription. The evolutionary conserved function of the ZRS is underscored by an ever increasing large number of point mutations that are scattered through large parts of ZRS region and cause congenital preaxial polydactylies (PPD) in humans and many other mammals [32]. In summary, these studies establish that the far upstream ZRS *cis*-regulatory region controls *Shh* expression in different tetrapod species and that point mutations cause PPD, while deletion of the central part of the ZRS results in limbless phenotypes.

We have generated a conditional *Hand2* mouse loss-of-function allele and use it to study the requirement of *Hand2* during limb bud initiation. Inactivation of *Hand2* in the forelimb field mesenchyme using the *Prx1*-Cre transgenic mouse strain disrupts the development of posterior skeletal elements. Complete and early inactivation results in a limb skeletal phenotype identical to limbs lacking *Shh*. Indeed, establishment of the *Shh* expression domain in the posterior limb bud is disrupted and early molecular markers of posterior identity are lost, while anterior markers expand posteriorly. This reveals the early requirement of *Hand2* for establishing posterior identity and activation of *Shh* expression. Using specific antibodies, we identify protein complexes containing both *Hand2* and *Hoxd13* transcriptional regulators in wild-type limb buds. Chromatin immunoprecipitation using *Hand2* antibodies reveals the specific enrichment of the ZRS in comparison to adjacent non-ZRS DNA sequences in wild-type limb buds. Functional analysis of the DNA-protein interactions in cultured fibroblasts reveals that *Hand2* and *Hoxd13* transactivate expression of a ZRS-luciferase reporter construct, while this is partially inhibited by Gli3R, which has been previously shown to interact with 5'*Hoxd* proteins [33]. Indeed, mouse limb buds deficient for both *Gli3* and *Hand2* lack AP asymmetry along the entire PD limb axis and display severe digit polydactyly with complete loss of identities. Our study uncovers the interactions of *Hand2* with the Gli3 and *Hoxd13* transcriptional regulators and the far-upstream ZRS *cis*-regulatory region that are required to polarize the nascent limb bud mesenchyme and establish *Shh* expression in the posterior limb bud.

Results

Limb bud-specific inactivation of *Hand2* results in skeletal defects identical to *Shh* deficient limbs

Mouse embryos lacking *Hand2* die during mid-gestation due to cardiovascular defects and limb bud development arrests prior to formation of limb skeletal elements [12,34]. Therefore, we generated a conditional *Hand2* loss-of-function allele by inserting two *loxP* sites into the locus ("floxed" allele: *Hand2^f* or *H2^f*), which

enables Cre-recombinase mediated deletion of the *Hand2* transcription unit (Figure S1). *Hand2* was inactivated in the limb bud mesenchyme ($H2^{\Delta\Delta c}$; Δc : conditional inactivation of the *Hand2*^f allele) using the *Prx1*-Cre transgene, which is expressed in the forelimb field mesenchyme from about E8.5 onwards (14 somites) [35,36]. The inactivation of *Hand2* was verified by monitoring the clearance of *Hand2* transcripts and proteins in forelimb buds and mesenchymal cells (Figure 1A and Figure S2A, S2B, S2C). Limb bud specific inactivation of *Hand2* ($H2^{\Delta\Delta c}$;

Figure 1A) causes distal truncations of the forelimb skeleton and loss of the autopod (Figure 1B). The skeletal phenotypes of *Hand2* deficient forelimbs are variable, but the most severely affected cases (39% of all limbs, n = 80; Figure S3A, S3D) are identical to *Shh* deficient limbs (Figure 1B). Indeed, *Shh* expression and SHH signal transduction are lacking from a similar fraction of all $H2^{\Delta\Delta c}$ limb buds (Figure 1C and Figure S3C). Therefore, the most severely affected $H2^{\Delta\Delta c}$ limb buds correspond to the limb-specific complete *Hand2* loss-of-function phenotype (Figure 1A–1C and

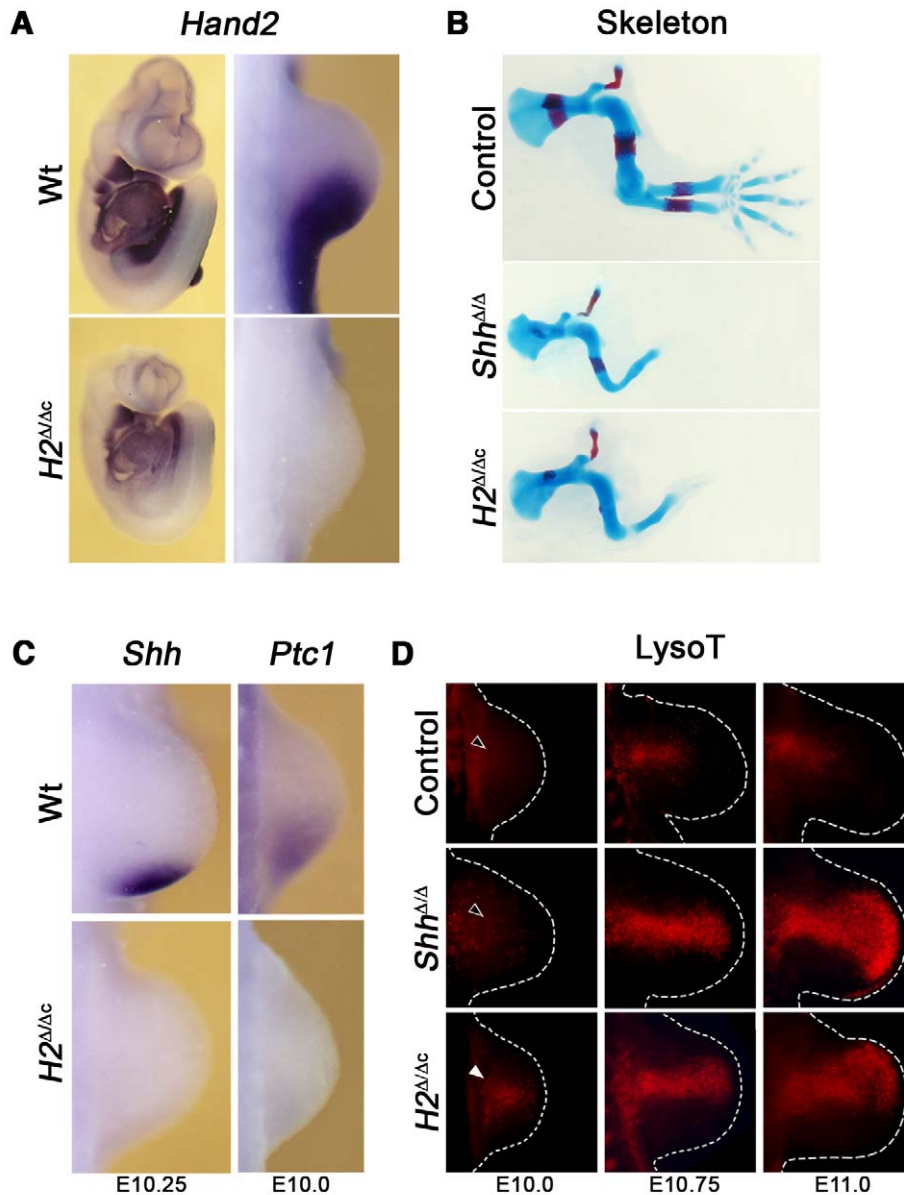


Figure 1. Early deletion of *Hand2* in mouse forelimb buds phenocopies the *Shh* loss-of-function skeletal phenotype. (A) Whole mount *in situ* hybridization detects *Hand2* transcripts in wild-type (Wt) and mouse embryos that lack the *Hand2* gene in their forelimb bud mesenchyme ($H2^{\Delta\Delta c}$) at E9.75 (28 somites). *Hand2* transcripts are absent from forelimb buds of $H2^{\Delta\Delta c}$ mouse embryos. (B) Skeletons of mouse forelimbs at E14.5, stained with alcian blue (cartilage) and alizarin red (bone). *Prx1*-Cre mediated inactivation of *Hand2* ($H2^{\Delta\Delta c}$) phenocopies the $Shh^{\Delta/\Delta}$ limb skeletal phenotype. Control: *Prx1*-Cre^{tg/+}. (C) *Shh* and *Ptc1* transcripts are absent from $H2^{\Delta\Delta c}$ limb buds at E10.25 (32 somites for *Shh*) and E10.0 (29 somites for *Ptc1*). (D) Detection of apoptotic cells by LysoTracker Red (LysoT). *Hand2* deficient limb buds are compared to control (*Prx1*-Cre^{tg/+} and $H2^{+/f}$) and $Shh^{\Delta/\Delta}$ limb buds at E10.0 (30 somites), E10.75 (37 somites), and E11.0. The white arrowhead points to the precocious initiation of cell death in $H2^{\Delta\Delta c}$ forelimb buds (compare white to open arrowheads; n = 2/4). In all panels, limb buds are oriented with the anterior to the top and the posterior to the bottom.

doi:10.1371/journal.pgen.1000901.g001

Figure S3). Between two and four digits form in hypomorphic $H2^{\Delta\Delta c}$ limbs (Figure S3A, S3D) as a likely consequence of residual *Hand2* expression, which triggers SHH signal transduction (Figure S3B, S3C).

In the most severely affected forelimb buds, cells along the entire PD axis, but in particular in the distal-anterior mesenchyme are eliminated by apoptosis (Figure 1D), which is distinct from the generalized apoptosis and developmental arrest of mouse embryos lacking *Hand2* constitutively (Figure S1D, S1E) [12]. In $H2^{\Delta\Delta c}$ forelimb buds, cell death is limited to the core mesenchyme at embryonic day E10.0 (Figure 1D, white arrowhead). In contrast, no significant apoptosis is detected in forelimb buds of wild-type and *Shh* deficient limb buds at these early stages (Figure 1D, open arrowhead). Therefore, *Hand2* is required for cell survival upstream of its role in activation of SHH signaling (Figure 1D, left panels). During progression of limb bud development, the apoptotic domain expands distal-anterior in $H2^{\Delta\Delta c}$ limb buds and becomes similar to the cell death domain observed in *Shh* deficient limb buds (Figure 1D, middle and right panels).

In mouse embryos, hindlimb development is delayed by ~12 hrs and activation of the *Prx1*-Cre transgene in the posterior mesenchyme is delayed by ~24 hrs in comparison to forelimb buds [35,36]. The resulting ~12 hrs delay in *Hand2* inactivation at equivalent stages in the posterior hindlimb bud allows formation of an autopod with 4–5 digits, while the tarsal bones are always fused (Figure 2A). Furthermore, inactivation of *Hand2* specifically in the distal forelimb bud mesenchyme from E10.5 onwards no longer alters skeletal development (data not shown). In agreement with the subtle skeletal alterations following *Prx1*-Cre-mediated *Hand2* inactivation in hindlimb buds (Figure 2A) *Shh* remains expressed, albeit at slightly lower levels than in wild-types (Figure 2B). Taken

together, these studies show that *Hand2* is essential to establish *Shh* expression in the posterior mesenchyme during initiation of limb bud development. Subsequently, it contributes to transcriptional up-regulation of *Shh* expression.

Hand2 is essential for establishment of posterior identity upstream of SHH signaling

Our further analysis focused on the most severe, complete *Hand2* loss-of-function phenotypes in forelimb buds (Figure 1). The early essential requirement of *Hand2* upstream of SHH in forelimb buds (for cell survival, Figure 1D) is further substantiated by molecular analysis, which reveals the lack of *Tbx3* and *Tbx2* expression [37] in the posterior mesenchyme of $H2^{\Delta\Delta c}$ forelimb buds. In contrast, their posterior expression is initiated but not up-regulated in *Shh*^{ΔΔ} forelimb buds (Figure 3A and 3B). The expression of 5' *HoxD* genes is activated but not propagated in *Hand2* deficient limb buds (Figure S4A, S4B), likely due to the disruption of SHH signaling (Figure 1C). Concurrently, the expression of anterior genes such as *Cry-μ*, *Alx4* and *Gli3* is ectopically activated or expands to the posterior margin in $H2^{\Delta\Delta c}$ forelimb buds earlier and/or more prominently than in *Shh*^{ΔΔ} limb buds (Figure 3C–3E and Figure S4C). This loss of posterior and gain of anterior molecular markers reveal the early essential requirement of *Hand2* for establishing posterior limb bud identity.

In wild-type limb buds, Hand2-containing chromatin complexes are bound to the ZRS cis-regulatory region that controls *Shh* expression

This analysis (Figure 1, Figure 2, Figure 3) led us to consider the possibility that *Hand2* might directly transactivate *Shh* expression, possibly in conjunction with 5' *Hox* genes, which are essential for *Shh* activation in mouse limb buds [24,26]. Chromatin immunoprecipitation (ChIP) studies showed previously that *Hoxd13* containing chromatin complexes are bound to the far up-stream ZRS cis-regulatory region that controls *Shh* expression in limb buds [27]. In addition, *Hoxd13* is able to transactivate a ZRS-luciferase reporter construct in transfected cells [27]. Therefore, the potential direct interactions of *Hand2* with *Hoxd13* proteins and the ZRS were assessed by luciferase transactivation assays in NIH3T3 cells, which are mouse fibroblasts commonly used to analyze the SHH pathway [38]. A luciferase reporter construct encoding the entire ZRS (ZRS-Luc) was generated by inserting the ~1.7 kb mouse ZRS region (Figure 4A and Figure S5) [28] upstream of an adenovirus minimal promoter (for details see Text S1). The basal activity of this ZRS-Luc reporter construct was set to 1 and transfection of either *Hand2* (~3-fold) or *Hoxd13* (~6.5-fold) induced luciferase activity and their co-transfection resulted in an ~10.5-fold increase (Figure 4B). *In silico* analysis revealed 6 *bona fide* *Ebox* sequence elements within the ZRS (Figure 4A and Figure S5). Inactivating point mutations in either individual or several of these *Ebox* elements reduce the activity of the ZRS, but not in a strictly *Hand2*-dependent manner as the transactivation by *Hoxd13* alone is also affected (data not shown). As *Hand2* and *Gli3R* act in a mutually antagonistic manner during initiation of limb bud development [11], the potential effects of *Gli3R* on transactivation were assessed. As neither the *Gli3* nor *Gli1* activator forms are able to activate the ZRS-Luc reporter on their own (data not shown), the ZRS likely lacks functional *Gli* binding sites [39], suggesting that any effects of *Gli3R* would be indirect. Indeed, co-expression of *Gli3R* results in significant inhibition of transactivation in the presence

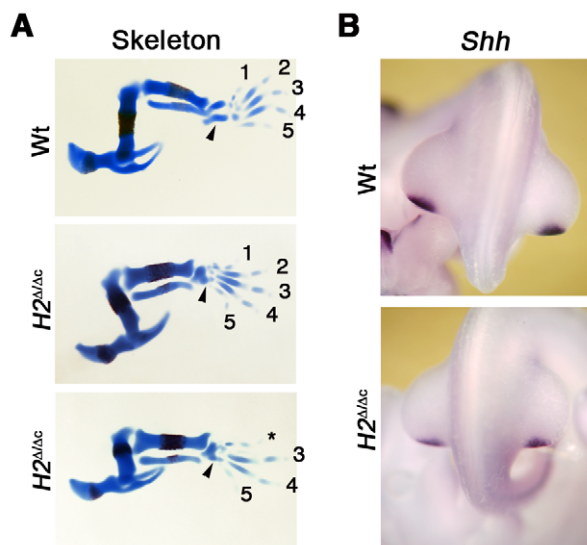


Figure 2. Delayed inactivation of *Hand2* in hindlimb buds results in rather normal *Shh* expression and development. (A) Hindlimb buds skeletons at E14.5, stained with alcian blue (cartilage) and alizarin red (bone). *Prx1*-Cre mediated inactivation of *Hand2* ($H2^{\Delta\Delta c}$) in hindlimb buds results in fusion of the tarsals (arrowheads) and formation of 5 ($n=11/24$) or 4 ($n=13/24$) digits. Please note that in latter case the formation of digit 2 and/or 3 (not shown), which depend mostly on long-range SHH signaling [7] is always affected. (B) *Shh* expression in wild-type and *Hand2* deficient hindlimb buds at E10.75 (37 somites). Note that the expression domain is correctly positioned in $H2^{\Delta\Delta c}$ hindlimb buds, but expression levels are reduced.

doi:10.1371/journal.pgen.1000901.g002

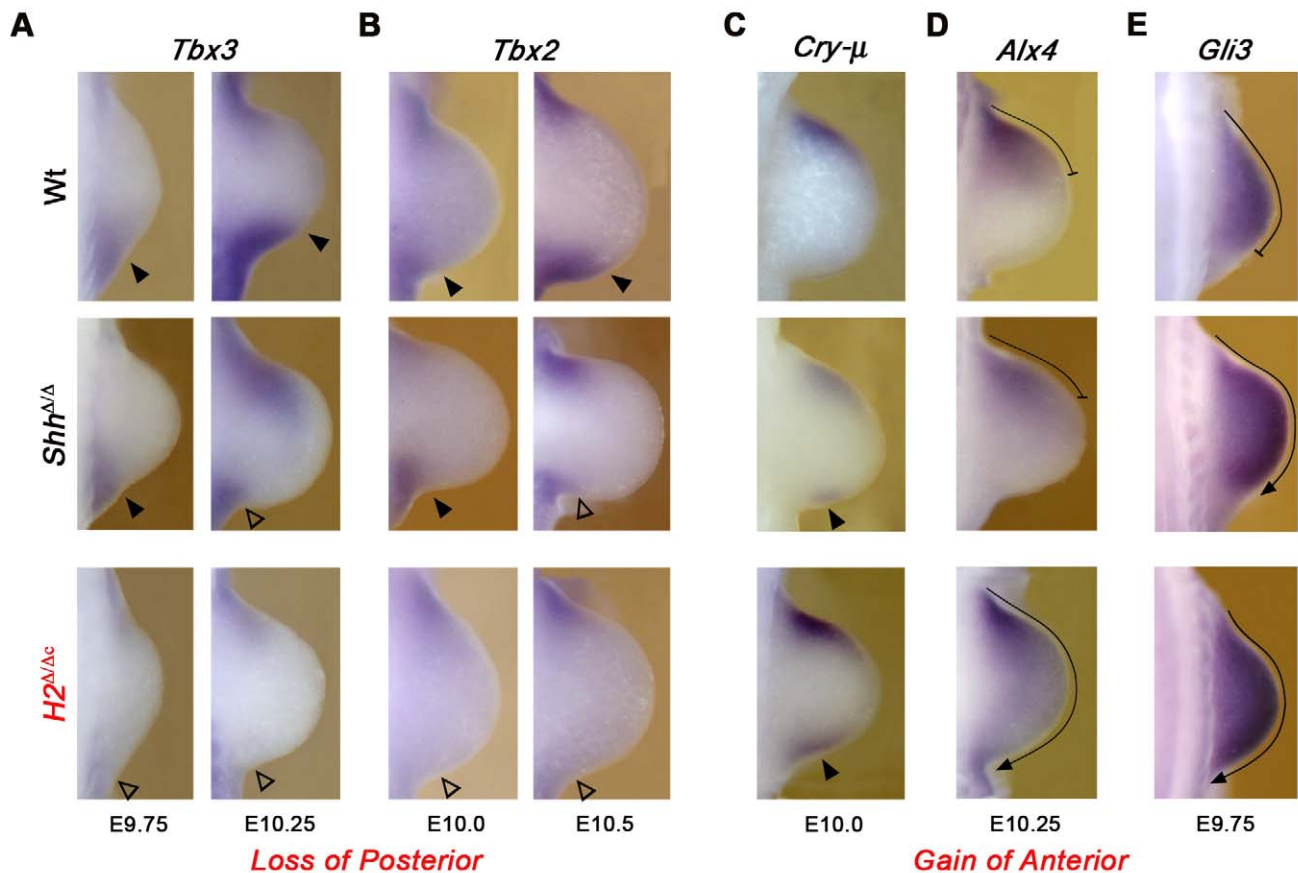


Figure 3. Establishment of posterior forelimb bud identity requires *Hand2*. (A,B) The loss of the posterior *Tbx3* and *Tbx2* expression domains in early *Hand2* deficient (*H2*^{Δ/Δc}) limb buds (from E9.75: 27 somites to E10.5: 35 somites) points to a failure in establishing posterior identity upstream of *Shh* activation. Open arrowheads: loss of expression in *Hand2* deficient forelimb buds; solid arrowheads: normal expression in wild-type and *Shh* deficient limb buds. By E10.25–E10.5 the posterior expression of *Tbx2* and *Tbx3* is also down-regulated in *Shh*^{Δ/Δ} limb buds. (C–E) Posterior expansion of anterior markers in *H2*^{Δ/Δc} limb buds. (C) *Crystallin-μ* (*Cry-μ*) is expressed ectopically in the posterior mesenchyme of *H2*^{Δ/Δc} limb buds at E10.0 (30 somites; indicated by solid arrowheads). The ectopic posterior *Cry-μ* expression is detected earlier than in *Hand2* than *Shh* deficient limb buds (not shown). The *Alx4* (D) and *Gli3* (E) expression domains are posteriorly expanded (indicated by arrows) in *Hand2* deficient limb buds at E9.75 (27 somites) and E10.25 (32 somites), respectively. Note that the posterior expansion of the *Gli3* expression domain is less pronounced in *Shh*^{Δ/Δc} than in *H2*^{Δ/Δc} limb buds. In all panels, limb buds are oriented with the anterior to the top and the posterior to the bottom. doi:10.1371/journal.pgen.1000901.g003

of *Hoxd13* (Figure 4B), in agreement with the proposal that *Gli3R* can bind to and potentially antagonize *Hoxd13* function [33]. In particular, *Gli3R* represses *Hand2*-*Hoxd13* mediated transactivation of the ZRS-Luc reporter by ~50% (Figure 4B).

The relevance of these interactions for limb bud development was determined by co-immunoprecipitation (Figure 4C and Figure S6) and ChIP analysis (Figure 4D and 4E). Immunoprecipitation of *Hoxd13* proteins in combination with Western blotting reveals the existence of protein complexes containing both *Hoxd13* and *Hand2* protein in wild-type limb buds (Figure 4C). The likely direct nature of these interactions is supported by efficient co-precipitation of epitope-tagged *Hand2* and *Hoxd13* proteins from transfected cells (Figure S6). These experiments establish that *Hand2* interacts directly with *Hoxd13* but not with *Gli3R* (Figure S6), which is relevant with respect to their genetic interaction (see below). As the available polyclonal *Hand2* antibodies specifically recognize and immunoprecipitate *Hand2* proteins (Figure S2B, S2C, S2D), ChIP on wild-type mouse limb buds was performed [40] to enrich *Hand2* containing chromatin complexes and the analysis of three independent, fresh chromatin preparations is shown in

Figure 4D and 4E. Conventional PCR using the amplicon “c” (Figure 4A) detected this ZRS region in chromatin precipitated with anti-*Hand2* antibodies (lanes α -*H2*, Figure 4D), while no such amplification was detected when non-specific IgGs were used (lanes α -IgG; Figure 4D). To further analyze this apparent association of *Hand2* containing chromatin complexes with the ZRS, three amplicons (“b”, “c”, “d”) probing different regions of the ~1.7 kb mouse ZRS (Figure 4A) were used for real-time PCR (Q-PCR) analysis. In addition, two amplicons located outside the mouse ZRS were chosen as likely negative controls (non-ZRS amplicons “a” and “e” in Figure 4A and 4E and Figure S5). Indeed, Q-PCR analysis revealed a minimally 14-fold enrichment of the amplicons located within the ZRS in comparison to the adjacent non-ZRS regions (Figure 4E). This enrichment is specific as ChIP using non-specific IgGs resulted in much lower Q-PCR amplification of all five regions. In particular, the enrichment of the ZRS in comparison to flanking non-ZRS regions is highly significant (amplicons “b” to “d” versus “a” and “e”; $p = 0.0018$), while the variability among the three ZRS amplicons is not significantly different. Interestingly, the ZRS region encompassing amplicon “b”, whose enrichment

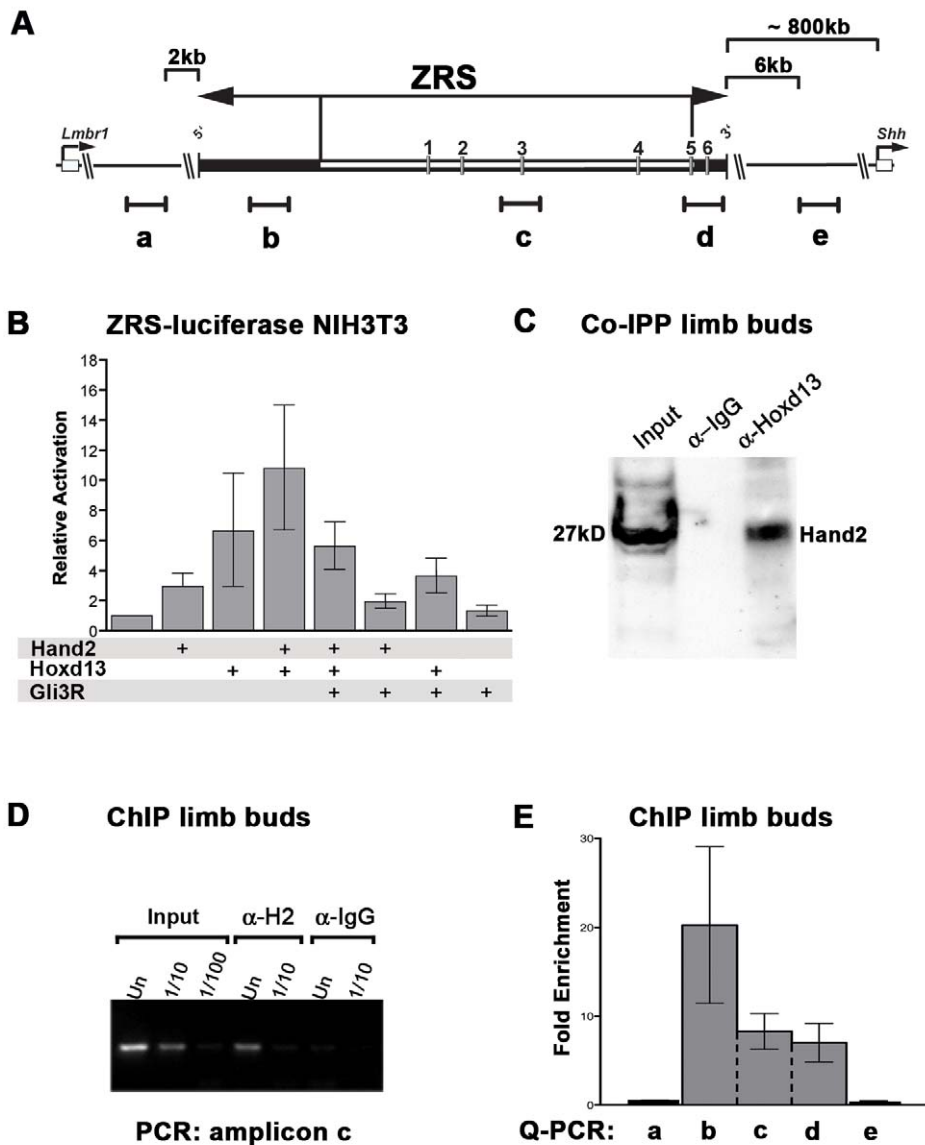


Figure 4. Hand2 interacts with Hoxd13 and is part of the chromatin complexes bound to the ZRS in limb buds. (A) Scheme of the ~1.7 kb mouse ZRS *cis*-regulatory and the flanking genomic regions. The ZRS is located within an intron of the mouse *Lmbr1* gene (indicated on the left) and located ~800 kb upstream of the *Shh* proximal promoter and coding exons (indicated on the right, see also Figure S5). The evolutionary conserved ZRS region drives expression of a *LacZ* reporter gene in a *Shh*-like pattern in mouse limb buds [28], while deletion of the MFC51 core region (indicated in white) disrupts *Shh* activation in limb buds [29]. Six *Ebox* sequences in the ZRS, which could potentially interact with Hand2 proteins are numbered "1" to "6". Black lines indicate the approximate positions and sizes of the PCR amplicons for ChIP analysis. Note that amplicons "b" to "d" reside within the mouse ZRS, while amplicons "a" and "e" are located ~2 kb upstream and ~6 kb downstream of the ZRS and serve as non-ZRS controls. (B) Luciferase transactivation assay in NIH3T3 fibroblasts. Cells were co-transfected with ZRS-Luc and the expression plasmids indicated. Bars represent standard deviations. $P < 0.0001$ for all samples except Gli3R alone: $P = 0.0519$. (C) Co-immunoprecipitation of Hand2 and Hoxd13 from wild-type limb buds (E10.5) using anti-Hoxd13 antibodies (α -Hoxd13) or IgGs (control). Hand2 proteins associated to Hoxd13 protein complexes were detected by Western blotting. (D,E) ChIP from wild-type limb buds (E11.0) to detect Hand2-containing chromatin complexes bound to the ZRS. (D) Analysis of amplicon "c" by conventional PCR (186 bp). Input: DNA isolated from cross-linked chromatin of E11.0 limb buds prior to ChIP was used as a positive control for PCR amplification. α -H2: ChIP using Hand2 antibodies. α -IgG: ChIP using non-specific goat IgGs as a control. Un: undiluted sample; dilutions as indicated. (E) Q-PCR analysis of three completely independent ChIP experiments using freshly cross-linked chromatin and α -Hand2 antibodies. The average values \pm standard error are shown. Values obtained by amplifying a particular region from ChIP experiments using non-specific goat IgGs were arbitrarily set at 1 and used to calculate the values for the α -Hand2 ChIP experiments. Statistical evaluation by the Mann-Whitney test shows that the amplicons within the ZRS ("b" to "d") are enriched in a statistically highly significant manner in comparison to the adjacent non-ZRS amplicons ("a" and "e"; $p = 0.0018$). doi:10.1371/journal.pgen.1000901.g004

is most variable, does not encode any *bona fide Ebox* elements (Figure 4A and 4E). This provides additional evidence for the fact that the interaction of Hand2-containing chromatin complexes with the ZRS may not depend only on *Ebox*

sequences. This ChIP analysis (Figure 4D and 4E) provides good evidence that the Hand2-containing chromatin complexes bind to the ZRS *cis*-regulatory region, but not to adjacent non-ZRS sequences.

Mouse limb buds deficient for both *Hand2* and *Gli3* lack AP asymmetry along the entire PD axis and are severely polydactylous

As embryos lacking *Hand2* in limb buds survive to advanced stages (Figure 1B), the functional relevance of the pre-patterning mechanism [11] can now be genetically investigated in *Hand2* and *Gli3* compound mutant ($H2^{\Delta/\Delta}Gli3^{Xt/Xt}$) embryos (Figure 5, Figure 6, Figure 7). In contrast to the *Hand2* deficiency, $H2^{\Delta/\Delta}Gli3^{Xt/Xt}$ limbs are severely polydactylous and display little phenotypic variability (Figure 5A and Figure S7A). In addition, the zeugopodal bones and elbow joints appear strikingly symmetrical (Figure 5A, white and black arrowheads in panel $H2^{\Delta/\Delta}Gli3^{Xt/Xt}$). These limb skeletal abnormalities are much more severe than the ones of $Gli3^{Xt/Xt}$ and $Shh^{\Delta/\Delta}Gli3^{Xt/Xt}$ limbs (Figure 4A, panel $Gli3^{Xt/Xt}$; see also [9,10]). While the skeletal elements of $H2^{\Delta/\Delta}Gli3^{Xt/Xt}$ limbs seem to lack AP asymmetry, survival of the zeugopod and autopod progenitors is restored and the primordia are expanded in contrast to $H2^{\Delta/\Delta}$ limbs (Figure S7B and data not shown). Moreover, the *Sox9* expression domain, which marks the pre-chondrogenic lineage [41], is expanded in $H2^{\Delta/\Delta}Gli3^{Xt/Xt}$ limb buds that tend to be larger than normal (Figure 5B, panel $H2^{\Delta/\Delta}Gli3^{Xt/Xt}$). However, no significant changes in proliferation were observed in $H2^{\Delta/\Delta}Gli3^{Xt/Xt}$ limb buds (data not shown). While the pre-chondrogenic condensations of all major skeletal elements are discernible by E10.75 in wild-type and *Gli3* deficient limb buds, *Sox9* expression remains diffuse and non-polarized in $H2^{\Delta/\Delta}Gli3^{Xt/Xt}$ limb buds (Figure 5B). During autopod develop-

ment, the pool of *Sox9* expressing digit progenitors is significantly expanded in $H2^{\Delta/\Delta}Gli3^{Xt/Xt}$ limb buds in comparison to *Gli3* mutants and wild-types (Figure 5B; compare limb buds at E11.5). The apparent symmetry of in particular the zeugopod in the $H2^{\Delta/\Delta}Gli3^{Xt/Xt}$ limbs contrasts with the normal AP asymmetry in $Gli3^{Xt/Xt}$ and $Shh^{\Delta/\Delta}Gli3^{Xt/Xt}$ limbs (Figure 5A) [9]. This observation indicates that *Hand2* and *Gli3* participate in establishment of the AP asymmetry of the proximal limb skeleton independent of SHH signaling. Indeed, the expression of *Runx2*, which marks proximal skeletal primordia [42], is altered in double mutant limb buds (Figure 5C). By E12.0, *Runx2* is expressed in the presumptive stylopod and zeugopodal domains of wild-type limb buds, while few *Runx2* positive cells are detected in *Hand2* deficient limb buds (Figure 5C). In contrast, the *Runx2* expression domain is expanded and lacks polarity in the proximal part of double mutant limb buds (Figure 5C, black arrowheads). Taken together, these results indicate that the skeletal phenotypes and the severe polydactyly of $H2^{\Delta/\Delta}Gli3^{Xt/Xt}$ limbs arise as a consequence of disrupting AP asymmetry (proximally as indicated by *Runx2*) and aberrant expansion of the skeletal progenitor pools (distally as indicated by *Sox9*).

Disruption of the self-regulatory system that interlinks the SHH, BMP, and FGF signaling pathways in limb buds

In $H2^{\Delta/\Delta}Gli3^{Xt/Xt}$ limb buds, *Shh* expression is not detected by *in situ* hybridization (Figure 6A) and its expression is ~10-fold lower than in wild-types (Figure 6C). Interestingly, the

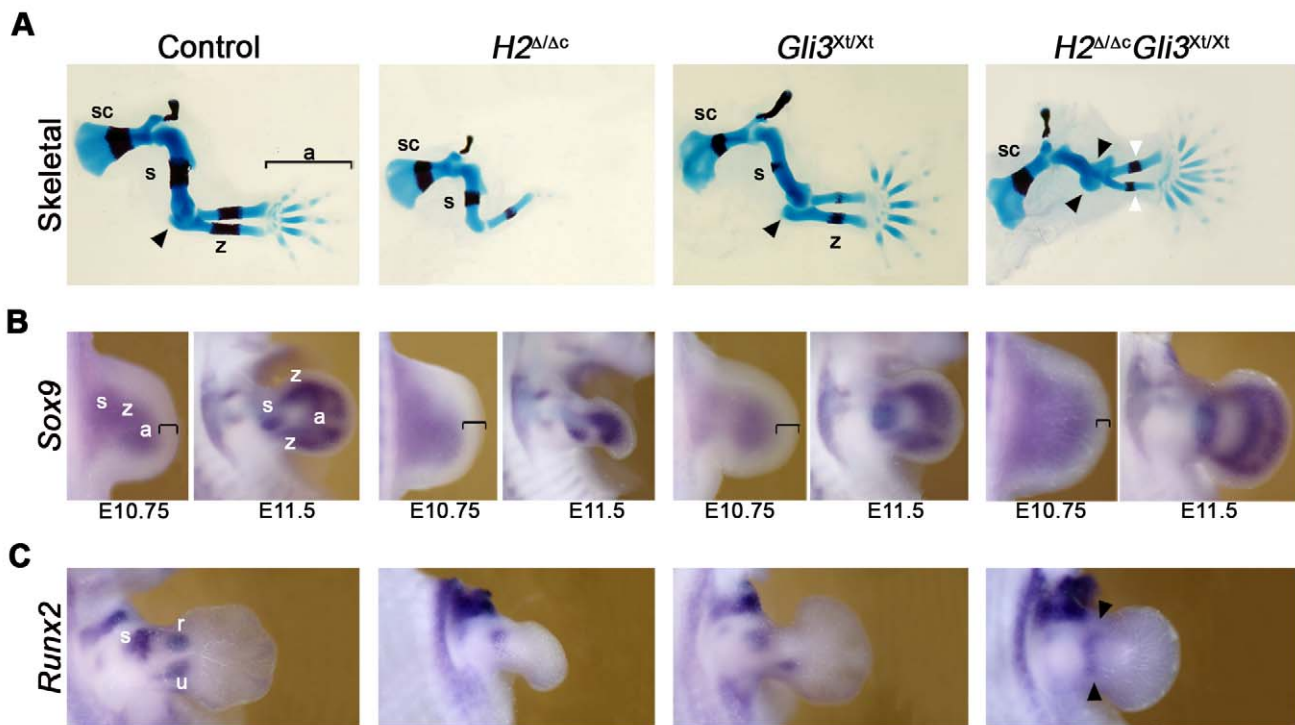


Figure 5. Forelimb buds lacking *Hand2* and *Gli3* lack AP polarity along the entire PD axis. (A) Skeletal preparations of $H2^{\Delta/\Delta}Gli3^{Xt/Xt}$, $H2^{\Delta/\Delta}$, and $Gli3^{Xt/Xt}$ single mutant and control ($H2^{\Delta/\Delta}$) forelimbs at E14.5. The black arrowheads point to the duplicated elbow-like structure while the white arrowheads point to the symmetrical zeugopodal skeletal elements in $H2^{\Delta/\Delta}Gli3^{Xt/Xt}$ limbs. Note the shortening of the stylopod in double mutant limbs. (B) Expression of *Sox9* in limb buds at E10.75 (38 somites) and E11.5. Black brackets indicate the non-expressing distal mesenchyme that is reduced in $H2^{\Delta/\Delta}Gli3^{Xt/Xt}$ limb buds. (C) *Runx2* expression in wild-type limb buds marks the presumptive stylopod (s) and zeugopodal domains (r/u) at E12.0. Note that establishment of anterior expression domain is delayed in $Gli3^{Xt/Xt}$ mutant limbs as it becomes visible by E12.5 (data not shown). Black arrowheads point to the apolar proximal expression of *Runx2* in $H2^{\Delta/\Delta}Gli3^{Xt/Xt}$ mutant limb buds. In wild-type limb buds, the presumptive expression domains for *Sox9* and *Runx2* are indicated as previously defined [42,63]. sc: scapula; s: stylopod; z: zeugopod; a: autopod; u: ulna; r: radius. All limb buds are oriented with the anterior to the top and the posterior to the bottom. doi:10.1371/journal.pgen.1000901.g005

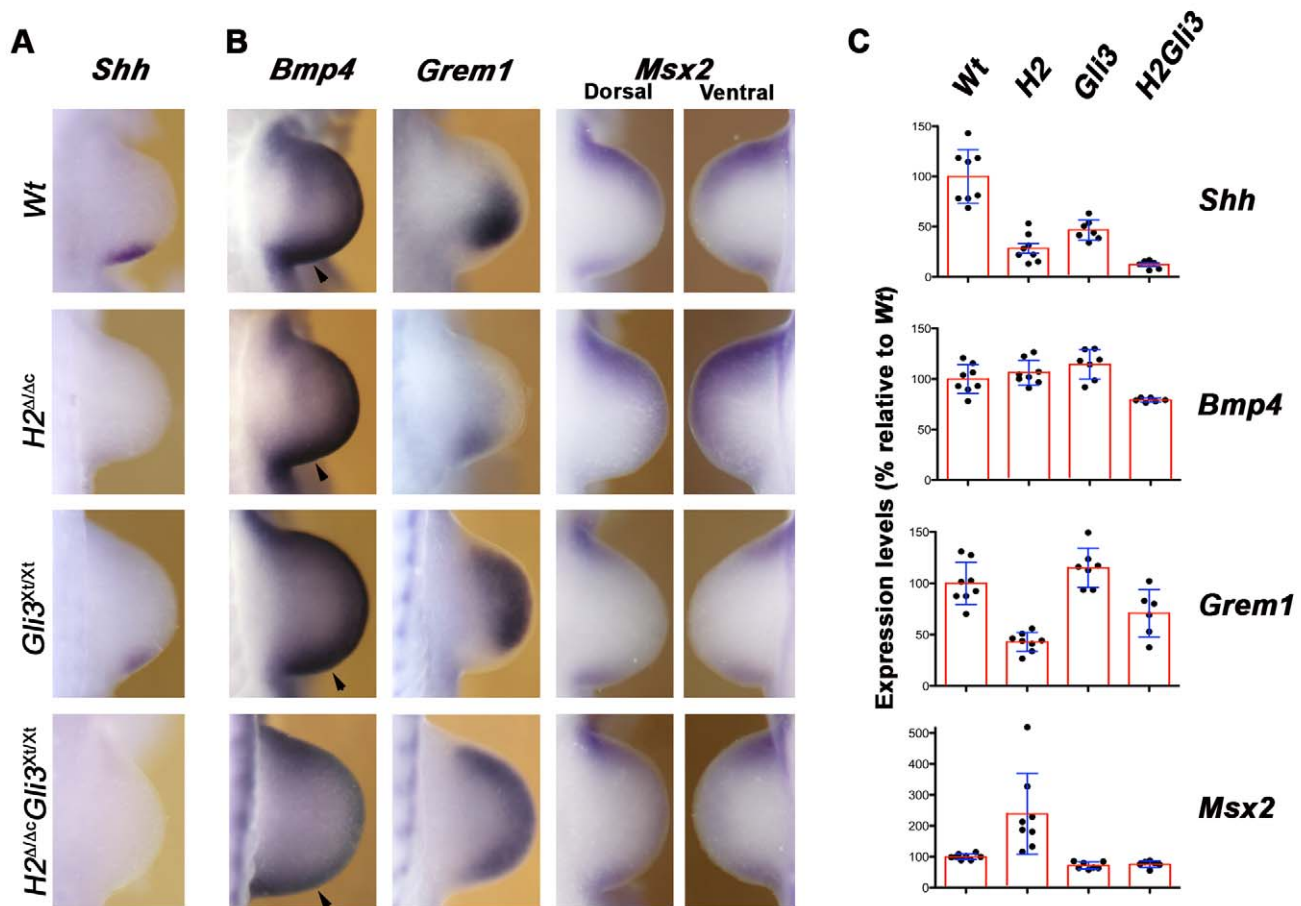


Figure 6. *Shh* expression and BMP pathway activity in $H2^{\Delta Ac}$ and $H2^{\Delta Ac} Gli3^{Xt/Xt}$ forelimb buds. (A) No *Shh* expression is detected in the posterior mesenchyme of $H2^{\Delta Ac}$ and $H2^{\Delta Ac} Gli3^{Xt/Xt}$ limb buds at E10.25 (32–33 somites). (B) *Bmp4*, *Grem1*, and *Msx2* expression at E10.5 (34–35 somites). Note that *Grem1* expression is activated, but not up-regulated and expanded distal-anterior in $H2^{\Delta Ac}$ limb buds. In contrast, the *Grem1* expression domain appears rather uniform in the majority of all $H2^{\Delta Ac} Gli3^{Xt/Xt}$ limb buds. (C) Q-PCR quantitation of *Shh*, *Bmp4*, *Grem1* and *Msx2* expression in single limb buds of mouse embryos of the indicated genotypes at \sim E10.5 (34–37 somites). Boxes show the average (\pm standard deviation), dots indicate levels in individual limb bud determined by triplicate analysis. The vertical axis indicates expression levels in percentages of wild-type levels (wild-type average set at 100%). Wt: wild-type (n=8 single limb buds analyzed); H2: $H2^{\Delta Ac}$ (n=8); Gli3: $Gli3^{Xt/Xt}$ (n=7); H2Gli3: $H2^{\Delta Ac} Gli3^{Xt/Xt}$ (n=6). All differences discussed in the text are statistically highly significant (p-values between $p < 0.001$ and $p < 0.05$ using Mann-Whitney tests). doi:10.1371/journal.pgen.1000901.g006

variability in *Shh* expression following *Prx1*-Cre mediated inactivation of *Hand2* (Figure 1C, Figure S3B, S3C, S3D, and Figure 6C) is no longer observed in $H2^{\Delta Ac} Gli3^{Xt/Xt}$ limb buds (Figure 6A and 6C), which agrees with the lack of significant variability in the resulting skeletal phenotypes (Figure 5A). This could be linked to the fact that posterior *Shh* expression is already reduced by \sim 50% in $Gli3^{Xt/Xt}$ limb buds (Figure 6A and 6C). The low *Shh* transcript levels detected in the most severely affected $H2^{\Delta Ac}$ and $H2^{\Delta Ac} Gli3^{Xt/Xt}$ limb buds (between 8% and 20%, Figure 6C) likely reflect basal expression not detected by *in situ* hybridization (Figure 1D, Figure 6A; see Discussion). *BMP4*-mediated up-regulation of its antagonist *Grem1* in the posterior mesenchyme is essential to initiate the self-regulatory signaling system that promotes distal limb bud development [43,44]. In $H2^{\Delta Ac}$ limb buds, *Bmp4* expression appears not significantly altered, while its expression is slightly reduced in $H2^{\Delta Ac} Gli3^{Xt/Xt}$ limb buds (panels *Bmp4* in Figure 6B and 6C). In particular, the posterior expression domain in double mutant limb buds appears smaller (arrowheads, panels *Bmp4* in Figure 6B), which results in rather symmetrical *Bmp4* expression along the AP limb bud axis.

Furthermore, *Grem1* expression is activated, but not up-regulated and distal-anteriorly expanded in *Hand2* deficient limb buds (panel *Grem1* in Figure 6B), similar to *Shh* deficient limb buds [44]. In double mutant limb buds, the *Grem1* expression domain appears symmetrical due to its anterior expansion. However, the rather variable *Grem1* transcript levels are overall reduced in $H2^{\Delta Ac} Gli3^{Xt/Xt}$ limb buds in comparison to wild-type and *Gli3* deficient limb buds (panels *Grem1* in Figure 6C). Finally, the expression of the direct BMP transcriptional target *Msx2* [43] is expanded in $H2^{\Delta Ac}$ limb buds, while its expression is significantly reduced in *Gli3* deficient and double mutant limb buds as a likely consequence of the alterations in *Grem1* (panels *Msx2* in Figure 6B and 6C). Taken together, these results corroborate the proposal that the initial phase of *Grem1* expression in the posterior mesenchyme depends on *BMP4* activity [43]. The rather symmetrical *Grem1* expression in $H2^{\Delta Ac} Gli3^{Xt/Xt}$ limb buds indicates that the second phase of SHH-dependent distal-anterior expansion of its expression in wild-type limb buds is a likely consequence of SHH-mediated inhibition of Gli3R activity [6].

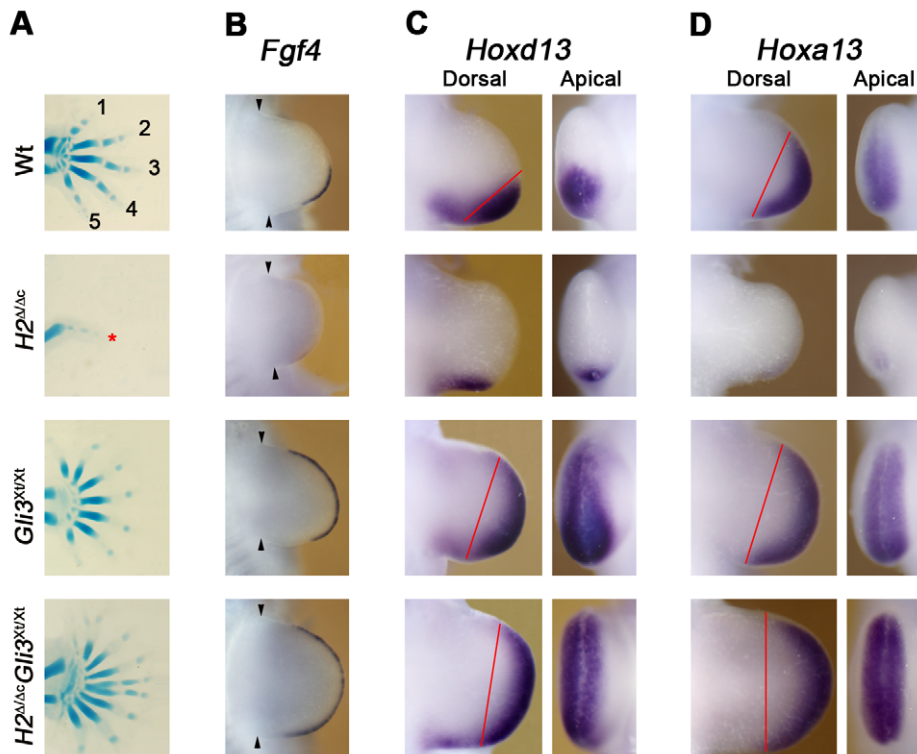


Figure 7. Apolar expression of *Fgf4*, *Hoxd13*, and *Hoxa13* in the autopod primordia of $H2^{\Delta\Delta c}Gli3^{Xt/Xt}$ forelimb buds. (A) Skeletal preparations of the autopod (E14.5) of $H2^{\Delta\Delta c}Gli3^{Xt/Xt}$, $H2^{\Delta\Delta c}$, and $Gli3^{Xt/Xt}$ single mutant and wild-type forelimbs. Digit identities are indicated by numbers 1 (thumb, anterior) to 5 (little finger, posterior). Black asterisks indicate digits with undetermined identities; red asterisk indicates the rudimentary digit formed in $H2^{\Delta\Delta c}$ forelimbs. (B) *Fgf4* expression in the AER of wild-type and mutant limb buds at E10.5 (36 somites). *Fgf4* is expressed at very low levels in the posterior of in $H2^{\Delta\Delta c}$ limb buds, but expands throughout the AER of $H2^{\Delta\Delta c}Gli3^{Xt/Xt}$ forelimb buds. Arrowheads indicate the anterior and posterior margins of limb buds. (C) *Hoxd13* expression at E10.75 (40 somites). The late *Hoxd13* expression domain in $H2^{\Delta\Delta c}Gli3^{Xt/Xt}$ limb buds appears symmetrical in contrast to e.g. *Gli3* deficient limb buds (expression borders are indicated by red lines). This is best seen by comparing apical views. (D) *Hoxa13* expression at E10.75 (41 somites). The *Hoxa13* expression domain appears also symmetrical in $H2^{\Delta\Delta c}Gli3^{Xt/Xt}$ limb buds, while some asymmetry is retained in *Gli3* deficient limb buds (red lines in dorsal views; best seen by comparing the apical views). doi:10.1371/journal.pgen.1000901.g007

Loss of AP asymmetry in the autopod of $H2^{\Delta\Delta c}Gli3^{Xt/Xt}$ limb buds

The lack of discernible AP identities in the autopod of $H2^{\Delta\Delta c}Gli3^{Xt/Xt}$ limb buds (Figure 7A) is confirmed by molecular analysis. In agreement with the rather symmetric distribution of *Bmp4* and *Grem1* in the distal limb bud mesenchyme (Figure 6B), *Fgf4* is expressed uniformly by the AER in double mutant limb buds (Figure 7B). The distal expression domains of the *Hoxd13* and *Hoxa13* genes mark the presumptive autopod territory and are required for specification and expansion of the digit progenitors [45,46]. Within the distal mesenchyme of $H2^{\Delta\Delta c}Gli3^{Xt/Xt}$ forelimb buds, the expression of *Hoxd13* is anteriorly expanded and appears apolar in comparison to wild-type and *Gli3* mutant limb buds (Figure 7C; best seen in the apical views). In addition, the AP asymmetry of the distal *Hoxa13* domain is also lost in double mutant limb buds (Figure 7D; best seen in the apical views). The expanded and apolar expression of these genes (Figure 7B–7D) together with the alterations in *Sox9*, *Runx2* (Figure 5B and 5C), *Bmp4* and *Grem1* (Figure 6B) reveal the striking loss of the asymmetrical expression of molecular and cellular markers of the AP axis along the entire PD axis in limb buds lacking both *Hand2* and *Gli3*.

Discussion

In this study, we uncover the key regulatory interactions involving *Hand2* that control establishment of posterior limb bud

identity upstream of SHH signaling, in particular the genetic interactions with *Gli3* that initiate AP axis polarity. Secondly, we reveal that *Hand2*, which like 5'*Hox* genes is essential for establishment of the *Shh* expressing limb bud organizer in the posterior-proximal mesenchyme, is part of the chromatin complexes bound to ZRS *cis*-regulatory region. The striking loss of posterior and gain of anterior molecular markers in *Hand2* deficient limb buds indicates that limb field symmetry may normally be broken by *Gli3*R-mediated posterior restriction of *Hand2* expression. This most likely parallels activation of 5'*HoxD* genes in the posterior mesenchyme [45]. In *Hand2* deficient limb buds, the SHH dependent establishment of the late 5'*HoxD* expression domains is disrupted, while in limb buds lacking both *Hand2* and *Gli3*, the late 5'*HoxD* expression domains expand uniformly throughout the distal autopod. Therefore, the down-regulation of 5'*HoxD* genes in *Hand2* deficient limb buds is a likely consequence of increased *Gli3*R activity due to lack of SHH signaling [23]. Furthermore, *Hand2* participates in transcriptional activation and/or upregulation of *Tbx2/3* and *Shh* expression in the posterior mesenchyme and is required for anterior restriction of *Gli3* and *Alx4* expression. In *Hand2* deficient limb buds, expression of the BMP antagonist *Grem1* is activated in the posterior mesenchyme under the influence of BMP signaling (ref. 43 and this study). This previous analysis and the observed anterior expansion of *Grem1* expression in $H2^{\Delta\Delta c}Gli3^{Xt/Xt}$ limb buds reveals that the transcriptional activation and positioning of

the *Grem1* expression domain is controlled by interaction of BMP4 (positive) with GLI3R (negative). In wild-type limb buds, the *Grem1* expression domain is always located distal-anterior to the *Shh* expressing cells and their descendants [47,48], while it remains proximal and low due to the lack of SHH signaling in *H2^{ΔΔ}* limb buds (this study). Taken together, these results provide further insights into the molecular mechanism controlling spatial and temporal aspects of BMP4-mediated initiation and SHH-dependent progression of *Grem1* expression, which acts as an essential node in the self-regulatory signaling system that controls limb development [1].

Hand2, the ZRS, and establishment of the *Shh* expression domain in the posterior limb bud mesenchyme

Our biochemical analysis of chromatin isolated from wild-type mouse limb buds reveals that Hand2-containing chromatin complexes are bound to the ZRS, which is the far upstream *cis*-regulatory region required for *Shh* expression in limb buds [28,29]. In particular, ZRS sequences are specifically and significantly enriched in Hand2 containing chromatin complexes in contrast to flanking regions. Furthermore, Hand2 is part of Hoxd13 protein complexes in limb buds and in transfected cells, the two proteins transactivate the expression of a luciferase reporter gene in a ZRS-dependent manner. Albeit the fact that such transactivation studies are of somewhat artificial nature, the conclusions reached by this analysis completely agree with the results of our genetic analysis of *Hand2* functions during mouse limb bud development. Early and complete genetic inactivation of Hand2 in limb buds disrupts establishment of the *Shh* expression domain in the posterior limb bud, while either incomplete or temporally delayed inactivation does no longer disrupt initiation of *Shh* expression (this study). This reveals the early essential requirement of Hand2 for establishment of the posterior *Shh* expression domain, while subsequently Hand2 appears to contribute to transcriptional up-regulation of *Shh* expression. This may happen as part of an auto-regulatory loop because SHH signaling in turn up-regulates *Hand2* expression most likely via repressing production of the Gli3R isoform [9,11,49]. The low levels of *Shh* expression detected by Q-PCR even in the most affected *H2^{ΔΔc}* and *H2^{ΔΔc} Gli3^{Xt/Xt}* limb buds, but not in *Shh* deficient limb buds (JDB and RZ, unpublished) are indicative of basal transcription of the *Shh* locus in the absence of *Hand2*, which is not detectable by *in situ* hybridization (this study). This basal expression may depend on Hox transcription factors [24,26] or other regulators of *Shh* expression in limb buds (see below). However, our study shows that Hand2 is essential to establish and upregulate *Shh* expression in the posterior mesenchyme, which defines the SHH signaling limb bud organizer [1]. This Hand2-mediated transactivation of *Shh* expression is a likely consequence of its direct interaction with the ZRS *cis*-regulatory region and is possibly enhanced by formation of transcriptional complexes with Hoxd13 protein in limb buds.

Genetic and experimental manipulation of paired appendage buds in mouse, chicken and zebrafish embryos have begun to reveal the factors required in addition to *Hand2* and *5' HoxD* genes for *Shh* activation. In particular, AER-FGF and retinoic acid signaling have also been implicated in the activation of *Shh* expression [21,50]. Deletion of both the *HoxA* and *HoxD* clusters in mouse embryos disrupts *Shh* activation and causes early arrest of limb bud development such that the limb skeleton is truncated at the level of the stylopod [24,26]. But in contrast to *Hand2*, loss-of-function mutations in these genes alone or in combination do not phenocopy the *Shh* loss-of-function limb skeletal phenotypes [51,52]. The Hand2 protein interacts with Hoxd13 and is part of the chromatin complexes bound to the ZRS in limb buds (this

study). However, other transacting factors will likely contribute to ZRS dependent activation of *Shh* transcription. In fact, the overlap of the *Hand2* and *Hoxd13* expression domains in the posterior limb bud mesenchyme is much bigger than the initial *Shh* expression domain. During limb bud initiation stages, the *Hand2* and *Gli3* expression domains overlap significantly, but then become rapidly mutually exclusive [11]. Therefore, these early dynamic changes in the expression domains of the *Hand2*, *Gli3* and *Hoxd13* transcriptional regulators may well alter their interactions and spatially restrict the formation of transcription initiating/enhancing Hand2-Hoxd13 chromatin complexes at the ZRS to the posterior limb bud (this study). These direct interactions would restrict the up-regulation of *Shh* expression to the posterior limb bud mesenchyme, thereby establishing the SHH signaling limb bud organizer. A recent study shows that the distant ZRS is in close proximity to the *Shh* transcription unit in both the anterior and posterior limb bud mesenchyme, but only loops out of its chromosomal territory in the posterior mesenchyme [31]. Interestingly, *Shh* is apparently transcribed by only a fraction of all ZPA cells at one particular time point, which indicates that the chromosomal conformation dynamics control *Shh* expression at the cellular level [31].

It is known that Hand2 binds DNA primarily as a heterodimer with E12 and/or the bHLH transcription factor Twist1 [16,19]. Interestingly, *Twist1* is also required during early limb bud development [18] and point mutations in the human *Twist1* gene alter its dimerization with Hand2, which causes congenital limb malformations [19]. Therefore, these additional factors may also participate in regulation of *Shh* expression. The expression of *Hand2* and *5' HoxD* genes is activated in parallel, but then they converge functionally on the ZRS to establish the *Shh* expression domain in the posterior limb bud (this study and ref. 24). Furthermore, the establishment of the posterior *Tbx2* and *Tbx3* expression domains is disrupted in *Hand2* deficient limb buds. The *cis*-regulatory elements controlling their expression are currently unknown, but it has been shown that *Tbx2* expression requires the overlying non-AER ectoderm [53]. Additional experimental and genetic evidence indicates that *Tbx2* and *Tbx3* act likely upstream of *Shh* to restrict its transcriptional activation to the posterior limb bud margin [53,54]. In particular, ectopic expression of *Tbx3* in early chicken limb buds induces an anterior shift of the entire limb bud together with transient anterior expansion of *Hand2* expression [55]. These studies indicate that *Tbx* genes are part of the molecular circuits that position the limb bud, specify posterior identity and restrict activation of *Shh* to its posterior margin.

Breaking limb bud symmetry

The genetic inactivation of the pre-patterning mechanism in *H2^{ΔΔc} Gli3^{Xt/Xt}* limb buds disrupts establishment of AP asymmetry and self-regulatory limb bud signaling [43], while PD axis outgrowth and formation of all three major limb skeletal segments are the likely consequence of uniform AER-FGF signaling [2]. This results in a shortened and symmetric stylopod, zeugopod and a polydactylous autopod with highly dysmorphic digits. Similar to *H2^{ΔΔc} Gli3^{Xt/Xt}* limb buds, limbs lacking *5' HoxD* genes and *Gli3* are also severely polydactylous but retain some polarity [56,57]. Therefore, the loss of AP polarity along the entire proximo-distal axis is more severe than the phenotypes observed in limb buds lacking *Gli3* alone or in combination with genes such as *Shh*, *Alx4* or *5' HoxD* genes [9,56–58]. Over-expression of *Hand2* in the entire limb bud mesenchyme results in a duplication of the anterior zeugopod (ulna) and posterior autopod (digits) [12], which indicates that disturbing the balance between Hand2 and Gli3

either by gene inactivation or over-expression alters AP polarity. Therefore, the balance of the opposing activities of Hand2 and Gli3R in concert with 5'HoxD genes may control specification of the AP limb axis independent and up-stream of SHH signaling. In mouse limb buds lacking the *Plzf* zinc finger protein, 5'*HoxD* genes are uniformly expressed from early stages onwards and AP polarity is partially lost in combination hindlimb digit polydactyly [59].

It remains unclear why the digit polydactyly in $H2^{\Delta\Delta c} Gli3^{Xt/Xt}$ forelimbs is more severe than the one of $Gli3^{Xt/Xt}$ (and $Shh^{\Delta\Delta} Gli3^{Xt/Xt}$ [9]) forelimbs. However, in $H2^{\Delta\Delta c} Gli3^{Xt/Xt}$ forelimb buds, the distal expression domains of *Hoxa13* and *Hoxd13*, which delineate the autopod territory and function in digit development (see [refs. 24, 26] for further detail) are anteriorly expanded in comparison to *Gli3* deficient limb buds. Such anterior expansion may point to an enlarged pool of autopod/digit progenitors, which could underlie the more severe digit polydactyly. As discussed before, this expansion of the *Hoxa/d13* expression domains and the presumptive autopod territory are a likely consequence of the early loss of AP polarity along the entire PD axis in double mutant forelimb buds in contrast to $Gli3^{Xt/Xt}$ mutants. In particular, the $H2^{\Delta\Delta c} Gli3^{Xt/Xt}$ forelimb skeletons bear some resemblance to the primitive paired appendages of Devonian fish and the polydactylous limbs of early tetrapods [60]. We shows that these rather "primitive" limb structures develop in the absence of pre-patterning (Hand2, Gli3) and the self-regulatory signaling system that interlinks the SHH, BMP and FGF signaling pathways, which are both key to normal limb skeletal development [1]. During tetrapod evolution, the symmetry of primitive polydactylous autopods from the Devonian period [61] was likely broken by beginning to set-up the regulatory interactions described in this study as they initiate posterior polarity up-stream or in parallel to their requirement for establishment of the SHH signaling limb bud organizer. The establishment of these transcriptional regulatory network acting upstream of SHH signaling might have enabled the development of the more refined and better functional pentadactylous limbs of modern tetrapods.

Materials and Methods

All animal experiments were performed in accordance with Swiss law and have been approved by the regional veterinary and ethics authorities.

Mice and embryos

The generation of *Hand2* conditional mutant mice is shown in Figure S1. *Hand2* mouse strains were kept in a mixed 129SvJ/C57BL6 genetic background. For details of the generation and analysis of *Hand2* mice and embryos see Text S1.

Immunoprecipitation (IP) and co-IP experiments

For IP, fore- and hind-limb buds from E11.0 embryos were collected in PBS and lysed in lysis buffer (Tris-HCl 10 mM pH 8.0; EDTA 1 mM; NaCl 140 mM; Triton 1%; SDS 0.1%; NaDeoxycholate 0.1%). Protein lysates (about 300 mg) were incubated overnight at 4°C with the anti-Hand2 (M-19, Santa Cruz; 1 mg) and protein G beads were added the next morning for about 5 hours at 4°C. After several washes in lysis buffer, beads were resuspended in Laemmli loading buffer and SDS-PAGE was performed under non-reducing conditions. Goat IgG antibodies were used as control. For Co-IP of endogenous embryonic proteins, 50 limb buds at E10.5 were dissected in PBS and processed as described [33]. The *Hoxd13* or control rabbit IgG antibodies used for co-IPs were covalently cross-linked to G

protein beads and bound proteins were detected with Hand2 antibodies (AF3876, R&D System).

Chromatin Immunoprecipitation (ChIP)

ChIP was performed using wild-type fore- and hindlimb buds at E11.0 (38–42 somites). For each experiment, 85 limb buds were dissected, pooled and the freshly cross-linked chromatin divided among the starting samples. The average size of the DNA fragments in the cross-linked and sonicated chromatin was ~500–2000 bp. Samples were processed as described [62] with the following modifications: protein G magnetic beads (Dynabeads, Invitrogen) were pre-absorbed with goat IgG (1–2 mg for 30 ml of beads for each sample) for minimally 1 hour at 4°C. After washing them with BSA-PBS (5 mg/ml), the beads were added to the chromatin extracts and gently rocked for 1 hour at 4°C. Afterwards, beads were spun down and the chromatin in the supernatant transferred to a new tube and incubated overnight with Hand2 antibodies (M-19, Santa Cruz; 1 mg) or goat IgG antibodies as control (1 mg). The following day, 25 ml of beads were added and the DNA-immunocomplexes were precipitated for 4 hours at 4°C. ChIP-enriched DNA samples were amplified by Q-PCR and conventional PCR. To compute the enrichment for a particular amplicon, its values were compared with the ones of a completely unrelated amplicon within the mouse *β-actin* gene that provides an additional negative control. The *β-actin* gene is located ~114 Mb downstream of the ZRS on mouse chromosome 5. The fold of enrichment was then calculated as the fold of increase in the specific signal in relation to the values obtained when using non-specific goat IgGs for ChIP (values set arbitrarily at 1). All oligos used are listed in Table S1. Three ChIP experiments were performed using completely independent and fresh (i.e. non-frozen) chromatin preparations. The values obtained were analyzed and the graphs shown in Figure 4D (means ± standard error) were drawn using the Prism Graphpad Software (La Jolla, USA). The statistical significance of all results was assessed using the Mann-Whitney test as part of the Prism software package.

Luciferase assays

Mouse NIH3T3 fibroblasts were plated on 24-well plates and transfected using Lipofectamine LTX (Invitrogen) including a total of 500 ng of DNA. Reporter constructs were co-transfected with 100 ng of *Hand2* and/or *Hoxd13* and/or *Gli3* expression constructs in combination with a *Renilla* luciferase vector. A detailed description of the generation of the expression constructs is available in Text S1. Cells were collected 28–30 hours post-transfection and luciferase reporter assays were performed using the Dual Luciferase Kit (Promega). Each assay was repeated at least 10 times. It is important to note that NIH3T3 cells do not express the endogenous *Hand2*, *Hoxd13* and *Gli3* genes (data not shown). For the co-immuno-precipitation assays in cells see Text S1.

Supporting Information

Figure S1 Generation and validation of the *Hand2* conditional allele. (A) Scheme depicting the *Hand2* gene targeting strategy. A targeting vector was constructed in order to flank both *Hand2* coding exons with *loxP* sites (blue triangles). An *EcoRV* (*ERV*) restriction site was inserted to enable screening of ES-clones by Southern blot analysis. The *PGK*-Neo-pA cassette was inserted into the construct 3' to the *loxP* site for positive selection. This selection cassette is flanked with two *FRT* sites (green triangles) to enable excision by the flipase (FLPe) recombinase. For genomic Southern

blot analysis, the 5' probe (violet box) and the 3' probe (orange box) were used. The PCR oligos and sizes of amplified bands are indicated. Arrows indicate the direction of transcription. To induce FRT and *loxP* mediated recombination at the *Hand2* locus, mice carrying the *Hand2* floxed-neo allele (*H2^{flneo}*) were intercrossed with FLPe and with *CMV-Cre* transgenic mice. (B) Southern blot analysis showing wild-type, the correctly recombined 4D7 ES-cell clone and DNA biopsies from mice heterozygous for the *H2^{flneo}* and the *Hand2* floxed (*H2^f*) allele. The 5' probe detects a 15 kb *ERV* fragment for the wild-type (Wt) locus, while an 8 kb *ERV* fragment is detected when the locus is correctly recombined. The 3' probe detects a 7.3 kb wild-type *PacI* fragment and a 9.3 kb fragment in the correctly targeted allele. Following excision of the *PGK-Neo-pA* cassette, the 9.3 kb is reduced to a 7.5 kb fragment in the *H2^f* allele. (C) PCR genotyping. (D) Morphology of mouse embryos at embryonic day E9.5–9.75 (25–27 somites). *Hand2* deficient embryos are growth retarded, the aortic and pericardial sac are dilated and branchial arches are malformed [13]. The heart (h), first (I) and second branchial arches (II) are indicated. Asterisks indicate the outgrowing forelimb buds. (E) LysoTracker Red (LysoT) analysis reveals the massive and generalized cell death in *Hand2* deficient embryos and limb buds at E9.5 (25 somites). a: anterior; d: dorsal; p: posterior; v: ventral.

Found at: doi:10.1371/journal.pgen.1000901.s001 (6.79 MB TIF)

Figure S2 Clearance of *Hand2* transcripts from mutant forelimb buds and specificity of α -Hand2 antibodies. (A) Q-PCR analysis to determine *Hand2* transcript levels in wild-type, *Hand2* floxed (*H2^f*), *Hand2* heterozygous and *Hand2* deficient limb buds at E10.25–10.5 (33–35 somites; n = 6–8). Note that no *Hand2* transcripts are detected in *Hand2* deficient limb buds. Bars: \pm standard deviation. asterisk: P = 0.0009. (B) Immunofluorescence using α -Hand2 antibodies (M-19, Santa Cruz) reveals the specific nuclear localization of Hand2 proteins in posterior (Wt-p) but not anterior (Wt-a) limb buds mesenchymal cells. No specific fluorescence is detected in mesenchymal cells isolated from *Hand2* deficient limb buds. (C) Hand2 proteins are cleared from *Hand2* deficient limb buds by embryonic day E10.5. Protein extracts were normalized for their vinculin content. (D) Immunoprecipitation (IPP) of Hand2 proteins from E11.0 limb buds. Hand2 proteins are detected by Western blotting. Control: α -IgG. Asterisks indicate the cross-reactivity with the light chains of the IgGs (control and α -Hand2) used for IPP.

Found at: doi:10.1371/journal.pgen.1000901.s002 (2.42 MB TIF)

Figure S3 Incomplete/delayed inactivation of *Hand2* in forelimb buds results in a hypomorphic phenotype. (A) Skeletal preparations of control (*Prx1-Cre* heterozygous) and *Hand2* deficient forelimbs at E14.5. Due to slight variability in *Prx1-Cre* mediated inactivation of the conditional *Hand2* allele in forelimb buds, three classes of skeletal phenotypes are observed. The most hypomorphic phenotype (Weak) results in formation of two misplaced zeugopodal bones, three anterior digits and a hypoplastic digit that resembles digit 4 (indicated by an asterisk). The arrowhead points to the twisted bones of the zeugopod. The less hypomorphic phenotype (Intermediate) results in formation of one zeugopodal bone and two digits. The null phenotype (Strong) is identical to the skeletal phenotypes observed in *Shh* deficient limb buds (Figure 1A). Asterisks indicate digits with unclear identities. (B) Analysis of *Hand2* expression reveals the variable nature of *Prx1-Cre* mediated inactivation of *Hand2* at E9.75 (28 somites). (C) This variability is also apparent when levels of SHH signal transduction are monitored by *Gli1* expression at E9.75 (27 somites). Complete absence of *Hand2* (B) and *Gli1* transcripts (C) was observed in 50%

of all *Prx1-Cre1*, *Hand2* deficient limb buds (n = 4/8). The others display varying degrees of *Hand2* and *Gli1* expression. All limb buds are oriented with the anterior to the top and the posterior to the bottom. (D) Table summarizing the frequencies of the three classes of limb skeletal phenotypes observed in *Hand2* mutant forelimbs. This variability is in agreement with the fact, that developmentally slightly later *Hand2* inactivation in hindlimb buds results in almost normal *Shh* expression and limb skeletal development (Figure 2). Taken together, these results indicate that *Hand2* needs to be inactivated very early and rapidly during the onset of limb bud development to disrupt establishment of the posterior *Shh* expression domain.

Found at: doi:10.1371/journal.pgen.1000901.s003 (3.68 MB TIF)

Figure S4 Activation of 5' *HoxD* genes and posterior expansion of *Gli3* expression in *Hand2* deficient limb buds. *Hoxd11* expression at E9.75 (27 somites) and E10.75 (36 somites). Expression of *Hoxd11* is initiated in limb buds lacking *Hand2* (arrowheads), but its up-regulation is disrupted. (B) *Hoxd13* expression is initiated, but rapidly down-regulated in *Hand2* deficient limb buds (arrowheads E10.5, 33 somites). (C) *Gli3* expression is expanded posteriorly in *Hand2* deficient limb buds at E10.0 (32 somites; compare white to black arrowhead). In *Shh* deficient limb buds, *Gli3* is not expanded to the posterior margin (compare white to open arrowheads). All limb buds are oriented with the anterior to the top and the posterior to the bottom. (D) Inactivation of *Hand2* alters *Gli3* protein processing. Protein extracts prepared from limb buds of the indicated genotypes at E10.5 (35 somites) were analyzed by immunoblotting using α -*Gli3* antibodies. The full-length *Gli3* protein is about 190 kD, while the processed *Gli3R* isoform is about 83 kD. Note that *Gli3R* form is more abundant in *Hand2* and *Shh* deficient than in wild-type limb buds. Samples are normalized for their vinculin contents. The asterisk points to an unrelated cross-reacting protein.

Found at: doi:10.1371/journal.pgen.1000901.s004 (5.95 MB TIF)

Figure S5 The genomic landscape encompassing the mouse ZRS. Scheme depicting part of mouse chromosome 5 (Ensembl: *Mus musculus* genomic region from position 29621310 to 29662806) analyzed in the ChIP experiments by Q-PCR. The *Lmbr1* locus encodes the mouse ZRS (1.67 kb) within intron 4, which is about 800 kb away from the *Shh* locus. The 6 *Ebox* elements (1 to 6) located in the ZRS are indicated. The framed orange and blue boxes indicate the 20 kb downstream and upstream flanking regions. These two regions are shown in the enlargements and potential *Ebox* elements are indicated. Coding exons are represented by filled boxes. Amplicon a is located about 2 kb downstream and amplicon e about 6 kb upstream of the ZRS (the primers used for Q-PCR amplification are indicated by green arrows).

Found at: doi:10.1371/journal.pgen.1000901.s005 (0.32 MB PDF)

Figure S6 Evidence that Hand2 interacts directly with the Hoxd13 but not Gli3R protein. Co-immunoprecipitation reveals the direct interaction of Hand2 with Hoxd13 in HEK293T cells (Hand2: Flag-epitope tagged; Gli3R: Myc-epitope tagged). In contrast, Gli3R is unable to directly interact with Hand2, but binds to Hoxd13 [12]. Protein extracts were immunoprecipitated (IP) using the following antibodies: α -Flag for Hand2, α -Hoxd13 for Hoxd13, α -Myc for Gli3R and immunoblotted (IB) using the appropriate antibodies.

Found at: doi:10.1371/journal.pgen.1000901.s006 (2.52 MB TIF)

Figure S7 Morphological defects in limb buds lacking *Hand2* and *Gli3*. (A) The forelimb morphology of double mutant mouse embryos at E14.5. Note the stunted forelimbs and the extreme

pre- and post-axial polydactyly in comparison to *Gli3*^{Xt/Xt} limb buds. White brackets indicate forelimb length. Asterisks indicate digits with undetermined identities. (B) The massive apoptosis of mesenchymal cells in *Hand2* deficient limb buds is suppressed in limb buds lacking both *Hand2* and *Gli3*. Apoptotic cells were detected by TUNEL fluorescence on limb bud sections at E10.25 (33 somites). Sections are oriented with the anterior to the top and posterior to the bottom.

Found at: doi:10.1371/journal.pgen.1000901.s007 (3.99 MB TIF)

Table S1 Oligos used for the study. All primers used for genotyping of mice and embryos, Q-PCR analysis of *Hand2* transcripts, Q-PCR analysis of the ChIP experiments are listed. Conditions for use are available upon request.

Found at: doi:10.1371/journal.pgen.1000901.s008 (0.04 MB DOC)

Text S1 Supporting materials and methods.

Found at: doi:10.1371/journal.pgen.1000901.s009 (0.08 MB DOC)

References

- Zeller R, Lopez-Rios J, Zuniga A (2009) Vertebrate limb bud development: moving towards integrative analysis of organogenesis. *Nat Rev Genet* 10: 845–858.
- Mariani FV, Ahn CP, Martin GR (2008) Genetic evidence that FGFs have an instructive role in limb proximal-distal patterning. *Nature* 453: 401–405.
- Towers M, Mahood R, Yin Y, Tickle C (2008) Integration of growth and specification in chick wing digit-patterning. *Nature* 452: 882–886.
- Zhu J, Nakamura E, Nguyen MT, Bao X, Akiyama H, et al. (2008) Uncoupling Sonic hedgehog control of pattern and expansion of the developing limb bud. *Dev Cell* 14: 624–632.
- Ahn S, Joyner AL (2004) Dynamic changes in the response of cells to positive hedgehog signaling during mouse limb patterning. *Cell* 118: 505–516.
- Wang B, Fallon JF, Beachy PA (2000) Hedgehog-Regulated Processing of Gli3 Produces an Anterior/Posterior Repressor Gradient in the Developing Vertebrate Limb. *Cell* 100: 423–434.
- Harfe BD, Scherz PJ, Nissim S, Tian H, McMahon AP, et al. (2004) Evidence for an expansion-based temporal Shh gradient in specifying vertebrate digit identities. *Cell* 118: 517–528.
- Hui C, Joyner A (1993) A mouse model of greig cephalopolysyndactyly syndrome: the extra-toes mutation contains an intragenic deletion of the Gli3 gene. *Nat-Genet* 3: 241–246.
- te Welscher P, Zuniga A, Kuijper S, Drenth T, Goedemans HJ, et al. (2002) Progression of Vertebrate Limb Development through SHH-Mediated Counteraction of GLI3. *Science* 298: 827–830.
- Litingtung Y, Dahn RD, Li Y, Fallon JF, Chiang C (2002) Shh and Gli3 are dispensable for limb skeleton formation but regulate digit number and identity. *Nature* 418: 979–983.
- te Welscher P, Fernandez-Teran M, Ros MA, Zeller R (2002) Mutual genetic antagonism involving GLI3 and dHAND prepatterns the vertebrate limb bud mesenchyme prior to SHH signaling. *Genes Dev* 16: 421–426.
- Charité J, McFadden DG, Olson EN (2000) The bHLH transcription factor dHAND controls *Sonic hedgehog* expression and establishment of the zone of polarizing activity during limb development. *Development* 127: 2461–2470.
- Yelon D, Baruch T, Halpern ME, Ruvinsky I, Ho RK, et al. (2000) The bHLH transcription factor Hand2 plays parallel roles in zebrafish heart and pectoral fin development. *Development* 127: 2573–2582.
- McFadden DG, McAnally J, Richardson JA, Charité J, Olson EN (2002) Misexpression of dHAND induces ectopic digits in the developing limb bud in the absence of direct DNA binding. *Development* 129: 3077–3088.
- Liu N, Barbosa AC, Chapman SL, Bezprozvannaya S, Qi X, et al. (2009) DNA binding-dependent and -independent functions of the Hand2 transcription factor during mouse embryogenesis. *Development* 136: 933–942.
- Dai YS, Cserjesi P (2002) The basic helix-loop-helix factor, HAND2, functions as a transcriptional activator by binding to E-boxes as a heterodimer. *J Biol Chem* 277: 12604–12612.
- Markus M, Benezra R (1999) Two isoforms of protein disulfide isomerase alter the dimerization status of E2A proteins by a redox mechanism. *J Biol Chem* 274: 1040–1049.
- Zuniga A, Quillet R, Perrin-Schmidt F, Zeller R (2002) Mouse Twist is required for FGF-mediated epithelial-mesenchymal signaling and cell survival during limb morphogenesis. *Mech Dev* 114: 51–59.
- Firulli BA, Krawchuk D, Centzone VE, Vargesson N, Virshup DM, et al. (2005) Altered Twist1 and Hand2 dimerization is associated with Saethre-Chotzen syndrome and limb abnormalities. *Nat Genet* 37: 373–381.
- Tickle C, Alberts BM, Wolpert L, Lee J (1982) Local application of retinoic acid in the limb bud mimics the action of the polarizing region. *Nature* 296: 564–565.
- Niederreither K, Vermot J, Schuhbaur B, Chambon P, Dolle P (2002) Embryonic retinoic acid synthesis is required for forelimb growth and anteroposterior patterning in the mouse. *Development* 129: 3563–3574.
- Buscher D, Bosse B, Heymer J, Ruther U (1997) Evidence for genetic control of Sonic hedgehog by Gli3 in mouse limb development. *Mech Dev* 62: 175–182.
- Zuniga A, Zeller R (1999) Gli3 (Xt) and formin (ld) participate in the positioning of the polarising region and control of posterior limb-bud identity. *Development* 126: 13–21.
- Tarchini B, Duboule D, Kmita M (2006) Regulatory constraints in the evolution of the tetrapod limb anterior-posterior polarity. *Nature* 443: 985–988.
- Knezevic V, De Santo R, Schughart K, Huffstadt U, Chiang C, et al. (1997) *Hoxd-12* differentially affects preaxial and postaxial chondrogenic branches in the limb and regulates *Sonic hedgehog* in a positive feedback loop. *Development* 124: 4523–4536.
- Kmita M, Tarchini B, Zakany J, Logan M, Tabin CJ, et al. (2005) Early developmental arrest of mammalian limbs lacking HoxA/HoxD gene function. *Nature* 435: 1113–1116.
- Capellini TD, Di Giacomo G, Salsi V, Brendolan A, Ferretti E, et al. (2006) Pbx1/Pbx2 requirement for distal limb patterning is mediated by the hierarchical control of Hox gene spatial distribution and Shh expression. *Development* 133: 2263–2273.
- Lettice LA, Heaney SJ, Purdie LA, Li L, de Beer P, et al. (2003) A long-range Shh enhancer regulates expression in the developing limb and fin and is associated with preaxial polydactyly. *Hum Mol Genet* 12: 1725–1735.
- Sagai T, Hosoya M, Mizushima Y, Tamura M, Shiroishi T (2005) Elimination of a long-range cis-regulatory module causes complete loss of limb-specific Shh expression and truncation of the mouse limb. *Development* 132: 797–803.
- Sagai T, Masuya H, Tamura M, Shimizu K, Yada Y, et al. (2004) Phylogenetic conservation of a limb-specific, cis-acting regulator of Sonic hedgehog (Shh). *Mamm Genome* 15: 23–34.
- Amano T, Sagai T, Tanabe H, Mizushima Y, Nakazawa H, et al. (2009) Chromosomal dynamics at the Shh locus: limb bud-specific differential regulation of competence and active transcription. *Dev Cell* 16: 47–57.
- Hill RE (2007) How to make a zone of polarizing activity: insights into limb development via the abnormality preaxial polydactyly. *Dev Growth Differ* 49: 439–448.
- Chen Y, Knezevic V, Ervin V, Hutson R, Ward Y, et al. (2004) Direct interaction with Hoxd proteins reverses Gli3-repressor function to promote digit formation downstream of Shh. *Development* 131: 2339–2347.
- Srivastava D, Thomas T, Lin Q, Kirby ML, Brown D, et al. (1997) Regulation of cardiac mesodermal and neural crest development by the bHLH transcription factor dHAND. *Nature Genetics* 16: 154–160.
- Logan M, Martin JF, Nagy A, Lobe C, Olson EN, et al. (2002) Expression of Cre recombinase in the developing mouse limb bud driven by a Pbx1 enhancer. *Genesis* 33: 77–80.
- Hasson P, Del Buono J, Logan MP (2007) Tbx5 is dispensable for forelimb outgrowth. *Development* 134: 85–92.
- King M, Arnold JS, Shanske A, Morrow BE (2006) T-genes and limb bud development. *Am J Med Genet A* 140: 1407–1413.
- Taipale J, Chen JK, Cooper MK, Wang B, Mann RK, et al. (2000) Effects of oncogenic mutations in *Smoothed* and *Patched* can be reversed by cyclopamine. *Nature* 406: 1005–1009.
- Vokes SA, Ji H, Wong WH, McMahon AP (2008) A genome-scale analysis of the cis-regulatory circuitry underlying sonic hedgehog-mediated patterning of the mammalian limb. *Genes Dev* 22: 2651–2663.

Acknowledgments

The *Gli3R*, *Hoxd13* and other protein expression constructs were kindly provided by J. Briscoe, J. Innis, and M. Williams. We are thankful to A. Zuniga and J.A. Cobb for providing the *Cry-μ* and *Runx2 in situ* probes. Chimeric mice were generated by D. Klewe-Nebenius, and C. Saegesser is acknowledged for animal care. The authors wish to thank M. Kmita, A. Zuniga, and all group members for helpful comments on the manuscript.

Author Contributions

Conceived and designed the experiments: AG DR MO RZ. Performed the experiments: AG DR MO XB JDB MT. Analyzed the data: AG DR MO XB JDB RP SM. Contributed reagents/materials/analysis tools: JDB RP SM. Wrote the paper: AG RZ. Involved in revision: DR MO JDB. Comments on manuscript: DR MO JDB MT RP SM. Involved in the design and execution of ChIP experiments: MT RP. Designed co-immunoprecipitation experiments from wild-type limb buds: SM.

40. Orlando V, Strutt H, Paro R (1997) Analysis of chromatin structure by in vivo formaldehyde cross-linking. *Methods* 11: 205–214.
41. Kawakami Y, Rodriguez-Leon J, Belmonte JC (2006) The role of TGFbetas and Sox9 during limb chondrogenesis. *Curr Opin Cell Biol* 18: 723–729.
42. Cobb J, Dierich A, Huss-Garcia Y, Duboule D (2006) A mouse model for human short-stature syndromes identifies Shox2 as an upstream regulator of Runx2 during long-bone development. *Proc Natl Acad Sci U S A* 103: 4511–4515.
43. Benazet JD, Bischofberger M, Tiecke E, Goncalves A, Martin JF, et al. (2009) A self-regulatory system of interlinked signaling feedback loops controls mouse limb patterning. *Science* 323: 1050–1053.
44. Zuniga A, Haramis AP, McMahon AP, Zeller R (1999) Signal relay by BMP antagonism controls the SHH/FGF4 feedback loop in vertebrate limb buds. *Nature* 401: 598–602.
45. Tarchini B, Duboule D (2006) Control of Hoxd genes' collinearity during early limb development. *Dev Cell* 10: 93–103.
46. Fromental-Ramain C, Warot X, Messadecq N, LeMeur M, Dollé P, et al. (1996) Hox-a13 and Hox-d13 play a crucial role in patterning of the limb autopod. *Development* 122: 2997–3011.
47. Scherz PJ, Harfe BD, McMahon AP, Tabin CJ (2004) The limb bud Shh-Fgf feedback loop is terminated by expansion of former ZPA cells. *Science* 305: 396–399.
48. Panman L, Galli A, Lagarde N, Michos O, Soete G, et al. (2006) Differential regulation of gene expression in the digit forming area of the mouse limb bud by SHH and gremlin 1/FGF-mediated epithelial-mesenchymal signaling. *Development* 133: 3419–3428.
49. Fernandez-Teran M, Piedra ME, Kathiriyi IS, Srivastava D, Rodriguez-Rey JC, et al. (2000) Role of dHAND in the anterior-posterior polarization of the limb bud: implications for the Sonic hedgehog pathway. *Development* 127: 2133–2142.
50. Lewandoski M, Sun X, Martin GR (2000) Fgf8 signaling from the AER is essential for normal limb development. *Nat Genet* 26: 460–463.
51. Chiang C, Litingtung Y, Harris MP, Simandl BK, Li Y, et al. (2001) Manifestation of the Limb Prepatterning: Limb Development in the Absence of Sonic Hedgehog Function. *Developmental Biology* 236: 421–435.
52. Kraus P, Fraidenraich D, Loomis CA (2001) Some distal limb structures develop in mice lacking Sonic hedgehog signaling. *Mech Dev* 100: 45–58.
53. Nissim S, Allard P, Bandyopadhyay A, Harfe BD, Tabin CJ (2007) Characterization of a novel ectodermal signaling center regulating Tbx2 and Shh in the vertebrate limb. *Dev Biol* 304: 9–21.
54. Davenport TG, Jerome-Majewska LA, Papaioannou VE (2003) Mammary gland, limb and yolk sac defects in mice lacking Tbx3, the gene mutated in human ulnar mammary syndrome. *Development* 130: 2263–2273.
55. Rallis C, Del Buono J, Logan MP (2005) Tbx3 can alter limb position along the rostrocaudal axis of the developing embryo. *Development* 132: 1961–1970.
56. Sheth R, Bastida MF, Ros M (2007) Hoxd and Gli3 interactions modulate digit number in the amniote limb. *Dev Biol* 310: 430–441.
57. Zakany J, Zacchetti G, Duboule D (2007) Interactions between HOXD and Gli3 genes control the limb apical ectodermal ridge via Fgf10. *Dev Biol* 306: 883–893.
58. Panman L, Drenth T, Tewelscher P, Zuniga A, Zeller R (2005) Genetic interaction of Gli3 and Alx4 during limb development. *Int J Dev Biol* 49: 443–448.
59. Barna M, Pandolfi PP, Niswander L (2005) Gli3 and Plzf cooperate in proximal limb patterning at early stages of limb development. *Nature* 436: 277–281.
60. Shubin N, Tabin C, Carroll S (1997) Fossils, genes and the evolution of animal limbs. *Nature* 388: 639–647.
61. Shubin N, Tabin C, Carroll S (2009) Deep homology and the origins of evolutionary novelty. *Nature* 457: 818–823.
62. Vokes SA, Ji H, McCuine S, Tenzen T, Giles S, et al. (2007) Genomic characterization of Gli-activator targets in sonic hedgehog-mediated neural patterning. *Development* 134: 1977–1989.
63. Sun X, Mariani FV, Martin GR (2002) Functions of FGF signaling from the apical ectodermal ridge in limb development. *Nature* 418: 501–508.

Manuscript in press.

(Release in April 2012)



GLI3 Constrains Digit Number by Controlling Both Progenitor Proliferation and BMP- Dependent Exit to Chondrogenesis

**Javier Lopez-Rios, Dario Speziale, Dimitri Robay, Martina Scotti,
Marco Osterwalder, Gretel Nusspaumer, Antonella Galli, Georg A.
Holländer, Marie Kmita and Rolf Zeller**

GLI3 Constrains Digit Number by Controlling Both Progenitor Proliferation and BMP-Dependent Exit to Chondrogenesis

Javier Lopez-Rios¹, Dario Speziale^{1,7}, Dimitri Robay^{1,4,7}, Martina Scotti^{2,7}, Marco Osterwalder¹, Gretel Nusspaumer³, Antonella Galli^{1,5}, Georg A. Holländer^{3,6}, Marie Kmita² and Rolf Zeller^{1,*}

¹Developmental Genetics, Department of Biomedicine, University of Basel, CH-4058 Basel, Switzerland

²Laboratory of Genetics and Development, Institut de Recherches Cliniques de Montréal, Montréal, Québec H2W1R7, Canada

³Department of Biomedicine and Children's Hospital, University of Basel, CH-4058 Basel, Switzerland

⁴Present address: Basilea Pharmaceutica International, CH-4005 Basel, Switzerland

⁵Present address: Department of Medicine and Genetics & Development, Herbert Irving Comprehensive Cancer Center, Columbia University Medical Center, New York NY 10032, USA

⁶Developmental Immunology, Department of Pediatrics, University of Oxford, Oxford, United Kingdom

⁷These authors contributed equally

*Correspondence: rolf.zeller@unibas.ch

SUMMARY

Inactivation of *Gli3*, a key component of Hedgehog signaling in vertebrates, results in formation of additional digits (polydactyly) during limb bud development. The analysis of mouse embryos constitutively lacking *Gli3* has revealed the essential GLI3 functions in specifying the antero-posterior (AP) limb axis and digit identities. We conditionally inactivated *Gli3* during mouse handplate development, which uncoupled the resulting pre-axial polydactyly from known GLI3 functions in establishing AP and digit identities. Our analysis revealed that *Gli3* directly restricts the expression of regulators of the G₁-S cell cycle transition such as *Cdk6* and constrains S-phase entry of digit progenitors in the anterior handplate. Furthermore, *Gli3* promotes the exit of proliferating progenitors toward BMP-dependent chondrogenic differentiation by spatio-temporally restricting and terminating the expression of the BMP antagonist *Gremlin1*. Thus, *Gli3* is a negative regulator of the proliferative expansion of digit progenitors and acts as a gatekeeper for the exit to chondrogenic differentiation.

Running Title: Dual Control of Digit Progenitor Expansion by *Gli3*

INTRODUCTION

Hedgehog signaling is a major regulator of organogenesis in both vertebrate and invertebrate embryos (Jiang and Hui, 2008; Varjosalo et al., 2006). Analysis of Sonic Hedgehog (SHH) signaling has provided insights into how SHH orchestrates vertebrate limb bud development (Chiang et al., 2001; Harfe et al., 2004; Riddle et al., 1993; Zeller et al., 2009). In the posterior mesenchyme, SHH is produced by the polarizing region (ZPA) to control antero-posterior (AP) axis specification and proliferative expansion of mesenchymal progenitors together with FGF and Wnt signals (ten Berge et al., 2008; Towers et al., 2008; Zhu et al., 2008). All three types of signals stimulate the expression of *Mycn*, which appears to be a key regulator of limb bud mesenchymal cell proliferation as its inactivation decreases proliferation, resulting in smaller limb skeletal elements and syndactyly (Ota et al., 2007).

SHH is part of a self-regulatory system that interlinks the ZPA with the apical ectodermal ridge (AER) and controls limb bud outgrowth by coordinating BMP, FGF and SHH signaling with the clearance of retinoic acid from the distal mesenchyme (Probst et al., 2011; Zeller et al., 2009). A key node in this system is the BMP antagonist Gremlin1 (GREM1), which keeps BMP activity low during limb bud outgrowth (Benazet et al., 2009). This feedback signaling system is self-terminating, as (1) the expanding population of *Shh* descendants is refractory to *Grem1* expression (Scherz et al., 2004), and (2) high AER-FGF signaling inhibits *Grem1* expression in the distal mesenchyme (Verheyden and Sun, 2008). AER-FGF signaling increases during limb bud

outgrowth, which eventually inhibits *Grem1* expression. This termination of *Grem1* expression results in a renewed raise of BMP activity (Benazet et al., 2009; Verheyden and Sun, 2008), which initiates condensation and chondrogenic differentiation of mesenchymal progenitors (Bandyopadhyay et al., 2006; Pizette and Niswander, 2000). In digit primordia, differential BMP signal transduction in the distal phalanx-forming region is likely required to determine the definitive identities (Suzuki et al., 2008; Witte et al., 2010).

In vertebrates, the expression of SHH target genes is regulated by the GLI1-3 transcription factors. In particular, SHH signal transduction at the primary cilia inhibits the proteolytic processing of GLI3 to a transcriptional repressor (GLI3R, Wen et al., 2010). This results in accumulation of GLI1-3 activators in the posterior limb bud, while GLI3R is the predominant GLI isoform in the anterior mesenchyme (Ahn and Joyner, 2004; Wang et al., 2000). A genome-wide screen for *cis*-regulatory regions bound by an epitope-tagged GLI3R transgene in mouse limb buds has identified ~200 candidate transcriptional targets, among them *Grem1* and the cell cycle regulator *Cdk6* (Vokes et al., 2008). Loss-of-function mutations in the mouse *Gli3* gene cause pre-axial and central polydactylies with soft-tissue fusions (polysyndactyly), a prominent feature shared with human congenital malformations caused by mutations in *GLI3* (Biesecker, 2006). Analysis of the *extra-toes* (*Xt*) loss-of-function mutation in mice has been instrumental to uncover essential requirements of *Gli3* (Hui and Joyner, 1993; Schimmang et al., 1992). In limb buds, *Gli3* is expressed from early stages onward and interacts with the *Hand2* and *5'Hoxd* transcription factors to polarize the nascent mesenchyme and restrict *Shh*

activation to the posterior mesenchyme (Galli et al., 2010; te Welscher et al., 2002a; Zakany et al., 2007). In *Gli3*-deficient mouse limb buds, posterior genes are expressed ectopically, while anterior genes are down-regulated (Buscher et al., 1997; Hill et al., 2009; Litingtung et al., 2002; McGlinn et al., 2005; te Welscher et al., 2002b; Zuniga and Zeller, 1999). Hence, *Gli3* participates in setting up the AP limb bud axis, but the extent to which posterior identity is retained in *Gli3*-deficient limb buds remained unclear (Galli et al., 2010; Hill et al., 2009). Limb buds deficient for both *Gli3* and *Hand2* lack AP polarity and are highly polydactylous (Galli et al., 2010), while the polydactyly of mouse limbs lacking both *Gli3* and *Shh* is indistinguishable from *Gli3* mutants (Litingtung et al., 2002; te Welscher et al., 2002b). Molecular analysis indicated that one major function of SHH is to counteract GLI3R-mediated repression of distal limb and digit development. Furthermore, the massive apoptosis observed in *Shh*-deficient limb buds has been linked to increased Gli3R levels and aberrantly high BMP activity (Bastida et al., 2004). Indeed, the incompletely penetrant anterior digit duplications in heterozygous *Xt^J* (*Gli3^{Xt^J/+}*) mice are enhanced by additional heterozygosity for a *Bmp4* loss-of function allele (Dunn et al., 1997). Similarly, transgene-mediated ectopic *Hoxd12* expression enhances the digit polydactyly as GLI3R forms a transcriptional activator complex with HOXD12 that promotes the formation of additional digits (Chen et al., 2004). The digit polydactyly of *Gli3*-deficient limbs is also enhanced by deletion of 5'*HoxD* genes as it results in an anterior gain of *Hoxd9* and *Hoxd10* expression (Sheth et al., 2007).

We generated a conditional loss-of-function *Gli3* allele and inactivated *Gli3* specifically in the developing handplate (autopod) of mouse limb buds. This allowed us to uncover the dual mechanism by which GLI3 controls digit morphogenesis and restrains the autopod to five digits (pentadactyly). In the anterior mesenchyme, GLI3 acts as a gatekeeper of the G₁-S transition by regulating the expression of cell cycle genes and S-phase entry. In addition, GLI3 restricts and terminates *Grem1* expression in the anterior autopod in a spatio-temporally controlled manner, which promotes the BMP-dependent exit of progenitors from proliferation to chondrogenic differentiation. Disruption of this dual role underlies the resulting pre-axial polydactylies, as progenitors continue to proliferate and the onset of chondrogenic differentiation is delayed in the absence of *Gli3*. This study shows how GLI3 tightly controls the kinetics and length of proliferative expansion and constrains the developing limb bud to pentadactyly.

RESULTS

Constitutive Loss of *Gli3* Alters the Anterior but not Posterior Autopod

To assess the extent of posterior development in *Gli3*-deficient forelimb buds, mesenchymal progenitors were marked by activation of a *LacZ* reporter gene in *Shh*-expressing cells and their descendants (Harfe et al., 2004). Despite the lack of *Gli3* and anterior ectopic SHH signaling (Figure S1), the descendants contributed equally to the posterior-most digits d5 and d4 and no ectopic anterior spot of LacZ-positive cells was detected in *Gli3*-deficient limb buds (Figure 1A; see also Harfe et al., 2004). The central and posterior digits 3-5 were readily identified by their morphology and extent of metacarpal ossification in *Gli3*-deficient limbs (Figure 1B). Several additional anterior digits formed, but the anterior-most digit 1 was lost in *Gli3*-deficient limbs (Figure 1B). These results showed that posterior cell fates were maintained and that the polydactyly arose from the anterior and central autopod in mutant limb buds. Real-time PCR (qPCR) and RNA *in situ* hybridization showed that the expression of SHH targets such as the transcriptional regulators *5'Hoxd*, *Hand2* and *Gli1* was increased in the anterior mesenchyme (Figure S1).

Conditional Inactivation of *Gli3* in the Developing Autopod

To study the spatio-temporal requirements of *Gli3*, we generated a conditional loss-of-function *Gli3^f* allele (Figure 1C and Figure S1). Cre-mediated recombination of the *Gli3^f* allele resulted in a deletion that encompassed the DNA binding and transactivation domains as in the constitutive *Gli3^{XtJ}* null allele, but only 15kb instead of 51kb were deleted (Maynard et al., 2002). An

additional *Gli3* null allele ($Gli3^{\Delta}$) was generated by germline recombination of the $Gli3^f$ allele. Genetic complementation with the $Gli3^{XtJ}$ allele showed that this $Gli3^{\Delta}$ allele reproduces the pleiotropic range of *Gli3* loss-of function phenotypes (Figure S1 and data not shown). Therefore, both *Gli3* null alleles were used interchangeably and are referred to as $Gli3^{\Delta}$ alleles. In addition, *Prx1*-Cre-mediated inactivation of *Gli3* from early limb bud stages onward ($Gli3^{\Delta/\Delta c}; P1\text{-Cre}$) caused an anterior polydactyly indistinguishable from $Gli3^{XtJ/XtJ}$ limbs (Figure 1D; compare to Figure 1B).

We inactivated the $Gli3^f$ allele specifically during autopod development in forelimb buds ($Gli3^{\Delta c}$ allele) using a mouse strain expressing the Cre-recombinase under control of the *Hoxa13* locus ($Hoxa13^{Cre/+}$, Figure 1E, Scotti et al., 2011). At gestational day E10.5, the *Gli3* transcript distribution was not affected, while by ~E11.75 *Gli3* transcripts had cleared from the distal autopod of $Gli3^{\Delta/\Delta c}$ forelimb buds (lower panels, Figure 1E). Immunoblotting showed that both the full-length GLI3 (GLI3FL) and GLI3R protein isoforms were no longer detectable in the distal part of the $Gli3^{\Delta/\Delta c}$ autopod, while levels in the proximal part remained similar to $Gli3^{\Delta/+}$ controls (Figure 1F, 1G). To exclude phenotypic and/or molecular variations due to heterozygosity for *Hoxa13* in $Gli3^{\Delta/\Delta c}$ forelimb buds, all other embryos (wild-type, $Gli3^{\Delta/+}$ and $Gli3^{\Delta/\Delta}$) analyzed also carried one $Hoxa13^{Cre/+}$ allele (Figures 2-7).

Inactivation of *Gli3* by *Hoxa13*-Cre Uncouples Pre-Axial Polydactyly from AP Axis Specification

Analysis of *Gli3*^{Δ/Δc} forelimbs at E16.5 revealed a distinct pre-axial polydactyly (n=42/42, Figure 2A). In general, the duplications affected digits 1 and 2 (asterisks in Figure 2A) and anterior character was retained in contrast to *Gli3*^{Δ/Δ} forelimbs. In contrast, all *Gli3*^{Δ/+}, *Hoxa13*^{Cre/+} forelimbs were phenotypically normal (n=10/16) or displayed only minor dysmorphologies (n=6/16, data not shown). Anterior ectopic or expanded mesenchymal expression of *Gli1*, *Hoxd12*, *Hoxd13* and AER-*Fgf8* hallmarks of the *Gli3* loss-of-function phenotype (panels *Gli3*^{Δ/Δ} Figure 2B-2E; Buscher et al., 1997; Zuniga and Zeller, 1999), but none of these genes were significantly altered in *Gli3*^{Δ/Δc} forelimb buds (panels *Gli3*^{Δ/Δc}, Figure 2B-2E). Rarely, very small ectopic patches of 5'*Hoxd* transcripts (*Hoxd13*: n=1/9; *Hoxd12*: n=2/6) were detected in *Gli3*^{Δ/Δc} forelimb buds (data not shown), but the anterior expression boundaries were otherwise maintained (panels *Gli3*^{Δ/Δc}, Figure 2B-2E). This indicated that anterior and posterior identities were retained in *Gli3*^{Δ/Δc} forelimb buds. At E11.75, the size of *Gli3*^{Δ/Δc} handplates was still normal in contrast to the enlarged autopod primordia in *Gli3*^{Δ/Δ} forelimb buds (Figure 2B-2E). Morphometric analysis revealed that only by E12.5, both *Gli3*^{Δ/Δc} (+38% ±14%) and *Gli3*^{Δ/Δ} handplates (+46% ±12%) were enlarged in comparison to wild-type controls (Figure S2 and data not shown). While the anterior-most digit in *Gli3*^{Δ/Δc} forelimbs was clearly dysmorphic, the analysis of molecular markers revealed the normal anterior digit 1 expression domains (Figure S2). Therefore, inactivation of *Gli3* during autopod development uncoupled the pre-axial polydactyly from alterations of the AP axis and showed that GLI3R is required to restrain the autopod to pentadactyly long after SHH-dependent specification of AP identities (Zhu et al., 2008).

Shared Molecular Signatures of the Two *Gli3*-Deficient Polydactylies

The transcriptomes of both types of *Gli3*-deficient anterior autopods were compared to wild-types at E11.75 to identify shared molecular alterations. The transcriptome of three independent anterior autopod samples per genotype was analyzed (Figure 3A). Hierarchical clustering revealed that the transcriptomes of *Gli3*^{Δ/Δc} and *Gli3*^{Δ/Δ} anterior autopods were more similar to each other than wild-type and *Gli3*^{Δ/+} control samples (all carrying the *Hoxa13*^{Cre/+} allele; Figure 3B). These microarray data sets were biologically significant as all known anterior alterations in *Gli3*^{XtJ/XtJ} limb buds (Figures S1 and McGlinn et al., 2005) and the normal expression of anterior genes in *Gli3*^{Δ/Δc} forelimb buds were detected (Figures 2 and Figure S2). Ingenuity pathway analysis and validation of the detected alterations by qPCR and RNA *in situ* hybridization revealed striking transcriptional changes. In particular, the core module that regulates the G₁-S transition of the cell cycle was specifically altered in both *Gli3*^{Δ/Δc} and *Gli3*^{Δ/Δ} anterior autopods (indicated by broken line, Figure 3C, Neganova and Lako, 2008), while *Mycn* and most other cell cycle regulators were not consistently changed (Figure 3C and Figure S3). The significant up-regulation and anterior expansion of the cyclin/kinase pair *Cdk6* (~1.9 fold) and *Ccnd1* (~1.3 fold) in the anterior handplate of both types of *Gli3*-deficient forelimb buds was confirmed by qPCR analysis (Figure 3D, E). The expression of *Cdkn2c*, encoding a CDK4/6 inhibitor (Sherr and Roberts, 1995), was reduced ~0.65 fold (Figure 3D). In summary, this transcriptome analysis revealed that the G₁-S transition of the cell cycle was specifically altered in the anterior of *Gli3*-deficient autopods.

Altered Cell Cycle Kinetics of Digit Progenitors in the Anterior Autopod

To directly assess the relevance of these transcriptional changes with respect to the cell cycle, mouse embryos were labeled with BrdU for one hour and anterior and posterior autopods dissected from age-matched *Gli3*^{ΔΔ} (n=5 at E11.75; ~50 somites) and control littermates (n=7). Dead cells (≤10% in all genotypes), erythrocytes and debris were excluded using the appropriate gates and intact single cells analyzed by flow cytometry (Figure 4A, B) to determine the fractions of cells in three distinct phases of the cell cycle (G₀-G₁; S and G₂-M; Figure 4A). Cells in S-phase contained high levels of BrdU and DNA, while cells in the G₀-G₁ (low DNA content) and G₂-M (high DNA content) phases had incorporated little or no BrdU (Figure 4A). No significant changes were detected between anterior and posterior parts of control autopods or with posterior parts of *Gli3*^{ΔΔ} mutant autopods (Figure 4A, B). This contrasted with the anterior part of *Gli3*-deficient autopods as the fraction of cells in S-phase was increased by ~25% (p≤0.01; Figure 4A, B). Concurrently, the fraction of cells in the G₀-G₁ transition of the cell cycle was decreased by ~17% (p≤0.01; Figure 4B). These alterations revealed that cell cycle entry was significantly enhanced in the anterior part of *Gli3*-deficient autopods (Figure 4A, B) in agreement with the specific transcriptional changes of regulators of the G₁-S transition (Figure 3C-E).

A previous genome-wide search for *cis*-regulatory sequences interacting with an exogenous epitope-tagged GLI3R protein in mouse embryos had identified *Cdk6* as a potential transcriptional target of GLI3 (Vokes et al., 2008). To gain

further insight into the possible direct regulation of *Cdk6* by GLI3, specific antibodies (Wen et al., 2010) were used for comparative chromatin immunoprecipitation (ChIP) analysis of wild-type and *Gli3*^{ΔΔ} forelimb bud extracts (Figure 4C). This analysis established that endogenous GLI3 proteins interact specifically with this genomic region located just up-stream of the *Cdk6* coding region in wild-type limb buds (~4-fold enrichment), while no interaction was detected in mutant limb buds (Figure 4C). The functional importance of this regulatory interaction was assessed by analyzing mouse forelimb buds lacking both *Gli3* and *Cdk6* (Figure 4D, E, Malumbres et al., 2004). While up to 7 digit rays formed in *Gli3*^{ΔΔ} forelimb buds (n=6/8), only six with duplicated distal-most phalanges formed in the majority of all *Gli3*^{ΔΔ}, *Cdk6*^{ΔΔ} forelimbs (n=12/17, Figure 4D). In contrast, the less pronounced pre-axial polydactyly in *Gli3*^{Δ/Δc} forelimbs was not affected by additional inactivation of *Cdk6* (n=6/6, Figure 4E). This genetic analysis established the sensitivity of the *Gli3*^{ΔΔ}, but not *Gli3*^{Δ/Δc} polydactyly to *Cdk6* inactivation. In agreement, FGF signaling, which stimulates the proliferation, was increased in the anterior of *Gli3*^{ΔΔ} but not *Gli3*^{Δ/Δc} forelimb buds (Figure 2E and Figure S3), while Wnt signaling was not altered (data not shown).

Decreased BMP Activity in the Anterior of *Gli3*-Deficient Limb Buds

Ingenuity pathway analysis also revealed major alterations of BMP signaling in anterior autopods (Figure S4). In particular, the expression of several targets of the BMP pathway such as *Msx2*, *Id1* and *Id3* was reduced ~2-fold in *Gli3*-deficient anterior autopods (Figure 5A, C and Figure S4). This reduction in BMP signal transduction was paralleled by a ≥2-fold increase in

Grem1 transcripts, while the expression of *Bmp* ligands was not consistently altered (Figure 5B, 5C and Figure S4). In *Gli3*^{ΔΔ} limb buds, *Grem1* expression is expanded anteriorly from the onset of limb bud development onward (te Welscher et al., 2002a), while in *Gli3*^{ΔΔc} forelimbs its anterior expansion occurred much later and concurrent with *Hoxa13*-Cre-mediated inactivation of *Gli3* (Figure 5B, compare to lower panels in Figure 1E). Furthermore, *Grem1* transcripts persisted in the anterior of both types of *Gli3*-deficient forelimb buds, while in wild-types transcripts became undetectable in the presumptive digit primordia by E12.5 (lower panels Figure 5B). CHIP analysis established that the endogenous GLI3 proteins interacted with a known *cis*-regulatory region within the *Grem1* *cis*-regulatory landscape (~6-8 fold enrichment, Figure 5D; Vokes et al., 2008).

***Gli3* Inactivation Delays the BMP-Dependent Exit of Proliferating Digit Progenitors to Chondrogenesis in the Anterior Mesenchyme**

As BMP signaling is required to initiate mesenchymal condensations and chondrogenic differentiation (Pizette and Niswander, 2000; Yoon et al., 2005), we analyzed the distribution of Sox9, which marks the pre-cartilaginous condensations of the forming skeletal primordia (Ng et al., 1997). In wild-type forelimb buds, five distinct Sox9-positive digit primordia were apparent by E12.5 (n=3/3, left panel Figure 6A). In contrast, only the posterior condensations were apparent in both types of *Gli3*-deficient autopods (n=3/3, Figure 6A). To correlate Sox9-positive with proliferating cells, the distribution of Ki67, which marks all proliferating cells (Gerdes et al., 1983), was assessed on parallel sections (Figures 6A, 6B). In wild-types, few Ki67-positive cells

were detected in the Sox9-positive condensations of the digit primordia, while the surrounding mesenchyme continued to proliferate (left panels, Figure 6B). In *Gli3*^{Δ/Δ} autopods, most cells in the anterior mesenchyme remained Ki67-positive (middle panels, Figure 6B) and in *Gli3*^{Δ/Δc} autopods, Ki67 persisted throughout the distal-most mesenchyme (right panels, Figure 6B). *Noggin* and *Col2a1*, two molecular markers of chondrogenic differentiation, delineated all digit primordia in wild-types, but only the posterior ones in *Gli3*-deficient autopods (Figure 6C, McGlinn et al., 2005). In *Gli3*-deficient forelimb buds, the anterior-most condensation appeared reduced and forked and the small primordia for digit 1 was absent (Figure 6C). Taken together, this analysis established that in *Gli3*-deficient forelimb buds, the anterior mesenchymal progenitors continued to proliferate and failed to initiate chondrogenic differentiation at the right time. To determine if this delayed exit toward chondrogenic differentiation was indeed caused by an excess of GREM1-mediated BMP antagonism, beads loaded with 0.5mg/ml BMP4 were implanted into the anterior of *Gli3*-deficient forelimb buds (Figure 6D). These grafts induced strong expression of both *Noggin* and *Col2a1* in the anterior mutant mesenchyme (right panels, Figure 6D), but in contrast to grafts into younger limb buds (see e.g. Bastida et al., 2004) cellular apoptosis was not increased (data not shown). Hence, a causal link between increased GREM1, aberrantly low BMP activity and delayed chondrogenic differentiation was established. In particular, *Grem1* expression in the anterior mesenchyme terminated around E13.0, which correlated well with the delay in differentiation of anterior digits in *Gli3*-deficient forelimb buds (data not shown).

As complete inactivation of *Grem1* alters limb bud development from early stages onward in the context of *Gli3* deficiency (Zuniga and Zeller, 1999), the phenotypic consequences of genetically reducing *Grem1* in *Gli3*^{ΔΔ} and *Gli3*^{ΔΔc} forelimbs were determined (Figure 7A, B). While *Gli3*^{ΔΔ}, *Grem1*^{Δ+} forelimb buds were identical to *Gli3*^{ΔΔ} forelimb buds (Figure 7A), the pre-axial polydactyly of *Gli3*^{ΔΔc} forelimbs (6-7 digit rays, n=12/12) was reduced to pentadactyly in most cases in *Gli3*^{ΔΔc}, *Grem1*^{Δ+} forelimbs (Figure 7B). In particular, distinct *Col2a1*-positive condensations were visible in the positions normally giving rise to digits 2 and 1 in *Gli3*^{ΔΔc}, *Grem1*^{Δ+} forelimb buds (upper right panel Figure 7B, compare to wild-type in Figure 7A). While an apparently normal digit 2 formed, duplicated distal phalanges persisted on the most-anterior digit in *Gli3*^{ΔΔc}, *Grem1*^{Δ+} forelimbs (n=11/17, lower right panel, Figure 7B). This analysis revealed the differential sensitivity of *Gli3*^{ΔΔ} and *Gli3*^{ΔΔc} polydactyly to the *Grem1* gene dosage, which is likely linked to the fact that *Grem1* is anteriorly expanded from the earliest stages onward in *Gli3*^{ΔΔ} forelimb buds (te Welscher et al., 2002a), while it expands only late during autopod formation in *Gli3*^{ΔΔc} forelimb buds (Figure 5B).

The genetic interaction of *Gli3* with *Bmp4* and effects on polydactyly were first analyzed in trans-heterozygous mouse embryos due to the early lethality of *Bmp4*-deficient mouse embryos (Dunn et al., 1997, see also Figure S5). Therefore we used *Hoxa13*-Cre to inactivate *Bmp4* (Liu et al., 2004) in a conditional manner during autopod development. Such conditional inactivation of *Bmp4* (*Bmp4*^{ΔΔc}) did not alter the anterior autopod likely due to redundancy among *Bmp* ligands (Bandyopadhyay et al., 2006), but a post-axial

condensation formed in some forelimbs (asterisks, Figure S5 and Figures 7C, D). In contrast, inactivation of *Bmp4* in the context of heterozygosity for *Gli3* significantly enhanced the pre-axial polydactyly (Figure 7C). While *Gli3*^{Δ/+} forelimbs were pentadactylous, the pre-axial polydactyly in *Gli3*^{Δ/+}, *Bmp4*^{Δ/Δc} forelimbs was increased to the maximal extent seen in *Gli3*^{Δ/Δc} forelimbs (n=10/12, Figure 7C, compare to left panels in Figure 7B). The elongated *Col2a1*-positive condensation that normally forms digit 2 was reduced to a forked rudiment in *Gli3*^{Δ/+}, *Bmp4*^{Δ/Δc} forelimb buds (asterisks, Figure 7C). Furthermore, the small anterior condensation giving rise to digit 1 (black arrowhead, Figure 7C) was absent in *Gli3*^{Δ/+}, *Bmp4*^{Δ/Δc} forelimb buds (upper right panel, Figure 7C). These results pointed to reduced and/or delayed initiation of chondrogenic differentiation. This polydactylous phenotype was not further enhanced by complete inactivation of both *Gli3* and *Bmp4* (n=14/14, Figure 7D). Overall, these results corroborate the proposal that aberrantly low BMP activity delays chondrogenic differentiation and contributes to the pre-axial polydactylies in *Gli3*-deficient forelimbs.

DISCUSSION

First, we show that constitutive loss of *Gli3* specifically alters the anterior of the developing limb bud, which indicates that the resulting pre-axial polydactyly is predominantly caused by disrupting the GLI3R isoform. In fact, it has been recently shown that GLI3R also mediates all essential *Gli3* functions during cortical neurogenesis in mouse embryos (Wang et al., 2011). Secondly, we establish that conditional inactivation of *Gli3* in the developing autopod uncouples the pre-axial polydactyly from the early GLI3 functions in establishment of AP identities (Galli et al., 2010; te Welscher et al., 2002a; Zakany et al., 2007). Therefore, the pre-axial polydactyly observed in *Gli3*^{Δ/Δc} forelimbs must be caused by alterations that occur long after the functions of *Gli3* in setting up the AP limb bud axis and the early specification of digit identities by SHH signaling (Zhu et al., 2008). In this context, GLI3R might be required only early and transiently to restrict the expression of posterior genes (Buscher et al., 1997; Zuniga and Zeller, 1999).

Most importantly, our study reveals the two distinct regulatory steps by which *Gli3* limits the proliferative expansion of the anterior limb bud mesenchyme and ascertains pentadactyly (Figure 7E). Initially, *Gli3* acts as a negative modulator of the G₁-S transition, most probably by directly regulating *Cdk6* transcription. These alterations of the G₁-S transition likely result in faster cycling rather than an increase in proliferating cells since the mitotic index was not increased (M.O. and J.L.-R., unpublished results). Subsequently, GLI3 limits the proliferative expansion of mesenchymal progenitors by restricting and ultimately terminating *Grem1* expression in a spatio-temporally

controlled manner in the anterior autopod (Figure 7E). The resulting increase in BMP activity promotes the exit of undifferentiated proliferating progenitors towards chondrogenesis. Therefore, GLI3 fulfills a dual role in constraining proliferation of mesenchymal progenitors by regulating both cell cycle entry and exit to chondrogenic differentiation. In support of a causal link between these two functions, it has been shown that *Cdk6* over-expression promotes proliferation and interferes with BMP2-induced osteoblast differentiation (Grossel et al., 1999; Ogasawara et al., 2004). Furthermore, these dual GLI3 functions are likely of general relevance as *Gli3* is required together with *Plzf* to initiate chondrogenic differentiation of stylopod and zeugopodal primordia in hindlimbs (Barna et al., 2005). Moreover, *Gli3* has been shown to balance proliferation with neural differentiation during central nervous system development (Blaess et al., 2008; Wang et al., 2011).

The gene networks regulating limb bud outgrowth and termination of the SHH-dependent signaling system that originates from the posterior autopod have been studied extensively (Figure 7E). The core module of this signaling system is the SHH/GREM1/AER-FGF feedback loop that keeps BMP activity low and promotes coordinated outgrowth of the limb bud (reviewed by Zeller et al., 2009). Its termination results in a renewed increase in BMP activity (Benazet et al., 2009), which likely promotes mesenchymal condensation and chondrogenic differentiation similar to what the present study establishes for the anterior autopod (Figure 7E). Indeed, genetic inactivation of both *Bmp4* and *Bmp2* interferes with formation of posterior digit primordia (Bandyopadhyay et al., 2006). Taken together these studies indicate that

BMP activity is low during the proliferative expansion of digit progenitors, but high levels are required for exit to chondrogenic differentiation (this study and Bandyopadhyay et al., 2006). Conversely, high BMP levels induce mesenchymal cell death during limb bud outgrowth and patterning (see e.g. Bastida et al., 2004), which in agreement with the present study indicates that proliferating progenitors depend on low BMP activity.

Genetic analysis revealed the differential sensitivity of the two types of *Gli3* deficiencies to *Cdk6* inactivation and *Grem1* gene dosage. The autopod of *Gli3*^{ΔΔ} forelimbs was enlarged and the G₁-S transition likely altered from early stages onward, which would render the resulting pre-axial polydactyly more sensitive to *Cdk6* inactivation. In contrast, the *Gli3*^{ΔΔ} polydactyly was not sensitive to heterozygosity for *Grem1*, which may again be a consequence of the early enlargement of the anterior autopod. This occurs during the period of robust and self-regulatory feedback signaling, which will rapidly compensate variations in BMP activity by adjusting *Grem1* expression (Nissim et al., 2006; Benazet et al., 2009). In contrast, the anterior autopod of *Gli3*^{ΔΔc} forelimb buds was only enlarged as feedback signaling terminated, which should render the system susceptible to aberrant *Grem1* expression. This was indeed evidenced by the fact that the pre-axial polydactylies in *Gli3*^{ΔΔc} forelimbs are sensitive to the *Grem1* gene dose. Therefore, the delayed exit from proliferation to BMP-dependent chondrogenic differentiation due to increased GREM1 activity is likely to contribute proportionally more to the enlargement of the anterior autopod in *Gli3*^{ΔΔc} than in *Gli3*^{ΔΔ} forelimb buds.

In light of the present study, alterations affecting cell cycle entry and exit to chondrogenic differentiation, rather than bona-fide patterning defects could underlie the congenital malformations observed in Greig's cephalopolysyndactyly and Pallister-Hall syndrome patients, which are caused by scattered point mutations and deletions in the human *GLI3* gene (reviewed by Biesecker, 2006). The highly variable limb polydactylies in these patients could be a consequence of variations affecting the duration of proliferative expansion of digit progenitors. In fact, Alberch and Gale (1983), using colchicine to inhibit proliferation in amphibian limb buds realized that local changes in cell proliferation affected the number and identities of digits. They concluded that the number of digits correlated well with the final size of the autopod field, i.e. the extent to which the progenitors expanded. In agreement, the constitutive loss of *Gli3* causes a more severe pre-axial polydactyly than later inactivation during autopod development. Therefore, the dual functions of *Gli3* in restricting S-phase entry and promoting exit to chondrogenic differentiation are an essential part of the morpho-regulatory systems (Figure 7E) that initiate and terminate the rather homogenous proliferative expansion of limb bud mesenchymal progenitors (Boehm et al., 2010; Gros et al., 2010) and constrain the autopod to pentadactyly.

EXPERIMENTAL PROCEDURES

Mouse Strains and Embryos

Studies with mice were performed in strict accordance with Swiss law and 3R principles. The *Gli3*^{XtJ} allele was maintained in a NMRI background. The *Gli3*^f, *Gli3*^Δ alleles and *Hoxa13-Cre* alleles were maintained in a mixed 129SvJ/C57BL/6J background. *R26R*^{LacZ/+}, *Shh*^{Cre/+}, *Prx1-Cre*, *Cdk6*, *Grem1*, *Bmp4* null and *Bmp4* conditional alleles were maintained in a C57BL/6J background. For all studies, wild-type and mutant embryos (age-matched: ±1 somite) of the same genetic background were used to exclude phenotypic variation. This analysis focused on forelimbs, as *Hoxa13-Cre* is active earlier in hindlimb buds resulting in a *Gli3* null phenotype.

Immunofluorescence and Immunoblot Analysis

Limb buds were fixed overnight in 4% paraformaldehyde at 4°C and Sox9 and Ki67 protein were detected on 7µm serial paraffin sections. Primary antibodies against Sox9 (1:500) and Ki67 (1:200; Millipore) were detected using goat anti-rabbit conjugated to Alexa Fluor-594 (1:500; Invitrogen). Nuclei were counterstained with Hoechst-33258. For immunoblot analysis, forelimb bud pairs were dissected at E11.75 (~52 somites) and 10µg protein was separated on 6% SDS-PAGE gels, followed by transfer to PVDF membranes (Millipore). GLI3 proteins were detected by chemo-luminescence using monoclonal anti-GLI3 antibodies (clone 6F5, 5µg/ml; Wen et al., 2010).

Microarray Analysis

Total RNA was isolated from the anterior handplates of forelimb bud pairs of three sex- and somite-matched embryos per genotype. Probes for the independent triplicates were labeled and hybridized to GeneChip Mouse Gene 1.0 ST Arrays (see Probst et al., 2011). Data were analyzed using the Partek Genomic Suite 6.5 software and Ingenuity Pathway Analysis software. The correlation coefficients (r) of biological triplicates of a particular genotype ranged from 0.994 to 0.998. To identify differentially expressed genes, two way ANOVA analysis was used. The microarray data files are available via MIAMExpress (accession no. E-MEXP-3495).

Quantitation of Transcript Levels by Real-Time PCR (qPCR)

The anterior halves of handplates at E11.75 (~52 somites) were dissected, total RNAs extracted, cDNA synthesized and analyzed by qPCR as described (Benazet et al., 2009; for primers see Supplemental Data). Relative transcript levels were normalized to the expression of two housekeeping genes, *Rpl19* and *Hprt1*. The expression levels of mutant samples were calculated in relation to wild-type controls (average set to 100%). All results (mean \pm SD) are based on analysis of 7 or 8 samples per genotype. The significance of all differences was assessed using the two-tailed, non-parametric Mann-Whitney test.

Flow Cytometric Analysis

Pregnant females were injected intra-peritoneally with 2mg of BrdU one hour before sacrifice. Forelimb autopod pairs of individual embryos (E11.75, ~50 somites) were dissected in ice-cold IMDM (Invitrogen) supplemented with

10% FCS (Hyclone) into anterior and posterior halves. Samples were dissociated into single cells using 1mg/ml collagenase D and 50µg/ml DNase I in 1xHBSS (Roche). Subsequently, cells were filtered through a 70µM mesh and decorated with FITC-conjugated anti-BrdU antibodies and 7-AAD (to determine DNA content, BD Bioscience). Samples were cooled on ice during the entire procedure. Flow cytometric analysis was done using a FACScalibur System (BD Biosciences) and primary data were processed using FlowJo software (Tree Star, Inc.). Initial analysis of DAPI uptake into apoptotic cells established that this dissociation caused less than 10% cell death. In particular, no differences in cell survival were apparent among the different genotypes. Forward and side scatter gates were set to exclude erythrocytes, cell debris and dead cells. No genotype-specific differences in size or complexity were detected. The significance of all differences was verified by two-tailed, non-parametric Mann-Whitney test.

Manipulation and Culture of Mouse Limb Buds

Mouse forelimb buds were cultured as described (Probst et al., 2011). Heparin beads were loaded with recombinant BMP4 (0.5 mg/ml in PBS; R&D Systems) and implanted into the anterior autopod of embryos at E12.0 (~56 somites). This BMP4 concentration was used as it neither stimulates *Grem1* expression (Nissim et al., 2006) nor causes significant cell death. Individual forelimb buds were cultured for 12-14 hours, fixed and analyzed by RNA *in situ* hybridization. Contralateral limbs with no beads or PBS-soaked beads served as controls.

REFERENCES

- Ahn, S., and Joyner, A.L. (2004). Dynamic changes in the response of cells to positive hedgehog signaling during mouse limb patterning. *Cell* 118, 505-516.
- Alberch, P., and Gale, E.A. (1983). Size dependence during the development of the amphibian foot. Colchicine-induced digital loss and reduction. *J Embryol Exp Morphol* 76, 177-197.
- Bandyopadhyay, A., Tsuji, K., Cox, K., Harfe, B.D., Rosen, V., and Tabin, C.J. (2006). Genetic Analysis of the Roles of BMP2, BMP4, and BMP7 in Limb Patterning and Skeletogenesis. *PLoS Genet* 2, e216.
- Barna, M., Pandolfi, P.P., and Niswander, L. (2005). Gli3 and Plzf cooperate in proximal limb patterning at early stages of limb development. *Nature* 436, 277-281.
- Bastida, M.F., Delgado, M.D., Wang, B., Fallon, J.F., Fernandez-Teran, M., and Ros, M.A. (2004). Levels of Gli3 repressor correlate with Bmp4 expression and apoptosis during limb development. *Dev Dyn* 231, 148-160.
- Benazet, J.D., Bischofberger, M., Tiecke, E., Goncalves, A., Martin, J.F., Zuniga, A., Naef, F., and Zeller, R. (2009). A self-regulatory system of interlinked signaling feedback loops controls mouse limb patterning. *Science* 323, 1050-1053.
- Biesecker, L.G. (2006). What you can learn from one gene: GLI3. *J Med Genet* 43, 465-469.
- Blaess, S., Stephen, D., and Joyner, A.L. (2008). Gli3 coordinates three-dimensional patterning and growth of the tectum and cerebellum by integrating Shh and Fgf8 signaling. *Development* 135, 2093-2103.

Boehm, B., Westerberg, H., Lesnicar-Pucko, G., Raja, S., Rautschka, M., Cotterell, J., Swoger, J., and Sharpe, J. (2010). The role of spatially controlled cell proliferation in limb bud morphogenesis. *PLoS Biol* 8, e1000420.

Buscher, D., Bosse, B., Heymer, J., and Ruther, U. (1997). Evidence for genetic control of Sonic hedgehog by Gli3 in mouse limb development. *Mech Dev* 62, 175-182.

Chen, Y., Knezevic, V., Ervin, V., Hutson, R., Ward, Y., and Mackem, S. (2004). Direct interaction with Hoxd proteins reverses Gli3-repressor function to promote digit formation downstream of Shh. *Development* 131, 2339-2347.

Chiang, C., Litingtung, Y., Harris, M.P., Simandl, B.K., Li, Y., Beachy, P.A., and Fallon, J.F. (2001). Manifestation of the Limb Prepattern: Limb Development in the Absence of Sonic Hedgehog Function. *Dev Biol* 236, 421-435.

Dunn, N.R., Winnier, G.E., Hargett, L.K., Schriek, J.J., Fogo, A.B., and Hogan, B.L.M. (1997). Haploinsufficient Phenotypes in *Bmp4* Heterozygous Null Mice and Modification by Mutations in *Gli3* and *Alx4*. *Dev Biol* 188, 235-247.

Galli, A., Robay, D., Osterwalder, M., Bao, X., Benazet, J.D., Tariq, M., Paro, R., Mackem, S., and Zeller, R. (2010). Distinct roles of Hand2 in initiating polarity and posterior Shh expression during the onset of mouse limb bud development. *PLoS Genet* 6, e1000901.

Gerdes, J., Schwab, U., Lemke, H., and Stein, H. (1983). Production of a mouse monoclonal antibody reactive with a human nuclear antigen associated with cell proliferation. *Int J Cancer* 31, 13-20.

Gros, J., Hu, J.K., Vinegoni, C., Feruglio, P.F., Weissleder, R., and Tabin, C.J. (2010). WNT5A/JNK and FGF/MAPK pathways regulate the cellular events shaping the vertebrate limb bud. *Curr Biol* 20, 1993-2002.

Grossel, M.J., Baker, G.L., and Hinds, P.W. (1999). cdk6 can shorten G(1) phase dependent upon the N-terminal INK4 interaction domain. *J Biol Chem* 274, 29960-29967.

Harfe, B.D., Scherz, P.J., Nissim, S., Tian, H., McMahon, A.P., and Tabin, C.J. (2004). Evidence for an expansion-based temporal Shh gradient in specifying vertebrate digit identities. *Cell* 118, 517-528.

Hill, P., Gotz, K., and Ruther, U. (2009). A SHH-independent regulation of Gli3 is a significant determinant of anteroposterior patterning of the limb bud. *Dev Biol* 328, 506-516.

Hui, C., and Joyner, A. (1993). A mouse model of greig cephalopolysyndactyly syndrome: the extra-toesJ mutation contains an intragenic deletion of the Gli3 gene. *Nat Genet* 3, 241-246.

Jiang, J., and Hui, C.C. (2008). Hedgehog signaling in development and cancer. *Dev Cell* 15, 801-812.

Litingtung, Y., Dahn, R.D., Li, Y., Fallon, J.F., and Chiang, C. (2002). Shh and Gli3 are dispensable for limb skeleton formation but regulate digit number and identity. *Nature* 418, 979-983.

Liu, W., Selever, J., Wang, D., Lu, M.F., Moses, K.A., Schwartz, R.J., and Martin, J.F. (2004). Bmp4 signaling is required for outflow-tract septation and branchial-arch artery remodeling. *Proc Natl Acad Sci USA* 101, 4489-4494.

Malumbres, M., Sotillo, R., Santamaria, D., Galan, J., Cerezo, A., Ortega, S., Dubus, P., and Barbacid, M. (2004). Mammalian cells cycle without the D-type cyclin-dependent kinases Cdk4 and Cdk6. *Cell* 118, 493-504.

Maynard, T.M., Jain, M.D., Balmer, C.W., and LaMantia, A.S. (2002). High-resolution mapping of the Gli3 mutation extra-toes reveals a 51.5-kb deletion. *Mamm Genome* 13, 58-61.

McGlinn, E., van Bueren, K.L., Fiorenza, S., Mo, R., Poh, A.M., Forrest, A., Soares, M.B., Bonaldo Mde, F., Grimmond, S., Hui, C.C., *et al.* (2005). Pax9 and Jagged1 act downstream of Gli3 in vertebrate limb development. *Mech Dev* 122, 1218-1233.

Neganova, I., and Lako, M. (2008). G1 to S phase cell cycle transition in somatic and embryonic stem cells. *J Anat* 213, 30-44.

Ng, L.J., Wheatley, S., Muscat, G.E., Conway-Campbell, J., Bowles, J., Wright, E., Bell, D.M., Tam, P.P., Cheah, K.S., and Koopman, P. (1997). SOX9 binds DNA, activates transcription, and coexpresses with type II collagen during chondrogenesis in the mouse. *Dev Biol* 183, 108-121.

Nissim, S., Hasso, S.M., Fallon, J.F., and Tabin, C.J. (2006). Regulation of Gremlin expression in the posterior limb bud. *Dev Biol* 299, 12-21.

Ogasawara, T., Kawaguchi, H., Jinno, S., Hoshi, K., Itaka, K., Takato, T., Nakamura, K., and Okayama, H. (2004). Bone morphogenetic protein 2-induced osteoblast differentiation requires Smad-mediated down-regulation of Cdk6. *Mol Cell Biol* 24, 6560-6568.

Ota, S., Zhou, Z.Q., Keene, D.R., Knoepfler, P., and Hurlin, P.J. (2007). Activities of N-Myc in the developing limb link control of skeletal size with digit separation. *Development* 134, 1583-1592.

Pizette, S., and Niswander, L. (2000). BMPs are required at two steps of limb chondrogenesis: formation of prechondrogenic condensations and their differentiation into chondrocytes. *Dev Biol* 219, 237-249.

Probst, S., Kraemer, C., Demougin, P., Sheth, R., Martin, G.R., Shiratori, H., Hamada, H., Iber, D., Zeller, R., and Zuniga, A. (2011). SHH propagates distal limb bud development by enhancing CYP26B1-mediated retinoic acid clearance via AER-FGF signalling. *Development* 138, 1913-1923.

Riddle, R.D., Johnson, R.L., Laufer, E., and Tabin, C. (1993). *Sonic hedgehog* mediates the polarizing activity of the ZPA. *Cell* 75, 1401-1416.

Scherz, P.J., Harfe, B.D., McMahon, A.P., and Tabin, C.J. (2004). The limb bud Shh-Fgf feedback loop is terminated by expansion of former ZPA cells. *Science* 305, 396-399.

Schimmang, T., Lemaistre, M., Vortkamp, A., and R  ther, U. (1992). Expression of the zinc finger gene *Gli3* is affected in the morphogenetic mouse mutant extra-toes (*Xt*). *Development* 116, 799-804.

Scotti, M., and Kmita, M. (2012). Recruitment of 5' *Hoxa* genes in the allantois is essential for proper extra-embryonic function in placental mammals. *Development* 139, doi 10.1242/dev.075408.

Sherr, C.J., and Roberts, J.M. (1995). Inhibitors of mammalian G1 cyclin-dependent kinases. *Genes Dev* 9, 1149-1163.

Sheth, R., Bastida, M.F. and Ros, M. (2007) *Hoxd* and *Gli3* interactions modulate digit number in the amniote limb. *Dev Biol* 310, 430-441.

Suzuki, T., Hasso, S.M., and Fallon, J.F. (2008). Unique SMAD1/5/8 activity at the phalanx-forming region determines digit identity. *Proc Natl Acad Sci USA* 105, 4185-4190.

- te Welscher, P., Fernandez-Teran, M., Ros, M.A., and Zeller, R. (2002a). Mutual genetic antagonism involving GLI3 and dHAND prepatterns the vertebrate limb bud mesenchyme prior to SHH signaling. *Genes Dev* 16, 421-426.
- te Welscher, P., Zuniga, A., Kuijper, S., Drenth, T., Goedemans, H.J., Meijlink, F., and Zeller, R. (2002b). Progression of Vertebrate Limb Development through SHH-Mediated Counteraction of GLI3. *Science* 298, 827-830.
- ten Berge, D., Brugmann, S.A., Helms, J.A., and Nusse, R. (2008). Wnt and FGF signals interact to coordinate growth with cell fate specification during limb development. *Development* 135, 3247-3257.
- Towers, M., Mahood, R., Yin, Y., and Tickle, C. (2008). Integration of growth and specification in chick wing digit-patterning. *Nature* 452, 882-886.
- Varjosalo, M., Li, S.P., and Taipale, J. (2006). Divergence of Hedgehog Signal Transduction Mechanism between *Drosophila* and Mammals. *Dev Cell* 10, 177-186.
- Verheyden, J.M., and Sun, X. (2008). An Fgf/Gremlin inhibitory feedback loop triggers termination of limb bud outgrowth. *Nature* 454, 638-641.
- Vokes, S.A., Ji, H., Wong, W.H., and McMahon, A.P. (2008). A genome-scale analysis of the cis-regulatory circuitry underlying sonic hedgehog-mediated patterning of the mammalian limb. *Genes Dev* 22, 2651-2663.
- Wang, B., Fallon, J.F., and Beachy, P.A. (2000). Hedgehog-Regulated Processing of Gli3 Produces an Anterior/Posterior Repressor gradient in the Developing Vertebrate Limb. *Cell* 100, 423-434.

Wang, H., Ge, G., Uchida, Y., Luu, B., and Ahn, S. (2011). Gli3 is required for maintenance and fate specification of cortical progenitors. *J Neurosci* *31*, 6440-6448.

Wen, X., Lai, C.K., Evangelista, M., Hongo, J.A., de Sauvage, F.J., and Scales, S.J. (2010). Kinetics of hedgehog-dependent full-length Gli3 accumulation in primary cilia and subsequent degradation. *Mol Cell Biol* *30*, 1910-1922.

Witte, F., Chan, D., Economides, A.N., Mundlos, S., and Stricker, S. (2010). Receptor tyrosine kinase-like orphan receptor 2 (ROR2) and Indian hedgehog regulate digit outgrowth mediated by the phalanx-forming region. *Proc Natl Acad Sci USA* *107*, 14211-14216.

Yoon, B.S., Ovchinnikov, D.A., Yoshii, I., Mishina, Y., Behringer, R.R., and Lyons, K.M. (2005). *Bmpr1a* and *Bmpr1b* have overlapping functions and are essential for chondrogenesis in vivo. *Proc Natl Acad Sci USA* *102*, 5062-5067.

Zakany, J., Zacchetti, G., and Duboule, D. (2007). Interactions between *HOXD* and *Gli3* genes control the limb apical ectodermal ridge via *Fgf10*. *Dev Biol* *306*, 883-893.

Zeller, R., Lopez-Rios, J., and Zuniga, A. (2009). Vertebrate limb bud development: moving towards integrative analysis of organogenesis. *Nat Rev Genet* *10*, 845-858.

Zhu, J., Nakamura, E., Nguyen, M.T., Bao, X., Akiyama, H., and Mackem, S. (2008). Uncoupling Sonic hedgehog control of pattern and expansion of the developing limb bud. *Dev Cell* *14*, 624-632.

Zuniga, A., and Zeller, R. (1999). Gli3 (Xt) and formin (ld) participate in the positioning of the polarising region and control of posterior limb-bud identity. *Development* 126, 13-21.

ACKNOWLEDGEMENTS

The authors are grateful to D. Klewe-Nebenius and C. Klasen (EMBL) for generating chimeric mice, and A. Offinger and her staff for excellent animal care. S. Scales (Genentech) provided the GLI3 antibodies. F. Imhof and A. Hermann participated in aspects of this study as part of their master research projects and E. Uenal performed the OPT analysis and volumetric measurements. P. Demougin from the University of Basel Lifesciences Training Facility performed the microarray hybridization and primary analysis. We thank J.D. Benazet, A. Zuniga and group members for critical input on the manuscript. JLR received an EMBO long-term and EU Marie Curie postdoctoral fellowship. This research is supported by grants of the Swiss National Science Foundation (grants no. 31003A_130803 to RZ and 310000_122558 to GAH), a EU reintegration grant (PERG-GA-2009-246576 to JLR), a Canadian Institute of Health Research grant (CIHR-82880 to MK) and the University of Basel. The authors declare no conflict of interest.

FIGURE LEGENDS

Figure 1. Pre-axial Polydactyly and Conditional Inactivation of *Gli3* during Mouse Autopod Development.

(A) *Shh*-Cre-mediated activation of a *LacZ* transgene inserted into the mouse *Rosa26* locus was used to map *Shh*-descendants in wild-type and *Gli3*-deficient forelimbs. Wild-type (Wt) genotype: *Shh*^{Cre/+}, *R26*^{LacZ/+}. *Gli3*^{XtJ/XtJ}. *Gli3*-deficient embryo carrying the *Shh*^{Cre/+} and *R26*^{LacZ/+} alleles.

(B) Forelimb skeletons at embryonic day E16.5. The mineralization of metacarpal bones (red; cartilage appears blue) in combination with the number and length of phalanges allows identification of posterior digits in wild-type (Wt) and *Gli3*-deficient (*Gli3*^{XtJ/XtJ}) embryos (see also Figure S1).

(C) Scheme depicting the *Gli3* locus and *Gli3* conditional allele. Deletion results in complete loss-of-function identical to the *Gli3*^{XtJ} null allele. Black triangles: *loxP* sites (see also Figure S1).

(D) Inactivation of *Gli3* in the limb bud mesenchyme from early stages onward using the *Prx1*-Cre transgene (*P1*-Cre) results in fore- and hindlimb polydactylies indistinguishable from *Gli3*^{XtJ/XtJ} limbs.

(E) Upper left panels: the *Hoxa13*-Cre transgene recombines the *R26*^{LacZ/+} reporter specifically in the distal part of the forming autopod. Upper right and lower panels: the clearing of *Gli3* transcripts was assessed by RNA *in situ* hybridization using Wt and *Gli3*^{ΔΔ} embryos as positive and negative controls (upper right panels). *Hoxa13*^{Cre/+}-mediated recombination of the *Gli3*^f allele produces the *Gli3*^{Ac} allele.

(F) Immunoblot analysis of full-length (GLI3FL) and processed GLI3 repressor (GLI3R) protein in forelimb handplates at E11.75. Protein extracts were normalized for Vinculin content (VCL).

(G) Immunoblot analysis of GLI3 protein in *Gli3*^{ΔΔ} forelimb handplates dissected into proximal (P) and distal (D) portions.

Digit nomenclatures in panels A, B, D and all subsequent Figures: normal digits with respect to position and morphology are indicated in black. Duplicated and/or additional digits in *Gli3*-deficient forelimbs are indicated in red. Red asterisks indicate hypomorphic digits or digits with uncertain identity.

*s: "split" digit due to duplication of distal phalanges.

Figure 2. *Hoxa13*-Cre-Mediated Inactivation of *Gli3* Uncouples Pre-Axial Polydactyly from the Loss of AP Axis Specification.

(A) Analysis of forelimb skeletons at E16.5.

(B-E) Analysis of the spatial distribution of *Gli1* (B), *Hoxd13* (C), *Hoxd12* (D) and AER-*Fgf8* transcripts (E) in forelimb buds (E11.75, 50-52 somites).

Ectopic (white arrowheads) and normal (black arrowheads) expression domains of *Gli1* and *Fgf8* are indicated. Broken lines mark the expanded (white) and normal (black) expression of 5'*Hoxd* genes in *Gli3*^{Δ/Δ} and *Gli3*^{Δ/Δc} forelimb buds. All forelimb buds analyzed carried one *Hoxa13*^{Cre/+} allele to exclude possible phenotypic variation due to heterozygosity for *Hoxa13* (see also Figure S2).

Figure 3. The G₁-S Transition of the Cell Cycle is Altered in the Anterior Mesenchyme of Both Types of *Gli3*-Deficient Forelimb Buds.

(A) Anterior forelimb autopods dissected for transcriptome analysis at E11.75. Lower panel: *Gli3* RNA *in situ* hybridization established clearance from the dissected anterior regions in *Gli3*^{Δ/Δc} mutants.

(B) Hierarchical clustering of the significant transcriptome alterations (p≤0.05 in all paired comparisons using two-way ANOVA tests). Red: genes up-regulated, blue: genes down-regulated.

(C) Ingenuity Pathway analysis was used to uncover the transcriptional alterations shared by *Gli3*^{Δ/Δ} and *Gli3*^{Δ/Δc} anterior forelimbs. The core module that regulates the G₁-S transition of the cell cycle is indicated by a broken line. Orange-red labeling of *Ccnd1* and *Cdk6* indicates significantly increased expression. *Cdk1*, *Mycn*: increased expression in only one *Gli3*-deficiency. *Myc*: alteration was not confirmed by qPCR. Blue labeling of *Cdkn2c*: significantly decreased expression.

(D) Validation of the alterations in *Cdk6*, *Ccnd1* and *Cdkn2c* transcript levels by qPCR (n=8, E11.75, ~52 somites). Statistically significant changes are indicated in blue (down-regulation) and orange-red (up-regulation). All results are represented as mean ±SD; p≤0.01.

(E) The spatial distribution of *Cdk6* and *Ccnd1* transcripts was analyzed by RNA *in situ* hybridization in combination with optical projection tomography (OPT), which results in improved spatial resolution of low and/or widely expressed genes. Limb bud morphology is shown in the blue channel, while

transcript distribution is shown in the red channel. Broken white lines indicate the anterior domains with expanded expression.

All forelimb buds analyzed were heterozygous for the *Hoxa13*^{Cre/+} allele.

Figure 4. Enhanced S-Phase Entry Contributes to the Pre-Axial Polydactyly in *Gli3*-Deficient Forelimb Buds.

(A) Flow cytometric cell cycle analysis of anterior and posterior limb bud cells in representative control (*Gli3*^{Δ/+}) and *Gli3*^{Δ/Δ} autopod samples at E11.75. Limb bud cells were gated to define three populations in the G₀-G₁, S or G₂-M phases of the cell cycle.

(B) Analysis of several *Gli3*^{Δ/Δ} (n=5) and control (Wt: n=3 and *Gli3*^{Δ/+}: n=4) samples to reveal cell-cycle alterations. Wt and *Gli3*^{Δ/+} forelimb autopods were pooled as controls, as no significant differences were detected by analyzing individual samples. All data are shown as mean ±SD. Two asterisks: p≤0.01; one asterisk: p≤0.05. A: anterior limb bud; P: posterior limb bud.

(C) ChIP-qPCR using anti-GLI3 detects interactions of the endogenous GLI3 proteins with the *Cdk6* locus. The blue region corresponds to a 3 Kb fragment identified by Vokes et al. (2008; mm9: chr5: 3,341,265-3,344,289) that includes the proximal promoter. Amplicons “2” and “3” are located in the critical region. All results are shown as mean ±SD (n≥3).

(D, E) Skeletal phenotypes resulting from additional inactivation of *Cdk6* in *Gli3*^{Δ/Δ} and *Gli3*^{Δ/Δ^c} forelimb buds.

All forelimb buds analyzed carried one *Hoxa13*^{Cre/+} allele. See also Figure S3.

Figure 5. Loss of *Gli3* Decreases BMP Activity in Anterior Forelimb Buds.

(A) *Msx2* expression in *Gli3*^{Δ/Δ} and *Gli3*^{Δ/Δc} forelimb buds (E11.75).

(B) Alterations in the expression of the BMP antagonist *Grem1* in forelimbs. Broken lines indicate the relevant anterior regions in wild-type (black) and *Gli3*-deficient forelimb buds (white). Open arrowheads point to *Grem1* expression in the proximal interdigital mesenchyme, which does not contribute to the digit primordia.

(C) qPCR analysis of two transcriptional BMP targets, *Msx2* and *Id1* and the BMP antagonist *Grem1* (n=8, E11.75). Statistically significant changes are indicated in blue (down-regulation) and orange-red (up-regulation). All results are represented as mean ±SD; p≤0.01.

(D) ChIP-qPCR using anti-GLI3 detects interactions of the endogenous GLI3 proteins with a conserved element within the *Grem1-Fmn1* regulatory landscape (indicated in green, Vokes et al., 2008; mm9: chr2: 113,481,000-113,481,438). Amplicons “2” and “3” are located in the critical region. All results are shown as mean ±SD (n≥3).

All forelimb buds shown were heterozygous for the *Hoxa13*^{Cre/+} allele. See also Figure S4.

Figure 6. The Exit of Proliferating Progenitors to Chondrogenesis is Delayed in the Anterior of *Gli3*-Deficient Autopods.

(A) Sox9 (red fluorescence) demarcates the forming digit primordia on sections of wild-type, *Gli3*^{Δ/Δ} and *Gli3*^{Δ/Δc} autopods (E12.5, ~60 somites).

(B) The Ki67 antigen (green fluorescence) marks proliferating cells, while the auto-fluorescent erythrocytes appear white. Cell nuclei appear blue due to counterstaining with Hoechst-33258. Upper panels: dotted rectangles indicate the position of the enlargements. Left and right lower panels: dotted white lines indicate the proximal limit of the mesenchymal zone with largely Ki67-positive cells.

(C) *Noggin* and *Col2a1* transcripts mark the ongoing chondrogenesis during digit formation at E12.5.

All relevant forelimb buds in panels A-C carried one *Hoxa13*^{Cre/+} allele.

(D) RNA *in situ* hybridization revealed the induction of *Noggin* (n=13/16) and *Col2a1* (n=10/13) expression (right panels) following implantation of BMP4-loaded beads (0.5mg/ml) into the anterior of *Gli3*^{Δ/Δ} forelimb buds at E12.0. Contra-lateral controls with no or PBS-soaked beads (left panels).

Figure 7. Reduction and Promotion of Pre-axial Polydactyly by Altering *Grem1*, *Bmp4* and *Gli3* Gene Dose

(A-F) Comparative analysis of genetic alteration of BMP pathway activity in the context of both types of *Gli3* deficiencies. *Col2a1* expression at E12.5 detects mesenchymal condensations (upper panels), which is compared with the resulting skeletal pattern at E16.5 (lower panels). Upper panels: arrowheads indicate the small condensation for digit 1, red asterisks point to reduced or forked digit primordia with uncertain identity. Lower Panels: black asterisks indicate post-axial condensations. Figure S5 shows the skeletal preparations of all genotypes analyzed.

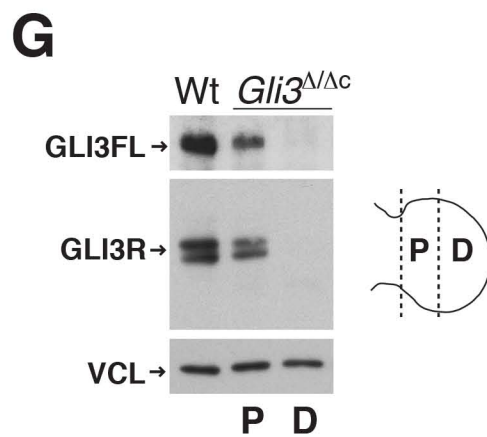
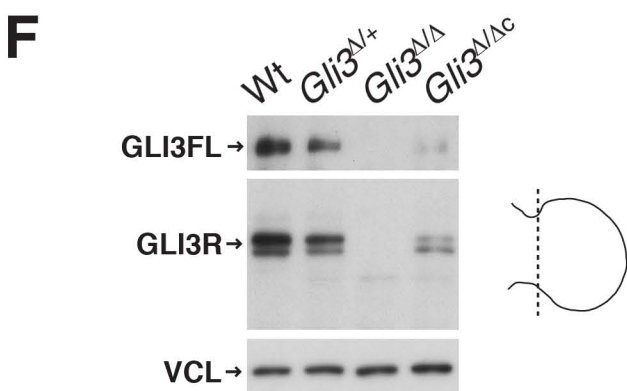
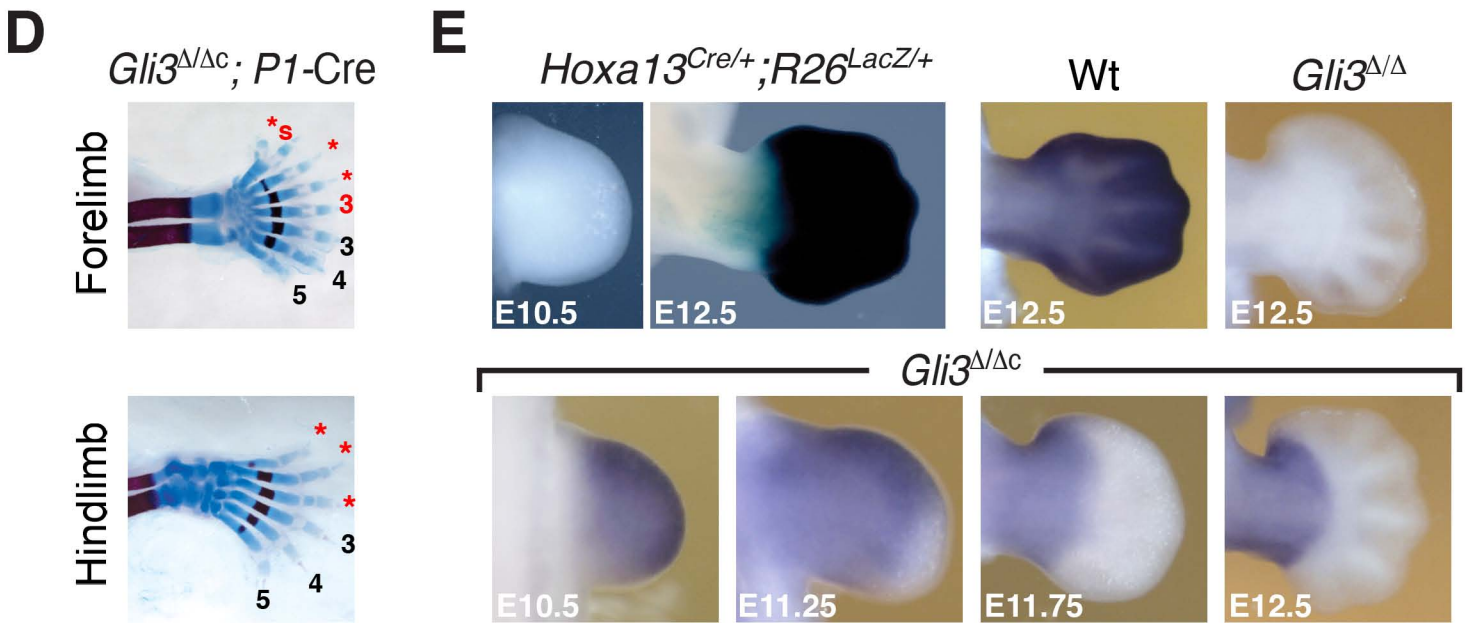
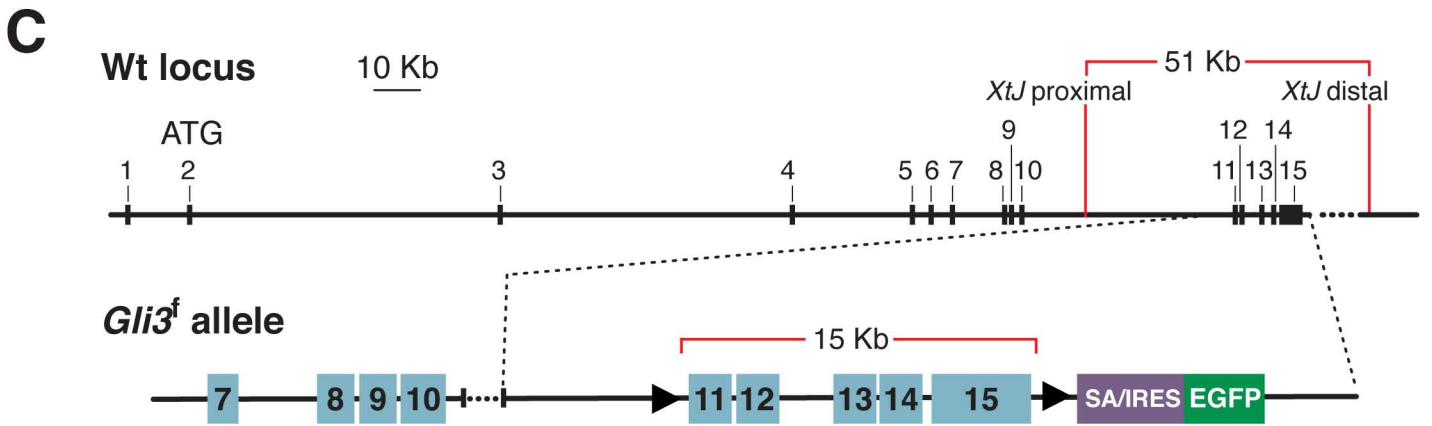
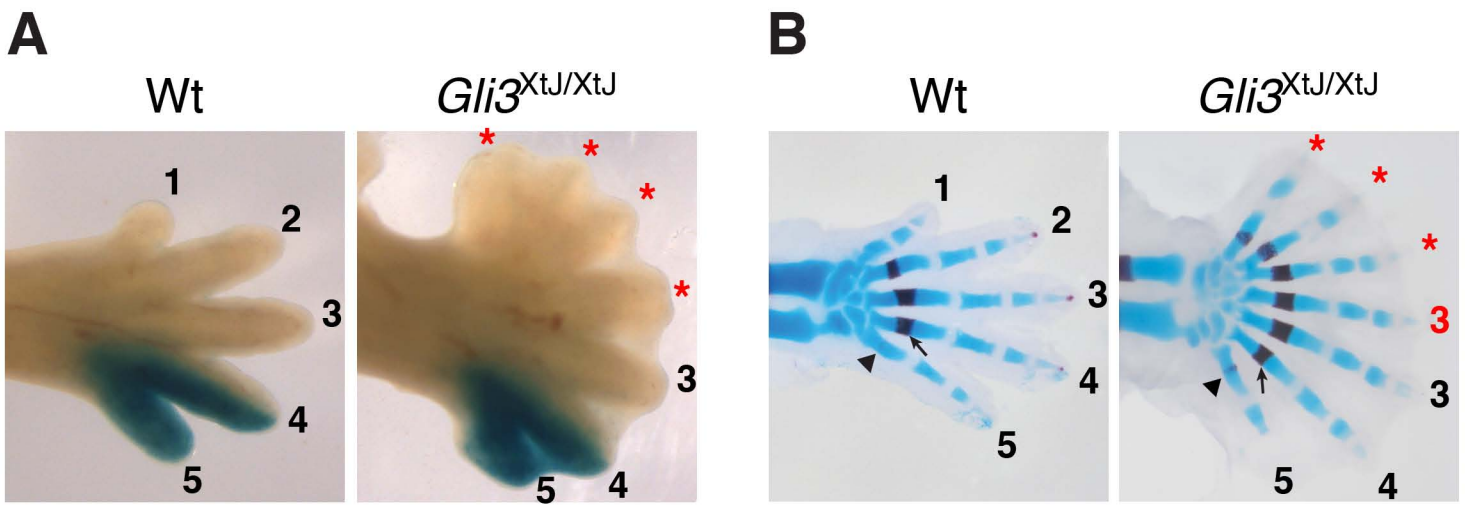
(A) Wild-type (i.e. *Hoxa13*^{Cre/+}) forelimbs compared to *Gli3*^{Δ/Δ} (n=6) and *Gli3*^{Δ/Δ}, *Grem1*^{Δ/+} forelimbs (n=9).

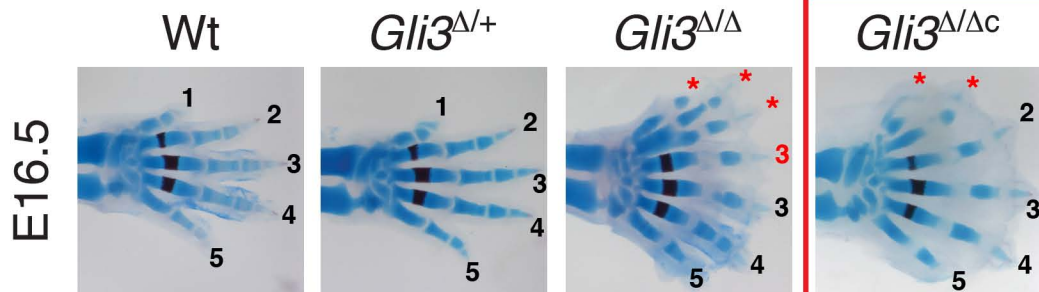
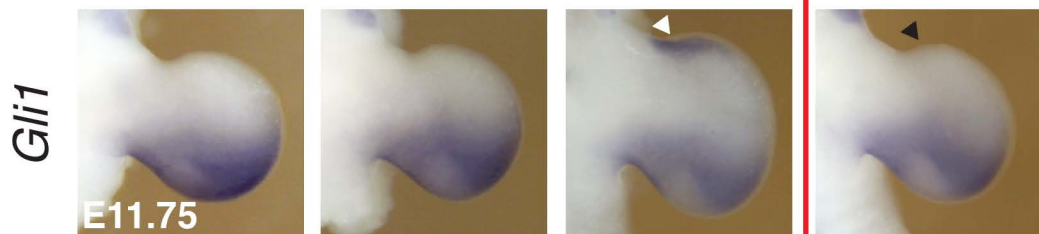
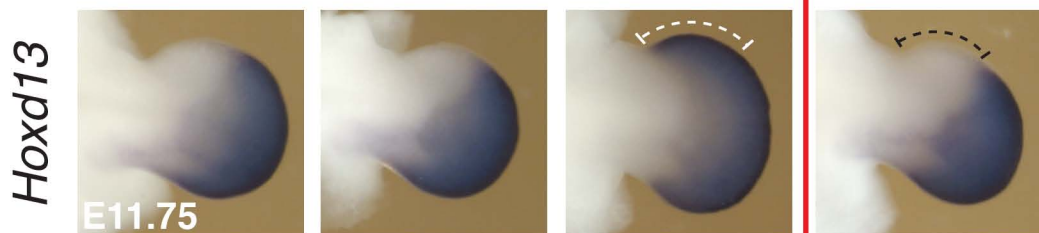
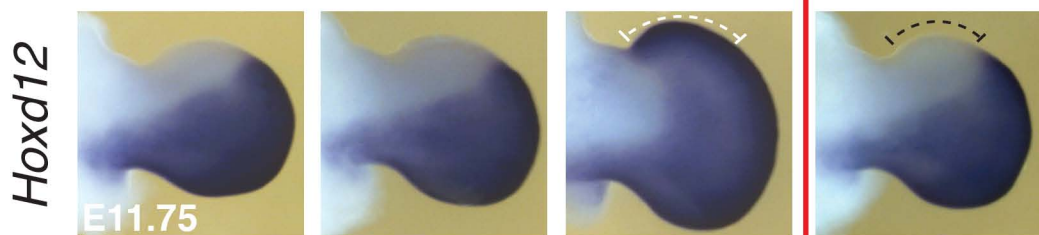
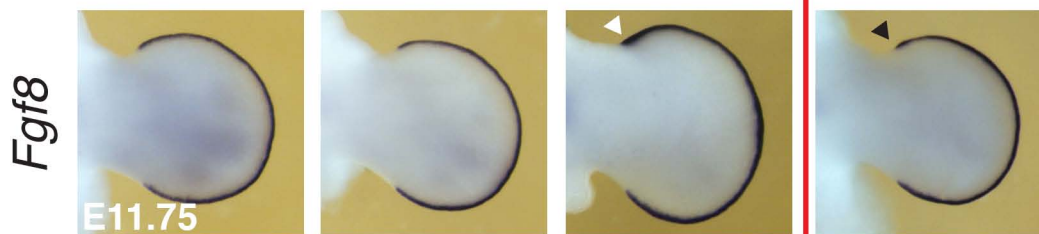
(B) Constitutive genetic inactivation of one *Grem1* allele in *Gli3*^{Δ/Δc} forelimb buds.

(C) *Gli3*^{Δ/+} forelimb buds carrying the *Hoxa13*^{Cre/+} allele compared with *Gli3*^{Δ/+}, *Bmp4*^{Δ/Δc} forelimbs in which one *Bmp4* allele was conditionally inactivated by *Hoxa13*-Cre.

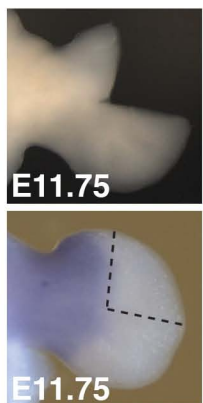
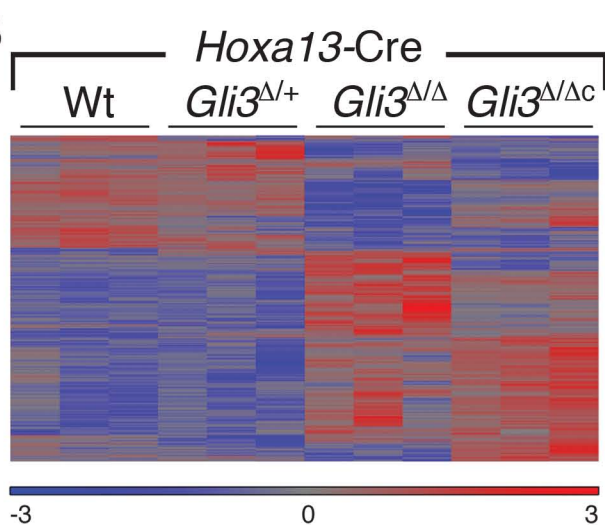
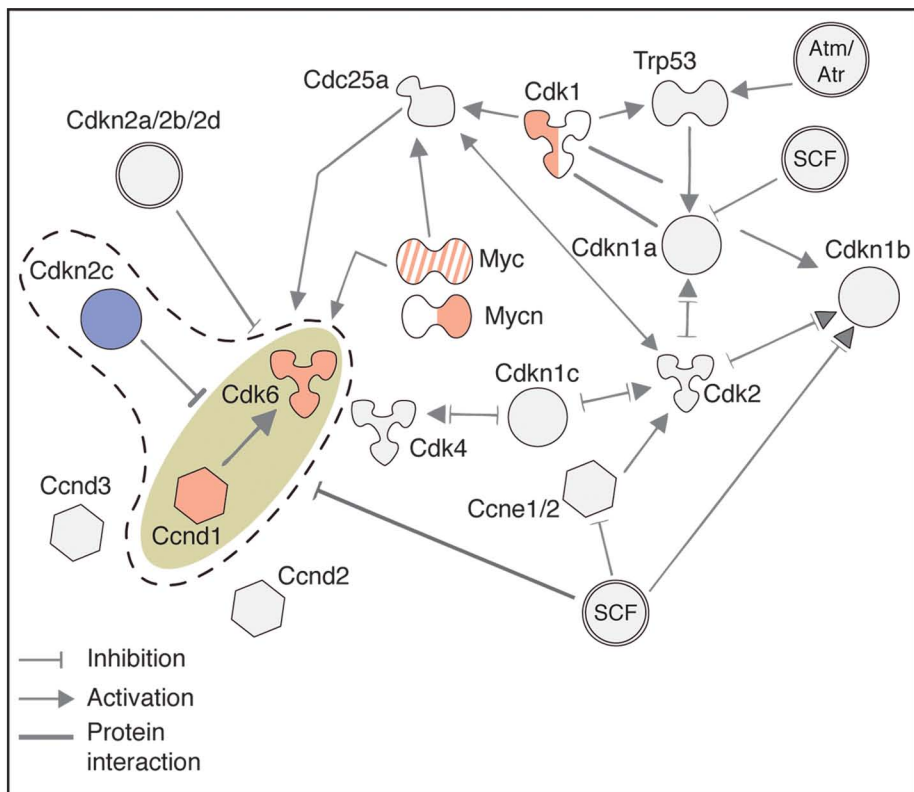
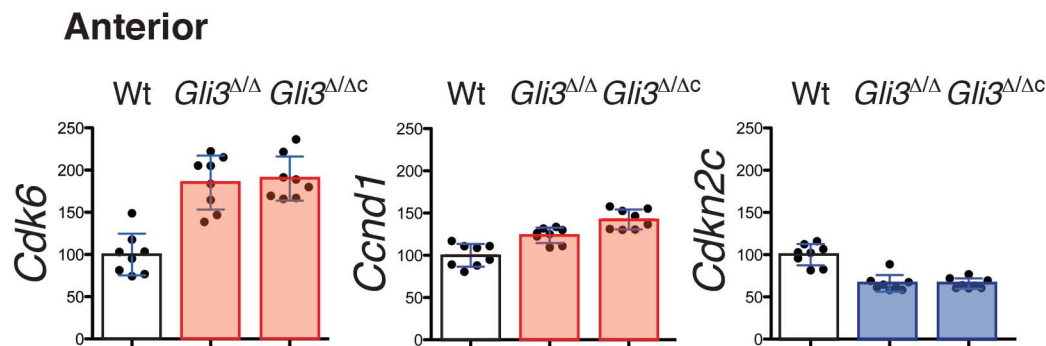
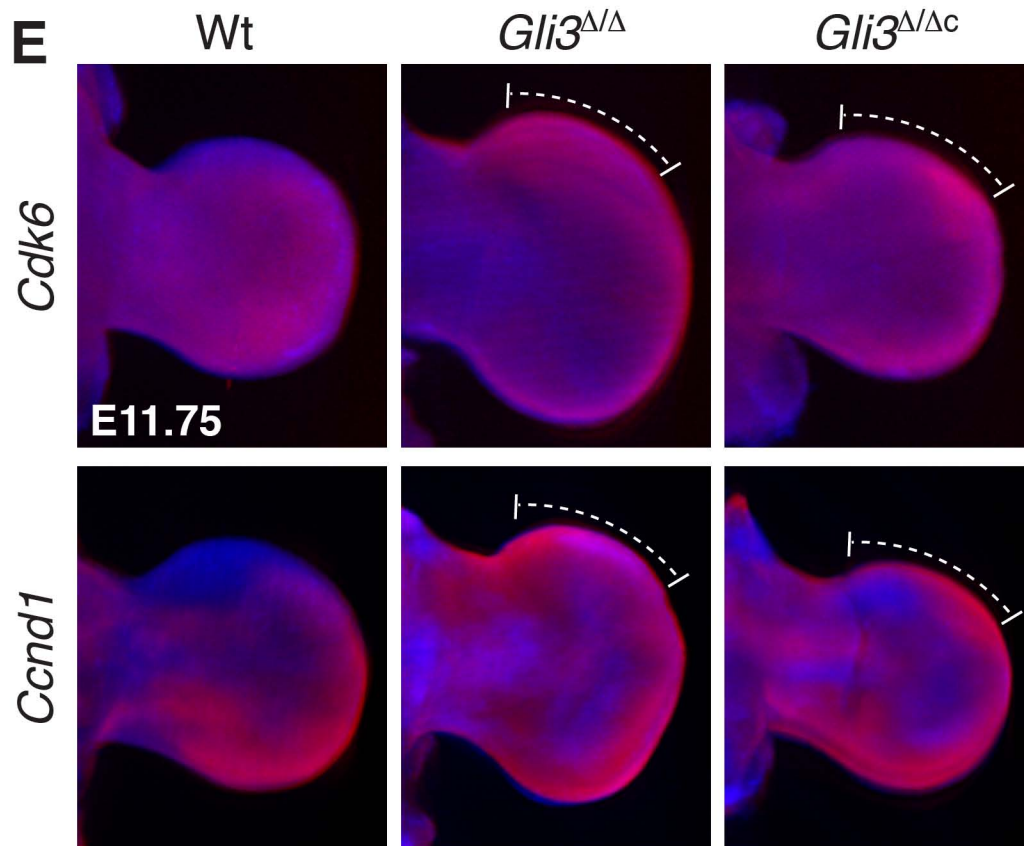
(D) *Gli3*^{Δ/Δc}, *Bmp4*^{Δ/Δc} forelimb buds.

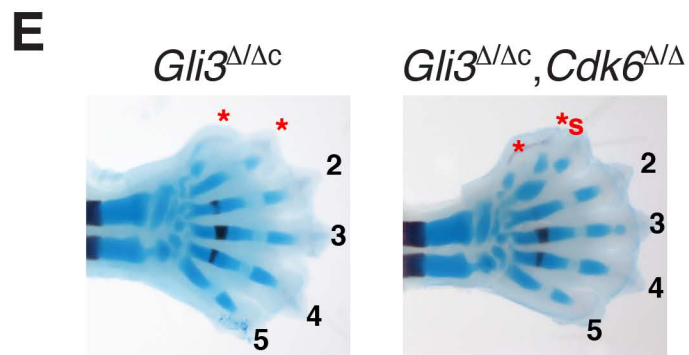
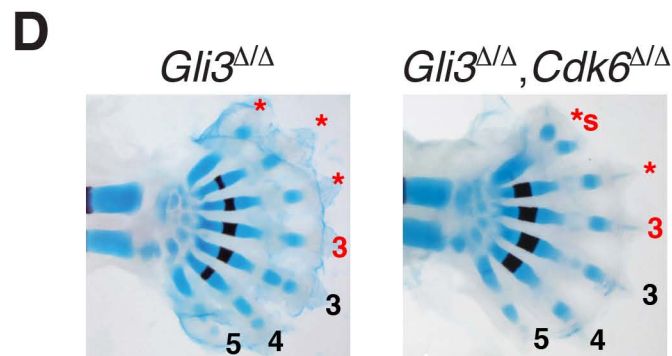
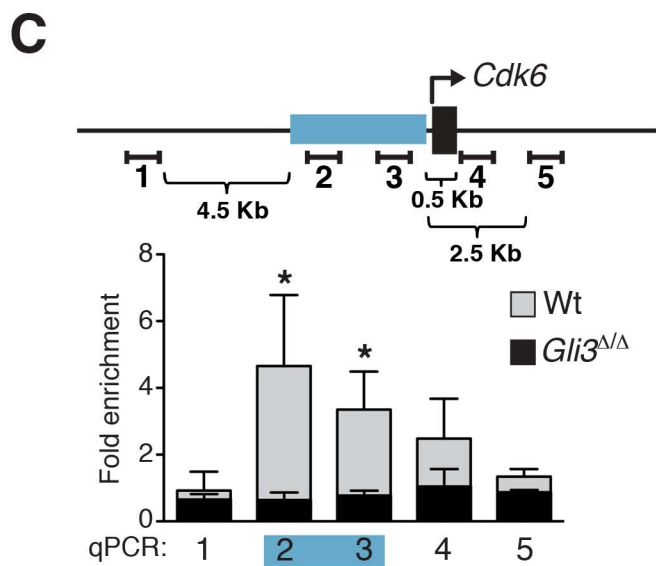
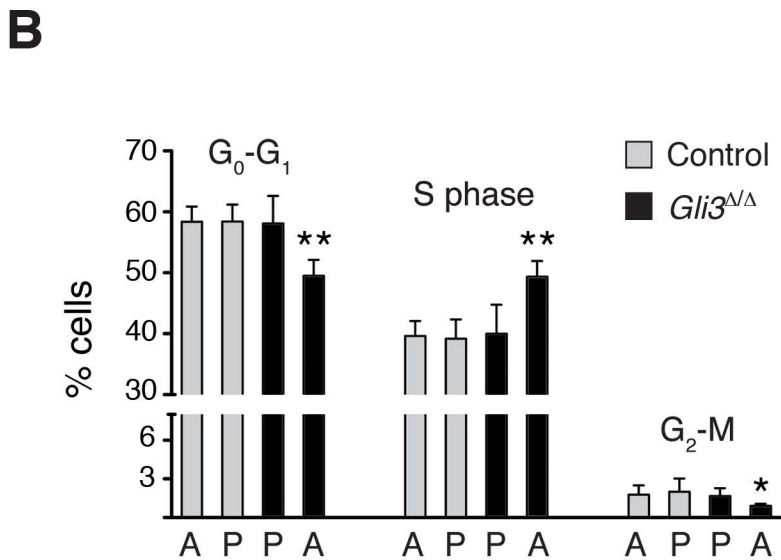
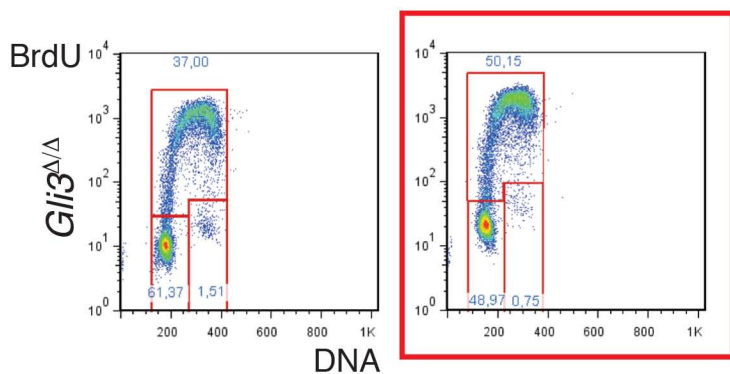
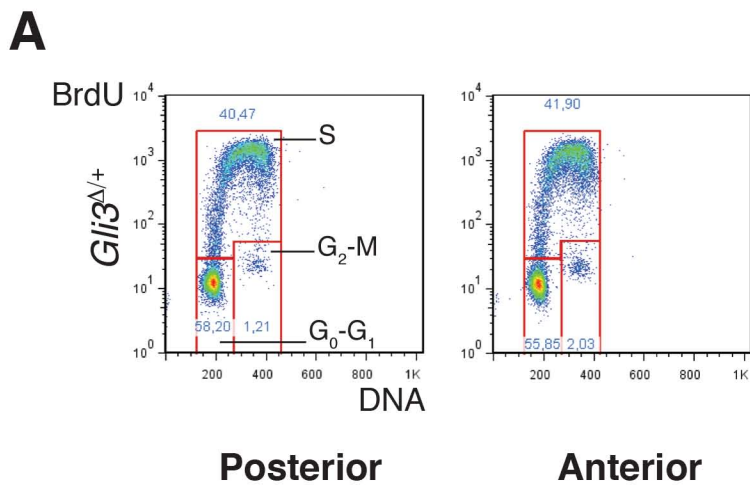
(E) Regulation of the proliferative expansion and chondrogenic exit of digit progenitors by GLI3R and SHH-dependent gene networks. Green: genetic interactions positively regulating proliferation; red: genetic interactions restraining the cell cycle and promoting exit to chondrogenic differentiation.

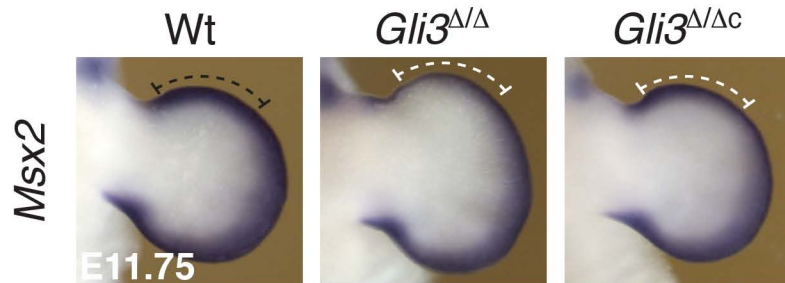
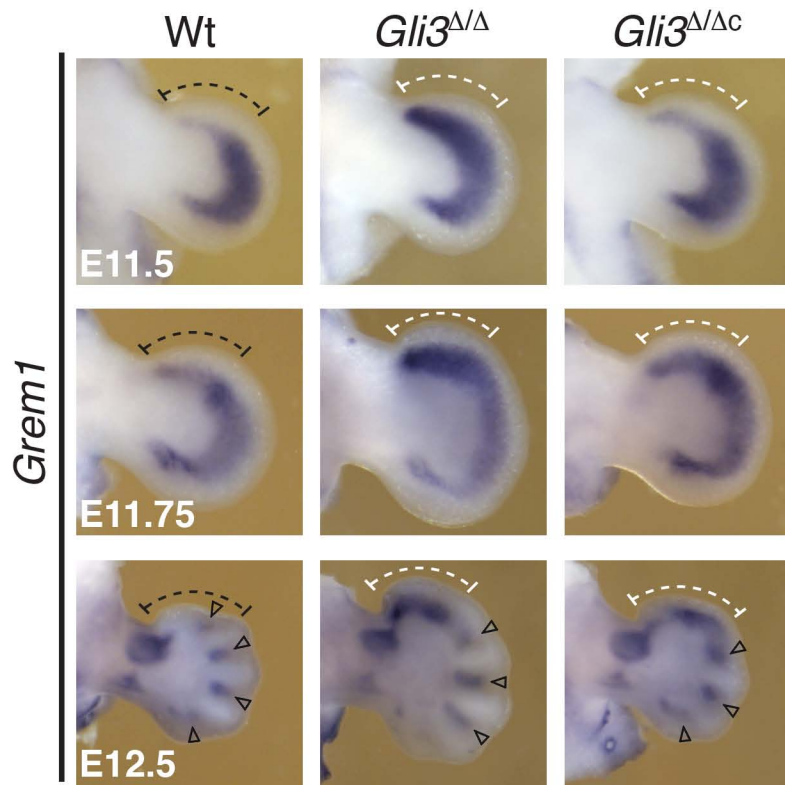
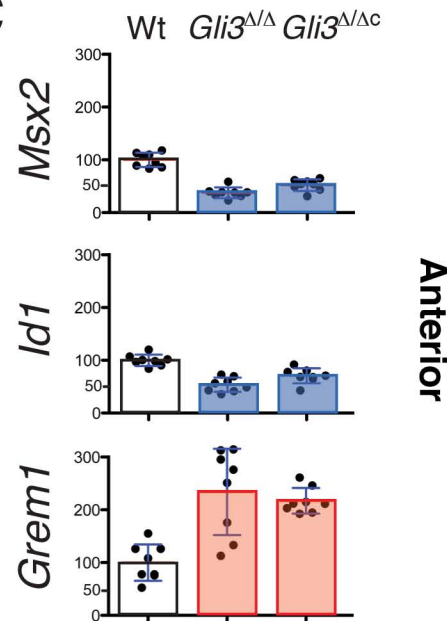
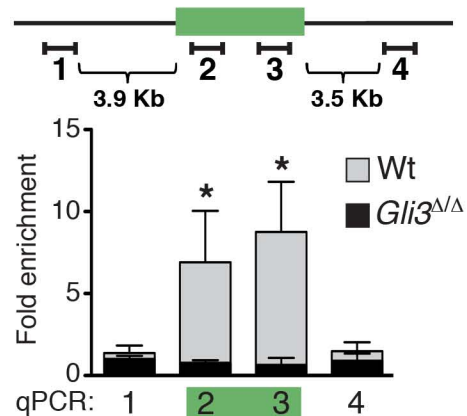


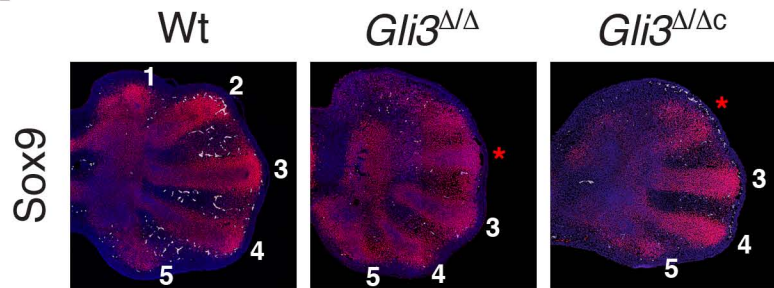
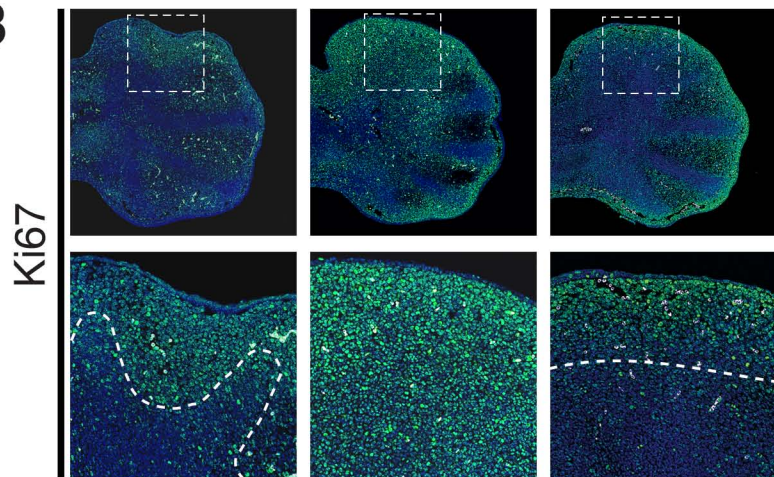
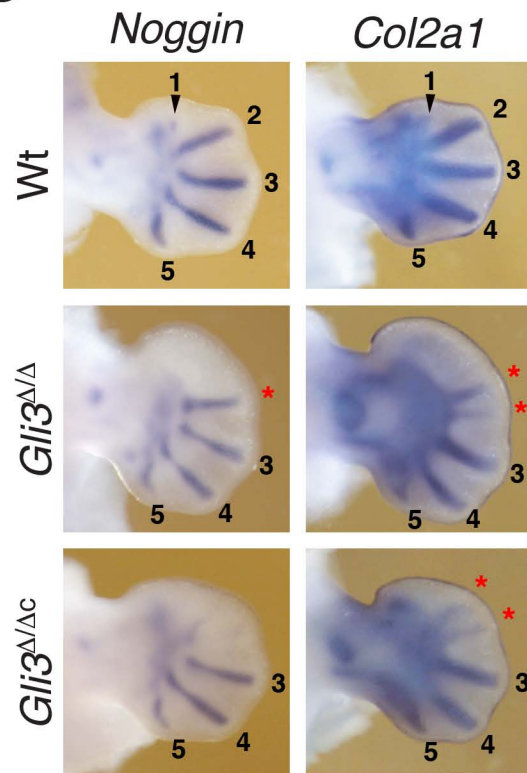
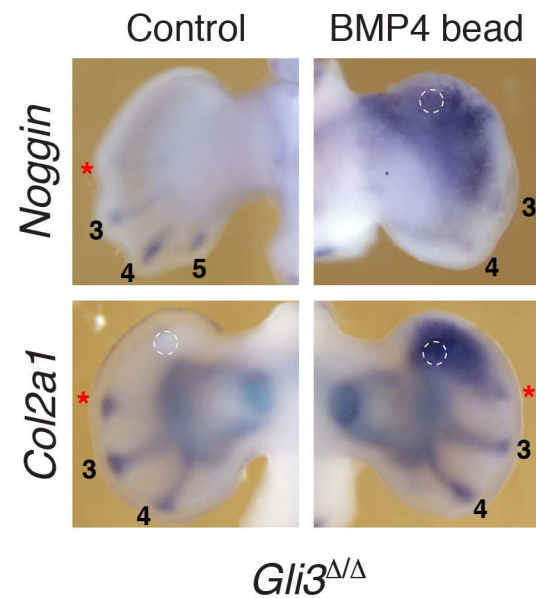
A**B****C****D****E**

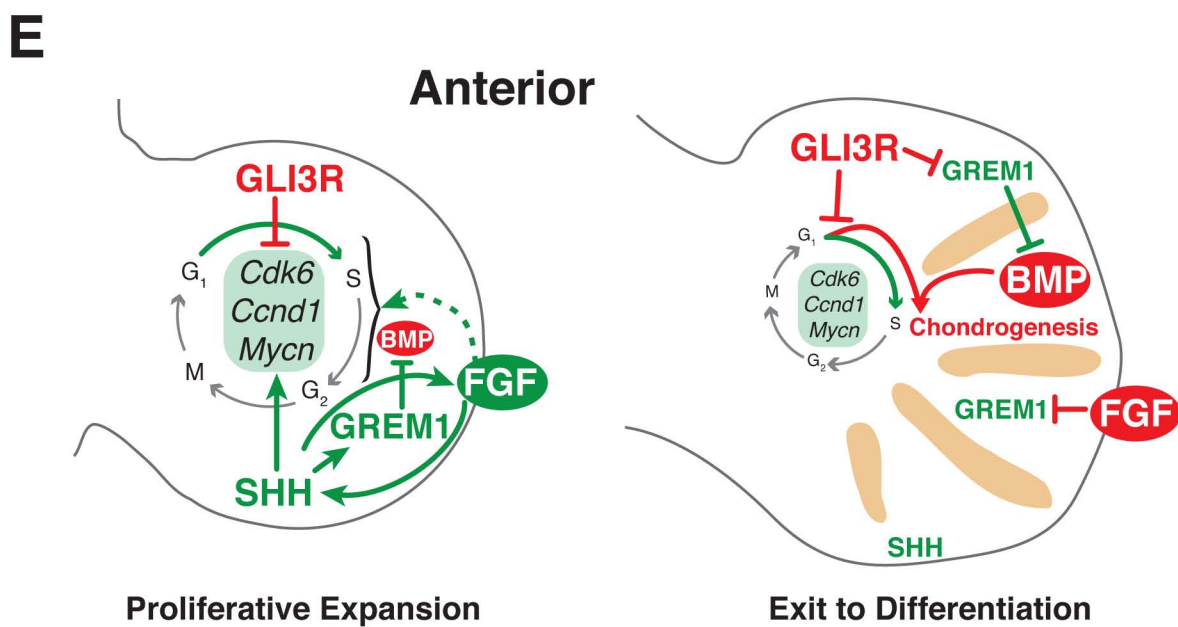
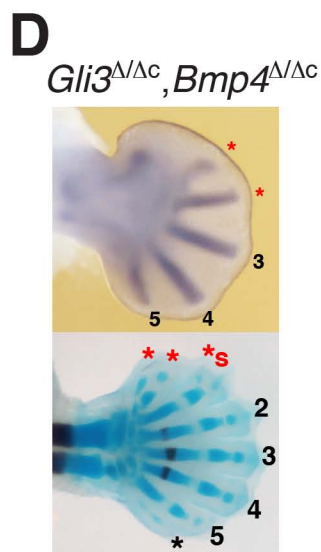
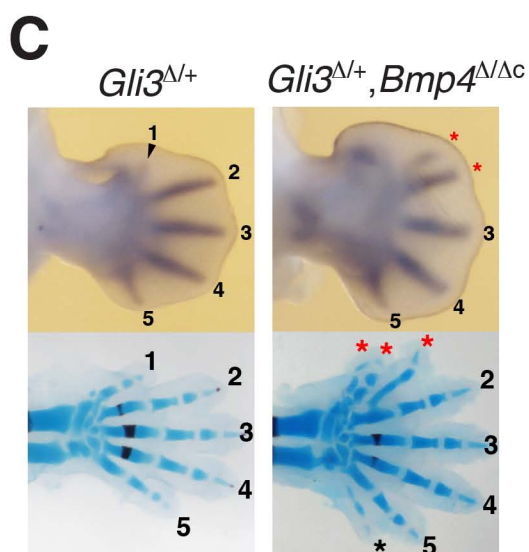
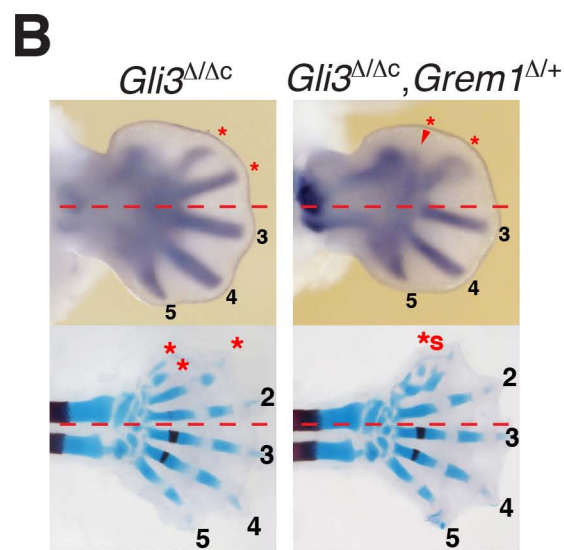
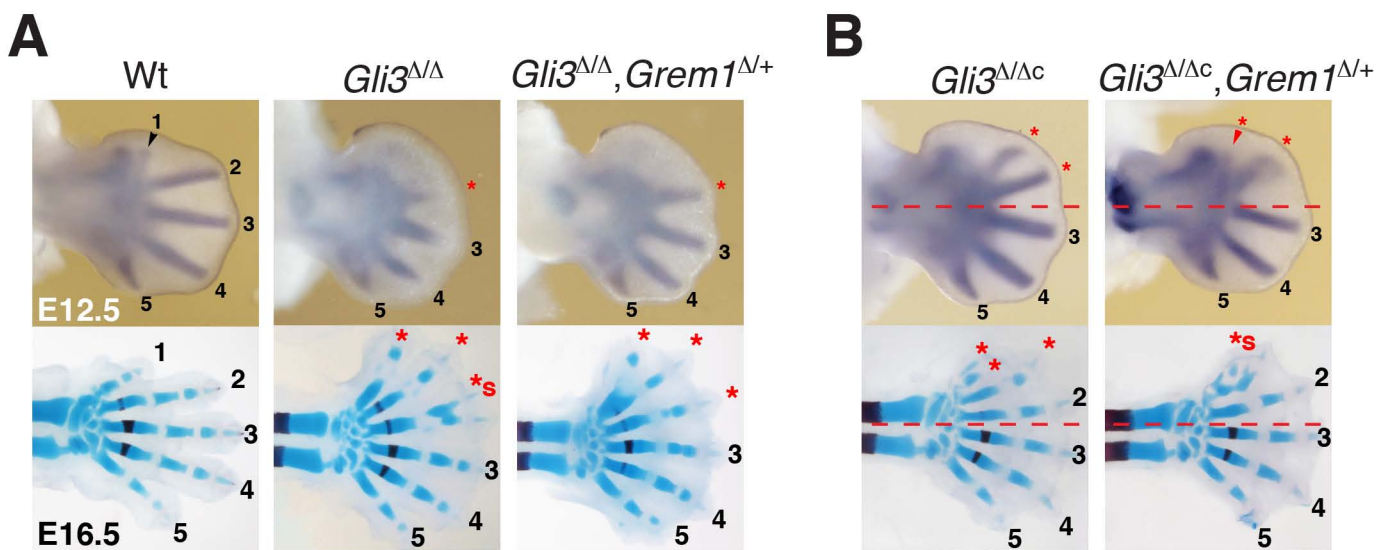
— *Hoxa13*-Cre —

A**B****C****D****E**



A**B****C****D**

A**B****C****D**



Supplemental Inventory

Figure S1, related to Figure 1. First part: molecular analysis of select genes in the anterior and posterior of $Gli3^{XtJ/XtJ}$ forelimb buds. Second part: generation and initial analysis of the conditional $Gli3$ loss-of-function allele.

Figure S2, related to Figure 2. Molecular and morphological analysis of the pre-axial polydactylies in $Gli3$ -deficient forelimb buds ($Gli3^{XtJ/XtJ}$ and $Gli3^{\Delta/\Delta c}$ alleles).

Figure S3, related to Figures 3,4. First part: molecular alterations in the expression of genes regulating the cell cycle in $Gli3$ -deficient forelimb buds. Second Part: FGF pathway activity is only increased in $Gli3^{\Delta/\Delta}$ but not $Gli3^{\Delta/\Delta c}$ forelimb buds.

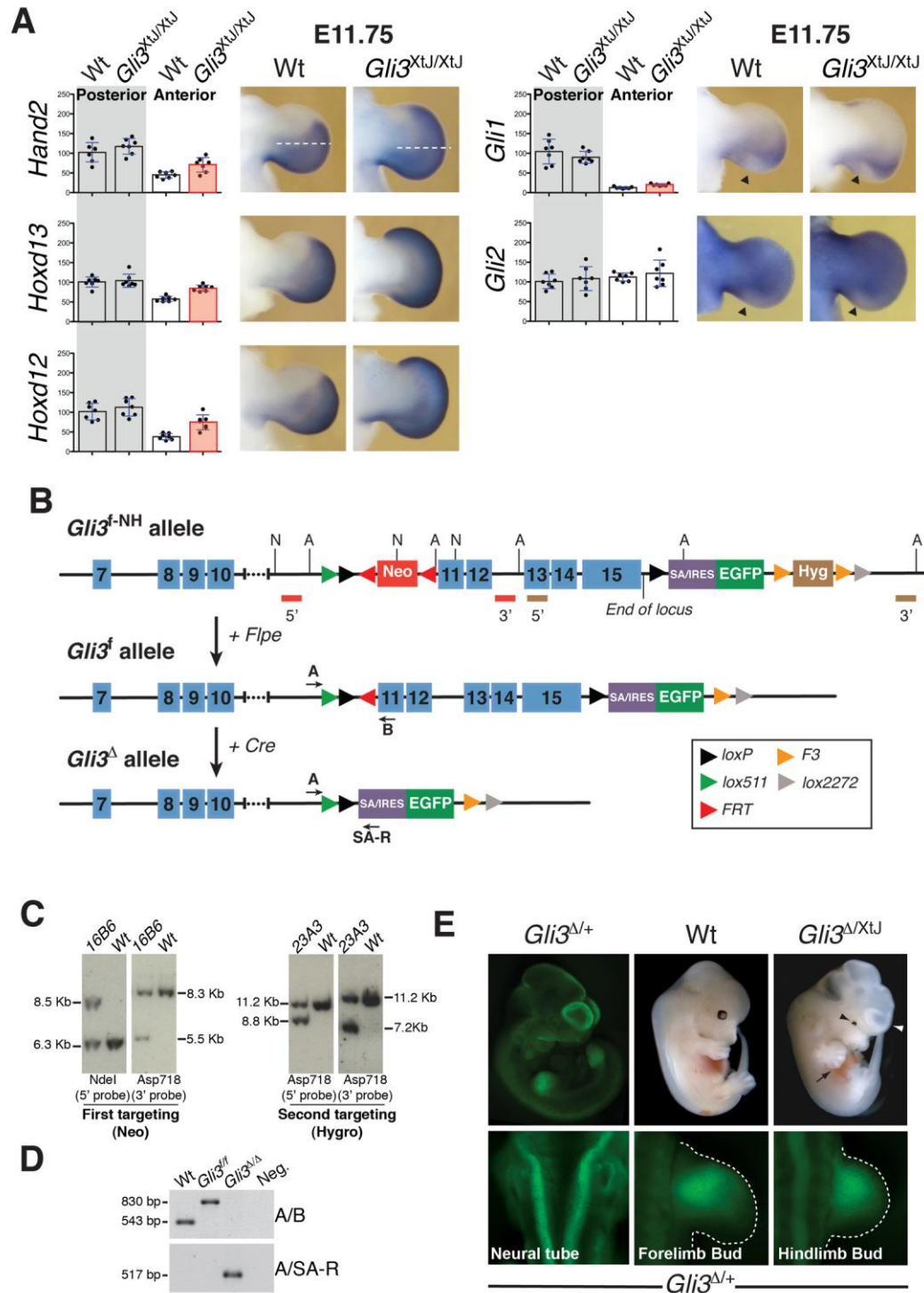
Figure S4, related to Figure 5. Ingenuity pathway analysis of the microarray, RNA *in situ* hybridization and qPCR analysis of the BMP pathway in $Gli3$ -deficient forelimb buds.

Figure S5, related to Figure 7. Analysis of $Gli3/Bmp4$ compound mutant forelimb buds.

Supplemental Experimental Procedures. Description of the generation and initial analysis of the $Gli3$ conditional loss-of-function allele. In addition, several methods and are described in more detail and all primers used are listed.

Supplemental References

Supplemental Data



(A) Quantitative and spatial analysis of the expression of key transcriptional regulators in the anterior and posterior mesenchyme of forelimb buds at E11.75 by qPCR and RNA *in situ* hybridization. The expression of *Hand2*, *Hoxd13*, *Hoxd12* and *Gli1* was increased specifically in the anterior part of *Gli3*-deficient autopods, while posterior expression was not significantly altered. SHH signal transduction was normal in the posterior mesenchyme of *Gli3*-deficient embryos, as both *Gli1* and *Gli2* transcription was not altered and the posterior-most cells underwent desensitization, which resulted in down-regulation of expression (arrowheads) identically to wild-type controls. The approximate plane of dissecting forelimb buds into anterior and posterior parts is indicated in the upper-most panels. Significant increases are shown in orange-red. Seven independent pairs of dissected forelimb buds at E11.75 were analyzed for each genotype. Relative expression levels were calculated by setting the expression levels in the posterior part of wild-type forelimb buds to 100%. All results are shown as mean \pm SD ($p \leq 0.01$). Wt: Wild-type.

(B) Scheme of the different *Gli3* alleles generated by two rounds of homologous recombination in ES cells. The heterotypic *lox511* and *lox2272* sites enable RMCE. In the parental *Gli3*^{f-NH} allele, two selection cassettes (*Neo* and *Hygro* flanked by *FRT* and *F3* sites) were removed to generate the definitive *Gli3*^f conditional allele. The *Gli3*^A null allele was generated by crossing mice carrying *Gli3*^f with a Cre-deleter mouse strain. This deletion placed *EGFP* under control of *Gli3* cis-regulatory regions (panel E). SA: Splice Acceptor; IRES: Internal Ribosome Entry Site.

(C) Characterization of the *Gli3*^{f-NH} allele in ES cells by Southern blot analysis. Examples for the first (clone 16B6) and second (clone 23A3) round of

targeting are shown. Correct 5' and 3' recombination was validated using probes outside the homology arms. The location of the relevant probes and restriction enzyme sites are indicated in panel B. N: *NdeI*; A: *Asp718*.

(D) PCR genotyping strategy for the *Gli3^f* and *Gli3^A* alleles.

(E) EGFP expressed under the control of *Gli3* *cis*-regulatory sequences in *Gli3^{Δ/+}* mouse embryos. *Gli3^{Δ/x^{tJ}}* trans-heterozygote mouse embryos displayed complete *Gli3* loss-of-function phenotypes. These included limb (arrow), brain (white arrowhead) and eye (black arrowhead) defects.

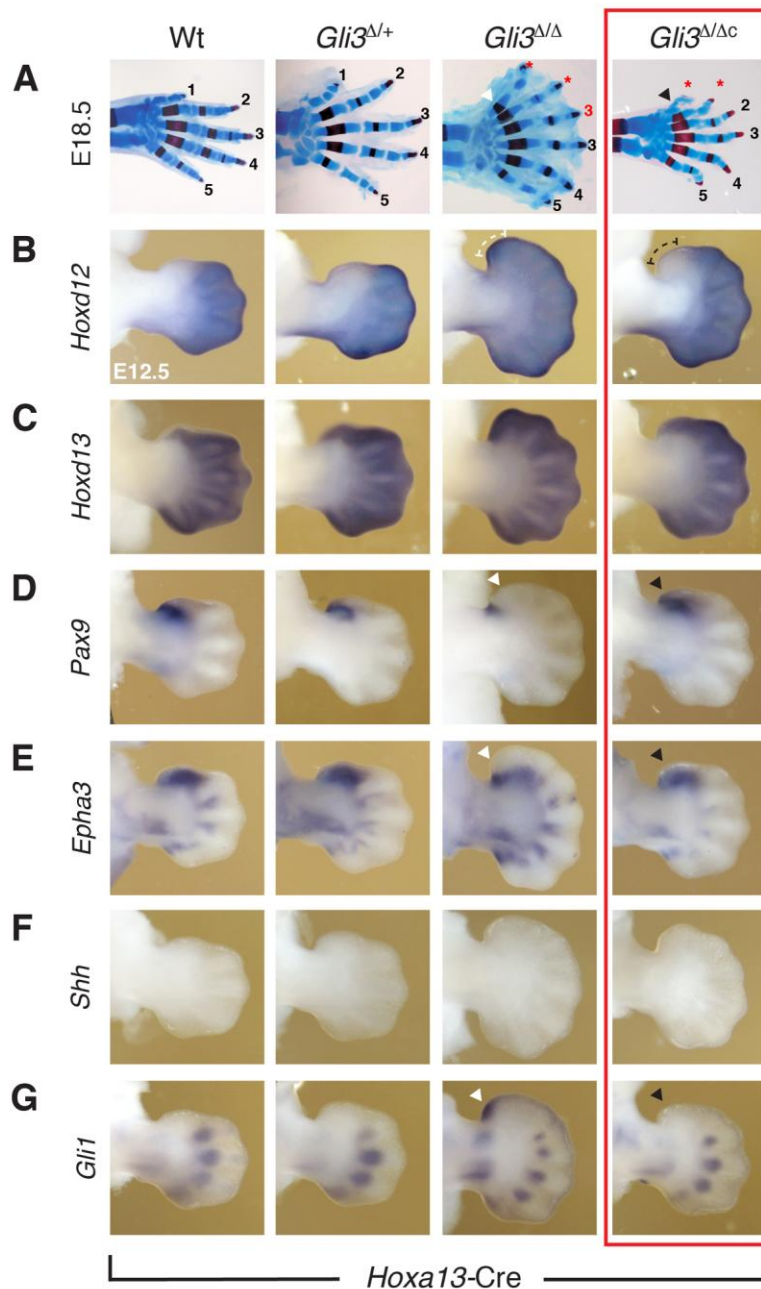


Figure S2 (related to Figure 2). Molecular and Morphological Characteristics of Pre-Axial Polydactyly in *Gli3*-Deficient Forelimb Buds.

(A) At E18.5, the lack of metacarpal mineralization and morphology of the anterior-most digit in *Gli3*^{Δ/Δc} forelimbs (black arrowhead) was reminiscent of digit 1 in wild-types. This contrasts with the anterior-most digit in *Gli3*^{Δ/Δ}

forelimbs (white arrowhead), in which the metacarpal bone had already initiated mineralization.

(B-G) Molecular analysis corroborated these morphological findings as the expression of genes marking the anterior digit 1 domain was maintained in *Gli3*^{Δ/Δc} in contrast to *Gli3*^{Δ/Δ} forelimbs at E12.5. In particular, the region that gives rise to the anterior-most digit is defined by absence of *Hoxd12* (black broken line) and the expression of *Hoxd13*, *Pax9* and *Epha3* (black arrowheads; Montavon et al., 2008; Woltering and Duboule, 2010). In *Gli3*^{Δ/Δ} forelimb buds *Hoxd12* expression was expanded anteriorly (white broken line) and the expression of both *Pax9* and *Epha3* was more restricted from the anterior-distal mesenchyme (white arrowheads). At this advanced stage, *Shh* expression was no longer detected in any of the genotypes. In contrast, low levels of *Gli1* transcript persisted in the anterior margin of *Gli3*^{Δ/Δ} (white arrowhead), but not *Gli3*^{Δ/Δc} (black arrowhead) forelimb buds. In addition, *Gli1* was expressed by all metacarpal primordia. All forelimb buds analyzed were heterozygous for the *Hoxa13*^{Cre/+} allele.

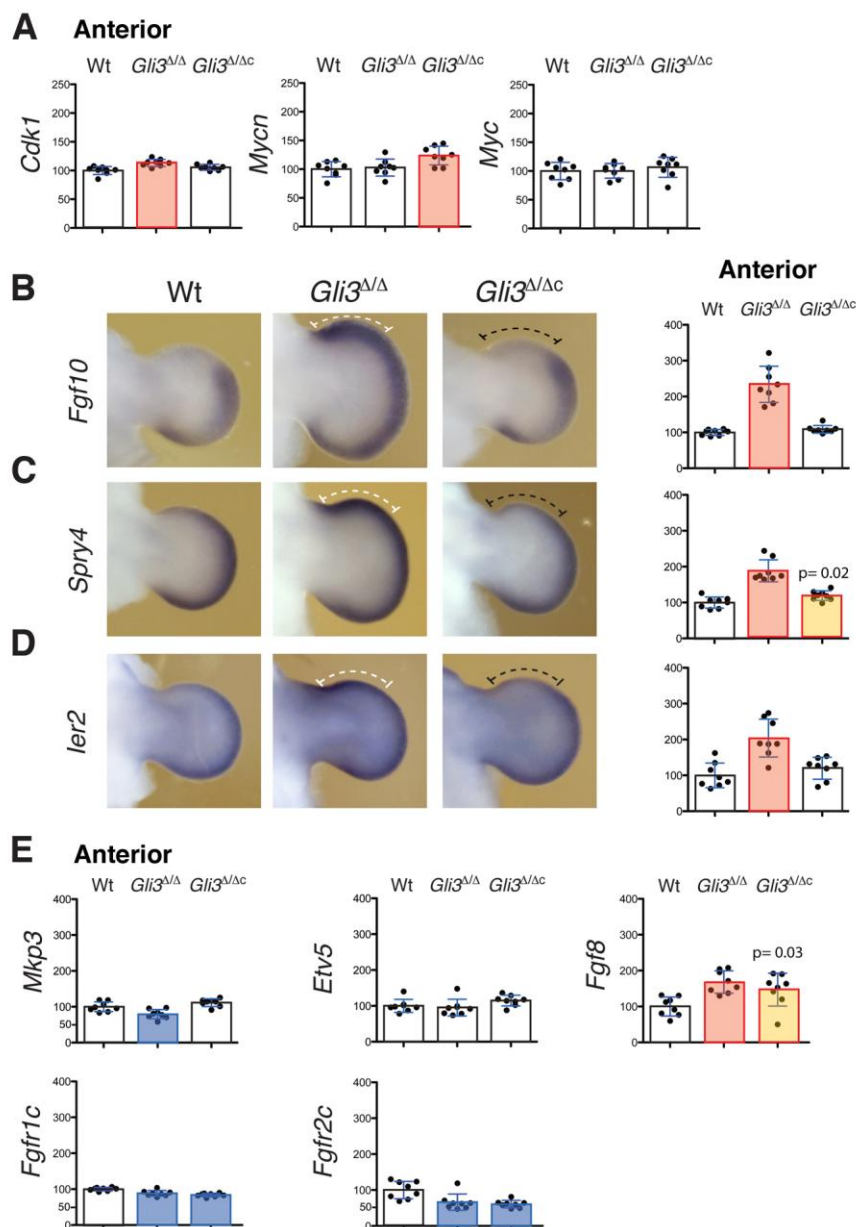


Figure S3 (related to Figures 3, 4). Differential Alterations of Cell Cycle Regulators and the FGF Pathway in *Gli3*-Deficient Forelimb Buds.

(A) *Cdk1* and *Mycn* expression were not consistently altered and the alterations detected in *Myc* by microarray analysis could not be confirmed by qPCR analysis.

(B-E) Spatial distribution and levels of *Fgf10*, *Spry4* and *Ier2* (immediate early response-2 gene), transcriptional targets of FGF signaling. This analysis

showed that FGF activity was significantly increased in *Gli3*^{Δ/Δ}, but not in *Gli3*^{Δ/Δc} forelimb buds at E11.75. Other targets of FGF signal transduction such as *Mkp3* (also known as *Dusp6*) or *Etv5* were not significantly altered in both types of *Gli3* deficiencies. Despite the normal length of the AER-*Fgf8* expression domain in *Gli3*^{Δ/Δc} forelimb buds (Figure 2E), its levels were increased as revealed by qPCR analysis. However, no obvious increase in FGF signal transduction (*Spry4*, *ler2*) was detected in *Gli3*^{Δ/Δc} forelimb buds. Eight independent pairs of dissected anterior forelimb buds at E11.75 were analyzed for each genotype by qPCR analysis. Statistically significant changes are shown in orange-red (up-regulated, p≤0.01), yellow (up-regulated, p≤0.05) and blue (down-regulated, p≤0.01). Data are represented as mean ±SD. All forelimb buds analyzed carried one *Hoxa13*^{Cre/+} allele.

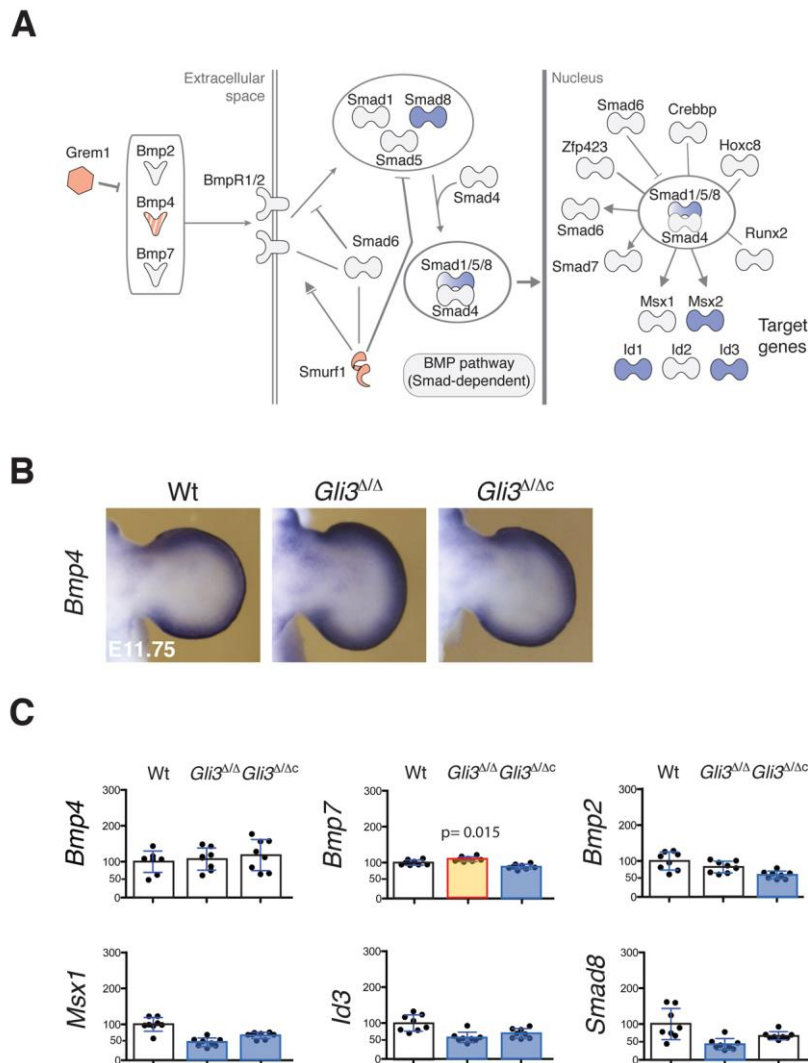


Figure S4 (related to Figure 5). Alterations of BMP Pathway Activity in *Gli3*-Deficient Forelimb Buds.

(A) Ingenuity Pathway analysis of canonical BMP signal transduction. Orange-red indicates transcriptional up-regulation and blue transcriptional down-regulation. *Bmp4* is indicated in striped orange-red as the slight up-regulation detected by microarray analysis was not confirmed by qPCR analysis. Several BMP transcriptional targets of the *Msx* and *Id* gene families (Hollnagel et al., 1999; Lallemand et al., 2005) were down-regulated.

(B) *Bmp4* expression was not significantly altered in forelimb buds at E11.75.

(C) Quantitation of transcript levels by qPCR in anterior autopods at E11.75 showed minor variations in *Bmp* expression. qPCR analysis confirmed the down-regulation of *Msx1* and *Id3* expression, which together with *Msx2* and *Id1* was indicative of reduced BMP activity. In contrast, *Smad8* was only reduced in the anterior of *Gli3*^{Δ/Δ} forelimb buds. Eight independent pairs of dissected forelimb buds at E11.75 were analyzed for each genotype. Statistically significant changes are shown in yellow (up-regulated, p≤0.05) and blue (down-regulated, p≤0.01). Data are shown as mean ±SD. All forelimb buds analyzed were heterozygous for the *Hoxa13*^{Cre/+} allele.

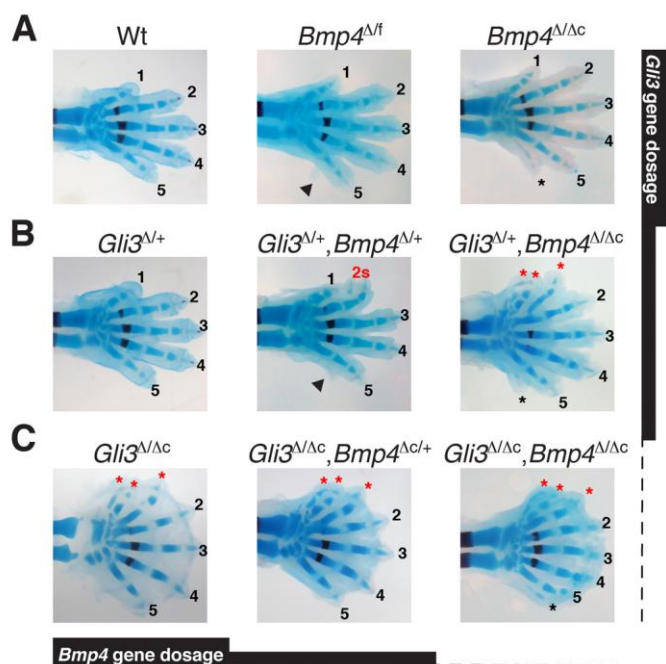


Figure S5 (related to Figure 7). Genetic Reduction of *Bmp4* and *Gli3* Reveals the Synergism in the Development of the Pre-Axial Polydactyly.

(A-C) Digit alterations for all genotypes of the *Gli3/Bmp4* intercroses at E16.5.

(A) Progressive genetic reduction of *Bmp4* reveals a dose-dependent effect on the formation of a post-axial condensation. The small postaxial outgrowth in *Bmp4*^{Δf} forelimbs is indicated by black arrowheads (n=7/10). The post-axial condensation in *Bmp4*^{ΔΔc} forelimbs is indicated by a black asterisk (n=5/8, Bandyopadhyay et al., 2006; Selever et al., 2004). f: floxed allele.

(B) The forelimb skeleton of *Gli3*^{Δ+} embryos is pentadactylous. Additional inactivation of one *Bmp4* allele results in duplicated anterior phalanges. Complete inactivation of *Bmp4* (*Gli3*^{Δ+}, *Bmp4*^{ΔΔc}) resulted in pre-axial polydactyly (red asterisks; n=10/12).

(C) *Hoxa13*-Cre mediated partial or complete inactivation of *Bmp4* in *Gli3*^{Δ/Δc} forelimbs results in pre-axial polydactyly (red asterisks; the black asterisk indicates the post-axial condensation).

All forelimbs were also heterozygous for the *Hoxa13*^{Cre/+} allele.

Supplemental Experimental Procedures

Generation of the *Gli3* Conditional Allele.

The *Gli3* genomic locus was engineered to insert *loxP* Cre-recombinase target sites upstream of the *Gli3* coding exon 11 and immediately downstream of the last exon (Figure S1B). The configuration of the *Gli3^f* allele allowed Cre-mediated recombination and thereby deletion of 60% of the *Gli3* coding exons, including the functionally essential parts of the GLI3 DNA binding domain (zinc fingers 2-5; Pavletich and Pabo, 1993). This strategy was chosen as it reproduces the exon deletion in the constitutive loss-of-function *Gli3^{XtJ}* allele (Maynard et al., 2002). While 51.5kb of genomic DNA are deleted in the *Gli3^{XtJ}* allele, the engineered deletion removes the same exons as part of a smaller 15kb deletion in the *Gli3^A* allele (Figure S1B). This much smaller deletion minimizes the possibility that *cis*-regulatory regions of e.g. neighboring genes could be affected (reviewed by Zeller and Zuniga, 2007). Moreover, we chose this strategy due to the particular nature by which proteolytic processing generates the Gli3R and Gli3FL protein isoforms. Deleting coding exons 11-15 would assure that neither of the two active isoforms could be generated after Cre-mediated recombination of the *Gli3* locus (Figure 1F).

Two successive rounds of targeting by homologous recombination in mouse R1-ES cells (Nagy et al., 1993) were required to engineer the *Gli3^{f-NH}* allele (Figure S1B). During the first targeting, the cassette was inserted at a *SacI* restriction site located 1.1kb upstream of coding exon 11 with the help of

homology arms of 5Kb and 4.8Kb on either side. In addition to a single *loxP* site, the construct encoded the *pGK-Neo* gene flanked by two *FRT* sites and a *lox511* heterotypic Cre-recombinase site for potential future use with RMCE (Branda and Dymecki, 2004). G418-resistant ES cell clones (286) were screened by Southern blot analysis (Figure S1C). Five ES cell clones were fully recombined at both 5' and 3' ends. Two of these ES cell clones with confirmed normal karyotype were electroporated a second time with a construct directed to introduce the second *loxP* site downstream of exon 15 together with a SA/IRES-EGFP reporter gene, a *pGK-Hygro* cassette flanked by *F3* sites for selection and a *lox2272* site for RMCE. The entire construct was inserted into a *BamHI* site located 500bp after the end of exon 15 with 7.2kb and 2.5kb homology arms. Hygromycin resistant ES cell clones (603) were screened by Southern blot analysis (Figure S1C). Eleven ES cell clones were correctly recombined and in seven of them, homologous recombination had occurred in *cis* to the first targeting. Two of the ES cell clones with confirmed normal karyotype were used to generate chimeric mice and germline transmission of the *Gli3*^{f-NH} allele was obtained for both. The *Gli3* floxed (*Gli3*^f) and null (*Gli3*^Δ) alleles (Figure S1D) were obtained by sequential crossing with FLPe and Cre-deleter mouse strains, respectively (Figure S1B; Rodriguez et al., 2000).

The *Gli3*^Δ allele is a complete loss-of-function allele, as it was non-complementing with the *Gli3*^{XtJ} allele (Figure S1E), and as *Gli3*^{Δ/Δ} mouse embryos displayed the full and pleiotropic phenotypes of the classical *Gli3*-deficiencies (Hui and Joyner, 1993; Johnson, 1967; Schimmang et al., 1992).

Also, *Prx1*-Cre-mediated inactivation reproduced the complete limb phenotypes of *Gli3*^{XtJ/XtJ} mouse embryos (Figure 1D). Attempts to inactivate the *Gli3*^f allele in a temporally controlled manner using a tamoxifen-inducible Cre-recombinase (Hayashi and McMahon, 2002) failed, as rapid and complete inactivation at the *Gli3* locus was not achieved (data not shown). Furthermore, the EGFP distribution in *Gli3*^{Δ/+} embryos was identical to the *Gli3* transcript distribution in wild-type embryos, which showed that no relevant *cis*-regulatory regions had been deleted (Figure S1E). The following primers were used to genotype the *Gli3*^f and *Gli3*^Δ alleles (Figure S1D):

Gli3-A: AGCTGGTAGCCTTAAAATAAGCCAA

Gli3-B: GCCTGAAAGAGGTCATCATCACC

SA-R: CGTGTCCTACAACACACTCCAA

***In Situ* Hybridization, LacZ Detection and Skeletal Preparations**

β-galactosidase activity was detected as described (Harfe et al., 2004). Mouse embryos were stained with Alcian blue and Alizarin red to differentiate cartilage (blue) and bone (red) and transcript distributions analyzed by whole-mount *in situ* hybridization (Zuniga and Zeller, 1999). For the OPT RNA *in situ* analysis shown in Figure 3E (Sharpe et al., 2002), forelimb bud samples were hybridized and processed for OPT scanning as described (Quintana and Sharpe, 2011; Summerhurst et al., 2008). Positive RNA *in situ* hybridization signals were imported into the red channel, while the autofluorescent signals that are used to reveal the overall limb bud morphology were imported into the blue channel.

Primers used for qPCR Analysis of Gene Expression

The following primers for qPCR were already described: *Bmp2*, *Bmp4*, *Bmp7*, *Grem1*, *Msx2*, *Fgf8*, *Gli1*, *Rpl19* (Benazet et al., 2009); *Hand2* (Galli et al., 2010); *Cdkn2c* (Uziel et al., 2005); *Cdk1* (Trowbridge et al., 2006); *Fgfr1c*, *Fgfr2c* (Fon Tacer et al., 2010); *Smad8* (Yew et al., 2005).

Gene	Forward Primer	Reverse Primer
<i>Hoxd13</i>	5'-AGGTGTAAGTGTGCCAAGGATCAG-3'	5'-AAGCCACATCTCCTGGAAAGG-3'
<i>Hoxd12</i>	5'-GCCCCTTCGCAGCAGAA-3'	5'-TGGAATCAGGCCCTTTCCTT-3'
<i>Gli2</i>	5'-GTGCACAGCAGCCCCACACTCTC-3'	5'-GGTAATAGTCTGAAGGGTTGGTGCCTGG-3'
<i>Cdk6</i>	5'-GCCCTTACCTCGGTGGTC-3'	5'-ACAGGGGTGGCATAGCTG-3'
<i>Ccnd1</i>	5'-CAGACGTTCAGAACCAGATTC-3'	5'-CCCTCCAATAGCAGCGAAAAC-3'
<i>Myc</i>	5'-TGAAGGCTGGATTTCTTTG-3'	5'-TTCTCTTCCTCGTCGCAGAT-3'
<i>Mycn</i>	5'-AACAAGGCGGTAACCACTTTCAC-3'	5'-TGCTGCTGATGGATGGGAAC-3'
<i>Fgf10</i>	5'-TTTGTGAGTTCTGCCTCCGTG-3'	5'-ACCCGTGGCTAACACACTTCAG-3'
<i>Spry4</i>	5'-TGTGACTCTGCAGCTCCTCAA-3'	5'-ATGAGGCTGGAGGTCCTGAACT-3'
<i>Ier2</i>	5'-GGCTTTAGGCATTATGCTCG-3'	5'-TCAGCCCCTTACACGATTTTC-3'
<i>Mkp3</i>	5'-GGCTGCTGCTCAAGAACTCAA-3'	5'-AAGCCACCTTCCAGGTAGAACG-3'
<i>Etv5</i>	5'-TGGCTCACGATTCTGAAGAGTTG-3'	5'-GGAACCTTGCTTCAGCTAACCAA-3'
<i>Msx1</i>	5'-TCAAGCTGCCAGAAGATGCTC-3'	5'-TTGGTCTTGTGCTTGCCTAGG-3'
<i>Id1</i>	5'-CTGAACGGCGAGATCAGTG-3'	5'-TTTTCTCTTGCCTCCTGAA-3'
<i>Id3</i>	5'-GAGGAGCTTTTGCCACTGAC-3'	5'-GAGAGAGGGTCCCAGAGTCC-3'
<i>Hprt1</i>	5'-GCAAACCTTGTCTTCCCTGGT-3'	5'-GGTCCTTTTACCAGCAAGCT-3'

Chromatin Immunoprecipitation (ChIP)

Forelimbs and hindlimbs of 10 wild-type (n=5 independent experiments) and *Gli3*^{ΔΔ} (n=3 independent experiments) embryos at E11.75 (~ 50 somites)

were dissected in cold PBS and disaggregated with a douncer. After crosslinking for 5 minutes (Visel et al., 2009), isolated nuclei were snap-frozen and kept at -80°C. Chromatin fragmentation was done using a Bioruptor sonicator, and each sample of sonicated chromatin was then processed for ChIP as described (Vokes et al., 2008) using a rabbit polyclonal anti-GLI3 antiserum (no. 2676, Genentech, Wen et al., 2010). To compute the level of enrichment for a particular amplicon, the values of both the ChIP and input samples were compared with those of an unrelated amplicon within the mouse β -actin locus serving as negative control (Galli et al., 2010). All results (mean \pm SD) are based on analyzing 3-5 independent experiments per genotype. The significance of all differences was assessed using the two-tailed, non-parametric Mann-Whitney test. All oligos used for amplification are listed below.

Primers used for ChIP-qPCR

Amplicon	Forward Primer	Reverse Primer
<i>Cdk6-1</i>	5'-AACTATTCCAGCCTGTTGTGTG-3'	5'-CAATGGATGCAGTCATGTGC-3'
<i>Cdk6-2</i>	5'-CCTGTGCAAGTTCCCTCTGT-3'	5'-GGGACTTGAAGCAAGAGTGC-3'
<i>Cdk6-3</i>	5'-AGATGGTCTGTCTCGCTGA-3'	5'-ATGGCAAGCTTAGTGGGAGA-3'
<i>Cdk6-4</i>	5'-ACCGGTGACTCTGTTAGACAGG-3'	5'-TTCAGAATAGCTTGGCTGCC-3'
<i>Cdk6-5</i>	5'-CACCTCAGGCACTGGATATGT-3'	5'-CTCACCAAGCTGGACTTACACA-3'
<i>Grem1-1</i>	5'-TCTTGTCTCTTCTGGACCGC-3'	5'-CATCAATCTGAGCTGCAGGA-3'
<i>Grem1-2</i>	5'-CCTCTTCCACAGTAGGCTCTTG-3'	5'-GGAAAGTGGGAGCTCAAACA-3'
<i>Grem1-3</i>	5'-ACAGTGCAGGTCTAAGCAATCC-3'	5'-CCTGCTATGTTTATGGGGACTT-3'
<i>Grem1-4</i>	5'-CATTGCTCTGTTGGAACAAGG-3'	5'-CAACACTTCCACCATGAGCTG-3'
β -actin	5'-ACACTGTGCCCATCTACGAGG-3'	5'-CGCTCGTTGCCAATAGTGATG-3'

Supplemental References

Branda, C.S., and Dymecki, S.M. (2004). Talking about a revolution: The impact of site-specific recombinases on genetic analyses in mice. *Dev Cell* 6, 7-28.

Fon Tacer, K., Bookout, A.L., Ding, X., Kurosu, H., John, G.B., Wang, L., Goetz, R., Mohammadi, M., Kuro-o, M., Mangelsdorf, D.J., *et al.* (2010). Research resource: Comprehensive expression atlas of the fibroblast growth factor system in adult mouse. *Molecular endocrinology* 24, 2050-2064.

Hayashi, S., and McMahon, A.P. (2002). Efficient recombination in diverse tissues by a tamoxifen-inducible form of Cre: a tool for temporally regulated gene activation/inactivation in the mouse. *Dev Biol* 244, 305-318.

Hollnagel, A., Oehlmann, V., Heymer, J., Ruther, U., and Nordheim, A. (1999). Id genes are direct targets of bone morphogenetic protein induction in embryonic stem cells. *J Biol Chem* 274, 19838-19845.

Johnson, D.R. (1967). Extra-toes: a new mutant gene causing multiple abnormalities in the mouse. *J Emb Exp Morph* 17, 543-581.

Lallemand, Y., Nicola, M.A., Ramos, C., Bach, A., Cloment, C.S., and Robert, B. (2005). Analysis of Msx1; Msx2 double mutants reveals multiple roles for Msx genes in limb development. *Development* 132, 3003-3014.

Montavon, T., Le Garrec, J.F., Kerszberg, M., and Duboule, D. (2008). Modeling Hox gene regulation in digits: reverse collinearity and the molecular origin of thumbness. *Genes Dev* 22, 346-359.

Nagy, A., Rossant, J., Nagy, R., Abramow-Newerly, W., and Roder, J.C. (1993). Derivation of completely cell culture-derived mice from early-passage embryonic stem cells. *Proc Natl Acad Sci USA* 90, 8424-8428.

Pavletich, N.P., and Pabo, C.O. (1993). Crystal structure of a five-finger GLI-DNA complex: new perspectives on zinc fingers. *Science* 261, 1701-1707.

Quintana, L., and Sharpe, J. (2011). Preparation of mouse embryos for optical projection tomography imaging. *Cold Spring Harb Protoc* 2011, 664-669.

Rodriguez, C.I., Buchholz, F., Galloway, J., Sequerra, R., Kasper, J., Ayala, R., Stewart, A.F., and Dymecki, S.M. (2000). High-efficiency deleter mice show that FLPe is an alternative to Cre-loxP. *Nat Genet* 25, 139-140.

- Selever, J., Liu, W., Lu, M.F., Behringer, R.R., and Martin, J.F. (2004). Bmp4 in limb bud mesoderm regulates digit pattern by controlling AER development. *Dev Biol* 276, 268-279.
- Sharpe, J., Ahlgren, U., Perry, P., Hill, B., Ross, A., Hecksher-Sorensen, J., Baldock, R., and Davidson, D. (2002). Optical projection tomography as a tool for 3D microscopy and gene expression studies. *Science* 296, 541-545.
- Summerhurst, K., Stark, M., Sharpe, J., Davidson, D., and Murphy, P. (2008). 3D representation of Wnt and Frizzled gene expression patterns in the mouse embryo at embryonic day 11.5 (Ts19). *Gene Expr Patterns* 8, 331-348.
- Trowbridge, J.J., Scott, M.P., and Bhatia, M. (2006). Hedgehog modulates cell cycle regulators in stem cells to control hematopoietic regeneration. *Proc Natl Acad Sci USA* 103, 14134-14139.
- Uziel, T., Zindy, F., Xie, S., Lee, Y., Forget, A., Magdaleno, S., Rehg, J.E., Calabrese, C., Solecki, D., Eberhart, C.G., *et al.* (2005). The tumor suppressors Ink4c and p53 collaborate independently with Patched to suppress medulloblastoma formation. *Genes Dev* 19, 2656-2667.
- Visel, A., Blow, M.J., Li, Z., Zhang, T., Akiyama, J.A., Holt, A., Plajzer-Frick, I., Shoukry, M., Wright, C., Chen, F., *et al.* (2009). ChIP-seq accurately predicts tissue-specific activity of enhancers. *Nature* 457, 854-858.
- Woltering, J.M., and Duboule, D. (2010). The origin of digits: expression patterns versus regulatory mechanisms. *Dev Cell* 18, 526-532.
- Yew, K.H., Hembree, M., Prasad, K., Preuett, B., McFall, C., Benjes, C., Crowley, A., Sharp, S., Tulachan, S., Mehta, S., *et al.* (2005). Cross-talk between bone morphogenetic protein and transforming growth factor-beta signaling is essential for exendin-4-induced insulin-positive differentiation of AR42J cells. *J Biol Chem* 280, 32209-32217.
- Zeller, R., and Zuniga, A. (2007). Shh and Gremlin1 chromosomal landscapes in development and disease. *Curr Opin Genet Dev* 17, 428-434.

CURRICULUM VITAE

Name: Marco Osterwalder

Address: Department of Biomedicine
Developmental Genetics
University of Basel
Mattenstrasse 28
CH-4058 Basel
Switzerland
Phone: +41 (0)61 695 3040
Email: M.Osterwalder@stud.unibas.ch

Date of Birth: August 22, 1982

Place of Birth: Muri (AG)

Nationality: Swiss

Native place: Gaiserwald/Waldkirch (SG)

School: *Primarschule:* Mühlau (AG); August 1989 – July 1994

Bezirksschule (Progymnasium): Sins (AG); August 1994 – June 1998

Military service: *Corps:* Fliegerabwehrtruppen
Function: Lenkwaffensoldat
Duration: 10/02/03 – 23/05/03

Academic Education:

Matura: **08/1998 - 07/2002:** Alte Kantonsschule Aarau,
Typus A

B.Sc. **10/2003 - 07/2006:** Biozentrum, University of Basel, Switzerland.

Awarded: Bachelor of Science in Molecular
Biology

M.Sc. **10/2006 - 10/2007:** Department Of Biomedicine (DBM),
Developmental Genetics, University of Basel,
Switzerland.

Research project:
“Function of Hand2 in early limb bud
polarisation”
under the supervision of Dr. Antonella Galli
and Prof. Dr. Rolf Zeller.

Awarded: Master of Science in Molecular
Biology

Ph.D. **02/2008 - 03/2012:** Department Of Biomedicine (DBM),
Developmental Genetics, University of Basel,
Switzerland.

SNF funded research project:
“Genome-wide identification of Hand2 target
regions in mouse embryos using dRMCE, a
new genetic tool”
under the supervision of Dr. Javier Lopez-Rios
and Prof. Dr. Rolf Zeller.

Awarded: Ph.D. in Cell Biology

Peer Reviewed Publications:

Galli, A., Robay, D., **Osterwalder, M.**, Bao, X., Benazet, J.D., Tariq, M., Paro, R., Mackem, S., and Zeller, R. (2010). Distinct roles of Hand2 in initiating polarity and posterior Shh expression during the onset of mouse limb bud development. **PLoS Genet** 6, e1000901.

Osterwalder, M., Galli, A., Rosen, B., Skarnes, W.C., Zeller, R. and Lopez-Rios, J. (2010). Dual RMCE for efficient re-engineering of mouse mutant alleles. **Nature Methods** (11):893-5.

Itou, J., Kawakami, H., Quach, T., **Osterwalder, M.**, Evans, S.M., Zeller, R., Kawakami, Y. (2012). Islet1 regulates establishment of the posterior hindlimb field upstream of the Hand2-Shh morphoregulatory gene network in mouse embryos. **Development**. [Epub ahead of print]

Lopez-Rios, J., Speziale, D., Robay, D., Scotti, M., **Osterwalder, M.**, Nusspaumer, G., Galli, A., Holländer, G., Kmita, M., and Zeller, R. (2012). GLI3 Constrains Digit Number by Controlling Both Progenitor Proliferation and BMP-dependent Exit to Chondrogenesis. **Dev Cell** (*in press*).

Non Peer Reviewed Publication:

Osterwalder, M., Lopez-Rios, J., and Zeller, R. Next generation engineering of conditional mouse alleles with loxP and FRT sites by dual RMCE. **Protocol Exchange**. doi:10.1038/protex.2010.210